

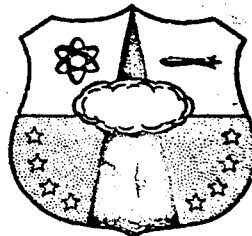


B

AIR FORCE DESIGN MANUAL
PRINCIPLES AND PRACTICES FOR
DESIGN OF HARDENED STRUCTURES

TECHNICAL DOCUMENTARY REPORT NUMBER AFSWC-TDR-62-138

December 1962



Research Directorate
AIR FORCE SPECIAL WEAPONS CENTER
Air Force Systems Command
Kirtland Air Force Base
New Mexico

Project Number 1080, Task Number 10802

(Prepared under Contract AF 29(601)-2390
by N.M. Newmark and J.D. Haltiwanger,
The Department of Civil Engineering,
University of Illinois, Urbana, Illinois)

GENERAL DISCLAIMER

This document may have problems that one or more of the following disclaimer statements refer to:

- This document has been reproduced from the best copy furnished by the sponsoring agency. It is being released in the interest of making available as much information as possible.
- This document may contain data which exceeds the sheet parameters. It was furnished in this condition by the sponsoring agency and is the best copy available.
- This document may contain tone-on-tone or color graphs, charts and/or pictures which have been reproduced in black and white.
- The document is paginated as submitted by the original source.
- Portions of this document are not fully legible due to the historical nature of some of the material. However, it is the best reproduction available from the original submission.

**HEADQUARTERS
AIR FORCE SPECIAL WEAPONS CENTER
Air Force Systems Command
Kirtland Air Force Base
New Mexico**

When Government drawings, specifications, or other data are used for any purpose other than in connection with a definitely related Government procurement operation, the United States Government thereby incurs no responsibility nor any obligation whatsoever; and the fact that the Government may have formulated, furnished, or in any way supplied the said drawings, specifications, or other data, is not to be regarded by implication or otherwise as in any manner licensing the holder or any other person or corporation, or conveying any rights or permission to manufacture, use, or sell any patented invention that may in any way be related thereto.

This report is made available for study upon the understanding that the Government's proprietary interests in and relating thereto shall not be impaired. In case of apparent conflict between the Government's proprietary interests and those of others, notify the Staff Judge Advocate, Air Force Systems Command, Andrews AF Base, Washington 25, DC.

This report is published for the exchange and stimulation of ideas; it does not necessarily express the intent or policy of any higher headquarters.

Qualified requesters may obtain copies of this report from ASTIA. Orders will be expedited if placed through the librarian or other staff member designated to request and receive documents from ASTIA.


A B S T R A C T


This is the second edition of the Air Force Design Manual. "Design of Protective Structures to Resist the Effects of Nuclear Weapons," AFSWC, TR-59-70, December, 1959 (Conf.). Its intended use is for the planning and design of structures to resist the effects of nuclear weapons ranging into the megaton class. The emphasis is primarily on underground construction. The material presented is derived from existing knowledge and theory, so that the manual is also a report of the state of the art.

Starting with general considerations of site selection and structural function, various phases of design are considered: free-field phenomena in air and ground, material properties, failure criteria, architectural and mechanical features, radiation effects, surface openings, conversion of free-field phenomena to loads on structures, and the design and proportioning of structural elements and structures.

PUBLICATION REVIEW

This report has been reviewed and is approved.


DONALD I. PRICKETT
Colonel USAF
Director, Research Directorate


JOHN J. DISHUCK
Colonel USAF
DCS/Plans & Operations

FOREWORD

This revised manual is the result of efforts of the staff of the Department of Civil Engineering of the University of Illinois. The work was accomplished under the general direction of Dr. N. M. Newmark, Professor of Civil Engineering and Head of Department, and the immediate supervision of Dr. J. D. Haltiwanger, Professor of Civil Engineering. Direct or indirect contributions have been received from many staff members and much of the material published in the first edition has been retained.

The principal authors of this revision were:

Dr. M. T. Davisson
Dr. J. D. Haltiwanger
Dr. J. G. Hammer
Dr. J. W. Melin
Dr. J. P. Murtha
Dr. W. C. Schnobrich
Dr. R. N. Wright, III

Major contributions to the work were made by Dr. Wright and Dr. Murtha.

Figures and text have been reproduced freely from various sources so as to present herein a complete procedure without requiring reference to other material that may not be readily available to the reader. In this regard special acknowledgment is due AFSWC and to N. M. Newmark and W. J. Hall for the use of material from AFSWC Report TDR-62-6, and acknowledgment is also due the Office of the Assistant Secretary of Defense for Installations and Logistics and to Newmark, Hansen and Associates for the use of material and numerous charts in Chapter 9 from the Protective Construction Review Guide.

This work was done under the auspices of the Structural Division, Research Directorate, Air Force Special Weapons Center, Kirtland Air Force Base, New Mexico.

TABLE OF CONTENTS

	<u>Page</u>
 CHAPTER 1. INTRODUCTION	
1.1 Objective	1-1
1.2 Sources	1-1
1.3 General Assumptions	1-2
1.4 Presentation	1-3
1.5 Notation	1-3
1.6 Accuracy and Precision.	1-3
1.7 Statistical Aspects	1-4
 CHAPTER 2. GENERAL CONSIDERATIONS	
2.1 Introduction	2-1
2.2 Pre-Design Considerations	2-2
2.2.1 Functions of the Facility.	2-2
2.2.2 Importance of the Facility	2-3
2.2.3 Probability and Proportions of Attack	2-3
2.2.4 Required Levels of Protection	2-4
2.2.5 Economic Considerations	2-5
2.3 Choice of Structural Configuration.	2-5
 CHAPTER 3. AIR BLAST PHENOMENA	
3.1 Introduction	3-1
3.2 Air Blast	3-2
3.2.1 Introduction	3-2
3.2.2 Overpressure	3-3
3.2.3 Dynamic Pressure	3-7
3.2.4 Effects of Surface and Topography.	3-20
3.3 Air Blast in Tunnels and Ducts.	3-22
3.3.1 Shock Formation in Straight Tunnels	3-24
3.3.2 Effect of Bends and Junctions.	3-28
3.3.3 Attenuation of Peak Overpressure in Straight Tunnels	3-30
3.3.4 Blast Loading on Doors and Blast Valves in Tunnels and Ducts.	3-32
3.4 References	3-35

TABLE OF CONTENTS (Cont'd)

	<u>Page</u>
 CHAPTER 4. FREE-FIELD GROUND MOTION	
4.1 Introduction	4-1
4.2 Air-Induced Ground Motion	4-2
4.2.1 Introduction	4-2
4.2.2 Stress Attenuation	4-5
4.2.3 Soil Properties	4-12
4.2.4 Displacement	4-26
4.2.5 Velocity	4-35
4.2.6 Acceleration	4-37
4.2.7 Outrunning Ground Motions	4-40
4.2.8 Examples of Air-Induced Displacement Computation	4-41
4.3 Direct-Transmitted Ground Shock	4-49
4.3.1 Introduction	4-49
4.3.2 Theoretical Basis of Predictions	4-51
4.3.3 Energy Equivalence	4-53
4.3.4 Experimental Results in Rock	4-54
4.3.5 Applicability to Other Materials	4-56
4.3.6 Tangential Motions	4-61
4.3.7 Effect of Layered Systems	4-62
4.4 References	4-64
 CHAPTER 5. DETERMINATION OF LOADS ON STRUCTURES	
5.1 Introduction	5-1
5.2 Above-Ground Structures	5-2
5.2.1 Introduction	5-2
5.2.2 Completely Closed Rectangular Structures	5-4
5.2.3 Above-Ground Open Rectangular Structures	5-10
5.2.4 Above-Ground Arches	5-16
5.2.5 Above-Ground Domes	5-22
5.3 Underground Structures	5-25
5.3.1 Introduction	5-25
5.3.2 Soil-Structure Interaction	5-29
5.3.3 Influence of Construction Methods	5-46
5.3.4 Fully-Buried Rectangular Structures	5-51
5.3.5 Fully Buried Arches	5-55
5.3.6 Fully Buried Domes	5-59
5.3.7 Underground Vertical Cylindrical Structures	5-60

TABLE OF CONTENTS (Cont'd)

	<u>Page</u>
5.4 Partially Buried Structures	5-71
5.4.1 Introduction	5-71
5.4.2 Rectangular Structures	5-72
5.4.3 Partially Buried Arches	5-77
5.4.4 Partially Buried Domes	5-80
5.5 References	5-82
CHAPTER 6. DYNAMIC PROPERTIES OF MATERIALS	
6.1 Introduction	6-1
6.2 Metals	6-1
6.2.1 General Discussion	6-1
6.2.2 Structural Steel	6-3
6.2.3 High Strength Low Alloy Steels	6-4
6.2.4 Reinforcing Steel	6-5
6.2.5 Brittle Behavior of Materials and Connections	6-7
6.3 Concrete	6-10
6.4 Timber	6-12
6.5 References	6-13
CHAPTER 7. FAILURE AND DESIGN CRITERIA	
7.1 Introduction	7-1
7.2 Failure vs Satisfactory Performance	7-2
7.3 Safety Factor	7-3
7.4 Design Criteria	7-4
7.5 Ductility Ratio	7-5
7.6 General Recommendations	7-9
7.7 References	7-11
CHAPTER 8. PROPERTIES OF STRUCTURAL ELEMENTS	
8.1 Introduction	8-1
8.2 Reinforced Concrete Beams and One-Way Slabs	8-1
8.2.1 Introduction	8-1
8.2.2 Flexural Strength of Beam Sections	8-3
8.2.3 Diagonal Tension	8-6
8.2.4 Pure Shear	8-7
8.2.5 Stiffness	8-10
8.2.6 Natural Period	8-10

TABLE OF CONTENTS (Cont'd)

	<u>Page</u>
8.3 Two-Way Slabs	8-13
8.3.1 Flexural Strength	8-13
8.3.2 Shear Strength	8-16
8.3.3 Supporting Beams	8-16
8.3.4 Stiffness	8-17
8.3.5 Natural Period	8-18
8.4 Reinforced Concrete Columns	8-19
8.4.1 Axially Loaded Reinforced Concrete Columns	8-19
8.4.2 Combined Flexure and Axial Loads . .	8-20
8.4.3 Period	8-21
8.5 Steel Beams	8-21
8.5.1 Introduction	8-21
8.5.2 Flexural Strength	8-22
8.5.3 Shear Strength	8-22
8.5.4 Local Buckling	8-23
8.5.5 Stiffness	8-24
8.5.6 Natural Period	8-25
8.6 Steel Columns	8-25
8.6.1 Axially Loaded Columns	8-25
8.6.2 Local Buckling	8-26
8.7 Circular Arches	8-27
8.7.1 Introduction	8-27
8.7.2 Natural Period	8-27
8.7.3 Resistance	8-31
8.7.4 Buckling	8-34
8.7.5 Ductility Factor	8-36
8.8 Domes	8-37
8.8.1 Introduction	8-37
8.8.2 Ductility	8-38
8.8.3 Natural Period	8-38
8.8.4 Compression Mode	8-39
8.8.5 Flexural Mode	8-41
8.8.6 Buckling	8-45
8.9 Silos and Tunnels	8-46
8.10 Footings.	8-47
8.10.1 Flexural Resistance	8-47
8.10.2 Shear	8-47
8.11 References	8-47

CHAPTER 9. DESIGN AND PROPORTIONING OF STRUCTURAL ELEMENTS

9.1 Introduction	9-1
----------------------------	-----

TABLE OF CONTENTS (Cont'd)

	<u>Page</u>
9.2 Reinforced Concrete Beams and One-Way Slabs	9-3
9.3 Reinforced Concrete Two-Way Slab and Supporting Beams	9-5
9.4 Steel Beams	9-6
9.5 Arches	9-7
9.6 Domes	9-10
9.7 Vertical Shafts and Silos	9-12
9.8 Footings	9-13
9.9 Columns	9-14
CHAPTER 10. EARTH SHOCK AND SHOCK MOUNTING	
10.1 Introduction	10-1
10.2 Shock Response Spectra	10-3
10.2.1 Response Spectra for Elastic Systems	10-3
10.2.2 Response Spectra for Inelastic Systems	10-7
10.3 Design of Simple Structures for Ground Shock	10-13
10.4 Design of Multi-Story Structures for Ground Shock	10-14
10.4.1 Design for Horizontal Motions	10-14
10.4.2 Design for Vertical Motions	10-17
10.5 Shock Effects on Mounted Equipment	10-18
10.5.1 Basic Considerations in Shock Mounting	10-19
10.5.2 Provision for Relative Distortion of Equipment and Structure	10-20
10.5.3 Nature of Elastic Systems Comprised of Mounted Equipment	10-20
10.5.4 Response of Light Equipment Mounted on Building Frame Members	10-23
10.5.5 Shock Effects on Heavy Equipment	10-24
10.6 Theoretical Approach for Complex Linear Systems	10-25
10.7 References	10-27
CHAPTER 11. ARCHITECTURAL CONSIDERATIONS	
11.1 General Approach	11-1
11.2 Entranceways	11-3
11.3 Doors	11-3
11.3.1 Protective Doors	11-3
11.3.2 Types of Doors	11-4
11.3.3 Functional Requirements	11-7
11.3.4 Important Door Characteristics	11-8

TABLE OF CONTENTS (Cont'd)

	<u>Page</u>
11.4 Ventilation and Blast Valves.	11-12
11.5 Foundations and Sealing	11-15
11.6 Structural Details	11-17
11.6.1 Concrete Construction	11-18
11.6.2 Steel Construction	11-19
11.7 Utility Systems	11-20
11.7.1 Utility Service Loads	11-21
11.7.2 Water Supply	11-22
11.7.3 Water Storage	11-22
11.7.4 Lighting, Electric Power	11-23
11.7.5 Sanitary Sewers	11-23
11.7.6 Fire Protection	11-23
11.7.7 Equipment Mounting, Utility Connections	11-24
11.7.8 Psychological Treatment	11-24
11.7.9 Miscellaneous Facilities	11-25
11.8 Costs	11-25
11.8.1 Gross Facility Estimate	11-25
11.8.2 Limited Cost Breakdown	11-27
11.8.3 Principal Factors Affecting Costs	11-29
11.9 References	11-34
CHAPTER 12. NUCLEAR RADIATION	
12.1 Introduction	12-1
12.2 Design Importance	12-2
12.3 Protection.	12-2
12.4 Radiation Characteristics	12-3
12.4.1 Kinds of Radiation	12-3
12.4.2 Units of Measure	12-5
12.5 Vulnerabilities	12-7
12.6 Prediction of Levels at Site	12-8
12.7 Gamma Radiation Shielding	12-12
12.8 Neutron Radiation Shielding	12-13
12.9 References	12-15
APPENDIX A. DESIGN EXAMPLES	
A.1 Buried Rectangular Structures	A-1
A.1.1 Design of Two-Way Roof Slab	A-2
A.1.2 Design of Supporting Beams	A-5
A.2 Buried Arch	A-7
A.3 Fully Buried Dome	A-8
A.4 Shallow Buried Dome	A-15

TABLE OF CONTENTS (Cont'd)

	<u>Page</u>
 APPENDIX B. DYNAMIC THEORY OF STRUCTURES	
B.1 Introduction	B-1
B.1.1 Single Versus Multi-Degrees-of-Freedom Systems	B-1
B.1.2 Importance of Equation of Motion	B-4
B.2 Methods of Analysis of Simple Systems	B-5
B.2.1 Introduction	B-5
B.2.2 Methods of Analysis	B-5
B.2.3 Approximate Analysis of Simple Systems Subject to Dynamic Loads	B-9
B.2.4 Sliding, Overturning and Rebound of Simple Systems	B-17
B.3 Notation	B-21
B.4 References	B-23
 APPENDIX C. THEORETICAL BACKGROUND FOR PREDICTIONS OF FREE-FIELD GROUND MOTIONS	
C.1 Introduction	C-1
C.2 Two and Three-Dimensional Studies of Air-Induced Ground Motions	C-5
C.2.1 Three-Dimensional Studies	C-5
C.2.2 Two-Dimensional Studies	C-5
C.3 Ground Motions by One-Dimensional Wave Theory	C-7
C.3.1 Uniform Elastic Medium	C-7
C.3.2 Layered Elastic Medium	C-13
C.3.3 Non-elastic Media	C-16
C.4 References	C-18
 APPENDIX D. NOMENCLATURE	
DISTRIBUTION	E-1

LIST OF TABLES

<u>Table No.</u>		<u>Page</u>
4-1	Ratio of Horizontal to Vertical Soil Pressures	4-67
4-2	Typical Seismic Velocities for Soils and Rocks	4-68
4-3	Approximate Overpressures at Which Outrunning of Ground Wave Occurs, Large Yield Surface Bursts	4-69
8-1	Values of k_c and k_s for Various Components of Displacement and Stress	8-52
11-1	Cost Data - Limited Cost Breakout	11-36 - 11-39
12-1	Estimated Medical Effects of Radiation Doses Expressed as Probability of Sickness or Death	12-16
B-1	Rate of Convergence	B-24
B-2	Stability and Convergence Limits	B-24

LIST OF FIGURES (Cont'd)

<u>Figure No.</u>	<u>Title</u>
3-18	Effects of Inclination and Length on Plate Drag Force at Low Mach Numbers
3-19	Drag Coefficients for Rectangular Bodies for Low Mach Numbers
3-20	Drag and Lift Coefficients for Structural Shapes of Infinite Length at Low Mach Numbers
3-21	Drag Coefficients as a Function of Reynolds Number for Low Mach Numbers
3-22	Maximum Peak Overpressure in a Tunnel Versus Incident Peak Overpressure for Three Angles of Incidence
3-23	Diffraction Effects at Wide Rectangular Slit
3-24	Transmitted Versus Incident Peak Overpressure for Equal Area T-Shaped Tunnel Junctions
3-25	Shape of Loading Function on Closure
3-26	Velocities of Incident and Reflected Shock Waves and of Rarefaction Wave Behind Reflected Shock Front Versus Incident Peak Overpressure for Square Wave
4-1	Typical Effect of a Visco-Elastic Medium on Wave Form and Peak Pressure
4-2	Change in Maximum Vertical Stress with Depth Due to Spatial Attenuation
4-3	Depth Attenuation Factor
4-4	Definition of Horizontal Pressure Coefficient K
4-5	Typical Soil Consolidation Curves
4-6	Triaxial Test Results
4-7	Confined Compression Test Results

LIST OF FIGURES

<u>Figure No.</u>	<u>Title</u>
3-1	Peak Overpressure at Ground Surface Versus Range for Various Yields -- Surface Burst at Sea Level
3-2	Reflection Factor Versus Peak Overpressure for Face-On Incidence
3-3	Reflection Factor for Various Peak Overpressures and Angles of Incidence
3-4	Normalized Overpressure Wave Forms -- 1 MT Surface Burst
3-5	Impulse and Duration Versus Overpressure -- 1 MT Surface Burst
3-6	Triangular Representations of Overpressure-Time Curves
3-7	Duration of Effective Triangles for Representation of Overpressure-Time Curves -- 1 MT Surface Burst
3-8	Two-Triangle Representation for Overpressure -- 1 MT Surface Burst
3-9	Three-Triangle Representation for Overpressure -- 1 MT Surface Burst
3-10	Overpressure Versus Dynamic Pressure
3-11	Normalized Dynamic Pressure Wave Forms -- 1 MT Surface Burst
3-12	Duration of Effective Triangles for Representation of Dynamic Pressure-Time Curves -- 1 MT Surface Burst
3-13	Two-Triangle Representation for Dynamic Pressure -- 1 MT Surface Burst
3-14	Three-Triangle Representation for Dynamic Pressure -- 1 MT Surface Burst
3-15	Initial Mach and Reynolds Numbers
3-16	Drag Coefficients for Equation (3-4)
3-17	Drag Coefficients for Equation (3-6)

LIST OF FIGURES (Cont'd)

<u>Figure No.</u>	<u>Title</u>
4-8	Selection of Constrained Modulus
4-9	Real and Linearized Stress-Strain Curves for Soil
4-10	Evaluation of Peak Relative Displacement
4-11	Air-Induced Surface Vertical Velocity
4-12	Change of Wave Form With Depth
4-13	Variation of Peak Pseudo Acceleration With Depth
4-14	Overpressure-Time Variation for Examples of Displacement Computation
4-15	Soil Parameters for Examples of Displacement Computation
4-16	Wave Form Arrival Times for Examples of Displacement Computation
4-17	Wave Form in Ground at Various Times
4-18	Displacement-Time Curves
4-19	Typical Wave Forms for Direct-Transmitted Ground Shock (From Ref. 4-3)
4-20	Peak Radial Acceleration Versus Radial Range on A Horizontal Radius -- Buried Nuclear Test in Tuff (From Fig. 4-1 of Ref. 4-30)
4-21	Variation of Peak Horizontal Radial Acceleration Scaled to Charge Size With Distance Scaled to Charge Size -- Buried HE Test in Sandstone (From Fig. 3-5, Ref. 4-27)
4-22	Peak Horizontal Acceleration Scaled to Charge Size for Rounds With Scale Charge Depth of 0.51 -- Dry Sand -- Buried HE (From Fig. 2-39, Ref. 4-31)
4-23	Peak Horizontal Acceleration Scaled to Charge Size for Rounds With Scale Charge Depth of 0.51 -- Dry Clay -- Buried HE (From Fig. 2-40, Ref. 4-31)

LIST OF FIGURES (Cont'd)

<u>Figure No.</u>	<u>Title</u>
4-24	Direct Shock Transmission in A Two-Layered System
5-1	Loading on Aboveground, Closed, Rectangular Structure
5-2	Loading on Aboveground, Partially Open, Rectangular Structure
5-3	Ideal Loading Scheme -- 180° Arch For Peak Incident Overpressures of 25 psi or Less
5-4	Non-Ideal Loading Scheme for 180° Arch for Peak Incident Overpressures of 100 psi or Less
5-5	Conventionalized Blast Loading on An Arch
5-6	Time-Dependent Loadings on Aboveground Arches
5-7(a)	Ideal Loading Scheme for 45° Dome for Peak Incident Overpressures of 25 psi or Less
5-7(b)	Non-Ideal Loading Scheme for 45° Dome for Peak Incident Overpressures of 100 psi or Less
5-8	A Blast Loading on An Above-Ground Dome
5-9	Force Field Assumed for Underground Structure
5-10	Assumed Variation of Shearing Stress Versus Displacement
5-11	Assumed Variation of Displacement and Shearing Stress With Depth
5-12	Variation of Pressure With Depth
5-13	Cross-Section of Underground Structure
5-14	Assumed Variation of Soil Displacement With Depth
5-15	Assumed Variation of Shearing Stress With Depth
5-16	Definition of Full Cover
5-17	Horizontal Dead Load Pressure Distribution Against Silo

LIST OF FIGURES (Cont'd)

<u>Figure No.</u>	<u>Title</u>
5-18	Magnitude of Horizontal Dead Load Pressure on Silo at Infinite Depth (Lower Limit)
5-19	Horizontal Dead Load Pressures on 50-Foot Diameter Silo for Various Angles of Internal Friction (Lower Limit)
5-20	Radial Design Pressure on A Vertical Silo At The Ground Surface
5-21	Typical Partially Buried or Mounded Rectangular Structure
5-22	Typical Partially Buried or Mounded Arch or Dome
6-1	Dynamic Increase in Yield Stress for Mild Steel
6-2	Yield Stress of A-7 and Reinforcing Steel
6-3	Influence of Temperature on Ductility
6-4	Influence of Loading Rate on Ductility
6-5	Effect of Rate of Straining on the Compressive Strength of Concrete
6-6	Relation Between Design Stress and Load Duration Timber
8-1	Flexural Capacity and Stiffness of Reinforced Concrete Beams
8-2(a)	Pure Shear Resistance of Reinforced Concrete Beams
8-2(b)	Diagonal Tensile Resistance of Reinforced Concrete Beams
8-3	Natural Period of Vibration for Reinforced Concrete Beams
8-4	Assumed Crack Pattern for Two-Way Slabs
8-5	Interaction Diagram for Reinforced Concrete Beam-Columns
8-6	Flexural Capacity and Stiffness of Steel Beams
8-7	Shear Capacity of Steel Beams
8-8	Natural Period of Vibration for Steel Beams

LIST OF FIGURES (Cont'd)

<u>Figure No.</u>	<u>Title</u>
8-9	Buckling Stresses for Axially Loaded A-7 or A-36 Steel Columns
8-10	Arch Notation Used in Analysis
8-11	A Blast Loading on An Above-Ground Dome
8-12	Effects of Line Load H -- Edge Free to Rotate
8-13	Effects of Line Load H -- Rotation of Edge Prevented
8-14	Effects of Edge Moments M_L -- Edge Free to Move
9-1	Maximum Response of Simple Spring-Mass System to Initially Peaked Triangular Force Pulse
9-2	Flexural Resistance of Simply Supported and Continuous One-Way Slabs ($\mu = 3.0$)
9-3	Resistance in Pure Shear of One-Way Slabs Without Inclined Web Steel ($\mu = 1.3$)
9-4	Pure Shear Resistance -- Factor for Slabs and Beams With Inclined Steel at Ends
9-5	Resistance in Diagonal Tension of One-Way Slabs ($\mu = 3.0$)
9-6	Web Reinforcement Factor
9-7	Resistance in Diagonal Tension for One-Way Slabs and Beams -- Factor For Influence of Flexural Steel
9-8	Flexural Resistance -- Two-Way Slab Factor
9-9	Flexural Resistance of Simply Supported or Continuous Reinforced Concrete Beams Supporting One-Way Slabs ($\mu = 3.0$)
9-10	Flexural Resistance -- Factor for Beams Supporting Non-Square Two-Way Slabs
9-11	Resistance in Pure Shear of Reinforced Concrete Beams Supporting One-Way and Square Two-Way Slabs ($\mu = 1.3$)
9-12	Resistance in Diagonal Tension of Reinforced Concrete Beams Supporting One-Way and Square Two-Way Slabs ($\mu = 3.0$)

LIST OF FIGURES (Cont'd)

<u>Figure No.</u>	<u>Title</u>
9-13	Resistance in Shear and Diagonal Tension -- Factor for Beams Supporting Non-Square Two-Way Slabs
9-14	Flexural Resistance of Steel Beams Supporting One-Way Slabs ($\mu = 3.0$)
9-15	Shearing Resistance of Simple and Continuous Steel Beams Supporting One-Way and Square Two-Way Slabs ($\mu = 3.0$)
9-16	Required Thickness of Fully-Buried Reinforced Concrete Arches for Dead Load
9-17	Required Thickness of Fully-Buried Reinforced Concrete Arches for Blast Load ($\mu = 1.3$)
9-18	Required Thickness of Fully-Buried Reinforced Concrete Arches for Blast Load ($\mu = 3.0$)
9-19	Required Thickness of Partially-Buried ($H_c = 0 \longrightarrow 0.062B$) Reinforced Concrete Arches ($\mu = 1.3$)
9-20	Required Thickness of Partially-Buried ($H_c = 0 \longrightarrow 0.062B$) Reinforced Concrete Arches ($\mu = 3.0$)
9-21	Required Thickness of Aboveground Reinforced Concrete Arches ($\mu = 1.3$)
9-22	Required Thickness of Aboveground Reinforced Concrete Arches ($\mu = 3.0$)
9-23	Required Area of Fully-Buried Steel Arches ($\mu = 3.0$)
9-24	Required Area of Fully-Buried Steel Arches ($\mu = 1.3$)
9-25	Required Area of Partially-Buried Steel Arches ($H_c = 0 \longrightarrow 0.062B$), ($\mu = 1.3$)
9-26	Required Area of Partially-Buried Steel Arches ($H_c = 0 \longrightarrow 0.062B$), ($\mu = 3.0$)
9-27	Required Area of Aboveground Steel Arches ($\mu = 1.3$)
9-28	Required Area of Aboveground Steel Arches ($\mu = 3.0$)

LIST OF FIGURES (Cont'd)

<u>Figure No.</u>	<u>Title</u>
9-29	Required Thickness of Partially-Buried R/C Domes ($\mu = 1.3$)
9-30	Required Thickness of Partially-Buried R/C Domes ($\mu = 3.0$)
9-31	Required Thickness of Aboveground R/C Domes ($\mu = 1.3$)
9-32	Required Thickness of Aboveground R/C Domes ($\mu = 3.0$)
9-33	Resistance of Square Column Footings
9-34	Resistance of Square Column Footings
9-35	Flexural Resistance of Wall Footings
9-36	Shear Resistance of Wall Footings Without Web Reinforcement
9-37	Strength of Axially-Loaded Rectangular Reinforced Concrete Columns
9-38	Ultimate Strength of Axially-Loaded I-Section Steel Columns
9-39	Rise Time Factor (K_r) Versus Rise Time
10-1	Typical Response Spectrum
10-2	Components of Ground Motion
10-3	Response Spectra
10-4	Inelastic Force-Displacement Relation
10-5	Elastic Response Spectrum
10-6	Replacement of An Inelastic Load-Deflection Relation By An Elasto-Plastic Relation
10-7	Elasto-Plastic Responses for A System With A Ductility Factor of 5
10-8	Acceleration Corresponding to Design Force Distribution Over Height of Building Frame
11-1	Estimated Cost of Bare Structure, Excluding Entrance Structures
11-2	Estimated Cost of Bare Structure, Including Special Entrance Structures

LIST OF FIGURES (Cont'd)

<u>Figure No.</u>	<u>Title</u>
11-3	Cost Ratio Versus Span For One-Story Rectangular Structures
11-4	Cost Ratio Versus Span For Dome Structures
11-5	Cost Ratio Versus Span For Arch (Igloo) Structures
11-6	Cost of Protective Doors
11-7	Cost Factor Versus Design Overpressure
12-1	Weapon Yield Versus Vulnerability Radius for Various Levels of Initial Gamma Radiation -- Surface Burst
12-2	Fallout Intensities (1 Hour Reference Dose) At Downwind Distances from GZ for Various Weapon Yields (Surface)
12-3	Accumulated Total Dose of Residual Radiation from Fission Products From 1 Minute After the Explosion
12-4	Shielding From Initial Gamma Radiation
12-5	Shielding From Residual Gamma Radiation
12-6	Attenuation of Fast Neutron Radiation -- Broad Beam in Thick Shie
B-1	Idealized Resistance Functions
B-2	Force Pulses
B-3	Maximum Response of Simple Spring-Mass System to Initially Peaked Triangular Force Pulse
B-4	Elasto-Plastic Replacement Resistance
B-5	Pressure-Response Curve For Decaying Resistance
B-6	Multiple Triangle Force Pulses
B-7	Delayed Rise Triangular Force Pulse
B-8	Acceleration-Time Diagram For Sliding Systems
B-9	Overturning Systems

LIST OF FIGURES (Cont'd)

<u>Figure No.</u>	<u>Title</u>
B-10	Design Chart For Elastic Rebound
C-1	Dilatational and Shear Wave Fronts for A Superseismic Plane Wave of Constant Velocity of Propagation
C-2	One-Dimensional Wave Conditions
C-3	One-Dimensional Wave In A Layered Medium

CHAPTER 1. INTRODUCTION

1.1 OBJECTIVES

The objectives of this manual are:

- a. To present the current "state of the art" of structural design to resist the effects of nuclear explosions.
- b. To guide and assist the designer who has some familiarity with nuclear blast phenomena, dynamic theory and limit design.
- c. To provide theory, data, background and references so that work undertaken by architect-engineer firms for the Air Force can follow standardized procedures.

This manual by original intent does not attempt to extend the theoretical frontiers per se. Rather, the intent is to select and apply existing theory and procedures so that the result is based upon the best available knowledge. The manual, therefore, draws liberally from the referenced sources. In some few cases (which are noted) portions of references were felt to be precisely suited to the discussion and are therefore included. Quite obviously, a manual prepared under these circumstances reflects to a considerable extent the experience and judgment of the authors. Periodic re-examination and re-evaluation will be required as more and better experimental and theoretical information becomes available.

1.2 SOURCES

Four general sources have been used in obtaining material for this

manual. They are

- a. Field Tests. Interim Technical and Weapon Test Reports.
- b. Laboratory Tests. Experimental laboratory work performed by universities, government laboratories, and private research activities.
- c. Theoretical studies.
- d. Extension of Work in Related Fields. Work done in such fields as seismology, geology, soil mechanics, and other branches of engineering and science.

1.3 GENERAL ASSUMPTIONS

The possible scope of this manual is limited only by the variety and range of the assumed design situations. An effort has been made to cover the more plausible situations and at the same time retain sufficient generality so that other applications could be made by the reader.

In general the weapons are assumed to be of Megaton range detonated as surface bursts. Both aboveground and belowground structures are given attention, although primary emphasis is placed on the belowground situation which is considered to be of greater importance to the Air Force.

Because of the present incomplete understanding of some of the aspects of protective construction, it has been necessary at some points in this manual to proceed on the basis of judgment in order to establish a design procedure. These assumptions are subject to revision as further knowledge is obtained, and the reader must guard against complacency in following procedures given.

1.4 PRESENTATION

This manual consists of twelve chapters and four appendices. Each chapter covers a fundamental aspect of the protective design problem and contains its own list of references. The page numbering, figures, equations, and references pertaining to a given chapter are presented together independently of the other chapters so that periodic revision can be made at a minimum of cost and effort.

1.5 NOTATION

Blast-resistant design involves many different scientific and engineering disciplines and it is not surprising to find a lack of standardization of symbols used. In some instances the same symbol is used for several different quantities. In a manual such as this which draws upon many different sources, the problem of establishing a uniform notation is a formidable one.

So far as possible, commonly accepted notation has been used. Each symbol is defined when first introduced, and a summary is given in Appendix D of those symbols used more-or-less generally throughout the manual. Special symbols used only within the confines of a few consecutive pages, as for example in a derivation, are not included in Appendix D.

1.6 ACCURACY AND PRECISION

In nuclear blast-resistant design it is not uncommon to work with quantities which may be in error by a factor of two or more. Having this to contend with, one becomes willing to accept errors of the order of 20% as tolerable.

It follows that extremely precise computations are not usually justified; the designer may only be deceiving himself if he strives for numerical precision with inaccurate basic data.

Throughout this manual some liberty has been taken to simplify computational methods when it was felt that their precision exceeded that of the input data being used. This is not so serious in design as it might be in analysis, because in design many of the uncertain values can be chosen so that the unknown error will introduce conservatism. In this manner the resulting design will be adequate for the assumed loading conditions, and probably adequate for something exceeding the assumed loading conditions.

1.7 STATISTICAL ASPECTS

There is a statistical uncertainty associated with any blast-resistant design. For loading conditions other than those assumed, the probability of survival will be altered and even less-known. It is therefore important that the loading condition selected be as realistic as possible. Selection of the most probable attack is not in the province of this manual, but it should be realized that the design can be no better than the loading assumptions, and a successful design can only be expected to withstand its specific design loads. All that can be asked of the designer is to produce a structure which will successfully withstand a predetermined set of loading conditions. This should be done with the realization that the structure may be vulnerable if the assumed loadings are unrealistic.

CHAPTER 2. GENERAL CONSIDERATIONS

2.1 INTRODUCTION

The design of structures to resist the effects of nuclear weapons must take into account all effects produced by such weapons, the proportions of these effects in any given case being a function of the type of burst and the weapon characteristics.

An air burst, in which the fireball does not come in contact with the ground surface, develops air shock waves, air-induced ground shock waves, flash heat, and radiation. A surface burst, in which the fireball comes in contact with the ground surface, develops the same effects as the air burst but the magnitudes of the effects are greater near ground zero. Furthermore, in a surface burst, a part of the energy is directly coupled from the weapon to the ground and is propagated as direct-transmitted ground shock. An added feature of the surface burst is that considerable dust and foreign material are carried into the air by the mushroom cloud, which results in a higher incidence of fallout radiation over a wide area by the contaminated particles.

An underground burst, in which the fireball escapes the ground surface by venting, produces very minor effects of air shock waves, flash heat, and direct radiation. Large direct-transmitted ground shock waves are produced together with the contamination of soil particles which are carried into the air for wide scattering.

The facility for which a design is to be prepared may be a standard installation for use in non-specific locations, or a unique installation for a specific location. Standard facilities can be designed only on the basis

of assumptions concerning the non-specific locations. Depending upon the general intended application of such a facility, reasonable or average conditions for the site should be assumed, and the basic design should be prepared with appropriate qualifications. Designing for the worst possible conditions may result in over-conservative, uneconomical, facilities in all other locations.

Unique designs for specific locations permit more realistic approaches to the nature of the loads, the site conditions, the subsoil properties, location of the water table, etc.

2.2 PRE-DESIGN CONSIDERATIONS

Among the many problems that must be considered by the designer of a hardened facility, the following are basic and of primary importance.

2.2.1 Functions of the Facility. The designer must begin by identifying the function of the facility and the means by which it can accomplish its purpose. The contents of the facility must be studied to determine the size and space requirements of the machinery and equipment of the installation, to include any special operating conditions such as vibration isolation, temperature and humidity controls, etc. Building services such as gas, power, water, sewage and communications are particularly susceptible to interruption at the connection points just outside the structure. Auxiliary services, or possibly independent self-contained services, may be a desirable feature to include in the design.

The space requirements for the occupying personnel depend somewhat upon the nature of the facility. If the facility must remain in operation

during an attack, the occupying personnel will be required to remain in their normal work areas, which demands that the entire facility provide the necessary levels of protection. However, if the facility may cease operation during and for a short time following an attack, a more desirable solution may be to include personnel shelters, either within or outside the facility.

2.2.2 Importance of the Facility. The importance of a facility is measured by the nature of its role in the success of a military mission, or the contribution it makes to the survival of a community during and/or following an attack. The relative importance assigned to the facility by the Department of Defense is used both in the target analysis to determine the probability of attack, and in the design to determine the levels of protection to be provided.

2.2.3 Probability and Proportions of Attack. The study of this subject is usually conducted by target analysis, and is not included in this manual. However, a brief discussion of the principles of target analysis will be of interest to the designer.

The first step in a target analysis is to evaluate the elements of the target. Common target elements include industrial centers, military installations, centers of communication, defense control centers, etc. For any given geographic area, each installation is evaluated on the basis of its function and importance, and is assigned a value representing the relative desirability of the installation as a target. When all of the significant installations of an area have been studied and evaluated as elements of the target, the entire complex of installations can be considered as a single target.

The target study considers the geographic size and setting of the target, topographic features of the target area, and the probable means of delivery of the weapon required to damage the target effectively. For the design of nuclear weapon-resistant facilities, the target analysis study leads to predictions of the levels of pressure, radiation, and heat effects to be expected at sites within the target area. Although the designer may not participate directly in the target analysis, his choice of the most desirable location to act in concert with the function and mission of the facility must be guided by an overall plan based on target analysis. This control is necessary to prevent a concentration of installations which would result in an increased priority for the target complex and overload the designs upon which the existing installations were constructed. Thus, the location of a new facility must not impair the survival of the existing facilities.

2.2.4 Required Levels of Protection. One of the most significant steps in the design is the establishment of the required levels of protection to be offered by the facility when subjected to the probable attack conditions. It is important to appreciate the concept of what constitutes "failure" as applied to facilities subjected to nuclear effects. This is discussed in Chapter 7.

It is evident that the levels of nuclear effects predicted by target analysis are based upon many uncertain variables. Therefore, the predicted values must take the form of a range of values rather than a single value, and a probability of occurrence attached to the limits of that range. From this, the designer must develop the design loads by their interrelation with the probability of occurrence.

Further uncertainty is involved in assigning the level of protection to be offered by the facility. Based upon the decisions concerning the function and importance of the facility, the survival condition of the structural elements and the levels of radiation exposure of the occupants must be established.

The application of a factor of safety to the predicted effects and the desired level of protection means that, during the subsequent design procedure, the ultimate behavior of the various elements should be used to avoid compounding the factor of safety which would result in over-conservatism and excessive costs.

2.2.5 Economic Considerations. As in all engineering projects, the justification of protective construction depends upon the economic balance between cost and benefit. The cost of a particular protective structure can be compared with an assessment of the benefits to be derived from such construction. However, to reduce disaster damage and possible loss of life to a dollar and cent basis is almost an impossible assignment.

Another aspect to the economic picture deals with the type of facility that must operate not only in times of emergency, but also in the normal course of events. For example, if survival of an attack dictates an underground installation for a critical facility that handles a considerable flow of material, the normal operating efficiency is certain to be reduced because of such things as inconvenience of access, space and expansion restrictions, etc.

2.3 CHOICE OF STRUCTURAL CONFIGURATION

Just as the function of the facility greatly influences the criteria

for design, so it also influences the type of structure that should be used. But by the same token, the severe conditions for which protective construction must be designed will often dictate a type of construction that in turn will exert considerable influence upon the execution of the function of the facility. Thus, the designer must be aware that certain conventional design arrangements and building practices must be modified to satisfy the protective design criteria.

The function of a facility identifies the nature of the equipment to be included, and by the nature of the equipment it can be determined whether the facility will be pressure-sensitive or shock-sensitive. This determination must consider both the nature of the equipment and the free-field pressures and motions. It is conceivable that a given structure with its contained equipment could be pressure-sensitive in one environment and shock-sensitive in another environment. If equipment is vulnerable to shock, it must be redesigned or insulated from the shock.

It should be apparent early in the preliminary designs whether the facility will be situated above ground or below ground. In general, placing a given facility below ground increases the operational problems; however, very few facilities can be designed as above ground structures to have the desired level of invulnerability. Burial of a facility will measurably reduce the loads for which it must be designed and increase the radiation shielding, but at the same time it will introduce new problems. Ground water problems may be encountered as well as numerous functional difficulties

attendant to the operation of a buried facility. Mechanical ventilation is probable in either case because above ground construction is almost certain to be windowless to provide the necessary protection, if not to eliminate the hazard of broken glass.

The geometry of the design should be, taking account of the functional requirements, such that the blast-induced loads are reduced as much as possible. Above ground structures should be of low silhouette, streamlined to reduce reflected pressures, and should present as small an area to the loading function as possible. Partially buried and mounded structures should also be streamlined to reduce the influence of reflected and drag pressures. In all cases, the geometrical proportions may have a strong influence not only on the cost but on the functional aspects of the facility as well.

Arches and domes are considered to be excellent geometric shapes from the standpoint of structural performance, but full space utilization may be difficult and the curved surfaces may cause higher construction costs. For rectangular structures, shear wall structures are lower in cost and superior in performance to rigid frame structures, but are restricted in application to those facilities that do not require open, continuous bays for work areas and are also more sensitive to the effects of shock. Rectangular roof systems may be of either slab or T-beam construction depending upon the economy of materials and methods vs. the head-room requirements.

Entrances and service openings are particularly critical elements of the design. Their size is controlled by the nature of the function of the

facility, and for large openings such as vehicle entrances, the associated problems are formidable. In addition to the requirement that the closure device successfully operate under the pressure and radiation effects to be imposed upon it, it must do so without jamming either due to its own deformation or any deformations of the structure itself. Another item to be considered is the method of actuating the closure of the openings, for the facility is certainly as vulnerable as its weakest element.

Subsoil conditions are very important for both above and below ground structures. Not only must consideration be given to bearing capacities and settlements under both normal and blast loads, but the properties of the soil as they influence the attenuation of stress with depth, the relation between vertical and horizontal pressures, and soil arching characteristics must also be investigated.

Weather conditions affect the subsoil properties by controlling the depth of frozen ground, the degree of saturation of the soil, and the position of the ground water table. The position of the ground water table requires special attention by the designer, for if the structure is located beneath its level, the floor slab must either be designed for the hydrostatic uplift or a suitable drainage system provided. In addition, the structure may need to be waterproofed.

A special type of facility may be settlement sensitive, such as a direction-oriented tracking station or missile guidance facility. In some cases it is difficult to design the facility to keep settlements within tolerable limits under normal loads. If such a structure is to be subjected to blast loads, the problem becomes even more difficult.

3.1 INTRODUCTION

Above-ground structures, above-ground portions of buried structures, and most buried structures encountered in practice will receive most of their loading from the air blast overpressure. In this chapter the characteristics of the air blast pressures from a surface burst are presented and the interaction of the air blast with objects is introduced. A discussion of the procedures used to obtain the air blast loading functions for structures and structural elements is contained in Chapter 5; in this chapter the background material required is presented.

It is not intended that this chapter serve as a self-contained, complete source of information on air blast phenomenology. A thorough discussion of the subject is available in Ref. 3-1. The objective of this chapter is to present information on air blast in a form readily adaptable to structural response computations, to amplify the presentation to include subjects such as the propagation of shock in tunnels, and to bring to the notice of the reader sources of additional information from the classified and unclassified literature.

Two major subdivisions of the air blast loading are considered in the following discussion: (1), the overpressure loading due to the greatly increased hydrostatic pressures which occur behind the shock front, and (2), the dynamic pressures due to the wind, or mass transfer of air, which is associated with air blast. The discussion will be concerned primarily with surface burst conditions since, for overpressures greater than about

10 psi, the range for a given overpressure level is greater for a surface burst than for an air burst. Thus it is assumed that a surface burst would probably be employed in an effort to destroy a hardened structure. For a positive height of burst the free-field pressure-time characteristics of the air blast pulse will be altered; information describing these changes is available in Ref. 3-1 and Ref. 3-2.

3.2 AIR BLAST

3.2.1 Introduction. Design loads for protective structures are derived from the assumed incident air blast pulse. Both overpressure and dynamic pressure pulses enter into the design loads of above ground portions of structures whereas only the overpressure pulse is considered in the design of underground installations. The purpose of this section is to discuss briefly the air blast parameters important in structural design and to present data sufficient for most design situations.

The blast parameters necessary for loading computations are the peak overpressure, p_{so} , the peak dynamic pressure, p_{do} , the durations of the positive phases of these pressures and the shape of the pressure-time curves. These parameters are functions of the yield, W , the height-of-burst, and the nature of the ground surface in the vicinity of the structure.

In this section the overpressure and dynamic pressure characteristics for surface bursts and ideal surface conditions will be presented. Ideal surface conditions consist of smooth, plane, rigid earth surfaces. Surface conditions are essentially ideal when the topography is flat and the surface is water, concrete or snow covered. The alterations in blast

characteristics caused by non-ideal surface conditions will also receive comment in a qualitative fashion. The peak overpressure, p_{so} , is used as the independent variable in most of the parameter charts presented herein. Time parameters are given for a yield of 1 MT and may be scaled to other yields by multiplying by the factor $(\frac{W}{1MT})^{1/3}$.

3.2.2 Overpressure. The parameters of interest in regard to the air blast overpressure include the peak side-on overpressure, or simply peak overpressure, which acts upon a surface parallel to the direction of propagation of the shock front, the peak reflected pressure which results when the blast wave impinges upon a surface, and the variation of these quantities with time. These significant parameters are discussed below in the stated order for conditions of surface burst and an ideal ground surface.

Figure 3-1 shows the relationship between weapon yield and horizontal range for various levels of peak overpressure for a surface burst. This figure is based on the results of theoretical calculations given in Ref. 3-6. These calculations are in general agreement with Ref. 3-2 for the lower pressure region. There are few measurements above 200 psi but the agreement between Fig. 3-1 and previous empirical studies in this higher region, such as Ref. 3-7, is satisfactory.

The reflected pressure produced when a shock wave impinges upon a surface is a function of the strength of the blast wave, p_{so} , and the angle of incidence, α , which is defined as the angle between the normal to the surface in question and the direction of propagation of the shock front.

For a normally incident shock, $\alpha = 0^\circ$, the peak reflected pressure,

p_{ro} , is given in Ref. 3-1 as

$$\frac{p_{ro}}{p_{so}} = 2 + (\gamma + 1) \frac{p_{so}}{2\gamma p_o + (\gamma - 1) p_{so}} \quad (3-1)$$

where p_o is the ambient atmospheric pressure and γ is the ratio of specific heats of the medium. This relation is based on the Rankine-Hugoniot equations which are derived for ideal polytropic gas.

For relatively low overpressures, $p_{so} < 60$ psi, the ratio of specific heats, $\gamma = \frac{c_p}{c_v}$, where c_p is the specific heat at constant pressure, and c_v the specific heat at constant volume, does not change markedly from its value at normal pressure and temperature, $\gamma = 1.4$. For such conditions Eq. (3-1) may be expressed as

$$\frac{p_{ro}}{p_{so}} = 2 + \frac{6p_{so}}{7p_o + p_{so}} \quad (3-2)$$

For overpressures in excess of 60 psi, the equation of state for air becomes significantly different from the ideal gas equation and a marked effect on the reflection factor, $\frac{p_{ro}}{p_{so}}$, results. Figure 3-2, from Ref. 3-8, indicates the variation of the reflected pressure for normally incident shocks with consideration of the effects of the pressure and temperature on the equation of state of air.

The effect of the angle of incidence, α , of the shock front on the surface of interest is shown in Fig. 3-3, taken from Ref. 3-9. It may be noted that Fig. 3-3 differs from Fig. 3.71b of Ref. 3-1. The latter shows a peak value in the reflection factor occurring at the critical angle

of incidence (40 to 65 degrees in the overpressure range of 2 to 20 psi). Reference 3-9 points out that there is a strong rarefaction just behind the Mach front and although the pressure reaches a value higher than that given by normal incidence, the pressure falls off rapidly with distance behind the Mach front. Further evidence of this observation has been obtained in efforts to measure the pressure directly with gages on the reflecting surface; measurements do not show higher values in the critical angle range, possibly because the pressure gradient is so great that the finite size of the gage averages out the pressure. Accordingly, the peaks in the reflection factors in the transition zone from regular to Mach reflection are not shown in Fig. 3-3. It is suggested that for practical uses the pressures be approximated as indicated by the dotted lines shown.

For lack of better data, it is recommended that, for peak overpressures greater than 60 psi, the reflection factor given in Fig. 3-2 be used for angles of incidence between 0 and 34 degrees, with a decrease thereafter as indicated in Fig. 3-3. Examples of the recommended approximation for overpressures of 200 and 1000 psi are shown in Fig. 3-3.

The time variation of the overpressure is also a significant parameter in air blast loading. The normalized curves of overpressure versus time for various peak overpressure levels, p_{so} , are shown in Fig. 3-4, taken from Ref. 3-10 and derived from data given in Refs. 3-1, 3-6, and 3-11. The abscissa, normalized time, is equal to the time of the overpressure of interest (for zero time taken as the time of arrival of the air blast) divided by the duration of the overpressure positive phase,

which is a function of the yield of the weapon and the range from ground zero. The ordinate, normalized pressure, is the overpressure at the time of interest as defined above, divided by the peak side-on overpressure which also is a function of the weapon yield and ground range.

The overpressure positive phase duration, D_p^+ , may be obtained from Fig. 3-5, taken from Ref. 3-6. The figure is plotted for a 1 MT surface burst; to scale to other yields, enter at the appropriate level of peak overpressure and multiply the value of D_p^+ from the figure by $(\frac{W}{1MT})^{1/3}$ to obtain the value of D_p^+ appropriate to the yield of interest. The value of p_{so} for any weapon yield and range may be obtained directly from Fig. 3-1. The overpressure impulse, I_p^+ , which is the area contained under the overpressure-time curve, is given in Fig. 3-5, and is scaled in the same fashion as the positive phase duration. It provides a measure of the momentum which may be imparted to an object by the air blast overpressure.

The overpressure-time curves of Fig. 3-4 are not in a form that is readily adaptable to use in computations of structural response to air blast loading. In order to represent simply the pressure-time variation for use in response computations, triangular representations equivalent to the theoretical exponential overpressure-time functions were developed in Ref. 3-10 from data appearing in Ref. 3-1 and 3-6.

Three single-triangle overpressure-time representations were developed, all with an initial pressure value equal to p_{so} but with the duration of pressure decay varied to give the following characteristics:

- (1) A single-triangle pulse of duration t_1 , which has the same total impulse as the actual pressure-time curve. It is applicable if the

maximum response of the structure occurs after the pressure pulse has passed.

(2) A single-triangle pulse of duration t_{∞} , which has the same slope as the initial decay of the actual pressure-time curve. It is applicable if the response of interest occurs early in the pressure history.

(3) A single-triangle pulse of duration t_{50} , which has the same time ordinate at 50 percent of peak overpressure as the actual pressure-time curve. It may be applied to response situations intermediate to those mentioned above.

The significance of t_1 , t_{50} , and t_{∞} is shown pictorially in Fig. 3-6, taken from Ref. 3-10. The values of t_1 , t_{50} , and t_{∞} are given as a function of the peak overpressure, p_{50} , in Fig. 3-7, also from Ref. 3-10. The durations shown are for a 1 MT surface burst; as indicated in the figure they may be scaled for other yields by multiplying by $(\frac{W}{1\text{MT}})^{1/3}$.

In situations where greater accuracy in analysis is desired than that possible using a single triangle representation of the overpressure-time variation, multiple-triangle representations have been developed in Ref. 3-10. A two-triangle representation is shown in Fig. 3-8, and a three-triangle representation is shown in Fig. 3-9. Both the two and three-triangle representations preserve the total impulse of the actual overpressure-time curve; it is, of course, possible to follow the actual variation of the overpressure-time curve more closely with the three-triangle representation. The times given in the cited figures may also be scaled to other yields by multiplication by $(\frac{W}{1\text{MT}})^{1/3}$.

3.2.3 Dynamic Pressure. The dynamic pressure, resulting from the winds associated with the air blast, produces loadings on above ground

structures comparable to the wind forces experienced during hurricanes - but the intensity of such drag forces produced by nuclear explosions can be much greater. Two factors must be considered in the evaluation of drag force on an object: (1), the dynamic pressure, which is a time dependent function of the weapon yield, ground range, height of burst, and surface conditions; and (2), the size, shape, and surface texture of the object interfering with the flow of air behind the shock front. The characteristics of the dynamic pressure under ideal surface conditions is discussed first; consideration of the effects of non-ideal surface conditions is deferred to Sec. 3.2.4. The influence of the object itself on the drag force, expressed in the form of a drag coefficient, is discussed in this section.

For ideal surface conditions the peak dynamic pressure may be expressed readily as a function of the peak overpressure. Figure 3-10, based on data from Ref. 3-6, presents the peak dynamic pressure, p_{do} , as a function of the peak overpressure to an overpressure level of 10,000 psi. It will be noted that the curve of Fig. 3-10 does not correspond exactly with the relation given between peak dynamic pressure and peak overpressure in Eq. (3.49-1) of Ref. 3-1 which is

$$p_{do} = \frac{5}{2} \frac{p_{so}^2}{7p_o + p_{so}} \quad (3-3)$$

Equation (3-3) is based on the Rankine-Hugoniot equations for an ideal gas; a more realistic representation of the behavior of air at high pressures and temperatures was used in Ref. 3-6 for the data for Fig. 3-10.

The variation of dynamic pressure with time is different quantitatively from the variation of overpressure with time, although the curves have the same general shape. Normalized curves of dynamic pressure versus

time for various values of peak dynamic pressure, p_{do} , are given in Fig. 3-11, based on data from Ref. 3-12. The abscissa, normalized time, is equal to the time from the arrival of the shock front at the point of interest divided by the duration of the dynamic pressure pulse, D_u^+ . The ordinate, normalized dynamic pressure, is equal to the transient value of the dynamic pressure, p_d , divided by the peak dynamic pressure, p_{do} . Beginning with a given value of weapon yield and ground range, the peak overpressure value is obtained from Fig. 3-1, the value for peak dynamic pressure is then obtained from Fig. 3-10, and the duration of the dynamic pressure, D_u^+ , is taken from Fig. 3-5. Note that the dynamic pressure duration must be scaled by the factor $(\frac{W}{IHT})^{1/3}$. Fig. 3-5 also presents the dynamic pressure impulse, I_u^+ , which also scales according to $(\frac{W}{IHT})^{1/3}$.

Triangular representations of the dynamic pressure-time variation have been prepared in a form comparable to that for the overpressure-time variation. Three single-triangle dynamic pressure-time representations, of durations t_i' , t_{50}' , and t_{∞}' are presented in Fig. 3-12 which is taken from Ref. 3-10. The durations t_i' , t_{50}' , and t_{∞}' have the same significance as the corresponding parameters of the single-triangle representations of the overpressure-time variation (refer to Fig. 3-6). Note that in Fig. 3-12 the durations t_i' , t_{50}' , and t_{∞}' are referred to the peak side-on overpressure, p_{50} , rather than the peak dynamic pressure, p_{do} . However, in the use of the single-triangle representations of dynamic pressure, the peak dynamic pressure from Fig. 3-10 is used as the initial ordinate.

A two-triangle representation of dynamic pressure, for use in response computations in which greater accuracy is desired than is possible

to obtain using a single triangle representation, is presented in Fig. 3-13. The two-triangle representation is based on the normalized dynamic pressure-time curves shown in Fig. 3-11; the first slope follows the actual decay closely in the initial stages, and the second slope is drawn to give the actual total impulse. Note that the parameters t_1^i , t_2^i and c_2^i are plotted against peak overpressure, p_{so} , in Fig. 3-13. However, the peak dynamic pressure, p_{do} , from Fig. 3-10 must be used in the computations for the ordinate of the two-triangle dynamic pressure representation. A three-triangle representation of the dynamic pressure is shown in Fig. 3-14 (from Ref. 3-10).

Drag Coefficients. When the time variation of dynamic pressure has been established, it is still necessary to define the loadings which the dynamic pressure produces. These loadings are determined by multiplying the dynamic pressure by an empirically developed drag coefficient. The drag coefficient, C_{do} , gives the relationship between the dynamic pressure and the total translational force on the object in the direction of the wind produced by the dynamic pressure.

$$F_d = C_{do} p_d A \quad (3-4)$$

where A can be either the area of the face upon which the wind impinges or the projected area of the body on a plane normal to the wind direction, depending upon the manner in which C_{do} is defined.

The lift coefficient, C_L , is used to define the total force produced on the object in the direction normal to the wind direction by

the dynamic pressure.

$$F_L = C_L p_d A \quad (3-5)$$

where A has the significance stated above.

Since the pressures acting on a structure are not uniform over any one face or generally the same on various faces, drag coefficients for surfaces are required to evaluate the loading on a particular surface or portion of a surface. A drag coefficient, C_{ds} , for a surface does not define the pressure distribution on the surface, but gives the total force due to the dynamic pressure acting on the surface.

$$F_s = C_{ds} p_d A_s \quad (3-6)$$

where F_s is the total force acting normal to the surface due to the dynamic pressure and A_s is the surface area. If the point-wise variation of pressure over a surface is required, i.e. for arch loadings, a drag coefficient, C_{dp} , which varies according to the point in question on the surface must be used.

$$p_d^i = C_{dp} p_d \quad (3-7)$$

where p_d^i is the loading at a particular point on the surface caused by the dynamic pressure. Obviously, some care is required to insure that a drag coefficient taken from one of the figures included herein is used only in the sense for which it was intended.

The evaluation of drag forces is not solely a problem of engineers

concerned with protective construction. Similar problems are encountered in designing structures to resist natural wind forces and in the design of aircraft. The body of information gathered in these studies provides our major source of information, but care must be used in applying it to nuclear blast conditions. The wind velocities associated with nuclear weapons can be much greater than those occurring naturally. While aeronautical studies have been extended to velocities greater than those occurring in nuclear explosions, the atmospheric conditions encountered near the surface due to a nuclear blast are far different from those encountered by a supersonic aircraft in the rarefied air at high altitudes. In addition, the wind velocities produced by a nuclear explosion are transient, the velocity changes rapidly with time, so flow conditions around an obstacle may not be similar, at the same wind velocity, to those established in a wind tunnel providing a constant wind velocity.

The parameters governing the value of a drag or pressure coefficient include the free-field parameters of the air: particle velocity (wind velocity), pressure level, temperature, and the rates of change of these quantities; and the obstacle parameters: body size, shape, surface texture, orientation relative to the direction of wind velocity, and shielding by the ground surface, other structures, or structural elements. The available information is not adequate to define the effects of all of these parameters; however, it is possible to recommend drag and pressure coefficients which will be conservative with regard to the neglected parameters. The parameter most difficult to account for is that of shielding. Some discussion of its influence appears in Chapter 5, but obviously neglect of shielding must always result in conservative design.

The sources used in the following discussion are Ref. 3-14 which summarizes much of the literature on drag forces, Ref. 3-15 which contains design recommendations for resisting natural wind forces and an extensive bibliography, and Ref. 3-16 which presents the results of shock tube studies of drag forces and gives some indication of the influence of transiency on drag forces.

The influence of free-field conditions on drag forces is expressed by two dimensionless numbers: the Reynolds number, R , and the Mach number, M . The Reynolds number expresses the relationship between the free-field fluid velocity, i.e. for air blast the particle velocity u , the kinematic viscosity of the fluid ν , and the characteristic body dimension L .

$$R = \frac{uL}{\nu} \quad (3-8)$$

The Reynolds number defines the flow pattern about the body; for low Reynolds numbers, smooth laminar flow occurs, and at high Reynolds numbers a turbulent wake forms behind the object. In a range of critical Reynolds numbers the flow may be unstable, varying with time from laminar to turbulent and back. The drag coefficient tends to be reduced as the Reynolds number increases at a fixed $\frac{u}{\nu}$ since the turbulent boundary layer transmits less drag force to the object.

The Mach number expresses the relationship between the particle velocity in the free-field and the velocity of sound, c_o , in the medium at the free-field conditions of temperature and pressure

$$M = \frac{u}{c_o} \quad (3-9)$$

The Mach number may fall into three important ranges: (1), the subsonic range, $M < \sim 0.5$, in which flow about the object is everywhere subsonic; (2), the transonic range $\sim 0.5 < M < \sim 2$, in which flow about the object is mixed subsonic and supersonic; and (3), the supersonic range, $M > \sim 2$, in which flow about the object is everywhere supersonic. The Mach number may be determined to the same precision with which the free-field conditions are known, but the extent of the transonic Mach range is entirely a function of the character of the object in the flow.

In order to estimate the range of Mach and Reynolds numbers likely to apply to air blast drag loadings, Fig. 3-15 shows the initial Reynolds number of a body of characteristic dimension $L = 1$ ft and the initial Mach number as a function of peak overpressure. These initial values are based upon the pressure, temperature, and particle velocity immediately behind the shock front as given by Ref. 3-6. The values are not applicable to the transient pressure during the decay of the overpressure, since the temperature and particle velocity cannot be assumed to be state functions of the transient pressure. These curves are based upon equations for properties of air as given in Ref. 3-13.

The Mach number, given by Eq. (3-9), is a function of the particle velocity and the speed of sound c_0 . The particle velocity and temperature immediately behind the shock front, from Ref. 3-6, were used to obtain the initial Mach number and initial Reynolds number, plotted in Fig. 3-15. These curves represent the maximum values of the Mach and Reynolds numbers which will occur for ideal surface conditions and may be used as a guide in the

selection of appropriate drag coefficients.

The curve of Mach number versus peak overpressure given in Fig. 3-15 indicates that drag coefficients in the transonic range will be of major interest. The shock tube studies of Ref. 3-16 extend only to $M = 0.45$, and the natural wind data of Ref. 3-15 is intended for application at Mach numbers near 0.1, so basic reliance must be placed on the transonic drag studies reported in Ref. 3-14. In the transonic range, flow separation occurs so the texture of surfaces parallel to the wind velocity will not have significant influence on the drag forces. For the same reason, the corner sharpness of obstacles which was found significant in Ref. 3-16 will not have the same importance and will be neglected here.

Figure 3-16, taken from data given in Ref. 3-14 and the curve for Mach numbers in Fig. 3-15, shows the drag coefficients corresponding to the initial Mach number for various objects as a function of peak overpressure. The curves are appropriate for use in evaluating the total translational force on an object using Eq. (3-4). For these curves incidence of the wind is assumed to be normal and A is the projected area of the object. The suggested application for each curve is as follows:

(a) This curve applies to a flat plate of infinite length oriented normally to the free-field velocity. Since the effects of depth of the body become insignificant as the Mach number approaches 1 this curve should be applicable to bodies of rectangular cross sectional outline and great length at right angles to the free-field velocity. Thus it can be applied to an exposed structural section such as a wide flange member or angle. Use of this curve is conservative if the free-field velocity is not

normally incident on the section, no better information on the effects of orientation is available than that given later from Ref. 3-15 for low Mach numbers. This latter information may be used with the realization that it leads only to an estimate of orientation effects.

(b) This curve applies to a disc oriented normally to the wind direction. Since the effects of length in the direction of the wind velocity are minor for Mach numbers greater than about 0.5, this curve may be applied to any body with a plane front face normal to the shock front with body length in the wind direction of the same order of magnitude as the minimum front face dimension. Curve (b) will become unreliable when the ratio between front face dimensions varies greatly from 1, in these cases the proper drag coefficient lies between curves (a) and (b).

(c) This curve applies to a long cylinder with the axis in the plane of the shock front. It may reasonably be applied to a semi-cylindrical structure lying on a surface; this is conservative since the surface boundary layer is neglected.

For a cylindrical section of less than 180 degree central angle, this curve is conservative. The scheme suggested in Fig. 5-4 for angular variation of the drag pressure can be applied as a guide to the point-wise distribution of pressure on the surface.

(d) This curve applies to a sphere. It may be used to establish a lower bound for the loading of a short cylinder with its axis in the plane of the shock front. It may also be used in conjunction with Fig. 5-7 to evaluate the drag pressures on a dome following the procedure outlined above for arches.

The curves of Fig. 3-16 yield the total drag force on an object, not the pressures on individual faces due to the dynamic pressure. The average pressures on faces exposed normally to the wind velocity can be determined from the drag coefficients given in curve (a) of Fig. 3-17, derived from data for discs in Ref. 3-14, and the curve of initial Mach number from Fig. 3-15. For faces separated from the flow stream (at Mach numbers greater than 0.5, this includes side and rear faces) curve (b) of Fig. 3-17 gives the rear surface drag coefficient. This curve was derived from data for discs in Ref. 3-14. This rear face drag coefficient also may be applied to side and top surfaces. Note that these negative pressures do not denote a suction on these faces, but rather that the overpressure level is reduced by the amount $C_{ds}p_d$. Curve (c) of Fig. 3-17 gives the ratio, p'_d/p_d , of the stagnation pressure to the dynamic pressure. The stagnation pressure is the maximum drag induced pressure on an obstacle. It is computed from Eq. 16-4 of Ref. 3-14:

$$\begin{aligned} \text{For } M < 1, \quad \frac{p'_d}{p_d} &= 1 + \frac{M^2}{4} + \frac{M^4}{40} + \\ &\hspace{25em} (3-10) \\ \text{For } M > 1, \quad \frac{p'_d}{p_d} &= 1.84 - \frac{0.76}{M^2} + \frac{0.166}{M^4} + \frac{0.035}{M^6} \end{aligned}$$

where p'_d is the stagnation pressure.

Reference 3-15 presents data for drag coefficients of normal structural forms for wind loadings. While the Mach number must be considered to be very low, the indicated effects of orientation and shape provide the only available basis for judgment. Figure 3-18, from Fig. 5 of Ref. 3-15,

shows the effect of orientation on the drag, lift, and center of action coefficients for flat plates of three ratios of length to height. The area used with the drag or lift coefficient to compute the total force remains the area of the plate face. Figure 3-19, from Table 2 of Ref. 3-15, presents some data on the effect of the length to height ratio on the drag coefficients of flat plates, flat plates on the ground, and rectangular parallelepipeds (not in contact with the ground). Figure 3-20, from Table 3 of Ref. 3-15, presents the drag coefficients and lift coefficients for long structural sections with axes in the plane of the shock front. Note that lift as well as drag must be considered for unsymmetrical or non-normally oriented structural shapes. Figure 3-21, from Fig. 6 of Ref. 3-15, presents drag coefficients as a function of Reynolds number for low Mach numbers. It may be considered applicable for pressure levels below the transonic Mach range, or roughly, below 20 psi.

It is believed that the drag coefficients and pressure coefficients from Figs. 3-16 and 3-17 provide the best available data for determining the forces due to the dynamic pressures from nuclear blasts. These drag coefficients are considered to be applicable for non-ideal as well as ideal surface conditions since the influence of non-ideal surface conditions is properly expressed in the dynamic pressure, p_d . However, the ratio between Mach number and overpressure, used to compute the curves of Fig. 3-16 and 3-17 is not reliable for non-ideal blast waves. In all instances the drag coefficients given in Fig. 3-16 and 3-17 are conservative compared to those given in Figs. 3-18 to 3-20. The normal incidence condition commonly provides

the peak drag force but members should be capable of resisting the lift forces occurring when incidence is non-normal. Although the applicability is questionable, some guidance as to the magnitude of the lift force can be obtained from Fig. 3-18 and 3-20.

References 3-1 and 3-17 contain recommendations concerning drag coefficients which may be compared with those obtained from Fig. 3-16 and 3-17. Reference 3-17 recommends drag coefficients of about 2 for structural shapes, 1.5 for box elements or flat plates, and about 0.8 for cylinders. Except for the box elements, these values are smaller than those given in Fig. 3-16. Reference 3-1 gives a drag coefficient of 1.0 for the front face of a box structure, which corresponds to that for a Mach number of 1 in Fig. 3-17, and the following variations with dynamic pressure for the drag coefficients for sides, top and rear face of a box structure:

<u>Dynamic Pressure</u>	<u>Drag Coefficient</u>
P_d	C_{ds}
0-25 psi	-0.4
25-50 psi	-0.3
50-130 psi	-0.2

The values given in Fig. 3-17 tend to be greater than the above for the higher pressures. The suggested drag coefficient for cylinders in Ref. 3-1 is 0.4 for pressures lower than 25 psi. Curve (c) of Fig. 3-16 appears quite conservative for low pressures.

In the use of the drag coefficients given in Fig. 3-16 and 3-17

the following procedure should be conservative. Obtain from Fig. 3-16 or 3-17 the maximum appropriate drag coefficient corresponding to the peak overpressure, p_{so} , or to a lower overpressure, and use this coefficient throughout the dynamic pressure history. If it is assumed that the Mach number from Fig. 3-15 is the same function of the transient overpressure that it is of the peak overpressure, a time dependent drag coefficient of interest may be obtained. The latter procedure is not strictly valid but it provides an indication of the degree of conservatism involved in the aforementioned simpler procedure.

3.2.4 Effects of Surface and Topography. The material previously presented on the variations of overpressure and dynamic pressure with range, yield, and time apply for ideal surface conditions - a smooth, plane, rigid reflecting surface. Ideal conditions may be considered to exist in areas of relatively flat topography where the surface material is not a good absorber and radiator of heat and is not picked up by the blast wave. Examples of ideal surfaces include water, snow, and concrete pavement. Two major types of deviation from ideal conditions may be defined: deviations produced by topography, i.e. non-planar surfaces; and deviations produced by the character of the surface material. It is not possible to give a quantitative formulation to the effects of non-ideal ground conditions since nature gives us an infinite variety of ground conditions, but the major features of the variations produced are discussed in the following paragraphs.

If the ground surface is not planar, but rather contains topographical features such as hills and valleys, the characteristics of

the overpressure pulse will be changed. Reference 3-3 summarizes an extensive experimental study of these phenomena. To note briefly the results, a decrease in ground slope results in a decrease in peak overpressure while an increase in ground slope produces an increase in peak overpressure. As the incident level of peak overpressure increases, the change in peak overpressure caused by a given change in slope becomes a smaller proportion of the incident overpressure. For a peak side-on overpressure greater than 25 psi, in the region of Mach reflection, a change of slope greater than 17 degrees is required to change the peak overpressure by 25 percent. If extreme slope conditions are present in the vicinity of the structure being designed, the reader may wish to refer to Ref. 3-3 for more detailed information. Unfortunately, the data presented there does not extend to peak overpressure levels in excess of 30 psi. As a guide, for lack of better information, the curves presented in conjunction with the material on Air Blast in Tunnels and Ducts in Sec. 3.3 may be used for large magnitude slope changes at high overpressure levels.

The character of the ground surface also influences the air blast parameters. A theoretical study of the effects of the surface, with correlations with field test results, may be found in Ref. 3-4. The significant surface effect, known as the precursor, can occur for low burst heights over heat absorbent, effective radiating surfaces such as dusty desert, coral, or asphalt. Thermal radiation from the fireball produces a heated layer of air adjacent to the surface through which the blast wave can

propagate more rapidly than in the ambient air. A non-ideal wave form with a slow rise to the first peak in overpressure, usually followed by a slow decay in pressure, and then a second peak results. This causes a decreased peak overpressure but a increased overpressure impulse, and the dynamic pressures tend to be greater than those associated with an ideal overpressure pulse. The increased dynamic pressures can be attributed to higher particle velocities and to mechanical effects such as the greater density of dust-laden air. The precursor effects tend to occur at overpressure levels between 10 and 250 psi for surface and low air bursts. An indication of the variation which may be expected in peak dynamic pressure is shown in Fig. 2-2.1 of Ref. 3-18. The figure is not reproduced herein since it must be emphasized that reliable techniques for establishing the peak values and time variations of overpressure and dynamic pressure under non-ideal conditions are not yet available. The best available information concerning these quantities may be found in Ref. 3-2, 3-4 and 3-5.

3.3 AIR BLAST IN TUNNELS AND DUCTS

When the air blast wave propagating over the surface is allowed to enter a tunnel or duct, a new wave front is formed inside the tunnel and this shock propagates throughout the tunnel. Energy losses and one-dimensional expansion will decrease the peak overpressure as the shock progresses along the tunnel. At the same time the peak overpressure may be increased or decreased as a result of the geometry of the tunnel complex.

For example, a gradual decrease in tunnel diameter would tend to increase the strength of the shock. On the other hand, bends, junctions, and increases in tunnel diameter would tend to decrease the shock strength at the wave front. Consequently, the design of interior doors, blast valves, etc., requires a detailed analysis of the air blast wave propagating in the tunnel system. Such an analysis will generally require consideration of factors such as entrance losses and shock formation in the tunnel, attenuation of peak pressures along straight sections of tunnel, effects of bends or junctions, effect of area changes along the tunnel, and perhaps the expansion of the pressure wave into chambers.

There do not exist at present sufficient empirical data or analytical methods to determine tunnel pressures for all possible cases even if the surface pressures are accurately known. There does exist sufficient information to allow designers to make reasonable estimates of tunnel pressures for many cases from free stream conditions at the tunnel entrance and a knowledge of the tunnel configuration. The primary sources of information are shock tube studies of model tunnel systems, (Refs. 3-19, 3-20, 3-21, and 3-22), and a semi-empirical solution in Ref. 3-20 for the maximum peak overpressure occurring in tunnels developed by Clark and Taylor at the Ballistic Research Laboratories. The maximum tunnel overpressures presented by Clark and Taylor are based on an analogy between the expansion of a pressure wave in a shock tube when the diaphragm separating the compression and expansion chambers is instantaneously ruptured and the entry of a pressure wave into a tunnel. The results obtained from this analogy are discussed below. The references mentioned above present data

on shock attenuation in straight tunnels and the effects of bends and junctions. Except for one study reported by Armour Research Foundation in Ref. 3-19 there is little information available concerning the effects of changes in cross-sectional area along a tunnel. Finally, information pertinent to the expansion of pressures into a large chamber is limited to incident peak pressures less than about 30 psi, Ref. 3-22 and 3-23, and specific chamber geometries. It is apparent that much more information than is presently available on the behavior of shock waves in tunnels is needed. Consequently, it must be assumed that some of the data presented herein will require re-evaluation as the results of new research become available.

In the following discussion the various factors affecting shock propagation in tunnel systems are reviewed and, where possible, data and procedures for predicting tunnel pressures are given.

3.3.1 SHOCK FORMATION IN STRAIGHT TUNNELS

The entry of a shock wave into a tunnel is accompanied by reflections and the formation of vortices near the portal. At some distance inside the entrance a more-or-less plane shock front is formed which continues to advance into the tunnel. The maximum peak overpressure will occur near this point in the tunnel where the new front is formed. As the shock wave progresses along a straight tunnel, the peak overpressure at the wave front continually decreases due to friction losses on the tunnel walls, the viscosity of the fluid, and the rate of pressure decay following the shock front. The magnitude of the maximum peak overpressure at the plane-shock-formation distance depends upon incident overpressure, the angle of

incidence between the tunnel axis and the direction of propagation of the air blast wave, and the topography of the ground surface near the portal.

Fig. 3-22 shows the relationship between the maximum peak overpressure in a tunnel and the incident peak overpressure for three angles of incidence. Each of the three cases is discussed individually below.

(a) Side-on Tunnel. In this case it is assumed that a tunnel or shaft is engulfed as the blast wave moves across the surface perpendicular to the tunnel axis. The diffraction of the wave over the entrance is somewhat similar to that shown in Fig. 3-23 which depicts the passage of a plane shock wave over an infinitely wide rectangular slit. Fig. 3-23(a) shows the expanding wave as it enters the tunnel or slit. The pressure jump across the front at point 2 is less than that at point 1 as a result of the expansion of the wave. In Fig. 3-23(b) the slit has been completely engulfed and the wave advancing into the slit has been reflected by the side walls. The front labeled 2, represents the original front which entered the slit. In Fig. 3-23(c) turbulent flow near the entrance is indicated by the vortices which are represented by the swirling flow. As these vortices shed and move down the tunnel, they cause pressure variations in the tunnel. The formation distance, or distance required for the wave fronts shown in Fig. 3-23(b) to coalesce, is not definitely known. However, gages located a distance of seven diameters from entrances in model tunnels used in shock tube studies, Ref. 3-20, indicate that the tunnel shock front has already formed at that distance.

The pressure relationship for the side-on case shown in Fig. 3-22 indicates that the maximum peak overpressure developed in the tunnel is

less than the incident peak overpressure as would be expected from Fig. 3-23(a). This relationship is based on shock tube studies of Ref. 3-22 in which the incident pressure varied from about 7 to about 850 psi. The measured maximum peak overpressures were generally within approximately 20 percent of those indicated by the relationship shown in Fig. 3-22. Since most of the data used in the BRL analogy is for a shock wave of constant pressure, the resulting relationships given in Fig. 3-22 are applicable only if the positive phase duration, t_o , satisfies the following criteria:

$$t_o \geq \frac{50 D}{c_o} \quad (3-11)$$

where D is the tunnel diameter in feet and c_o is the ambient sound velocity in feet per second. For weapons with a yield greater than one MT, the positive phase duration is about one second as a minimum. Consequently, Eq. (3-11) indicates that the relationships given in Fig. 3-22 are applicable to tunnels with a diameter of less than about 22 feet.

(b) Face-on Tunnel. In this case the tunnel axis is coincident with the direction of propagation of the air blast wave on the surface and the surface geometry at the tunnel entrance exerts a considerable influence on the development of the tunnel shock. If the tunnel is centered in a large reflecting area such as a sheer cliff, the entrance of the tunnel is immediately immersed in an extensive reflected pressure region when the incident wave strikes the face of the cliff. If the reflected pressure region is not relieved by diffraction around the cliff or by other means before the tunnel shock is completely formed, the maximum peak overpressure

in the tunnel will exceed the incident peak overpressure. In this case the formation distance was found from shock tube studies, Ref. 3-22, to range from 5 to 10 tunnel diameters. At the other extreme, if there is no reflecting area at an entrance such as the entrance of a pipe, the tunnel would merely confine the incident pulse to a one-dimensional expansion. This would result in a maximum overpressure in the tunnel approximately equal to the free stream overpressure at the entrance.

The relationship between maximum peak overpressure in the tunnel and the incident overpressure shown in Fig. 3-22 is the best fit to shock tube data. It assumes that the tunnel entrance is surrounded by a large, vertical, smooth reflecting surface. This relationship is based on data collected by BRL for incident pressures ranging approximately from 4 to 90 psi and limited ARF data from Ref. 3-19 for pressures up to about 200 psi. No data is available for higher pressures, the dashed part of the curve shown in Fig. 3-22 is an extrapolation.

The face-on pressure relationship is strictly valid provided that the distance between the edge of the tunnel and the edge of the reflecting surface is at least five tunnel diameters. Any rigid surface capable of withstanding the reflected pressure can be considered an adequate reflecting surface; unless it has a roughness with perturbations comparable in size to the tunnel diameter the surface can be considered smooth. Finally the same duration criterion, Eq. (3-11), given for the side-on case applies. In any event, the face-on case as described forms an upper limit since smaller distances between the tunnel and the edge of the reflecting area

or smaller durations than required by Eq. (3-11) will result in lower pressures in the tunnel.

(c) Oblique Case (45°). In this case the angle between the tunnel axis and the direction of propagation of the air blast wave is 45° . The relationship given in Fig. 3-22 between maximum peak overpressure in the tunnel and incident peak overpressure was derived in Ref. 3-24 from shock tube studies of model tunnels reported in Ref. 3-19. The slope of the resulting curve was slightly adjusted to conform to the more reliable relationships for the side-on and face-on cases. Since the range of available shock tube data is limited, the oblique case relation is shown as an extrapolation (dashed curve) for both higher and lower pressures.

3.3.2 EFFECT OF BENDS AND JUNCTIONS.

(a) 90° Bends. If a sharp turn or bend is incorporated in a tunnel system, it will reduce the peak pressure at the shock front provided there is no change in the cross-sectional area of the tunnel. Shock tube studies performed by the Ballistic Research Laboratories, Ref. 3-21, indicate that a single, sharp 90° bend in a tunnel will reduce the peak pressure by approximately six percent. Thus the peak pressure, p_n , after n such turns is

$$p_n = p_{so} (0.94)^n \quad (3-12)$$

where p_{so} is the peak overpressure in the tunnel just ahead of the first turn. Eq. (3-12) assumes that there are no losses from either friction or pressure attenuation between bends. It further assumes that the positive

phase duration is greater than $500/C_0$. The shock tube data, upon which Eq. (3-12) is based, were restricted to pressures less than 20 psi and they indicated that the attenuation might be less for lower pressures (about 4 psi).

The effect of tunnel bends was studied by Armour Research Foundation, Ref. 3-19. In these tests the model tunnels were artificially roughened and included two 90° bends separated by a length of 10 diameters. The results indicate a peak pressure reduction due to the bends of about 20 percent, if approximate losses resulting from friction are subtracted from total peak pressure losses. Eq. (3-12) gives about 12 percent reduction for two turns. In the Armour tests, p_{50} varied from 30 to 225 psi and they indicated that the pressure attenuation increased slightly with increasing peak pressure. It is apparent that the pressure attenuation resulting from bends also should be related in some degree to the radius of curvature of the bend. In the ARF tests the radius of curvature of the bend was one-half the tunnel diameter, Ref. 3-19. The exact value used in developing Eq. (3-12) was not reported. Reference 3-19 also states that pressure attenuation is insignificant if the radius of turn is greater than about five times the tunnel diameter. However, no indication is given as to the manner in which the attenuation varies with change in radius of curvature.

(b) T-Shaped Tunnel Junctions. Fig. 3-24 shows the relationships between incident and transmitted peak overpressure in the various branches of a T-shaped tunnel junction. These relationships are valid only when the intersecting tunnels are of equal cross-sectional areas and the positive phase durations exceeds $500/C_0$. The curve labeled 1 in Fig. 3-24 is based

on the Ballistic Research Laboratories shock tube analogy and has been substantiated by shock tube studies for peak overpressures up to about 60 psi in Ref. 3-20. The curves labeled 2 and 3 in the Fig. 3-24 are empirical and are based on shock tube studies, Ref. 3-20.

If a tunnel is side-on to a main tunnel of much larger diameter, the situation is similar to the entry of the air blast wave into a side-on tunnel at the surface. In such cases the relationship shown for a side-on tunnel in Fig. 3-22 can be used to calculate the peak overpressure in the side-on tunnel. Correspondingly little, if any, decrease in the peak overpressure in the main tunnel would be expected.

3.3.3 ATTENUATION OF PEAK OVERPRESSURE IN STRAIGHT TUNNELS.

In paragraph 3.3.1 it was noted that the attenuation of peak overpressure in a tunnel depends on wall friction, fluid viscosity and the time rate of decay of pressure at the shock front. This problem has recently been studied at the Armour Research Foundation (ARF) and Ballistic Research Laboratories (BRL) and their results were published in Ref. 3-19 and 3-21 respectively. The results of these two studies give a slightly different picture of the pressure attenuation, and an absolute comparison of the results is impossible without test data more detailed than that given in the published reports. In the ARF tests of Ref. 3-19, model tunnels having diameters of 2, 3.5 and 8 inches with both smooth and artificially roughened walls were tested in the shock tube. These tests resulted in relationships between shock strengths and scaled length, L/D , where L is distance along the tunnel and D is tunnel diameter. In this

dimensionless form only the smooth wall data were independent of diameter. BRL studied, in Ref. 3-21, the attenuation in smooth model tunnels that is dependent on the initial slope of the pressure decay curve. The BRL study also includes an approximate analytical solution for pressure attenuation in which no account is made of entropy, viscosity, or heat transfer to the tunnel walls. The results of the BRL analytical study were compared with shock tube tests using smooth wall tunnel models.

Subsequent to the publication of Ref. 3-22, Mr. R. O. Clark developed the following expression for the peak pressure, p_{sx} , expected at a distance L from a tunnel entrance:

$$p_{sx} = p_{so} e^{-\left[\frac{A}{D} + \frac{1}{t}\right]KL} \quad (3-13)$$

where p_{so} = peak overpressure at the tunnel entrance

D = tunnel diameter

$$K = \frac{u + c_1 - c_o}{(u + c_1 + c_o)(c_1 + u)}$$

$$u = \frac{5p_{so}}{7p_o} \frac{c_o}{\sqrt{1 + 6p_{so}/7p_o}}, \text{ particle velocity}$$

$$c_1 = \text{sonic velocity immediately behind the front} \\ = c_o \sqrt{\left[\frac{p_{so} + p_o}{p_o}\right] \left[\frac{p_{so} + 7p_o}{6p_{so} + 7p_o}\right]}$$

c_o = sonic velocity ahead of the front

t = initial tangent duration of the overpressure-time relationship

A = a constant. $A = 28$ describes the average of the empirical data.

$A = 16$ describes the upper envelope of the data.

In Eq. (3-13) the pressure attenuation resulting from wall friction and fluid viscosity is taken as $e^{-AKL/D}$ and the attenuation associated with the steepness of slope of the pressure-time curve as $e^{-KL/t}$.

Eq. (3-13) along with the previously referenced results of Armour Research Foundation form at present the only bases for predicting pressure attenuation for design purposes. If Eq. (3-13) is used, the following values of the various parameters are suggested:

$$A = 16$$

$$t = t_{\infty} + 1/4 \frac{c_1 + u}{c_0} KL \text{ (second)}, \text{ where } t_{\infty} \text{ may be obtained from Fig. 3-7}$$

$$p_{so} = \text{maximum peak overpressure in a tunnel from Fig. 3-22}$$

The parameter K varies from 15.4×10^{-5} to 7.4×10^{-5} sec. per ft. for values of p_{so} from 50 to 1000 psi and in this range $K = 10^{-4}$ is a reasonable average value for use.

It should be noted here that Eq. (3-13) appears to indicate slightly more attenuation for tunnel distances less than about 30 diameters, than reported by ARF.

3.3.4 BLAST LOADING ON DOORS AND BLAST VALVES IN TUNNELS AND DUCTS.

The shape of the assumed pressure-time relationship for a closure device in an elementary tunnel configuration is shown in Fig. 3-25. This loading consists of the overpressure-time relationship that would exist at a distance L from the entrance if the tunnel were not sealed plus a reflected pressure spike.

If the tunnel length is greater than about five times the tunnel

diameter, D , the peak overpressure at a distance L can be determined from the data presented in Paragraph 3.3.3. The shape of the overpressure-time curve at this distance can be assumed to be the appropriate idealized shape from Fig. 3-4 if better estimates of those shapes are not available. Theoretical considerations, Ref. 3-21, indicate that an increase in duration of the positive phase accompanies that part of the pressure attenuation associated with the rate of decay of the pressure behind the shock front. The new duration, t_o' is given by the following equation:

$$t_o' = t_o + \int_0^L K \left[\frac{c_1 + u}{c_o} \right] dx \quad (3-14)$$

where t_o is positive phase duration at the tunnel entrance. The remaining terms in Eq. (3-14) are functions of the peak pressure at the shock front and are defined in Paragraph 3.3.3. As a conservative estimate, Eq. (3-14) may be taken as

$$t_o' = t_o + KL \left[\frac{c_1 + u}{c_o} \right] \quad (3-15)$$

The peak reflected pressure, p_{ro} , can be taken from Fig. 3-2. The duration of the reflected pressure spike, t_p , is given as follows

$$t_p = \frac{L}{c_r} + \frac{L}{U_r} \quad (3-16)$$

where U_r is the net velocity of the reflected shock wave and c_r is velocity of a rarefaction wave in the compressed gas in the tunnel, U_r , c_r and U , the incident shock velocity, are plotted in Fig. 3-26 as a function of the

incident peak overpressure on the door. These velocities should be used for relatively short tunnels only. If the tunnel leading to the closure is very long, the velocity of the reflected and rarefaction waves will vary with pressure.

If the door is mounted flush at the entrance of the tunnel, the loading function depends upon the orientation of the tunnel entrance with respect to the direction of travel of the air blast wave. For example, a horizontal door placed flush at the ground surface would be loaded only by the incident overpressure-time curve. On the other hand, a door in an entrance that is constructed in a vertical cliff may experience a loading pulse similar to that for the front surface of an above ground rectangular structure.

If the distance from the tunnel entrance to the closure device is less than about five times the tunnel diameter, the conservative approach would be to use a loading equal to that at $5D$ unless the door is approximately flush, i.e., $L \approx 0$.

3.4 REFERENCES

- 3-1 "The Effects of Nuclear Weapons", U. S. Dept. of Defense and Atomic Energy Com., April 1962. (UNCLASSIFIED)
- 3-2 "Capabilities of Atomic Weapons", AFM-136-1A, Armed Forces Special Weapons Projects, Washington, D. C., June 1960. (CONFIDENTIAL)
- 3-3 Willoughby, A. B., Kaplan, K. and Condit, R. I., "Effects of Topography on Shock Waves in Air", AFSWC TR-57-9, August 1956. (CONFIDENTIAL)
- 3-4 "Surface Effects on Blast Loadings", AFSWC TR-60-54, Armour Research Foundation, May 1958. (SECRET)
- 3-5 Moulton, J. F., "Nuclear Weapons Blast Phenomena", DASA 1200, Vol. I (SECRET), Vol. II (SECRET), Vol. III (CONFIDENTIAL), March 1960.
- 3-6 Brode, H. L., "Weapons Effects for Protective Design Ground Support Systems Weapons Effects", P-1951, Rand Corporation, Santa Monica, California, 31 March 1960. (UNCLASSIFIED)
- 3-7 Broyles, C., "Air Blast Phenomena from Surface Bursts", Symposium on Air Blast Effects, AFSWP 898, February 1957, pp. 109-116. (SECRET)
- 3-8 Brode, H. L., "Reflection Factors for Normally Reflected Shocks in Air", The Rand Corporation, Research Memorandum RM-2211, 14 July 1958. (UNCLASSIFIED)
- 3-9 Smith, L. G., "Photographic Investigation of the Reflection of Plane Shocks in Air", OSRD Report No. 6271, (ASTIA A.T.I. 18454), 1 November 1945. (UNCLASSIFIED)
- 3-10 Newmark, N. M. and Hall, W. J., "Preliminary Design Methods for Underground Protective Structures", AFSWC-TDR-62-6, June 1962. (SECRET)
- 3-11 Brode, H. L., "Numerical Solution of Spherical Blast Waves", Journal of Applied Physics, Vol. 26, No. 6, pp. 766-775, June 1958. (UNCLASSIFIED)
- 3-12 Brode, H. L., "Theoretical Description of the Blast and Fireball for a Sea Level Megaton Explosion", The Rand Corporation, Research Memorandum RM-2248, 2 Sept. 1959. (SECRET RD)

- 3-13 Keyes, F. G., "A Summary of Viscosity and Heat-Conduction Data for H_2 , A, H_2 , O_2 , CO, CO_2 , H_2O , and Air", Transactions ASME, Vol. 73 (1951), p. 589. (UNCLASSIFIED)
- 3-14 Hoerner, S. F., "Fluid Dynamic Drag", Published by Author at 148 Busteed Drive, Midland Park, New Jersey, 1958. (UNCLASSIFIED)
- 3-15 "Wind Forces on Structures", Transactions ASCE, Vol. 126 (1961), p. 1124. (UNCLASSIFIED)
- 3-16 "Transient Drag and its Effect on Structures", Final Report on Contract No. AF 33(616)-2285 for WADC by the American Machine and Foundry Co., February 1955. (SECRET)
- 3-17 Newmark, N. M., "Analysis and Design of Structures to Resist Nuclear Blast", Bulletin 106, Part 2, Virginia Polytechnic Institute, August 1954. (UNCLASSIFIED)
- 3-18 "Design of Structures to Resist Nuclear Weapons Effects", ASCE Manual of Engineering Practice No. 42, 1961. (UNCLASSIFIED)
- 3-19 Swatosh, J. J., Jr. and Birukoff, R., "Blast Effects on Tunnel Configurations", SWC TR-59-48, Air Force Special Weapons Center Kirtland Air Force Base, New Mexico, October 1, 1959. (UNCLASSIFIED)
- 3-20 Clark, R. O. and Taylor, W. J., "Shock Pressures in Tunnels Oriented Face-On and Side-On to a Long Duration Blast Wave", BRL 1280, Ballistic Research Laboratories, Aberdeen Proving Ground, Maryland, June 1960. (UNCLASSIFIED)
- 3-21 Clark, R. O. and Coulter, G. A., "Attenuation of Air Shock Waves in Tunnels", BRL 1278, Ballistic Research Laboratories, Aberdeen Proving Ground, Maryland, June 1960. (UNCLASSIFIED)
- 3-22 "First Information Summary of Blast Patterns in Tunnels and Chambers", DASA 1171, Ballistic Research Laboratories, Aberdeen Proving Ground, Maryland, March 1960 (Draft Copy). (UNCLASSIFIED)
- 3-23 Sinnamon, G. K., Austin, W. J. and Newmark, N. M., "Air Blast Effects on Entrances and Air Intakes of Underground Structures", WT-726, Operation UPSHOT-KNOTHOLE, University of Illinois, Urbana, Illinois, 1 February 1955. (UNCLASSIFIED)
- 3-24 Newmark, Hansen and Associates, "Protective Construction Review Guide (Hardening)", Volume I, prepared for the Office of the Assistant Secretary of Defense, Installations and Logistics, Revised 1 June 1961. (UNCLASSIFIED)

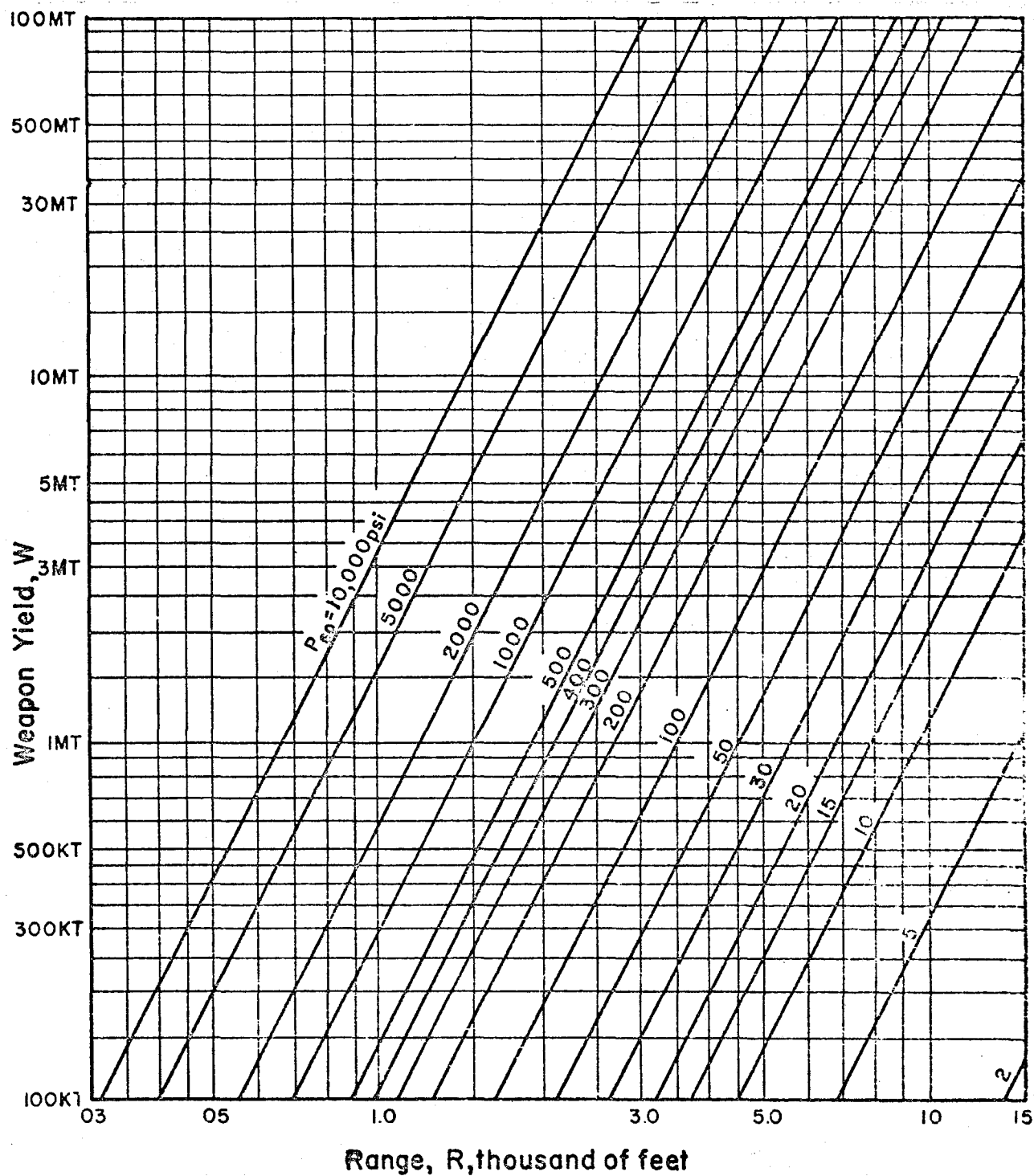


FIG. 3-1 PEAK OVERPRESSURE AT GROUND SURFACE
VERSUS RANGE FOR VARIOUS YIELDS —
SURFACE BURST AT SEA LEVEL.

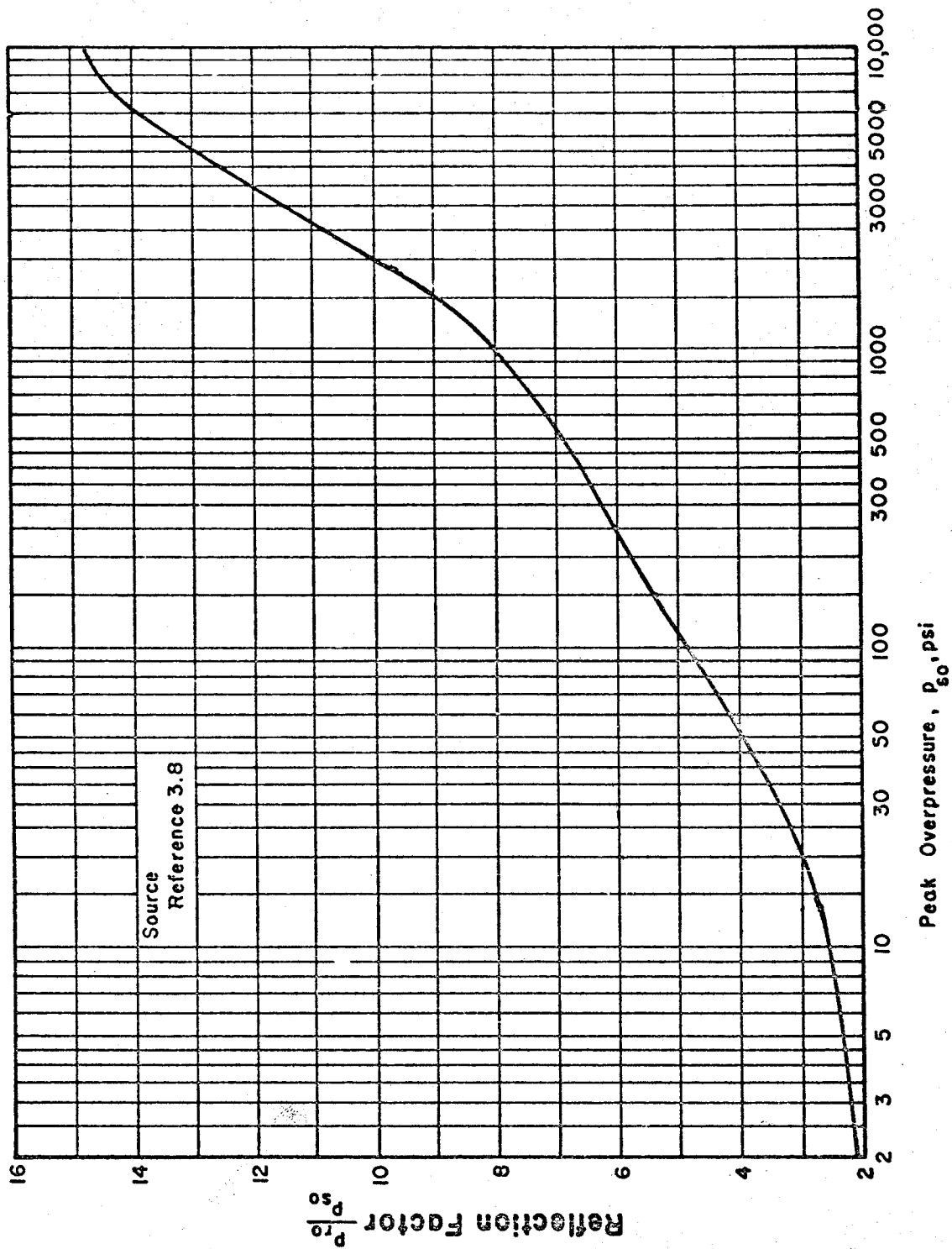


FIG. 3-2 REFLECTION FACTOR VERSUS PEAK OVERPRESSURE
FOR FACE-ON INCIDENCE

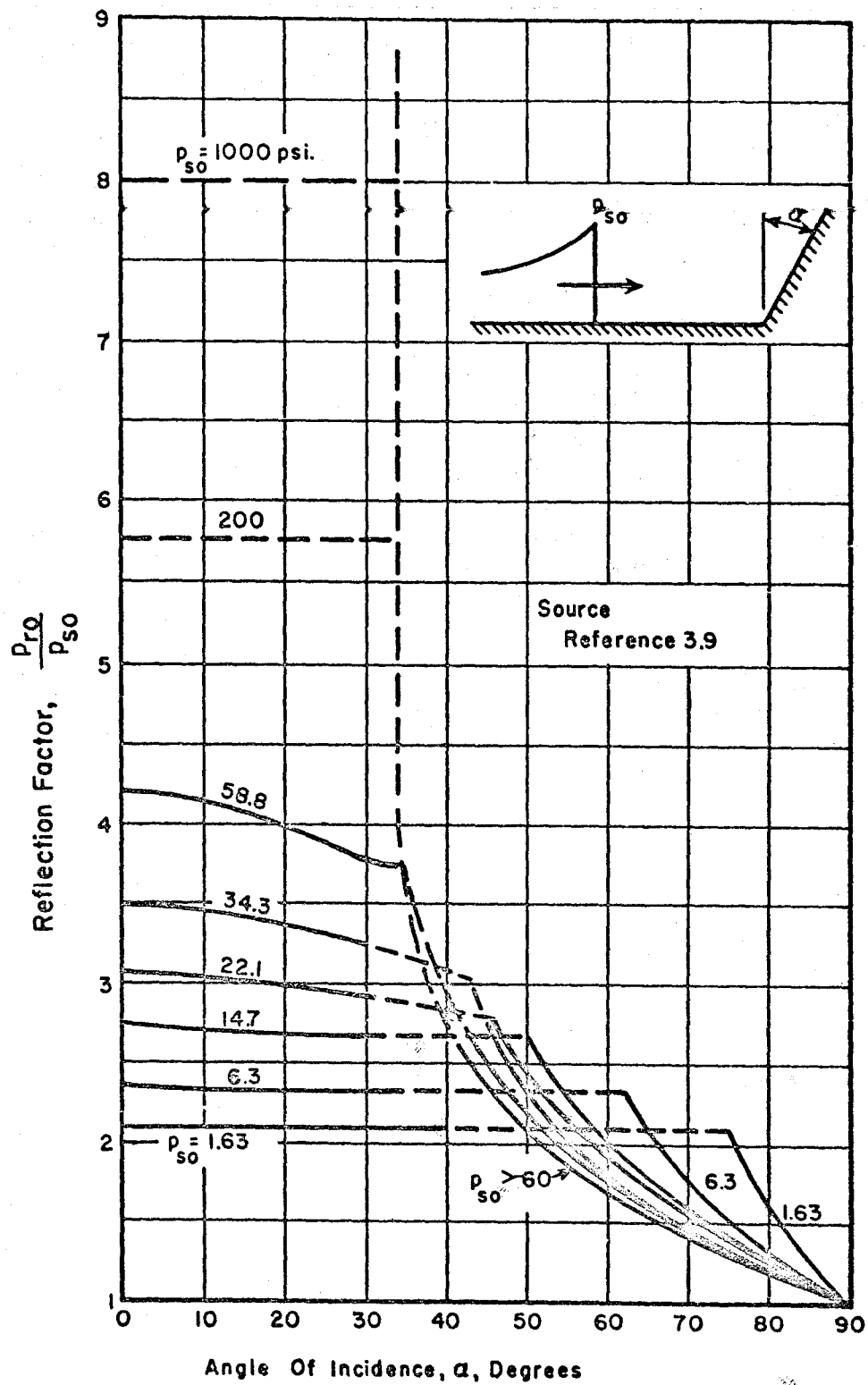


FIG. 3-3 REFLECTION FACTOR FOR VARIOUS PEAK OVERPRESSURES AND ANGLES OF INCIDENCE

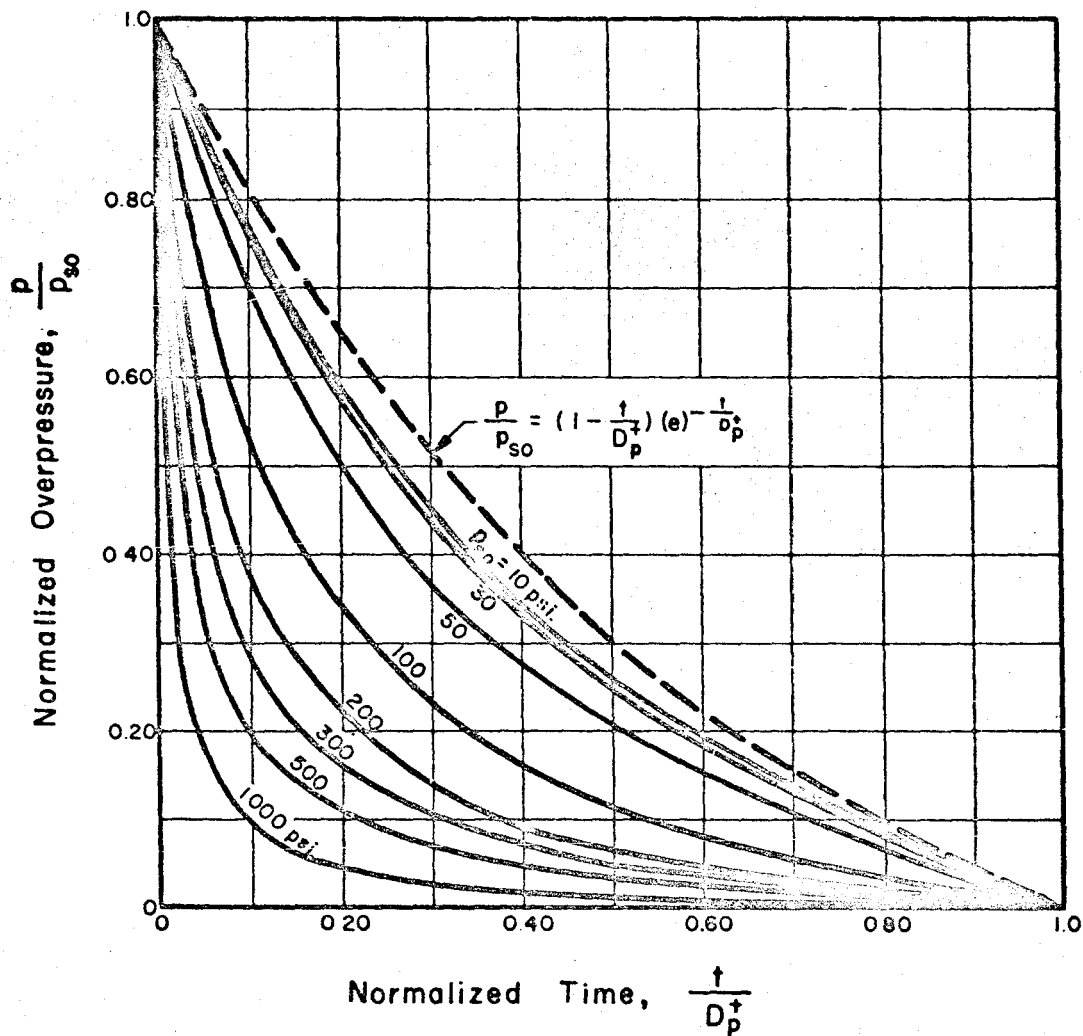


FIG. 3-4 NORMALIZED OVERPRESSURE WAVE FORMS — 1 MT SURFACE BURST

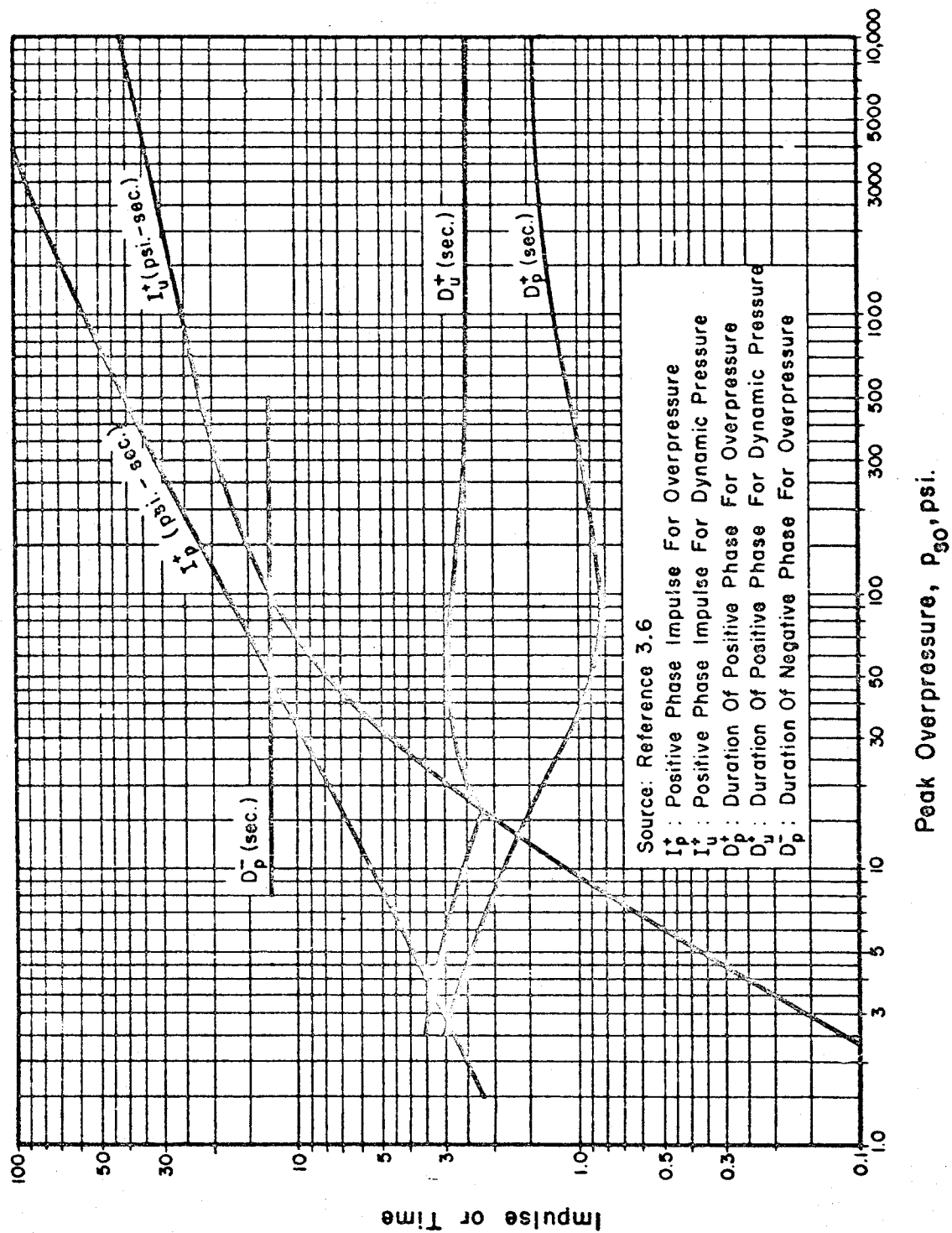
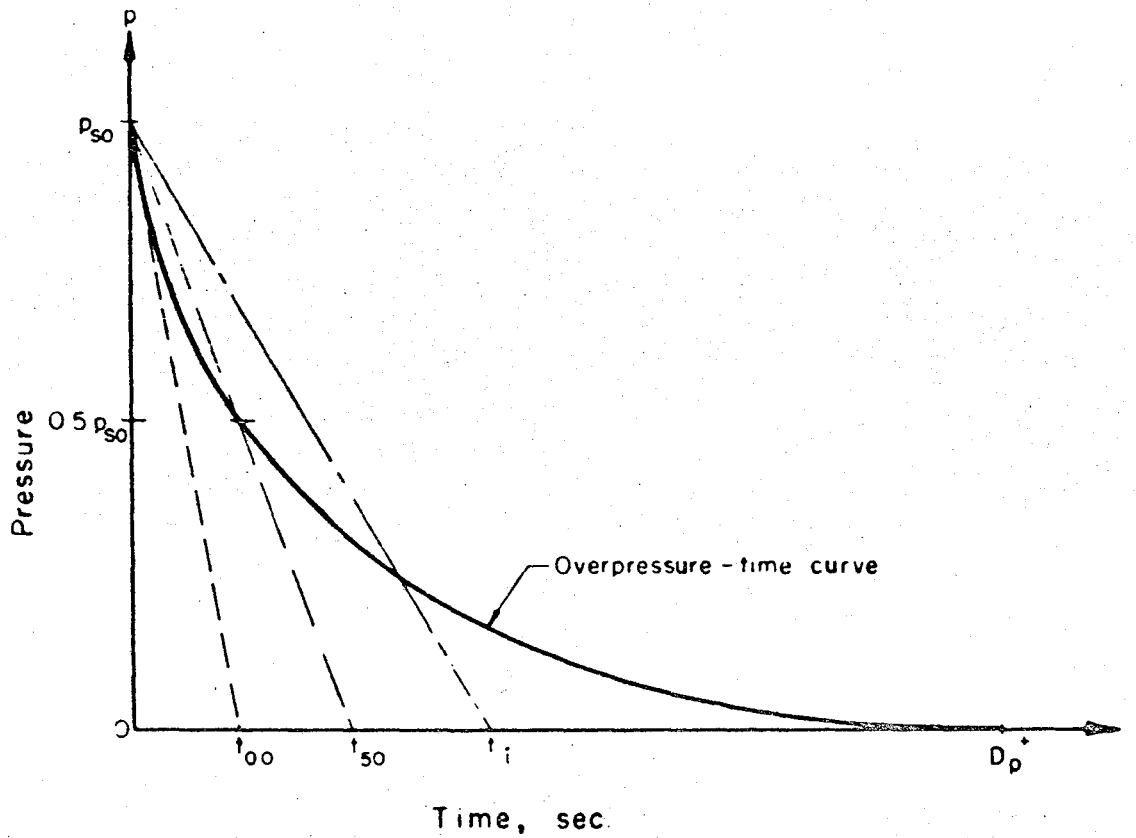


FIG. 3-5 IMPULSE AND DURATION VERSUS OVERPRESSURE —
1 MT SURFACE BURST



The same types of triangular representations were used for dynamic pressure-time curves, designated as t'_{00} , t'_{50} , and t'_i , but for convenience of use the pressures are expressed in terms of peak overpressure instead of peak dynamic pressure. For dynamic pressure the duration of the positive phase is designated as D_u^+ .

FIG. 3-6 TRIANGULAR REPRESENTATIONS
OF OVERPRESSURE-TIME CURVES

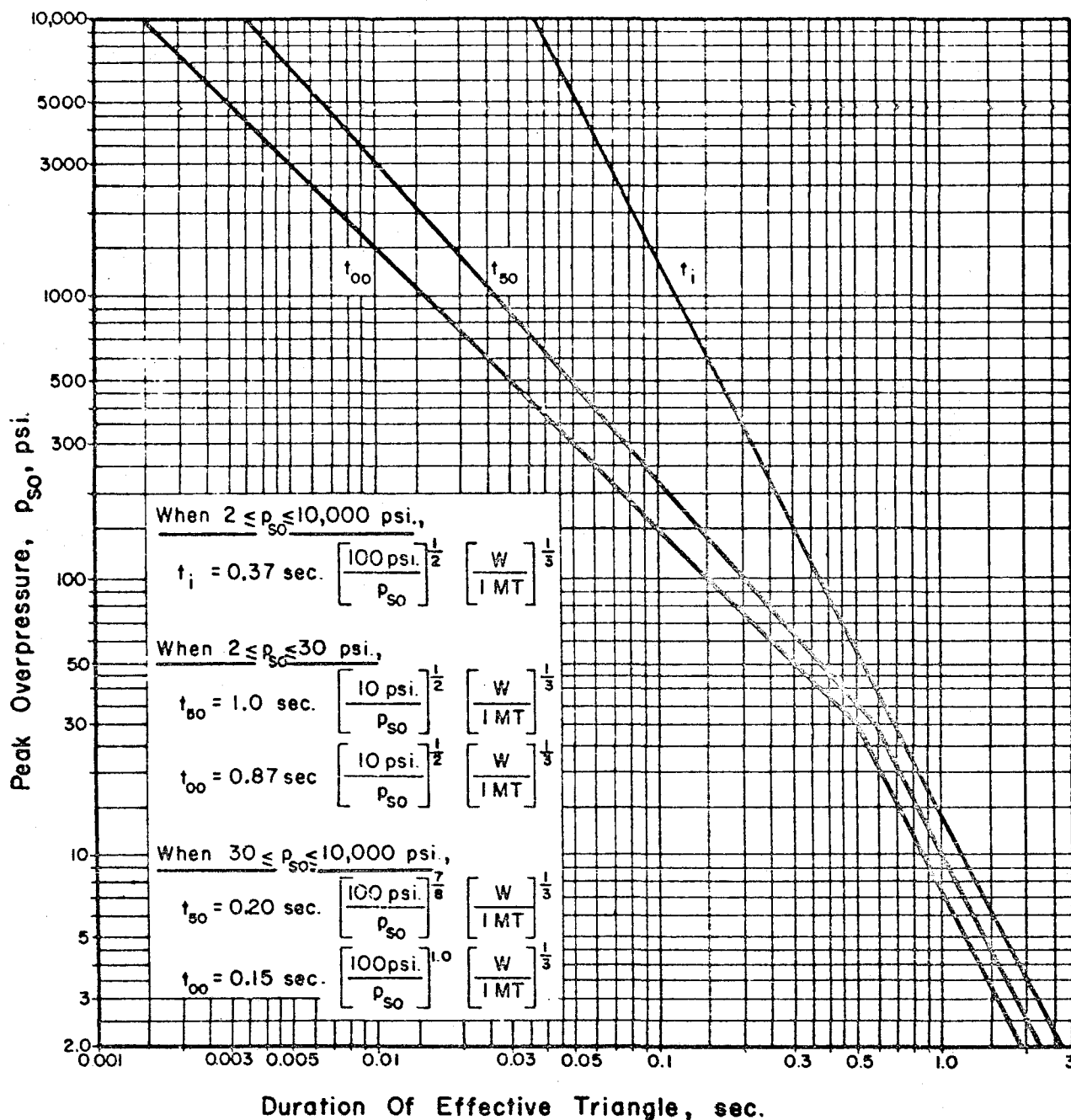
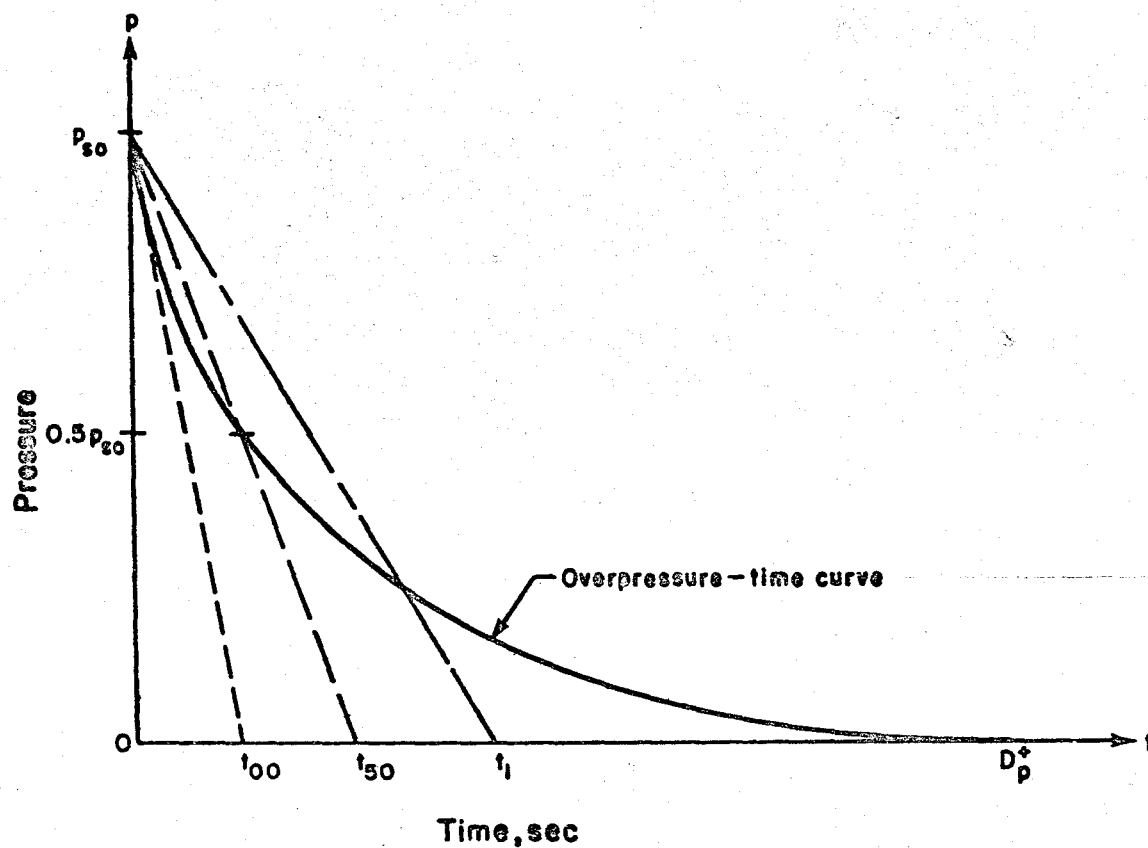


FIG. 3-7 DURATION OF EFFECTIVE TRIANGLES FOR REPRESENTATION OF OVERPRESSURE-TIME CURVES — 1 MT SURFACE BURST



The same types of triangular representations were used for dynamic pressure-time curves, designated as t'_{00} , t'_{50} , and t'_1 , but for convenience of use the pressures are expressed in terms of peak overpressure instead of peak dynamic pressure. For dynamic pressure the duration of the positive phase is designated as D_t^+

**FIG. 3-6 TRIANGULAR REPRESENTATIONS
OF OVERPRESSURE-TIME CURVES**

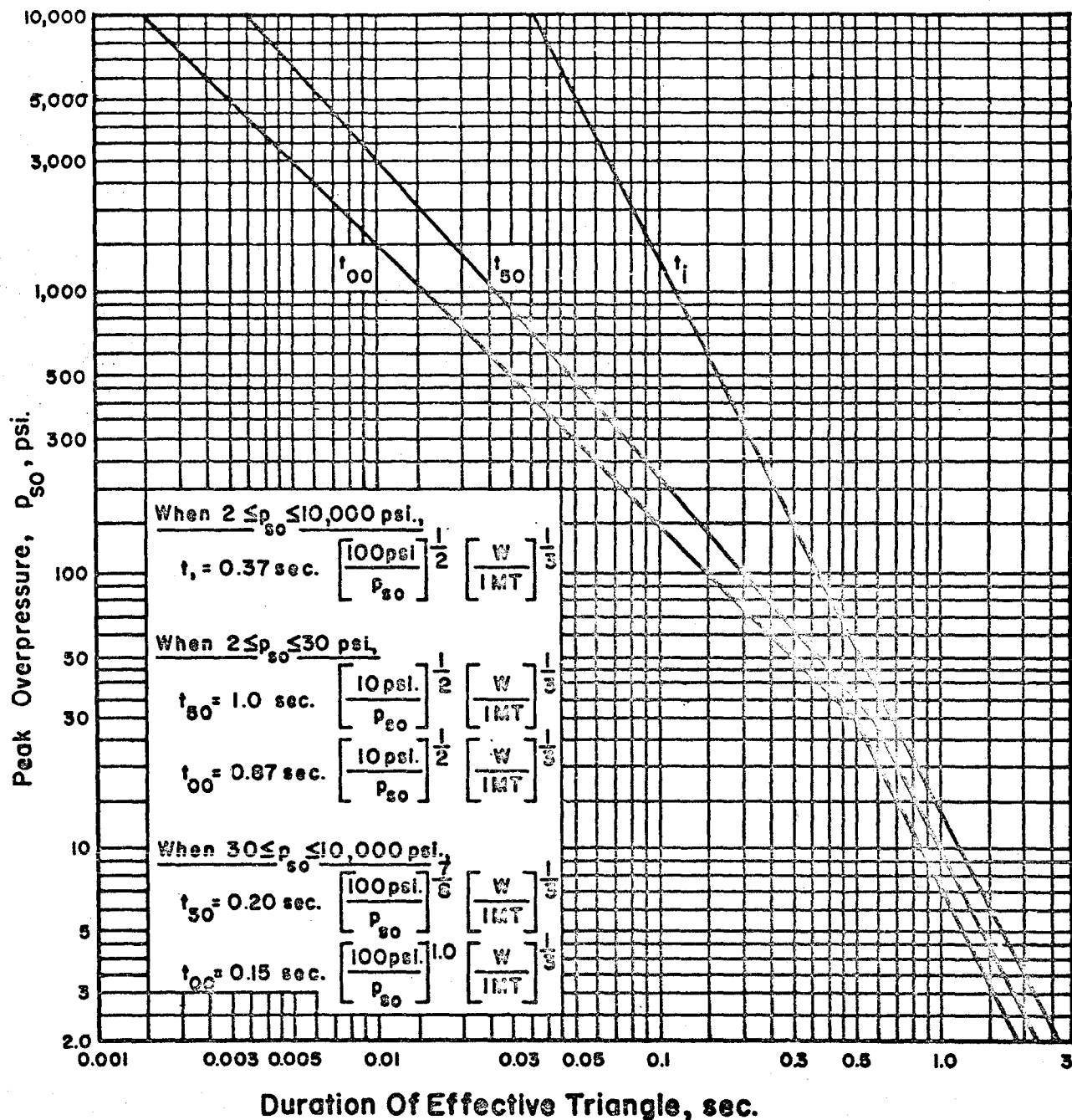


FIG. 3-7 DURATION OF EFFECTIVE TRIANGLES FOR REPRESENTATION OF OVERPRESSURE-TIME CURVES — 1 MT SURFACE BURST

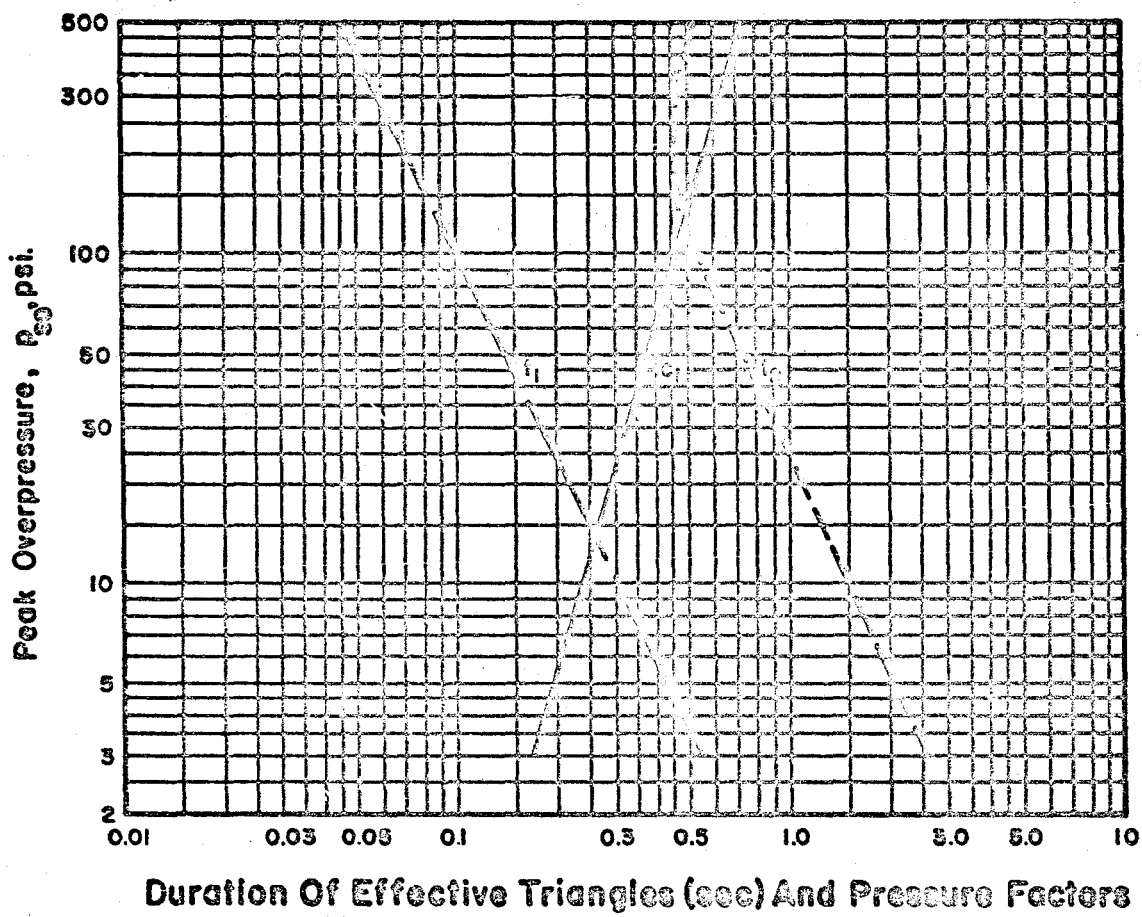
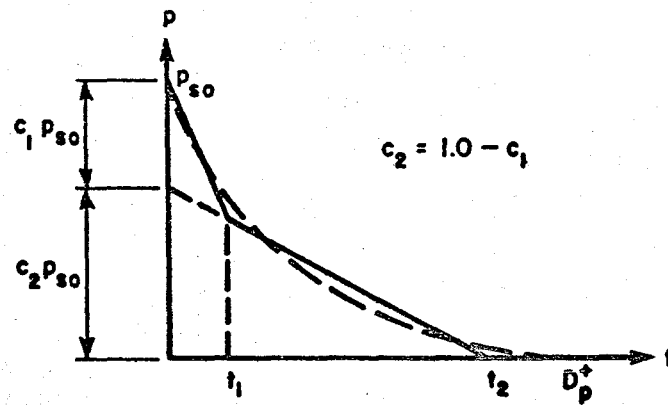


FIG. 3-8 TWO-TRIANGLE REPRESENTATION FOR
 OVERPRESSURE—1MT SURFACE BURST

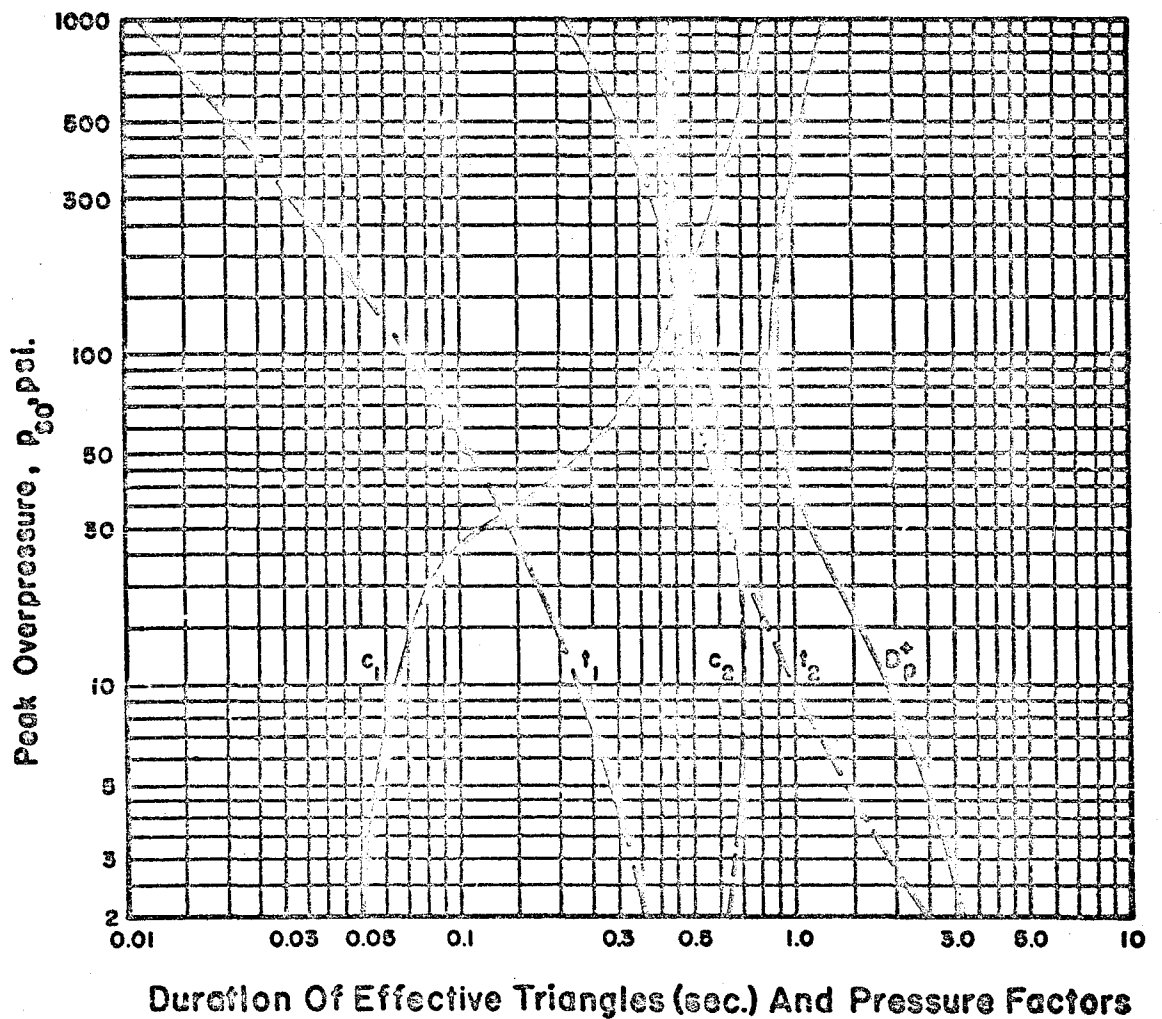
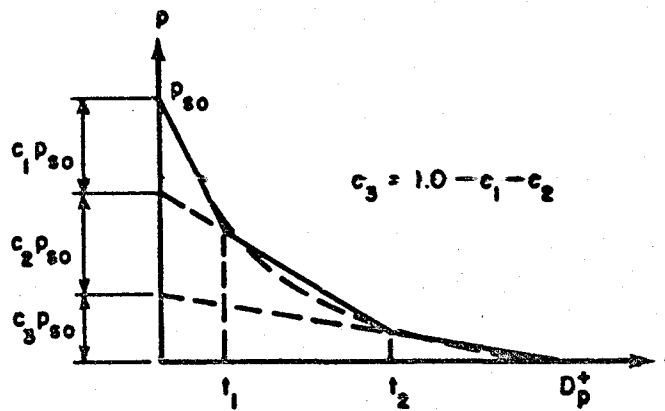


FIG. 3-9 THREE-TRIANGLE REPRESENTATION FOR OVERPRESSURE — IMT SURFACE BURST

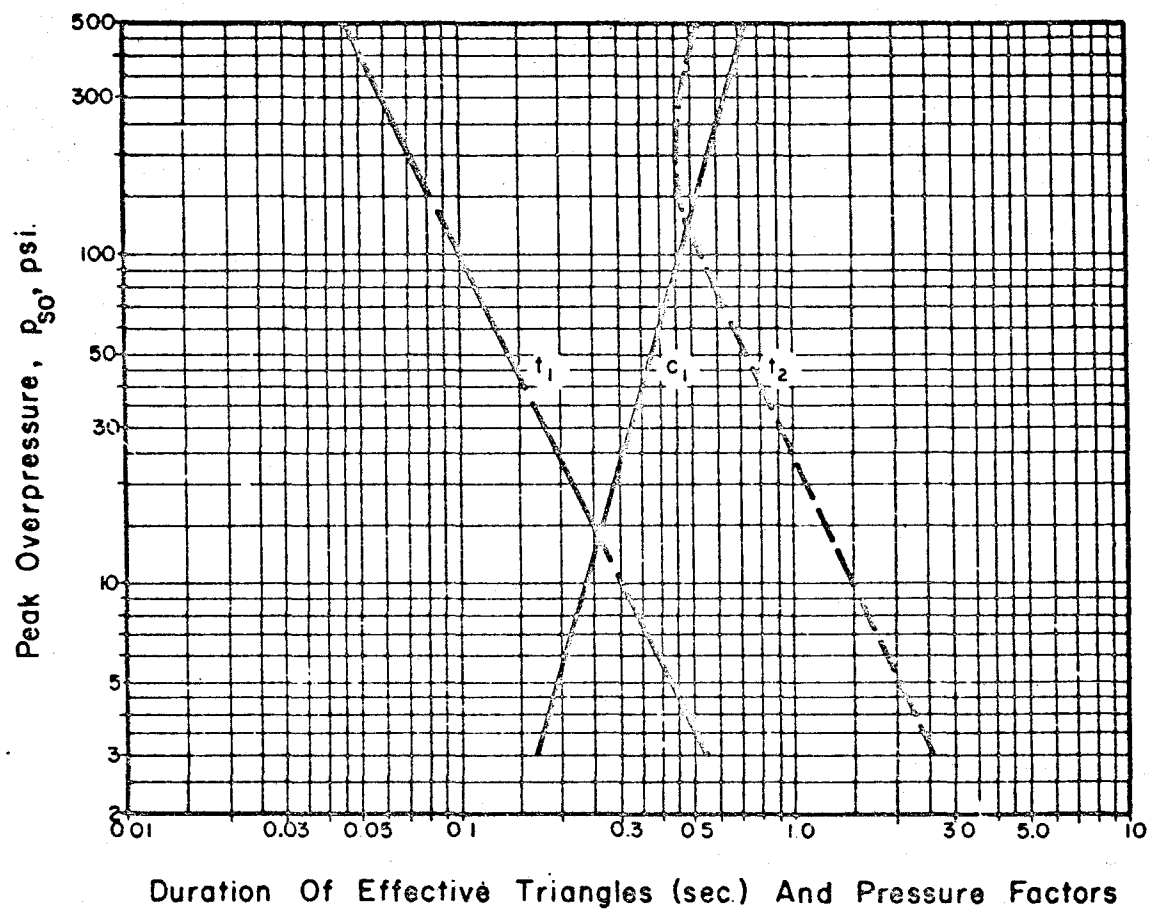
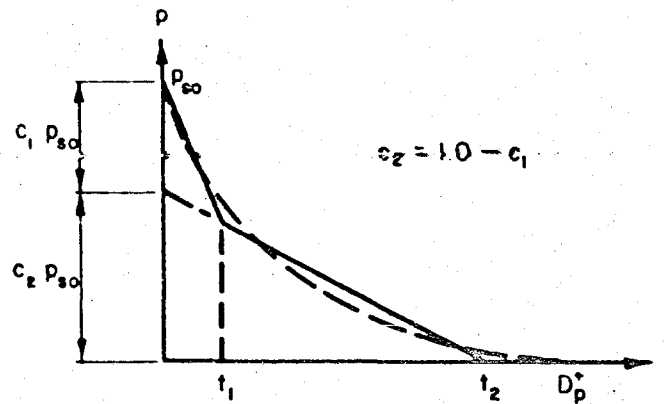


FIG. 3-8 TWO-TRIANGLE REPRESENTATION FOR
 OVERPRESSURE—1 MT SURFACE BURST

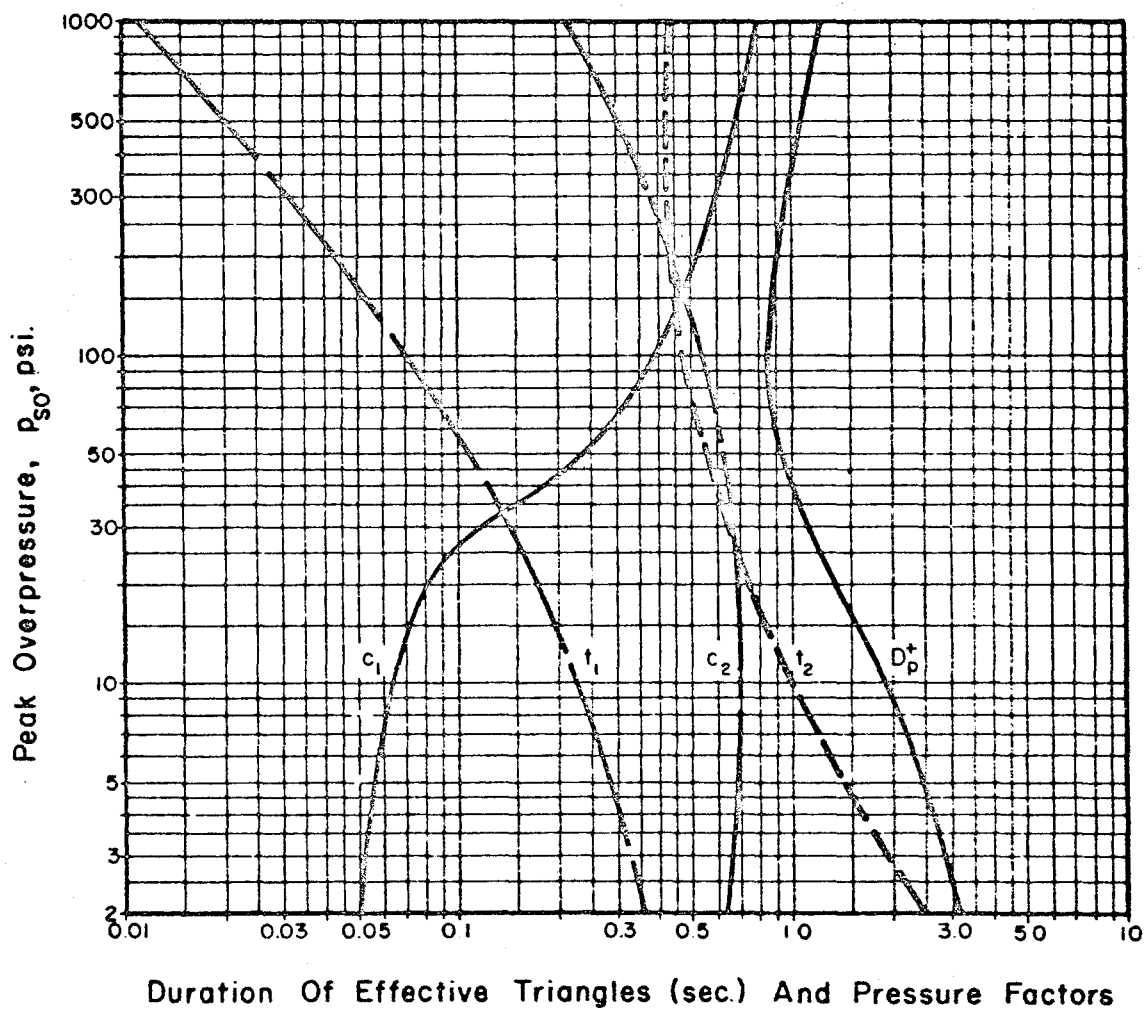
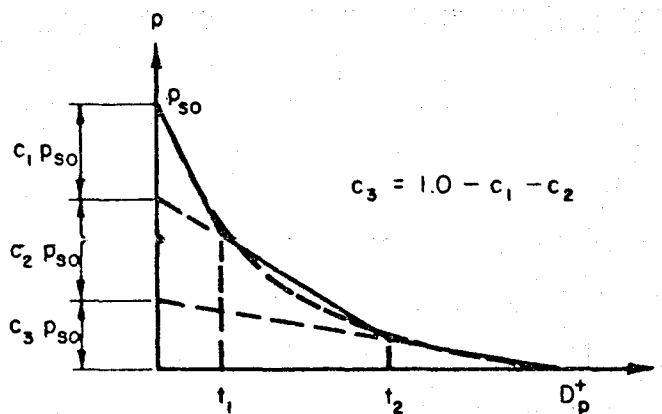


FIG. 3-9 THREE-TRIANGLE REPRESENTATION FOR OVERPRESSURE — 1 MT SURFACE BURST

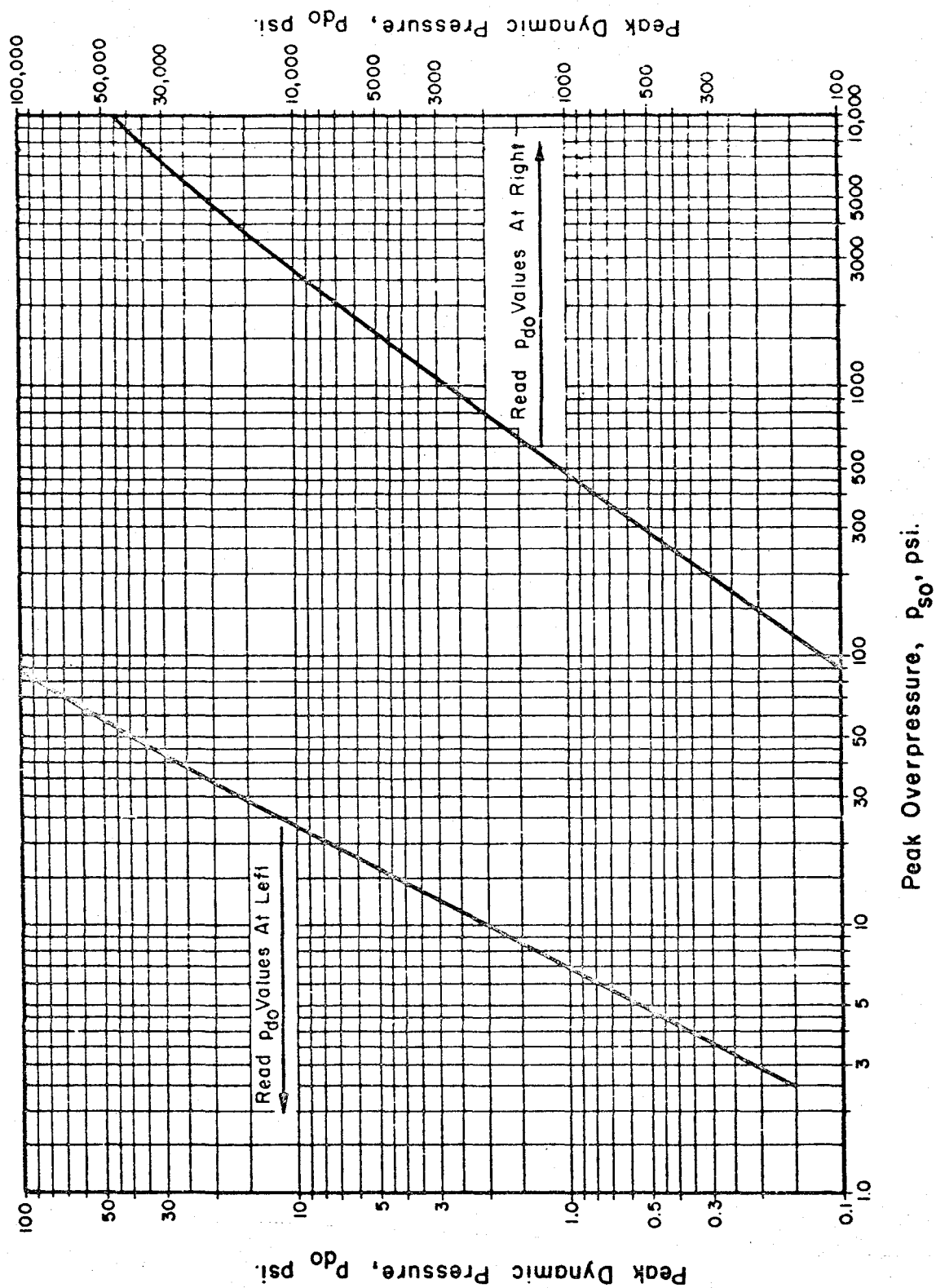


FIG. 3-10 OVERPRESSURE VERSUS DYNAMIC PRESSURE

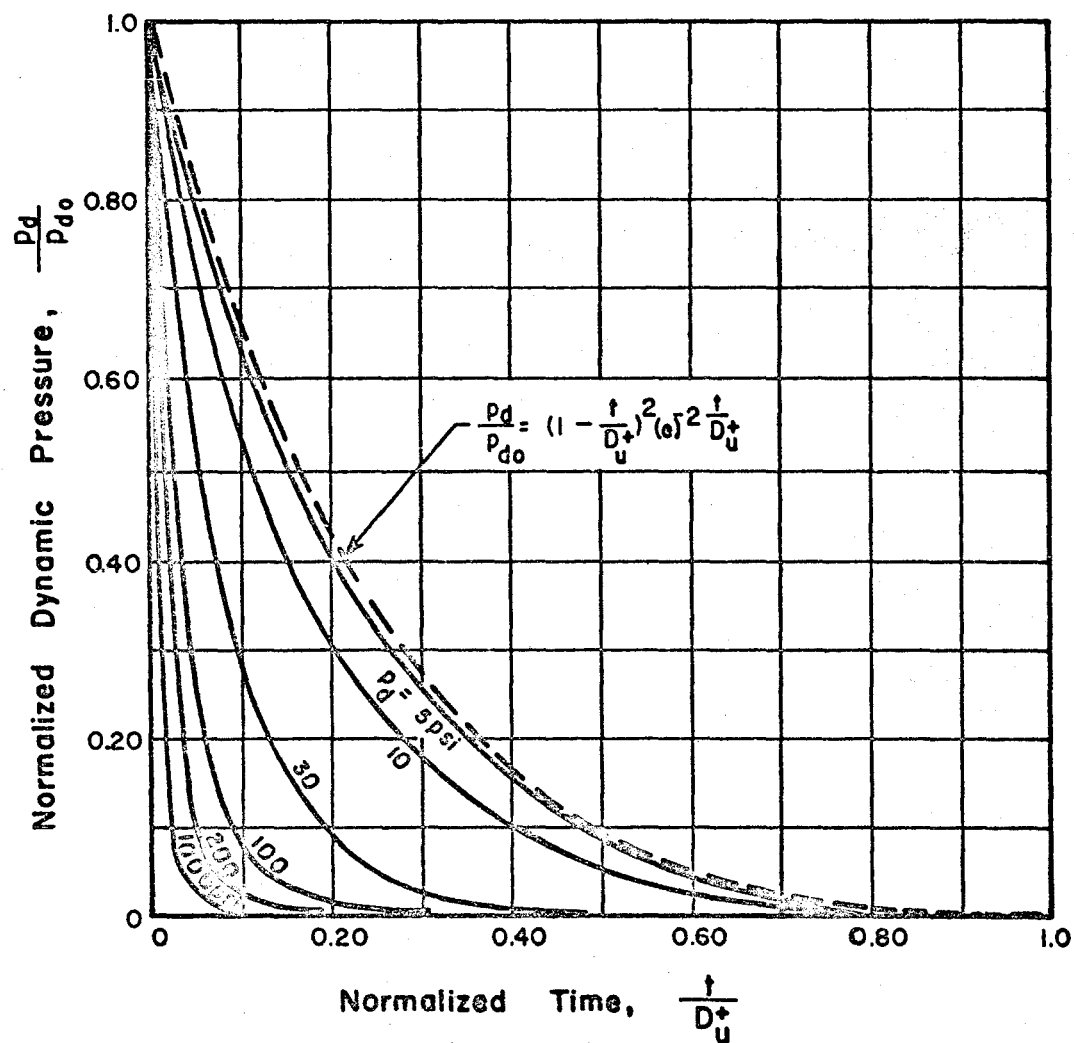


FIG. 3-II NORMALIZED DYNAMIC PRESSURE
WAVE FORMS — 1 MT SURFACE
BURST

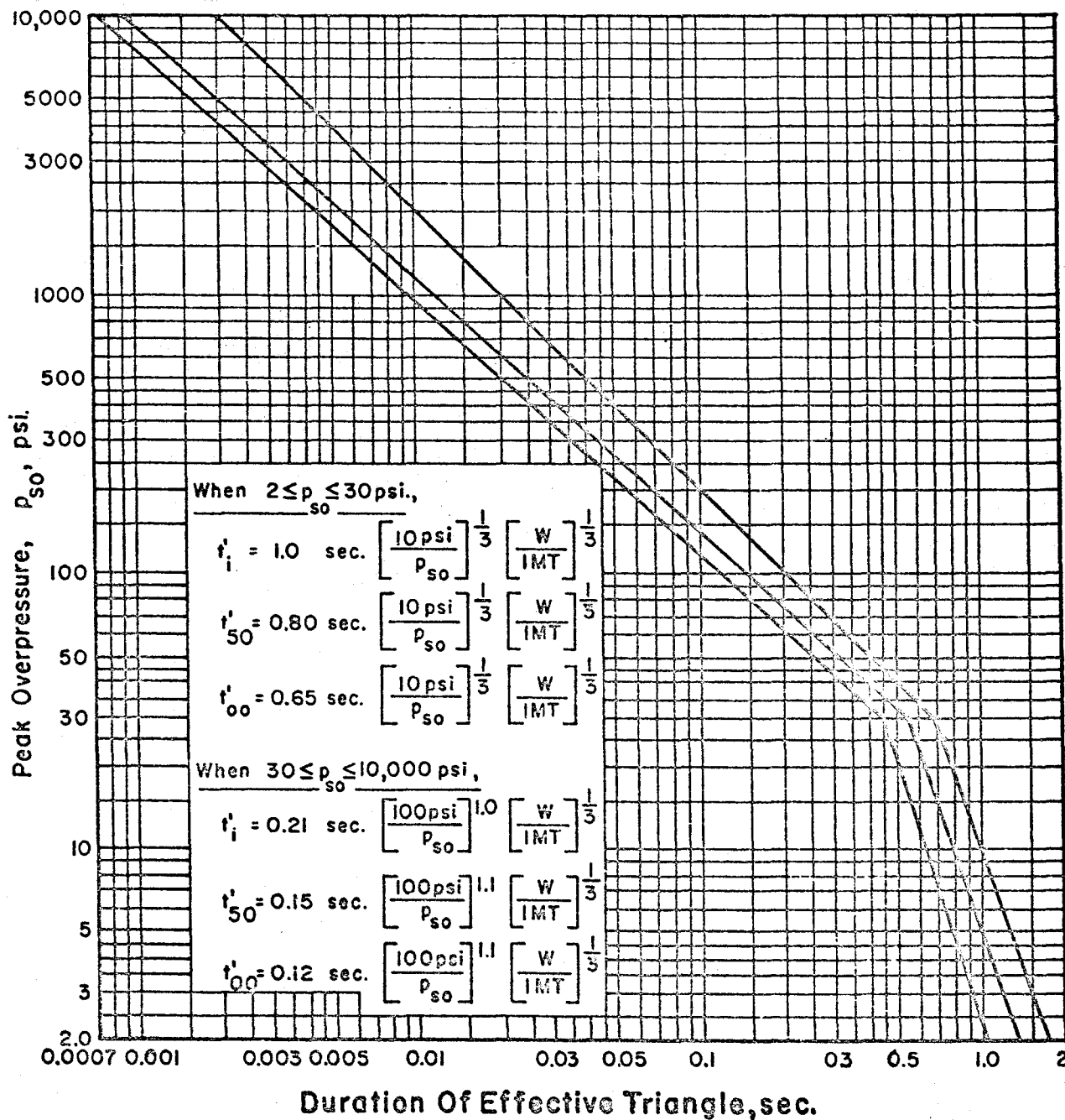
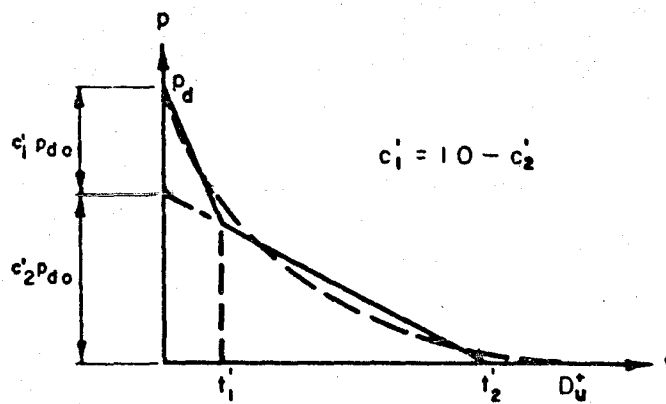


FIG. 3-12 DURATION OF EFFECTIVE TRIANGLES FOR REPRESENTATION OF DYNAMIC PRESSURE-TIME CURVES—IMT SURFACE BURST



NOTE:

For p_{d0} Versus p_{s0} See Figure 3-10

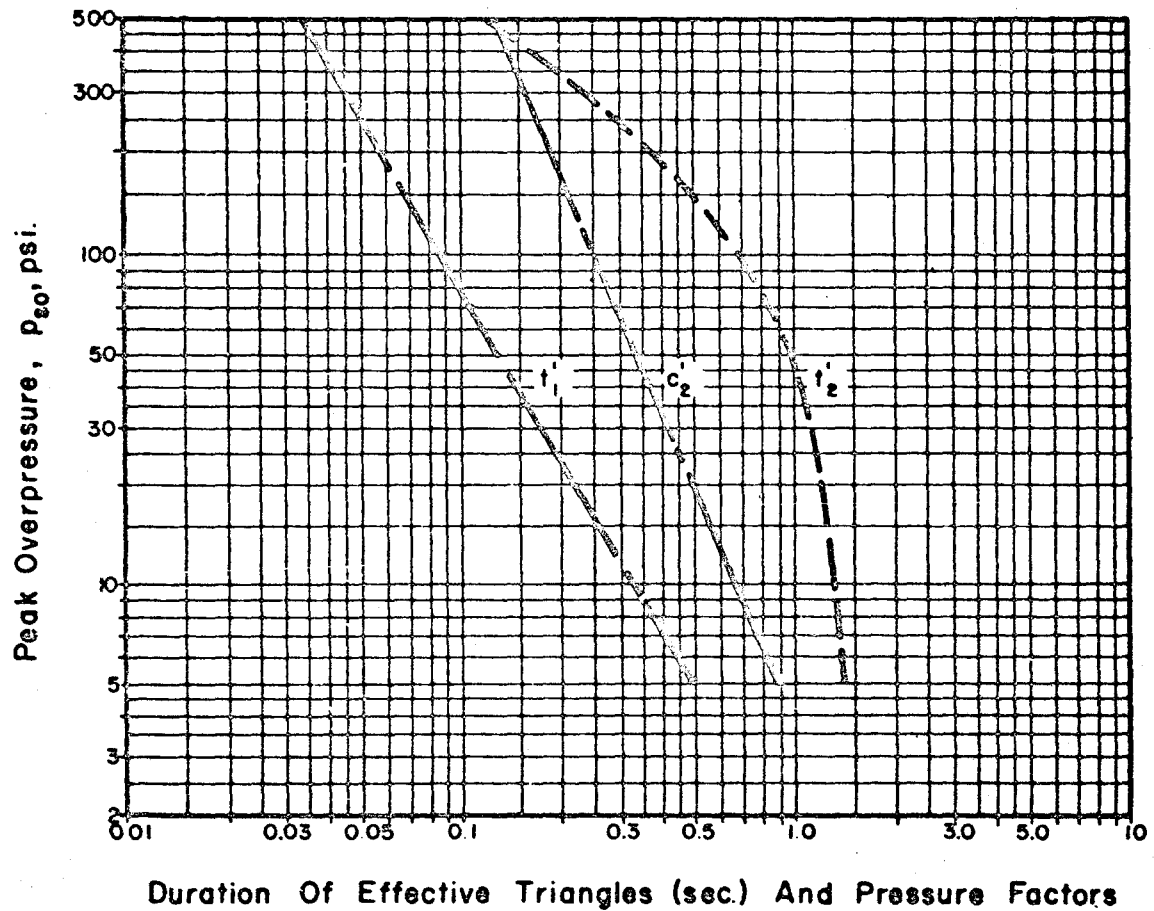
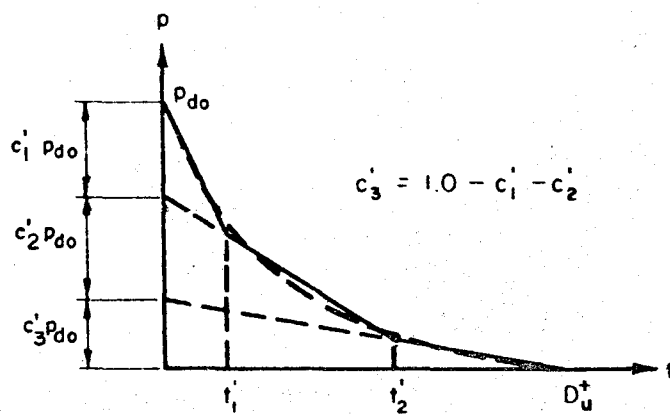


FIG. 3-13 TWO-TRIANGLE REPRESENTATION FOR DYNAMIC PRESSURE — 1 MT SURFACE BURST



NOTE:

For p_{d0} Versus p_{s0} See Figure 3-10

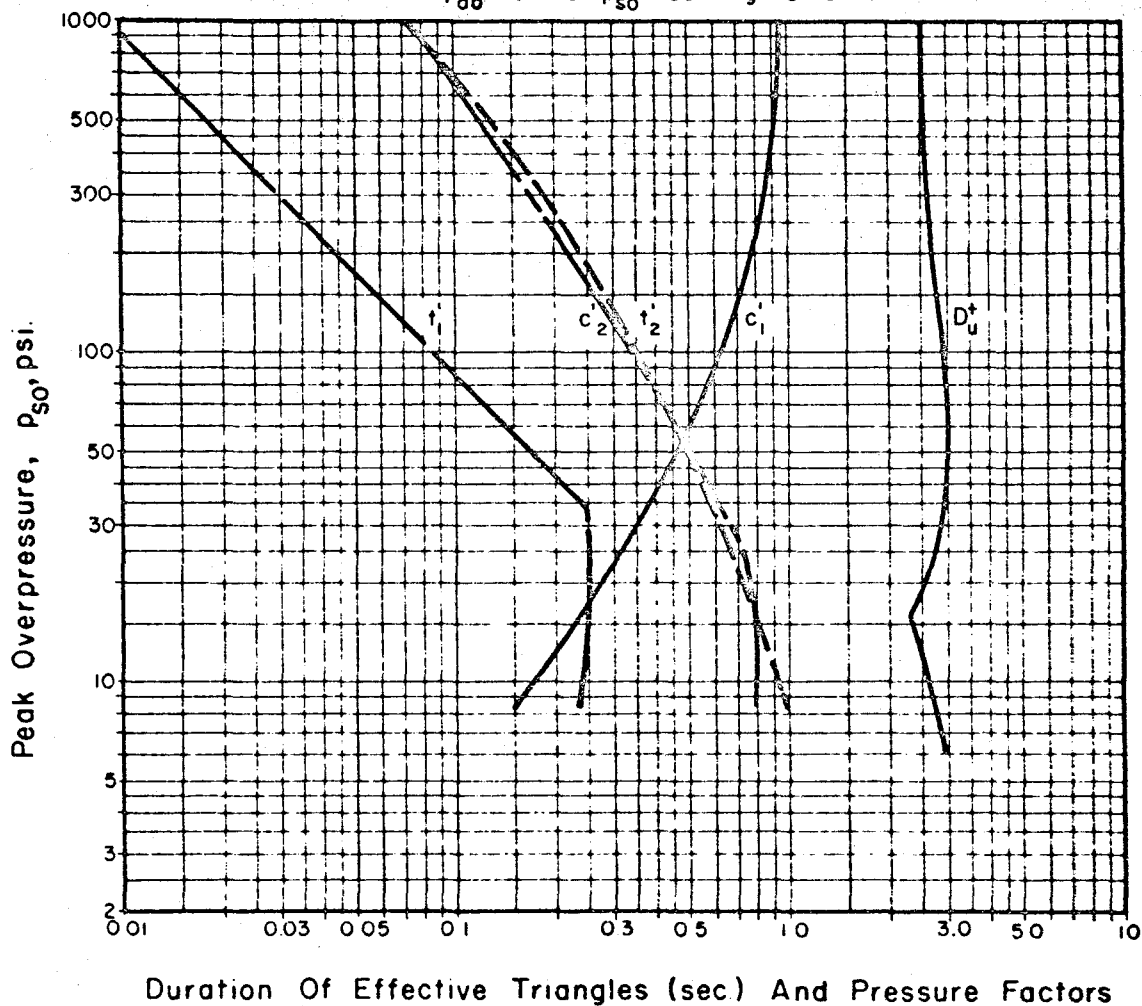


FIG. 3-14 THREE-TRIANGLE REPRESENTATION FOR
DYNAMIC PRESSURE—1 MT SURFACE
BURST

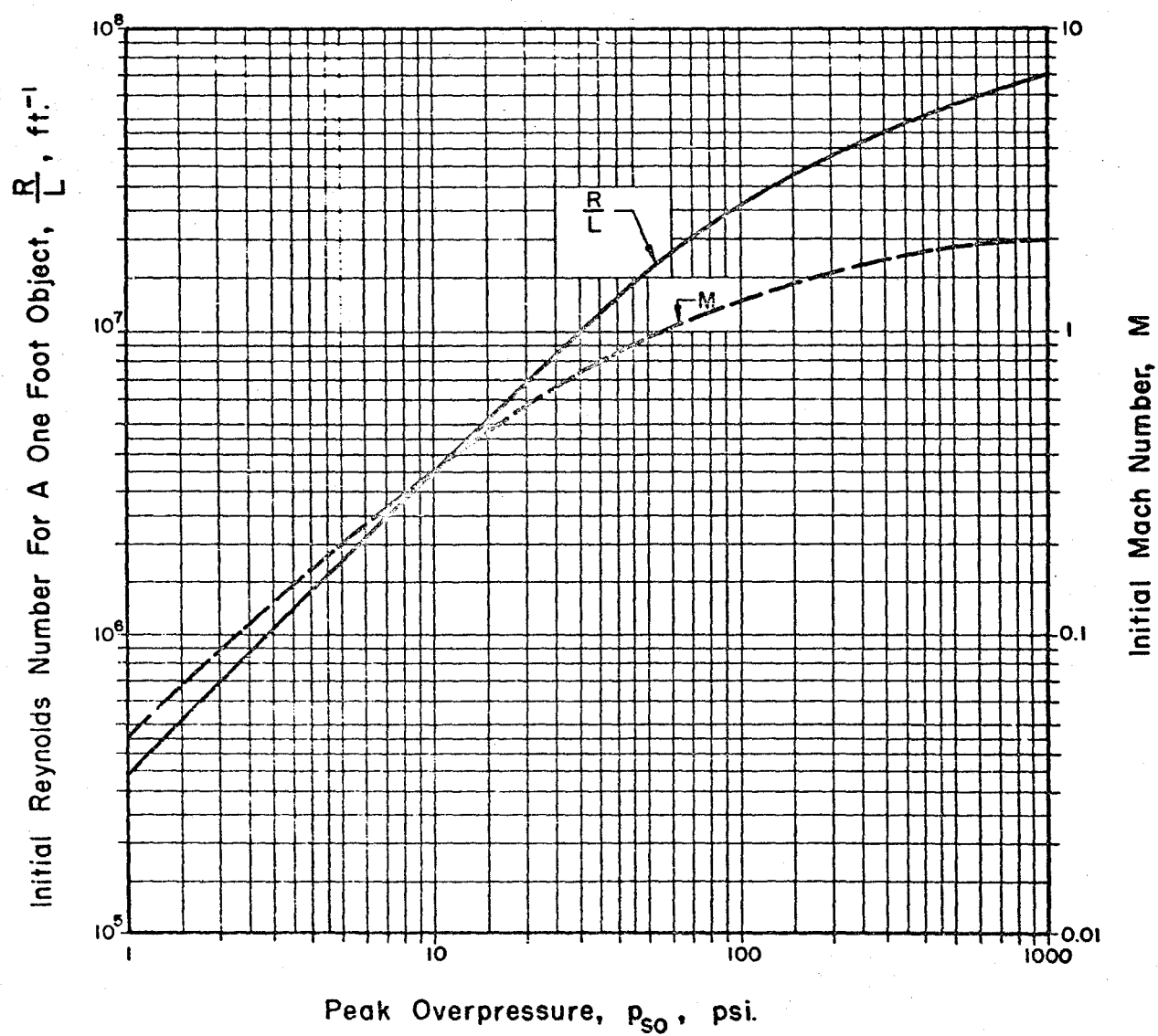


FIG. 3-15 INITIAL MACH AND REYNOLDS NUMBERS.

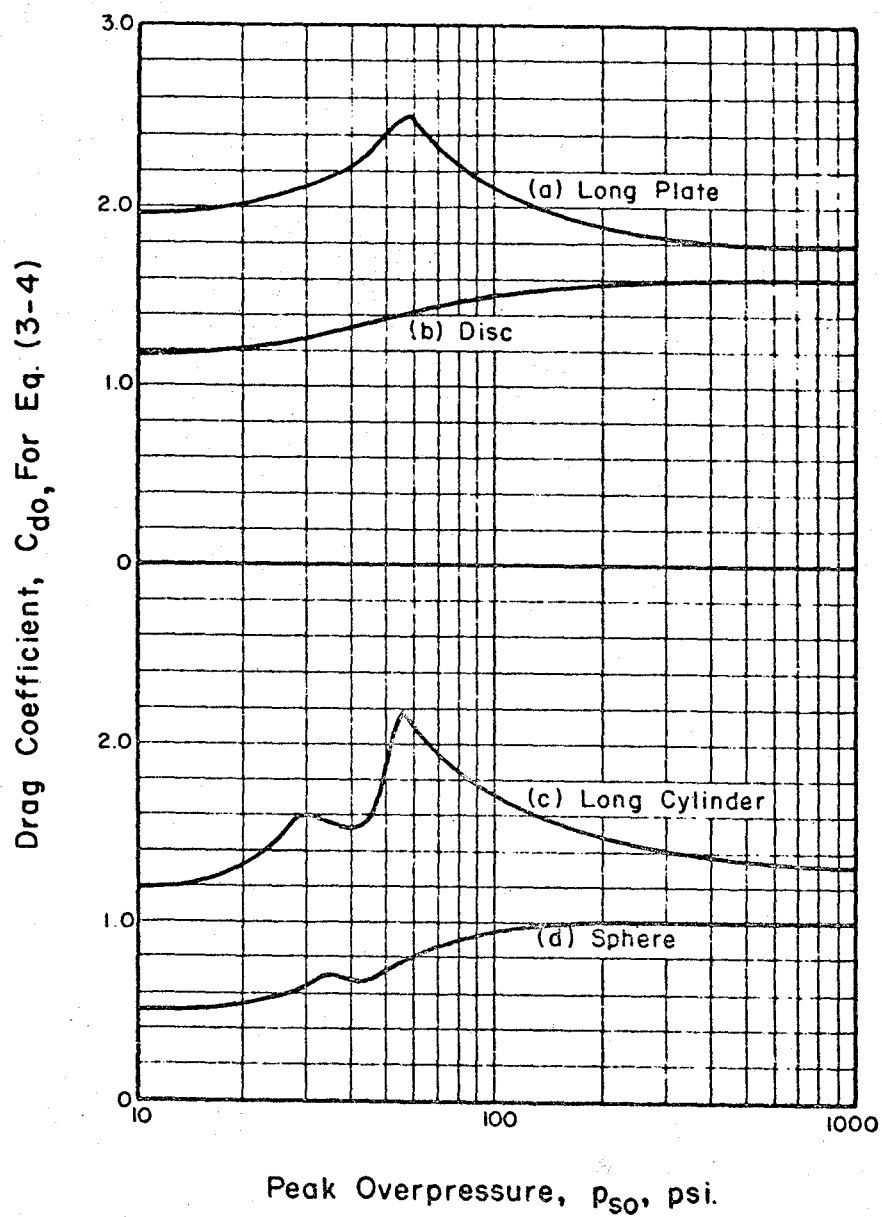


FIG. 3-16 DRAG COEFFICIENTS FOR EQUATION (3-4).

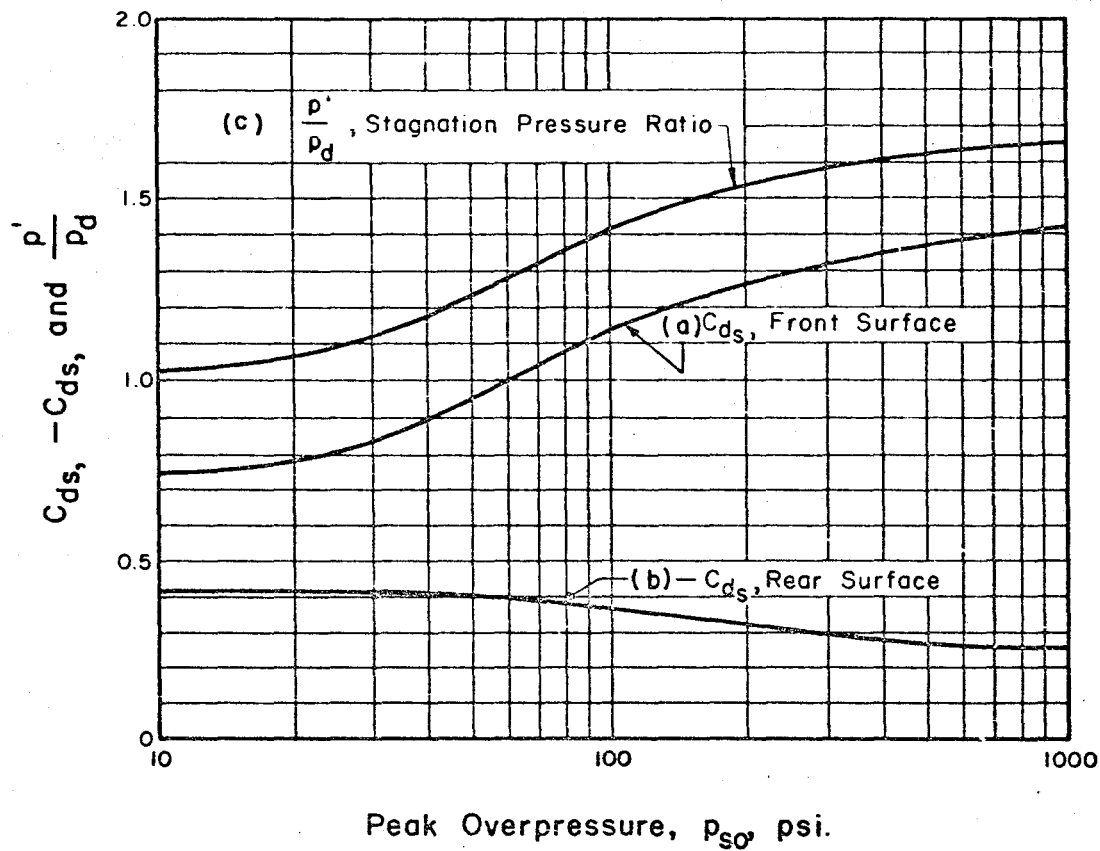


FIG. 3-17 DRAG COEFFICIENTS FOR EQUATION (3-6).

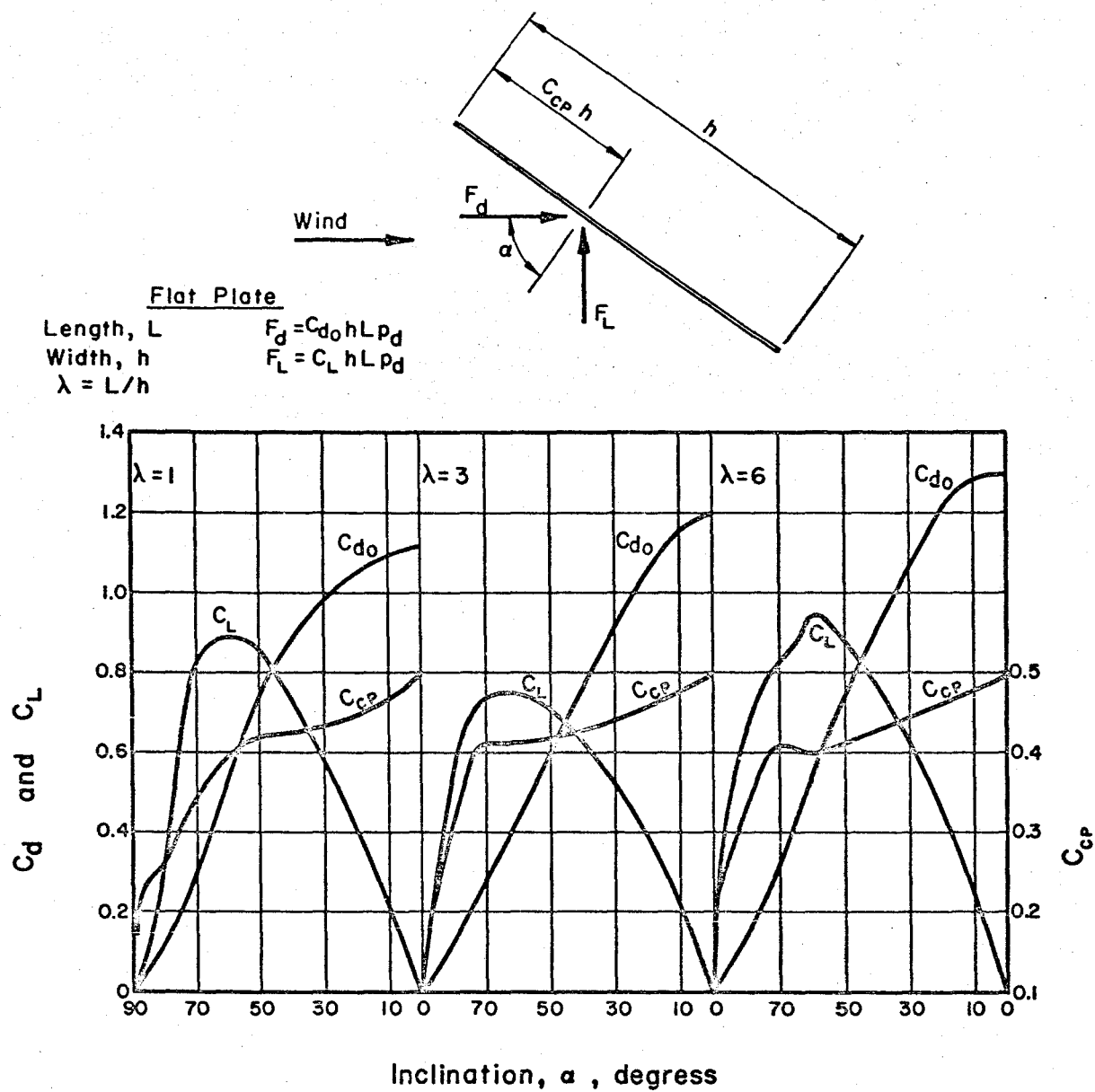
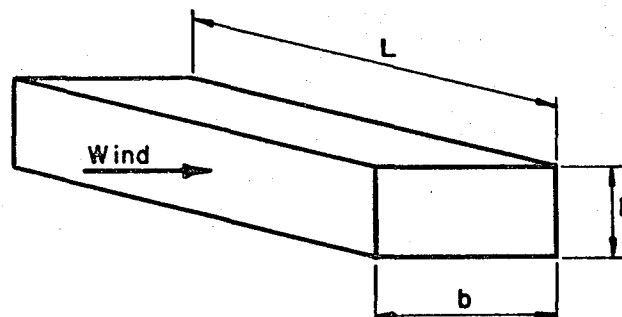


FIG. 3-18 EFFECTS OF INCLINATION AND LENGTH ON PLATE DRAG FORCE AT LOW MACH NUMBERS.



Drag Coefficient For Normal Incidence On Front Face.

	Flat Plate							Flat Plate On Ground			Parallel- epiped		
$\lambda = L/h$	1.0	2.0	5.0	10	20	40	∞	1.0	10	∞	∞	∞	∞
$\gamma = b/h$	0	0	0	0	0	0	0	0	0	0	0.1	1.0	6.0
Front Face, C_{d_s}	0.76						0.60	0.72		0.60			
Rear Face, $-C_{d_s}$	0.36						1.38	0.38		0.60			
C_{d_0} For Total Drag	1.12	1.19	1.20	1.23	1.42	1.66	1.98	1.10	1.20	1.20	1.95	2.03	0.90

FIG. 3-19 DRAG COEFFICIENTS FOR RECTANGULAR BODIES FOR LOW MACH NUMBERS.

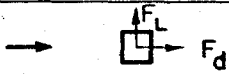










Profile And Wind Direction	C_{d_0}	C_L
	2.03	0
	1.96 2.01	0
	2.04	0
	1.81	0
	2.00	0.3
	1.83	2.07
	1.99	-0.09
	1.62	-0.48
	2.01	0
	1.99	-1.19
	2.19	0

FIG. 3-20 DRAG AND LIFT COEFFICIENTS FOR
STRUCTURAL SHAPES OF INFINITE
LENGTH AT LOW MACH NUMBERS.

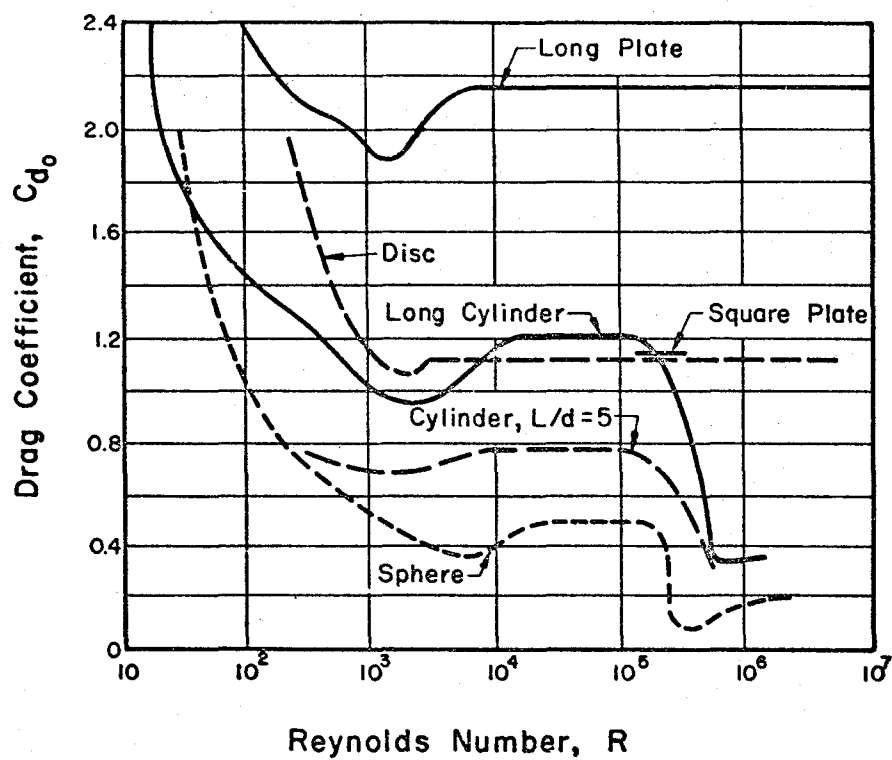


FIG. 3-21 DRAG COEFFICIENTS AS A FUNCTION OF REYNOLDS NUMBER FOR LOW MACH NUMBERS.

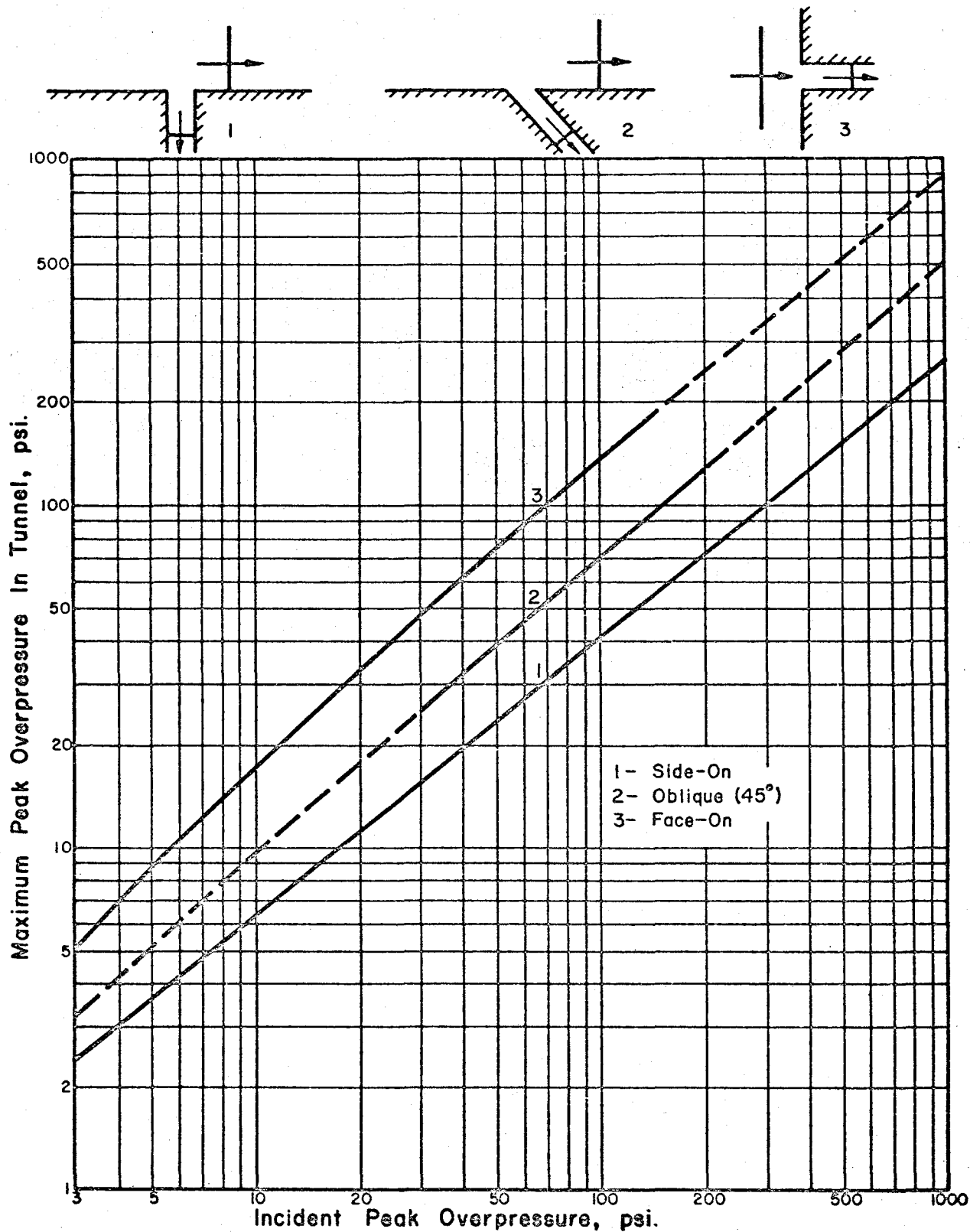
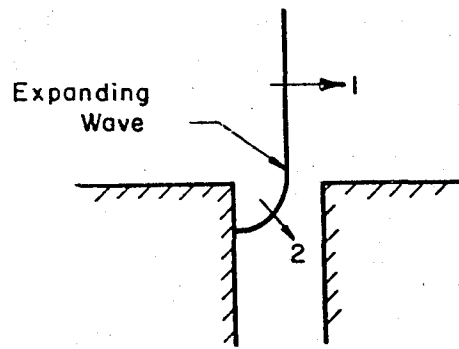
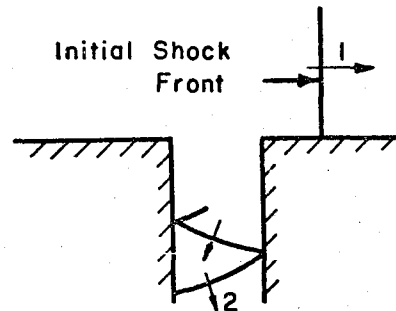


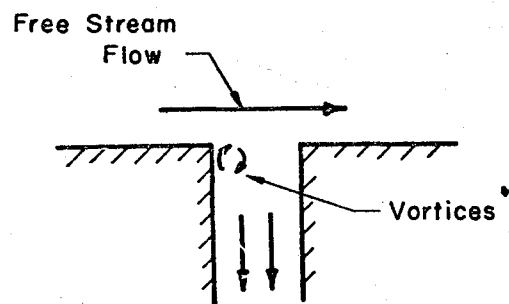
FIG. 3-22 MAXIMUM PEAK OVERPRESSURE IN A TUNNEL VERSUS INCIDENT PEAK OVERPRESSURE FOR THREE ANGLES OF INCIDENCE



(a) Shock Front Expanding Into A Slit.



(b) Reflection Inside The Slit.



(c) Pseudo Steady State Condition.

FIG. 3-23 DIFFRACTION EFFECTS AT WIDE RECTANGULAR SLIT.

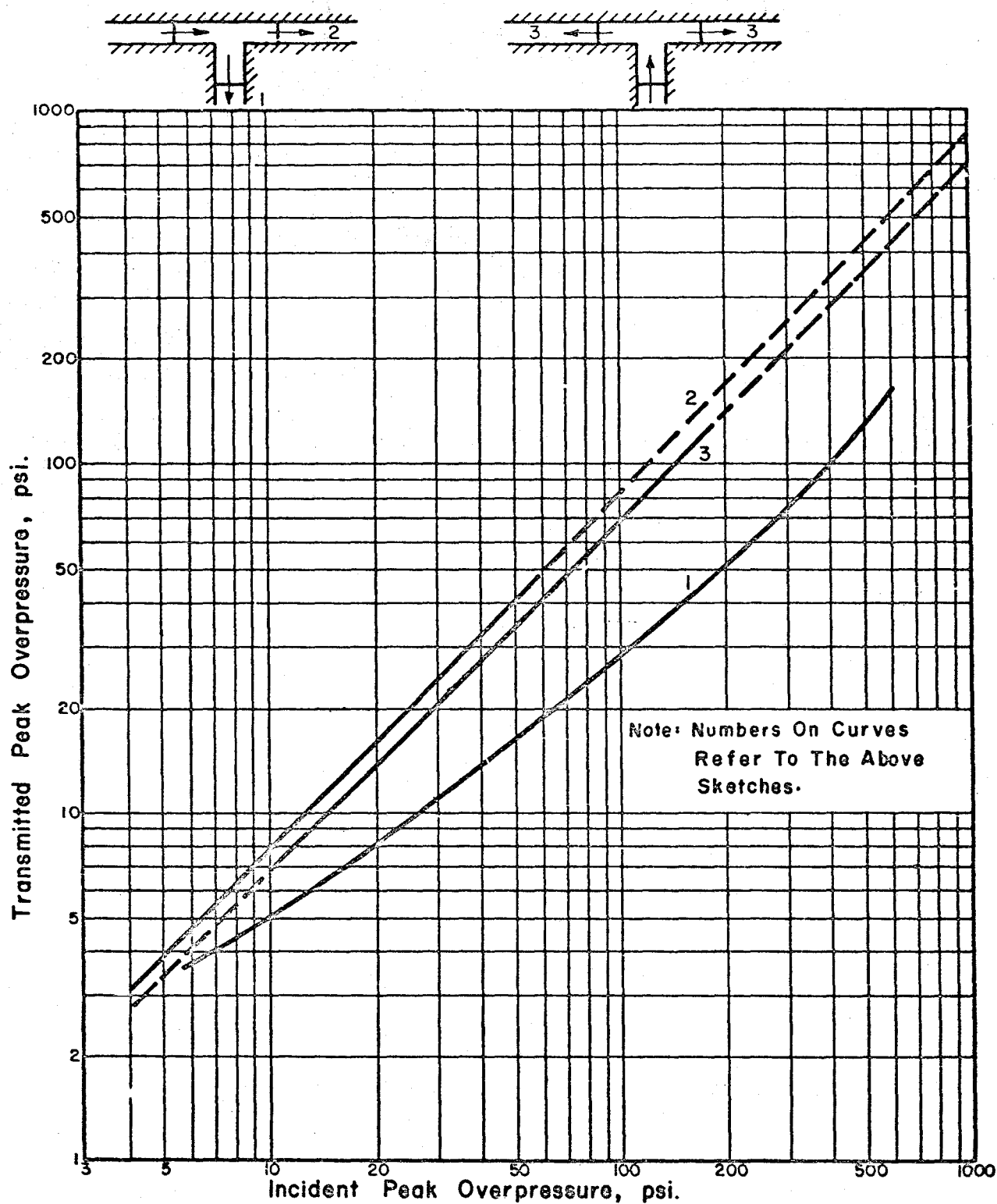


FIG. 3-24 TRANSMITTED VERSUS INCIDENT PEAK OVERPRESSURE FOR EQUAL AREA T-SHAPED TUNNEL JUNCTIONS

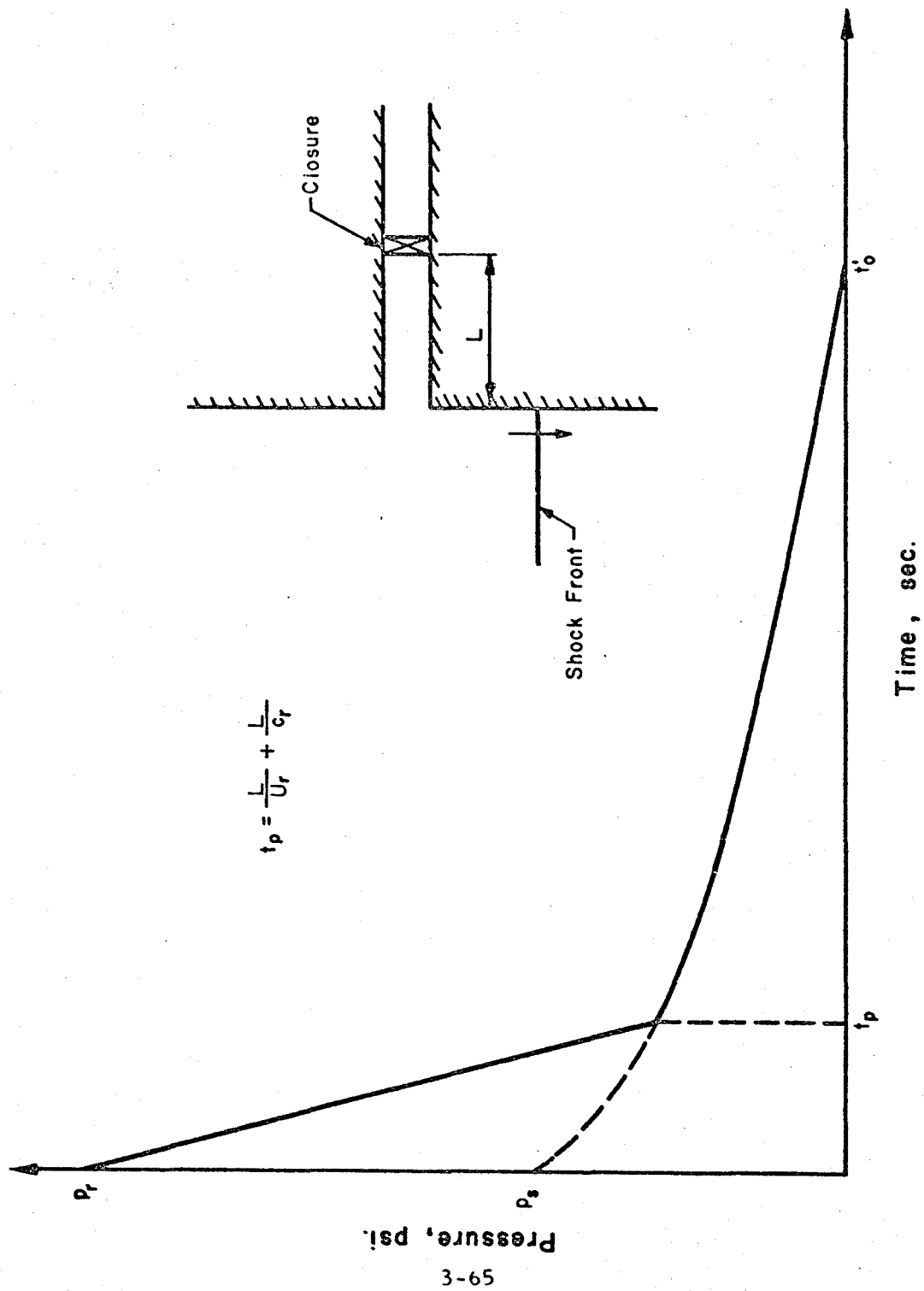


FIG. 3-25 SHAPE OF LOADING FUNCTION ON CLOSURE

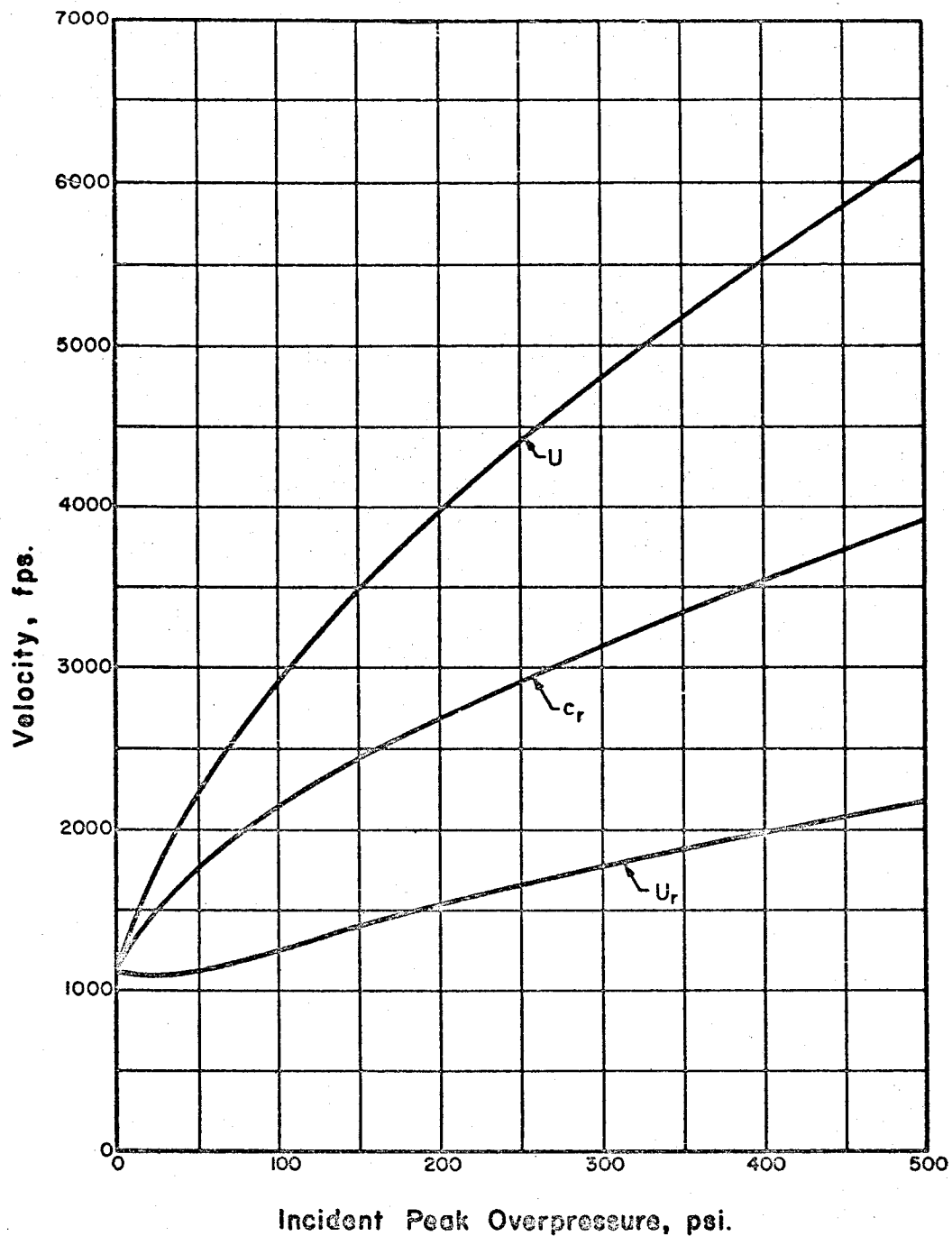


FIG. 3-26 VELOCITIES OF INCIDENT AND REFLECTED SHOCK WAVES AND OF RAREFACTION WAVE BEHIND REFLECTED SHOCK FRONT VERSUS INCIDENT PEAK OVERPRESSURE FOR SQUARE WAVE.

CHAPTER 4. FREE-FIELD GROUND MOTION

4.1 INTRODUCTION

Free-field motions are discussed in two separate categories, air-induced ground motions produced by the air-blast energy, and direct-transmitted ground motions produced by the energy imparted to the earth at the point of detonation. The ground motion observed at a given point is a complex combination of air-induced and direct-transmitted effects and is generally dependent upon the distance from ground zero, the depth of the point, geologic conditions, weapon yield, and height of burst.

The expressions and techniques recommended herein for use in design are based upon field test observations and theoretical studies. Neither the theoretical background nor the available field test data is sufficiently complete to make the predictions of response as precise as those commonly used in engineering design for static loads. Most of the design expressions are based upon elastic one-dimensional wave theory, covered in Appendix C, which is only an approximation of the deformation conditions in the earth. More exact theories are available, but the use of these more complex formulations of blast-induced ground motions cannot now be justified in the light of the present inadequate knowledge of the dynamic stress-strain properties of earth media.

The experimental data available comes largely from measurements made at the Nevada Test Site and the Eniwetok Proving Ground. The soil formations in these areas are far from representative of those occurring in most parts of the United States. The scatter in the data is great

because of the inherent variability of the loading and the soil conditions, and because of the adverse conditions under which such measurements must be made. The design expressions and techniques recommended herein are as good as can be offered at present.

Research in all phases of the area is now in progress, e.g. in the theory of the propagation of waves through non-uniform non-elastic media, in the stress-strain-time characteristics of earth media, and in laboratory and field investigations of the response of dynamically loaded solids. It may be assumed that the recommendations presented herein will be modified as our knowledge in the area is increased.

Section 4.2 deals with the evaluation of ground motions induced by the air-blast; Section 4.3 discusses the ground motions caused by direct-transmitted energy from the point of detonation; and Appendix C presents the theoretical background upon which most of the computations are based. No effort is made to provide a thorough discussion of nuclear weapons effects, since the reader is expected to have access to and a working knowledge of Ref. 4-1.

4.2 AIR-INDUCED GROUND MOTION

4.2.1 Introduction. Air-induced ground motions are functions of the air-blast characteristics above the point of interest and the properties of the earth medium. Considering the air-blast characteristics, the air-induced ground motions can be grouped into two general categories, those occurring under superseismic conditions (i.e., when the velocity of the air blast front exceeds the dilatational wave propagation velocity of the medium),

and those occurring under outrunning conditions (i.e., when the air-blast velocity falls below the dilatational wave propagation velocity of the medium). For the superseismic condition the surface overpressure-time variation directly above the point of interest controls the ground motion and the deformation conditions correspond reasonably well to those assumed in one-dimensional wave theory. (Refer to the discussion of wave propagation theories in Appendix C.) For the condition of outrunning ground motion, the air-induced disturbance travels more rapidly in the ground than the air-blast travels along the surface. This condition results in an alteration of the deformation conditions in the ground and considerably complicates the computation of response.

Extensive research in recent years has resulted in reasonably reliable techniques for the evaluation of air-blast characteristics, and considerable progress has been made in the study of the response of solids of known properties to moving surface pressures; but the knowledge of the properties of earth media, particularly the stress-strain relations as a function of time rate of loading, is not yet sufficiently advanced to make possible full use of our ability to compute the response of a medium. Section 4.2.3 deals with the present state of our knowledge concerning the dynamic stress-strain properties of earth media, and discusses the available techniques for evaluating the properties of a given natural deposit. It must be emphasized that no computation of ground motion will be more reliable than the soil parameters used as a basis for the computation. The soils investigation and analysis must form a major portion of the design effort for any protective installation.

The major portion of this section is concerned with the presentation of the expressions and techniques required for the evaluation of ground motions for superseismic conditions. A brief discussion of the outrunning condition is presented with some essentially empirical expressions for estimation of the ground motions in Section 4.2.7.

Air-induced ground motion phenomena are not yet completely understood. The expressions presented herein have their theoretical foundation in the one-dimensional wave theory which is often an exceedingly crude representation of the actual state of deformation in the earth. Theoretical studies which consider the ground to be loaded by a two or three dimensional representation of the air-blast loading offer considerable promise of increasing our understanding of ground response but as yet expressions of sufficiently simple form to be practicable for application in design have not resulted from these studies. Most of the experimental data available that are pertinent are reviewed in Ref. 4-2 and 4-3. With the exception of surface or near surface observations; there are relatively few measurements against which to check theoretical studies. For those underground measurements which do exist, the records are difficult interpret since they reflect not only the measurement technique, but also the non-homogeneous properties of the soil. Reference 4-2 provides a detailed correlation of the measurements of ground motions with the theoretical studies, but the scatter in the measurements for theoretically similar conditions indicates the difficulty of describing simply the behavior of complex, non-homogeneous earth media. Furthermore, most of the experimental data were obtained

in the unique soil deposits of the Nevada and Pacific Proving Grounds.

As a result, the techniques presented for the estimation of ground motions are based largely on elementary theoretical considerations, consideration of the available test data, and the best available judgment.

4.2.2 Stress Attenuation. The theory of one-dimensional wave propagation in an infinite homogeneous medium, discussed in Appendix C, gives no attenuation of stress with increasing depth. Attenuation is known to occur and it can be attributed to two causes, absorption of energy by the medium through inelastic deformations and by three dimensional or spatial dispersion of the air blast energy.

Attenuation from Inelastic Deformations

As noted above, no attenuation of the pressure with increasing depth occurs for an elastic medium under one-dimensional loading. However, in a medium which is not perfectly elastic, but rather elasto-plastic and/or visco-elastic in its stress-strain-time behavior, the peak pressure will attenuate with increasing depth as a result of non-conservative energy absorption by the medium. Several studies of the response of inelastic media have been performed. In Refs. 4-4, 4-5, and 4-6 the governing equations for the response of visco-elastic media for one, two and three dimensional loadings are presented. However, solutions sufficiently detailed to provide information in a form usable by designers of protective facilities are not yet available. The shortage of detailed solutions results from the computational problems involved in evaluating the solutions and from the lack of knowledge of the proper formulation for the dynamic stress-strain-time properties of earth materials. References 4-7 and 4-8 present one-

dimensional formulations of the problem of pressure attenuation due to inelastic behavior of a medium for which results have been obtained.

In the latter reports attenuation was studied by means of a mathematical model consisting of discrete masses connected by springs and dashpots. The behavior of the model requires that a finite rise time be used for the overpressure-time function studied, which limits the closeness with which an air blast pressure-time curve can be approximated. Illustrative of the effect of a visco-elastic medium on the wave form is Fig. 4-1 (Fig. 9 of Ref. 4-8). This effect is characterized by a reduction in peak pressure, an increase in rise time, and a decrease in the decay rate beyond peak pressure with increasing depth.

Spatial Attenuation

The attenuation of stress with depth resulting from three-dimensional dispersion as a shock wave propagates across the ground surface has been studied, Refs. 4-7 and 4-8, by assuming the soil to be an elastic, homogeneous, isotropic, massless medium bounded by a horizontal plane surface which was loaded by static, distributed, vertical loads on a finite area of the surface. These assumptions permitted the use of Boussinesq's Equations, Ref. 4-9, for the determination of the stress at any point within the semi-infinite medium. Consequently, assuming the distribution of overpressure on the surface at any particular time to be known, the corresponding subsurface stresses were computed by treating the surface loads as instantaneous static loads. Since the medium was assumed to be massless, the shock transmission velocity was infinite; therefore, it was possible to study the variation of stress with time

at a given point by stopping the shock front at successive times in its progress across the surface of the medium and computing the subsurface stresses by integrating Boussinesq's equations over the varying distributed surface loading.

The effect of spatial attenuation on the maximum stress based upon the computational technique described above is shown in Fig. 4-2 for weapon yields of 40 KT, 1 MT and 5 MT, for surface pressures of 100 and 200 psi, to depths of 200 ft. By study of these results it was possible to express the spatial attenuation as a function of yield, peak over-pressure and depth, see Eq. (4-1).

Formulation of Stress Attenuation with Depth

The peak stress value in the medium decreases with increasing depth from the maximum value of p_{so} at the surface. The attenuation is a result of spatial dispersion of the energy of the blast and of inelastic behavior of the medium. If, as recommended in Ref. 4-7, only the attenuation due to spatial dispersion is considered, the peak pressure values determined should be conservative.

If only spatial attenuation is considered, using the approximate technique of Ref. 4-7, the attenuation curves of Fig. 4-2 can be represented by the expression

$$\alpha_z = \frac{\text{Attenuation Factor}}{1 + \frac{z}{L_w}} \quad (4-1)$$

where

$$L_w = 230 \text{ ft.} \left[\frac{100 \text{ psi}}{P_{so}} \right]^{1/2} \left[\frac{W}{1MT} \right]^{1/3}$$

which is plotted in Fig. 4-3.

The peak vertical stress at depth z can now be expressed as a function of the peak side-on overpressure and the attenuation factor.

$$\frac{\text{Peak Vertical Stress}}{P_{vp}} = \alpha_z P_{so} \quad (4-2)$$

Note that to correspond to common soil mechanics convention for stress, compressive stress is considered to be positive. To avoid confusion with the equations in Appendix C for the one-dimensional wave theory, for which tensile stresses are considered to be positive, the symbol p is used for compressive stress. Note too, that the increment of stress herein discussed is not the total stress effective at the depth in question, but the stress due to the air blast loading.

Horizontal Stress

Generally the horizontal stress, p_h , in the soil is taken as some constant, K , times the vertical stress, p_v , or $p_h = K p_v$. The magnitude of K depends on the properties of the soil, the degree of saturation, the stress level, and the conditions of lateral strain imposed on the soil element.

If in the soil element shown in Figure 4-4 an increment of

vertical stress p_v is applied, producing an increment of vertical strain ϵ_z , the lateral strain ϵ_h will depend on the increment of lateral stress p_h induced. As discussed in Section 4.2.1, the ground displacements due to air-blast are considered to be one-dimensional with only vertical strain occurring; therefore, the K-values of practical importance are those corresponding to zero lateral strain, $\epsilon_h = 0$. For this case, K is denoted as K_0 and is defined as the ratio of the principal stresses, p_h/p_v . Where outward lateral strains are induced, p_h reaches a minimum value, K_a , in the active state. If a passive state is induced by increasing p_h to its maximum value, inward strains occur and K is denoted by K_p . A K-value of unity indicates that the material behaves hydrostatically.

In situ, the value of K_0 may exceed unity on account of various events in geological time. Furthermore, the in situ K_0 -value is not generally known. Fortunately, the value of K_0 only for an added increment of stress is required to compute air-induced horizontal stresses. The K_0 for an increment of stress can be determined with more precision than the K_0 for the in situ condition.

A saturated soil may be considered to be a composite column consisting of water and a dry soil skeleton with grain to grain contact. For saturated soils of low dry density, the water has a bulk modulus many times that of the soil skeleton. A stress suddenly applied to an element of such a soil is transmitted almost entirely through the water phase; hence, K_0 assumes a value of nearly unity if no drainage by consolidation occurs. Relatively permeable soils of high dry density behave in a similar

manner because the loading rates of interest will not allow drainage. By contrast, relatively high dry density soils of low permeability, e.g. shale, may behave quite differently. The soil skeleton may be stiffer than the water phase and transmission of an applied stress through the water phase may be restricted. Therefore, the K_0 -value is bounded by unity, the value for water, and approximately 0.5, the value for the dense soil alone.

Under static loads and drained conditions, K_0 assumes a value corresponding to that of the soil skeleton. A large amount of data is available concerning the value of K_0 for static loading, under both drained and undrained conditions. This is in contrast to the very small amount of data available for dynamic loading conditions.

Soils have been grouped into a few convenient categories in Table 4-1. Recommended dynamic K_0 -values are given therein along with typical values for the drained and undrained static conditions. The terms soft, medium, stiff and hard have been used to describe the consistency of the soil. These may be indexed numerically by the unconfined compression strength in tons per square foot, and more crudely by the Standard Penetration Test, see Ref. 4-10. The following tabulation gives the consistency limits:

<u>Consistency</u>	<u>Unconfined Compression Strength - q_u - tsf</u>	<u>Standard Penetration Test - N - Blows per ft</u>
Very soft	< 0.25	< 2
Soft	0.25-0.50	2-4
Medium	0.50-1.00	4-8
Stiff	1.00-2.00	8-15
Very Stiff	2.00-4.00	15-30
Hard	> 4.00	> 30

For the depths and pressures of interest, K_0 -values for rock may be determined from the elastic properties of rock cores. Measurement of vertical and circumferential strains (Ref. 4-11) on a rock core tested in unconfined compression at the stress levels of interest will furnish the data necessary to compute Poisson's ratio, ν . Then, for zero lateral strain and an elastic material, $K_0 = \frac{\nu}{1-\nu}$. It should be remembered that information obtained from rock cores represents the behavior of a sound mass of the rock. The test data should be correlated with the elastic properties of the rock determined by the seismic survey (discussed in Section 4.2.3). The seismic survey automatically accounts for irregularities in the rock mass and a correlation of these two sets of data, and any other information available, is needed to detect unsound rock conditions. Some information on the elastic properties of various rock types is available in Refs. 4-12, 4-13, 4-14, 4-15, and 4-16.

The preceding discussion of horizontal stresses and K_0 -values does not apply to increments of stress increase exceeding about 1000 psi.

Reflections of Stress at Boundaries Between Layers

Wave theory for elastic media predicts that reflection will produce significant changes in the stress level at an interface between strata of differing elastic properties. The reflection phenomenon is discussed in Appendix C for the one dimensional elastic wave.

Experimental data from nuclear field tests (e.g., Ref. 4-2) have not shown significant reflections of stress waves. In addition, laboratory tests on soil with differences in seismic velocity and density of adjacent

layers have yielded similar results. These observations appear to indicate either inability to measure stress in a real soil mass or that layering does not produce stress reflections of magnitude comparable to theoretical values in real earth media. Accordingly, it is recommended that the effects of layering on the stress distribution with depth be neglected until such time as more positive recommendations can be made.

4.2.3 Soil Properties

Introduction. Protective construction, whether above or below the ground surface, is susceptible to all the difficulties and uncertainties inherent in foundation engineering. Therefore, the usual subsurface investigations required for static loading conditions are still required; furthermore, they must be greatly supplemented in order to predict the behavior of the structure under dynamic loads.

The following discussion does not dwell on the ordinary foundation engineering problems because they are adequately treated elsewhere (see e.g. Ref. 4-10). Instead, the additional soil parameters necessary for ground motion predictions are discussed. Assuming free-field ground motions to be one-dimensional (vertical strain only), the most important soil parameter is the constrained modulus of deformation, M , under dynamic loads. For zero lateral strain (K_0 condition of Section 4.2.2), the constrained modulus becomes

$$M = \frac{p_v}{\epsilon_z} \quad (4-3)$$

In the pages that follow, brief discussions of the several components of a complete subsurface exploration are presented, including not only field and laboratory experimental programs, but also interpre-

tive studies. Particular attention is devoted to the determination of the constrained modulus of deformation that should be used to estimate the magnitudes of air-blast-induced deformations.

Subsurface Exploration. Reference 4-11 contains a detailed guide to field explorations. The same general outline will be followed herein. Each step discussed below may occur in one or more phases as the process of selecting a site proceeds from initial spotting on a map to final approval as a site for construction.

Geology. The geological study should consist of a general reconnaissance of the area to determine regional and local geological structure in addition to drainage and groundwater conditions. In particular, fault zones should be located because they may be the seat of undesirable differential motions under blast loading. Information necessary for the development of a water well is also usually required.

Personnel for the geological investigation should consist of a geologist working in conjunction with a foundation engineer, or an engineering geologist competent in both areas.

Geophysical Survey. A seismic refraction survey (see Ref. 4-17) should be performed after the geological study and before or in conjunction with the exploratory boring operation. The survey will serve to verify the stratification determined geologically and to detect fault zones or other discontinuities. Of major importance for free-field ground motion predictions are the elastic properties in the vertical direction. These should be determined from vertical dilatational and shear waves in an up-hole survey. The borings used for up-hole logging may be the ones

drilled for soil sampling purposes if the two investigations can be coordinated.

Most materials, soils included, decrease in stiffness or modulus as the applied stress level is increased. Seismic refraction investigations involve setting off a charge of explosive and recording the time required for the induced pulse to travel between two points on the ground surface a known distance apart. The velocity, c , of a wave in an elastic medium is related to the elastic constants of the medium which in turn are related to the constrained modulus. The constrained modulus, M , is related to the velocity, c , by

$$M = \frac{\gamma c^2}{g} = \rho c^2 \quad (4-4)$$

$$\text{where } c^2 = \frac{E(1-\nu)}{\rho(1+\nu)(1-2\nu)}$$

and γ is the in-place density of the soil, g is the acceleration of gravity, and E is Young's modulus. Because seismic pulses are at a very low stress level, the constrained modulus so obtained will be higher than the modulus applicable to blast loading. Therefore, the constrained modulus determined by seismic means represents essentially an upper bound to the modulus applicable to blast conditions.

Exploratory Borings. The purpose of exploratory borings is to define the nature and extent of the soils (and rock) comprising the soil profile. Standard penetration tests should be run in conjunction with the boring program in soils amenable to such tests.

While almost any drilling technique yielding a soil sample will serve to define the soil profile, the most important physical properties

of the soil can be determined only from undisturbed samples. A sample of soil extracted from the ground will exhibit lower shear strength and higher compressibility than the in situ soil if it has been subjected to distortion (disturbance). Therefore it is essential that drilling and sampling techniques yielding a minimum of disturbance be used. Reference 4-18 covers this subject thoroughly and, in addition, is a good source of general reference material on drilling and sampling methods.

The type of drilling and sampling equipment used will vary according to anticipated subsoil conditions at the site. It is suggested that rotary equipment capable of drilling 6 in. diameter (or larger) holes 200 ft. (or more) deep should be the minimum acceptable, and that a hydraulic feed travel of at least 5 ft. should also be required. Combinations of several drilling methods may be required at some sites.

Sampling procedures should be the best available for the material being sampled. In soft to medium overburden soils, a piston sampler of 3 inch minimum diameter is preferable. For stiff and hard soils, the Pitcher Sampler (Ref. 4-19) has been used with notable success. In granular soils, a split spoon sample along with the standard penetration test is acceptable. For rock, NX cores (2-1/8" dia.) should be obtained when at all feasible.

No general recommendations can be given as to the location, depth, and number of borings needed at a given site; these are decisions that should be left to the discretion of the foundation engineer. Coordination of the exploratory borings with the geophysical survey can lead to economies and should be attempted. If the boreholes are to be used in the seismic survey, steps should be taken to insure that the holes stay open. Ground water conditions should be observed during the boring operations to detect

artesian water, a perched water table, or any other occurrence of note. If required, permeability studies may be made with the use of the boreholes. One borehole should be converted to an open tube piezometer for recording the ground water level over a period of time.

Sewage and waste disposal studies, in place density of surface soils, borrow pit investigations and other miscellaneous studies may be performed at the same time as the exploratory borings.

Field Classification. All soil and rock materials should be classified according to the recommendations in Ref. 4-11. The Unified Soil Classification System is used for all soil materials; field procedures for its use are given in Reference 4-20. Adherence to the standard system will enhance communications and interchanges of information. The soil and rock samples should be identified and classified as they are taken from the ground. The field classification so recorded should be immediately available to all interested parties.

Laboratory Investigation. The general scheme of the laboratory testing program is discussed in Ref. 4-11; therefore it will only be outlined in the following paragraphs. Test procedures for determination of the constrained modulus have not yet been well established; therefore the following recommended procedures are subject to modification as improvements become available.

All soil samples should be subjected to a laboratory identification and classification routing using the Unified System, Ref. 4-20. In addition, the natural water content should be determined on representative portions of all specimens. The unconfined compressive strength, q_u ,

should be determined by test or estimate for all samples not used for other tests.

Representative samples from the different strata should be used for the following tests:

1. Determination of density, γ
2. Grain size distribution
3. Liquid and plastic limit
4. Specific gravity of solids
5. Triaxial tests. Most tests will be of the consolidated undrained type, Q_c . Other types of tests should be performed at the foundation engineer's discretion.
6. Consolidation tests. Most tests are not loaded to a pressure sufficiently high to define the load-deformation curve properly. A pressure of at least 100 tons per square foot should be attained in such tests. The indicated maximum previous load, p_o^1 , and overburden pressure, p_o , should be determined.
7. Swell pressures should be determined in the consolidation test for materials likely to be subjected to an environment conducive to swelling.
8. Vibration, sonic, bulk modulus, confined compression or other tests for determination of the constrained modulus.

These will be discussed separately in later paragraphs.

Miscellaneous laboratory tests on selected soils may be performed as required, e.g. CBR, slaking, compaction, and permeability.

Rock cores should be subjected to careful laboratory classification, identification and description. Adsorption tests should be performed on representative cores of the various rock strata. Unconfined compression tests, direct tension tests, and torsion tests should then be performed on these samples. Companion samples should be subjected to axial strain under unconfined conditions. These cores should be instrumented to record vertical and horizontal strains as a function of axial stress. Young's modulus, E , and Poisson's ratio, ν , can be determined from the test results and used to calculate the constrained modulus according to Eq. (4-5).

$$M = E \frac{(1 - \nu)}{(1 + \nu)(1 - 2\nu)} \quad (4-5)$$

Constrained Modulus Tests. For rock, the constrained modulus can be determined from Eq. (4-5) as described immediately above. However, the modulus cannot be evaluated with the same confidence for soils. Several tests are currently being used to determine the constrained modulus of soils; none of them are entirely satisfactory. New techniques are being developed and it is anticipated that the tests discussed below will undergo considerable modification in the near future. A knowledge of several soil phenomena is necessary to understand and interpret the constrained modulus tests; these are listed below:

1. Sample disturbance, mentioned previously, often produces irreversible changes in the properties of a soil removed from the ground. Direct laboratory determinations of soil properties are seldom possible; however, good sampling techniques and corrections based on judgment and experience can lead to reasonably reliable test interpretations.

Removal of a sample from the ground involves stress changes and corresponding deformations and distortions. Dissolved gases entrapped in the pore water tend to come out of solution. A rapid recompression will compress this gas, plus the water and soil; consequently, a lower modulus will be observed in the tests than in situ where only water and soil, without the additional gases, are being compressed. Figures 4-5(a) and 4-5(b) respectively, typical void ratio, e , versus log of the effective vertical pressure, p , curves for a normally loaded, and an apparently preloaded, soil. The solid lines represent the curves obtained from the best available undisturbed samples in ordinary consolidation tests. The coordinates e_0 and p_0 represent the void ratio and overburden pressure in situ respectively. The dashed lines through these points represent the probable field behavior of the samples. The dotted curves represent test results on disturbed samples. Note how disturbance masks the probable true in situ behavior of the soil. In Fig. 4-5(b), the coordinate p_0' represents the probable pressure to which the sample was previously loaded.

2. The preload indicated in Fig. 4-5(b) does not necessarily mean that the sample was subjected to a higher pressure earlier than now exists in situ. Chemical alteration, cementation and other effects may cause the sample to be cemented and thus more stiff than if these alterations had not occurred. Regardless of the cause of the indicated preload, the change

in load-deformation characteristics is the same and is the phenomenon of importance. For pressures lower than p_o' , the soil has a higher modulus than at pressures above p_o' .

3. The modulus of a soil is known to increase with lateral confinement, at least in the upper few hundred feet of the earth's crust. Fig. 4-6 shows typical stress-strain curves, p_v vs. ϵ_z , obtained from triaxial tests where the lateral pressure, p_h , was held constant. The initial tangent modulus, (M_i) , is defined as the slope of the initial part of the $p_v - \epsilon_z$ curve.

The difference between the initial tangent modulus obtained in the triaxial test and the constrained modulus may be approximately observed by running tests with constant ratios of lateral to vertical stress. For comparison, the typical results of such tests have also been plotted on Fig. 4-6. Note the increased modulus as the ratio of horizontal stress to vertical stress is increased. If K_o , Section 4.2.2, were a constant with change in stress level, and if this ratio were applied in the triaxial cell, then the modulus so obtained would be the constrained modulus.

4. Fig. 4-7 shows typical results of undrained confined compression tests. The modulus generally increases with the strain rate.
5. A saturated soil may be thought of as a composite column consisting partly of water and partly of the soil skeleton.

The constrained modulus of water is equal to the bulk modulus or approximately 300,000 psi. Generally the soil skeleton will have a very much lower modulus. The combined effect will generally be a lower modulus than 300,000 psi. However, the modulus will generally exceed 100,000 psi and probably 150,000 psi. If the modulus of the soil skeleton exceeds that of water, then the combined modulus will exceed 300,000 psi.

Unsaturated soils have a constrained modulus only a small fraction of that of water for degrees of saturation below approximately 95 percent. This is because the soil is now a composite column consisting essentially of air and the soil skeleton. Reference 4-21 discusses this subject more thoroughly.

With the above discussion as background, the interpretation of the following constrained modulus tests is facilitated.

Vibration. The vibration test is performed on a cylinder of soil that may be subjected to a confining pressure. Dilatational and shear waves are propagated at various frequencies until resonance is found. Young's modulus and the shear modulus are derived from the data (Ref. 4-22) and are used to calculate Poisson's ratio. Equation (4-5) may then be used to calculate the constrained modulus. The vibration test applies more energy to the soil than is used in a seismic refraction survey, but stress levels very much below the stresses of interest are induced. The effects of sample disturbance

tend to reduce the modulus while the low stress level causes an observed modulus higher than the modulus of interest. The two factors tend to balance each other with the modulus so determined being less than but closer to the seismic modulus limit than any other type of test. Elastic behavior is assumed throughout.

Sonic. Sonic tests measure the travel time of a pulse through a soil sample and thus give the velocity of wave propagation in the soil. The stress level is very low and the results and interpretation are similar to that of seismic data.

Unconfined Compression. When a sample can be tested in no other way, the initial tangent modulus from the stress-strain curve in an unconfined compression test will yield at least some information. Because of the lack of confining pressure, the results will be quite low compared to the in situ value. Reference to Eq. (4-5) indicates that a Poisson's ratio of 0.3 and 0.4 would cause the constrained modulus to be 34 percent and 114 percent respectively, greater than the initial tangent modulus. Considering sample disturbance and the lack of confining pressure, a reasonable interpretation of the test would be to consider the constrained modulus to be two or three times the initial tangent modulus from an unconfined compression test.

Triaxial. The initial tangent modulus from a triaxial test is more reliable than that from an unconfined test because of the confining pressure effects. It is recommended that the constrained modulus be taken as twice the initial tangent modulus.

Confined Compression. One dimensional tests may be performed in consolidation equipment, in the sampling tube itself, or by various other means. The test has the advantage of being capable of rapid loading with

very little lateral strain. Furthermore, it may be carried to the stress levels of interest and the percent recovery observed upon unloading, thereby giving information on both the total and residual strains. The test has the disadvantage of unknown friction effects on the sides of the sample, some lateral deformation due to an imperfect fit of the sample in the ring and unknown lateral stress conditions. It is recommended that the test results be taken at face value and then altered as warranted by the condition of the sample as the foundation engineer's judgment deems proper.

Evaluation of Data. It is presumed that the foundation engineer will have evaluated and reported the data obtained in a manner suitable to the ordinary engineering aspects of the job. In addition, the geology should be fitted regionally and pinpointed locally using the field reconnaissance, geophysical exploration and boring data. Particular attention should be given to the location of fault zones.

The evaluation of the constrained modulus is the most important step with respect to the dynamic loading problem. Only one comparison of the procedures described herein for computing ground motions with field test data exists. It is recommended that the foundation engineer study the comparison between predictions given in Ref. 4-22 and the measurements as reported in Ref. 4-23.

Recognizing the large uncertainties that exist, the following procedure may be used to estimate the in situ modulus that should be used to compute displacements. This procedure is substantially that presented in Ref. 4-24.

1. As shown in Fig. 4-8, draw both the overburden pressure, p_o , versus depth relationship and the preload pressure, p_o' , versus depth relationship.
2. Draw the attenuated peak stress, $\alpha_z p_{so}$, versus depth relationship. See Section 4.2.4.
3. Mark the depths at which the overstress ratio, o_s of (Eq. 4-6), or the preconsolidation ratio, o_p of (Eq. 4-7), is less than unity. Also mark the depths at which the ratios exceed three.

$$o_s = \frac{\alpha p_{so}}{p_o} \quad (4-6)$$

$$o_p = \frac{\alpha p_{so}}{p_o} \quad (4-7)$$

4. Draw the constrained modulus versus depth relationship using all the test data. Use marks distinguishing each type of test.
5. Below the permanent water table, use a modulus of 150,000 psi unless the test data give a higher value.
6. The seismic data will represent an upper bound that is closely approached by the vibration test data. The unconfined and triaxial tests will form a lower bound with the confined compression tests usually somewhat higher. The two bounds define the area within which the in situ modulus should fall.

7. References 4-22 and 4-24 indicate that where σ_s or σ_p are less than unity, the soil behaves elastically with a modulus approximately equal to that determined in the vibration test which is less than the upper modulus bound by about 20 to 25 percent of the range between the bounds.
8. Where σ_s or σ_p exceeds 3, the modulus approaches the lower bound and may be nearly that of the confined compression tests which is greater than the lower modulus bound by approximately 20 to 25 percent of the range between the bounds.
9. Where σ_s or σ_p are between unity and three, there is a transition in the modulus that should be determined on the basis of judgment.
10. Assume complete rebound for soils below the permanent water table and where σ_s or σ_p are less than unity. Assume 70 to 80 percent recovery where σ_s or σ_p exceed three. Make a transition between the two limits. Dynamic confined compression tests or other tests can yield useful information on the percent recovery upon unloading.

The above procedure is in the infancy of its development. Note that the foundation engineer's judgment is an indispensable element in the selection of the constrained modulus that should be used in the computation of displacements under blast loading.

In the computation of vertical displacements, the soil profile is divided into layers of thickness depending upon the conditions, and the strain computed for each layer from Eq. 4-8.

$$\epsilon_z = \frac{p_v}{M} \quad (4-8)$$

An idealized p_v versus ϵ_z curve should be developed for each layer consistent with the stress level reached in each respective layer. Figure 4-9 indicates by dashed lines the probable real behavior of the soil under dynamic loading. The solid lines represent the idealized curve with M_p being the slope during increasing stress and M_r the slope during rebound.

4.2.4 Displacement. In general the displacement quantities of interest include maximum transient absolute displacements residual absolute displacements, maximum transient relative displacements and residual relative displacements. In the discussion of the evaluation of displacement which follows, it is assumed that the soil parameters for each subsurface layer appropriate to the in situ lateral constraint, peak stress level, and loading rate have been evaluated using the methods discussed in Section 4.2.3. Figure 4-9 shows the relationship between the linearized stress-strain curve considered in the computations and the probable real stress-strain curve, and indicates the significance of the various soil parameters.

The stress distribution in the soil is based upon the one-dimensional wave propagation theory discussed in Appendix C. The only peak stress attenuating mechanism considered is spatial attenuation; Eq. (4-2) is used to define the variation of peak stress with depth. As mentioned before, no reflections are considered to take place at boundaries between soil strata of different physical properties.

Vertical Displacements

The most general technique of displacement computation involves computing the displacement for a given point at a particular instant in time by summing the strains from infinite depth to the point of interest. Repetition of the process at regular time intervals will result in curves of vertical displacement versus time for the points of interest.

The most significant steps involved in such computations are concerned with establishing the stress distribution with depth at a given time, and with determining the strain at a given depth as a function of the stress and stress history.

The pressure distribution with depth is not easily determined. The subsurface wave form produced by a decaying air blast wave is extremely complex. The beginning of the pressure wave travels at higher velocity than the peak pressure, as does the unloading wave. The situation is too complex for computations of the pressure distribution to be practicable; instead approximations which will facilitate computations and lead to reasonable results are made.

The increase in wave length caused by the greater velocity of the wave front than the wave peak can have a considerable effect on displacement. The velocity of the wave front, termed c_i , can be computed from the initial tangent modulus of deformation M_i , and the soil mass density, ρ .

$$c_i^2 = \frac{M_i}{\rho} \quad (4-9)$$

Disturbance of soil samples is likely to cause the laboratory values

of M_i to be unreliable. The wave front velocity, c_i , should lie between the seismic velocity as determined by seismic surveys and the wave peak velocity c_p , $c > c_i > c_p$. If the velocities c_i and c_p for the medium are known and the rise time of the blast wave at the surface is assumed to be zero, the distance $z_i - z_p$ is given by

$$z_i - z_p = z_p \left(\frac{c_i}{c_p} - 1 \right)$$

where z_i and z_p are the depths of penetration of the wave front and peak pressure, respectively. If c_i and c_p are poorly defined, the same rough estimate used in the evaluation of peak acceleration (Sec. 4.2.6) may be applied - that the rise time, t_r , at a particular depth is one half of the transit time, t_t , required for the peak pressure to reach the depth. Applying this estimate the distance from the wave peak to the initial point of the wave is

$$z_i - z_p = z_p$$

It is reasonable to consider the pressure to vary linearly from zero to the peak pressure value over this distance.

The peak pressure p_{vp} is assumed to vary with depth due to attenuation as given by Eq. (4-2).

The distribution of pressure with depth above the point of peak pressure is difficult to specify rigorously. The overpressure decay propagates more rapidly than the peak pressure, reflects when it meets the peak, reflects again when it reaches the surface, etc. The accuracy

with which the soil properties can be described does not justify an attempt to trace out this behavior.

It is recommended that the air blast wave be represented as shown in Fig. 4-14 since the use of linearized approximations of the surface overpressure-time curve may lead to inconsistencies in the pressure-time variation at depth. Figures 3-4, 3-5, and 3-7 provide the information necessary for constructing the surface overpressure-time curve. To handle the decay portion of the pressure-depth curve in the medium it will be adequate to consider the pressure vs. depth curve at a particular time to be linear.

The strain distribution is established from the stress-strain characteristics of the soil and the pressure distribution. The relations between pressure and strain can be determined from the linearized stress-strain curve, Fig. 4-9.

If p_v , the vertical stress at depth z , has never been exceeded at the point in question, the corresponding vertical strain is

$$\epsilon_z = \frac{p_v}{M_p} = \frac{p_v}{\rho c_p^2} \quad (4-10)$$

where M_p is the modulus corresponding to p_{vp} (see Fig. 4-9).

If p_v is smaller than a previous value, that is if pressure is decaying or an unloading wave has reached the point, the strain is

$$\epsilon_z = \frac{p_{vp}}{M_p} - \frac{p_{vp} - p_v}{M_r} = \epsilon_{zr} + \frac{p_v}{M_r} = \epsilon_{zr} + \frac{p_v}{\rho c_r^2}$$

Thus the strain is not solely a function of the stress level but also a function of the stress history. If the ratio of residual strain to peak strain is selected as the parameter defining the unloading stress-strain curve of the soil;

$$k_p = \frac{\epsilon_{zr}}{\epsilon_{zp}} = 1 - \frac{M_p}{M_r}$$

then, if p_v is smaller than the peak stress value p_{vp} at the point, and occurs later than p_{vp}

$$\epsilon_z = \frac{p_v}{M_p} + \frac{k_p (p_{vp} - p_v)}{M_p}$$

$$\epsilon_z = \frac{p_v (1 - k_p) + k_p p_{vp}}{\rho c_p^2} \quad (4-11)$$

where

$$c_p^2 = \frac{M_p}{\rho}$$

The peak transient and the residual vertical displacement of a point can be obtained from the displacement - time curve for the point. The peak transient relative displacement, ^{between} two points may be obtained by determining the maximum difference in displacement at any one time. It should be noted that the time of maximum relative displacement between two points is not necessarily the time of peak displacement for either point, and that the maximum relative displacement is greater than the difference between peak transient displacements, but less than the peak strain occurring at either point multiplied by the vertical distance separating the points.

Figure 4-10 illustrates the relationship between peak displacement and peak relative displacements. An example of the computation of displacements is given as Example 4.1 of Section 4.2.8.

Certain approximate techniques for computing displacement can be appropriate. If the soil conditions below a particular point can reasonably be considered to be uniform to a depth equal to the length of the pressure wave in the soil, the peak transient displacement of the point can be computed from the air blast impulse as follows.

$$d_p = \frac{1}{2} \frac{p_{so} t_i}{\rho c_p} \quad (4-12)$$

where $\frac{1}{2} p_{so} t_i$ represents the total impulse, and t_i is given in Fig. 3-7.

The residual displacement, d_r , is given by

$$d_r = k_p d_p$$

where $k_p = \epsilon_{zr}/\epsilon_{zp}$ as shown in Fig. 4-9.

If a layer of relatively compressible soil of thickness significantly less than the length of the wave in the soil overlies bedrock, Eq. (4-12) does not apply. The peak relative displacement between the surface and the bedrock is closely approximated by the summation of the strains between the two points occurring when the pressure peak reaches the bedrock. To obtain an upper bound on the peak transient displacement of the surface the peak transient displacement of the top of the bedrock layer may be computed using (Eq. 4-12) and added to the peak relative displacement between the surface and the bedrock.

A technique for such computation of relative displacement is recommended in Ref. 4-25. The strain distribution with depth is taken as the strains corresponding to the envelope of an attenuated peak pressure. If the soil does not exhibit creep or viscous flow such a computation will give a conservative estimate of the peak relative displacement. It cannot be stated that the result will be conservative for a creep sensitive soil. Example 4.2 demonstrates the application of this technique.

A similar technique for computation of relative displacements is recommended in Ref. 4-24. The peak relative displacement is again assumed to occur as the pressure peak reaches the deeper point, but the strains are considered to decrease immediately as the pressure decays after the passage of the peak. The pressure distribution in the soil is sketched in to meet the air overpressure value for the time in question. The strain distribution is then computed using Eq. (4-11), and the strains are summed to yield the relative displacement. Example 4.3 demonstrates the application of the technique.

Preliminary Design Expressions

The above techniques of displacement computation require a thorough evaluation of the soil properties prior to their application. For use in the preliminary stages of design, before complete soil information is available, the following relations from Ref. 4-3, based upon the one dimensional elastic wave theory and studies of field test results, may be used. The use of these relations generally involves the use of an effective wave propagation velocity, c , the selection of which may be guided by seismic

surveys and engineering judgment based upon the geology of the area.

Table 4-2 gives ranges of seismic velocity for various media.

The elastic component of vertical displacement at the surface may be obtained from Eq. (4-12). Using t_i from Fig. 3-7, and a ρ value corresponding to a density of 115 pcf, which is a representative value for soils,

$$\text{Elastic Vertical Displacement at the Surface} \\ d_{se} = 9 \text{ in.} \left[\frac{p_{so}}{100 \text{ psi}} \right]^{1/2} \left[\frac{1000 \text{ fps}}{c} \left[\frac{W}{1MT} \right] \right]^{1/3} \quad (4-13)$$

where c is an average seismic velocity associated with M_r if c is taken as c_r , as shown in Fig. 4-9 by

$$c^2 = c_r^2 = \frac{M_r}{\rho}$$

The residual displacement at the surface has been empirically correlated in Ref. 4-3 with test data to give the following:

$$\text{Approximate Surface Residual Displacement} \\ d_{rs} = \frac{p_{so} - 40}{30} \text{ in.} \left[\frac{1000 \text{ fps}}{c} \right]^2 \quad (4-14)$$

for $p_{so} > 40 \text{ psi}$ (d_{rs} assumed to be zero
for $p_{so} < 40 \text{ psi}$)

where c = surface seismic velocity

For Nevada Test Site conditions use of $c = 1000 \text{ fps}$ gives an upper bound to observed residual surface displacements.

The peak total surface displacement is equal to the sum of the elastic and residual components as given by Eqs. (4-13) and (4-14).

For competent soils, residual deflections at depths in excess of 100 ft. have been observed to be negligible. If the residual displacement is considered to vary linearly with depth to zero at depth 100 ft., the expression for residual displacement at depth z becomes

Approximate Residual Displacement at Depth z

$$d_{rz} = d_{rs} \left[1 - \frac{z^*}{100 \text{ ft}} \right]$$

$$z^* = z \text{ ft.} \quad 0 < z < 100 \text{ ft.}$$

$$z^* = 100 \text{ ft.} \quad z > 100 \text{ ft.}$$

(4-15)

The elastic component of relative displacement between the surface and a point at depth z can be estimated from the bounding statement previously mentioned; the maximum average strain between the two points must be less than the maximum strain at the surface. If attenuation with depth is neglected, and $z = z^*$

$$d_{pe} < \frac{p_{so}}{\rho c_r} z^*$$

For a soil density of 115 pcf the expression becomes

$$d_{pe} < 4.8 \text{ in.} \left[\frac{p_{so}}{100 \text{ psi}} \right] \left[\frac{1000 \text{ fps}}{c_r} \right]^2 \frac{z^*}{100 \text{ ft}}$$

The elastic relative displacement can be considered to be about half of the bounding value given above, or

Approximate Elastic Relative Displacement

$$d_{pe} \approx 2.4 \text{ in.} \left[\frac{P_{so}}{100 \text{ psi}} \right] \left[\frac{1000 \text{ fps}}{c_r} \right]^2 \frac{z^*}{100 \text{ ft}} \quad (4-16)$$

A reasonable estimate of the maximum relative vertical displacement between two points is given by the sum of the results of Eqs. (4-15) and (4-16).

Horizontal Displacements

The techniques for evaluating vertical displacements are based upon the one-dimensional wave theory and, therefore, yield no information concerning the horizontal displacements. Some efforts to determine horizontal displacements from ideal plane wave theory have been made, but the ratios of horizontal to vertical displacements determined on this basis bear little relation to those measured in field tests. For this reason it appears appropriate to use a single ratio of horizontal to vertical displacement.

In Ref. 4-3 the suggested ratio of peak horizontal to peak vertical displacement is given as 1/3 for supersismic conditions. This ratio appears reasonably conservative since the horizontal displacements observed in field tests are reported in Ref. 4-2 to range from 1/100 to 1/10 of the peak vertical displacement; yet it is considerably smaller than the ratio may be according to the idealized plane wave theory.

4.2.5 Velocity. The peak vertical velocity, v_p , can be expressed in terms of the peak vertical stress by use of the results of the one-dimensional wave theory of Appendix C.

$$v_p = \frac{P_{vp}}{\rho c}$$

The value used for c should correspond to the constrained modulus of deformation appropriate to the stress level and loading rate. The evaluation of moduli of deformation was discussed in Section 4.2.3. If the modulus of deformation corresponding to the stress level p_{vp} is denoted as M_p , the appropriate wave propagation velocity c_p is given by

$$c^2 = c_p^2 = \frac{M_p}{\rho}$$

Considering the attenuation of peak stress with depth given by Eq. (4-2) the peak velocity equation for any depth z becomes

$$\begin{array}{c} \text{Peak Vertical Velocity} \\ v_p = \frac{\alpha_z p_{so}}{\rho c_p} \end{array} \quad (4-17)$$

For a representative value of soil density of 115 pcf, Eq. (4-17) becomes

$$\begin{array}{c} \text{Peak Vertical Velocity for Soil} \\ v_p = 4.0 \text{ fps} \left[\frac{p_{so}}{100 \text{ psi}} \right] \left[\frac{1000 \text{ fps}}{c_p} \right] \alpha_z \end{array} \quad (4-18)$$

or $v_p = 50 \text{ in./sec} \left[\frac{p_{so}}{100 \text{ psi}} \right] \left[\frac{1000 \text{ fps}}{c_p} \right] \alpha_z$

A plot of Eq. (4-18) is given by Fig. 4-11 for $\alpha_z = 1$, or surface conditions.

The peak horizontal velocity, v_{hp} , is not defined by the one-dimensional wave theory approach. Considerable variation exists among the empirical rules of thumb suggested; Ref. 4-3 recommends $v_{hp} = 2/3 v_p$, while Ref. 4-2 shows that the ratio v_{hp}/v_p measured in field tests under superseismic conditions has a maximum value of approximately 1/9. Since

most field test velocity measurements are based upon integration of acceleration records, a process often involving rather arbitrary variations of the base line, it is recommended that the more conservative ratio of 2/3 be applied.

4.2.6 Acceleration. The peak vertical downward acceleration is a function of the shape and duration of the rise to the velocity peak. Field test observations show little dependence of the air blast rise time on yield or peak side-on overpressure level; it is more nearly a function of the ground surface conditions. The minimum value of rise time of the air blast pressure is of the order of 0.001 seconds. For a linear rise of surface pressure and particle velocity the peak acceleration can be expressed by

$$a_p = v_p / t_r$$

where t_r is the rise time to peak velocity; at the surface this is equal to the rise time of the air blast. If an air blast rise time of 0.001 seconds is used, and the results are increased by about 20 percent to account for non-linearity of the rise, the equation for peak surface downward acceleration becomes

Peak Downward Vertical Acceleration at the Surface

$$a_p = 150 \text{ g} \left[\frac{P_{so}}{100 \text{ psi}} \right] \left[\frac{1000 \text{ fps}}{c_p} \right] \quad (4-19)$$

The value for c_p in Eq. (4-19) should correspond to the soil conditions at the surface. Since the surface acceleration appears to be partially dependent upon yield and other factors as well as peak surface velocity, it is recommended that no value of c_p greater than 2000 fps be used in

Eq. (4-19), regardless of higher measured values of surface seismic velocity. With $c_p = 1000$ fps, the results of Eq. (4-19) agree well with surface acceleration data from the Nevada Test Site. It should be noted that Eq. (4-19) is derived from Eq. (4-18) and should be applied only to soils. A similar expression may be developed for rock beginning with Eq. (4-17).

Peak downward vertical acceleration attenuates sharply with depth. The equation given in Ref. 4-2 for a_p at 5 ft. depth, which is based upon correlation with field test results, gives values roughly one quarter as great as those of Eq. (4-19). The sharp attenuation is due more to the increase of rise time with depth than to attenuation of the peak vertical velocity. The change in the pressure distribution with respect to depth and time with increasing depth is shown schematically in Fig. 4-12. The stretching out of the pressure distribution is due to the non-linearity of the stress-strain curve for soil. Non-linearity of the pressure rise with time becomes more pronounced with increasing depth. Accordingly, it is recommended that the peak acceleration value at depth be taken as twice that appropriate to a linear rise.

Peak Vertical Downward Acceleration at Depth

$$a_p = 2g \frac{v_p}{t_r} \frac{1}{32.2 \text{ ft/sec}^2} \quad (4-20)$$

The selection of an appropriate value for t_r requires some judgment; obviously it should never be less than the air blast rise time. Assuming an air blast rise time of 0.001 seconds, the rise time at depth would be (see Fig. 4-12)

$$t_r = 0.001 + \frac{z}{c_p} - \frac{z}{c_i}$$

When the values for c_p and c_i are not well defined, an approximate evaluation of the peak acceleration can be made. As a guide to the rise time, t_r , Ref. 4-3 suggests that the rise time be taken as one half of the time required for the peak stress to reach the depth of interest

$$t_r = \frac{1}{2} \frac{z}{c_p}$$

Substitution of this value for t_r into Eq. (4-20) for t_r , with v_p taken from Eq. (4-18), yields

$$a_p = 5 g \left[\frac{p_{so}}{100 \text{ psi}} \right] \left[\frac{100 \text{ ft}}{z} \right] \alpha_z \quad (4-21)$$

The restrictions on unit weight of the medium inherent in Eq. (4-18) apply equally to Eq. (4-21). In no instance should an a_p from Eq. (4-21) greater than the surface value from Eq. (4-19) be used. Equation (4-21) gives infinite acceleration at zero depth since it neglects the air blast rise time. Reference 4-2 presents an equation for peak vertical downward acceleration at 5 foot depth which gives a smaller acceleration value for a seismic velocity of 1000 fps than Eq. (4-21). However, for depths in excess of 10 feet the results of Eq. (4-21) agree well with the test data shown in Ref. 4-2. It is recommended that a smooth transition between the results of Eq. (4-21) and Eq. (4-19), such as is shown in Fig. 4-13 be applied.

The peak horizontal acceleration can be taken equal to the peak vertical acceleration as recommended in both Ref. 4-2 and 4-3.

4.2.7 Outrunning Ground Motions. Outrunning ground motion occurs when the air shock velocity U decays below the dilatational wave velocity of the medium. The approximate pressure level at which outrunning occurs for various media is given in Table 4-3, taken from Ref. 4-2. It should be noted that outrunning ground motions and direct-transmitted ground shock are different phenomena. Outrunning ground motion is produced when the air-induced ground motion begins to propagate more rapidly than the air blast shock front, but it is an air induced phenomenon. Direct transmitted ground shock, discussed in Section 4.3 is ground motion propagated through the medium from the region of the crater.

Reference 4-3 deals with outrunning ground motion by applying amplification factors to the air-induced ground motions computed for superseismic conditions. Peak velocity and acceleration values are amplified by the factor β .

<u>Condition</u>	<u>β</u>
Superseismic $c < U$	1
Outrunning	
Transeismic $U < c < 1.5 U$	c/U
$1.5U < c < 2 U$	1.5
Subseismic $2 U < c$	$1 + U/c$

It is considered in Ref. 4-3 that peak displacement values are not strongly affected by outrunning.

In Ref. 4-2 a considerably different approach to the evaluation of outrunning ground motions is employed. Expressions for acceleration, velocity, and displacement for outrunning conditions are established by

correlation of test data. The data show great scatter making correlation difficult; however, it is indicated that the outrunning ground motions are proportional to the scaled ground range rather than overpressure. A discussion of the technique used to establish the range for outrunning based upon seismic survey of the medium is also presented.

4.2.8 Examples of Air-Induced Displacement Computation.

Air Blast Conditions

$$P_{so} = 300 \text{ psi}$$

$$W = 5 \text{ MT}$$

The overpressure time variation is established using Figs. 3-4, 3-5, and 3-7.

From Fig. 3-5, $D_p^+ = 0.97 \text{ sec.}$ $\left[\frac{5}{1}\right]^{1/3} = 1.66 \text{ sec.}$ The wave form can then be taken from Fig. 3-4. As a guide for representing the curve shape at higher pressures the t_{∞} and t_{50} lines are sketched. From Fig. 3-7

$$t_{\infty} = 0.050 \left[\frac{5}{1}\right]^{1/3} = 0.086 \text{ sec.}$$

$$t_{50} = 0.078 \left[\frac{5}{1}\right]^{1/3} = 0.134 \text{ sec.}$$

Attenuation of Peak Pressure with Depth

$$\text{Eq. (4-1)} \quad \alpha_z = \frac{1}{1 + \frac{z}{L_w}}$$

$$L_w = 230 \text{ ft} \left[\frac{100 \text{ psi}}{P_{so}}\right]^{0.5} \left[\frac{W}{1 \text{ MT}}\right]^{1/3} = 227 \text{ ft}$$

The values of α_z may be computed or taken from Fig. 4-3.

Soil Parameters

Fig. 4-15 shows the variation of the propagation velocities for the wave front, c_f , and the wave peak, c_p , and the densities of the materials. This information would be obtained from the site exploration and evaluation programs.

Location of Wave Form with Time

The transit times for the wave front and wave peak are computed by considering the propagation velocities at the centers of 20-foot increments of depth (from Fig. 4-15) to represent the average propagation velocities through each increment. The resulting curves of arrival time for the wave front and wave peak are shown in Fig. 4-16.

Example 4.1. Computation of Displacement-Time Curves

Stress Distribution with Time

The stress distribution in the ground at regular intervals of time are determined using Fig. 4-16 to define the location of the wave form. The variation of stress with depth is assumed to be linear between the following critical points: zero stress at the wave front, the attenuated peak stress $\alpha P_{z\ SO}$ at the wave peak and the side-on overpressure from Fig. 4-14 at the surface. These stress distributions are shown in Fig. 4-17.

Computation of Displacement

To compute displacement as a summation of strains, the strain at the center of each 20-foot increment of depth is assumed to represent the average strain in that depth increment. The strain ϵ_z and the increment of displacement Δd are computed from:

For stress increasing

$$\epsilon_z = \frac{p_v}{\rho c_p^2} \quad (4-10)$$

$$\Delta d = \frac{p_v \Delta z}{\rho c_p^2}$$

For stress decreasing, and with $p_{vp} = \alpha_z p_{so}$ Eq. (4-11) becomes

$$\epsilon_z = \frac{p_v(1 - k_p) + k_p \alpha_z p_{so}}{\rho c_p^2}$$

$$\Delta d = \frac{p_v(1 - k_p) + k_p \alpha_z p_{so}}{\rho c_p^2} \Delta z$$

k_p is the ratio of residual strain to peak strain, $\frac{\epsilon_{zr}}{\epsilon_{zp}}$

For $z < 100$ ft., $k_p = 0.30$ - compressible overburden

For $z > 100$ ft., $k_p = 0$ - sound rock

The k_p for the overburden is taken as 0.3 since the overstress ratio σ_s exceeds three for nearly the full 100 feet to sound rock (see Sec. 4.2.3).

To find the peak displacement at a given depth a displacement-time curve is constructed. For each instant of time considered:

- Determine the variation of stress with depth (Fig. 4-17).
- Determine the increment of displacement in each increment of depth using the appropriate relation for stress increasing or stress decreasing.
- The displacement of the point in question equals the sum of all displacement increments occurring below the point. This provides one point on the displacement-time curve (Fig. 4-18).

Repeating the above steps at additional instants of time permits a curve such as Fig. 4-18 to be drawn.

Residual Displacement

$$\epsilon_{zr} = \frac{k_p \alpha_z p_{so}}{\rho c_p^2}$$

$$\Delta d_r = \frac{k_p \alpha_z p_{so}}{\rho c_p^2} \Delta z$$

The residual displacement is completely defined by the soil properties and the curve of attenuated peak pressure with depth. The residual displacement at any depth is obtained by summing the increments of residual displacement occurring below the point in question.

The resulting displacement-time curves for this example are plotted in Fig. 4-18. The curve of relative displacement between the surface and 100 foot depth is the difference between the surface and 100 foot depth displacement-time curves. The peak displacement values of interest are:

Peak Surface Displacement	4.9 in.
Residual Surface Displacement	1.6 in.
Peak Relative Displacement 0 to 100 ft	4.9 in.
Peak Displacement at 100 ft. depth	0.3 in.
Residual Displacement at 100 ft. depth	0.0 in.

Example 4.2 Approximate Computations of Peak Relative Displacement Assuming Strains Corresponding to Simultaneous Peak Stress Values.

Considering the strain values to correspond to the attenuated peak stress and the strain at the center of a 20 foot increment of depth to represent the average strain in the increment of depth:

Peak Displacement

$$\epsilon_z = \frac{\alpha_z p_{so}}{\rho c_p^2}$$

$$\Delta d = \frac{\alpha_z p_{so}}{\rho c_p^2} \Delta z$$

Residual Displacement

$$\epsilon_{zr} = \frac{k_p \alpha_z p_{so}}{\rho c_p^2}$$

$$\Delta d_r = \frac{k_p \alpha_z p_{so}}{\rho c_p^2} \Delta z$$

The sum of the displacement increments between the surface and 100 foot depth yields the peak and residual relative displacements between the surface and 100 foot depth.

Peak Relative Displacement 5.3 in.

Residual Relative Displacement 1.6 in.

Note that the peak value is greater than the value determined in Example 4.1, but the residual value is unchanged.

The peak absolute displacement can be conservatively estimated by assuming that the peak displacement at 100 foot depth occurs simultaneously with the peak relative displacement. The peak displacement at 100 foot depth can be estimated using Eq. (4-12) as shown in Example 4.4.

Example 4.3 Approximate Computations of Peak Relative Displacement

The peak relative displacement between two depths is computed assuming the peak value to occur when the stress wave peak reaches the greater depth. The wave peak reaches 100 foot depth at $t = 0.053$ from Fig. 4-16. Using the same techniques of strain and displacement computation discussed in Example 4.1, the resulting peak and residual relative displacements from the surface to 100 foot depth are:

Peak Relative Displacement 4.2 in.

Residual Relative Displacement 1.6 in.

The peak relative displacement value is less than that determined in Example 4.1 since the peak relative displacement actually occurs before the wave front attains a depth of 100 feet as may be seen in Figs. 4-17 and 4-18.

The peak absolute displacement of the surface can be estimated by assuming the peak displacement at 100 foot depth to occur simultaneously with the peak relative displacement. The process is conservative in that the times of peak values are unlikely to coincide. The peak displacement at 100 foot depth can be estimated using Eq. (4-12) as shown in Example 4.4.

Example 4.4 Application of Equations Based Upon One-Dimensional Wave Theory to Displacement Prediction.

The displacement equation, Eq. (4-13), is based upon the total impulse of the air-blast wave and implicitly assumes the soil to be uniform with depth and no attenuation of stress with depth to occur. If Eq. (4-13) is directly applied to determine the peak elastic surface displacement and an average value for c corresponding to c_p , for an average value of

$c_p = 2000 \text{ f}_{ps}$ and $k_p = 0.3$ is used:

$$c_r = \frac{c_p}{\sqrt{1 - k_p}} = \frac{2000}{.836} = 2390$$

$$d_{se} = 9 \text{ in.} \left[\frac{p_{so}}{100 \text{ psi}} \right]^{1/2} \left[\frac{1000 \text{ fps}}{c} \right] \left[\frac{W}{1MT} \right]^{1/3} \quad (4-13)$$

$$d_{se} = 11.2 \text{ in. at surface}$$

If Eq. (4-12) is used to compute the peak displacement at a depth of 100 feet with $c = 10,000 \text{ fps}$ for the sound rock:

$$d_p = \frac{1/2 p_{so} t_i}{\rho c} \quad (4-12)$$

$$\text{for } t_i = 0.37 \text{ sec. and } \gamma = 150 \text{ pcf}$$

$$d_p = 2.1 \text{ in. at 100 ft. depth}$$

The above results do not agree with the results of Example 4.1, but the equations are applied to a case which does not correspond well with the homogeneous medium assumed, and the attenuation of stress and impulse with depth not considered.

The empirical relation for residual surface displacement

$$d_{rs} = \left[\frac{p_{so} - 40}{30} \right] \text{ in.} \left[\frac{1000 \text{ fps}}{c} \right]^2 \quad (4-14)$$

yields for

$$c \approx 2000 \text{ fps}$$

$$d_{rs} = 2.2 \text{ in.}$$

The elastic component of relative displacement can be estimated from Eq. (4-16).

$$d_{pe} = 2.4 \text{ in.} \frac{p_{so}}{100 \text{ psi}} \left[\frac{1000 \text{ fps}}{c_r} \right]^2 \frac{z^*}{100 \text{ ft}}$$

The c_r value can be determined from $c_r^2 = c_p^2 / (1 - \nu_p)$. Using $c_p = 1000 \text{ fps}$, the surface value, $c_r = 1200 \text{ fps}$.

The resulting elastic component of relative displacement from the surface to 100 foot depth is 5.0 inches. This value is somewhat greater than the 3.1 inches for the corresponding quantity from Example 4.1. The difference results from considering the value $c_r = 1200 \text{ fps}$ to apply for the full 100 foot depth increment.

The above computations indicate that the equations for displacement prediction can give extremely conservative results when applied to situations corresponding poorly to the conditions for which the equations were derived. Consideration of the soil conditions of this example, Fig. 4-15, indicates that displacement equations based upon impulse should not be used at depths less than 100 feet since homogeneous soil conditions do not exist above that level. Careful applications of the equations can yield results comparable to those of Example 4.1.

Consider Eq. (4-12)

$$d_p = \frac{1/2 p_{so} t_i}{\rho c}$$

The term $1/2 p_{so} t_i$ represents the impulse effective in producing displacement at this depth. The wave length in the rock for a wave propagation velocity of 10,000 fps and the equivalent triangular pulse, $t_i = 0.37 \text{ sec.}$, is 3700 feet. Applying an average spatial attenuation to the peak overpressure, say

that corresponding to a depth of 2000 ft.

$$d_p = \frac{1/2 \alpha_z p_{so} t_i}{\rho c}$$

$$= \frac{\frac{1}{2} \left[\frac{1}{1 + \frac{2000}{227}} \right] 300 \times 0.37 \times 1728}{\frac{150}{32.2} \times 10,000} = 0.21 \text{ in.}$$

which corresponds closely to the value determined in Example 4.1.

The peak surface displacement will correspond closely to the peak relative displacement between the surface and 100 feet. The average peak strain between the surface and 100 foot depth can be computed based upon an average attenuated pressure, say the value for $z = 50$ feet, and an average wave propagation velocity, say the value at $z = 50$ feet or $c_p = 2000$ fps

$$\text{Average } \epsilon_{zp} = \frac{\alpha_z p_{so}}{\rho c_p^2} = \frac{246 \times 144}{\frac{115}{32.2} \cdot 2000 \cdot 2000} = 2.48 \times 10^{-3} \text{ in./in.}$$

$$\text{Peak Relative Displacement} = \epsilon_{zp} \Delta z = 2.48 \times 10^{-3} \times 100 \times 12 = 3.0 \text{ in.}$$

This technique is comparable to that used in Examples 4.2 and 4.3 where the computation is more precise because of the incremental form of the computations.

4.3 DIRECT-TRANSMITTED GROUND SHOCK

4.3.1 Introduction. As mentioned earlier, ground shock effects, though of a highly complex nature in the general case, are commonly divided into two categories, namely the air-induced effects and the direct-transmitted effects. Methods whereby the air-induced effects, i.e. those motions induced

at points beneath the ground surface as a result of air blast pressure passing over the ground surface, may be predicted were presented in Section 4.2. Direct-transmitted effects, i.e. those ground motions produced by the energy imparted directly to the ground at the point of detonation, will be discussed in this section.

Present knowledge of direct-transmitted shock effects is substantially less extensive than the knowledge of air-induced effects. This situation is a result of a number of factors, principal among which are the following: (1) Field test data for direct shock effects is far less extensive than for air-induced effects. (2) Field test data that are available, with only a very few exceptions, are from buried high explosive detonations. (3) Extrapolation from high explosive shock effects to nuclear shock effects requires the introduction of a yield equivalence factor, about which substantial uncertainties exist. (4) Extrapolation from the effects produced by buried charges to effects produced by surface charges requires the introduction of another yield equivalence factor to estimate the percentage of the energy in a surface burst which is propagated directly into the ground. (5) The test data that are available, even from HE detonations, produce very little information concerning the variation with time of the direct-transmitted shock pulses. In general, only maximum values of strain or acceleration were measured.

Despite the difficulties enumerated above, efforts to establish prediction methods for the effects of direct-transmitted ground shock have met with some moderate degree of success, at least when applied to a limited

range of rock materials. In general, the prediction methods are based on elementary concepts developed from one dimensional wave theory in a uniform elastic medium as presented in Appendix C. The elementary relationships for displacement, velocity, and acceleration developed on this basis were modified by empirically determined factors so as to yield results compatible with the limited amount of applicable test data available.

4.3.2 Theoretical Basis of Predictions. On the basis of a plane wave theory for a uniform elastic medium, it can be shown that:

$$v_r = \frac{\sigma_r}{\rho c} = \left(\frac{\sigma_r}{E}\right) \left(\frac{E}{\rho c}\right) = \epsilon c \quad (4-22)$$

where v_r is the velocity of the particle in the medium, σ_r is the stress intensity in the direction of shock wave propagation, ρ is the density of the medium, c is the velocity of wave propagation, E is the modulus of elasticity of the material, and ϵ is the strain in the medium in the direction of shock wave propagation.

The applicability of this relationship to direct-transmitted ground shock effects, which more properly should be characterized by a spherical wave propagating through soil or rock whose properties are neither elastic nor uniform, is highly questionable. The legitimacy of this approximation is particularly questionable close to the point of detonation where the curvature of the advancing shock front becomes significant. At greater distances, it may be reasonable. However, despite the obvious inadequacies of this basis, it does serve to insure proper scaling relationships between the particle motion parameters with which we are concerned and it also serves as a framework around which to develop empirical relations expressing

shock effects as functions of weapon yield, range, and other pertinent parameters.

To continue on the basis of plane wave theory, if the time dependent characteristics of the velocity pulse, the peak value of which is given by Eq. (4-22), are known, it is possible to compute the corresponding maximum acceleration and maximum displacement in the medium. Fig. 4-2 of Ref. 4-3, which is reproduced herein as Fig. 4-19, shows typical qualitative wave forms for direct-transmitted ground motions. Virtually no information is available as to the quantitative shape of these pulses; however, Ref. 4-25 indicates that the duration (t_1) of the velocity pulse can be estimated within a factor of about two, as being equal to one-half the transit time of the pulse from the point of detonation to the point at which the motion is sought. Similarly, Ref. 4-26 also approximates the rise time (t_r) from zero velocity to maximum velocity as about one-sixth the transit time of the velocity pulse.

The maximum acceleration can, of course, be computed from the slope of the velocity curve. The minimum possible acceleration would be consistent with a linear variation of the velocity with time between zero and its maximum value. However, it seems reasonable to expect that at some point during this time, the slope of the velocity pulse will be greater than that corresponding to a linear variation. Ref. 4-3 suggests that the velocity pulse be assumed parabolic in shape; consequently, the acceleration would then be twice that corresponding to a linear variation of velocity. This reasoning leads to the following expression for maximum direct-transmitted acceleration

$$a_r = \frac{v_r}{(t_r/2)} = \frac{12c^2}{R} \epsilon \quad (4-23)$$

where a_r is maximum radial acceleration, v_r is maximum radial velocity, R is the slant range from point of detonation, and the other quantities are as previously defined.

Similarly, if the velocity pulse were known quantitatively throughout, the maximum particle displacement in the medium in a direction parallel to shock propagation could be determined by integrating the velocity-time pulse. Having available only the qualitative pulse indicated herein in Fig. 4-19, it has been suggested that the pulse be assumed parabolic in shape, in which case its area is equal to two-thirds of the positive phase length (t_1) multiplied by the maximum velocity. This leads to the following expression for maximum radial displacement.

$$d_r = \frac{2}{3} v_r t_1 = \frac{1}{3} R \epsilon \quad (4-24)$$

4.3.3 Energy Equivalence. Most of the test data available from which direct-transmitted shock effects may be estimated are from buried high explosive detonations. To extrapolate from these data to estimate shock effects produced by surface nuclear detonations requires not only that the equivalence factor relating buried HE to buried nuclear be established, but also that the equivalence factor relating buried, fully contained detonations to surface detonations of the same charge also be known.

To relate fully contained nuclear charges to fully contained HE charges, a yield effectiveness factor of 0.16 is recommended ($w_N \approx 0.16 w_{HE}$). To relate a surface nuclear burst to a fully contained nuclear burst, a

factor of 0.06 may be used (surface $w_N \approx 0.06$ fully contained w_N). Accordingly, the equivalence factor relating a surface nuclear burst to a fully contained HE burst becomes $0.06 \times 0.16 \approx 0.01$ (surface $w_N \approx 0.01$ fully contained w_{HE}). Significant differences of opinion exist regarding equivalence factors. At this time, however, the above factors are considered to be reasonable estimates.

4.3.4 Experimental Results in Rock. Two primary sources for the study of direct-transmitted shock effects exist. The earliest of these is the "rock" part of the Underground Explosion Test program (UET) reported in Ref. 4-27. This was a study of the effects of buried high explosive detonations in rock. The size of the charges varied from 320 lbs. to 320,000 lbs. of TNT.

The second source is the more recent test of a small nuclear detonation in tuff in Shot Rainier of Operation Plumbbob and is reported in Ref. 4-30. While the quantity of the data accumulated in the UET tests far exceeds that acquired in the Rainier test, the latter is probably the best source from which to extrapolate for the effects of surface nuclear explosions. Using the Rainier results as a basis for extrapolation eliminates the uncertainties associated with the equivalence factor relating confined nuclear to confined HE. However, it should be noted that the Rainier test involved only one material, namely tuff, while the UET studies included several rock types as well as a companion study of the effects of detonations buried in soils of several types. Thus, the UET test results, when compared with those of the Rainier test, should serve to indicate the range of applicability of motion prediction expressions as developed from the Rainier data.

Rainier Effects. As indicated above, the Rainier shot of Operation Plumbbob consisted of the detonation of a small nuclear device in tuff having a seismic velocity of approximately 6000 fps. The most significant results obtained in this test are portrayed in Fig. 4.1 of Ref. 4-30, which is reproduced in substance herein as Fig. 4-20. Reference to this figure will indicate that the maximum observed radial acceleration produced by this detonation can be represented approximately by the following expression:

$$a_r W^{1/3} = (2 \times 10^{11}) g (R/W^{1/3})^{-4}$$

or

$$a_r = 2000 g \left(\frac{W}{1KT} \right) \left(\frac{100 \text{ ft}}{R} \right)^4 \quad (4-25)$$

Noting the compatibility relationships that must exist between acceleration, velocity, and displacement at a point, and also that the available data from the Rainier test as well as from other sources (particularly Refs. 4-26 and 4-27) indicate that velocity (or strain) and displacement vary as $(1/R)^n$ where, approximately, $1 < n < 2$ for displacements and $1.5 < n < 2.5$ for velocity, Ref. 4-3 suggests that Eq. (4-25) be modified as follows:

$$a_r W^{1/3} = (1.35 \times 10^{10}) g (R/W^{1/3})^{-3.5}$$

or

$$a_r = 1350 g \left(\frac{W}{1KT} \right)^{5/6} \left(\frac{100 \text{ ft}}{R} \right)^{3.5} \quad (4-26)$$

Equations (4-25) and (4-26), which represent the data given on Fig. 4-20, are for a fully contained detonation. Using an equivalence factor of 0.06, as discussed earlier, to convert from buried effects to the effects

of a surface detonation, and converting the weapon yield from kilotons to megatons, Eq. (4-26) becomes

$$a_r = 40,500 \text{ g } \left(\frac{W}{1\text{MT}}\right)^{5/6} \left(\frac{100 \text{ ft}}{R}\right)^{3.5} \quad (4-27)$$

or perhaps more conveniently:

$$a_r = 12.7 \text{ g } \left(\frac{W}{1\text{MT}}\right)^{5/6} \left(\frac{1000 \text{ ft}}{R}\right)^{3.5} \quad (4-28)$$

where W is given in megatons of surface nuclear yield.

It is obvious that these expressions are applicable only to the tuff in which the accelerations on which they were based were measured. To generalize these equations so that they may be applied to other materials, it is possible to scale them in terms of the seismic velocity, c . Equation (4-23) indicates that acceleration should be a function of c^2 . Rewriting Eq. (4-28) as a function of c^2 , noting that it was derived for a material with a seismic velocity of about 6000 fps, yields the following expression:

$$a_r = 0.36 \text{ g } \left(\frac{W}{1\text{MT}}\right)^{5/6} \left(\frac{1000 \text{ ft}}{R}\right)^{3.5} \left(\frac{c}{1000 \text{ fps}}\right)^2 \quad (4-29)$$

By substituting Eq. (4-29) into Eqs. (4-22), (4-23), and (4-24), corresponding expressions for radial velocity and displacement may be obtained.

$$v_r = 0.95 \text{ fps } \left(\frac{W}{1\text{MT}}\right)^{5/6} \left(\frac{1000 \text{ ft}}{R}\right)^{2.5} \left(\frac{c}{1000 \text{ fps}}\right) \quad (4-30)$$

$$d_r = 3.8 \text{ in. } \left(\frac{W}{1\text{MT}}\right)^{5/6} \left(\frac{1000 \text{ ft}}{R}\right)^{1.5} \quad (4-31)$$

4.3.5 Applicability to Other Materials. Though Eqs. (4-29, 30,

and 31) appear to be applicable to any material whose "elastic" properties can be characterized by seismic velocity, c , the fact remains that they were derived on the basis of test results in one material (Tuff, $c = 6000$ fps) only. Because of the lack of a sound theoretical basis, the applicability of these equations to other materials can be checked only by comparing them with test results in other materials.

Unfortunately, test data against which to compare the Rainier-based equations are very limited. In Operation Redwing several nuclear devices were exploded in rock and measurements were made of the resulting ground motions (Ref. 4-32). However, the yield was so small in comparison with that for which the instrumentation was planned that gages responded only in the very low regions of the response ranges for which they were adjusted. Consequently, quantitatively, these data should be considered unreliable. Though the scatter of the results is quite large, Fig. 3.5 of Ref. 4-32 does indicate that maximum radial acceleration varies roughly as $R^{-3.5}$ or R^{-4} , which agrees quantitatively with the Rainier data.

Probably a better comparison can be made with tests reported in Refs. 4-27 and 4-31, which present the results of HE tests in rock and in soil, respectively. The charge sizes varied from 320 lbs. to 320,000 lbs. of TNT. Though these tests were for high explosives rather than nuclear, data are extensive and several comparisons can be drawn.

Reproduced herein as Fig. 4-21 is Fig. 3.5 of Ref. 4-27 on which are presented the radial accelerations produced in sandstone by several HE detonations. The average of these accelerations was represented by:

$$a_r W^{1/3} = (2.9 \times 10^6) g \left(\frac{W}{R} \right)^{4.1} \quad (4-32)$$

where W is in pounds of TNT. To study the applicability of the Rainier-based relations to sandstone, it is of interest to reduce Eq. (4-26) (on which Eqs. 4-29, 30 and 31 were based) to its equivalent in terms of pounds of TNT. Converting Eq. (4-26) to pounds of TNT, using an equivalence factor between HE and nuclear of 0.16, yields:

$$a_r = (3.5 \times 10^5) g (W)^{5/6} \left(\frac{1}{R}\right)^{3.5} \quad (4-33)$$

which, for comparison with Eq. (4-32), can also be written as

$$a_r W^{1/3} = (0.35 \times 10^6) g \left(\frac{W^{1/3}}{R}\right)^{3.5} \quad (4-34)$$

where W is in pounds of TNT.

To be directly comparable, note must be taken of the fact that Eq. (4-26) and, consequently Eqs. (4-33) and (4-34), were obtained for tuff with a seismic velocity of 6000 fps while Eq. (4-32) is for a sandstone having an average seismic velocity of about 9000 fps. To correct for this, Eq. (4-34) can be generalized, in terms of c, as follows:

$$a_r W^{1/3} = (1.0 \times 10^4) g \left(\frac{R}{W^{1/3}}\right)^{-3.5} \left(\frac{c}{1000 \text{ fps}}\right)^2 \quad (4-35)$$

Using for sandstone a c of 9000 fps, Eq. (4-35) becomes

$$a_r W^{1/3} = (8.1 \times 10^5) g (R/W^{1/3})^{-3.5} \quad (4-36)$$

which is plotted on Fig. 4-21 for ease of comparison. Reference to this figure will indicate that, for scaled ranges less than about 10, Eq. (4-36) represents quite well an average of the sandstone data and, for scaled ranges greater than about 10, it represents a reasonable upper bound. Thus, on this

basis, the Rainier-based relations appear to be generally applicable to sandstone as well as to tuff, from which they were developed.

The applicability of the Rainier-based equations to other materials can also be studied on the basis of strains. Fig. 3-1 of Ref. 4-27 presents average values of strains as functions of scaled range for three materials as follows:

For Granite: $\epsilon = (1.2 \times 10^4) (R/W^{1/3})^{-2.0}$ Micro in./in. (4-37)

($c \approx 12,000$ fps)

For Sandstone: $\epsilon = (1.9 \times 10^4) (R/W^{1/3})^{-2.4}$ Micro in./in. (4-38)

($c \approx 9,000$ fps)

For Limestone: $\epsilon = (0.4 \times 10^4) (R/W^{1/3})^{-2.0}$ Micro in./in. (4-39)

($c \approx 17,000$ fps)

To determine strains on the basis of the Rainier data, the acceleration, as given by Eq. (4-33), may be substituted into Eq. (4-23), which, with $g = 32.2$ ft/sec/sec., yields:

$$\epsilon = (1.0 \times 10^6) (R/W^{1/3})^{-2.5} \left(\frac{1}{c}\right)^2 \quad (4-40)$$

If average values of c (as taken from Ref. 4-27) of 12,000 fps, 9000 fps, and 17,000 fps are used for granite, sandstone, and limestone respectively, Eq. (4-40) gives, for comparison with Eqs. (4-37, 38, and 39), the following:

Granite: $\epsilon = (0.7 \times 10^{-4}) (R/W^{1/3})^{-2.5}$ Micro in./in. (4-41)

Sandstone: $\epsilon = (1.24 \times 10^{-4}) (R/W^{1/3})^{-2.5}$ Micro in./in. (4-42)

Limestone: $\epsilon = (0.35 \times 10^{-4}) (R/W^{1/3})^{-2.5}$ Micro in./in. (4-43)

This comparison can hardly be said to indicate general applicability of the Rainier data to other materials; however, it should not be concluded on this basis alone that the Rainier data are inapplicable to materials other than tuff, since Eq. (4-40) is based on several assumptions, the most uncertain of which are the time-variation of the velocity pulse and the yield equivalence factor between HE and nuclear effects.

Some insight into the applicability of the Rainier data to soils can be obtained by study of the results of HE tests in dry clay and dry sand as reported in Ref. 4-31. On the basis of information given on pages 1-5 and 1-6 of Ref. 4-31, it appears that the seismic velocity of both the sand and the clay was about 1000 to 1500 fps at the shallow depths at which acceleration measurements were made. These acceleration measurements are reported in Figs. 2-39 and 2-40 of Ref. 4-31 for dry sand and dry clay, respectively, and are reproduced herein in Figs. 4-22 and 4-23.

To compute accelerations for these soils on the basis of the Rainier data, use can be made of Eq. (4-35) with c -values of 1000 to 1500 fps. In this manner the following relations are obtained.

For $c = 1000$ fps:

$$a_r W^{1/3} = (1.0 \times 10^{-4}) g (R/W^{1/3})^{-3.5} \quad (4-44)$$

For $c = 1500$ fps:

$$a_r W^{1/3} = (2.25 \times 10^4) g (R/W^{1/3})^{-3.5} \quad (4-45)$$

For comparison, these equations are plotted on Figs. 4-22 and 4-23. Though the point scatter is very large for these soils, the above equations indicate general compatibility between the Rainier extrapolation and the measured accelerations in the two media.

On the basis of the preceding discussion, it appears that, while the uncertainties are still very large and additional studies, both experimental and theoretical, are still needed, the Rainier-based relations (Eqs. 4-29, 4-30 and 4-31) can be used to estimate the radial motions produced in a variety of media by surface nuclear detonations. It should, however, be emphasized that the results obtained in a given instance may be very substantially in error, easily by a factor of 2 or 3, and possibly higher, particularly when applied to materials other than that for which the basic relation for acceleration was empirically determined.

4.3.6 Tangential Motions. The previous discussion was concerned only with radial motions produced by direct-transmitted shock. Unfortunately, there is virtually no data on the corresponding tangential motions. However, until additional information becomes available it is recommended that, as for air-induced effects, the tangential displacement, velocity, and acceleration be taken as 1/3, 2/3, and 1 times the radial displacement, velocity, and acceleration, respectively.

Ref. 4-3 states that it is desirable to consider the direct-transmitted effects as being applicable only at some distance below ground surface, except

perhaps at close-in ranges. At large ranges, it is suggested that the expressions developed above be applied only below a surface subtending an angle of about 20 degrees with the ground surface.

4.3.7 Effect of Layered Systems. As in the case of air-induced shock, no attempt is made to consider possible stress reflections between soil strata of different properties; however, the effect of stratification should be considered in arriving at effective seismic velocities to be used in estimating direct transmitted accelerations and velocities. The following procedure is taken directly from Section 4.5.8 of Ref. 4-3.

For estimating the velocities and accelerations only, not displacements, in a two-layered system, the method illustrated in Fig. 4-24 based on ray-paths may be used as a best approximation at present. The principle used is based on an effective value of c , designated as \bar{c} , for which the transit time by a direct wave from the source to the target is the same as for the fastest transit time of a shock wave in the complex layered system.

Reference to Fig. 4-24 will show the following relationships to exist.

$$\sin \theta = c_1/c_2$$

and

$$\frac{R}{\bar{c}} = \frac{(2H-z) \sec \theta}{c_1} + \frac{R - (2H-z) \tan \theta}{c_2}$$

Thus:

$$\frac{c_1}{\bar{c}} = \frac{c_1}{c_2} + \frac{2H-z}{R} \sqrt{1 - \left(\frac{c_1}{c_2}\right)^2} \quad (4-46)$$

It will be noted that if

$$\frac{2H-z}{R} \rightarrow 0, \bar{c} \rightarrow c_2$$

and if

$$c_1 = c_2, \bar{c} \rightarrow c_1$$

As an example, if $H = 100$ ft, $z = 60$ ft, $R = 2000$ ft, $c_1 = 2000$ fps, and $c_2 = 8000$ fps, then one finds from Eq. (4-46) that $\bar{c} = 6300$ fps. Velocities and accelerations could, therefore, be estimated by using this value of \bar{c} for c in Eqs. (4-29 and 4-30).

4.4 REFERENCES

- 4-1 "The Effects of Nuclear Weapons", U. S. Dept. of Defense, and Atomic Energy Commission, U.S. Government Printing Office, Washington, D. C., April 1962. (UNCLASSIFIED)
- 4-2 Sauer, F. M., "Ground Motion Produced by Aboveground Nuclear Explosions", AFSWC-TR-59-71, April 1959. (SECRET FRD)
- 4-3 Newmark, N. M., Hall, W. J., "Preliminary Design Methods for Underground Protective Structures", AFSWC-TDR-62-6, June 1962. (SECRET)
- 4-4 Cinelli, G. and Fugelso, L. E., "Theoretical Study of Ground Motion Produced by Nuclear Blasts", AFSWC-TR-60-8, 30 October 1959. (UNCLASSIFIED)
- 4-5 Weidlinger, Paul, "A Study on the Effect of a Progressing Surface Pressure on a Viscoelastic Half-Space", SR-22, The Mitre Corporation, Bedford, Massachusetts, 20 February 1961. (UNCLASSIFIED)
- 4-6 Baron, M. L., Bleich, H. H. and Weidlinger, Paul, "Theoretical Studies on Ground Shock Phenomena", SR-19, The Mitre Corporation, Bedford, Massachusetts, October 1960. (UNCLASSIFIED)
- 4-7 Newmark, N. M., "Considerations in the Design of Underground Protective Structures", Vol. III, Final Report of Special Studies Related to the WS 107A-2 Launcher Installation, American Machine and Foundry Company, 20 June 1958. (SECRET)
- 4-8 Smith, R. H. and Newmark, N. M., "Numerical Integration for One-Dimensional Stress Waves", Civil Engineering Studies, Structural Research Series No. 162, University of Illinois, Urbana, Illinois, August 1958. (UNCLASSIFIED)
- 4-9 Timoshenko, S. and Goodier, J. N., "Theory of Elasticity", McGraw-Hill Book Company, Inc., New York 1951. (UNCLASSIFIED)
- 4-10 Terzaghi, K. and Peck, R. B., "Soil Mechanics in Engineering Practice", John Wiley and Sons, Inc., 1948. (UNCLASSIFIED)
- 4-11 "ICBM Standard Guide of Field Procedures", Air Force Ballistic Missile Division. (UNCLASSIFIED)
- 4-12 Wuerker, R. G., "Annotated Tables of Strength & Elastic Properties of Rocks", Petroleum Branch, AIME, 1956. (UNCLASSIFIED)

- 4-13 "Physical Properties of Some Typical Foundation Rocks", compiled by G. G. Balmer, U. S. Bureau of Reclamation, Concrete Laboratory Report No. Sp-39, 1953. (UNCLASSIFIED)
- 4-14 Judd, W. R. and Huber, C., "Correlation of Rock Properties by Statistical Methods", Aero-Astronautics Dept., The RAND Corporation, Santa Monica, P-2224, 1961. (UNCLASSIFIED)
- 4-15 Obert, L., Windes, S. L. and Duval, W. I., "Standardized Tests for Determining the Physical Properties of Mine Rock", U. S. Bureau of Mines, R.I., 3891, 1946. (UNCLASSIFIED)
- 4-16 Windes, S. L., "Physical Properties of Mine Rock", Part I, U. S. Bureau of Mines, R.I. 4459, 1949. (UNCLASSIFIED)
Windes, S. L., "Physical Properties of Mine Rock", Part II, U. S. Bureau of Mines, R.I. 4727, 1950. (UNCLASSIFIED)
Blair, P. E., "Physical Properties of Mine Rock", Part III, U. S. Bureau of Mines, R.I. 5130, 1955. (UNCLASSIFIED)
- 4-17 Dobrin, M. B., "Introduction to Geophysical Prospecting", McGraw-Hill, New York, Second Edition, 1960. (UNCLASSIFIED)
- 4-18 Hvorslev, M. J., "Subsurface Exploration and Sampling for Civil Engineering Purposes", Waterways Experiment Station, Vicksburg, November 1949. (UNCLASSIFIED)
- 4-19 Mobile Drilling Inc., Indianapolis, Indiana, Catalog No. 615. (UNCLASSIFIED)
- 4-20 "Earth Manual", U. S. Bureau of Reclamation, Denver, 1960. (UNCLASSIFIED)
- 4-21 Johnson, S. J., "An Alternative Method for Determining the Constrained Modulus and the Coefficient of Elastic Vertical Compression", Moran, Proctor, Mueser and Rutledge, August 1961. (UNCLASSIFIED)
- 4-22 Hammer, M. J. and Wilson, S. D., "Subsurface Investigations and Ground Motion Studies at Nevada Test Site", AFBMD Contract AF 04(647)650, January 13, 1961. (SECRET)

Unclassified Appendices

- A - Geology, Nevada Test Site
- B - Geophysical Investigations, Nevada Test Site
- C - Exploratory Drilling and Sampling, Nevada Test Site
- D - Laboratory Testing Equipment, Procedures & Test Results, Nevada Test Site

- 4-23 Perret, W. R., "Ground Motion Studies at High Incident Overpressure", Operation Plumbbob, Project 1.5, WT-1405, Sandia Corporation, 20 June 1960. (UNCLASSIFIED)
- 4-24 Wilson, S. D. and Sibley, E. A., "Ground Displacements Resulting From Air-Blast Loading", Paper presented at the Houston Convention of the American Society of Civil Engineers, 1962. (UNCLASSIFIED)
- 4-25 WS-133 A, Operational Sites Final Report Phase I, Surface and Subsurface Evaluation, Contract No. AF 04 (647)-494, Addendum No. 1 - Section III Subsurface Data, Air Force Ballistic Missile Division, July 1960. (CONFIDENTIAL)
- 4-26 "An Engineering Manual on Design of Underground Installations in Rock", prepared by U. S. Bureau of Mines for the Corps of Engineers, Draft Copy, March 1957. (CONFIDENTIAL)
- 4-27 Engineering Research Associates, "Underground Explosion Test Program, Final Report, Vol. II, Rock", 30 April 1953. (UNCLASSIFIED)
- 4-28 Wright, J. K. and Herbert, J. D., "Measurement of Ground Shock in Homogeneous Media, Surface Movement", FWE-161, July 30, 1958. (CONFIDENTIAL)
- 4-29 Moulton, J. F., "Nuclear Weapons Blast Phenomena", Prepared for Defense Atomic Support Agency by U. S. Naval Ordnance, DASA 1200, Vol. I (SECRET RD), Vol. II (SECRET FRD), Vol. III (CONFIDENTIAL FRD), March 1960.
- 4-30 Perret, W. R., and Preston, R. G., "Preliminary Summary Report of Strong-Motion Measurements from a Confined Underground Nuclear Detonation", ITR-1499, Operation PLUMBBOB, June 15, 1958. (UNCLASSIFIED)
- 4-31 Engineering Research Associates, "Underground Explosion Test Program, Final Report, Vol. I, Soil", 30 August 1952. (UNCLASSIFIED)
- 4-32 Adams, W. M., Flanders, F. L., Perret, W. R. and Preston, R. G., "Preliminary Summary Report of Strong-Motion Measurements, Underground Nuclear Detonations", Project 26.0, Operation HARDTACK, ITR-1711, January 1960. (UNCLASSIFIED)

TABLE 4-1 RATIO OF HORIZONTAL TO VERTICAL SOIL PRESSURES

Soil Description	K_o , For Stresses Up to 1,000 psi		
	Dynamic	Static	
	Undrained	Undrained	Drained
Cohesionless Soils, Damp or Dry	1/4	1/3-dense 1/2-loose	1/3-dense 1/2-loose
Unsaturated Cohesive Soils of Very Stiff to Hard Consistency	1/3	1/2	1/2
Unsaturated Cohesive Soils of Medium to Stiff Consistency	1/2	1/2	1/2
Unsaturated Cohesive Soils of Soft Consistency	3/4	1/2 to 3/4	1/2 to 3/4
Saturated Soils of Very Soft to Hard Consistency and Cohesionless Soils	1	1	1/2-stiff 3/4-soft
Saturated Soils of Hard Consistency. $q_u = 4$ tsf to 20 tsf.	3/4 to 1	1	1/2
Saturated Soils of Very Hard Consistency. $q_u > 20$ tsf.	3/4	1	1/2
Rock	Obtain from tests on rock cores and correlate with seismic data.		

TABLE 4-2 TYPICAL SEISMIC VELOCITIES FOR SOILS AND ROCKS

Material	Seismic Velocity fps
Loose and Dry Soils	600 - 3,300
Clay and Wet Soils	2,500 - 6,300
Coarse and Compact Soils	3,000 - 8,500
Sandstone and Cemented Soils	3,000 - 14,000
Shale and Marl	6,000 - 17,500
Limestone - Chalk	7,000 - 21,000
Metamorphic Rocks	10,000 - 21,700
Volcanic Rocks	10,000 - 22,600
Sound Plutonic Rocks	13,000 - 25,000
Jointed Granite	8,000 - 15,000
Weathered Rocks	2,000 - 10,000

Based on information taken from: "Subsurface Exploration and Sampling of Soils for Civil Engineering Purposes", by Juul Hvorslev, ASCE Research Report, printed by Waterways Experiment Station, Vicksburg, Mississippi, 1948, p. 30, Fig. 4.

TABLE 4-3 APPROXIMATE OVERPRESSURES AT WHICH OUTFRUNNING OF GROUND
WAVE OCCURS, LARGE YIELD SURFACE BURSTS

<u>Formation</u>	<u>Overpressure* (psi)</u>
Alluvium	less than 40
Gravel (dry)	10 - 100
Gravel (wet)	40 - 500
Sandy clay	100 - 500
Sandstone	500 - 2000
Shale	650 - 2500
Limestone	1500 up
Metamorphic	1000 up
Granite	3000 up

Source: Ref. 4-2

*Outrunning conditions may be anticipated at over-
pressures less than those tabulated.

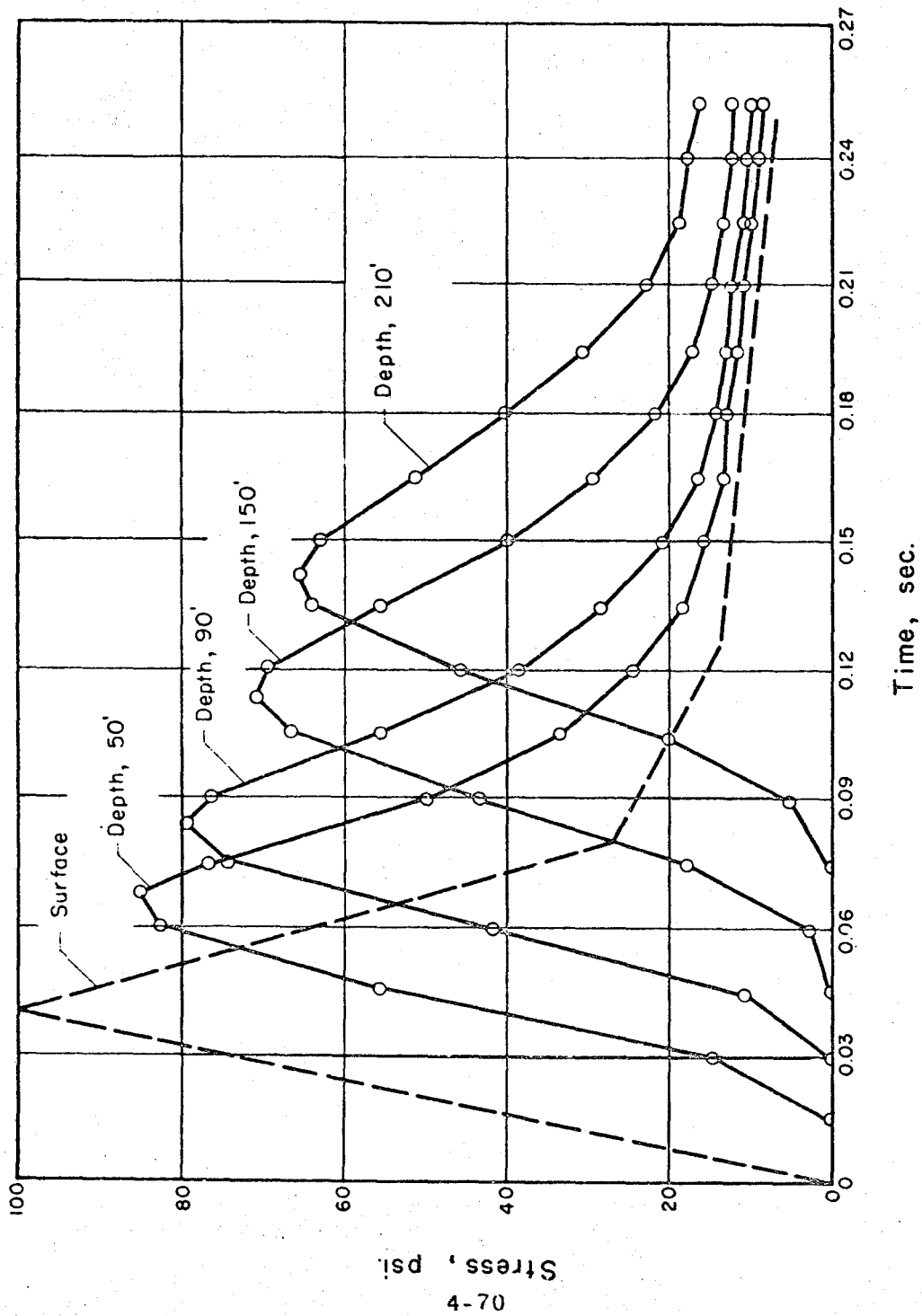


FIG. 4-1 TYPICAL EFFECT OF A VISCO-ELASTIC MEDIUM ON
WAVE FORM AND PEAK PRESSURE.

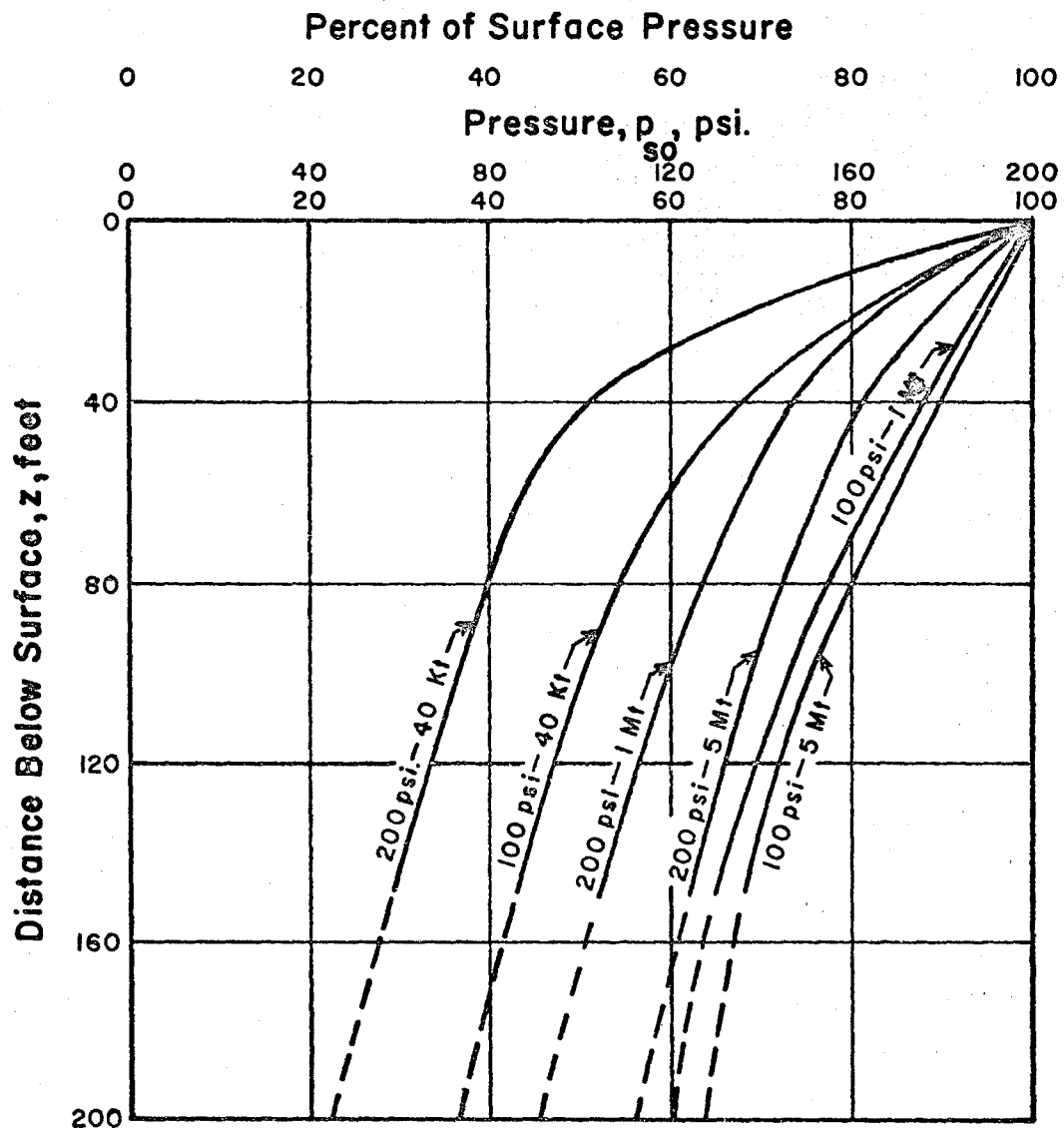


FIG. 4-2 CHANGE IN MAXIMUM VERTICAL STRESS
WITH DEPTH DUE TO SPATIAL ATTENUATION

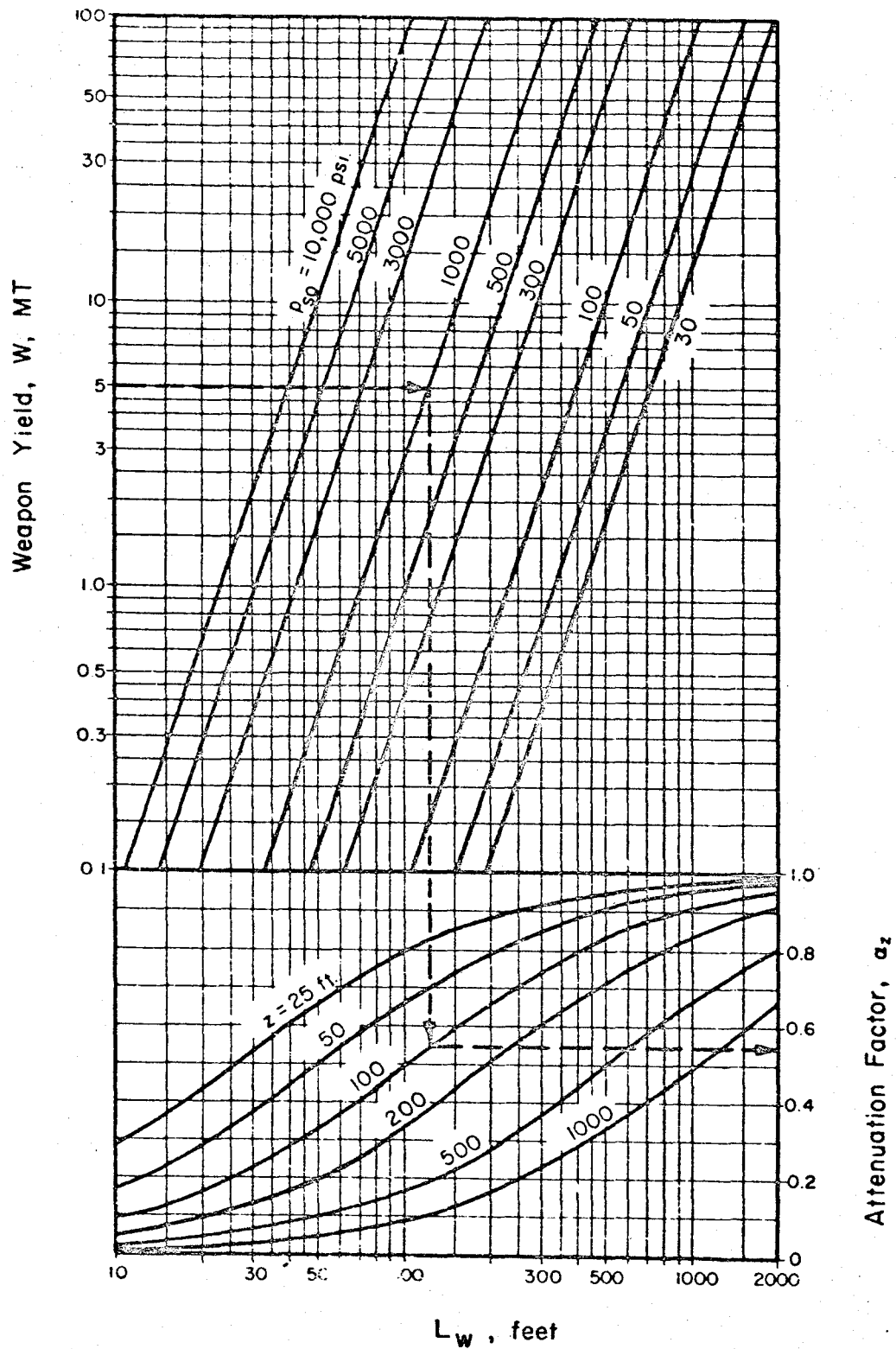
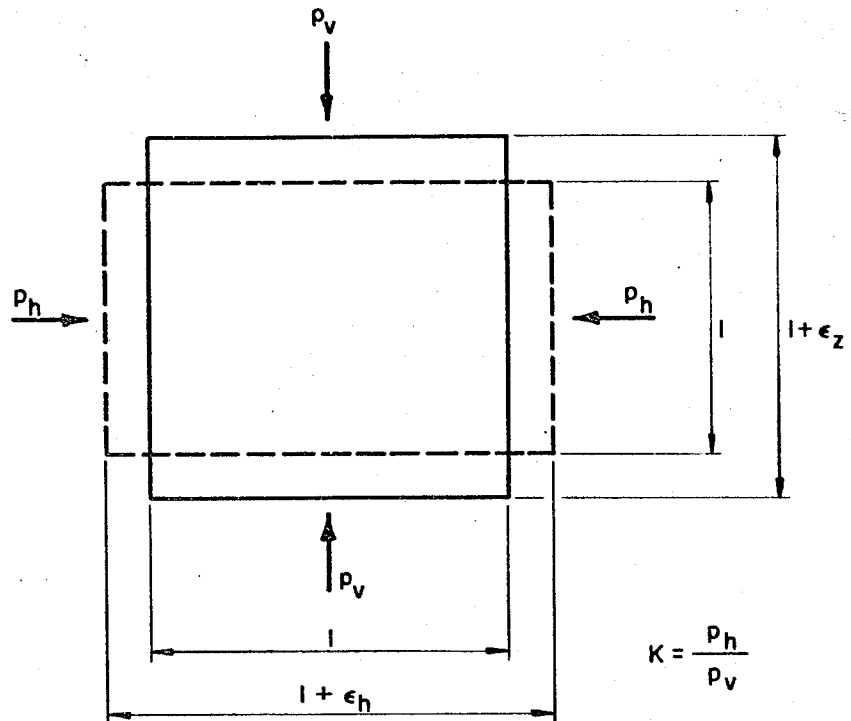
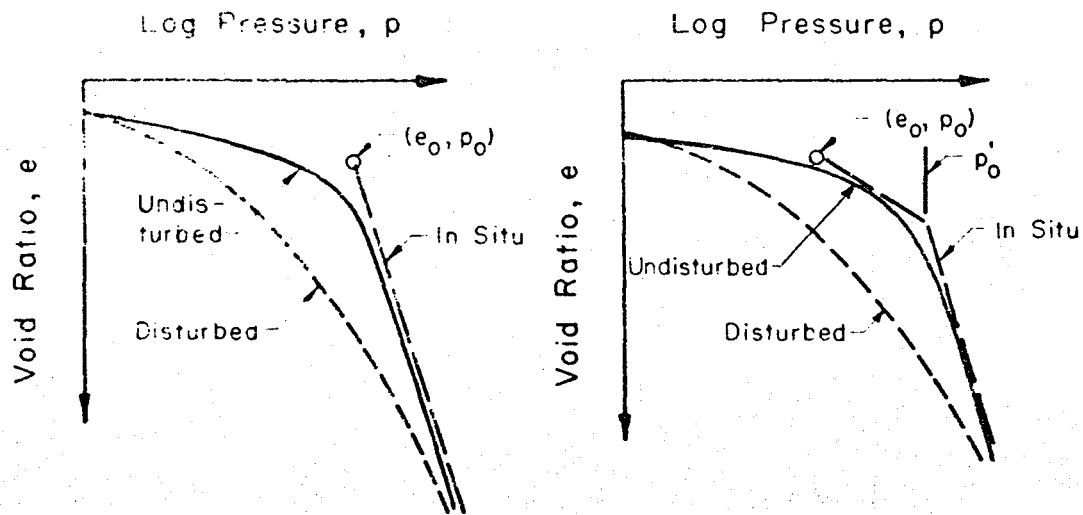


FIG. 4-3 DEPTH ATTENUATION FACTOR



- (1.) If $\epsilon_h = 0$, $K = K_0 = \frac{p_h}{p_v}$
- (2.) If ϵ_h is Positive, K Approaches The Lower Limit, K_a , The Active Case.
- (3.) If ϵ_h is Negative, K Approaches The Upper Limit, K_p , The Passive Case.

FIG. 4-4 DEFINITION OF HORIZONTAL PRESSURE COEFFICIENT K .



(a) Normally Loaded

(b) Preloaded

FIG. 4-5 TYPICAL SOIL CONSOLIDATION CURVES.

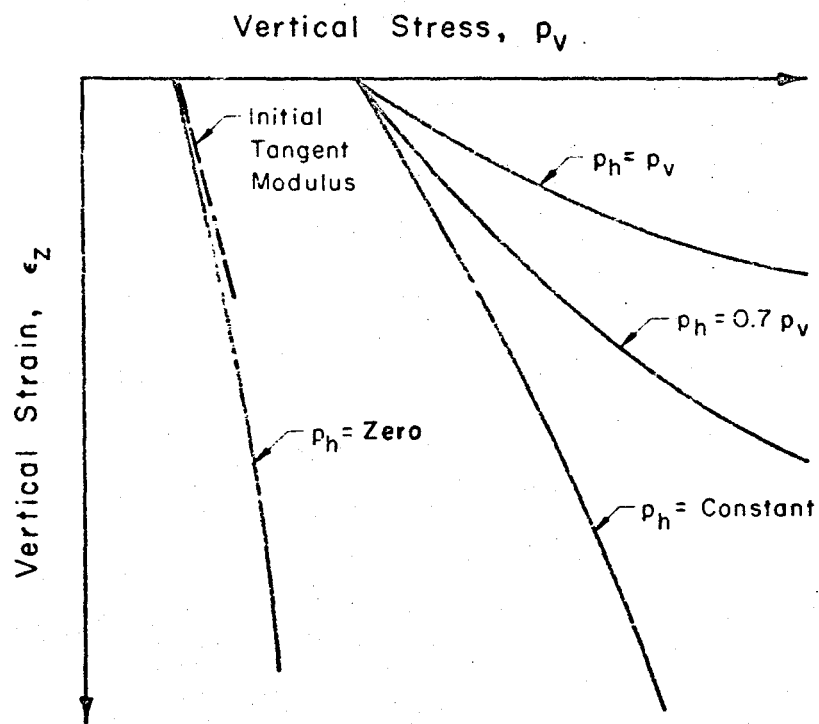


FIG. 4-6 TRIAXIAL TEST RESULTS.

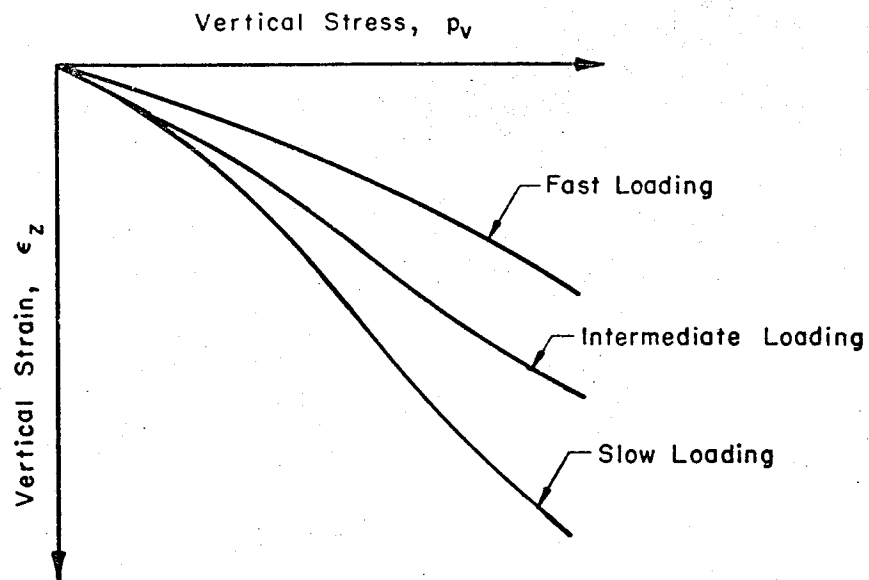


FIG. 4-7 CONFINED COMPRESSION TEST RESULTS.

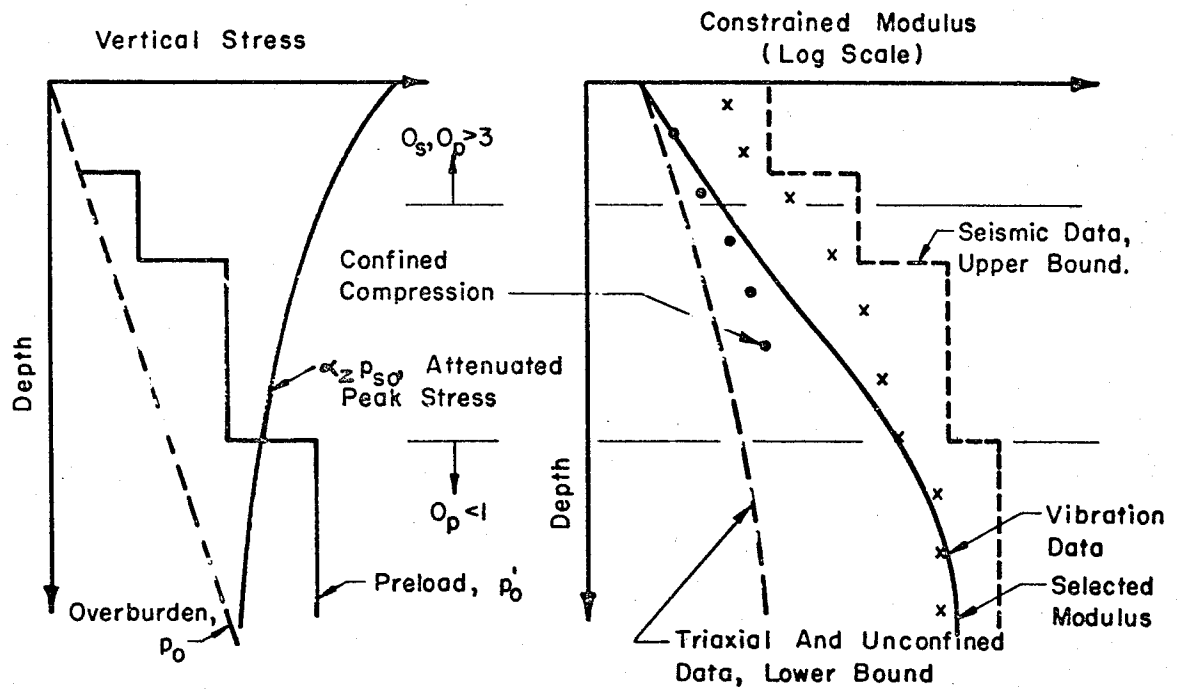


FIG. 4-8 SELECTION OF CONSTRAINED MODULUS.

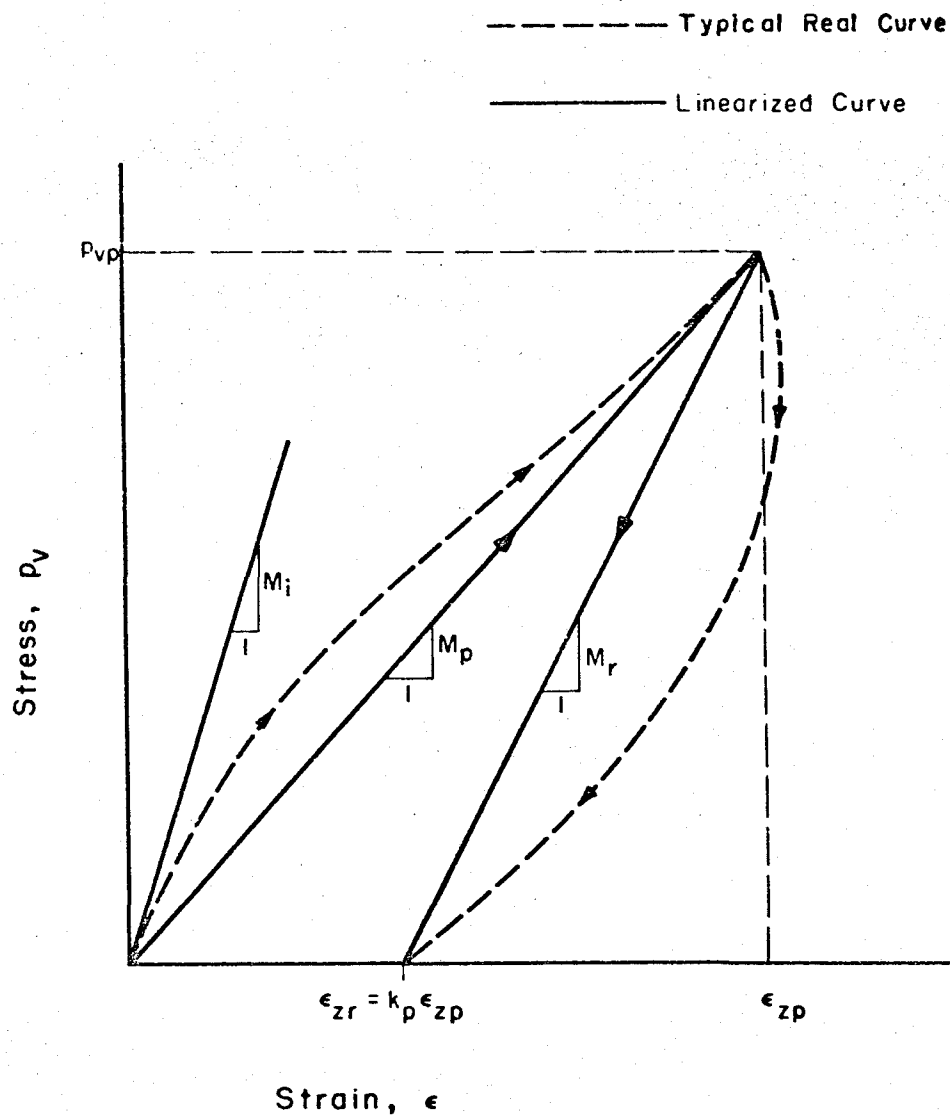


FIG. 4-9 REAL AND LINEARIZED STRESS-STRAIN CURVES FOR SOIL.

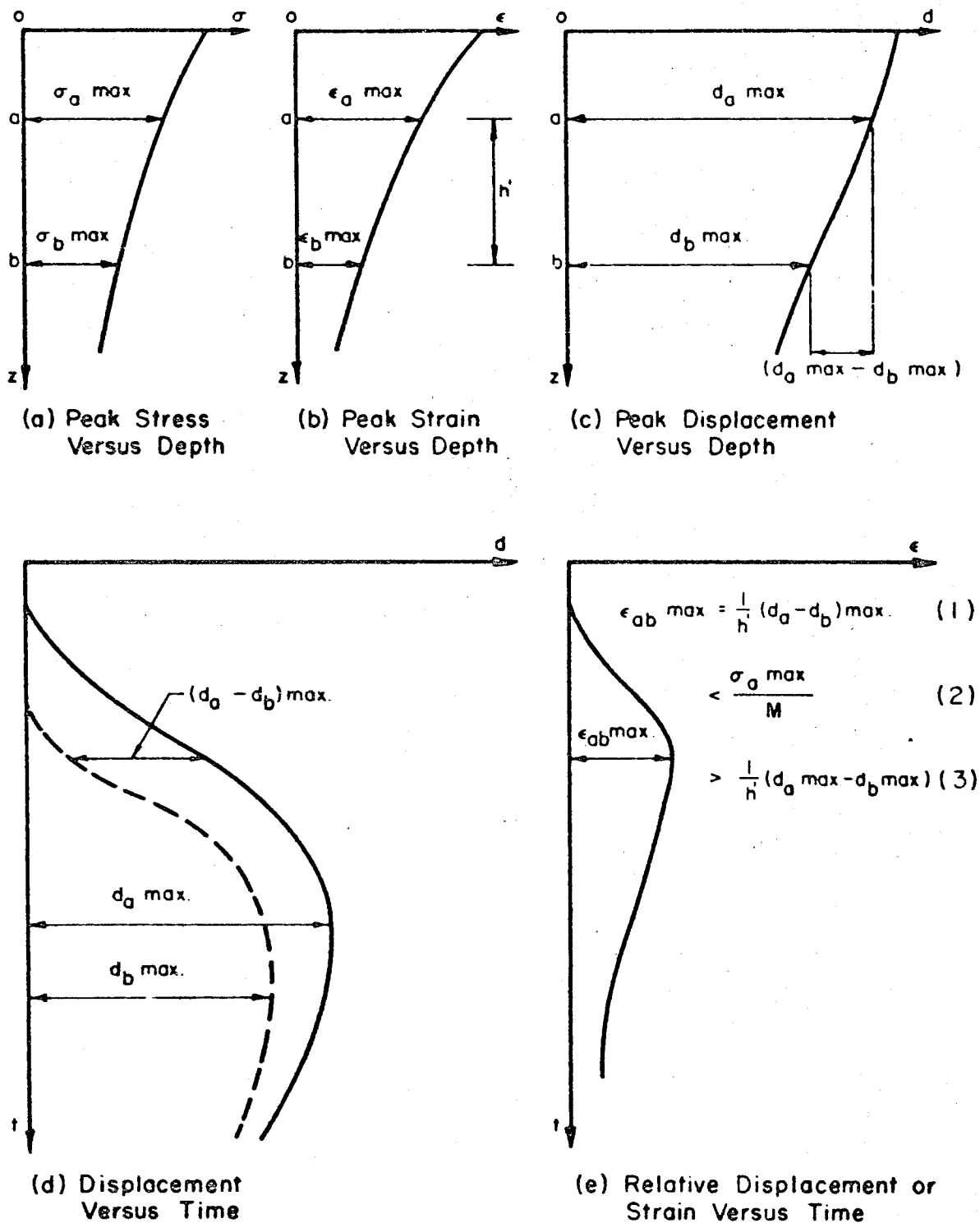


FIG. 4-10 EVALUATION OF PEAK RELATIVE DISPLACEMENT

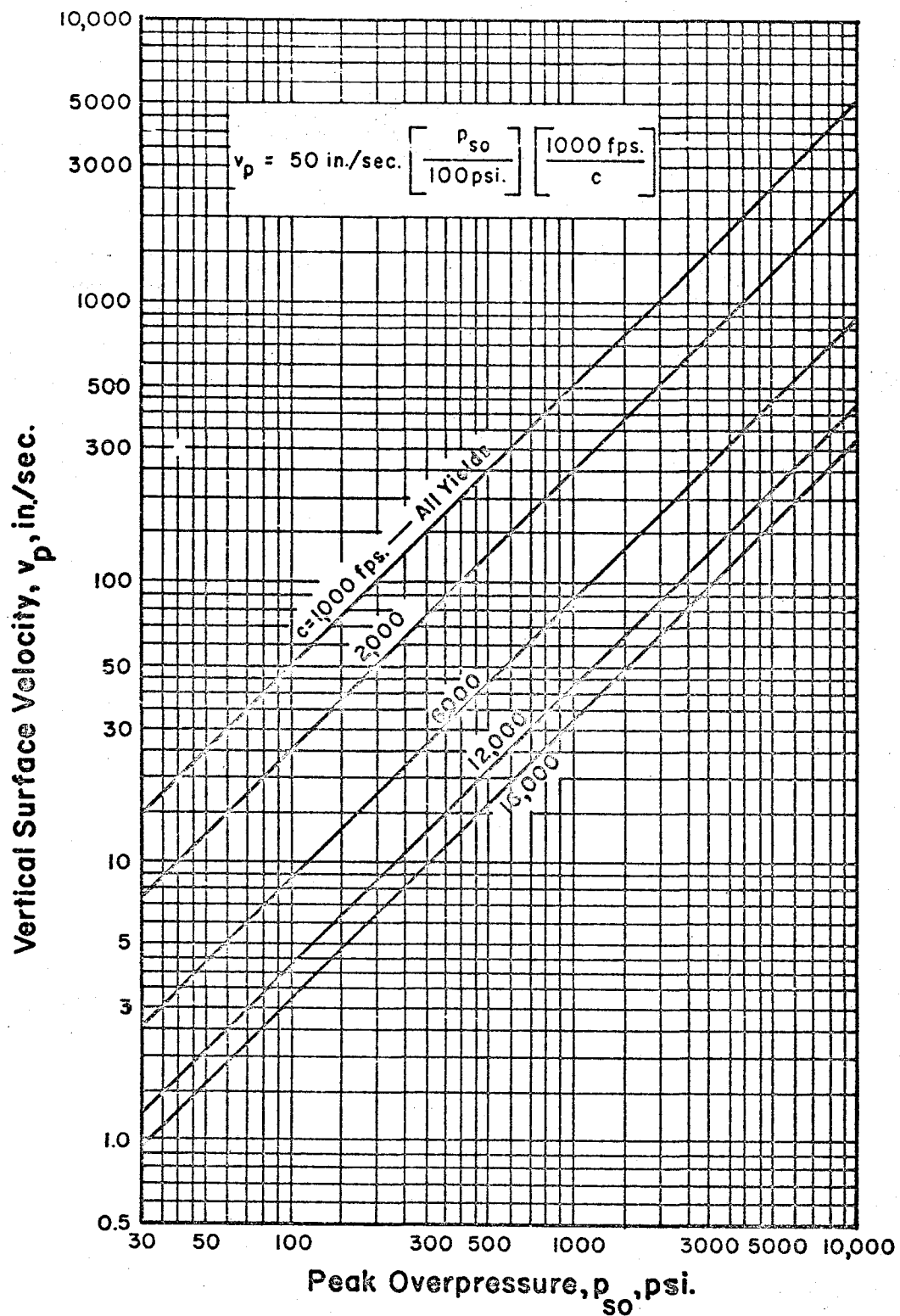


FIG. 4-II AIR-INDUCED SURFACE VERTICAL VELOCITY

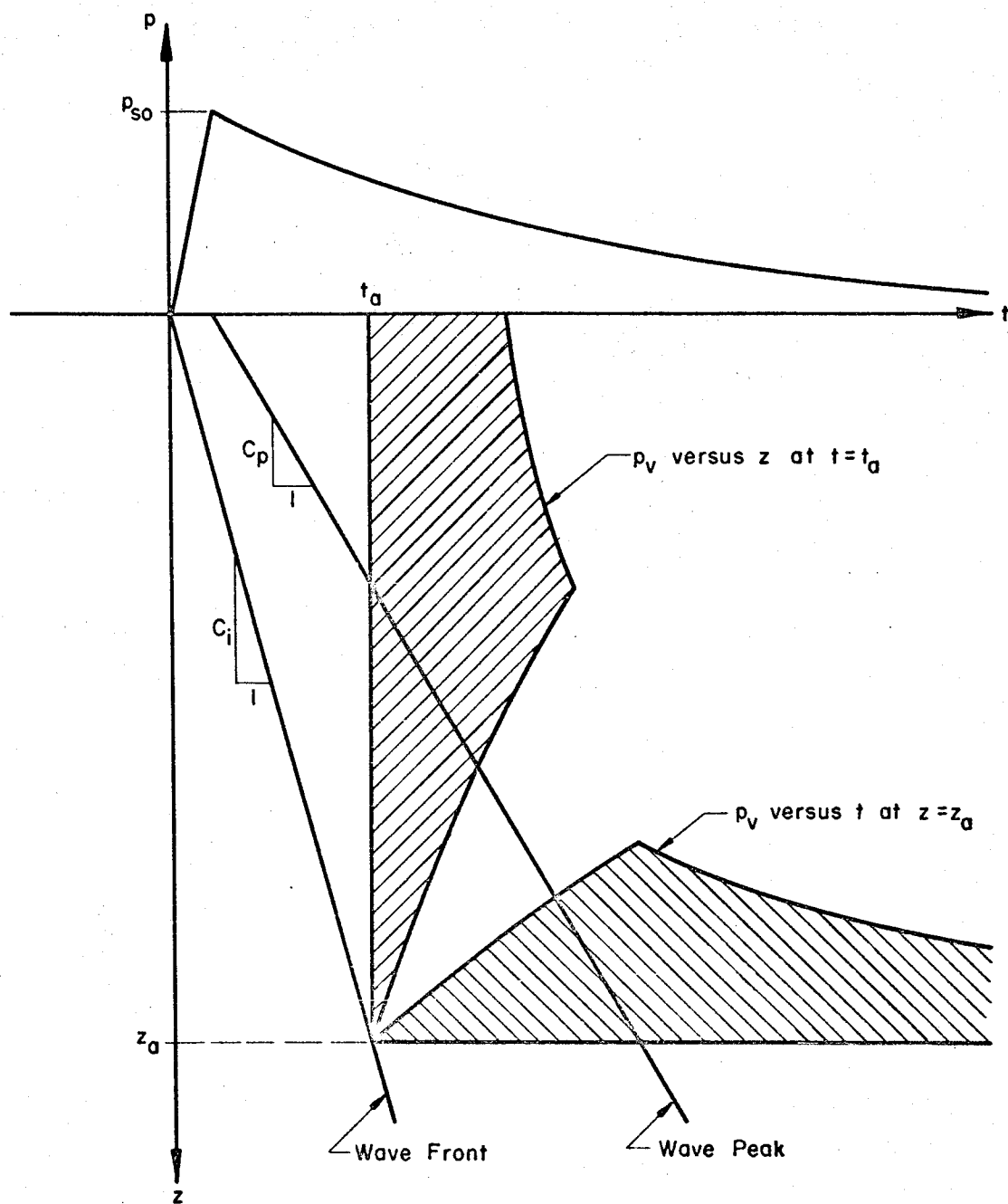


FIG. 4-12 CHANGE OF WAVE FORM WITH DEPTH.

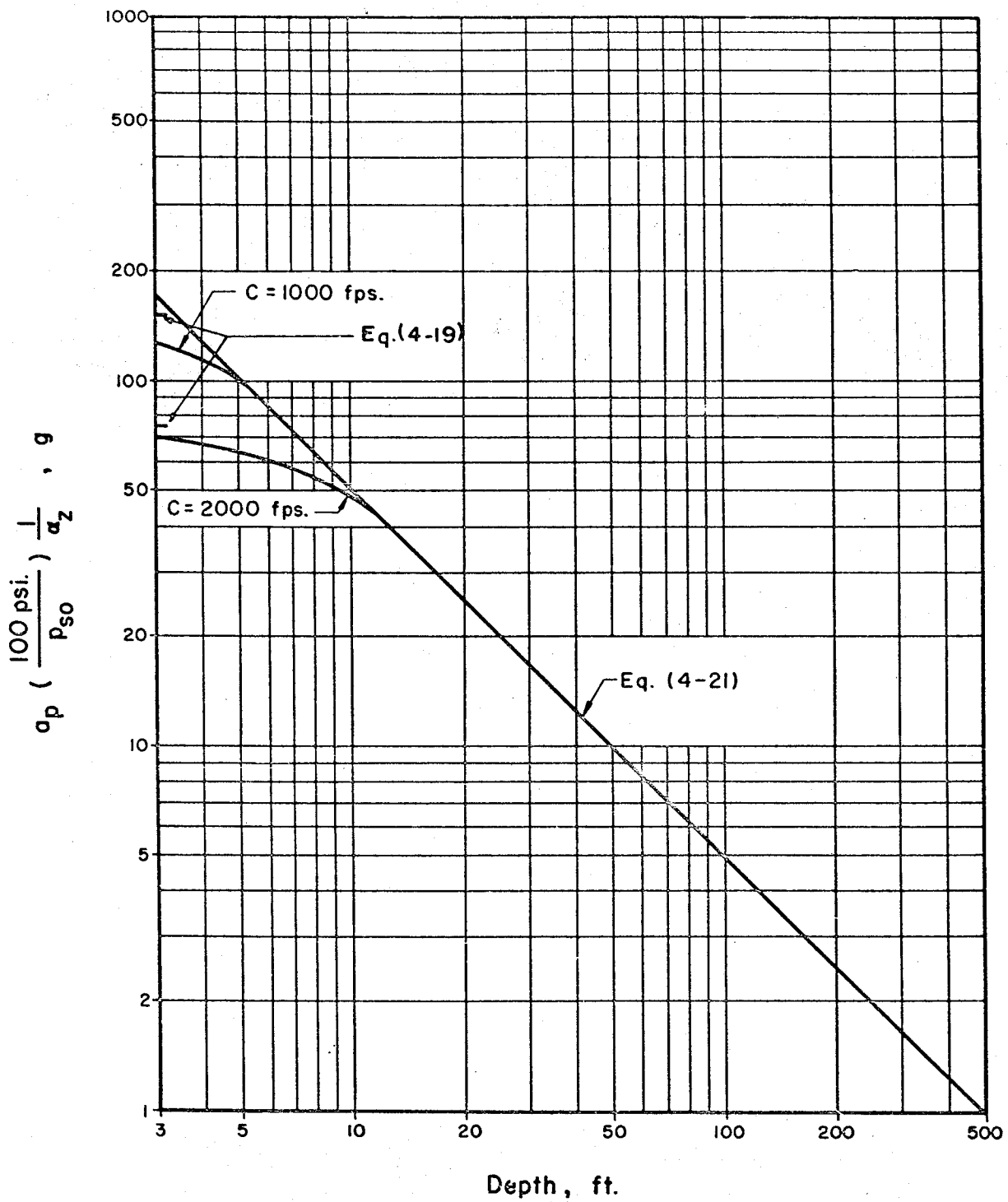


FIG. 4-13 VARIATION OF PEAK PSEUDO ACCELERATION WITH DEPTH

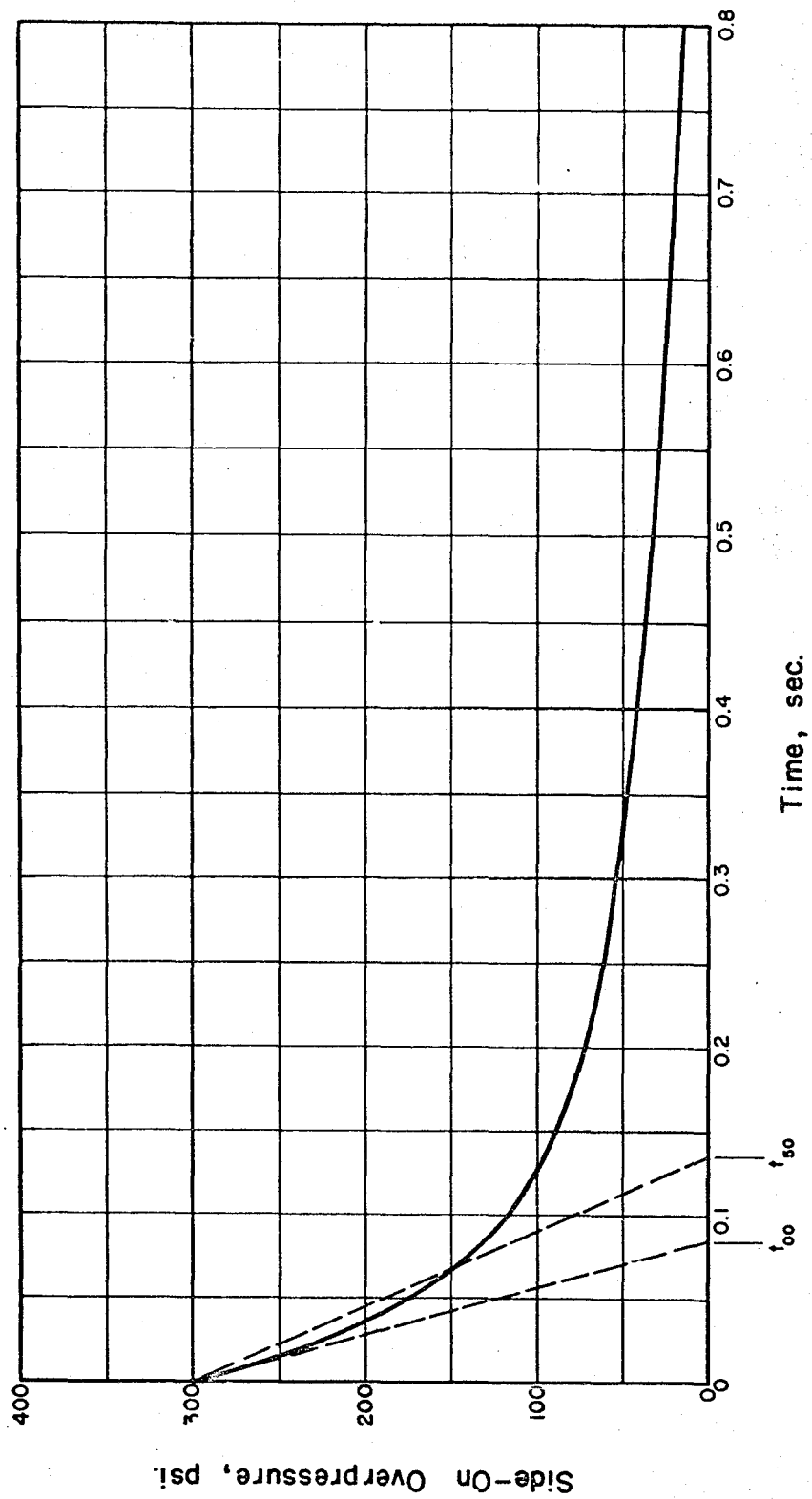


FIG. 4-14 OVERPRESSURE-TIME VARIATION FOR EXAMPLES OF DISPLACEMENT COMPUTATION.

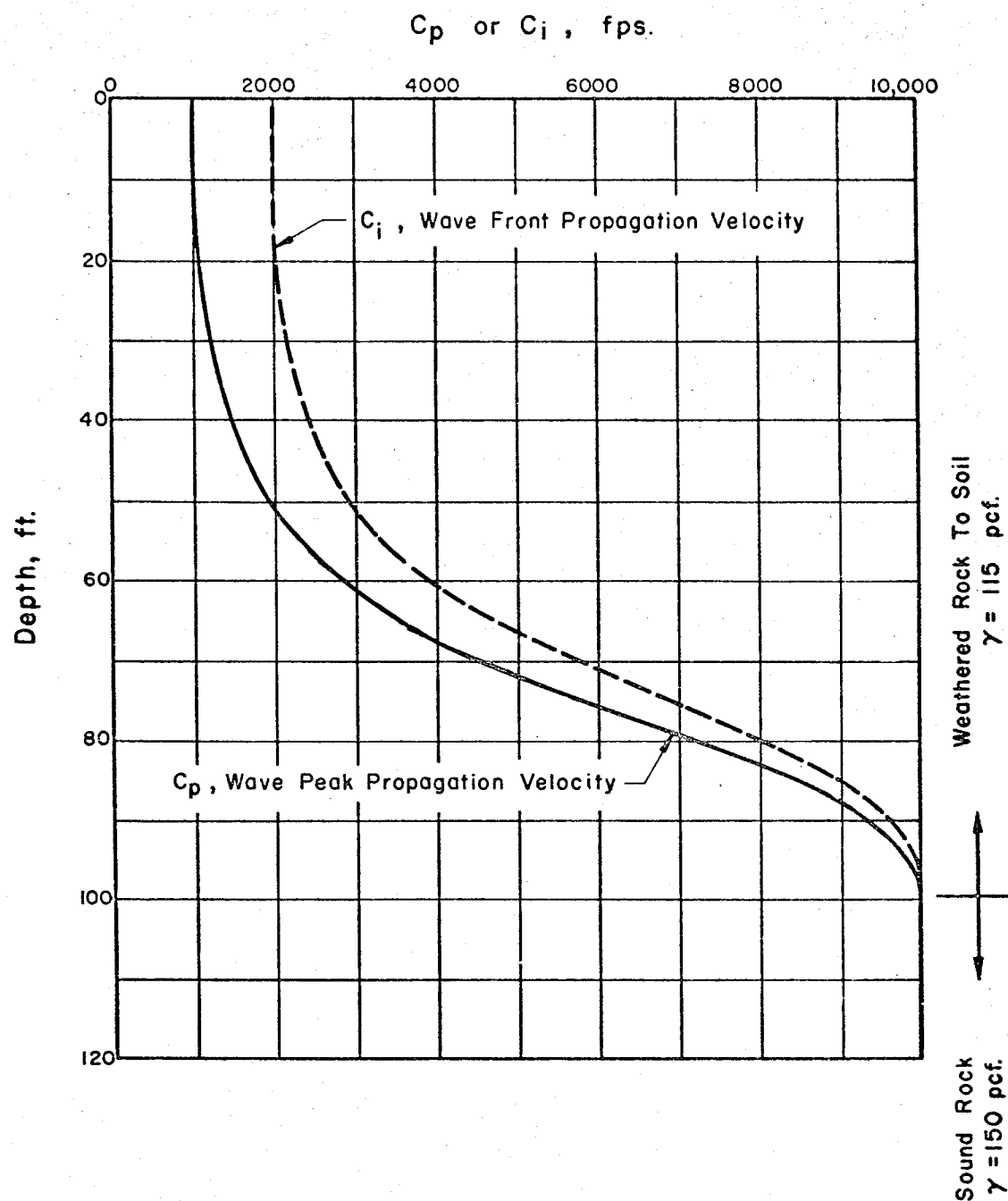


FIG. 4-15 SOIL PARAMETERS FOR EXAMPLES OF DISPLACEMENT COMPUTATION.

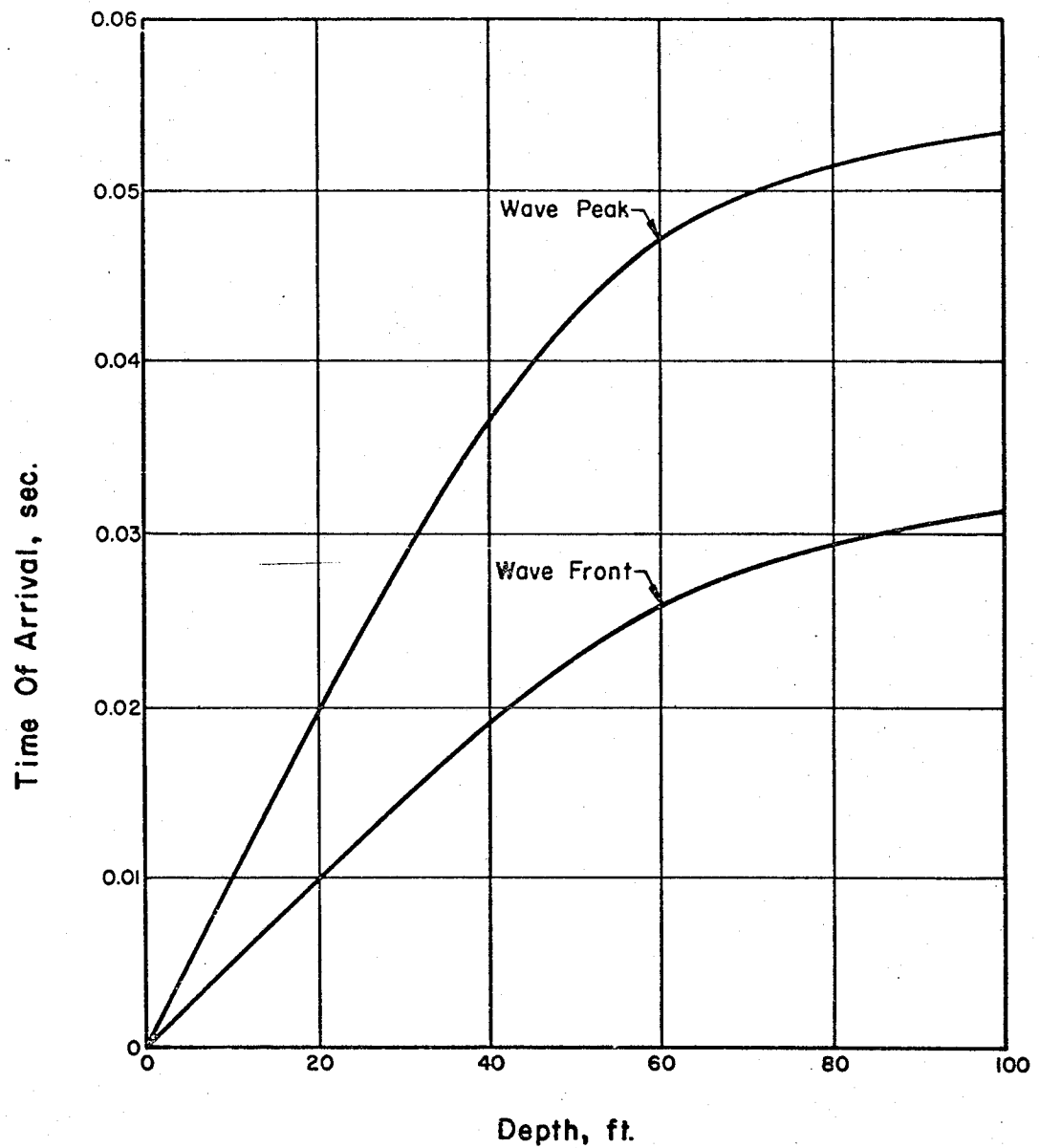


FIG. 4-16 WAVE FORM ARRIVAL TIMES FOR
EXAMPLES OF DISPLACEMENT
COMPUTATION.

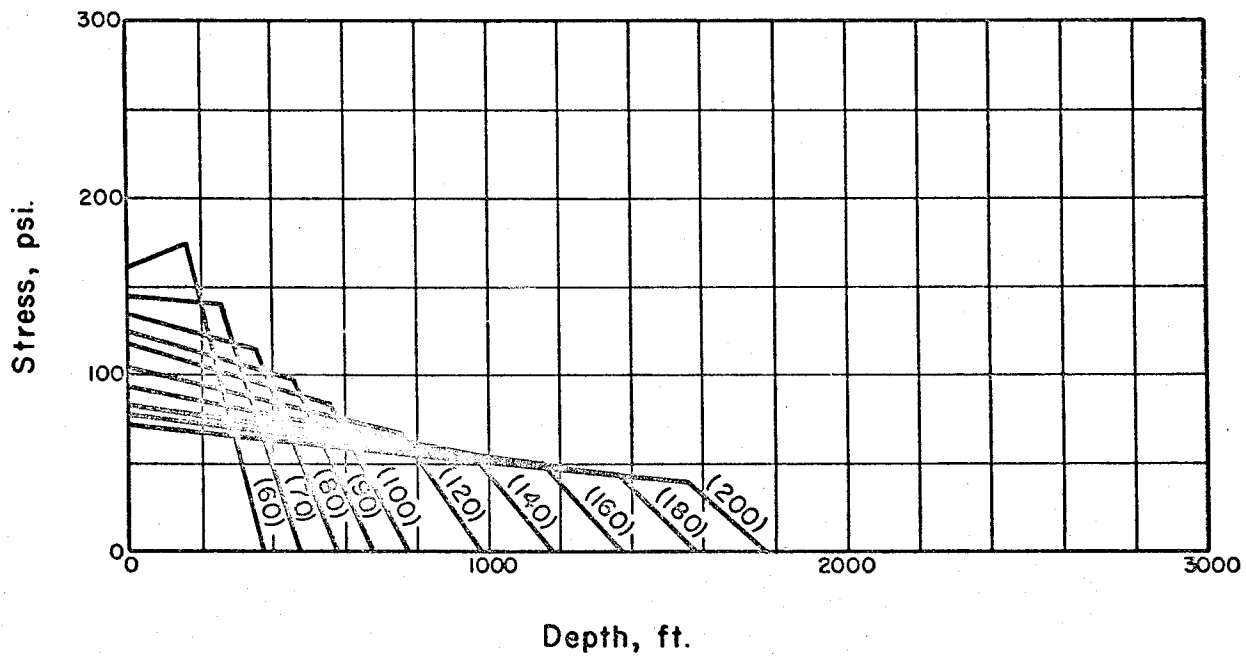
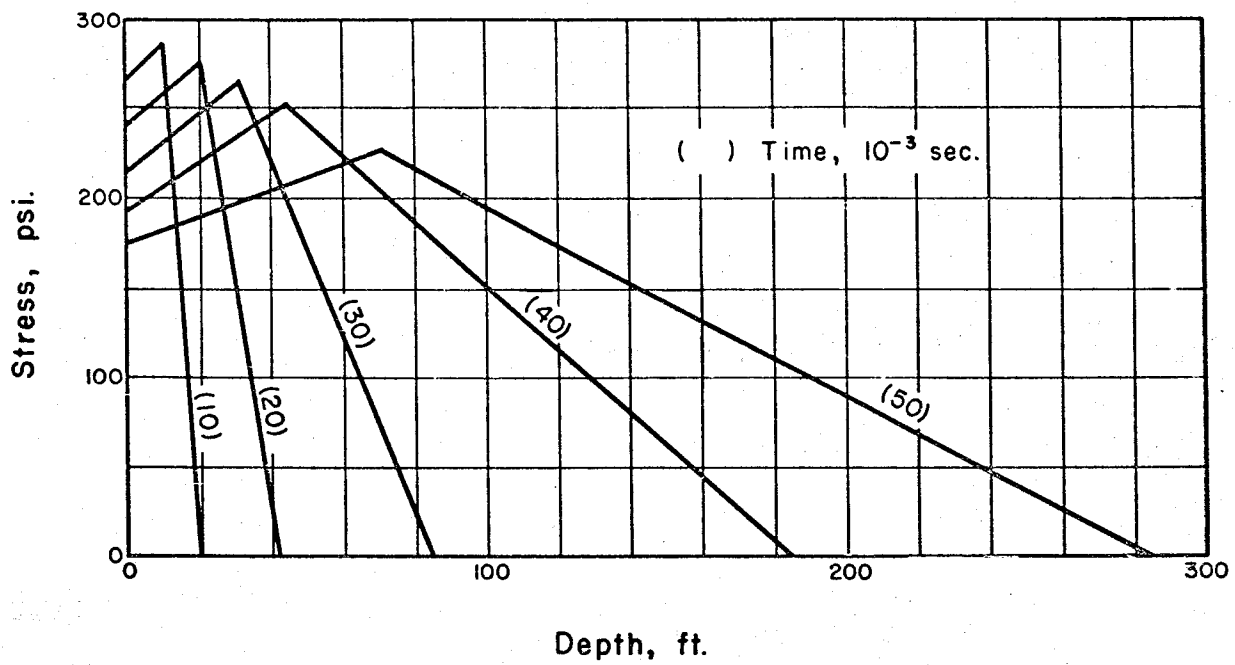


FIG. 4-17 WAVE FORM IN GROUND AT VARIOUS TIMES

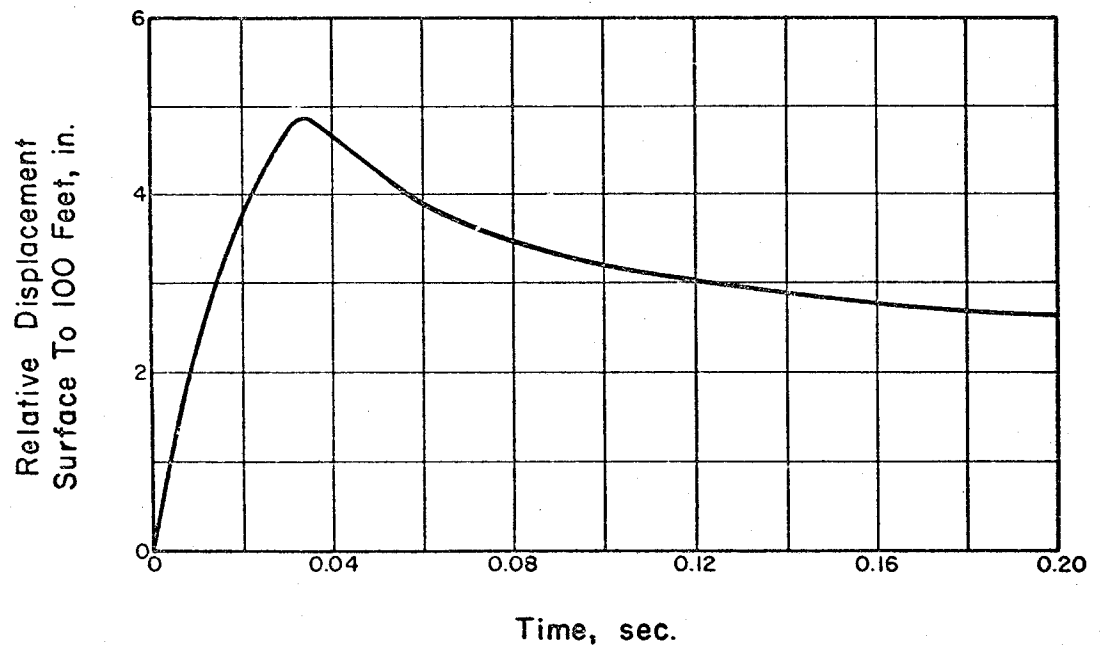
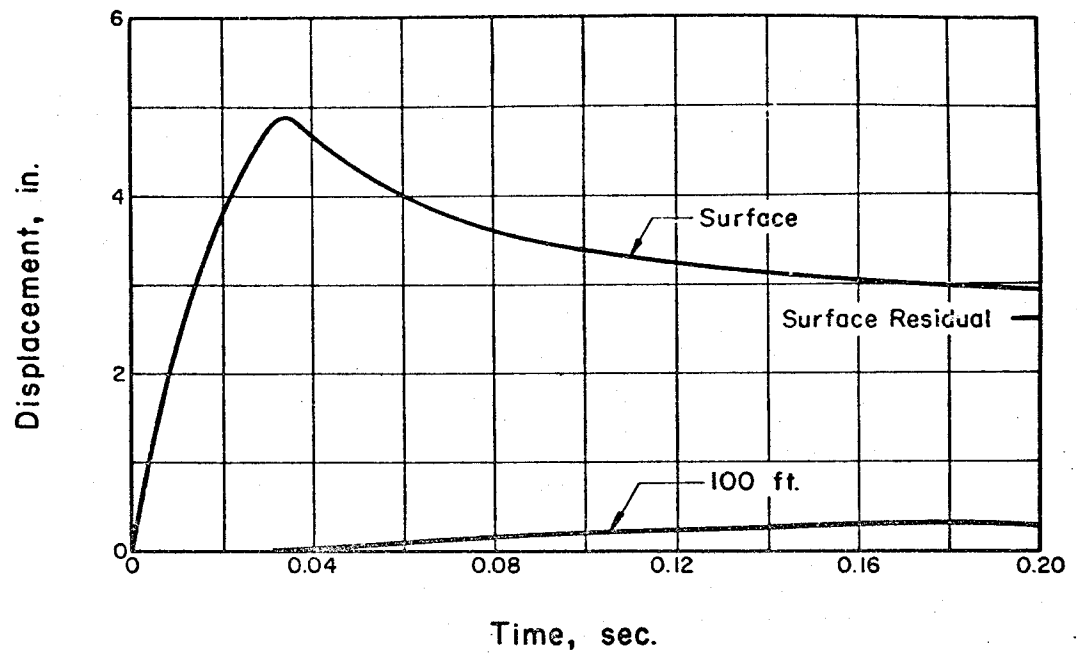


FIG. 4-18 DISPLACEMENT—TIME CURVES

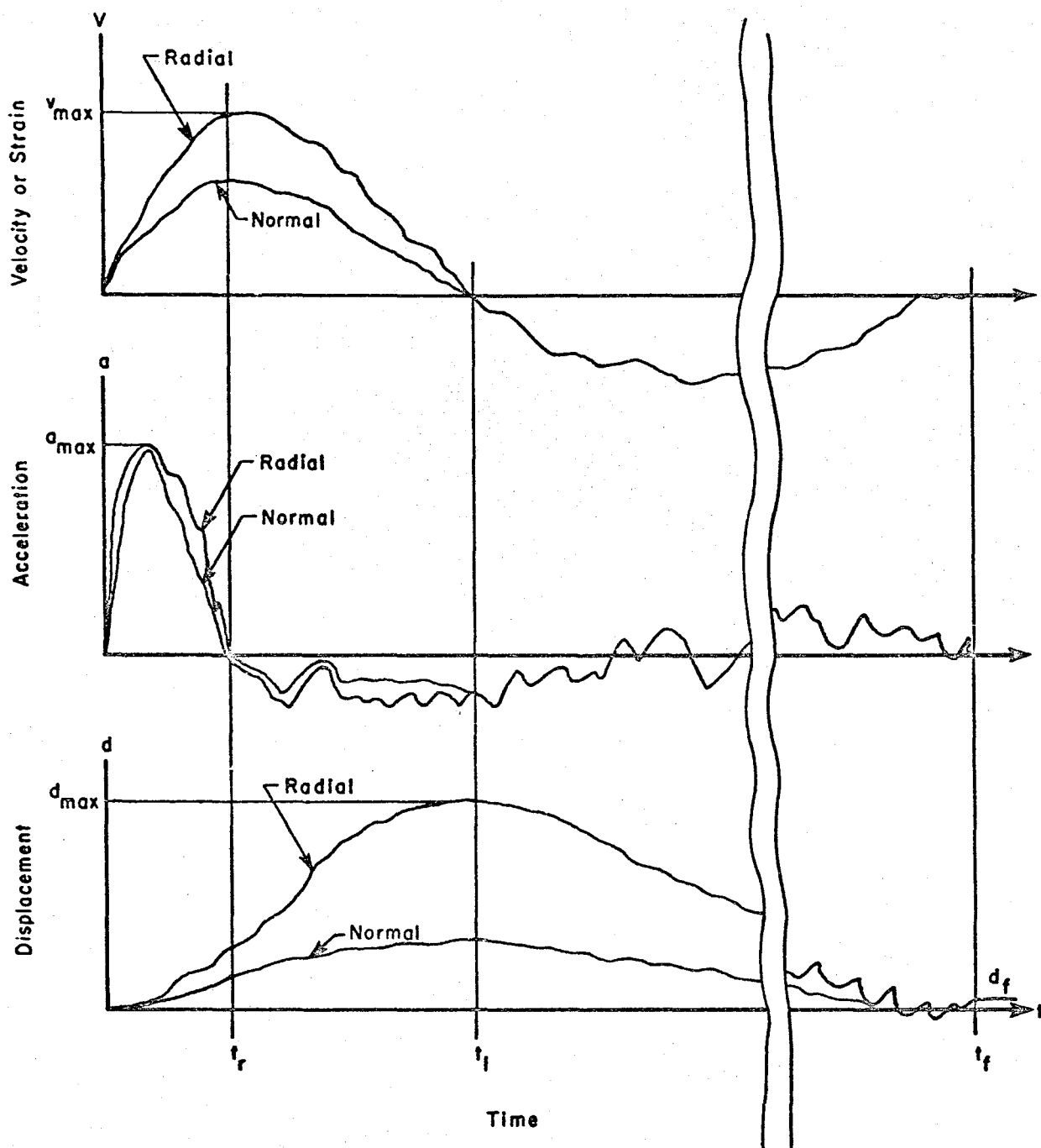


FIG. 4-19 TYPICAL WAVE FORMS FOR DIRECT-TRANSMITTED GROUND SHOCK. (From Ref. 4-3)

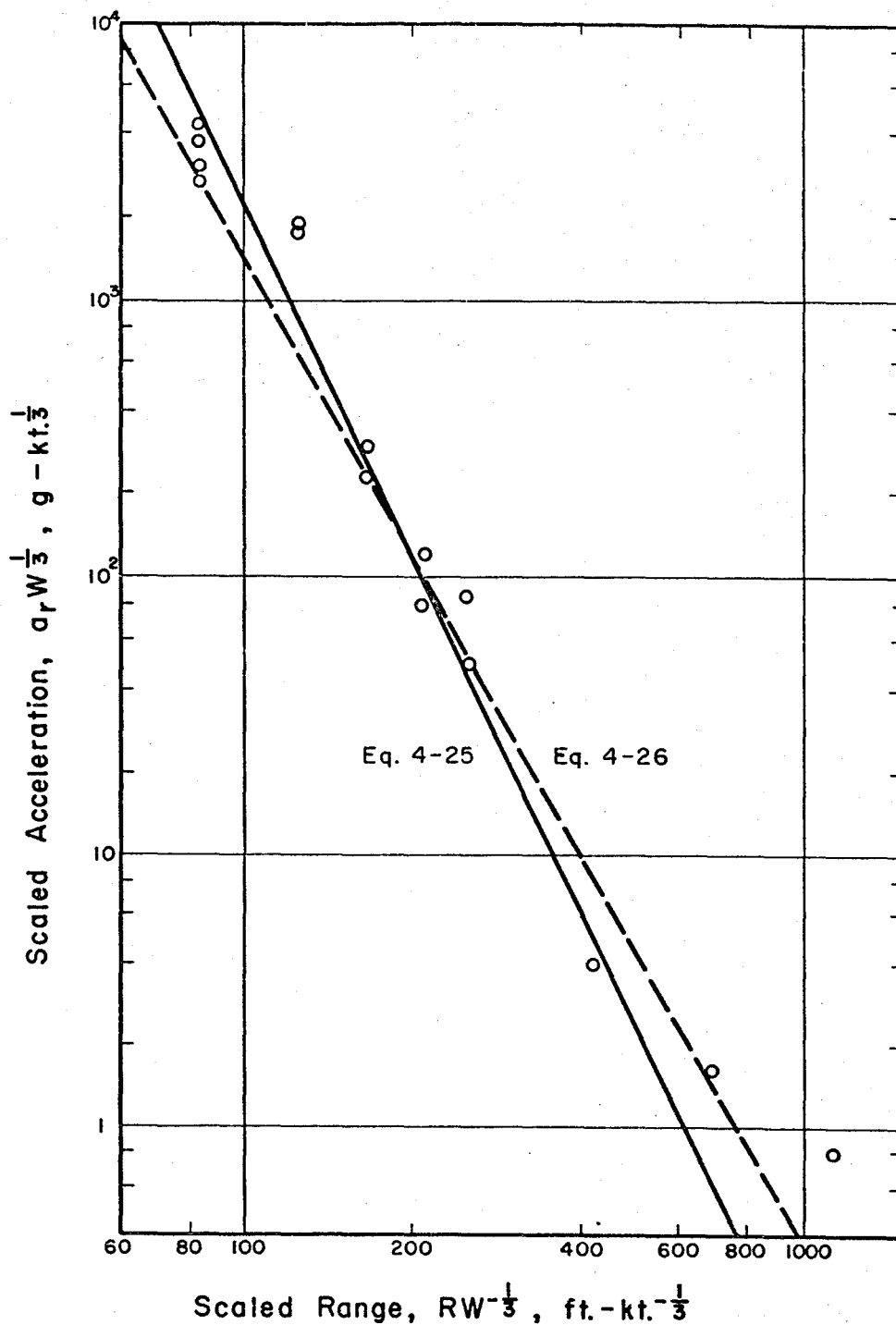


FIG. 4-20 PEAK RADIAL ACCELERATION VERSUS RADIAL RANGE ON A HORIZONTAL RADIUS — BURIED NUCLEAR TEST IN TUFF. (From Fig. 4-1 Of Ref. 4-30)

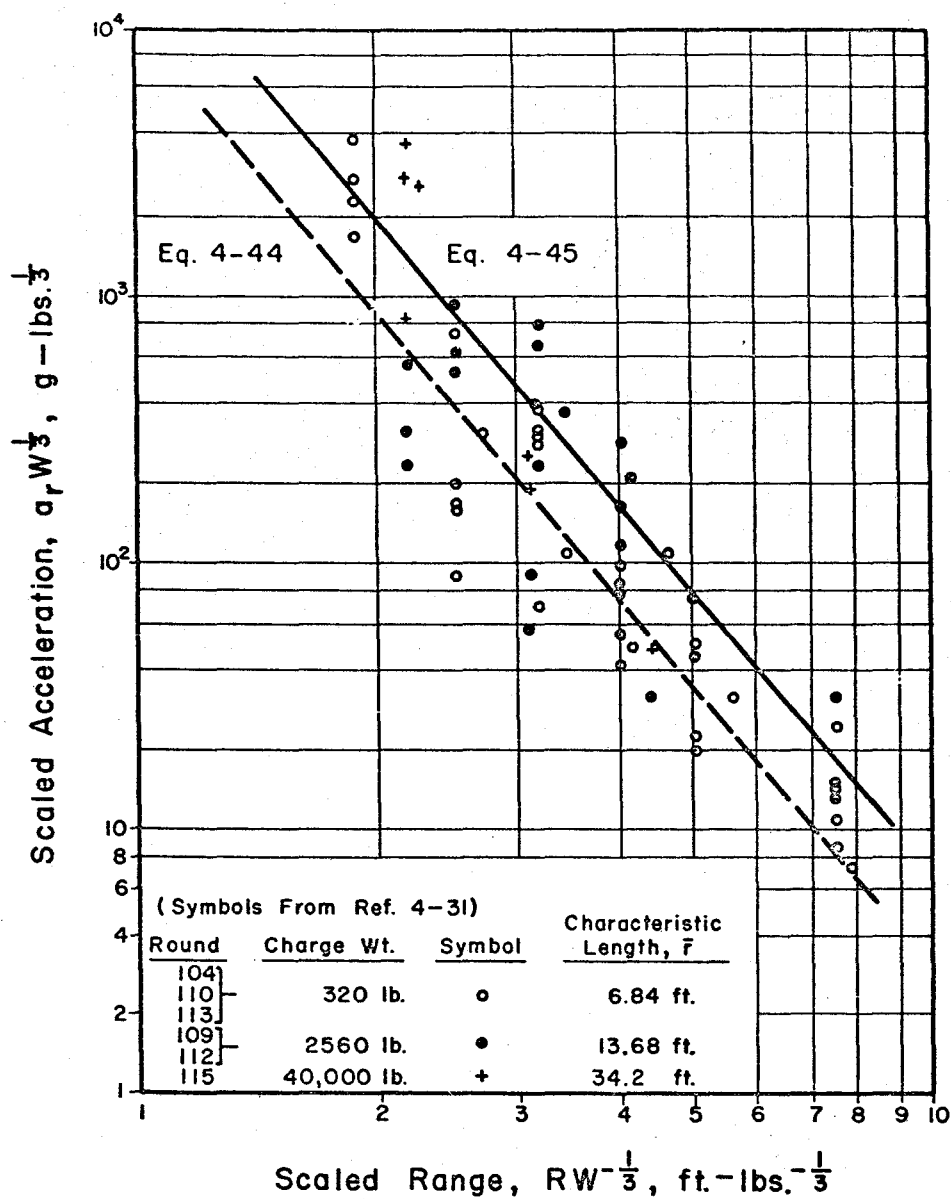


FIG. 4-22 PEAK HORIZONTAL ACCELERATION
 SCALED TO CHARGE SIZE FOR ROUNDS
 WITH SCALE CHARGE DEPTH OF 0.51—
 DRY SAND — BURIED HE. (From Fig.
 2-39, Ref. 4-31)

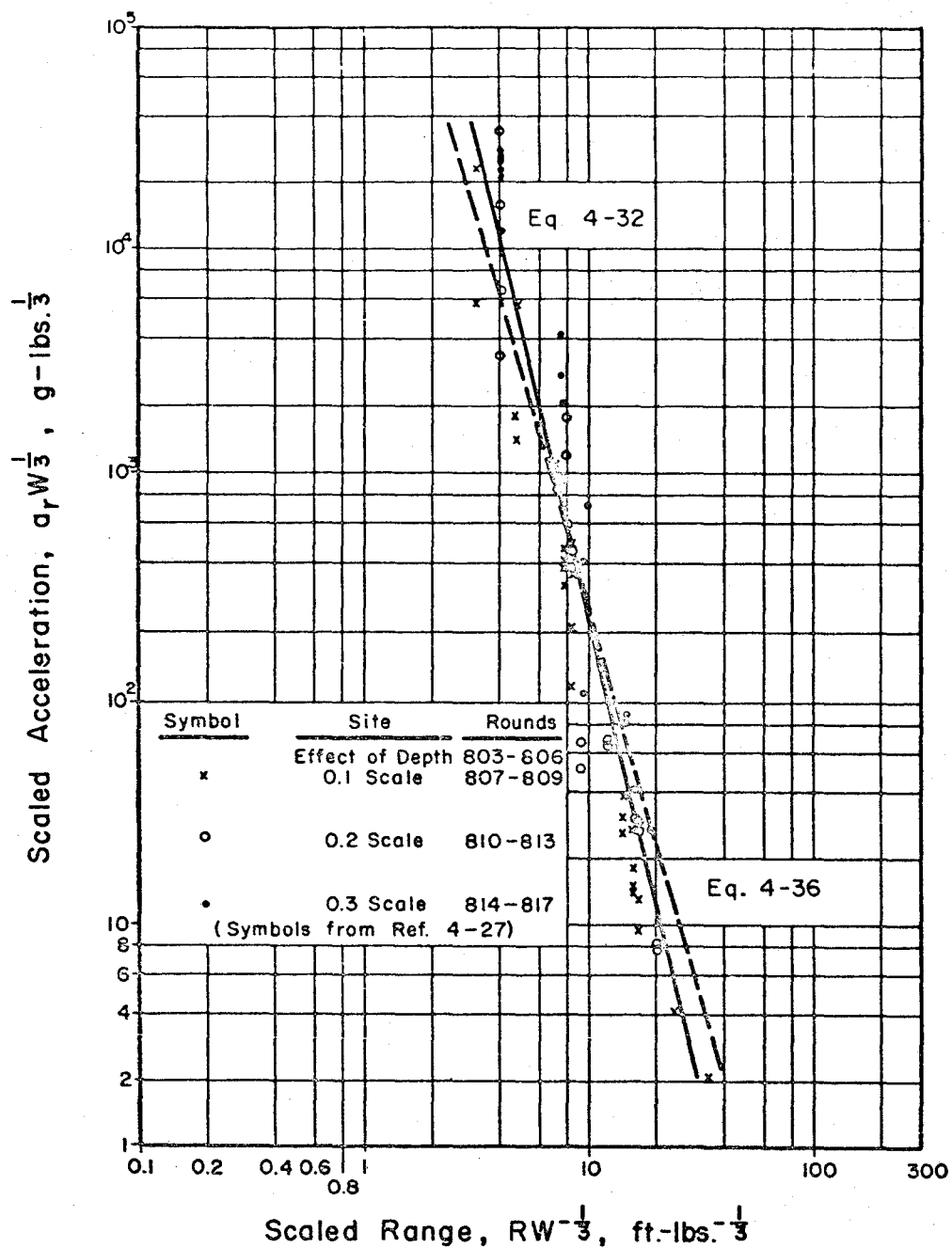


FIG. 4-21 VARIATION OF PEAK HORIZONTAL RADIAL ACCELERATION SCALED TO CHARGE SIZE WITH DISTANCE SCALED TO CHARGE SIZE — BURIED HE TEST IN SANDSTONE.
(From Fig. 3-5, Ref. 4-27)

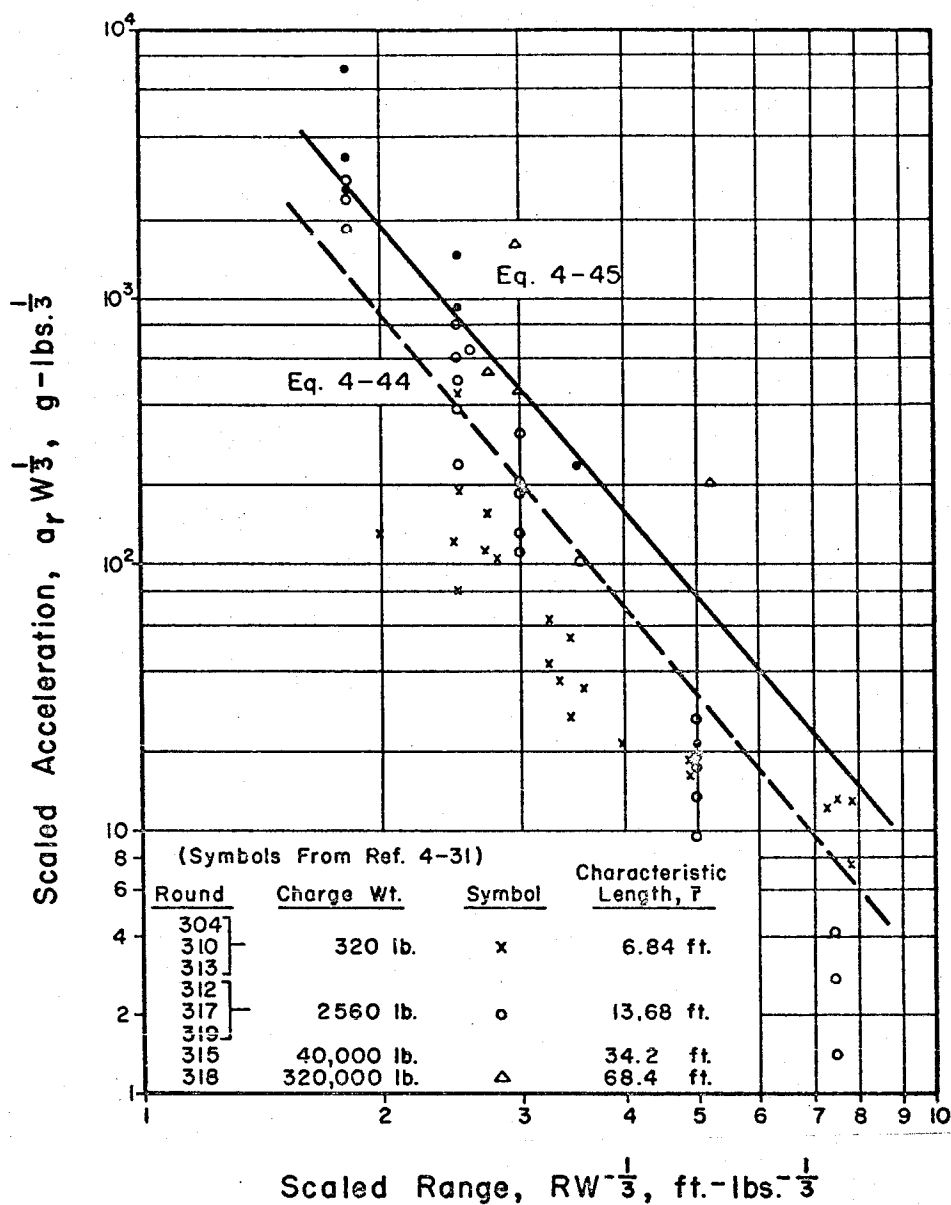
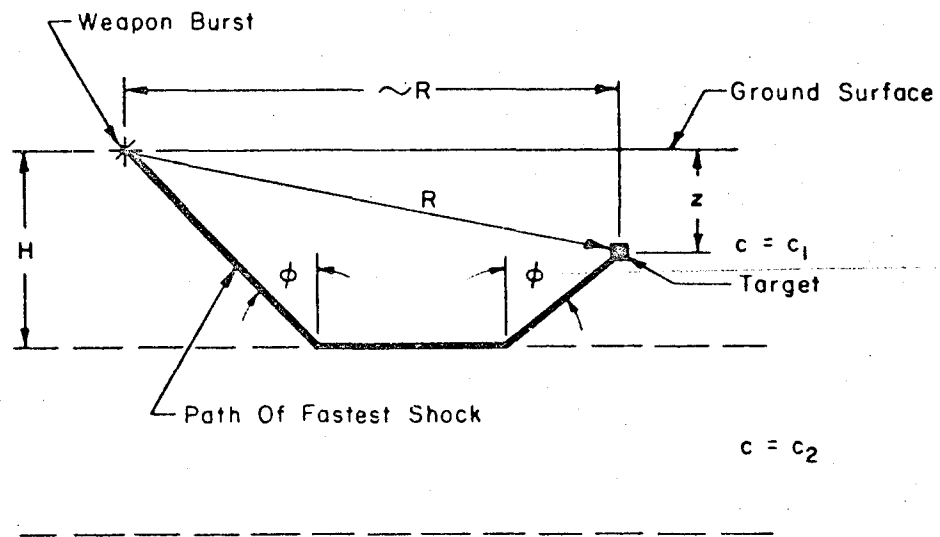


FIG. 4-23 PEAK HORIZONTAL ACCELERATION
 SCALED TO CHARGE SIZE FOR ROUNDS
 WITH SCALE CHARGE DEPTH OF 0.51 —
 DRY CLAY — BURIED HE. (From Fig.
 2-40, Ref. 4-31)



Note:

- (a) R Is Much Greater Than $2H$, or
- (b) If Target Is In Faster Layer, Use $\bar{c} = c_2$

FIG. 4-24 DIRECT SHOCK TRANSMISSION IN A TWO-LAYERED SYSTEM

CHAPTER 5. DETERMINATION OF LOADS ON STRUCTURES

5.1 INTRODUCTION

In addition to the normal dead loads and live loads for which conventional structures must be designed, protective structures must resist forces which may be imparted to them as a result of a nuclear explosion. This chapter is devoted to a discussion of the nature of the blast-induced forces which a protective structure may be expected to experience. These forces usually will be much larger, perhaps by several orders of magnitude, than the conventional dead and live loads; however, there are exceptions. In any event, the total force for which a structure should be designed must include the usual dead and live loads in addition to the blast forces. It is assumed herein that the procedures for determining dead loads and normal live loads are familiar to the reader; consequently, this chapter will, with minor exceptions, be restricted to considerations of blast-induced forces.

The nature of the forces produced on a structure by a nuclear explosion depends on a multiplicity of factors, principal among which are the following: (1) the location of the structure with respect to ground surface - completely above ground, completely buried, or partially above ground and mounded with earth; (2) the geometrical configuration of the structure - rectangular, arched, domed, or a framework; (3) the orientation of the structure with respect to the direction of shock propagation; and (4) the location of the structure with respect to the point of detonation of the weapon.

For structures either partially or completely below ground, additional factors must be considered. Included among these are: (1) the shape of the earth surface above the structure; (2) the depth of earth cover over the structure; (3) the type of soil in which the structure is placed and the location of the water table; (4) the flexibility of the structure relative to that of the soil in which it is placed, and (5) the construction methods (particularly the backfill procedures) employed in the erection of the structure.

It should be noted here, and it will be emphasized repeatedly throughout this chapter, that our knowledge of the nature of the forces produced on structures by a nuclear explosion is still incomplete. This is particularly true of buried structures for which, to define correctly the nature of the blast loading, it is necessary to understand the complex interaction of the structure and the blast-loaded soil in which it is placed. For such structures, even though there has been a substantial amount of both theoretical and experimental research directed toward this problem, it is still necessary in many instances to rely heavily on the judgment of men who have accumulated a substantial background of experience in this area.

The loading recommendations given herein are, to the fullest extent possible, based on the results of theoretical studies and field and laboratory test observations. In those cases where the recommendations are based primarily on judgment, this is indicated.

5.2 ABOVE-GROUND STRUCTURES

5.2.1 Introduction. When a structure is placed above ground in

the environment of the air blast wave from a nuclear detonation, time-dependent forces are imparted to the structure. These forces are dependent both in peak value and in variation with time on the characteristics of the overpressure and dynamic pressure in the free-field and the geometrical configuration of the structure. The characteristics of the free-field pressures are treated in Chapter 3 and are not repeated here.

Conventionalized loadings of above-ground structures, including the effects of structural geometry, are presented in considerable detail in a number of publications, perhaps the most readily available of which is The Effects of Nuclear Weapons (Reference 5-1). However, for convenience, these loadings are reviewed herein and the influence of variations in some of the more uncertain, but nonetheless significant, parameters is discussed.

For any given set of free-field overpressure and dynamic pressure pulses, the forces imparted to an above-ground structure or structural element can be divided into three general components: (1) the force resulting directly from the overpressure, (2) the force resulting from the dynamic pressure, and (3) the reflected pressure which results when a shock front impinges upon an interfering surface. The relative significance of each of these three components is dependent upon the geometrical configuration and size of the structure or structural element, and the orientation of the structure relative to the direction of shock wave propagation. In this section consideration will be given to the loads for which rectangular structures, frameworks, arches, and domes should be designed when placed completely above the ground surface.

As a matter of interest, it should be noted that above-ground protective structures cannot usually be economically justified at over-pressure levels in excess of about 30 psi. For pressure levels above this value, equal protection can usually be achieved at lower cost by placing the structure in a buried or partially buried configuration. It is, however, recognized that the functional requirements of some installations may well require that above ground structures or above ground portions of underground structures be designed to withstand pressures of several hundred psi.

5.2.2 Completely Closed Rectangular Structures. The completely enclosed above-ground rectangular structure is the structural form and environment for which the blast loading can be defined with the greatest confidence. For design purposes, it is necessary to consider the following three loadings for such a structure: (1) the load on the front, or windward, face; (2) the load on the rear, or leeward, face; and (3) the load on the roof of the structure. Since, in general, the shock may approach the structure from any direction, it is usually necessary that all walls of the structure be designed as though they were windward faces. Consequently, the load on the leeward face is of interest only to the extent that it must be considered in combination with the load on the windward face to arrive at the net translational force on the entire structure.

Windward Face. The conventionalized loading on the windward face of a closed rectangular structure is illustrated in Fig. 5-1(a). It should be noted that the maximum pressure is taken equal to the reflected pressure

determined as discussed in Chapter 3.

For an overpressure pulse which rises instantaneously from zero to its peak value, the rise time to peak reflected pressure on the wall surface can also be taken as zero. However, for a case in which the rise to peak overpressure is accomplished in a finite time, the maximum intensity of reflected pressure as well as the time variation of reflected pressure prior to the attainment of its maximum value is uncertain. The peak reflected pressure can be taken conservatively as that for an overpressure rise time of zero. For a vertical wall surface, the time variation of reflected pressure prior to its maximum value is normally not of particular consequence; it can usually be taken with little error as a linear variation from zero to maximum in a time equal to the rise-time of the overpressure pulse.

The magnitude of the rise-time of the overpressure pulse is ill-defined but, in most instances, is small enough that it can be taken as zero without introducing significant error. An indication of the magnitude of this rise time, as it varies with overpressure level for an ideal pulse is given in Fig. 2-2.3 of Ref. 5-4.

It should be noted that the linear decay of reflected pressure loading from its maximum, as shown in Fig. 5-1(a), cannot be representative of every point on the windward wall surface. Similarly, considerable uncertainty exists concerning the time required for the pressure to decay from the peak reflected value to a value equal to the sum of the overpressure

and drag pressure. As indicated in the figure, it is recommended that this reflected pressure decay time be taken as $3S/U$ where S is the least distance from the stagnation point on the windward surface of the structure to the edge of the structure and U is the velocity of shock propagation of the overpressure pulse. The stagnation point is defined as the point on the surface of the structure most remote from any free edge of the structure. For an above-ground structure with its foundation flush with the ground surface, this would be equal either to the height of the structure or to half the width of the structure, whichever is less.

As mentioned above, this conventionalized reflected pressure loading cannot be representative of all points on the front face of the structure since, after reaching a maximum value, the decay of reflected pressure at any point is dependent on the distance of that point from the free edge of the structure. Consequently, at any given instant of time, it should be possible to plot contours of equal reflected pressure on the front face, such contours increasing in value from a minimum adjacent to the edge of the structure to a maximum at the point of stagnation. The idealization depicted in Fig. 5-1(a) is recommended as a reasonable approximation of the average load on the front face. After the reflected pressure effects have vanished, the load on the windward wall is, as indicated on the figure, equal simply to the overpressure plus the drag pressure.

If the front face of the structure is inclined with respect to the ground surface, the blast wave does not impinge on all elements of the wall surface at the same time; rather, the wave front traverses the wall in a finite time equal to the horizontal projection of the wall divided by the

shock front velocity. The general nature of the loading on such an inclined surface can still be characterized as indicated in Fig. 5-1(a); however, the variation with time during the build-up to maximum pressure as well as the decay from this maximum to the quasi-steady-state condition is subject to a greater uncertainty than exists in the case of the vertical wall surface. It is recommended that, for such a case, the rise time to maximum reflected pressure be taken equal to the transit time of the shock pulse across the inclined surface plus the rise time of the overpressure pulse, which is usually taken to be zero. Similarly, it is recommended that a linear decay from peak reflected pressure to the quasi-steady-state condition in a time interval equal to $3S/U$ be used. S is equal to the distance from the stagnation point to the edge of the surface, such distance being measured on the wall surface rather than along its projection on a vertical surface.

On an inclined surface it should also be noted that the reflection factor, by which the peak overpressure is multiplied to obtain the peak reflected pressure, and the drag coefficient, by which the dynamic pressure is multiplied to determine the drag pressure, vary with the slope of the inclined surface. The influence of the angle of incidence on the magnitudes of these two pressure coefficients is discussed in Chapter 3.

Leeward Face. The conventionalized loading on the rear, or leeward, face of an above-ground closed rectangular structure is depicted in Fig. 5-1(b). No pressure is felt on the rear face until the shock front reaches that point. Consequently, using the same time reference as for the front face, pressure begins to build up on the back face at a time equal to

L/U , the length of the structure parallel to the direction of shock propagation divided by the velocity of shock propagation. At some later time, after the rear face has become completely engulfed in the blast, the pressure reaches a maximum value equal to the side-on overpressure reduced by an amount equal to the drag pressure which acts as a suction in the direction of shock propagation. Since the overpressure pulse does not impinge on this leeward face, there is no reflected pressure. The pressure on the rear face is considered, as indicated in the figure, to build-up linearly in a time equal to $5S/U$ where S and U are defined in the same manner as for the front face. Clearly, the linear variation of pressure with time assumed during this build-up period cannot be real; its actual nature is uncertain. As in the case of the reflected pressure decay on the front face, the assumed linear variation with time is not indicative of any particular point on the rear face. Those parts of the rear face adjacent to the free edges of the structure will first receive the influence of the shock pulse and, as the pressure flows around the structure, the entire rear face is loaded. The pressure variation as shown is recommended as a reasonable average condition to be considered for the entire rear face. It should also be noted that there is some difference of opinion as to the time required for the build-up of pressure on the rear face. The recommended value of $5S/U$ is taken from Ref. 5-2, while Ref. 5-1 recommends a value of $4S/U$.

Appropriate drag coefficients are given in Chapter 3 for computation of the drag loading on the rear face.

For large yield weapons and structures of normal proportions, it is usually satisfactory to ignore the variation in free-field conditions

between the front and rear faces of the structure. To be "correct", one should consider the decrease in free-field overpressure and dynamic pressure consistent with an increase in range equal to the length of the structure in the direction of shock propagation. This decrease is usually so small as to be of no consequence. It should be noted that, for very large structures and for very small weapons, particularly if the overpressure levels of interest are quite high, the change in free-field conditions between the front and rear faces may be significant. In such cases, these variations should certainly be taken into account.

Net Translational Force on Entire Structure. To determine the translational force for which the entire structure must be designed, it is necessary only to add at each instant of time the loading as determined above for the windward and leeward faces. To facilitate this addition, the front and rear face loadings should be plotted to the same time scale. It is usually convenient to use as zero time the instant at which the advancing shock front first contacts the windward wall surface.

Roof Loading. As the shock front traverses the structure, a pressure is imparted to the roof equal at any given time to the magnitude of the overpressure present at that time at any specified point on the roof, reduced somewhat by a negative drag pressure, or suction, associated with the passage of air particles over the surface. The magnitude of this negative drag coefficient varies with pressure level; appropriate values are given in Chapter 3.

Since a finite time is required for the shock pulse to traverse the roof of the structure, it is clear that the rise time to maximum pressure

is something in excess of the rise time of the overpressure pulse. Because of the lateral extent of the roof surface parallel to the direction of shock propagation, the real loading is a complex function of both the location on the roof surface and the time-dependent variation of the overpressure pulse. It is adequate for design purposes to use an average roof loading as depicted in Fig. 5-1(c) which rises linearly from zero to a maximum value in a time equal to the transit time of the pulse across the roof plus the rise time of the overpressure pulse, which is generally taken to be zero. Beyond the maximum, it is equal at all times to the overpressure reduced, as mentioned above, by the negative drag loading. If, as is usually the case, the roof structure consists of separate panels supported on the walls or columns, the lateral dimension used in computing the transit time should be taken as the dimension, parallel to the direction of shock propagation, of the roof panel being designed rather than the entire length of the roof structure.

5.2.3 Above-Ground Open Rectangular Structures. In the preceding section consideration was given to the loads for which a completely enclosed above-ground rectangular structure subjected to an air blast pulse from a nuclear explosion should be designed. If the structure, instead of being completely enclosed, has openings in the walls and/or the roof, the blast-induced forces, though still consisting of the three components of overpressure, drag pressure, and reflected pressure, are substantially modified. The extent to which the loading is modified is dependent primarily on the percentage of the wall surface area that is open, thereby permitting the blast wave to pass through the structure rather than around and over it.

The most significant influence of wall openings is that they permit a build-up of pressure inside the structure; consequently a tendency towards equalization of the overpressure effects on all elements of the structure exists. Clearly, if the percentage of open wall area is very small, the time required for a build up of internal pressure will be so long as to have virtually no influence on the loads for which the structure or its elements should be designed. For such a case, the structure should be designed as a completely closed one. At the other extreme, if the structure consists primarily of open framing, exemplified by the steel frame of an ordinary warehouse, the effect of the wall area becomes undetectable and the entire structure is engulfed both internally and externally as the advancing shock front passes through it. For such a structure, the forces which must be considered in design are those imparted only to the relatively small individual structural elements of the frame.

Between these two extremes there exists a broad spectrum of structural types in which varying percentages of wall area may be considered to be open. On the basis primarily of theoretical studies, as indicated in Ref. 5-1, it has been generally accepted that if the open wall area constitutes less than approximately thirty percent of the gross wall surface area, the structure may be considered effectively as a closed structure and should be designed for the loads as discussed in Sec. 5.2.2. For structures in which the wall openings constitute an area in excess of about thirty percent of the gross wall area, it is similarly recommended that the structure be considered an open structure which should be designed for the loads as discussed below.

Clearly, the distinction between an open structure and a closed structure is somewhat arbitrary; however, it is conservative since the design loadings for a closed structure are substantially more severe than those for an open structure of the same geometrical dimensions and a thirty-percent wall opening is adequate to permit the build up of the internal pressure necessary to counteract the effect of the externally applied overpressure.

The loading on the windward wall elements of an open structure can be determined in the same manner as the loading on the windward wall face of the closed structure if the influence of the structural dimensions on the time variation of the loading components is taken into account. That is to say, the dimension L which influenced the time at which pressure began to build up on the leeward face of the closed structure should, for an open structure, be replaced by the front wall thickness to define the time at which pressure begins to build up on the leeward side of the front wall. Similarly, the dimension S which defines the time required for the peak reflected pressure to decay to the pseudo-steady-state condition for the windward wall of the closed structure, should now be computed as the least distance from the stagnation point of a particular wall element to the edge of that element, be it the edge of the structure or the edge of a wall opening. The net effect of these changes for most structures that can be characterized as "open structures" is virtually to eliminate the effect of overpressure as a loading component on the front wall surface, and to reduce severely the duration of the reflected pressure component, leaving primarily a drag loading equal to the dynamic pressure multiplied by a drag coefficient, the

appropriate value of which can be determined from data given in Chapter 3. For a bare structural frame, the complete neglect of overpressure and reflected pressure as loading components is entirely reasonable.

One rather important difference should be noted at this point between the design of wall elements for completely closed structures and completely open structures. For a completely closed structure, the controlling design loading for a wall always acts on the outside of the wall element, though, as discussed in Chapter 9, consideration must always be given to the possibility of elastic rebound for short duration loadings. For a partially open structure, since the blast wave passes through the structure, the leeward wall will be loaded from inside the structure in somewhat the same manner as the windward wall is loaded on the outside. This is indicated in Fig. 5-2, which was taken from Ref. 5-1 generalized to include a rise time of the overpressure pulse. Consequently, the wall elements of partially open structures should be designed to resist loadings applied in either direction.

The net translational force for which the entire structural frame should be designed can be taken as the summation in time of the loadings on the individual components engulfed by the advancing shock front. For a partially open structure in which the primary elements are the windward and leeward walls, the net translational force can be taken as the sum, in time, of the loads on these surfaces.

For an open structural frame in which, as mentioned before, only the drag loadings on the individual structural elements need be considered,

the net translational force should be taken as the summation in time of the loadings on each exposed structural element including columns, truss members, purlins, girts, bracing elements, etc. To attempt to arrive at the loading in such a rigorous manner would imply greater knowledge of the true loading than really exists. Consequently, it is usually reasonable to determine the net translational force on an open frame structure as being equal to the dynamic pressure multiplied by the total area of all structural elements projected on a vertical plane, multiplied by an average drag coefficient for the structural elements which takes into account the influence of the geometrical shapes of the structural elements. Such a procedure results in a slightly more severe loading than would be obtained if the loadings on each structural element were summed in time to obtain the total loading; however, this effect is off-set at least to some extent by the neglect of spikes of reflected pressure and overpressure experienced by each of the elements as they are engulfed in the shock wave.

There are other factors involved in the determination of the loading on an open structure which have been neglected in the procedure above. Principal among these are the effects of shielding of one element of a structure by another element between it and ground zero. Clearly, if one element is placed against and directly behind another element, the loading on the two elements should be determined as though they were one element. If the distance between the two elements is increased, they begin to experience individual loadings. However, each of these loadings is affected by the presence of the other member. Such interference is particularly noticeable in the reflected pressure and drag loadings.

The drag coefficients recommended in Chapter 3 for use with various structural configurations assume these structural elements to be alone in the path of the advancing shock wave. If the two elements are closely spaced, the shock wave is disturbed and consequently the drag coefficients are modified. Similarly, particularly for the shielded element, if the shock front has been substantially disturbed, reflected pressure effects may be virtually non-existent.

While these effects are known to exist, they have not been sufficiently well defined to permit their inclusion in the determination of loadings on above ground open structures. Fortunately, they are normally of relatively little significance. It has been demonstrated that if the distance between elements in the direction parallel to shock propagation is equal to or greater than approximately 10 times the lateral dimension of the windward element, the effects of shielding become very small and can, therefore, be neglected. In this connection, it should also be noted that in open frame structures the effects of shielding can usually be neglected even though the distance between individual structural elements may be much less than ten times the lateral dimension mentioned above. If the orientation of the structure with respect to the blast propagation direction is changed slightly, these closely spaced elements are no longer arranged in a plane parallel to the direction of shock propagation; consequently, each of them is subjected to the full intensity of the advancing shock front without significant interference by other members.

In the preceding discussion, frequent reference has been made to an open structural frame. Actually, there are few such structures - perhaps water towers, antenna towers, outdoor cranes, and the like.

Practically, there are many such structures existing in the form of ordinary mill buildings which consist of simple structural frames with light, frangible, wall covering. Such wall covering may be of corrugated metal, asbestos, or perhaps unreinforced masonry. Such walls usually are incapable of resisting even very low pressures and are blown off the frame early in the history of loading. In the process of breaking, the wall covering does impart an impulse to the structural frame. In most cases, this impulse is so small that it can be neglected. However, if the wall covering is such that an appreciable impulse is required to fracture it, an estimate should be made of this failure impulse which should then be added at time zero to the drag loading determined for the exposed structural frame.

5.2.4 Above-Ground Arches. The loading on an above-ground arch is similar in many respects to that discussed in Section 5.2.2 for an above-ground rectangular structure. However, because of the curvature of the arch, the angle of the incidence between the advancing shock front and the surface being loaded changes continuously around the arch. This complicates the loading for which an arch must be designed.

Since it is not possible to control the direction from which an advancing air blast wave will engulf the structure, an arch should be designed for the case of the shock front advancing normal to the longitudinal axis of the arch, since this is the orientation for which the loading is most severe.

Design of the end walls should be based on a loading appropriate to the structural configuration of the end walls.

As in the case of a rectangular structure, the load at any point on the surface of an arch is composed of the three components, namely, reflected pressure, overpressure, and dynamic pressure. Brief consideration of each of these components may be appropriate.

As the advancing shock front makes contact with, and passes across the arch, each point on the arch is subjected to a radially applied pressure equal to the overpressure in the shock wave at that particular point and time. During transit of the shock front across the arch, constantly varying, nonuniform radial loads are applied to the arch as overpressure. After the arch has become completely engulfed in the shock wave, the effect of overpressure can be considered in most instances as a uniform radially applied pressure equal to the time-dependent overpressure of the engulfing wave. If the span of the arch is very large and the duration of the overpressure pulse is very small, it may be desirable to take account of the variation with time of the overpressure intensity around the arch.

As the shock wave engulfs the arch, each point of the arch is also subjected to a drag force, the intensity of which is dependent upon the magnitude of the dynamic pressure and the drag coefficient which, in turn, varies from point to point around the arch because of the change in angle of incidence. Consequently, the effect of drag loading on an arch is to produce a nonuniform, time-dependent, radial

pressure around the arch, not only during transit of the shock front, but even after the arch is completely engulfed in the blast wave.

The response of an above-ground arch to reflected pressures is similar to the response to drag loading. As the advancing shock front intersects or impinges on successive points along a circumference of the arch, pressures are increased by reflection, but to varying degrees depending on the angle of incidence between the shock front and the tangent to the arch at the point of interest. Consequently, the effects of reflection are greatest at the base of the arch where the tangent is most nearly vertical, and decrease as the shock front advances to the crown of the arch, at which point the shock front is traveling parallel to the arch surface and, consequently, reflection effects vanish.

Another factor of considerable importance is the general character of the shock front. The simplest loading is that associated with an ideal shock in which the rise to peak overpressure is instantaneous, followed by the theoretical exponential decay. For load pulses in the precursor region, or where there is a significant finite time involved in the rise from zero to peak overpressure, the arch loading is more complex. In such regions the reflected pressure is reduced, while the dynamic pressure, though virtually impossible to predict with confidence either in magnitude or in time variation, is probably substantially increased.

The preceding paragraphs indicate quite clearly, that the "real" load which may be expected on an arch subjected to the effects

of an air blast pressure pulse is an extremely complex function and one which, at present, is incapable of rigorous definition. A very substantial amount of effort has been devoted to the study of this question. Probably the most extensive work is that done by the American Machine and Foundry Company as summarized in Ref. 5-3. Somewhat more idealized loadings of the same general character as those presented in Ref. 5-3 are given in Ref. 5-4 and are reproduced herein as Figs. 5-3 and 5-4.

Design procedures for complex loadings of a form similar to those depicted in Figs. 5-3 and 5-4 have been developed by AMF and presented in Ref. 5-3.

In Ref. 5-5, Newmark and Merritt recommended a highly simplified loading for the design of above-ground arches. The simplified loading has as its basis the assumption that an above-ground arch loaded by a shock wave traversing the arch in a direction normal to its longitudinal axis will respond in two primary modes; namely, a breathing mode consistent with a uniformly applied radial pressure, and an antisymmetrical flexural mode corresponding to a load applied radially inward on the windward side of the arch and radially outward on the leeward side of the arch. The first of these modal loadings, referred to hereafter as the compression loading, is illustrated in Fig. 5-5(a) and is identified as a uniform radial load of magnitude p_c . The second modal loading, identified hereafter as the flexural mode, is an antisymmetrical load of magnitude p_f as illustrated in Fig. 5-5(b). Both of these modal components vary with time as described in the following paragraphs, and as shown in Fig. 5-6.

For the compression mode, Fig. 5-6(a), the uniform radial pressure p_c is assumed to increase linearly from zero to a maximum value of p_{so} , the free-field side-on overpressure, in a time t_r as given by:

$$t_r = (1 - \beta/\pi) \tau \quad (5-1)$$

where τ is the transit time of the shock wave across the structure and β is half the central angle of the arch. At times greater than t_r , the uniform radial component of loading, p_c , is assumed to decay with time in the same manner as the free-field overpressure.

For the flexural mode, the pressure pulse may be considered as consisting of two components - an initial component resulting from the unsymmetrical loads imparted to the arch as the shock wave passes over the arch, and a drag component resulting from the continuing drag loading after the arch has been engulfed by the shock wave. These components are shown in Figures 5-6(b) and 5-6(c). While unnecessary for the above-ground case, the total flexural load has been divided into these two components to facilitate a subsequent discussion of loading on partially buried arches.

The initial component of the flexural mode, $p_{f1}(t)$, increases linearly to a maximum value of

$$p_{im} = \left[(1/2) + (\beta/\pi) \right] p_{so} - \frac{p_{dm}}{2 + 6(\beta/\pi)} \quad (5-2)$$

at a time $\tau/2$ and decays linearly to zero at time $(1 + 3\beta/\pi)\tau$ as shown in Fig. 5-6(c). The drag component of the flexural loading, $p_{f2}(t)$ is

shown in Fig. 5-6(b) as increasing linearly to a maximum value of

$$p_{dm} = (\beta/\pi) C_d p_d \quad (5-3)$$

at a time $(1 + 3 \beta/\pi)\tau$ and thereafter remains approximately equal to

$$p_{f2}(t) = \left[(\beta/\pi) C_d p_d(t) \right] \quad (5-4)$$

where $p_d(t)$ is the time-dependent dynamic pressure defined in Chapter 3, and C_d is the appropriate drag coefficient.

The drag coefficient can be taken as approximately 0.4 for a nearly ideal blast wave when the peak overpressure is less than about 100 psi. For non-ideal wave forms, such as caused by a precursor, the dynamic pressure may be two to three times the theoretical values. These effects are believed to be caused by a combination of air heating by the thermal pulse and the large quantities of entrained dust. It is recommended that C_d be increased to about 1.0 in such cases.

In the simplified loadings recommended by Ref. 5-5, portrayed here in Figs. 5-5 and 5-6, time zero is taken in all instances to be the time at which the shock front first reaches the windward surface of the arch.

The resultant combined flexural loading is obtained as a summation with time of the two loading components p_{f1} and p_{f2} as portrayed in Figs. 5-6(b) and 5-6(c). Thus

$$p_f(t) = p_{f1}(t) + p_{f2}(t) \quad (5-5)$$

For most design cases, the simplified loadings taken from Ref. 5-5 are thought to be reasonable and are recommended here for general

use. The extent of the simplifications involved in this loading are obvious. When, in the opinion of the designer, the circumstances warrant a more rigorous design procedure, it is recommended that recourse be taken in the methods of Ref. 5-3. It should be noted that the loadings used in the procedures of Ref. 5-3, which are of the same general nature as those depicted herein in Figs. 5-3 and 5-4, are a more realistic representation of the real loads to which an above-ground arch will be subjected; however, uncertainties of substantial magnitudes still surround the parameters used to define this more complex loading. Furthermore, the complexity of both the loading and of the design procedure may imply a greater precision in the design than really exists.

5.2.5 Above-Ground Domes. The loads induced on above-ground domes by air blast are similar in their characteristics to the loads induced on above-ground arches. The three-dimensional curvature of domes serves to complicate further the definition of the loading of a particular point on a dome as compared to that of a similarly located point on an arch; however, similar parameters can be used to define the loading.

Reported in Ref. 5-6 are the results of pressure measurements taken on the surface of 50-foot base diameter, 90° central angle, reinforced concrete domes tested in Operation Plumbbob. The measurements taken in these tests are summarized in Ref. 5-3, in which they are used to develop the design loading schemes as given in Section 1.5.1 of that reference. As for above-ground arches, similar definitions of dome loadings, though somewhat more idealized, are presented in unclassified

form in Ref. 5-4. The recommended loadings of Ref. 5-4 are reproduced herein as Figs. 5-7(a) and 5-7(b). Reference to these figures will indicate that these loadings recognize the point-wise variation with time of the pressure on the dome surface. They also take into account the apparently significant influence of the character of the free-field pressure pulse on the loadings imparted to the dome surface; for an ideal free-field pressure pulse, the effect of reflections as the advancing shock front impinges on the windward surface of the dome becomes a significant part of the loading, whereas for the non-ideal free-field pulse the effects of reflections of pressure tend to diminish, or even disappear.

In Ref. 5-5, Merritt and Newmark present, as they did for arches, a simplified design loading for above-ground domes. In this reference, modal loadings for a dome were defined in the same manner as for an arch, as discussed in the preceding section. The compression mode loading is identical to that prescribed for an arch. The recommended flexural mode loading, while varying in time exactly as prescribed for an arch (see Fig. 5-6), takes as its maximum value one-half the maximum value of the pressure locally applied by the shock at the most windward point on the surface of the dome. This maximum pressure is a function of the angle of incidence on the dome surface. Its magnitude is taken equal to the reflected pressure consistent with the overpressure level and the slope of the surface.

A review of the loading schemes outlined above suggests that the loading recommended in Refs. 5-3 and 5-4 is more complex than is warranted by the present state of knowledge, whereas the loading recommended by Ref. 5-5 is perhaps an oversimplification of the real loading. It is suggested that a reasonable design loading may be obtained by modifying the load recommendations of Ref. 5-5 to acknowledge both the latitudinal and longitudinal variations of the load-time function associated with the reflected pressure and drag pressure components of the load. In other words, whereas Ref. 5-5 assumes the flexural mode loading to be uniform inward on the windward side and uniform outward on the leeward side of the dome, it is recommended herein that variations over the dome surface be taken into account.

As in Ref. 5-5, it is recommended that the loading be composed of two parts, one part being consistent with the compression mode of response and the other being consistent with antisymmetrical or "flexural" mode of response. These loadings are illustrated in Fig. 5-8. The uniform compression component of load has a maximum value equal to the free-field side-on overpressure, p_{so} . It has a rise time equal to that given in Eq. (5-1) for an arch, after which the pressure decays with time as does the free-field overpressure.

The unsymmetrical, or flexural, load should vary in time with both latitude and longitude. The surface variation in this loading can be taken as indicated in Fig. 5-8(c) and the variation in time can be

taken exactly as described for the flexural loading component of an arch in Fig. 5-6. As for an arch, it is convenient to split the unsymmetrical loading into two components; one of these components corresponding to the unsymmetrical loading which exists during the transit of the shock front across the dome while the other component corresponds to the continuing force resulting from drag.

The total unsymmetrical loading, $p_f(t)$, is equal to the time-wise summation of the initial component, $p_{f1}(t)$, and the drag component, $p_{f2}(t)$. For a dome, p_{im} , the maximum value of p_{f1} , should be computed as the maximum reflected pressure on the windward part of the dome. Similarly, the drag coefficient, C_d , used to determine the drag loading component, p_{f2} , should be chosen consistent with the slope of the dome surface at its base. The selection of a pressure reflection factor and a drag coefficient consistent with the slope of the dome surface at its springing line is discussed in Chapter 3.

Even though the loading scheme recommended above is a highly simplified approximation of the real loading, it is sufficiently complex to cause some difficulty in design. Recognizing this, design procedures taking into account the nonuniform nature of the flexural mode loading have been developed and are presented in Chapter 8.

5.3 UNDERGROUND STRUCTURES

5.3.1 Introduction. When a structure is located beneath the surface of the ground, the load produced on it by a nuclear explosion

becomes dependent upon the nature of the free-field pressure pulse in the soil in the vicinity of the structure; the type, size, and orientation of the structure; the construction procedures used; the nature of the supports or foundations of the structure; and the depth to which the structure is buried in the soil.

The characteristics of the free-field blast-induced pulse in the soil were treated in Chapter 4 and will not be repeated here. The other factors mentioned above which influence the loading on a buried structure will be discussed in the sections that follow and recommendations will be given for loadings to be used for design purposes.

The blast-induced pressure experienced by a structure that is below the level of the natural ground surface is dependent, among other factors, on the character of the overpressure pulse on the surface of the ground. The dynamic pressure ceases to be of importance since dynamic pressures produce drag loadings only on structures interfering with the motion of the air particles in the shock pulse. As the surface overpressure wave passes over a buried structure, a pressure wave is propagated into the soil. This pressure wave traverses the structure, loading it unevenly and unsymmetrically during transit of the pressure front across the structure. For the structure to deform under such loads, it is necessary that the soil adjacent to the structure also undergo deformation. If the structure is buried deeply enough, the resistance of the soil to such deformation is sufficient to prevent the structure from deforming significantly in flexural modes.

Typical of this situation is a buried arch being traversed normal to its longitudinal axis by a pressure pulse. Even though buried, the windward side of the arch is subjected to load before the leeward side is loaded. Consequently, the windward side of the arch tends to move inward thereby forcing the leeward side outward against the soil. If the leeward side of the arch is to be displaced in this manner, it is necessary that the soil adjacent to it be pushed upward and outward, thereby developing a soil resistance related to the passive soil resistance. If the arch is buried deeply enough, this passive resistance is sufficient to keep the arch from deforming in the manner described. Consequently, though the arch is obviously subjected to unsymmetrical and nonuniform loads, these loads are assumed to be of little or no consequence from a design point of view. This presumes, of course, that the arch does possess the limited amount of flexibility needed to permit the deformations required to develop the passive soil resistance.

Similarly, even after the pressure wave has completely engulfed the arch, the load intensity on the crown of the arch, which would be consistent with the free-field vertical blast-induced pressure at the depth of the crown, would be substantially larger than the pressures exerted at the springing line of the arch, which would be consistent with the horizontal pressure in the soil at a depth corresponding to the depth of the arch foundation. Under such a loading, it would be expected that the crown of the arch would deflect downward, forcing

the arch haunches to deflect outward into the soil. If the depth of soil is sufficient to prevent significant deformations of the arch in this manner, the load distribution around the arch must tend to equalize; then, for design purposes, the nonuniformity of loading can be neglected.

In cases such as those described above, be the structure an arch, dome or of other type, it is assumed that only a uniform pressure consistent with the free-field pressures existing in the soil at the depth of the structure need be considered for design. A structure which is buried deeply enough to meet this criterion has come to be called a "fully buried structure". Only structures meeting this criterion will be treated in this section. Structures buried at shallower depths, or structures located on the ground surface and mounded with earth, are discussed in the following section. The critical depth required to constitute the fully buried case is dependent on the type of structure being considered. Recommendations for these critical depths are given later for each of the structural types considered.

It is difficult to define with confidence and precision the loads for which structures meeting the fully buried criterion should be proportioned even though the loading depends primarily on the uniform free-field soil pressure. This difficulty derives from the fact that, under the influence of uniform free-field pressures, the structure tends to deflect away from the soil adjacent to it causing the contact pressure between the soil and the surface of the structure to be reduced by the

development of arch action in the soil. It is also possible for a very rigid structure surrounded by a very compressible soil that, under the action of the free-field soil pressures, the soil surrounding the structure deforms more than the structure, thereby producing on the structure pressures larger than those existing in the free-field. In a ductile structure, such increased loads, though they may develop, are considered to be relieved by deformation of the structure. Properly designed protective structures should possess enough ductility to prevent this increase in load.

The arching influences on the pressures for which buried structures should be designed are not well understood for the static case and are more uncertain under dynamic loading conditions. This subject is discussed in Section 5.3.2 and recommendations, though admittedly somewhat crude, are given whereby the effects of arching can be taken into account when establishing design loads for buried structures.

Another factor of possible consequence is the build-up, or reflection, of pressure as the underground shock front impinges on the surface of the buried structure. The influences of this phenomenon are also treated in Section 5.3.2.

5.3.2 Soil-Structure Interaction. In its broadest sense, the term "soil-structure interaction" includes all aspects of the complex relationship between the blast-induced free-field pressures in soil and the pressures for which a structure placed in this environment should be designed. Stated most simply, it concerns the extent to which deformations, under load, of a structure or structural element influence or modify the

intensity and distribution of the contact pressures between the structure and the soil adjacent to it.

Some aspects of the general interaction problem are treated in subsequent sections. Specifically, consideration is given, for each of the several primary structural types, to depths of earth cover required to reduce to relative unimportance the sensitivity of a buried structure to the inherent initial dissymmetries of blast loading. Two other aspects of the interaction problem that are not treated elsewhere, but which require discussion, are: (1) reflection of pressure at a soil structure interface, and (2) modification of contact pressure between soil and structure by the development of soil arching.

Reflection at Soil-Structure Interface. As discussed in Appendix C in relation to the propagation of a stress wave across the boundary between two soil strata of different elastic properties, the pressure in the free-field should be changed in intensity when it impinges on the surface of a structure. Specifically, for the ideal elastic case, a reflection, or build-up, of pressure should result when a stress wave in soil comes into contact with a more resistant material such as a structure. The theoretical magnitude of the reflection, as discussed in Appendix C, is dependent upon the relative acoustic impedance, ψ , of the two materials.

Considerable discussion is given to this question in Sect. 20.3.1 of Ref. 5-19 wherein the available data, both theoretical and experimental, were reviewed. Without question, theory indicates that a magnification of the free-field pressure should exist as the pressure wave makes contact with

the structure. Field test data were cited in which pressures on the walls of a buried box substantially higher than those in the free-field were known to have existed. However, Ref. 5-19 theorizes that these higher pressures were probably air blast reflections and are, therefore, not pertinent to the problem being discussed.

Other instances also exist in which measured pressures on the surface of a structure exceeded those in the adjacent free-field; specifically, in Ref. 5-11, several gages on the surfaces of buried arches gave such readings. It is interesting to note, however, that other gages similarly located on the same arches failed to indicate these higher pressures; consequently, these data are considered inconclusive.

Still other test data indicate no such reflections. Of particular pertinence are the field tests discussed in Refs. 5-20, 5-21, and 5-22 in which the pressures experienced by a series of small drums with heads of varying stiffnesses were determined. No significant evidence of reflections of pressure on the drum heads was observed.

Though admittedly uncertain and tentative, and recognizing the inadequacies of available data, the existing evidence is believed to support a conclusion that, despite theory, no significant pressure reflections at soil-structure interfaces exist.

Arching. The redistribution of the free-field stresses around a structure due to the presence of the structure is associated with transfer of stress from relatively flexible areas to relatively rigid areas and is

called "arching". The arching phenomena observed statically may not be the same under dynamic conditions because of differences in both the stiffness and strength of soil and the response of buried structures under dynamic and static conditions.

In considering the behavior of underground structures subjected to blast forces, the flexibility or compressibility of the structure has a major effect on the loading that the structure receives. If the structure is highly compressible (as soft rubber), there is essentially an open hole and the loading that the structure receives is virtually zero. On the other hand, if the structure is very rigid relative to the soil, the loading it receives may be even larger than the free-field pressure. The normal forces which would exist in the free-field without the structure, are transferred around the structure by means of the shearing and compressive resistance of the soil. It is significant that there can be no arching in a material which has no shearing resistance, e.g. water. Hence, arching is essentially a utilization of the shearing resistance of the soils to carry compressive stresses. Therefore, arching is a function at least of the shearing strength of the soil and the flexibility of the structure.

Unfortunately, there is little useful experimental data available that will assist in understanding soil-structure interaction and arching phenomena. A description of the static arching problem is available in Ref. 5-16 by Terzaghi. Some of the initial experimental data from weapons tests were presented in Refs. 5-8, 5-23, and 5-24. A series of tests on small underground drums was directed specifically at the interaction

problem and is discussed in Refs. 5-20, 5-21 and 5-22. A summary of the information available in the literature is presented in a report by Armour Research Foundation (Ref. 5-25). The Armour design approach is described in Refs. 5-9, 5-26 and 5-27; however, it may not be conservative enough for dynamic conditions. A modification of the Armour treatment of arching is presented in Ref. 5-7; the essential features of it are given herein, in many instances, verbatim.

Basic Considerations. Consider the roof of an underground structure which is subjected to a vertical static surface pressure p_s causing the roof to deflect an amount u_0 .

As the deflection takes place it is assumed that slip planes occur in the soil vertically toward the surface above the perimeter of the structure.

Consider the forces on a differential element within the slip planes at a distance x measured vertically upward from the structure (Fig. 5-9).

For vertical equilibrium

$$A_1 \frac{dp}{dx} dx = \tau dx S$$

or

$$\frac{dp}{dx} = \tau \frac{S}{A_1} \quad (5-6)$$

where

A_1 = area of structure within slip planes

S = circumference of structure within slip planes

If the ratio A_1/S is defined as R , Eq. (5-6) becomes

$$\frac{dp}{dx} = \frac{\tau}{R} \quad (5-7)$$

where R has for the following relations:

- (a) When A_1 is a square, $A_1 = L^2$, $S = 4L$, $R = L/4$
- (b) When A_1 is a circle, $A_1 = \frac{\pi L^2}{4}$, $S = \pi L$, $R = L/4$
- (c) When A_1 is a strip of unit width between parallel slip planes,
 $A = L$, $S = 2$, $R = \frac{L}{2}$

L is the horizontal distance between slip planes and is the smaller of the two plan dimensions of the structure.

It is assumed that the horizontal pressure, q , within the soil is always some constant K times the vertical stress, p ; hence

$$q = Kp \quad (5-8)$$

It is further assumed that the variation of the shearing stress along the slip planes at some point x is a function of the displacement u of the differential element. However, it is also assumed to be consistent with the Coulomb theory that the shearing stress τ can never exceed τ_{\max} , where

$$\tau_{\max} = c + q \tan \phi \quad (5-9)$$

and where

c = cohesion of soil

ϕ = angle of shearing resistance

From Eq. (5-8), Eq. (5-9) becomes

$$\tau_{\max} = c + Kp \tan \phi \quad (5-9a)$$

It is further assumed that this maximum shearing stress τ_{\max} does not exist all along the entire slip plane but occurs whenever the displacement u becomes greater than some proportion of the span L . Until $\tau = \tau_{\max}$, it is assumed that the variation of τ with u is linear.

These assumptions yield a stress deformation relationship for τ as given in Fig. 5-10.

It is now assumed that the variation of u with depth is exponential in x or

$$u = u_0 e^{-\beta x/L} \quad (5-10)$$

where

$\beta = \text{constant}$

$u_0 = \text{average uniform displacement of roof (equal to displacement of soil at } x = 0)$

These assumptions lead to a variation of the shearing stress and displacement with depth as shown in Fig. 5-11.

From Fig. 5-11 it should be noted that for the two ranges of u

$$u \leq \alpha L, \tau = \frac{u}{\alpha L} \tau_{\max} \quad (5-11)$$

$$u \geq \alpha L, \tau = \tau_{\max}$$

Hence from Eq. (5-10), Eqs. (5-11) becomes

$$u \leq \alpha L, x \geq x_1, \tau = \frac{u_0 e^{-\beta x/L}}{\alpha L} \tau_{\max}$$

$$u \geq \alpha L, x \leq x_1, \tau = \tau_{\max}$$

Consider now the behavior of the differential element shown in Fig. 5-9 for the two ranges of u

Case 1. $u > \alpha L, \tau = \tau_{\max}$

From Eq. (5-7)

$$\frac{dp}{dx} = \frac{\tau_{\max}}{R}$$

or from Eq. (5-9a)

$$\frac{dp}{dx} = \frac{c}{R} + \frac{K}{R} (\tan \phi) p \quad (5-12)$$

For convenience redefine the new constants

$$A = \frac{c}{R} \quad (5-13)$$

$$B = K \frac{\tan \phi}{R}$$

Equation (5-12) then becomes

$$\frac{dp}{dx} = A + B p \quad (5-14)$$

The solution to Eq. (5-14) is

$$Bx = \log (A + Bp) - \log C_1$$

where C_1 is a constant of integration

Hence

$$A + Bp = C_1 e^{Bx} \quad (5-15)$$

For the boundary condition at $x = 0$ the soil pressure is p_o , the pressure on the structure.

Hence, for

$$x = 0, p = p_o, \text{ and}$$

$$C_1 = A + Bp_o \quad (5-16)$$

Substituting Eq. (5-16) into (5-15) yields

$$A + Bp = (A + Bp_o) e^{Bx} \quad (5-17)$$

or

$$\text{Log } (A + Bp) = \text{Log } (A + Bp_o) + Bx$$

$$\text{Log } \frac{A + Bp}{A + Bp_o} = Bx \quad (5-18)$$

Equation (5-18) gives the variation of pressure with depth for

Case 1 where u is greater than αL and $\tau = \tau_{\max}$.

Case 2. $u \leq \alpha L, \tau = \frac{u_o e^{-\beta x/L}}{\alpha L} \tau_{\max}$

From Eqs. (5-7) and (5-9a) the governing equation for this case becomes

$$\frac{dp}{dx} = \frac{u_o}{\alpha L} e^{-\beta x/L} \left(\frac{c}{R} + \frac{K \tan \phi}{R} p \right) \quad (5-19)$$

From Eq. (5-13)

$$\frac{dp}{dx} = \frac{u_o}{\alpha L} e^{-\beta x/L} (A + Bp) \quad (5-20)$$

The general solution to Eq. (5-20) is

$$\frac{1}{B} \log (A + Bp) = -\frac{u_o}{\alpha \beta} e^{-\beta x/L} + \frac{1}{B} \log C_2 \quad (5-21)$$

where C_2 is a constant of integration.

From the condition at

$$x = 0, \text{ where } p = p_o$$

there results

$$A + Bp_o = C_2 e^{-Bu_o/\alpha \beta} \quad (5-22)$$

Inserting the results of Eq. (5-22) in Eq. (5-21) yields

$$\frac{1}{B} \log \left(\frac{A + Bp}{A + Bp_o} \right) e^{-Bu_o/\alpha \beta} = -\frac{u_o}{\alpha \beta} e^{-\beta x/L}$$

which can be put in the form

$$\frac{\alpha \beta}{Bu_o} \log \frac{A + Bp}{A + Bp_o} = 1 - e^{-\beta x/L} \quad (5-23)$$

Equation (5-23) gives the variation of pressure with depth for

Case 2, where

$$u \text{ is less than } \alpha L \text{ and } \tau = \frac{u_o}{\alpha L} e^{-\beta x/L} \tau_{\max}$$

A typical plot of Eqs. (5-18) and (5-23) for the behavior of the two cases is given in Fig. 5-12.

It is convenient now to introduce the x variable θ such that

$$\begin{aligned}\theta &= Bx, \text{ for Case 1} \\ \theta &= \frac{B u_o}{\alpha \beta} (1 - e^{-\beta x/L}), \text{ for Case 2}\end{aligned}\tag{5-24}$$

θ has a physical significance since it indicates the variation of the pressure with depth, or it may be called an arching factor. Since Fig. 5-12 indicates the two bounds for all possible cases which could exist, the pressure variation with depth must lie between these two curves for a behavior consistent with the previous assumptions.

Introducing the arching factor θ in Eqs. (5-18) and (5-23) yields

$$\log \frac{A + Bp}{A + Bp_o} = \theta$$

which can be transformed to

$$p = \frac{A}{B} (e^{\theta} - 1) + p_o e^{\theta}\tag{5-25}$$

Consider the arching which will take place in a soil which has no cohesion. For this case $c = 0$ and from Eq. (5-13) $A = 0$ and Eq. (5-25) becomes

$$p = p_o e^{\theta}\tag{5-26}$$

where θ is given by Eq. (5-24).

An interesting result can be obtained for the limiting condition of Case 2 for a cohesionless soil. For this situation

$$\theta = \frac{B u_o}{\alpha \beta} (1 - e^{-\beta x/L})$$

which from Eq. (5-10) can be written

$$\theta = \frac{Bu_o}{\alpha \beta} \left(1 - \frac{u}{u_o}\right)$$

As x increases u/u_o decreases, and θ approaches $Bu_o/\alpha \beta$, a constant.

Hence, for deeply buried structures such that x can in fact be large

$$\theta = \frac{Bu_o}{\alpha \beta} \quad (5-27)$$

Since θ is a constant, p is also a constant for large x (see Eq. 5-26).

The important significance of the limiting condition of Case 2 in understanding soil structure interaction is that it indicates that arching is a function of the depth of cover, the soil properties, and the resistance of the structure. It further indicates that for granular soils there is a maximum amount of arching which can occur regardless of the depth of burial at which the structure is located.

For Case 1, which is the other limiting condition, there results for a cohesionless soil

$$p = p_o e^{Bx} \quad (5-28)$$

Hence the surface overpressure which the structure can resist depends on the depth of cover. This implies that arching continues to increase with depth of cover. This is the concept put forth in the Armour theory and

tends to support their statement that the theory is an upper bound.

The two limiting cases are as follow: (1) arching increases very rapidly with depth as indicated by Case 1, (2) arching approaches a constant for Case 2. Practical cases will lie between these limits. However, it is believed that design conditions for dynamic loading are closer to Case 2, based on the results of the tests discussed in Refs. 5-20, 5-21 and 5-22.

Underground Flat Roofs. For a design procedure to estimate the arching on roofs of underground structures, the following is suggested. This procedure is limited to large yield weapons and to conditions which may be considered quasi-static.

Consider the roof on a structure with span length L which undergoes a maximum centerline deflection δ_o due to a uniform roof pressure p_o (Fig. 5-13). This deflection, δ_o , corresponds to the quantity, u_o , as used in Eq. (5-10). Let p_{vp} be the free-field maximum vertical pressure assumed to be constant over the depth h . τ is the shearing force on the slip planes (as illustrated in Fig. 5-13), h the total depth of the structure and H an elevation dimension above the structure.

Let

$L = B$ for a long tunnel of width B

$L = D$ for a square or circular plane structure of
diameter or side D

Take H to be the smaller of the following:

$$h - 0.25L \text{ or } 2L$$

Now assume that the shear displacement of the soil along the slip planes varies over the distance H as shown in Fig. 5-14. From the figure, the

displacement δ_n at some elevation $x = nH$ is

$$\delta_n = (1-n) \delta_o \quad (5-29)$$

where

$$\delta_n = \alpha L$$

and α is a constant taken as 0.02.

Hence,

$$n = 1 - \frac{0.02 L}{\delta_o}$$

n may be neglected in Eq. (5-29) for $\delta_o < 0.02 L$.

From these results the variation of τ is as follows (Fig. 5-15)

$$x \leq nH, \quad \tau = \tau_{\max}$$

$$x \geq nH, \quad \tau = \left[1 - \frac{x-nH}{(1-n)H} \right] \tau_{\max} \quad (5-30)$$

where τ_{\max} is defined by Eq. (5-9a)

Let $\bar{\tau}$ be the average value of τ in Fig. 5-15.

Hence

$$\bar{\tau} = \frac{1}{H} \left(nH + \frac{H-nH}{2} \right) \tau_{\max}$$

$$= \frac{1+n}{2} \tau_{\max}, \quad \text{for } n \geq 0 \quad (5-31)$$

and

$$\bar{\tau} = \frac{1}{2} \frac{\delta_o}{0.02 L} \tau_{\max} \quad \text{for } n < 0 \quad (5-32)$$

Define the difference between p_{vp} and p_o as

$$p_{vp} - p_o = \frac{H}{R} \bar{\tau} \quad (5-33)$$

where $\bar{\tau}$ = the average shearing stress on the slip plane between

$$x = 0 \text{ and } x = H$$

$R = B/2$ for a long tunnel of width B

$R = D/4$ for a square or circular plan structure of diameter or side D . In general, R is the area divided by the perimeter of the structural plan of the structure.

From the above, by substituting Eqs. (5-31) and (5-9a) into Eq. (5-33), it can be shown that the following equation relates p_{vp} and p_o

$$p_{vp} - p_o = \frac{H}{R} \frac{1+n}{2} \left[c + (K \tan \phi) \frac{p_{vp} + p_o}{2} \right] \quad (5-34)$$

provided that, as an approximation, $(p_{vp} + p_o)/2$ is used for p in Eq. (5-9a).

Hence, for $\delta_o \geq 0.02L$, and a cohesionless soil:

$$\frac{p_o}{p_{vp}} = \frac{1 - \frac{1+n}{4} \frac{H}{R} K \tan \phi}{1 + \frac{1+n}{4} \frac{H}{R} K \tan \phi}, \text{ for } n \geq 0 \quad (5-35)$$

Equation (5-35) may be taken as the design equation to estimate the arching effect of the free-field stress; however, in no case should p_o/p_{vp} be taken less than 0.1. K may be taken as K_o given in Table 4-1 of Chapter 4.

For $\delta_o < 0.02L$ use Eq. (5-36)

$$\frac{p_o}{p_{vp}} = \frac{1 - \frac{H}{4R} \frac{\delta_o}{0.02L} K \tan \phi}{1 + \frac{H}{4R} \frac{\delta_o}{0.02L} K \tan \phi} \quad (5-36)$$

Underground Arches. The method described above may be used to estimate the arching effect on underground arches by taking the deflection δ_o as the displacement of the crown downward due to the circumferential strains plus the estimated downward displacement of the footings. The displacement of the crown due to rib shortening may be taken as pr/DE times the rise of the arch, but in no case should pr/DE be more than the circumferential strain consistent with stability of the arch. H for the arch may be taken as the average depth of earth cover over the arch, or twice the arch span, whichever is smaller.

In the above expressions

p = free-field stress

r = radius of arch

D = average thickness of arch

E = modulus of elasticity of arch

Influence of Footing Motions. Little information is available on the design of foundation for structures subjected to blast. A number of research programs are currently in progress to provide information in this area, but it will be some time before the results are generally available. The judgment of a competent foundation engineer must be relied on for numerical results in design.

The usual criteria stated in terms of allowable footing pressure or allowable pile load are not applicable; the soil generally has greater shearing strength or bearing capacity under rapid loading than under static loading. A bearing failure corresponding to overturning of a wedge or cylinder of soil beneath the footing is partly resisted by the inertia of the large mass of soil that must be moved, and this must be taken into account in designing the footings. Moreover, it is important to note that a blast loads a large area of soil nearly uniformly to pressures sometimes considerably greater than those allowed by static design considerations. The presence of this loading affects the bearing capacity for additional load, but not necessarily reduce it. In no case is it necessary for blast loading that the total area of the footings supporting the walls and columns of the structure exceed the area of the roof. At worst, even in a soft soil, the structure can be built as a box with a base slab of the same strength as the roof. If properly designed for the expected blast forces, such a structure will move with the surrounding soil mass, regardless of the blast pressure to which it is subjected.

In many soil materials, the resistance to penetration of the foundations increases with the movement as friction develops in the material. In such cases, if moderate amounts of motion are permissible, no special provision for bearing pressure under dynamic load need be made. Some special studies have been made recently for buried structures to investigate the possibility that the loading imparted to the structure may be reduced appreciably by the foundation motion; if true, foundation movement may serve

to aid in arching. These studies, as yet incomplete, do indicate a beneficial effect from permitting reasonable foundation motions, and partially explain some of the results observed in field tests. These results are only preliminary and until such time as further studies are made, and more data become available, only a qualitative indication of the results, as noted above, is desirable.

5.3.3 Influence of Construction Methods. Generally, two methods of inserting an underground structure into the ground can be defined, namely, cut-and-cover and tunnelling. The following discussion is reasonably independent of the method used. Several of the most important features of construction will be discussed in relation to their effect on the engineering behavior of the completed structure. These features should be considered in the design stage. In addition, the specifications should be written to allow for an expedient solution of anticipated construction difficulties. The design should be made, and construction executed, in relation to the conditions as they actually exist in the field. If the conditions assumed on the basis of the foundation investigation are found to differ from those actually existing, then an appropriate re-evaluation is necessary.

On the face of an excavation, the normal and tangential stresses become zero; some loosening of the surrounding soil occurs because of the inward strain associated with the stress relief. Spalling or raveling may occur because of the stress differences induced by the excavation; this effect generally increases with time after excavation. Additional sloughing may occur because of the loss of apparent cohesion associated with desiccation

of the exposed faces of the excavation. For circular excavations, the soil and/or rock will carry by hoop action some of the stress changes associated with the excavation. However, reveling or drying that causes caving in one area of the excavation may cause progressive caving throughout the excavation. A progressive loosening of the surrounding soil follows the foregoing events.

Experience has shown that earth materials that will ravel or cave should be effectively braced as rapidly as possible. The fact that such materials will stand temporarily after excavation is fortuitous; the stand-up time should be used for placement of the bracing. The loads that a bracing system must carry have also been shown by experience to increase as the inward strain of the soil increases beyond the relatively small amount required for the development of the active earth pressure state. Therefore, the immediate placement of tight bracing will decrease the strength of the bracing required. Further benefits are obtained by not allowing the soil surrounding the excavation to be loosened.

In the subsoil investigation, assumptions will have been made as to the thickness and horizontal extent of the different strata. If structures are located where, there is local stratification, it is desirable that the properties be the same horizontally in all directions. Furthermore, no structures should be located across or near fault zones if it can be avoided. The geologic details should be checked as the excavation proceeds. Conditions other than those assumed beforehand should be noted and appropriate action taken where required. Any geologic detail causing a loss of homogeneity in horizontal directions should be noted. Where blasting is necessary, smooth

wall techniques should be employed. The blasting technique should cause a fracture of the soil or rock only within the zone to be excavated. Blasting techniques should keep overbreak and fracturing to an absolute minimum outside the zone of excavation.

It is necessary that the designers, inspectors, and builders of underground structures to resist blast loading become familiar with the purpose of the structure. The structure and the surrounding soil will be subjected to very large loads and will act together. This is in contrast to the structures with which we are more familiar. Ordinarily a structure must resist only the load of the soil surrounding it. Under blast loads, the soil, which is a structure in itself, must interact with a man-made structure. The construction technique must be such that the desirable properties of the soil medium are retained. Overbreak, fracturing, loosening, lost ground, etc. are factors that must be avoided; either singularly or collectively they can produce a nonhomogeneity that was not considered in the design and that could cause the structure to fail its intended purpose under blast loading.

The final analysis of an underground structure should be performed after construction if the analysis is to have real meaning. All of the effects of construction should be included, preferably analytically, although it is recognized that qualitative reasoning must be used alone in many cases. A construction diary that carefully delineates the soil and rock conditions as they are exposed along with a description of the earth movements that occur is necessary for an intelligent re-evaluation of the hardness of the site at a later date.

Several of the items discussed in the following paragraphs must be considered in the details of design. Many of these items cannot be evaluated quantitatively; therefore, qualitative reasoning must be used. Several of the details are concerned with dewatering, waterproofing and the connection of one structure to another. Of very great importance are the differential motions that may take place between different structures under blast loading.

A loose backfill can lead to excessive settlements under the weight of the backfill alone; negative skin-friction on structures such as missile silos can result. In addition, the negative skin-friction under blast loading will be more severe for loose than for compact backfills. Where electro-magnetic shields are used, negative skin-friction can cause an undesirable rupture at a weld or connection to another structure.

For cut-and-cover structures, the behavior under blast loading will be influenced by the properties of the backfill. Generally, the fill should be compact and uniform in physical properties. It should be brought up uniformly around the structure to avoid the deformations usually associated with structures filled on one side only. In the case of an arch or dome, a non-uniformly built-up backfill can deflect the structure into a buckling mode and thus lead to premature collapse under blast-load conditions.

Improper dewatering has been a major cause of construction difficulties on the present missile sites, although the ground water conditions were adequately defined before construction. Adequate appreciation was not given to the fact that improper dewatering techniques could be harmful to the physical properties of the soil structure itself. In order to maintain

the integrity of the soil structure, it is necessary to anticipate the need for dewatering and to carry out dewatering before excavation proceeds. The technique frequently employed is to attempt excavation and not to bother with dewatering until the need is obvious. Unfortunately, this is much too late if the integrity of the soil structure is to be maintained. If ground water is not controlled, the soil surrounding the structure can be loosened differentially and erosion or lost ground can occur. Furthermore, a small amount of erosion or piping of a pervious layer can lead to overbreak in the overlying layers. Where raveling occurs, backpacking should be employed behind the bracing to maintain a tight contact between bracing and the soil. The hay or straw normally used in backpacking is quite inadequate for the purposes of protective construction. It is necessary that grout or other competent material be used for backpacking; otherwise, a non-homogeneity will occur.

The dewatering technique used is necessarily governed by the site conditions. Dewatering is ordinarily accomplished with successive layers of single stage pumps. Because many of the underground structures go to a great depth, deep well dewatering techniques often can be employed to advantage. Care must be exercised to insure that damage does not occur as a result of piping and lost ground. A common cause of piping is the washing of fines from a well in order to increase the yield. Lost ground because of pumping may be acceptable at distances away from the structure, but it is definitely undesirable adjacent to the structures.

A backfill that is impervious and properly compacted will drastically limit the supply of water surrounding the structure available for seepage through leaks in the structures. If the backfill happens to be

pervious, and is connected to an aquifer, then a ready supply of water is available and waterproofing details must be very carefully designed. It must be determined whether a stratum is an aquifer or merely contains a pocket of water. This information is useful for dewatering during construction as well as an indicator of the water supply available to leaks after the construction is complete. Generally, an impervious backfill is desirable.

Swelling soils can cause serious construction problems. They are often found in arid or semi-arid climates, but also occur elsewhere. In several of the present missile silos, a thin bottom slab was used that rested on swelling soils. Because a very great pressure reduction had occurred on the subsoil, it tended to suck-in water; however, the low permeability of swelling soils requires a long period of time for satisfaction of the suction forces. As migrating water was sucked into the soil, swelling progressed and a failure of the bottom slabs was observed. Two techniques usually used to prevent swelling are to keep the imposed pressures on the soil high and to prevent a supply of moisture from getting to the troublesome soil.

The foregoing discussion of the effects of construction should be considered during site selection. Although the hardness of a site may be adequate if construction can be accomplished, the cost of construction in a particular location must be considered in the selection of the site. The construction difficulties should not be minimized during the process of site selection.

5.3.4 Fully-Buried Rectangular Structures. The earth cover required to meet the "fully-buried" criterion for a rectangular structure is at the present time subject to very substantial uncertainties. Estimates

of the minimum earth cover consistent with this case are given in Refs. 5-4 and 5-7 and are reproduced herein as Fig. 5-16. These recommendations are admittedly crude, being based on limited theoretical studies and judgment. Unfortunately, there are no full-scale field test results which can be used to evaluate the validity of these recommendations. Because this depth-of-cover criterion, given in Fig. 5-16, is the best information currently available, it is recommended for use until such time as additional information makes refinement possible. Among the refinements that seem particularly needed is the inclusion of a parameter expressing the influence of soil type. Certainly the depth of earth required to develop a passive resistance capable of preventing substantial lateral deflection of the structure must be, at least in part, dependent upon the shearing strength of the soil. Unfortunately, at the present time, knowledge of the dynamic behavior of soil and soil masses is so limited that the inclusion of a soil type factor in the depth of cover requirements is not justified.

Accepting the criterion given above, the blast-induced loads for which the several structural components of a fully buried rectangular structure should be designed can be estimated as follows:

Horizontal Elements. If the roof of the structure is flush with the ground surface, it is subjected only to the direct effects of the air blast overpressure. As the shock front crosses the structure, the roof is subjected to a constantly varying load, and many of the theoretically infinite number of modes of vibration of the roof are excited. However, theoretical studies and field tests (see Ref. 5-8) indicate that the response of the roof in the higher modes of vibration is far over-shadowed by the response

in its fundamental mode under the action of the overpressure pulse after the roof slab has been completely enveloped by the air blast wave. Actually, because of the variation in overpressure with the distance from ground zero, the roof slab is never subjected to an absolutely uniform load; however, roof elements capable of resisting air blast overpressures of interest are necessarily of relatively short spans and the variation of overpressure across this span can be neglected safely.

If the roof of the structure is located at some depth below the ground surface, account must be taken of changes in the pressure pulse as it propagates downward through the earth, and also of the effects of soil arching. As discussed above for the roof slab flush with the ground surface, there is a short period of nonuniform loading during passage of the pressure wave across the roof of the structure; however, the effects of this nonuniform loading can be neglected and the roof can be assumed to respond only in its primary mode under the action of a uniformly distributed load which varies in time as the pressure wave in the free-field at a depth below the surface equal to that of the roof. Therefore, if the effects of arching were neglected, a buried flat roof should be designed for a load pulse modified from the surface overpressure in its time variation and having a peak value attenuated for depth as discussed in Chapter 4. However, to neglect the effects of soil arching could be unnecessarily conservative, as demonstrated in the studies of Armour Research Foundation reported in Ref. 5-9. Consequently, the roof should more appropriately be designed for a pressure pulse uniformly distributed across the roof which varies in time as does

the free-field pulse in the soil at the depth of the roof, but which may be reduced in intensity because of soil arching as discussed in Section 5.3.2.

As a general rule a buried rectangular structure will have as its base a slab similar to that used for the roof. It is recommended that such a base slab be designed for the same loading for which the roof is designed. This recommendation is made despite the fact that the free-field pressure pulse at the depth of the base will be somewhat different from that at the roof. Furthermore, modification of the pressure on the base slab by arching has not been investigated even to the limited extent that arching over the roof has been studied. However, it does not seem reasonable to expect that the forces on the base slab can differ very much from those on the roof.

Vertical Elements. The blast-induced loads for which the walls of a buried rectangular structure should be designed are somewhat more uncertain than those for the roof and base slabs. Significant studies by the Armour Research Foundation on this question are reported in Ref. 5-9, wherein the influence of the shearing stresses developed in the soil as it follows the deflecting wall panel is investigated. The predicted surfaces of sliding within the soil were located on the basis of model tests in which the existence of such surfaces was quite clearly demonstrated.

Though the studies of Ref. 5-9 throw considerable light on the interaction of a vertical wall element and the soil adjacent to

and above it, it is not recommended that the procedures suggested therein be used at present as a basis for design. The reluctance to recommend those procedures derives from the fact that they require an understanding of the dynamic behavior of soils which does not now exist. Furthermore, the relationship between horizontal and vertical blast-induced pressures in soil in the free-field are at the present time so uncertain that it is not considered justifiable to modify the free-field horizontal pressures to consider the effects of arching. Consequently, it is recommended that walls of fully-buried structures be designed for a uniformly distributed load which varies in time as the attenuated vertical pressure pulse at a depth equal to mid-height of the wall element, and which is related in intensity to the free-field vertical pressure by the lateral pressure coefficients given in Table 4-1. This procedure is considered to be consistent with the present state of knowledge and, though possibly conservative, is probably not unduly so. It is also noted that this procedure neglects the effects of the unsymmetrical load generated as the shock front envelopes the wall surface. The neglect of the unsymmetrical load is justified on the same basis that similar effects for horizontally oriented elements were neglected.

5.3.5 Fully Buried Arches. As discussed in Sect. 5.3.1, an arch is subjected, at least initially, to nonuniform intensities of load regardless of the depth to which the arch is buried. As the shock propagates across the arch, the windward face is loaded prior to the leeward face and, as a consequence, the windward side tends to deflect inward thereby

forcing the leeward side outward into the soil. Even after the shock front has crossed the arch, nonuniform, though symmetrical, loadings tend to continue since the crown of the arch is subjected to a load comparable to the vertical soil stress at a depth equal to the location of the arch crown while the sides of the arch are subjected to pressures related more closely to the horizontal soil stresses which are usually substantially less than the vertical stresses. However, as discussed previously, despite the initial existence of such nonuniform loads, deflections of the arch consistent with them cannot develop if the restraining effect of the soil is great enough to resist these deformations. Consequently, below some critical depth at which the soil resistance becomes adequate to prohibit the development of significant flexural deformation, the pressures on the surface of the arch will tend to be equalized as arch deformations try to develop. For this case, the arch can be designed to resist a uniform radial pressure, the initial nonuniformities of load being neglected.

Below the critical depth defined above, arches are said to be "fully-buried". At the present time, the available information is inadequate to define with complete confidence the depth required to constitute the fully-buried case. The present generally accepted criterion is that given in Refs. 5-4 and 5-7, which is reproduced herein as Fig. 5-16. This recommendation is based in large measure on judgment, supported by a few field tests and theoretical investigations. Among the most significant field tests are those reported in Refs. 5-10, 5-11 and 5-12. The most extensive theoretical study is that reported by Whipple in Refs. 5-13 and 5-14. While none of

these references, either individually or collectively, are adequate to establish a criterion for full burial of an arch, they do serve to indicate the reasonableness and probable conservatism of the criterion given in Fig. 5-16.

The concrete arches of Ref. 5-11 met the criterion completely, and the corrugated steel arches of Ref. 5-10 conformed very closely with the fully buried criterion of Fig. 5-16. Neither of these arches experienced any significant damage and they exhibited no significant amounts of unsymmetrical response. In Ref. 5-12, corrugated metal arches identical to those reported in Ref. 5-10 were tested in Operation Hardtack under conditions which met the fully-buried criterion given herein. These arches suffered complete collapse, but collapse occurred at overpressure levels which, when applied as uniform radial pressures, would have produced circumferential compressive stresses in the arch considerably in excess of the yield strength of the material.

In Refs. 5-13 and 5-14 Whipple reports the results of a theoretical study of the response of shallow buried arches to the loads induced by the passage of an air blast wave over the ground surface. This study, while representing the arch in an admittedly crude manner as a series of four rigid lengths with masses and resistances concentrated at their inter-sections, does take into account the effects of the soil mass surrounding the arch both as to a reduction in load on the windward side as the soil tends to follow the deforming arch as well as the increase in resistance afforded by the development of passive pressure in the soil on the leeward side. The result of this investigation, though it includes many assumptions and

idealizations such as the overly simplified representation of the arch and the uncertainties inherent in the dynamic properties of the deforming soil, does serve to indicate that the criterion for full burial shown in Fig 5-16 is generally adequate and is usually somewhat conservative.

Accepting this criterion for full burial as reasonable, all arches buried at depths equal to or greater than this can then be designed for a uniform radial pressure equal in intensity and in variation with time to the blast-induced free-field vertical pressure in the soil at a depth equal to the average depth of cover over the arch. Designing the arch for this load may be overly conservative since it neglects the effects of soil arching as the structure deflects radially inward under the uniform radial loading. Consequently, Ref. 5-7 recommends that the intensity of the loading defined above be decreased because of arching effects while the time variation of the load remains unchanged. The magnitude of the reduction due to arching can be computed in the same manner as for the roof of an underground rectangular structure as discussed in Sect. 5.3.2.

As the footings of an arch are forced into the soil on which they rest by the thrust imparted from the loaded arch surface, the entire arch tends to move away from the soil through which the load is being transmitted. As a consequence, such footing motion tends to enhance the development of soil arching around the structure; the extent to which arch action may be increased by footing motion is also discussed in Sect. 5.3.2.

Any reference to the possible effects of construction procedures on the loads that may be felt by a buried arch has been excluded from the preceding paragraphs. It has been assumed in this discussion that reasonable

and proper construction procedures have been employed and that the backfill around the arch has been compacted so as to be quite uniform around the entire arch. It has also been assumed that during the construction and backfilling operations, procedures have been such as to prevent the arch from becoming severely "out-of-round"; excessive out-of-roundness may well invite a premature buckling failure of the loaded arch.

5.3.6 Fully Buried Domes. The discussions of the preceding section are applicable with only minor modification to fully-buried domes. The information available for establishing the depth of soil cover required to constitute the fully-buried case for a dome is even more limited than for an arch. Based primarily on judgment, and with a recognition of the greater inherent strength of a dome and the smaller influence of unsymmetrical and nonuniform loads, Ref. 5-7 recommends that the depth of cover required to constitute the fully buried case for a dome be taken identical to that stipulated in Fig. 5-16 for an arch. There is now no basis, either theoretical or experimental, on which to modify this criterion to reflect the differences known to exist between the response of arches and domes; it is recommended that this criterion be used until additional information makes rational modification possible.

For domes meeting this criterion of full burial, the blast loading for which they should be designed should be determined in the manner discussed in the preceding section for fully-buried arches.

It should be emphasized again that the design loadings recommended herein presume at least a reasonable amount of flexibility to make load equalization possible.

5.3.7 Underground Vertical Cylindrical Structures. There are no test data and very limited theoretical studies upon which to base recommendations for the loadings for which this very important structural type should be designed. The most recent studies are given in Ref. 5-18 which is reproduced, in many instances almost verbatim, herein. An earlier study of this problem reported in Ref. 5-15 may be consulted for additional background material.

No specific recommendations were made for the determination of the dead loads for which previously discussed structural types should be designed. For the usual cut-and-cover arch, dome, or rectangular structure, the static loads are normally quite small in relation to the blast-induced forces to which these structures may be subjected. For deeply buried structures or a vertical silo, the static forces may become the controlling design criteria because of attenuation of blast-induced pressures with depth and the increase of static forces with depth.

Dead Load Soil Pressures on Silos. The static forces that a vertically oriented silo in soil must resist are in many cases at least as uncertain as the blast-induced forces. They depend primarily on the soil type, location of the water table, and the construction procedures used to build the silo. Considering the wide variety of soil conditions that may be encountered and the endless variation in construction techniques that may be employed, it is impossible herein to give specific recommendations whereby the dead load soil pressures on such silos may be established. However, general guide lines are available and are summarized to indicate the nature of these forces.

By means of procedures given in Article 74 of Ref. 5-16, an estimate can be made of the lower limit of the static radial pressures that exists on the walls of a cylindrical shaft in granular material. The following recommendations for dead load pressures on silos in granular materials are taken from Ref. 5-18, having been developed on the basis of Terzaghi's work as presented in Ref. 5-16.

Consider a vertical shaft of radius r in a granular material, as shown in Fig. 5-17 where the pressure distribution is shown schematically on the wall of the shaft. The radial pressure at a depth z is noted by the symbol p_z . Because of soil movements during construction operations, the lateral pressure may be considerably below the lateral pressure "at rest", and there is a tendency for the lateral pressures to arch around the wall of the shaft. The pressure distribution recommended for use in designing the structure for dead load is shown in Figs. 5-17 and 5-18. Figure 5-17 gives, as a function of the ratio of the depth z to the silo radius r , the ratio of the pressure p_z at depth z to the pressure at an infinite depth, p_∞ . The curve shown has the equation:

$$\frac{p_z}{p_\infty} = \frac{z/r}{(z/r) + 2.5} \quad (5-37)$$

The pressure at an infinite depth is shown in Fig. 5-18 in terms of the density, or weight per unit volume of the soil, w , and the radius of the silo, r , as a function of the angle of internal friction ϕ . Values of ϕ below thirty degrees are not found for sand. Values of ϕ for silt may range down to twenty-five degrees. These curves are not applicable for internal

friction angles of less than twenty-five degrees.

As an indication of the way in which these figures are used, there is shown in Fig. 5-19 the horizontal dead load pressures on a fifty-foot diameter silo in soils having various angles of internal friction. The curves shown are prepared for a material of a density of 120 lb./cu.ft., and the pressures are given in psi as a function of the depth below the surface in feet. There is given below each of the curves the pressure at an infinite depth computed from the coefficients in Fig. 5-18. It can be seen from Fig. 5-19 that for a soil having an internal friction angle of 35 degrees, although the pressure at an infinite depth is 13.9 psi, the pressure at a depth of 150 feet is only 10 psi and the pressure at 50 feet is about 6.3 psi.

The calculations described are for essentially dry materials. For undrained conditions and an impervious structure, the pressures of the water below the water table must also be considered. It is appropriate, in conditions where water is present, to reduce the unit weight of the material below the water table to the submerged unit weight.

Static soil pressures in granular materials computed in the manner just described should be considered applicable only if the construction techniques are such that deformations in the soil adjacent to the silos sufficient to develop the full internal shearing strength of the soil are permitted; consequently, as mentioned previously, they represent a lower limit of the static soil pressures that may act on the silo wall. The upper limit for these static pressures would be consistent with a construction

procedure which permitted no inward deformation of the soil as the silo excavation progressed. Static soil pressures for such a case could be determined as the "at rest" pressures on the basis of procedures given in any standard soil mechanics reference. Perhaps a more reasonable estimate, though it would require a knowledge of the construction techniques employed, would be that recommended for the design of bracing in open-cuts as given by Terzaghi & Peck in Ref. 5-17. Such a procedure would assume a plane vertical cut in the soil; however, the diameter of the silo is usually sufficiently large so that the error from this source is probably of little consequence considering the empirical nature of the procedure.

The preceding discussion of static soil pressures is applicable only to granular materials. No reliable theory for the radial pressure on a vertical cylinder in clay is available that takes into account the internal strength of the clay. Ref. 5-15 suggests that the plastic nature of clay causes the radial pressures at considerable depth to approach the "at rest" condition with the passage of time. By "considerable depth" is meant a depth such that the stresses due to overburden approach those at which creep is likely to begin. This depth, H_c , is given roughly by:

$$H_c = 1.5 q_u / w \quad (5-38)$$

where q_u is the unconfined compressive strength in the soil and w is its unit weight. Above this critical depth, the static radial pressures may be substantially less than the "at rest" pressure. Because of the influence of construction procedures, it is impossible to make specific recommendations in this regard.

In the final analysis, considering the complexities of this problem and the uncertainties inherent in all of the parameters of consequence, it will probably be desirable for each site to be studied by persons qualified by experience and training to consider the probable influences of the several parameters involved before static load pressures to be used in design are determined.

Lateral Blast-Induced Soil Pressure. As an air blast wave passes over the ground surface a pressure pulse generated by it propagates downward through the soil. As this pressure pulse in the soil encounters the vertical cylinder, it imparts a force to the cylinder. During transit of the shock across the cylinder, the loads imparted are obviously of a nonuniform, unsymmetrical nature.

After the shock front has completely traversed the cylinder, then, neglecting the variation of pressure with range over the relatively small distances consistent with silo diameters, the silo is subjected to a uniform radial pressure equal, or at least directly related to, the free-field horizontal soil pressure. The unsymmetrical loading that occurs during transit of the shock front across the silo exists, of course, at all depths below ground surface; however, as the silo tries to deform under the action of these unsymmetrical loadings, it tends to move away from the areas of high pressure intensity and move into the soil in areas of low blast pressure intensity. Such deformations develop resistances in the soil which reduce the significance of these nonuniform loads. Indeed, below some critical depth, the available soil resistance is sufficient to preclude the development

of significant flexural deformations of this type in the silo in the same manner discussed in preceding sections for fully buried arches and domes. Consequently, below this critical depth, as yet undefined, the silo can be designed for a uniform radial pressure related in magnitude directly to the free-field horizontal soil pressures and varying in time as the free-field soil pressure at the depth of interest.

Near the ground surface, the available soil resistance is normally inadequate to resist the flexural deformations resulting from the unsymmetrical loads imparted to the structure during transit of the shock front. As a consequence, above the critical depth discussed in the preceding paragraph, it is necessary to design the structure not only for uniform radial pressure but also for a nonuniform time dependent force.

If both the soil and the silo liner were of ideally elastic materials, it would be possible to determine on a theoretical basis the ratio between the uniform radial pressure on the silo and the free-field lateral pressure in the soil. The significant parameters would be the difference between the elastic moduli of the soil and silo liner material and the difference in the Poisson's ratios of the two materials. After studying the question of blast-induced radial pressures on silo liners in this manner, it was concluded in Ref. 5-18 that, in general, the reduction in pressure produced by the compressibility of the silo liner is negligible. Furthermore, because the value of Poisson's ratio for soil is usually not well defined, it was suggested that no attempt be made to take into account the

compressibility of the silo liner and that the silo be designed for a uniform radial pressure equal to the free-field horizontal pressure in the soil at the depth of interest. Thus, below the critical depth, the time dependent blast-induced radial pressure may be taken equal in magnitude to the free-field vertical pressure at the depth of interest multiplied by the appropriate lateral pressure coefficient K_0 as given in Table 4-1.

The critical depth below which nonuniform loads can be neglected for design purposes can not at present be well defined, there being neither theoretical studies nor experimental data on which to base an estimate. Relying primarily on judgment, Ref. 5-18 suggests that it be taken as a depth below ground surface equal to one diameter of the silo being designed. Above this point the silo should be designed to withstand the effects not only of a uniform radial pressure but also of a nonuniform radial pressure. The two components, as suggested in Ref. 5-18, are illustrated in Fig. 5-20.

One component is a uniform compression, $p_c(t)$, acting around a circumference; the other is a varying pressure, $p_f(t)$, consisting of four half-sine waves around the circumference, alternately inward and outward. It is suggested that the maximum amplitude of each component be taken equal to one-half of the peak side-on overpressure at the ground surface. When designing the structure, the stresses produced by these two components of loads should be considered to be additive, and the silo should be so proportioned that the sum of the stresses does not exceed the yield strength of the material. The uniform radial component, $p_c(t)$, should be assumed to vary in time as does the surface overpressure pulse and should be considered constant in magnitude above the critical depth. The sinusoidally varying component, $p_f(t)$, should

be considered to have a rise time equal to one-half the transit time of the shock front across the silo and a total duration equal to the transit time. Further, it should be assumed to have a peak value at ground surface equal to one-half the surface side-on overpressure and should be assumed to diminish in intensity linearly to a value of zero at the critical depth.

Clearly, these recommendations result in a discontinuity in design loading at a depth equal to one silo diameter since, immediately above this point, the design pressure would be a uniform radial pressure equal in magnitude to one-half the surface overpressure while, immediately below this critical depth, the recommended load is a uniform radial pressure equal to the attenuated free-field horizontal pressure at that depth. Such a discontinuity should not occur in a silo; consequently, it is suggested that the section resulting from a design based on the loading recommended below the critical depth be considered to control at the critical depth.

For both dead load and blast load, irregularities in loading may occur over the entire height of the cylinder because of variations in the properties of the soil or for other reasons. These irregularities are likely to be entirely accidental and unpredictable in character and location. To provide for them, it is recommended that an irregularity with a maximum value equal to ten percent of the lateral dead load design pressure be considered; this pressure should be assumed to vary sinusoidally around the circumference as recommended for the live load flexural component. This recommendation is applicable primarily below the critical depth, since above that point sufficient flexural resistance would automatically have been incorporated in the design of the silo by consideration of the sinusoidally varying live

load distribution described in the preceding paragraphs.

If the roof of the silo is supported by the silo walls, the blast load imparted to the roof is carried by axial compression in the silo wall and should be treated as discussed in the following section. If, on the other hand, the roof of the silo is supported on a circumferential ring footing outside of, but adjacent to, the silo wall, it is necessary to consider its effect on the radial pressures for which the upper portion of the silo wall should be designed.

Because of the influence of the actual geometry of the individual structure under consideration, it is impossible here to give specific recommendations for the increase in radial pressures on the silo resulting from this feature. However, in general, it can be assumed that the silo roof footing will generate radial pressures on the silo wall surface directly beneath the footing equal to the bearing pressure beneath the footing multiplied by the lateral pressure coefficient given in Table 4-1. The depth of the silo over which these increased radial pressures should be considered effective is uncertain; it is recommended, however, that they be considered to vary linearly from a maximum value at a point immediately beneath the footing to zero at a distance below the footing equal to the width of the footing.

Vertical Force on Silos. During the passage of the shock front across the silo and after the silo has been completely enveloped in the shock wave, longitudinal compressive forces in the silo wall will be generated from two primary sources. If the silo roof is supported directly on the silo wall, then the blast pressure on the roof is imparted directly

to the silo wall as an axial compressive stress. Also, because of the differences in the elastic properties of the silo wall and the soil in which it is embedded, the soil adjacent to the wall tends to move with respect to the wall, thereby inducing vertical forces in the wall as a result of the skin friction existing between the earth and the wall.

The first of these components of compressive force can be easily evaluated since at any instant in time it is equal to the total overpressure acting on the silo roof divided by the silo wall cross-sectional area. The second component is much more complex and, at the present time, incapable of precise definition. In computing the skin friction force, account must be taken of the magnitude of the skin friction and the direction of relative motion of the silo and of the earth adjacent to it. Both of these factors vary with time differently at all points over the entire length of the silo. In general, the magnitude of the skin friction force is dependent upon the radial pressure which, at any given instant of time, varies with depth. Also, depending upon the total length of the silo, its foundation conditions, and the length of the pressure wave in the soil, it is entirely possible that the direction of relative motion between the silo and the soil at points near the bottom of the silo may be opposite to the direction of relative motion at that same instant of time at points near the top of the silo.

The existence of these uncertainties, unfortunately, does not eliminate the need for a procedure whereby the magnitudes of the compressive forces induced by skin friction can be estimated. Recognizing this need, as well as the extremely complex nature of the problem, the following

procedure taken from Ref. 5-18 is suggested. The procedure, though obviously approximate, is thought to be reasonable and probably conservative.

In general, the vertical force transmitted by friction on the silo walls can be computed from the magnitude of the shearing resistance of the soil adjacent to the silo and the lateral force. The shearing force transmitted to the silo wall cannot exceed the coefficient of friction multiplied by the lateral force. However, the coefficient of friction used should be less than the tangent of the angle of internal friction of the undisturbed soil, because the soil adjacent to the silo is generally disturbed by the construction operations. If no other measure of the shearing resistance of the disturbed soil is available, it seems reasonable to take the angle of internal friction to be five degrees less than that of the general mass of the material. For cohesive materials the shearing resistance should not be taken as more than one-half the unconfined compressive strength of the material. It is suggested that the maximum vertical force in the silo wall and the maximum pressure on the foundation be computed on the basis of the following conservative assumptions:

- (1) Assume that a reversal in the direction of the shearing force occurs at about mid-height of the effective length of the silo. The effective length is the total height minus the portion near the top having a sloping or wedged profile.

- (2) The maximum vertical stress in the wall occurs at the point where the shearing force reverses in direction. This maximum stress is computed for the combined roof loading plus the total shearing force of the

upper part where the shearing stresses are acting downward.

(3) The total load on the base of the silo is equal to the total load at the top plus the net force transmitted by shear. The net force transmitted by shear is near zero in homogeneous material, but it may be considerably different from zero if the soil properties change with depth.

If the soil deposit is stratified, or if, for any other reasons, the soil properties vary significantly over the depth of the silo, the procedure outlined above is not applicable and could lead to rather large errors. For such nonuniform soils, no simple procedures can be given. Taking into account the variations in soil properties, as well as the foundation conditions of the silo, the depth at which the direction of relative motion of soil and silo reverses must be evaluated. The maximum vertical force in the silo wall will exist at this point, and can be computed as the sum of the roof load and the total skin friction force above this point.

5.4 PARTIALLY BURIED STRUCTURES

5.4.1 Introduction. Included in this section is a discussion of the blast-induced loadings that might be expected on those structures which, though either totally or partially covered with earth, fail to have sufficient earth cover to meet the criteria for full burial discussed in the preceding sections. Consequently, for those structures consideration must be given not only to the uniform confining pressure for which the fully buried

structures were designed, but also to the nonuniform unbalanced load associated with both the passage of the shock front across the structure and with the continuing drag pressures that persist after the structure has been completely engulfed in the blast wave.

For structures in this category there are virtually no data, either theoretical or experimental, from which design loadings can be inferred. There have been a limited number of tests of mounded arches in which the mound proportions were such as to place the structure in the classification defined here as partially buried structures; however, the results of these few tests are inadequate as a basis for the formulation of design loading criteria because the extent of such tests has been insufficient to identify in any quantitative sense the effect of the several parameters considered to be important.

Unfortunately, as mentioned in the case of the vertical silos, a lack of knowledge eliminates neither the problem nor a need for a solution to it. Consequently, recommendations are presented in the following paragraphs for procedures whereby design loads for partially buried structures of each of the several common types may be estimated. It must be emphasized that no rigorous defense of these recommended procedures can now be given; they are presented as recommendations only and are highly susceptible to revision and refinement as additional information in this area becomes available.

5.4.2 Rectangular Structures. For obvious reasons, when a rectangular structure is covered by earth, it is necessary that we consider only the completely closed case. In general, the blast pressures for which

the roof and base slabs of such a structure must be designed are unaffected by the fact that the structure as a whole fails to meet the fully buried criterion. Certainly, this is true in all cases for the base of the structure and in most cases for the roof of the structure. Of course, if the side slopes of the covering earth mound extend over the roof, the reflected and drag pressures that exist on the windward side of the embankment may be transmitted in some manner to the roof.

Roof Loading. Consider a partially buried rectangular structure such as is illustrated in Fig. 5-21. If a normal to the windward slope at its junction with the top of the mound intersects the windward wall instead of the roof (line DG, for example), the roof may be considered to be unaffected by the pressures on the windward slope, and may be designed for a uniform distributed load identical to that recommended in Sect. 5.3.4 for a roof that is flush with the natural ground surface.

If, however, the mound configuration is such that the above described normal intersects the roof (line EH, for example), the influence of the forces on the windward slope must be considered. The following procedure, though without rational basis, is suggested.

(1) Assume that part of the roof on the leeward side of point H to be unaffected by forces on the windward slope and take its loading to be identical to that described in the preceding paragraph.

(2) For that part of the roof on the windward side of point H, consider the loading to vary with time as the loading on the windward slope but to be reduced in intensity by the factor K_v where

$$K_v = \frac{s}{\sqrt{s^2 + 1}}$$

Thus, if $\bar{p}(t)$ is the time-dependent pressure on the windward slope, determined by the methods of Sect. 5.2.2 to include the effects of overpressure, drag, and reflection, then the blast-induced load on that part of the roof windward of point H can be taken as $K_v \bar{p}(t)$. However, in no case should the roof loading windward of point H be taken as less severe than that recommended above for the leeward part of the roof.

Base Loading. If the mound configuration is such that the roof loading is unaffected by pressures on the side slopes, it is reasonable that the loading on the base slab be taken equal to that on the roof.

If, on the other hand, the mound configuration is such that the pressures on the windward slope do influence the roof design load, the corresponding base load is more uncertain. Without question, the nature of the roof loading must influence the load on the base, but the extent and character of this influence is at present unknown. Considering the inherent rigidity of a buried rectangular structure, any non-uniformities of roof loading should be evened out on the base. Consequently, while no load forms for the base can at present be given, it is recommended that the base be proportioned to give a uniform structural resistance equal to the average resistance of the roof.

Wall Loading. In the absence both of research studies and experience, it is impossible to present with confidence recommended design

loadings for walls of mounded rectangular structures. At one extreme, if the mound side slope is nearly vertical and in close proximity to the wall, the design load for the wall is, for practical purposes, equal to the load on the windward slope of the mound. At the other extreme, if the side slopes of the mound are very flat, the effect of the load on these slopes can be neglected, thereby constituting the fully-buried case for which wall loadings have been recommended in Sect. 5.3.4.

For the general case such as is illustrated in Fig. 21, the wall loading is somewhere between the two extremes identified above. Though their significance cannot now be specified, the following parameters are among the more important factors that influence the blast-induced pressure of the wall of a mounded rectangular structure: (1) the location of the structure relative to natural ground surface, (2) the location of the top of the mound relative to the structure, (3) the steepness of the mound side slopes, (4) the distance between the wall and the mound side slope, and (5) the type of soil and the backfill procedures used in the mound.

Until information becomes available on which to base more rational recommendations, the following design loadings are suggested, though they are thought to be conservative. The conservatism stems from a neglect of any attenuation or modification of the pressure pulse as it propagates from the mound surface to the wall and also from the neglect of the fact that, as the loaded wall begins to deflect, the pressure on the wall may be reduced by soil arching. The suggested procedure is as follows:

(1) Draw lines normal to the windward slope of the mound at the top and bottom of the slope as shown in Fig. 5-21 at points C and D or E.

(2) Take the loading on that part of the wall included between these two lines (FG or FB) to vary with time as the pressure on the windward slope but to be reduced in intensity by the factor K_h where

$$K_h = \frac{1}{\sqrt{s^2 + 1}}$$

Thus, if $\bar{p}(t)$ is the time-dependent pressure on the windward slope, then the corresponding pressure function on that part of the wall being considered can be taken as $K_h \bar{p}(t)$. Regardless of the mound configuration, the load function should never be taken as less severe than $K_o p_s(t)$ where K_o is as given in Table 4-1 and $p_s(t)$ is the surface overpressure-time function.

(3) Take the loading on that part of the wall above the part discussed in (2) to be $K_o p_s(t)$.

(4) Take the loading on that part of the wall below the part described in (2) to be $K_o p_v(t)$ where $p_v(t)$ is free-field vertical pressure function in the soil attenuated from the natural ground surface.

It is recognized that the loading criteria suggested above will result in a discontinuity of criteria when the mound has a slope of 1 on 4 which corresponds to the fully buried case. While recognizing this inconsistency, the basis of the procedures outlined above is not considered sufficiently rational to warrant the introduction of refinements to overcome the difficulty.

5.4.3 Partially Buried Arches. In Sects. 5.2.4 and 5.3.5 recommendations were given for design loadings for arched structures completely above ground and fully buried, respectively. For an arch which is either completely or partially covered by an earth mound, but for which the earth cover is insufficient to meet the requirements for full burial as set forth in Sect. 5.3.5, the blast-induced forces must be intermediate between those for the two limiting conditions just specified.

As indicated previously, no data are available to serve as a basis for the formulation of design loading recommendations for partially buried arches. The recommendations that follow are based primarily on judgment as influenced by the obvious need for a smooth transition in loading, as the earth cover is increased, from the loading stipulated for the completely above ground case to that for the fully buried case.

A method for extrapolating from the above ground case to obtain the blast loadings on a partially buried arch is given in Ref. 5-5. A study of these recommendations indicates several weaknesses, the most important of which follow:

- (1) The nonuniform components of load similar to those illustrated in Figs. 5-6(b) and (c) generated by the reflected and drag pressures on the soil mound are extremely sensitive to changes in the depth of earth cover.

- (2) The unsymmetrical loading identified in (1) is highly sensitive to changes in slope of the sides of the earth mound especially when the slopes approach those taken to be comparable in their effect to a flat surface, i.e., 1 on 4.

(3) The procedure of Ref. 5-5 fails to recognize that, if the side slopes are very steep, the effect of cover over the arch in reducing the unsymmetrical component is negligible.

In an attempt to overcome these weaknesses of the procedures given in Ref. 5-5, it is recommended that the methods outlined in the paragraphs that follow be used to interpolate between the above ground and the fully buried cases to obtain reasonable estimates of design loads for the partially buried arch.

As for the above ground case, partially buried arches must be designed not only for a uniform radial pressure related to the surface air blast overpressure, but also for an unsymmetrical or flexural component of loading related to the reflected and drag pressures on the earth mound. The uniform compression loading should be taken equal to that for the above ground case as illustrated in Fig. 5-6(a). The unsymmetrical loading components have the same characteristic form as in the above ground case, as illustrated in Figs. 5-6(b) and (c), but are reduced in intensity because of the existence of the earth mound over the arch.

Because of its nature, it seems reasonable that the drag component of the flexural loading should depend primarily on the steepness of the side slopes of the earth mound as well as the location of the side slope laterally with respect to the arch. Based on the criterion for full burial defined in Fig. 5-16, flexural loading may be completely neglected if the side slopes are flatter than one on four. Furthermore, if the side slopes are as steep as one on two, a further increase in slope will have only little effect on the loading.

Consider the mounded arch shown in Fig. 5-22; if, in this case, s is less than 4 but greater than 1, the drag component of flexural load should vary between zero and the above ground value shown in Fig. 5-6(b). As a reasonable interpolation between these two limits, it is suggested that the peak value of the drag component of loading be taken as

$$p_{dm} = \left(\frac{\beta_s}{\pi} C_d p_d \right) \alpha \quad (5-39)$$

where $\alpha = (4 - s)/3$, β_s = half of the central angle of the circular arc most nearly coincident with the actual ground surface, and C_d = the drag coefficient corresponding to the steepness of the actual side slope.

In the above, s should be taken as 4 if equal to or greater than 4, and as 1 if equal to or less than one, and as its actual value if between these limits.

The peak drag loading given by Eq. (5-39) can be assumed to occur at a time

$$t_r = \left(1 + 3 \frac{\beta_s}{\pi} \right) \tau \quad (5-40)$$

after which it can be taken as

$$p_{f2}(t) = \left[\frac{\beta_s}{\pi} C_d p_d(t) \right] \alpha \quad (5-41)$$

where the terms are as previously defined.

The initial component of the flexural loading of a partially buried or mounded arch is dependent on both the average depth of cover of the arch and the location and steepness of the side slopes. To interpolate reasonably between the above ground case and the fully buried case, it is suggested

that the value of the initial component be taken as increasing linearly to a maximum of

$$p_{im} = \left[1 - 4 \left(\frac{H_{av}}{L} \right) (1 - \alpha^2) + \alpha \left(\frac{\beta_s}{\pi} \right) \right] p_{so} - \frac{1}{2 + 6 \frac{\beta_s}{\pi}} p_{dm} \quad (5-42)$$

in which all terms are as previously defined. In this equation, the quantity $\left[(H_{av}/L) (1 - \alpha^2) \right]$ should never be taken as less than 0.125 nor greater than 0.25. If its actual value is outside these bounds, the nearest adjacent bound should be used.

The maximum value of the initial component of flexural loading can be taken as occurring at a time $\tau/2$ after which it decays linearly to zero at a time $(1 + 3 \beta_s/\pi)\tau$.

The influence of the steepness of the side slopes and the depth of cover over the arch on the two components of flexural loading are evident in the terms (H_{av}/L) and α as they appear in Eqs. (5-39), (5-41), and (5-42). The influence of the lateral location of the side slopes with respect to the arch is not immediately evident; actually, the influence of this parameter is reflected in the magnitude of β_s since, as the lateral distance between the side slopes is increased, the value of β_s must necessarily be decreased. Used with the restrictions imposed in their presentation, the procedures just described will, at the two extremes, yield loads identical to those previously recommended for the completely above ground and the fully buried cases and will provide a smooth transition in load between these two bounds. No other arguments can be given at present to justify their use.

5.4.4 Partially Buried Domes. A dome that has some earth cover, but less than that stipulated for the fully buried case in Sect. 5.3.6, is

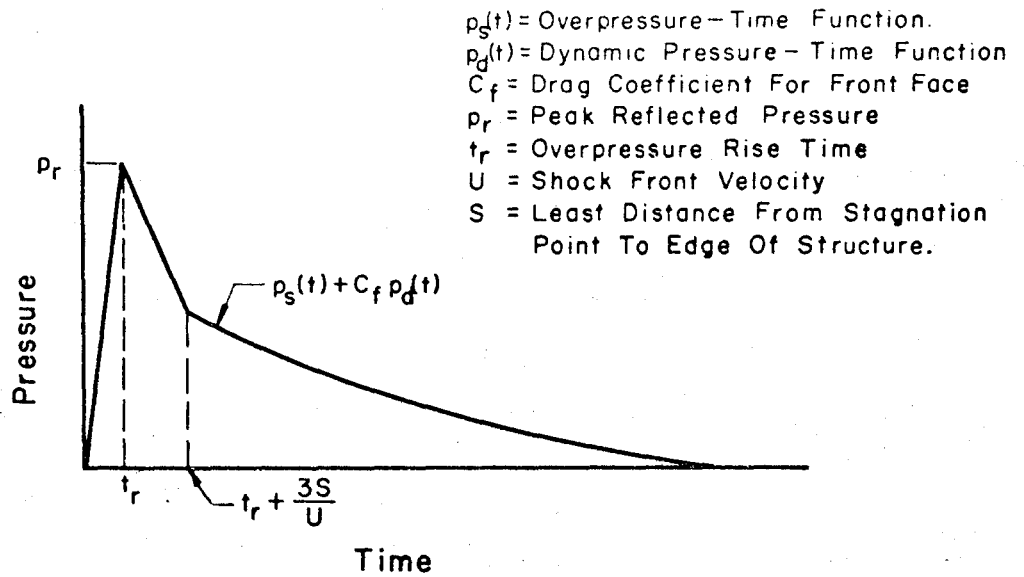
generally referred to as being partially buried or mounded. For such domes, the uniform compression component of load should be taken equal to that recommended for the fully buried case. In addition, it must also be designed for flexural load comparable in its general form to that required for an above ground dome in Sect. 5.2.5. However, the flexural loading can be reduced in intensity for a mounded dome because of the influence of the soil cover. Lacking better knowledge of the nature of the loading, it is recommended that the procedures suggested in Sect. 5.4.3 for flexural load interpolation between the above ground and the full buried arches be applied also to partially buried domes.

5.5 REFERENCES

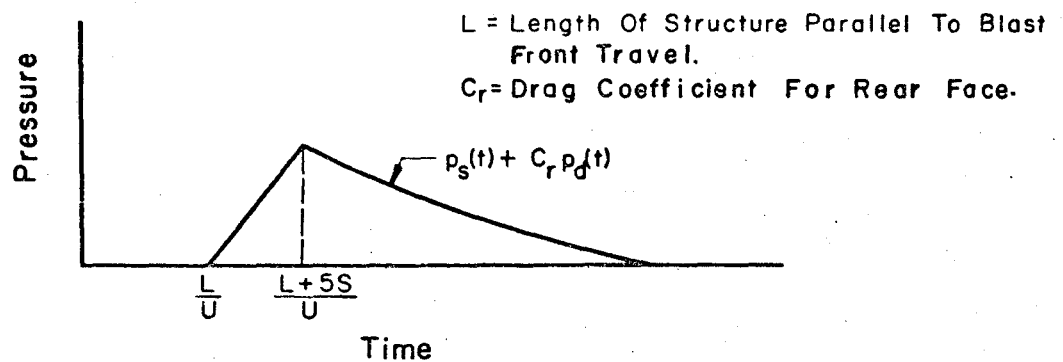
- 5-1 "The Effects of Nuclear Weapons", by U. S. Department of Defense for U. S. Atomic Energy Commission, April 1962. (UNCLASSIFIED)
- 5-2 Newmark, N. M., "An Engineering Approach to Blast Resistant Design", Transactions, ASCE, V. 121, pp. 45-63, New York, 1956. (UNCLASSIFIED)
- 5-3 Morrison, T. G., "Protective Construction, Part II of III", Contract No. AF 33(616)-2522, Project No. 1080, Task No. 10802, American Machine and Foundry Company, Mechanics Research Division, Dec. 1958. (SECRET)
- 5-4 "Design of Structures to Resist Nuclear Weapons Effects", ASCE Manual of Engineering Practice No. 42, 1961. (UNCLASSIFIED)
- 5-5 Merritt, J. L. and Newmark, N. M., "Design of Underground Structures to Resist Nuclear Blast", Vol. 2, Final Report, Contract DA-49-129-eng-312, Dept. of Civil Engineering, University of Illinois, for Office Chief of Engrs., April 1958. (UNCLASSIFIED)
- 5-6 Grubaugh, R. E., Morrison, T. G., Kocke, R. S., Neidhardt, G. L., and Tuggle, W., "Full Scale Field Tests of Dome and Arch Structures", Operation PLUMBBOB, ITR 1425, October 1957. (CONFIDENTIAL)
- 5-7 Newmark, N. M., Hall, W. J., "Preliminary Design Methods for Underground Protective Structures", AFSWC-TDR-62-6, June 1962. (SECRET)
- 5-8 Sinnemon, G. K., "Air Blast Effects on Underground Structures", Project 3.4, Operation TEAPOT, ITR-1127, University of Illinois, May 1955. (CONFIDENTIAL RD)
- 5-9 "Analysis of Underground Roof and Wall Panels Subjected to Nuclear Blast", Contract No. AF 33(600)-37360, Task 5, Armour Research Foundation, April 1960. (CONFIDENTIAL)
- 5-10 Albright, G. H., "Evaluation of Earth-Covered Prefabricated Ammunition Storage Magazines as Personnel Shelters", Operation PLUMBBOB, ITR 1422, November 1957. (CONFIDENTIAL)
- 5-11 Flathe, W. J., Breckenridge, R. A., and Wiehle, C. K., "Blast Loading and Response of Underground Concrete-Arch Protective Structures", Operation PLUMBBOB, ITR 1420, November 1957. (CONFIDENTIAL)

- 5-12 Albright, G. H., Rush, P. J., DeDoux, J. L., True, V., White, C. R., "Response of Earth-Confined Flexible-Arch-Shell Structures in High-Overpressure Region", Operation HARDTACK, ITR 1626-1. (SECRET)
- 5-13 Whipple, C. R., "The Dynamic Response of Shallow-Buried Arches Subjected to Blast Loading", Report for Air Force Special Weapons Center, Contract No. AF 29(601)-2591, Project No. 1080, University of Illinois, 1961. (UNCLASSIFIED)
- 5-14 Whipple, C. R., "Numerical Studies of the Dynamic Response of Shallow Buried Arches Subjected to Blast Loading", Draft of Report for Air Force Special Weapons Center, Contract No. AF 29(601)-2591 and AF 29(601)-4508, Project No. 1080, University of Illinois, 1961. (UNCLASSIFIED)
- 5-15 Newmark, N. M., "Final Report of Special Studies Related to the WS 107A-2 Launcher Installation", Vol. III, American Machine and Foundry Co., Greenwich, Connecticut, 1958. (SECRET)
- 5-16 Terzaghi, K., "Theoretical Soil Mechanics", John Wiley and Sons, New York, 1943, Chapter X. (UNCLASSIFIED)
- 5-17 Terzaghi, K., and Peck, R. B., "Soil Mechanics in Engineering Practice", John Wiley and Sons, New York, 1948. (UNCLASSIFIED)
- 5-18 Newmark, Hansen and Associates, "Protective Construction Review Guide (Hardening)", Vol. I, prepared for Office Secretary of Defense, under Contract SD-52, 1961. (UNCLASSIFIED)
- 5-19 Newmark, N. M. and Merritt, J. L., Draft, Chapter 20 - "General Loading Phenomena and Structural Behavior", "Underground Phenomena and Effects from Nuclear Explosions, Part IV, Effects on Underground Structures and Equipment", Contract No. DA-49-146-XZ-027, June 1961. (OUO)
- 5-20 Bultmann, E. H., McDonough, G. F., and Sinnamon, G. K., "Loading on Buried Structures at High Incident Overpressures", Project 1.7, Operation PLUMBBOB, WT-1406, University of Illinois, February 1959. (CONFIDENTIAL)
- 5-21 Bultmann, E. H., McDonough, G. F., and Sinnamon, G. K., "Loading on Buried Structures in High-Overpressure Regions", Project 1.9 Operation HARDTACK, WT-1614, University of Illinois, January 1960. (SECRET)
- 5-22 McDonough, G. F., "Dynamic Loads on Buried Structures", Ph.D. Thesis, University of Illinois, 1959. (UNCLASSIFIED)
- 5-23 Newmark, N. M. and Sinnamon, G. K., "Air Blast Effects on Underground Structures", Project 3.8, Operation UPSHOT-KNOTHOLE, WT-727, University of Illinois, January 1954. (CONFIDENTIAL RD)

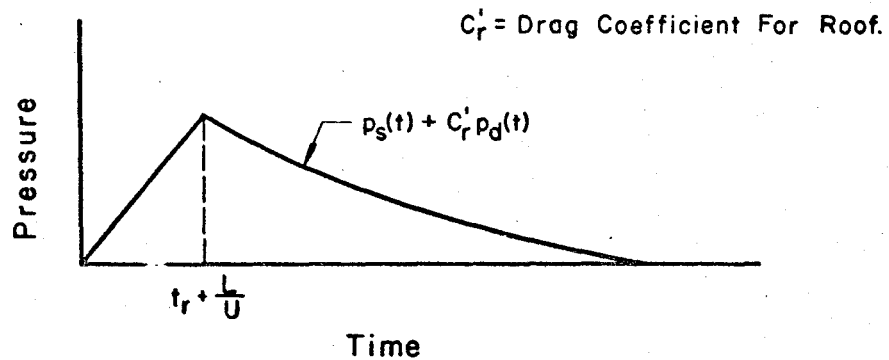
- 5-24 Bultmann, E. H., Jr., Sevin, E. and Schiffman, T. H., "Blast Effect on UPSHOT-KNOTHOLE and TEAPOT Structures", Project 3.4, Operation PLUMBB08, ITR-1423, Armour Research Foundation and Structures Division, AFSWC, October 1957. (CONFIDENTIAL RD)
- 5-25 "Experimental Methods of Determining the Behavior of Underground Structures Under Dynamic Loads", Draft of Final Report for OCDM, Contract No. CDM-SR-60-47, ARF Project No. K200, Armour Research Foundation, January 1961. (UNCLASSIFIED)
- 5-26 "Underground Structures Subjected to Nuclear Explosions", Contract No. AF 33(600)-27802, ARF Project No. K122K5, Armour Research Foundation, November 1958. (CONFIDENTIAL)
- 5-27 Selig, E. T., McKee, K. E., and Vey, E., "Underground Structures Subject to Air Overpressure", Proceedings American Society of Civil Engineers, Vol. 86, EM 4, August 1960, pp. 87-103. Trans. ASCE V 126, Part I, pp. 1627-1649. (UNCLASSIFIED)



(a) Windward Wall Loading

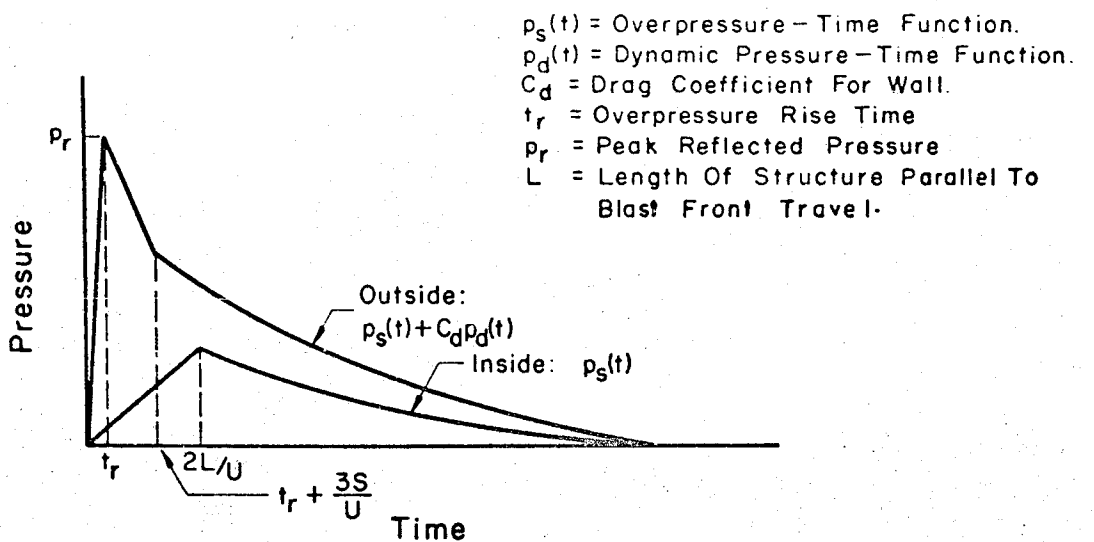


(b) Leeward Wall Loading



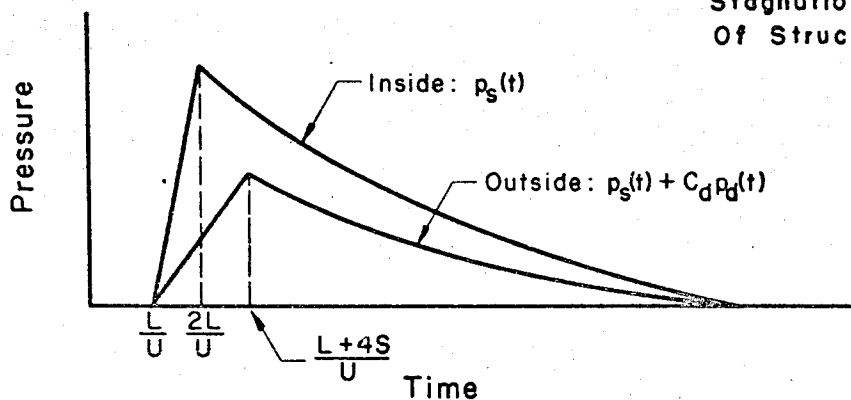
(c) Roof Loading

FIG. 5-1 LOADING ON ABOVEGROUND, CLOSED, RECTANGULAR STRUCTURE.

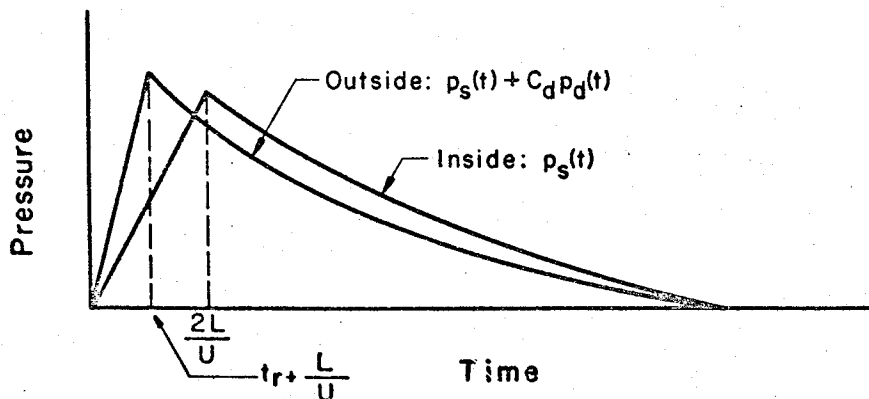


(a) Windward Wall Loading

U = Shock Front Velocity.
 S = Least Distance From Stagnation Point To Edge Of Structural Elements.

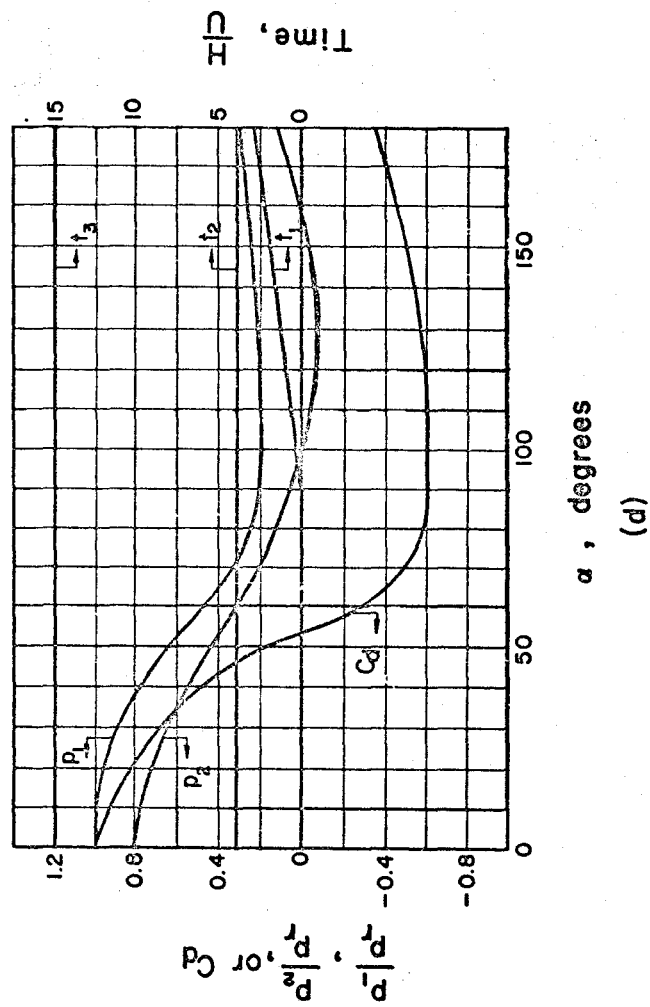
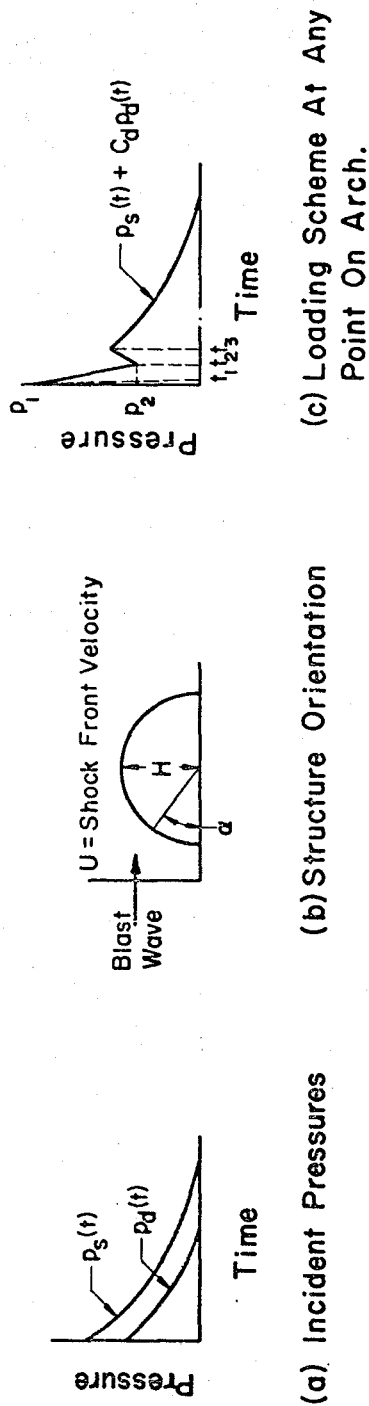


(b) Leeward Wall Loading



(c) Roof Loading

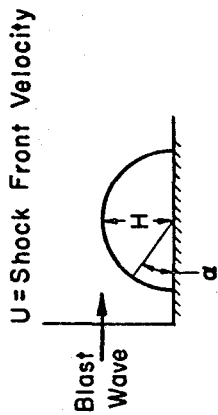
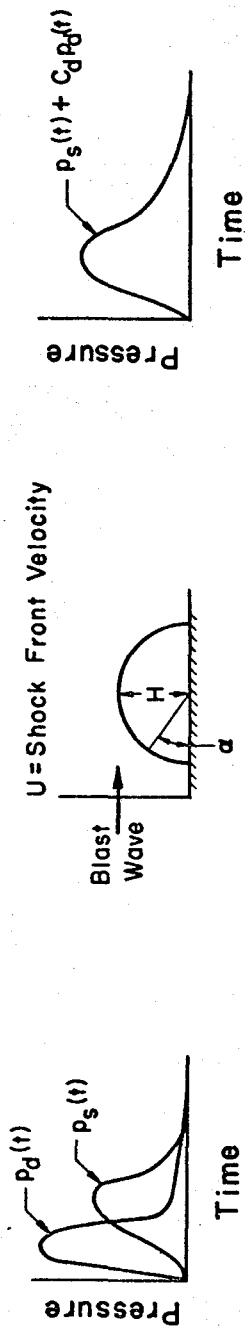
FIG. 5-2 LOADING ON ABOVEGROUND, PARTIALLY OPEN, RECTANGULAR STRUCTURE.



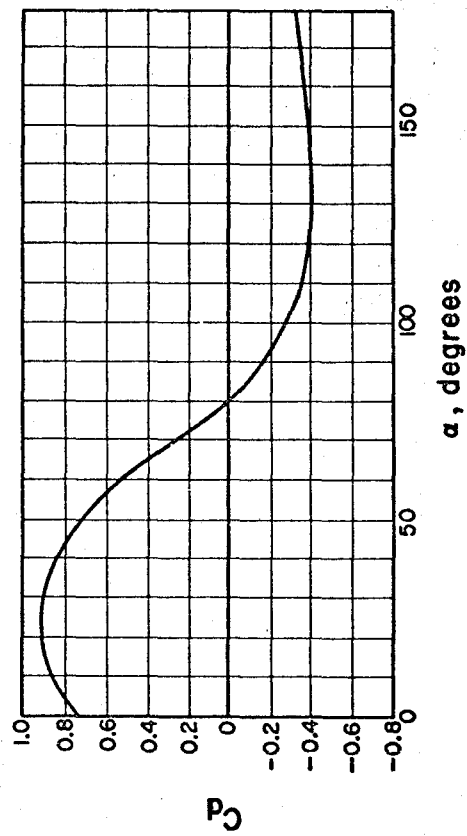
NOTES:

1. Time Units Are Expressed As A Ratio Of Height Of Arch, H , To Velocity Of The Shock Front, U .
2. p_1 And p_2 Related To p_r , The Ideal Reflected (0°) Coefficient. These Could Be Related To p But Relationship To p_r Was Felt More Appropriate For Front Face Loading. Same Relationship Used On The Back Face For Consistency.

FIG. 5-3 IDEAL LOADING SCHEME — 180° ARCH FOR PEAK INCIDENT OVERPRESSURES OF 25 PSI. OR LESS.

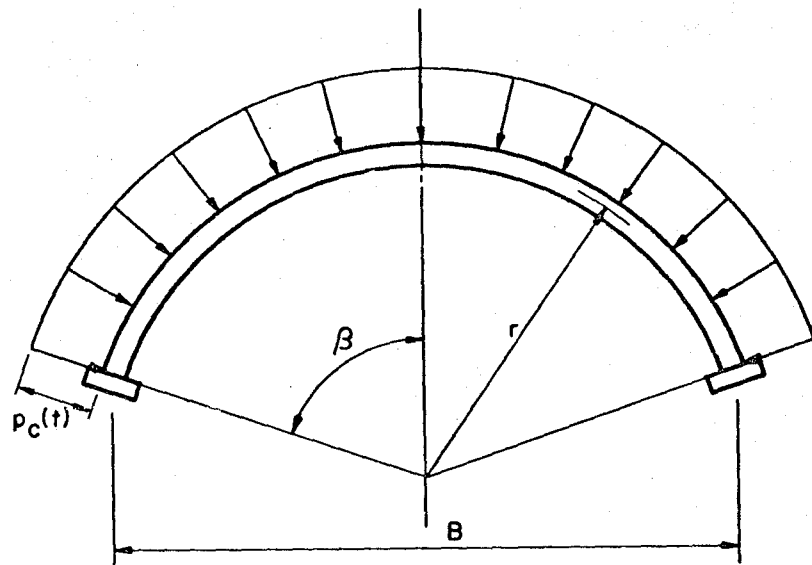


(a) Incident Pressures. (b) Structure Orientation. (c) Loading Scheme At Any Point On Arch.

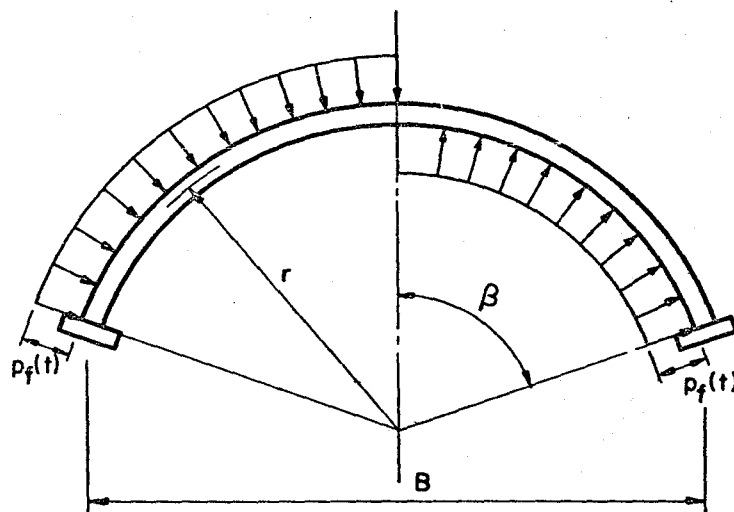


(d)

FIG. 5-4 NON-IDEAL LOADING SCHEME FOR 180° ARCH FOR PEAK INCIDENT OVERPRESSURES OF 100 PSI. OR LESS.

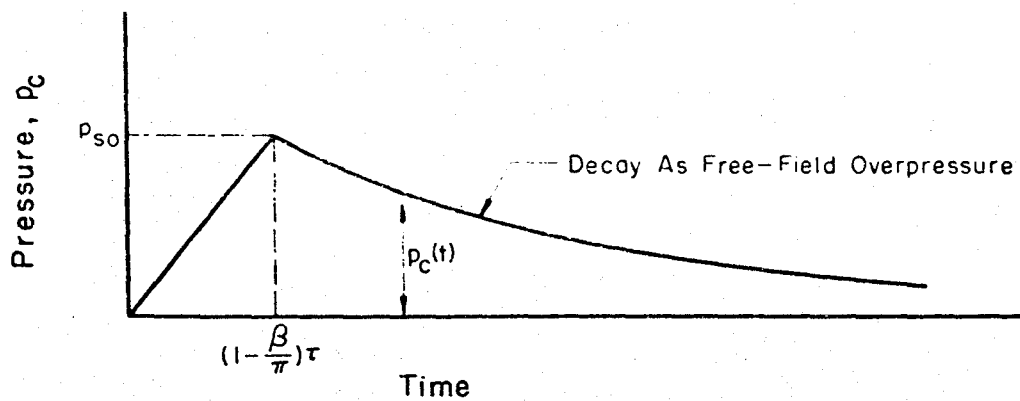


(a) Uniform Compression Loading. (See Fig. 5-6 For Variation With Time.)

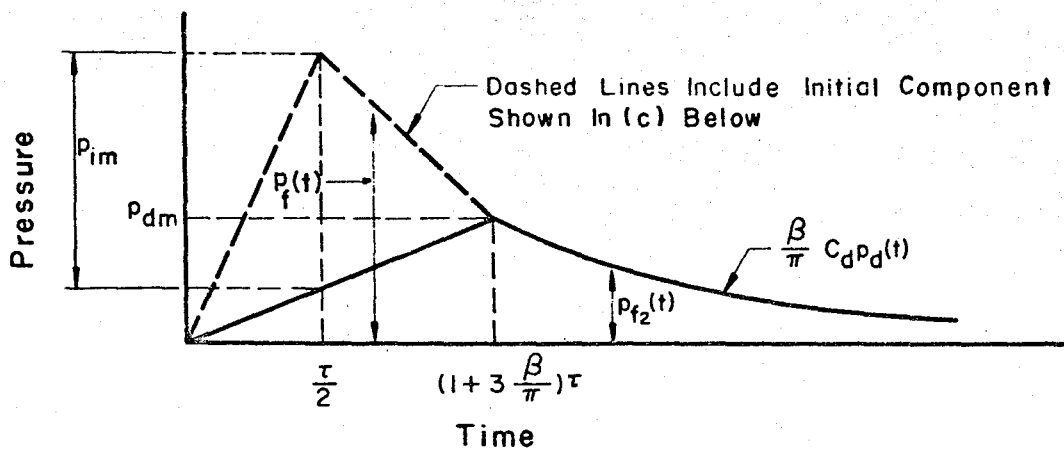


(b) Flexural Loading. (See Fig. 5-6 For Variation With Time.)

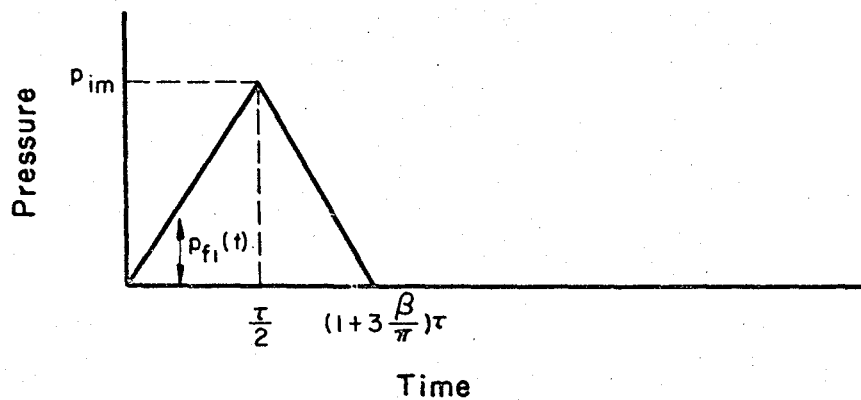
FIG. 5-5 CONVENTIONALIZED BLAST LOADING ON AN ARCH.



(a) Uniform Compression Loading



(b) Drag Component Of Flexural Loading



(c) Initial Component Of Flexural Loading

FIG. 5-6 TIME-DEPENDENT LOADINGS ON ABOVEGROUND ARCHES.

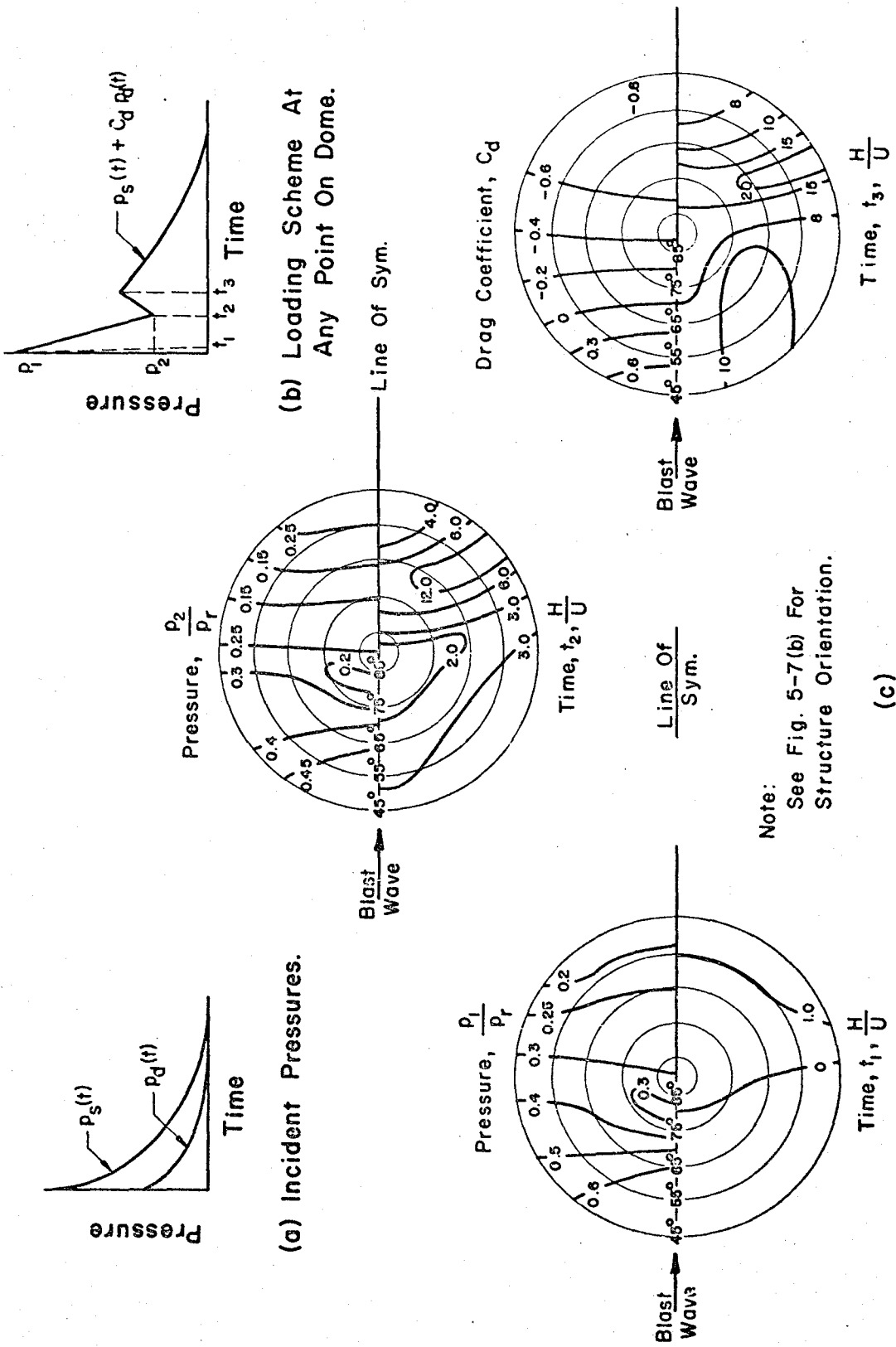
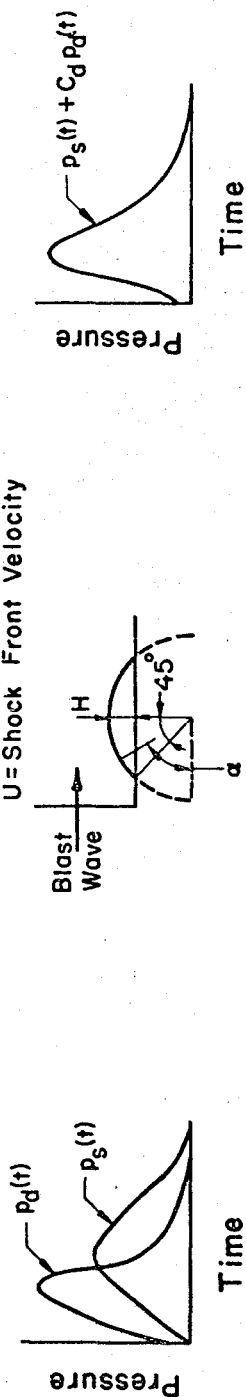
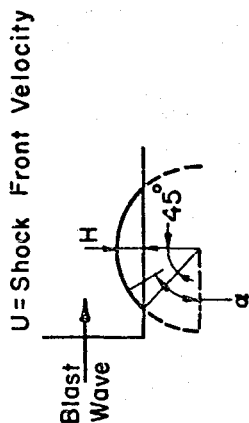


FIG. 5-7(a) IDEAL LOADING SCHEME FOR 45° DOME FOR PEAK INCIDENT OVERPRESSURES OF 25 PSI. OR LESS.



(a) Incident Pressures.



(b) Structure Orientation.

(c) Loading Scheme At Any Point On Dome.

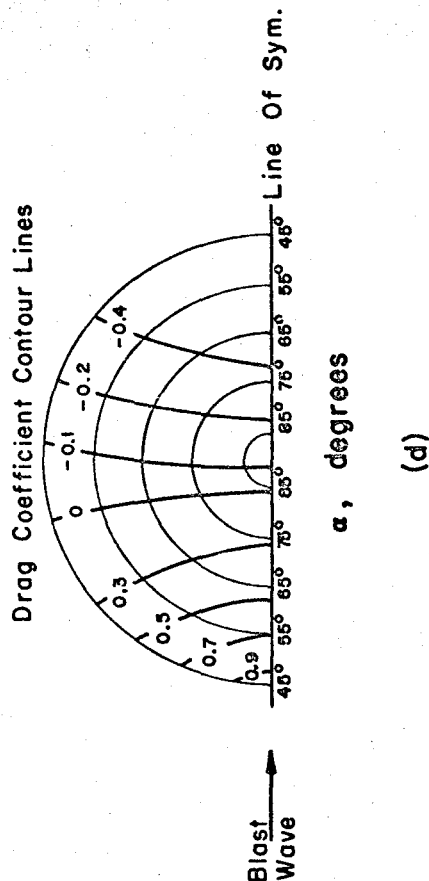
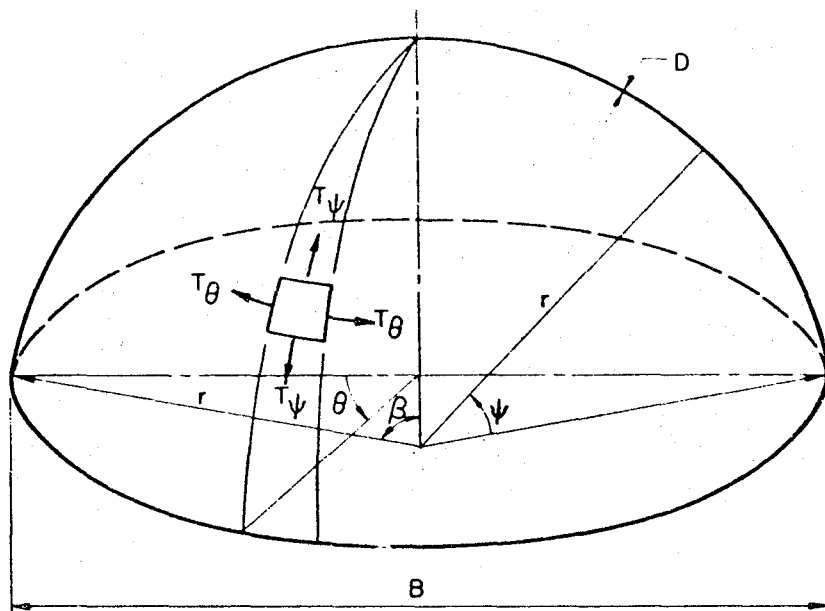
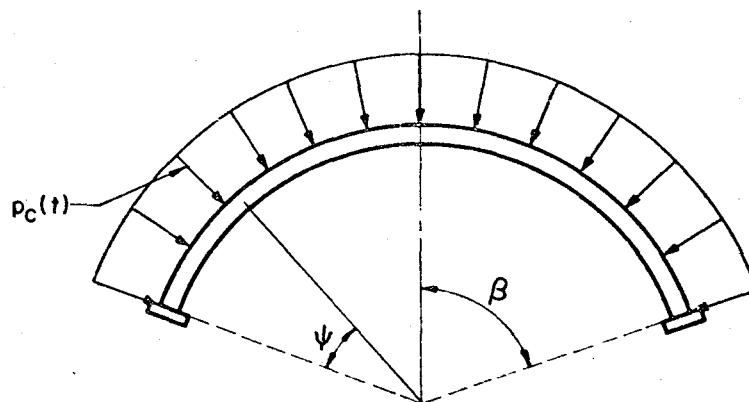


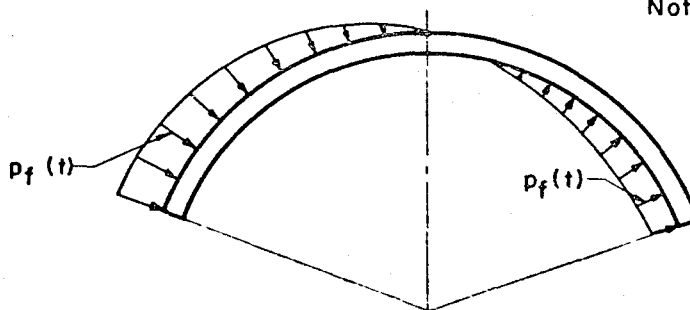
FIG. 5-7(b) NON-IDEAL LOADING SCHEME FOR 45° DOME FOR PEAK INCIDENT OVERPRESSURES OF 100 PSI. OR LESS.



(a) Dome Notation



(b) Uniform Radial Component. (For Variation With Time See Fig. 5-6(a) For Arch.)



Note:

$p_f(t)$ Varies Sinusoidally With Latitude From Maximum At $\psi=0$ To Zero At $\psi=\beta$; It Also Varies Sinusoidally With Longitude From Maximum At $\theta=0$ To Zero At $\theta=90^\circ$.

(c) Flexural Component. (For Variation With Time See Figs. 5-6 (b and c) For Arch.)

FIG. 5-8 A BLAST LOADING ON AN ABOVE-GROUND DOME.

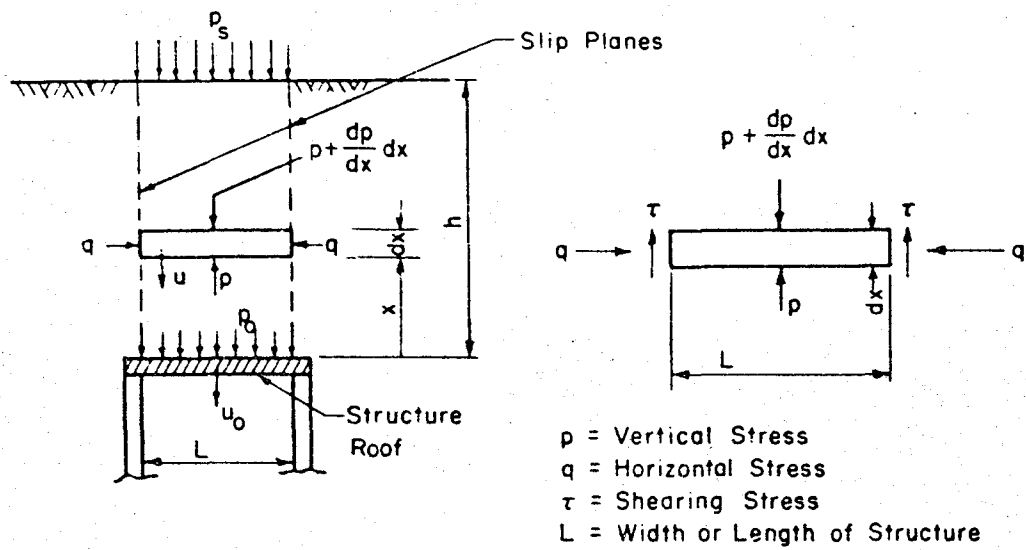


FIG. 5-9 FORCE FIELD ASSUMED FOR UNDERGROUND STRUCTURE

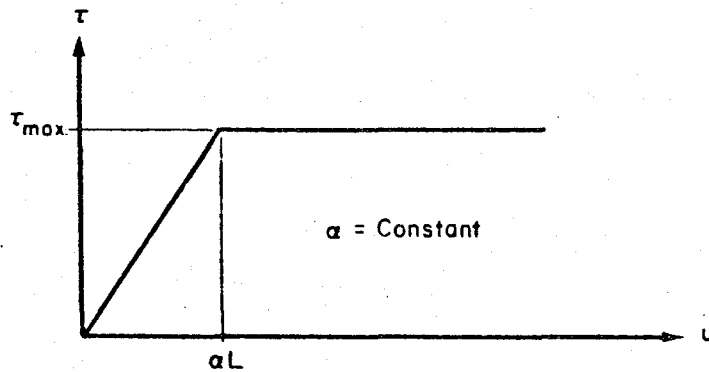


FIG. 5-10 ASSUMED VARIATION OF SHEARING STRESS VERSUS DISPLACEMENT

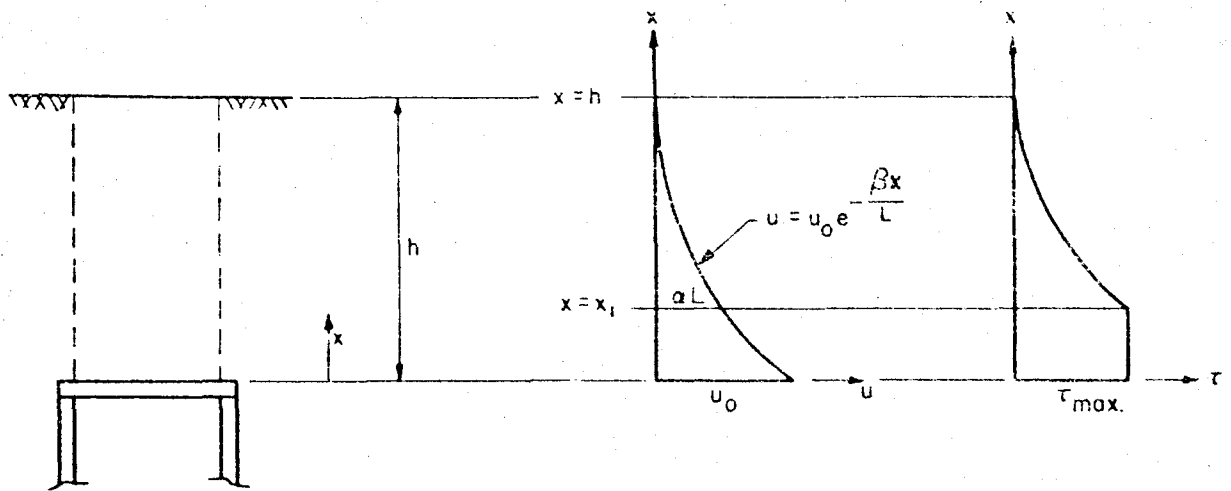


FIG. 5-II ASSUMED VARIATION OF DISPLACEMENT AND SHEARING STRESS WITH DEPTH.

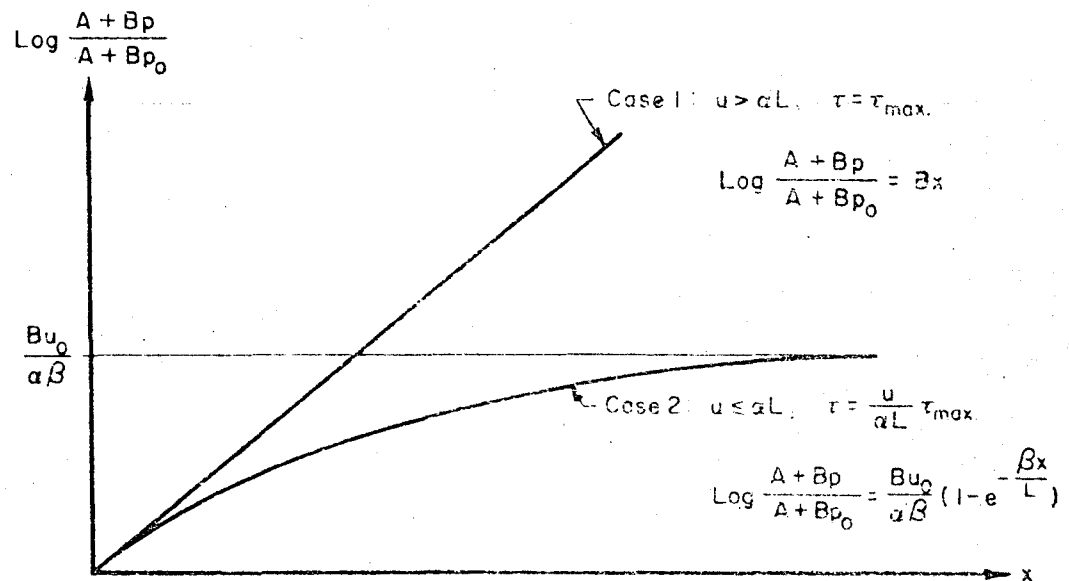


FIG. 5-12 VARIATION OF PRESSURE WITH DEPTH

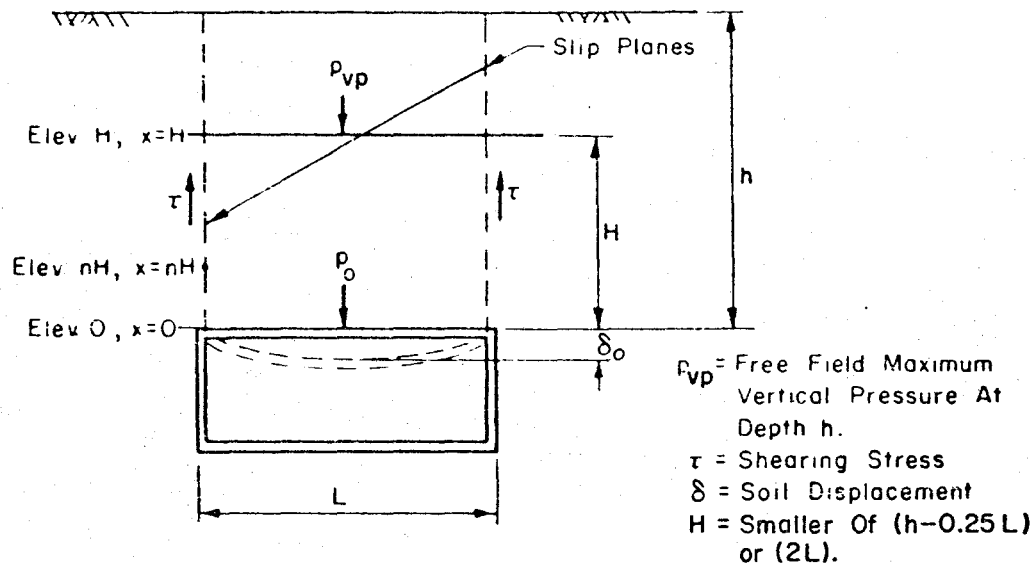


FIG. 5-13 CROSS-SECTION OF UNDERGROUND STRUCTURE

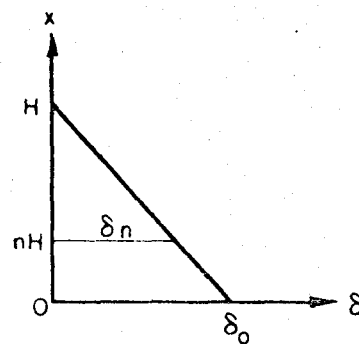


FIG. 5-14 ASSUMED VARIATION OF SOIL DISPLACEMENT WITH DEPTH

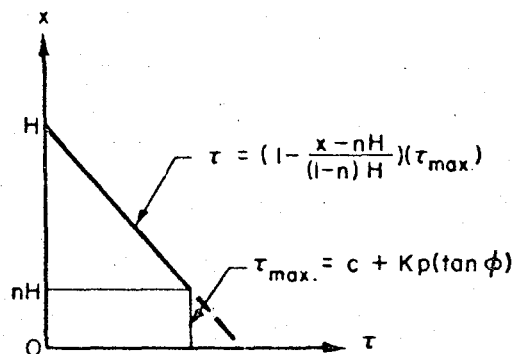
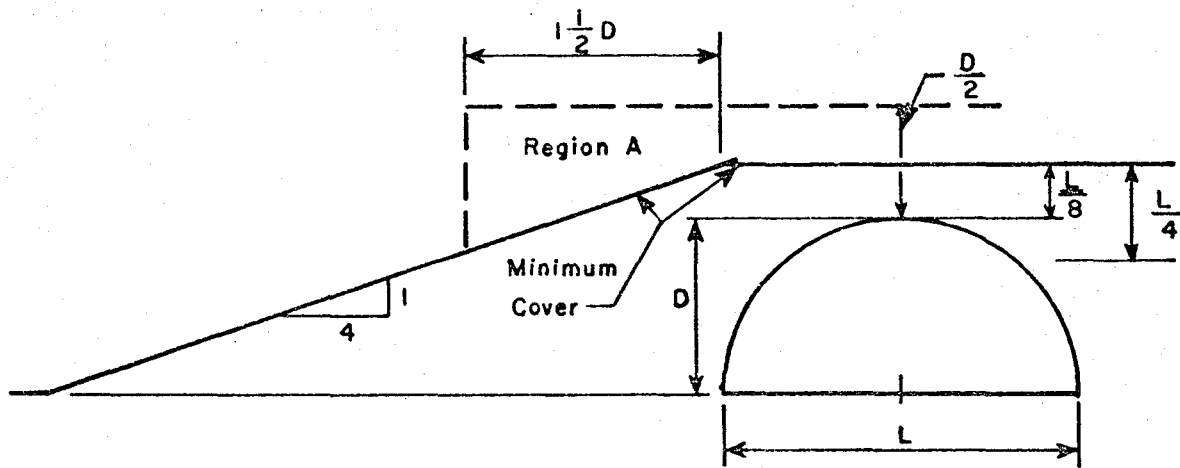
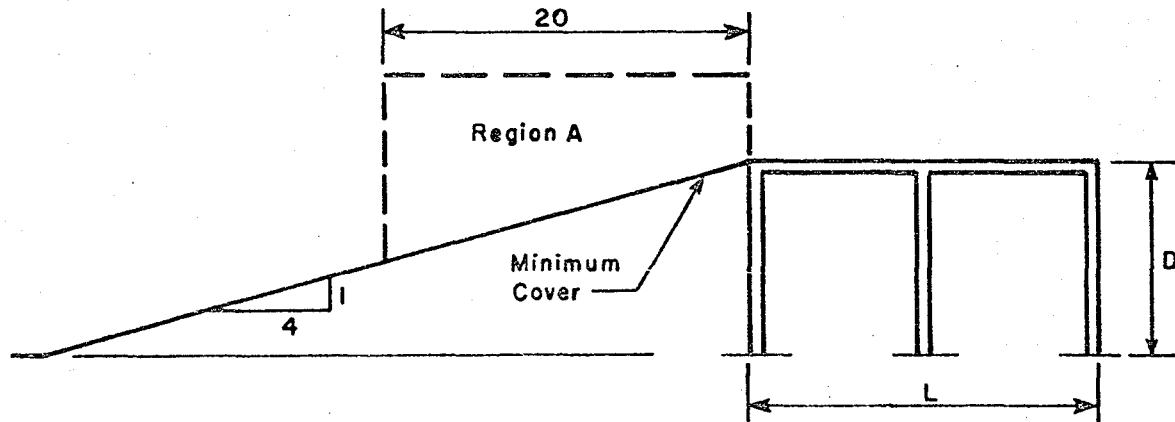


FIG. 5-15 ASSUMED VARIATION OF SHEARING STRESS WITH DEPTH



(a) Arch or Dome



(b) Rectangular Structure

In Region A, maximum slope permitted is 1 on 2 Elsewhere no Limitations apply, except cover must be greater than minimum shown.

FIG. 5-16 DEFINITION OF FULL COVER

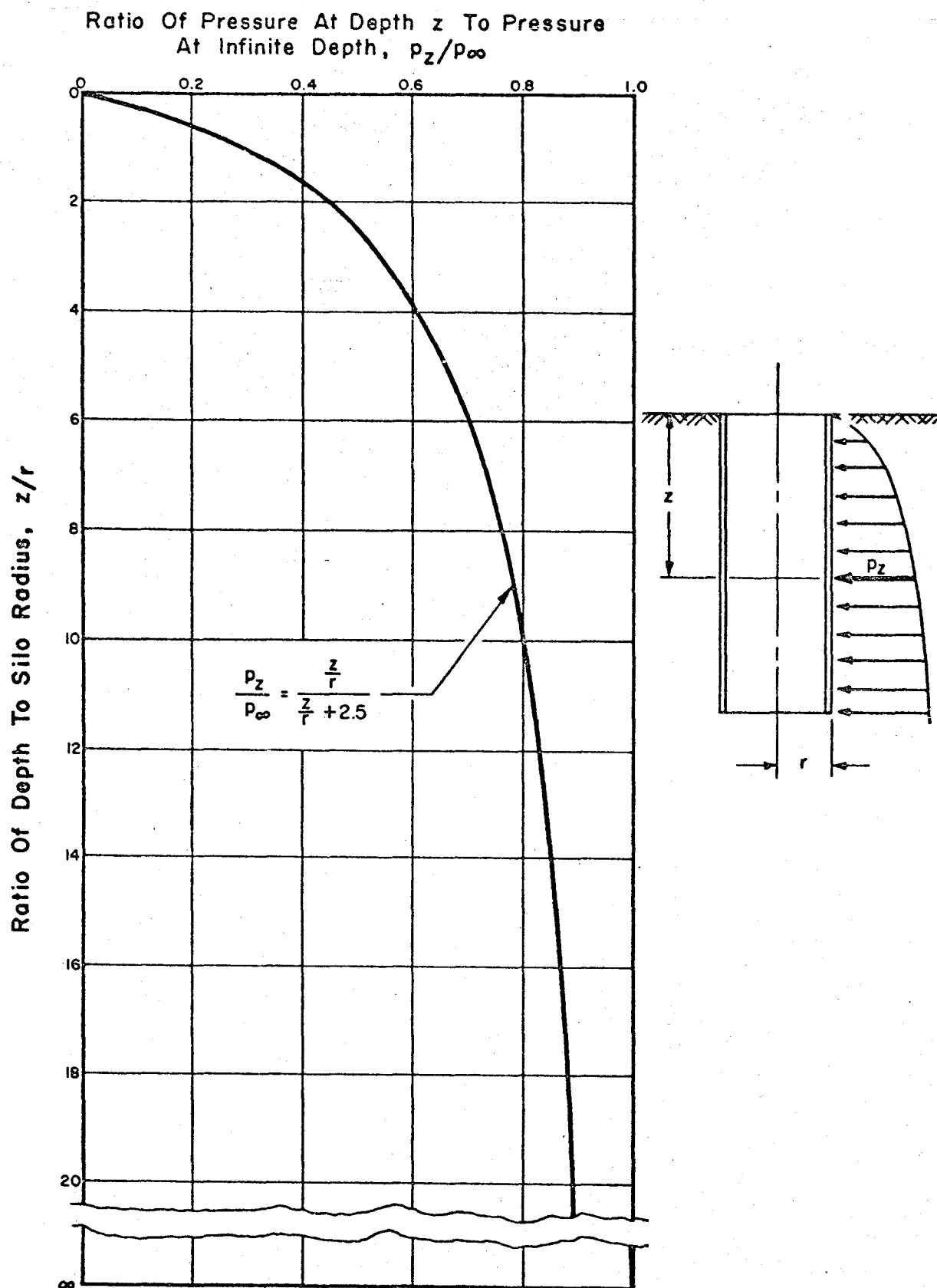


FIG. 5-17 HORIZONTAL DEAD LOAD PRESSURE DISTRIBUTION AGAINST SILO

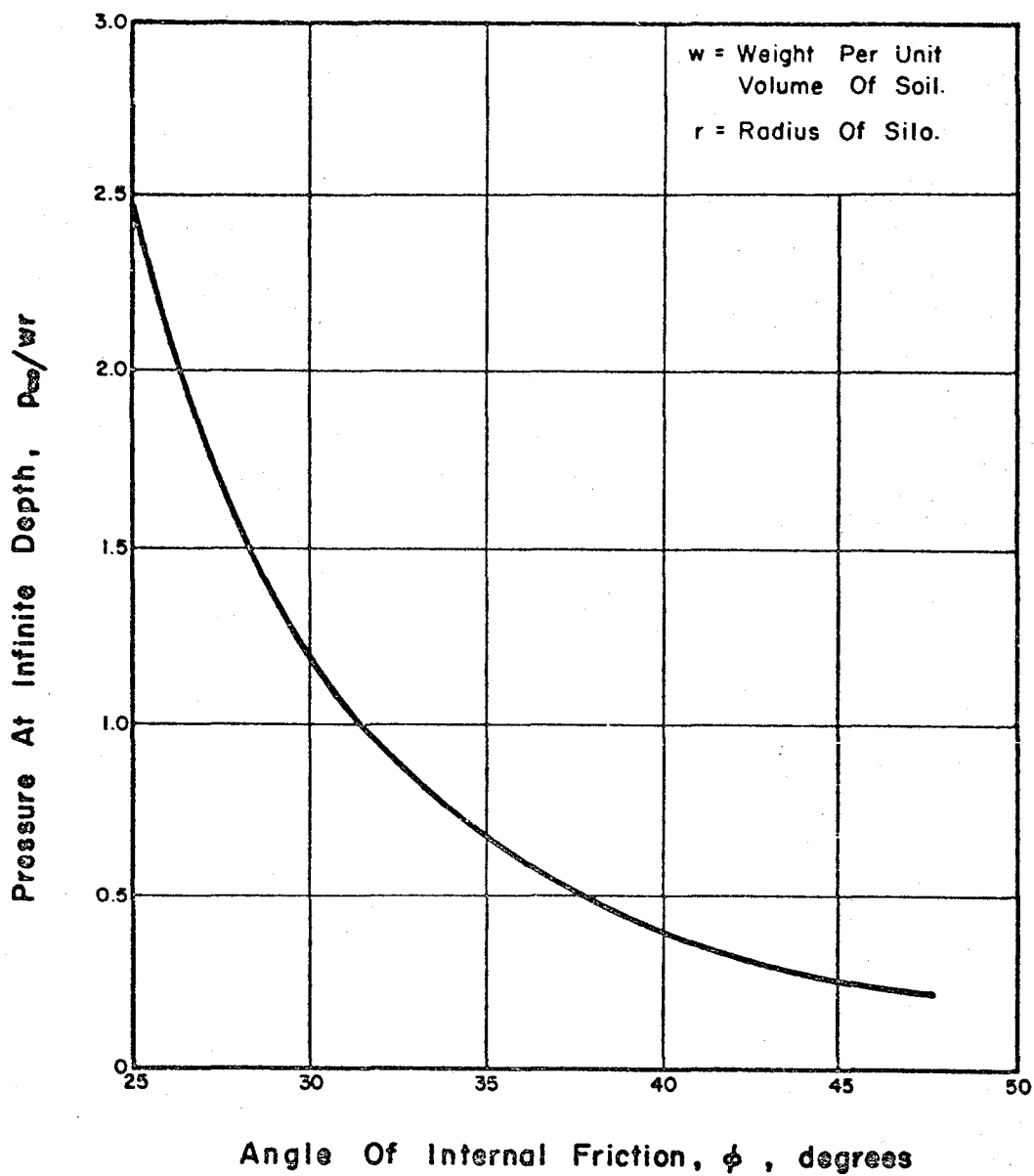


FIG. 5-18 MAGNITUDE OF HORIZONTAL DEAD LOAD PRESSURE ON SILO AT INFINITE DEPTH (LOWER LIMIT).

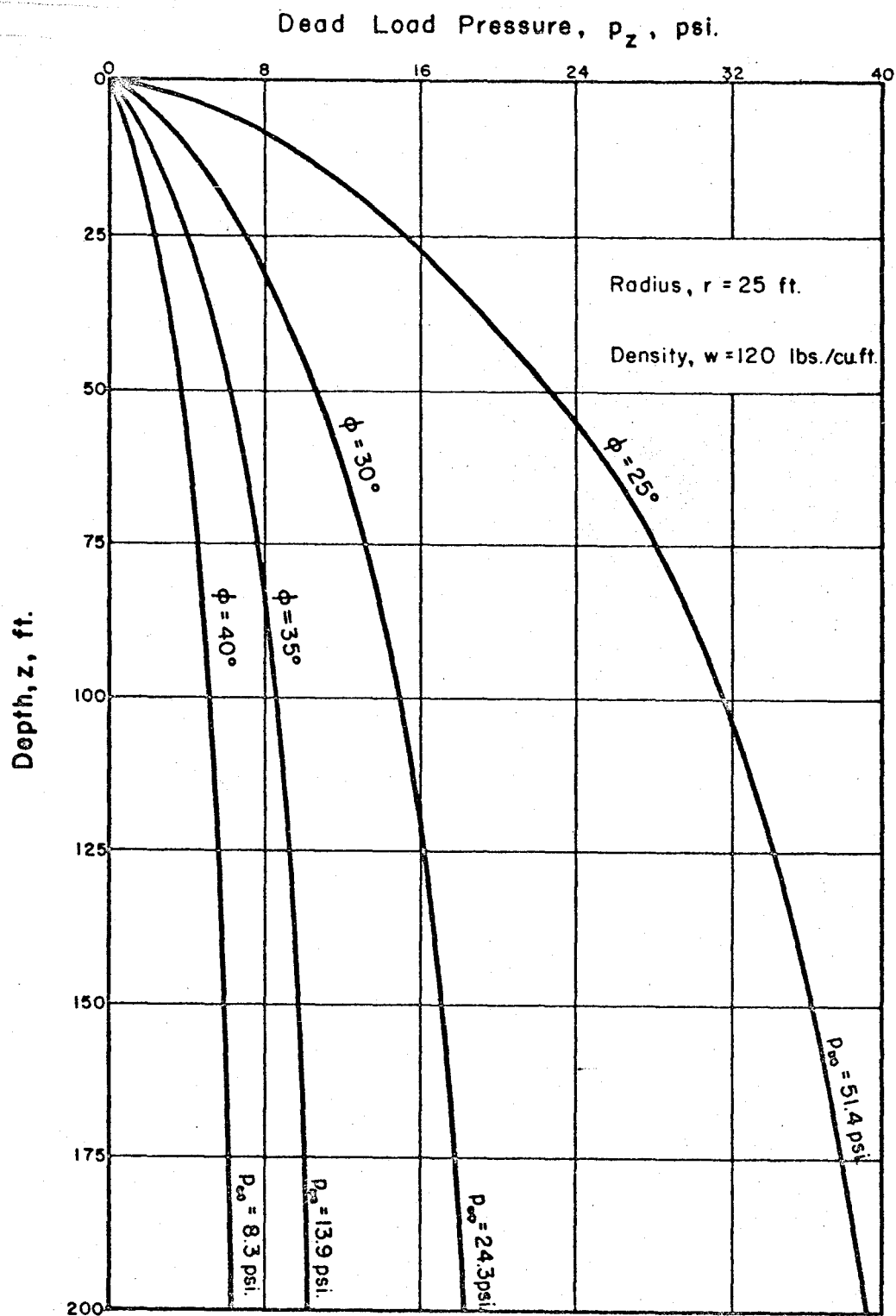
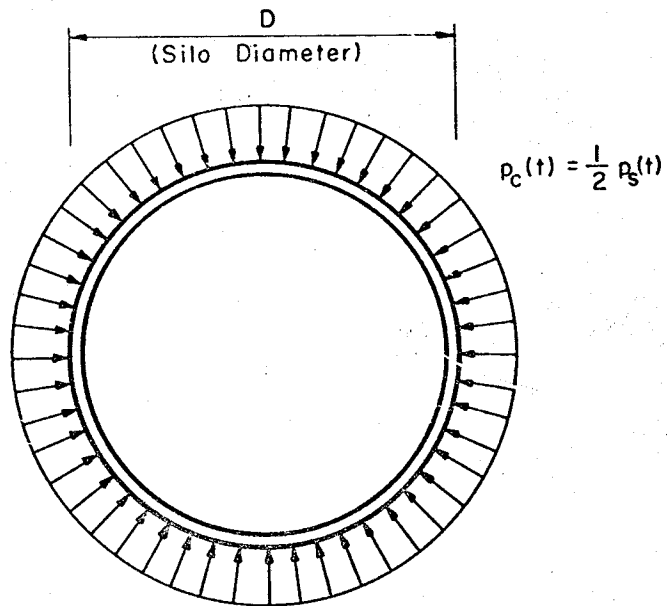
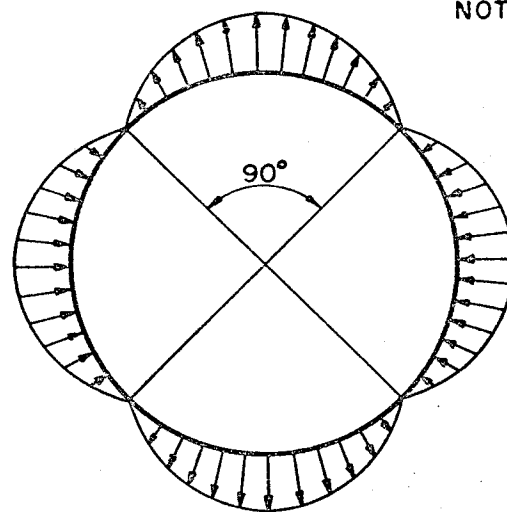


FIG. 5-19 HORIZONTAL DEAD LOAD PRESSURES ON 50-FOOT DIAMETER SILO FOR VARIOUS ANGLES OF INTERNAL FRICTION (LOWER LIMIT).



(a) Uniform Component, $p_c(t)$



NOTE:

$p_f(t)$ Varies Sinusoidally
Around A Circumference
As Shown, And Linearly
With Depth From Max-
imum At Ground Surface
To Zero At Depth = D .

(b) Non-Uniform Component, $p_f(t)$

FIG. 5-20 RADIAL DESIGN PRESSURE ON A VERTICAL
SILO AT THE GROUND SURFACE.

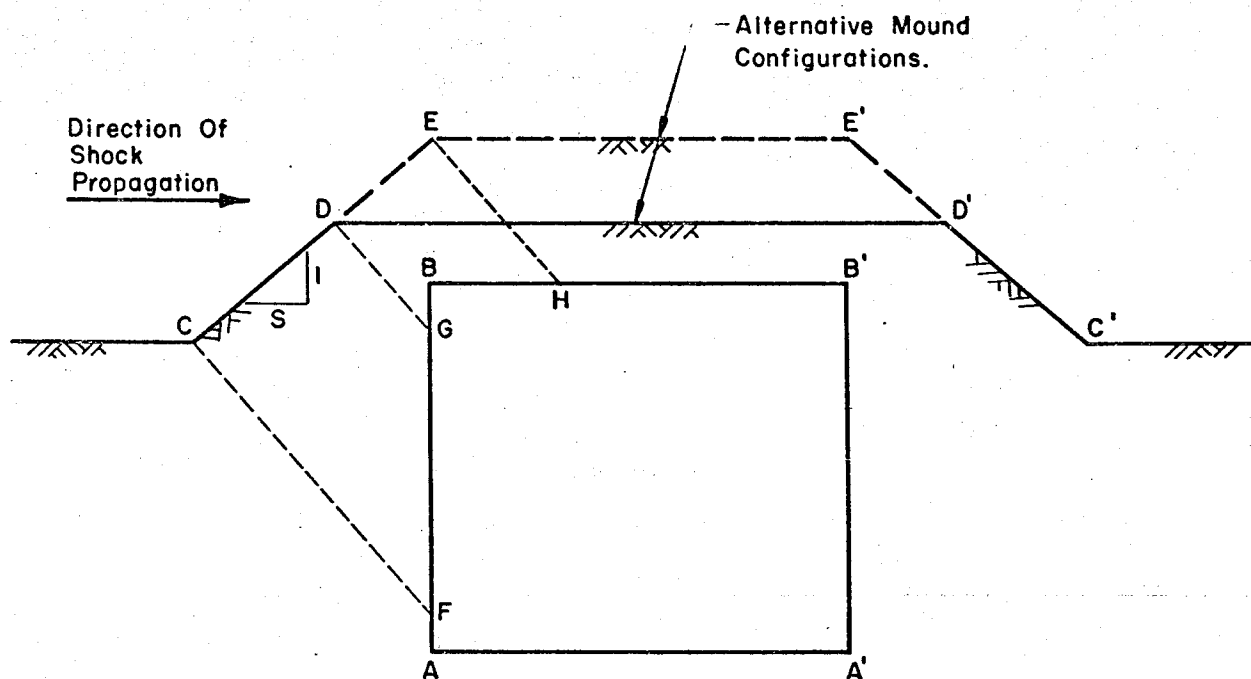


FIG. 5-21 TYPICAL PARTIALLY BURIED OR MOUNDED RECTANGULAR STRUCTURE.

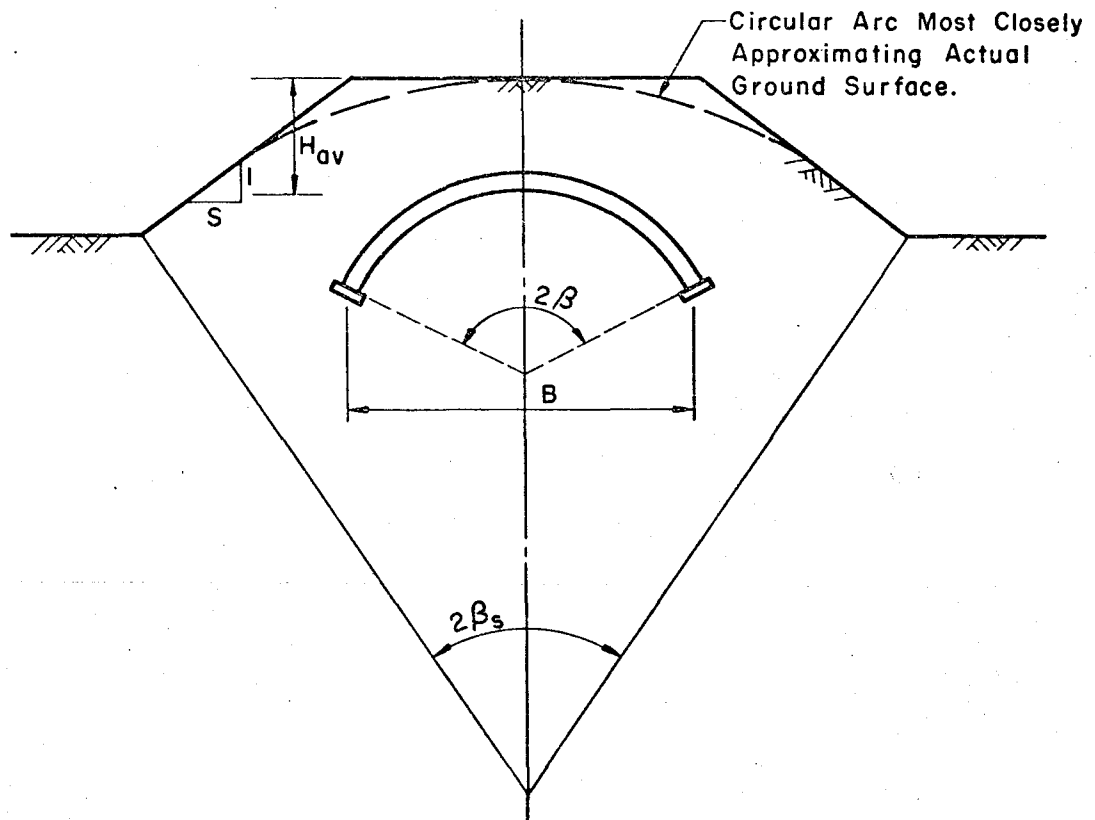


FIG. 5-22 TYPICAL PARTIALLY BURIED OR MOUNDED ARCH OR DOME.

CHAPTER 6. DYNAMIC PROPERTIES OF MATERIALS

6.1 INTRODUCTION

Material properties under dynamic loads are of interest in two respects. First, the normal static stress-strain relationship may be altered permitting different deformations and energy absorption. Secondly, the dynamic loading may affect the circumstances under which brittle failure can occur. Such conditions as severe restraint, residual stresses, discontinuities, flaws, and thickness of materials and joints must be studied in their interrelation and influence on cracking tendency. Experimentation and study continue, with many questions as yet not answered. The purpose of this chapter is to discuss the problems and to summarize the present state of knowledge of dynamic material behavior.

6.2 METALS

6.2.1 General Discussion. Metals can be grouped into two classes with respect to their behavior under dynamic loading. In the first class are those metals with continuous unbroken stress-strain curves showing no sharp yielding zone. This group includes all metals with a basic crystal structure which is face-centered cubic, i.e., aluminum, copper, etc., and in addition those steels which are heat-treated or worked until they lose their definite yield points. Metals of this group do not generally exhibit significant changes in their mechanical properties under dynamic loadings of the type encountered in blast resistant design. The second group includes those metals which have a body-centered cubic crystalline lattice. This group includes the standard structural alloy steels, etc. Metals of this group show a

marked variation in mechanical properties with changes in rate of loading. In studying the influence of rapid loading on the behavior of these latter metals two types of investigations have been employed. In one, a constant strain-rate function is applied to the specimen and its rate is varied between tests (Refs. 6-1, 6-2, 6-3). In the other a loading pulse with a sharp rise is applied to a specimen which has very little mass (Refs. 6-4, 6-5, 6-6).

Under the strain-rate testing, the stresses associated with the initiation of yielding are found to increase as the strain-rate increases. The magnitude of this increase is a direct function of the strain-rate. The few strain-rate tests that have been reported have been constant strain-rate tests.

The other data existing are those from the loading tests. In this case, a load causing stresses in excess of those normally associated with yielding is applied rapidly to a test specimen which has little mass. The specimen responds directly to the loading with strains increasing elastically with stress. During this time the loading test is essentially equivalent to a constant strain-rate test. If the peak value of the stress is equal to or greater than the yield stress established by the strain-rate associated with the rate of loading, the material will yield with no delay. If the stress is less than that value, the straining will stop for some finite time after the load has reached its peak before yielding commences. There is thus a critical value of peak stress for each strain-rate to yield relationship which determines if the time delay occurs. During this delay time the specimen supports a stress in excess of that commonly associated with static yielding at a strain corresponding to elastic behavior (Refs. 6-5, 6-6). This delay time decreases as the excess stress increases until zero delay

time is reached at a stress equal to the yield stress value for the strain-rate applied.

In Fig. 6-1 the ratio of dynamic yield stress to the static yield stress (values corresponding to maximum strain-rate permissible under ASTM specification) is plotted against time to initiate yielding, measured from zero time. In applying these data to the design of structural systems it must be remembered that it is the response of the system which determines the dynamic effect felt by the material. The delayed yield behavior can only be found in essentially massless systems. In actual members possessing mass and susceptible to inertia loading the time-rate effect of delaying the yield does not ordinarily manifest itself and can be neglected.

Strain-rates govern the dynamic material properties of most systems. In an actual member, the strain-rate varies with both time and position in the member. For typical members or systems, the response generally carries the member to yielding at a time when the strain-rate is near the maximum. Although time to yielding can be computed, sufficient data are not available to determine the effects of this time variation of strain-rate. Thus average values are used, realizing that they are in general conservative.

In the response to dynamic loadings the Modulus of Elasticity of steel has been demonstrated not to change significantly.

6.2.2 Structural Steel. In Fig. 6-2 the dynamic stresses associated with the initiation of yielding are plotted for varying times to yield. The static or base value of yield stress is taken as that corresponding to a time to yield of one second. At this rate the value of 37 ksi was selected based upon a study by Jackson and Moreland (Ref. 6-7) which shows that approximately

90 percent of A-7 steel should have a yield stress in excess of this value. The approximate time to yield is in the range 0.2-0.3 times the fundamental period of vibration of the member being loaded. Using this relation it can be seen from Fig. 6-2 that for structures with a period of approximately 100 msec or greater a dynamic yield stress of 45,000-50,000 psi is reasonable, while for structures with a period of less than 100 msec a value greater than 50,000 psi is indicated. Although this hedges somewhat on the longer periods, it is reasoned that the conservatism of using constant strain-rate data and the low static stress allow such a selection. A more refined yield value might be selected after a detailed analysis of the original design; however, this does not seem justified by the nature of the problem.

The results cited above are considered to apply equally well to steels under the new ASTM Specification A-36.

For shear, numerous data and theoretical studies indicate that the dynamic shear yield value is about 0.6 times the dynamic tension yield value, and failure in shear takes place at about 0.75 times the tensile strength.

6.2.3 High Strength Low Alloy Steels. The results of laboratory tests indicate that the steels with higher static yield stresses do not achieve as high a percentage of increase in yield stress under dynamic loadings as do weaker steels. For the low carbon steels of this group which exhibit the flat yield zone, although little specific test data are available, the yield stress may be increased slightly as the rate of loading increases. A limited number of strain-rate tests conducted by Jones and Moore (Ref. 6-2) show a flattening out of the dynamic yield increase at higher strain rates.

For this reason, until more complete data become available, increases above 5 percent are questionable. As with A-7 steel, the yield stress in shear is taken as 0.6 times the dynamic yield stress in tension.

6.2.4 Reinforcing Steel. Behavior of intermediate and structural grade reinforcing steels at the strain-rates associated with the response to blast loadings is analogous to the behavior of A-7 steel. Figure 6-2 gives the dynamic stresses associated with the initiation of yielding versus the time to yield. For intermediate grade, the static yield value is taken as 45,000 psi. This value represents an average value. For smaller bars the tendency is toward higher values and for the larger bars, lower values (Ref. 6-23).

From Fig. 6-2 the following dynamic yield values are indicated:

Intermediate Grade $f_{dy} = 50,000 - 60,000$ psi

Structural Grade $f_{dy} = 40,000 - 50,000$ psi

Because of the variability of static properties of reinforcing bars, further increases in these values cannot be generally recommended. For grades of reinforcing steels which do not exhibit definite yield zones, negligible dynamic increases occur, as mentioned in Sect. 6.2.1. For those grades of reinforcing which have higher initial yield values than intermediate grade and finite yield zones, dynamic increases consistent with the approach used for low alloy steels can be used.

In regard to the dynamic properties of reinforcing bars, the question of the effect of welding is of interest. There has been recently concluded at the University of Illinois a series of tests in which this question was studied (Ref. 6-24). Tests were made on No. 6 deformed bars

of two grades: ASTM Designation A15 (Intermediate Grade) and ASTM Designation A-431 (a high strength steel). Bars of both grades were tested in the as-rolled condition and also after having been joined by 60-degree, single-Vee butt welds with a 1/8 inch gap between the welded parts. The bars were tested under slowly applied loads as well as under rapidly applied loads. For the rapid load tests, an infinite duration pulse was used. The time required to reach failure in the high strength bar tests varied from 0.005 to 0.012 sec., and the time to yield for the intermediate bars was about 0.003 to 0.004 sec.

Interpreting the results of these tests, Ref. 6-24 states that "...these tests have shown the high-strength reinforcing bars having the same physical and chemical properties of those used in this program can be welded to produce a bar having properties under slow and rapid loading not significantly different from those of the as-rolled unwelded bar. On the other hand, these results provide a warning that weld defects, perhaps even minor ones, can greatly reduce the ultimate strength and elongation under rapid loading".

Concerning the tests on the intermediate grade bars, Ref. 6-24 states that the welded specimens developed yield points under rapid loading from 26 to 32 percent higher than that for the welded bars tested slowly, while the increase in yield due to rapid loading of the as-rolled bars was usually about 33 percent.

Thus, it may be concluded that if the welds are properly made, butt-welded reinforcing bars behave in essentially the same manner as unwelded bars with both slow and rapid loading. However, weld defects can

precipitate brittle failures, particularly under dynamic loads, at stress levels below the yield strength of the as-rolled bar.

6.2.5 Brittle Behavior of Materials and Connections. Under dynamic loadings the enhanced possibility, under certain conditions, of brittle failure of welded connections requires that more than usual consideration be given the connections. The chemical composition of the metal is of primary importance; certain composition steels, such as those of high carbon content, are more susceptible to brittle fracture. Attention should be given not only to the welds, but also to the procedure and conditions under which the welding is done. A brittle condition or unusual stress concentration in rivets and bolts can be a source of failure, but the punching and preparation of holes may be of more significance in this respect. In addition, edge conditions may determine the strength. These statements may seem contradictory to the phenomenon of connections offering increased resistance when specimens deform rapidly, but insight into the brittle behavior of materials substantiates all of these apparently conflicting statements. It should be noted that much of the material on brittle failures is relatively new, and with a shortage of tests under a wide range of conditions, there is still a large area of theory which is not completely understood or agreed upon.

Figure 6-3 is a typical qualitative plot of test results for assessing the tendency toward brittle fracture. The stress required for plastic flow depends upon both rate of loading (or strain-rate) and temperature. The ductility transition temperature zone is an attempt to mark the boundary between brittle and ductile behavior. It moves to the right (higher tempera-

ture) with an increase in notch severity and/or increase in rate of loading. Although there is a "fracture appearance transition temperature" at a higher energy range, this "fracture transition" is almost insensitive to the notch severity and rate of loading. It is of less importance since service failures were found to have little manifestation of ductility. This may be explained by the fact that brittle behavior below the ductility transition temperature may initiate a crack and spontaneous cleavage propagation may follow at stresses above 10,000 psi. This is generally true for fractures initiated in the laboratory by impact methods; however, recent results make this particular stress level questionable. Static loads under the same conditions of brittleness, temperature and initiated crack could cause a cleavage crack to grow if a sufficient region of the structure had reached a stress equal to yield.

Although a notch may cause stress concentrations, this is not the primary reason for its embrittling action. A state of stress exists at a notch where the ratio of maximum shearing stress to maximum principal stress becomes small thus inducing brittle behavior. Such embrittling may also be the result of cold-working, punching, shearing, flame-cutting, "arc-striking", high degrees of restraint and residual stresses.

The significant effect of an increase in strain-rate is that the yield stress increases more rapidly than the ultimate stress. Such an increase in the ratio of yield stress to ultimate stress introduces the possibility of local fracture of a brittle nature in an ordinarily ductile material. Also, the "transition temperature" can increase with increased strain-rate under fixed conditions of stress and strain, and brittle failure

can occur at higher temperatures.

Strain-rates may become exceedingly high where there are stress concentrations. The resultant strain-rate at such points is the product of the initial strain-rate and the stress concentration factor.

Figure 6-4 shows a comparison of the effect of impact and slow loading on energy absorption for fracture of notched specimens of 0.16% C plain carbon steel. Considerable variation in energy absorption occurs between 0° and +40°F. There is a linear relation between the log of the strain-rate and the reciprocal of the absolute temperature of transition.

Records of service failures substantiate that embrittlement results from defects in materials and poor workmanship, along with low temperatures and impact loads. No brittle failures are likely at temperatures higher than the effective transition even with the presence of defects or flaws.

Almost without exception, the origin of cracks in welded ships, for example, were at weld defects. This would indicate that designing connections for structures to undergo dynamic loading requires a thorough understanding of sound welding procedures and factors affecting weldability.

As has been noted, the fabrication methods of edges with their consequent physical and geometrical properties have a profound effect on the probability of brittle failures.

Since the shanks of bolts and rivets are not "cold-worked" or "notched" during fabrication, and since they are basically shear components, brittle failure of these items in the manner of defective welds is unlikely. High-strength bolts are an exception in that they are basically in

tension, but by the nature of their structural function the impact loading does not have the same relation to the basic stresses as in the case of bolts in shear. Thus it seems likely that high-strength bolts in shear would not be as susceptible to brittle failure as other connections. This has been confirmed by the A.R.E.A.'s conclusions that such joints are superior to riveted joints and they are not affected adversely by extremely low temperatures.

Rivets and bolts undergoing impact loads must have consideration given to the materials used, the time-rate of loading anticipated and the lowest ambient temperature of the structural elements. In addition, consideration should be given to the type of loading normally carried prior to the anticipated dynamic loading. For example, a member normally subjected to reversals of load may suffer from fatigue and thus become more susceptible to brittle fracture. These considerations determine how critical will be the connection material properties, fabrication methods and workmanship. Information on significant properties of the materials and prescribed fabrication procedures are normally available from manufacturers, societies, and institutes concerned with the use of the material in question.

6.3 CONCRETE

Tests reported in Refs. 6-17 and 6-18 show that with increased rates of straining concrete properties vary as shown in Fig. 6-5. In the referenced tests, two basic concrete strengths were tested. The "weak" concrete had an f'_c of approximately 2500 psi while the "strong" concrete

had an f'_c of approximately 6000 psi. The curve of Figure 6-5 represents an average of the effect upon these two strengths. In the general region of interest, the increase in the ultimate strength ranges from 20 to 40 percent. Flexural members are generally proportioned such that the reinforcing steel governs the resistance capacity. For such members concrete strength variations of the amounts given above have little or no effect upon the resistance capacity. Therefore, there is little necessity for using increased concrete flexural strength values for dynamic loads. There may, however, be good reason for using increased compressive strengths in columns and similar members.

It should also be noted that the dynamic increases in compressive strength discussed above should be considered as being applicable to the static strength at the time of loading, not the so-called standard or 28-day static strength. Thus, from an attack point of view, it would be proper to take into account an increase in strength due to aging before applying the dynamic increase factor. For design, it is probably also reasonable to consider at least some increase due to aging; however, the amount of time that should be assumed to exist between the construction of a facility and the date of potential loading by blast is a subject of which is beyond the scope of this manual.

Shear properties of concrete should increase under dynamic conditions. Little data exists on this subject. Because of the brittle nature of this mode of failure, no allowance should be made for any increases that might occur.

6.4 TIMBER

Tests conducted by the Forest Products Laboratory (Refs. 6-19, 6-20) demonstrated the increased load capacity of timber members under short duration loadings. The tests studied the influence of rate and duration of loading on the compression parallel to the grain and the modulus of rupture and found that these values increased 100 percent for the loadings of the order of one second as compared to the long-duration loadings which are the basis of the working stress code values (see Fig. 6-6). A limited amount of supporting data indicate that the same relationship holds for the other properties. This effect of load-duration has been recognized for some time and allowance for it is made in present timber design codes. Although under blast loadings the rate of loading is more rapid, the stress level is held for some finite duration as opposed to the increasing load to failure of the Forest Products Laboratory tests. These counteracting influences are assumed to balance out and the 100 percent increase is considered realistic. Thus the dynamic design stresses are approximately twice the normal design stresses given in timber codes. These normal design stresses have a factor of safety of a minimum value of 1-1/4 and a most probable value of 2-1/2. However, it is felt that there is not enough uniformity in ultimate strengths to permit a reduction in safety factor in addition to the 100 percent increase recommended for dynamic loading.

6.5 REFERENCES

- 6-1 Manjoine, M. J., "Influence of Rate of Strain and Temperature on Yield Stresses of Mild Steel", Journal of Applied Mechanics, Vol. II, No. 4, December 1944. (UNCLASSIFIED)
- 6-2 Jones and Moore, "An Investigation of the Effect of Rate of Strain on the Results of Tension Tests of Metals", ASTM Proceedings, Vol. 40, 1940. (UNCLASSIFIED)
- 6-3 Fry, L. H., "Speed in Tension Testing and Its Influence of Yield Point Values", ASTM Proceedings, Vol. 40, 1940. (UNCLASSIFIED)
- 6-4 Clark, D. S., and Wood, D. J., "Time Delay for the Initiation of Plastic Deformation at Rapidly Applied Constant Stress", ASTM Proceedings, 1949. (UNCLASSIFIED)
- 6-5 Vreeland, T., Wood, D. J. and Clark, D. S., "A Study of the Mechanism of the Delayed Yield Phenomenon", Metal Prog., October 1952. (UNCLASSIFIED)
- 6-6 Massard, J. M., "The Stress-Deformation Characteristics of Some Mild Steel Subjected to Various Rapid Uniaxial Stressing", Ph.D. Thesis, University of Illinois, 1955. (UNCLASSIFIED)
- 6-7 Johnston, Yang, and Beedle, "An Evaluation of Plastic Analysis as Applied to Structural Design", Progress Report No. 8 on Welded Continuous Frames and Their Components. (UNCLASSIFIED)
- 6-8 Parker, Earl R. Baker, "Brittle Behavior of Engineering Structures", John Wiley and Sons, 1957. (UNCLASSIFIED)
- 6-9 Stour and Doty, "Weldability of Steels". (UNCLASSIFIED)
- 6-10 Welding Research Council, "Control of Steel Construction to Avoid Brittle Failure". (UNCLASSIFIED)
- 6-11 Harris, L. A., and Newmark, N. M., "The Effect of Fabricated Edge Conditions on Brittle Fracture of Structural Steels", University of Illinois, 1957. (UNCLASSIFIED)
- 6-12 Hechtman, R. A., "A Study of the Effects of Heating and Driving Conditions on Hot-Driven Structural Steel Rivets", University of Illinois, 1948. (UNCLASSIFIED)
- 6-13 Seely and Smith, "Advanced Mechanics of Materials", Second Edition, John Wiley and Sons, 1952. (UNCLASSIFIED)

- 6-14 McDonald, D., Ang, A., and Massard, J. M., "An Investigation of Riveted and Bolted Column-Base and Beam-to-Column Connections under Slow and Rapid Loading", University of Illinois, 1958. (UNCLASSIFIED)
- 6-15 "Procedure Handbook of Arc Welding Design and Practice", 11th Edition, The Lincoln Electric Co., 1957. (UNCLASSIFIED)
- 6-16 "Current Structural Bridge Steels, A Survey of Usage and Economy", Bridge Division, Bureau of Public Roads. (UNCLASSIFIED)
- 6-17 Watstein, D., "Effect of Straining Rate on the Compressive Strength and Elastic Properties of Concrete", Proceedings ACI, 1953. (UNCLASSIFIED)
- 6-18 McHenry and Shideler, "Review of Data on Effect of Speed in Mechanical Testing of Concrete", Bulletin D9, Portland Cement Association. (UNCLASSIFIED)
- 6-19 Wood, L. W., "Relation of Strength of Wood to Duration of Load", Forest Products Laboratory Report R1916. (UNCLASSIFIED)
- 6-20 Tiska, J. A., "Effect of Rapid Loading on the Compressive and Flexural Strength of Wood", Forest Products Laboratory Report 1767. (UNCLASSIFIED)
- 6-21 Nadai, A., "Theory of Flow and Fracture of Solids", McGraw-Hill Book Company. (UNCLASSIFIED)
- 6-22 "Design of Structures to Resist the Effects of Atomic Weapons, Strength of Materials and Structural Elements", Manual Corps of Engineers, U. S. Army, EM 1110-345-414, March 1957. (UNCLASSIFIED)
- 6-23 Gaston, J. R., Siess, C. P., and Newmark, N. M., "An Investigation of the Load-Deformation Characteristics of Reinforced Concrete Beams up to the Point of Failure", University of Illinois, 1952. (UNCLASSIFIED)
- 6-24 Siess, C. P., "Behavior of High Strength Deformed Reinforcing Bars Under Rapid Loading", University of Illinois, prepared for the Committee of Concrete Reinforcing Bar Producers, American Iron and Steel Institute, February 1962. (UNCLASSIFIED)

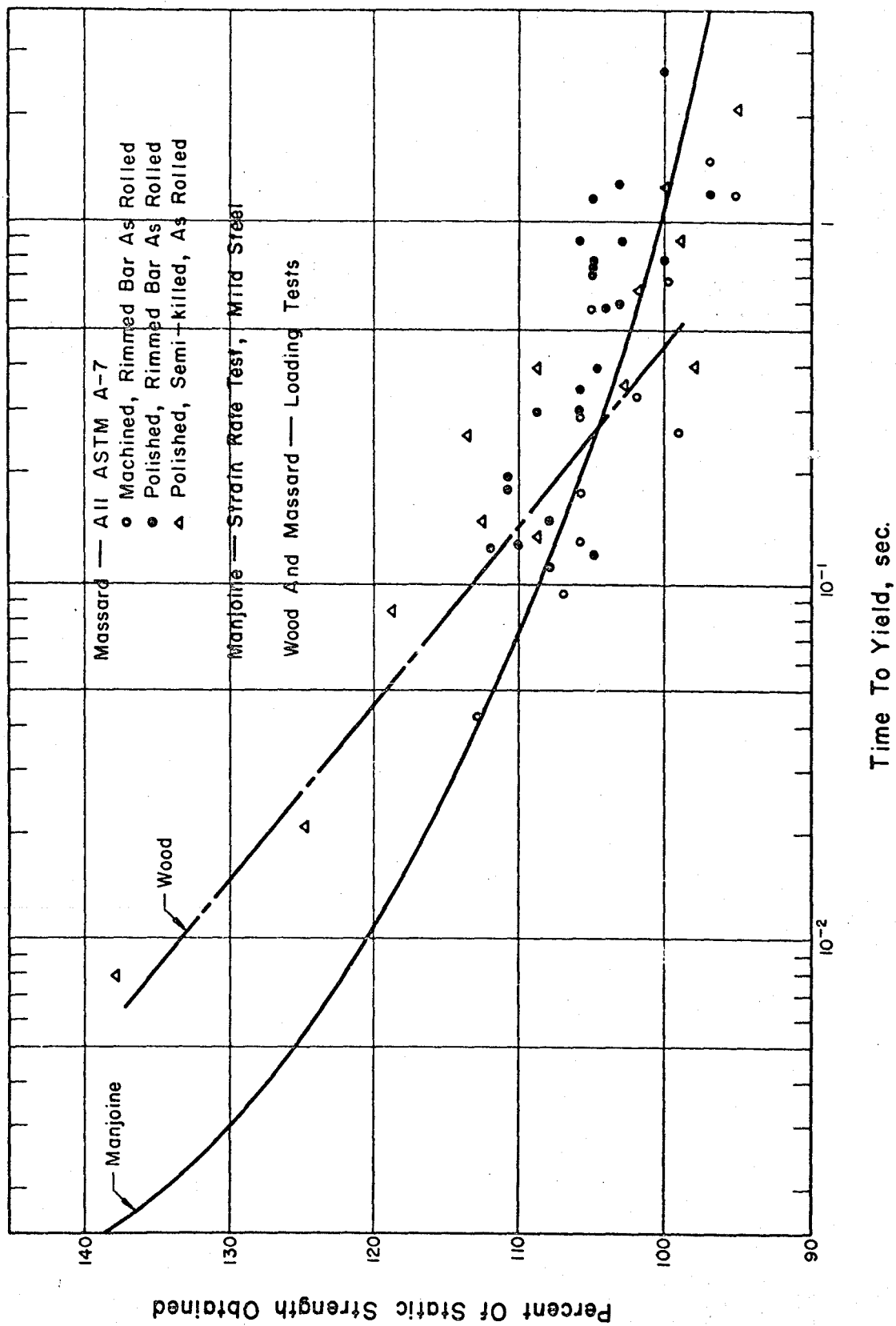
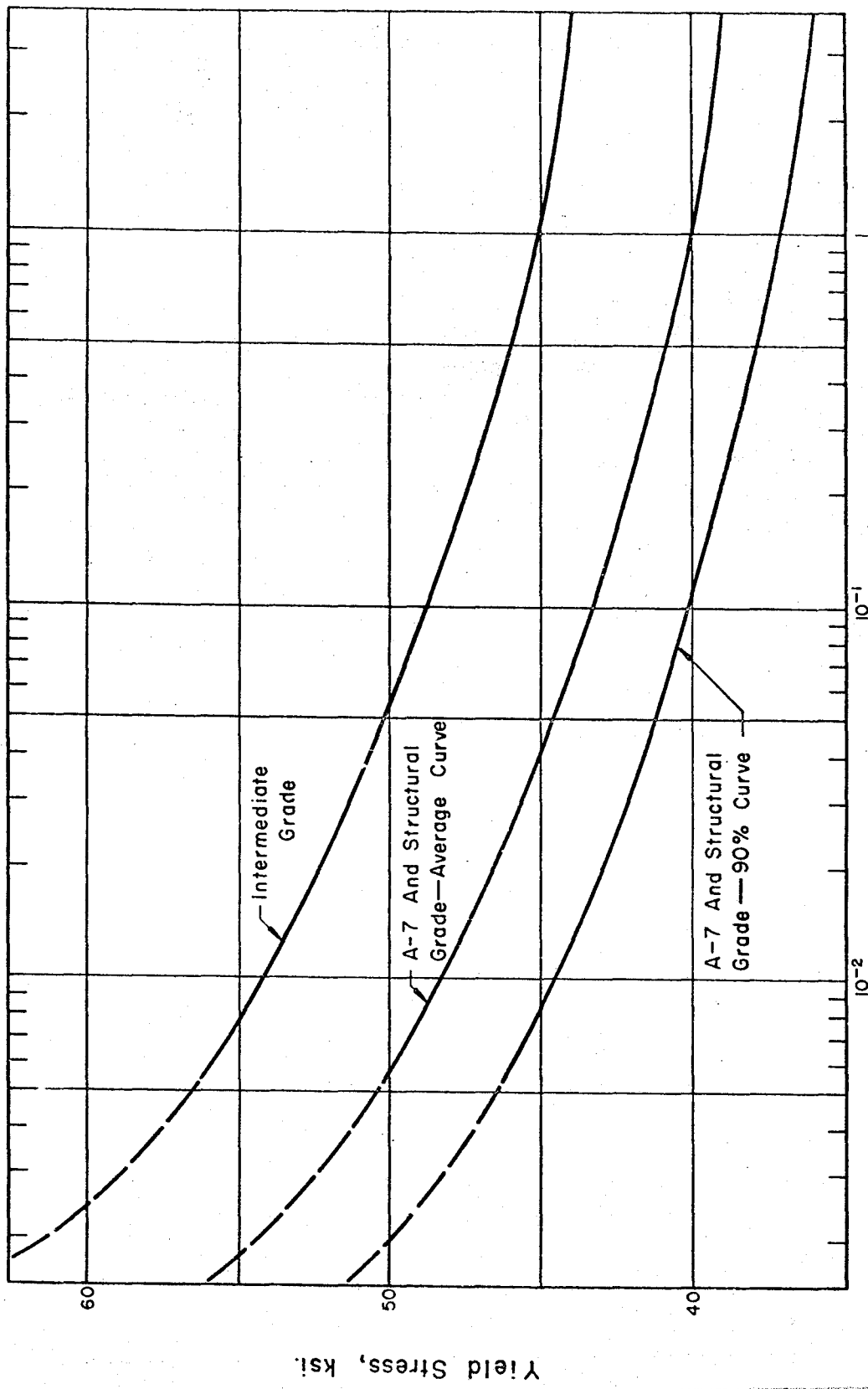


FIG. 6-1 DYNAMIC INCREASE IN YIELD STRESS FOR MILD STEEL



Time To Yield, sec.

FIG. 6-2 YIELD STRESS OF A-7 AND REINFORCING STEEL

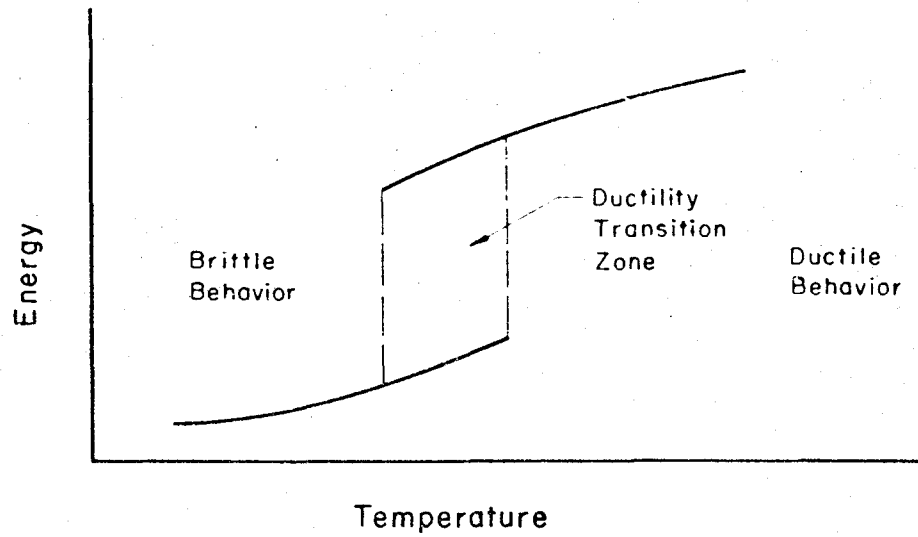


FIG. 6-3 INFLUENCE OF TEMPERATURE ON DUCTILITY.

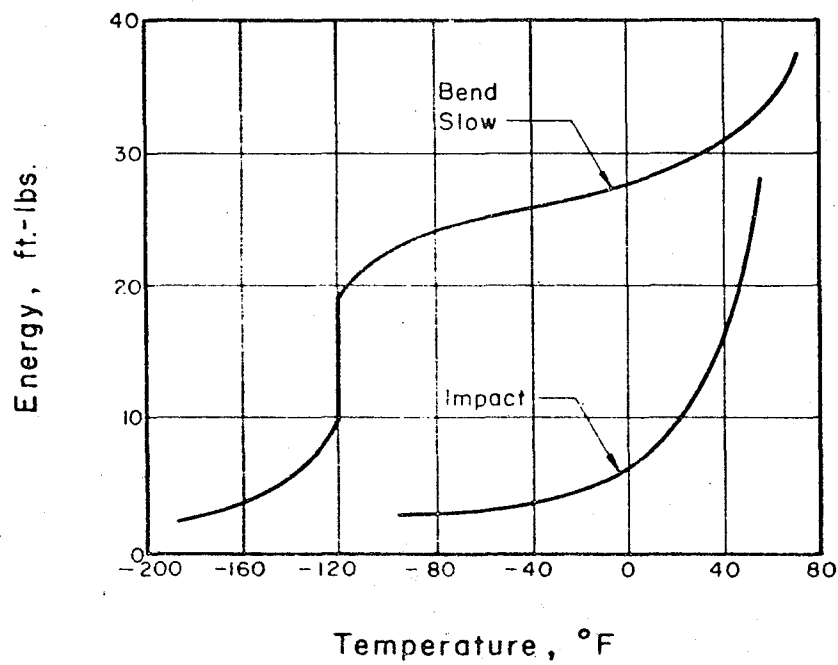


FIG. 6-4 INFLUENCE OF LOADING RATE ON DUCTILITY.

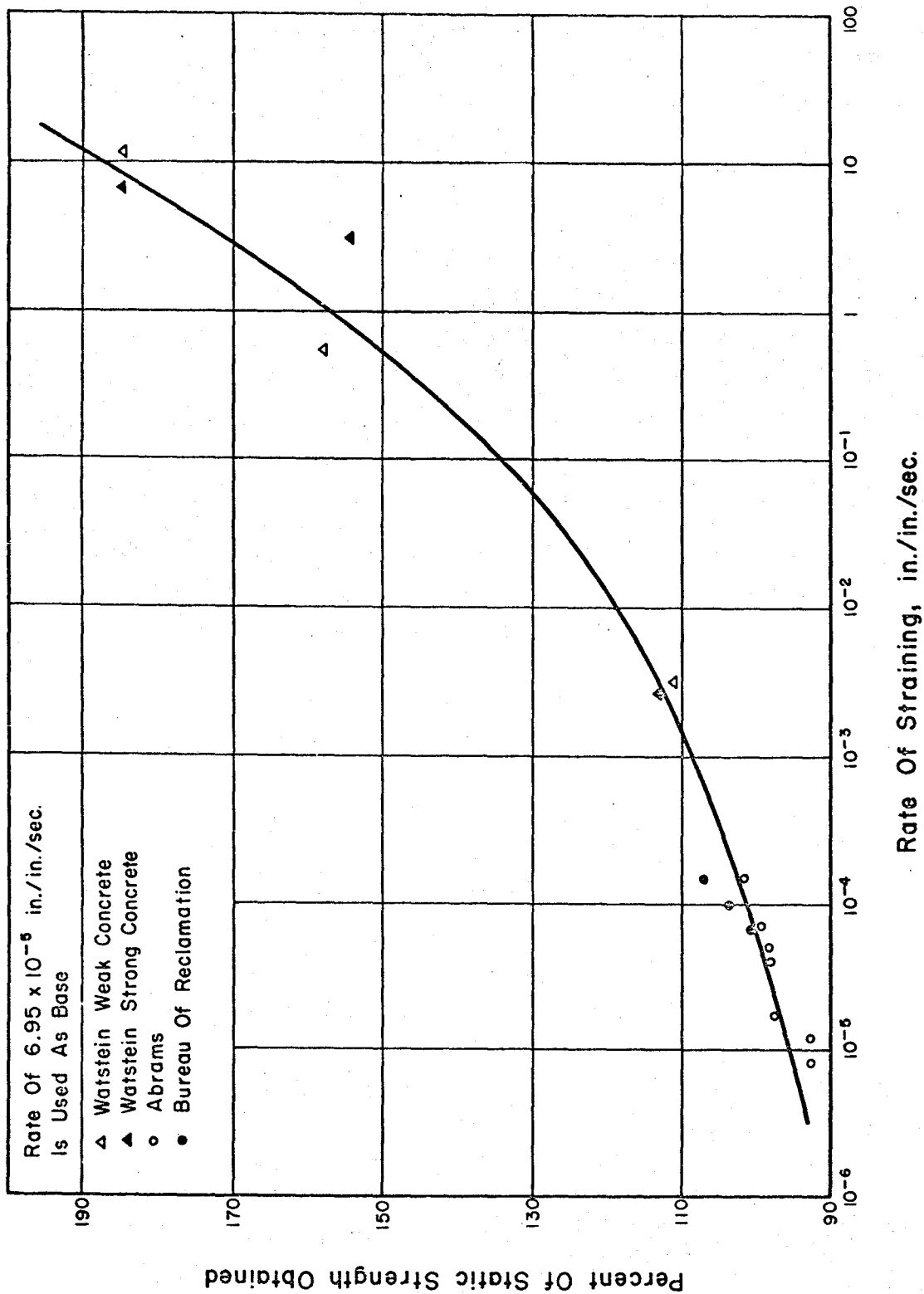
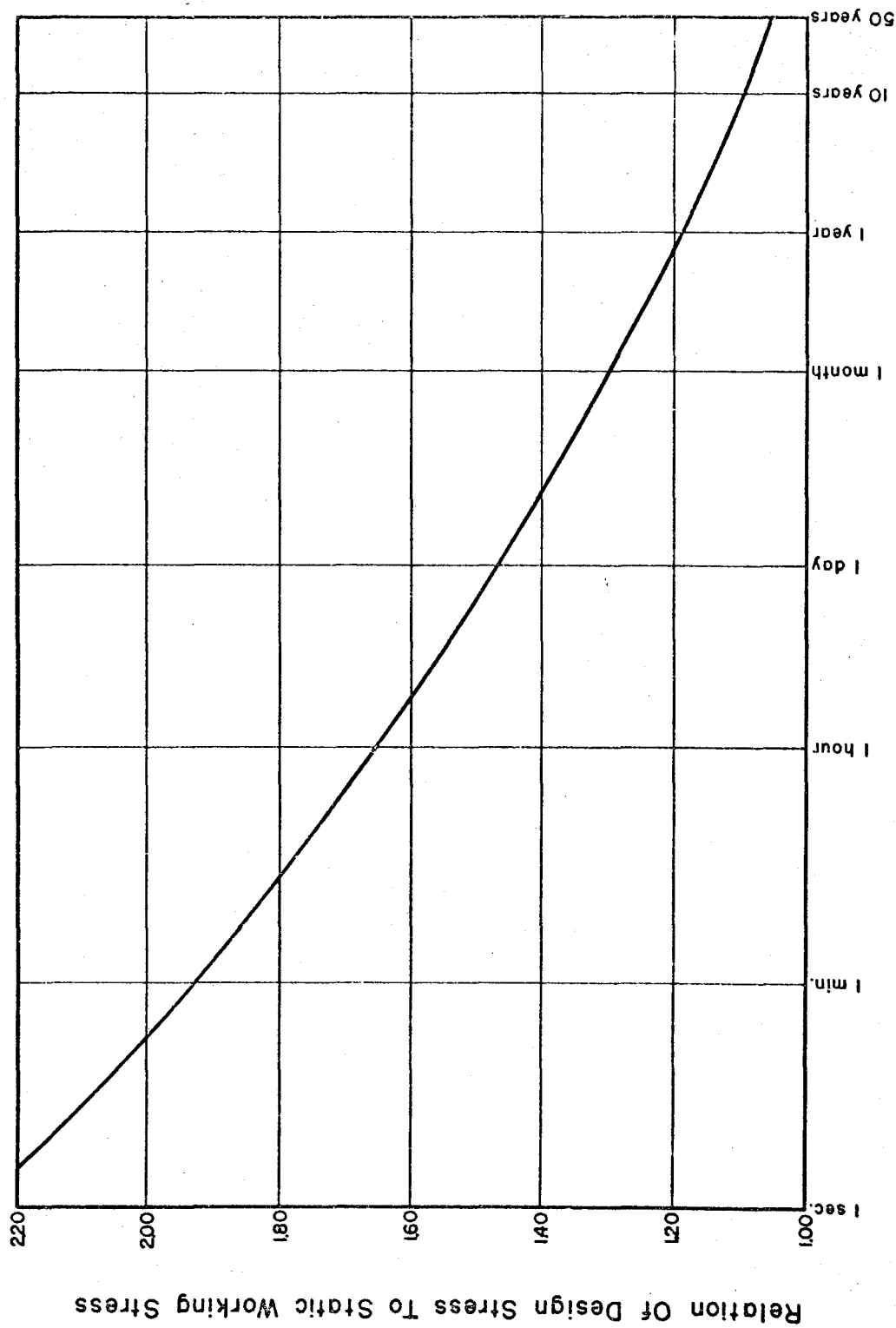


FIG. 6-5 EFFECT OF RATE OF STRAINING ON THE COMPRESSIVE STRENGTH OF CONCRETE



Duration Of Maximum Load

**FIG. 6-6 RELATION BETWEEN DESIGN STRESS AND LOAD DURATION
TIMBER**

CHAPTER 7. FAILURE AND DESIGN CRITERIA

7.1 INTRODUCTION

Having established the environment in which the structure must be placed, it is necessary to give consideration to the performance that will be required of the structure. Actually, it is convenient to think of satisfactory performance versus failure, and to think of failure as any performance which does not meet the standards that have been set as minimum requirements. The performance requirements, of course, can be set for a given structure without any knowledge of the loads to be encountered. Combining the performance requirements with loading criteria and with material and structural properties leads to a design.

It is apparent that at each step of the design procedure, further elements of uncertainty are introduced. By the time the design is complete, the probability of non-failure is indeterminate but is related to and derived from: 1) the probability that the assumed loading conditions will actually prevail; 2) the probability that the structure will behave in the manner assumed; and 3) the probability that the structural materials themselves will exhibit the properties of strength, ductility, etc. which were assumed.

It is thus seen that the concept of a safety factor is rather meaningless, and that one must turn to an ultimate or limit design which is closely allied with some idea of minimum acceptable structural performance, or conversely with some definition of failure.

The purpose of this chapter is, therefore, to discuss the concept of failure in its broadest sense and to show how criteria for design must be carefully fitted to the failure concept for the specific case being considered.

7.2 FAILURE VS SATISFACTORY PERFORMANCE

For use herein, failure might be defined as non-ability of a structure to perform its minimum assigned function during some specified period of time (Ref. 7-4). In this sense a structure could be considered to have failed in a number of situations of which the following are illustrative:

- (a) Structural collapse.
- (b) Excessive structural distortion so that equipment etc. become non-operative.
- (c) Failure to protect human occupants from nuclear effects.
- (d) Failure to protect equipment and supplies from nuclear effects.

Which type of failure is critical must be decided in each individual case and may require command decisions, particularly if the safety of personnel is involved.

In defining failure, the complete operating function of the structure must be considered:

- (a) Is the structure to withstand one attack or several repeated attacks?

- (b) How soon after an attack is the structure required to function?
- (c) Is such operation in a normal or emergency, buttoned-up condition?
- (d) How long is the structure required to perform its function after an attack?
- (e) Is saving operating personnel an end in itself or is the operation the primary objective?
- (f) What is the absolute minimum performance which will be acceptable?

Satisfactory performance is then considered to be anything short of failure, and an arbitrarily sharp cut-off is assumed between success and failure.

7.3 SAFETY FACTOR

As previously stated, the concept of a safety factor is vague in nuclear blast-resistant design. The design is essentially an ultimate design aimed at the standards of performance required. There is a certain probability that a given set of structural performance requirements may be met by a given structure resisting a given loading pattern. There is then a further probability that the given loading pattern will be the one which occurs. The first of these two probabilities can be made to be very close to 100% by uniformly conservative assumptions in material and structural behavior; the second probability is one over which the designer has no control. This lack of control should not be of concern, however, if it is accepted that

the design must lead only to satisfactory structural performance against one predetermined set of loading conditions. If these conditions are taken as the design conditions and a design is made on the basis of ultimate structural and functional performance, the resulting "factor of safety" can be interpreted as being unity.

It does not seem that a factor of safety larger than one is desirable for nuclear blast-resistant design since the design is based on assumed loads which may never be realized. If, for some reason a greater factor of safety were required, the loading assumptions should be increased and an ultimate design made to achieve the required performance based upon the increased loading.

7.4 DESIGN CRITERIA

The design criteria are selected: 1) to meet the performance requirements, and 2) to let failure occur in a preferred, predetermined fashion.

In considering the performance requirements, design criteria include:

- (a) Maximum permissible absolute and relative displacements and distortions (both elastic and permanent).
- (b) Maximum permissible stresses (or strains) and minimum strengths.
- (c) Maximum permissible radiation in the interior.
- (d) Maximum permissible accelerations and velocities to which structure and its contents may be subjected.

- (e) The number of times the structure is expected to withstand the assumed loading conditions.
- (f) When and how long the structure must perform its function.
- (g) The requirements for area, cube, operational function, habitability, etc.

The structure could be proportioned so that the assumed loading conditions:

- (a) Cause impending failure by fatigue.
- or (b) Barely produce yielding at one section or at more than one section.
- or (c) Cause excessive elasto-plastic displacements.
- or (d) Produce a condition of impending instability.

It is usually desirable to insure that if failure does occur it will be in a predicted fashion. This can be decided either with the aim of reducing the violence of suddenness of failure or of controlling failure in a manner which is well understood.

7.5 DUCTILITY RATIO

The preceding discussion shows the importance of defining satisfactory performance (or failure) and the need for describing this by some physical measurement. It is customary to speak of structural response in a general way to mean the "aggregate overall general effect produced by the loads on the structure" (Ref. 7-3). More specifically, the term "response"

is used to describe the deflection of a structure at a given time.

If the structure is a simple single-degree-of-freedom system, the response is simply the value of the displacement coordinate at the time of interest. For a more realistic, complex structure having many degrees of freedom and as many displacement coordinates as degrees of freedom, the overall response is complex. What is generally done is to assume a manner of deflection which is consistent with the loading and the mode of the fundamental period of vibration of the structure. Then some one coordinate can be chosen which is representative of the overall response in this mode.

Assuming the effective response to be describable by one coordinate, the concept of a ductility ratio for a structure becomes meaningful. The ductility ratio μ is the ratio of the maximum response to that response at which linear behavior stops (or inelastic behavior starts). Thus a μ of 5 would mean that the maximum response of the structure was 5 times the response at which the structure first yielded. A μ of less than unity would mean that the structure remained elastic.

Ductility ratios are used in describing the response of structural elements as well as of composite structures. It is customary to design for the required strength and a ductility ratio as large as the performance requirements will permit. Members having large ductility ratios are capable of greater absorption of strain energy and thus are more efficient in resisting transient loading. Furthermore, for buried structures, ductility in a structure is essential to permit the structural deformations required to take full advantage of the inherent strength of the soil that surrounds

the structure. Soil resistance can be mobilized only after deformations are imposed upon it.

The ductility factor that corresponds to collapse for various structures ranges from slightly greater than one for brittle structures to values of the order of 20 to 30 for very ductile structures. In some cases it can even be higher. The ductility factor used in a given design can have an important effect on the resistance that must be designed into a structure. This effect is discussed in Chapter 9 and Appendix B.

It should be emphasized that the choice of the ductility factor to be used in the design of a particular facility, or components thereof, may be controlled by functional requirements rather than by ductility limit of the material at failure. For example, if the facility must withstand numerous repetitions of the design load, the ductility factor would have to be considerably smaller than the value that would be acceptable for a one-time loading. Similarly, the amount of cracking and spalling of concrete increases as the amount of inelastic strain and the number of load applications are increased. Consequently, in a given structure the damage that might be done to equipment or personnel by pieces of spalled concrete might require the specification of a low ductility factor to avoid the formation of spalls, even though a high ductility factor may be permissible from the standpoint of maintaining structural integrity. In still other cases it may be necessary for operational reasons to limit the displacements that will develop under the design loads. Thus, it is necessary that ductility factors used in the design of elements of a structure be chosen

consistent with the operational requirements of the element with an upper limit being placed on the factor by the ultimate ductility of the material.

If functional requirements do not impose more stringent restrictions, it is recommended that a value of $\mu = 1.3$ be taken for relatively brittle structures because there is practically no structure which does not have some inelastic deformation even up to the point of yielding. For moderately brittle structures μ can be taken in the range from about 2 to 3, and for quite ductile structures μ can be taken in the range from 10 to 20. In general, for reinforced concrete structures or for steel structures, the ultimate ductility factor for flexural members is less for deep members than for shallow members; and in reinforced concrete in particular, it is less for heavily reinforced members than for lightly reinforced members. The ductility factor for compression members should be taken in the brittle range, about 1.3 (Ref. 7-1). For reinforced concrete beams and one-way slabs μ is approximately $\frac{10}{\phi - \phi'}$, where ϕ is the percent tensile reinforcement and ϕ' is the percent compressive reinforcement. However, the value of μ should not exceed 30.

For reinforced concrete beams with structural grade steel reinforcement, tests indicate the following: (Ref. 7-3)

(a) Concrete strength has little effect on the energy absorbing capacity of beams failing initially in tension but does have an effect on the energy absorbing capacity of beams failing in compression.

(b) The ductility of a beam depends on the percent of reinforcing steel. The addition of compression steel enables a larger angle change to take place before the concrete crushes, and thereby increases the deflection

corresponding to collapse (i.e. a larger value for μ).

(c) The compression reinforcement must be well tied in order to produce the greater permissible μ .

The following representative values of μ correspond to collapse and are based upon test data (Ref. 7-3):

	<u>Max. Value of μ</u>
R-C Beams (tension steel only)	$\frac{10}{\phi}$
R-C Beams (tension and compr. steel)	$\frac{10}{\phi - \phi'}$
Steel Beams (lateral load)	26
(Note: To develop this ductility, the flanges must be thick enough to prevent local plastic buckling.)	
Steel Beams (lateral and axial load)	8
Welded Portal Frames (vert. load)	6 - 16
Composite T Beam	8

7.6 GENERAL RECOMMENDATIONS

The following recommendations are taken from Ref. 7-2.

Any structural or material property which may cause brittle behavior should be eliminated. The percentage of tensile reinforcement in reinforced concrete should be in the range from 0.25 to 1.5%. The percentage

of web reinforcement should be not less than 0.5% if web reinforcement is required at all. Where practicable, web reinforcement should be used in structures where a shearing mode of failure may develop. Structural and intermediate grade steel are preferred. Details of fabrication must be such that severe stress concentrations and the possibility of introducing large residual stresses are avoided. In members subjected primarily to flexure, a minimum of 0.25% compressive reinforcement should be used. If axial forces predominate, the amount of compressive reinforcement should equal the amount of tensile reinforcement. Plain bars should not be used for reinforcement.

The above recommendations apply to a combination of the blast loads and the usual dead and live loads. In addition, the structure must satisfy at common factors of safety the requirements for the conventional dead and live loads expected.

Basic dynamic material properties were discussed in Chapter 6.

7.7 REFERENCES

- 7-1 Newmark, Hansen and Associates, "Protective Construction Review Guide, (Hardening)", Volume I, prepared for the Office of the Assistant Secretary of Defense under Contract SD-52, 1961. (UNCLASSIFIED)
- 7-2 Merritt, J. L. and Newmark, N. M., "Design of Underground Structures to Resist Nuclear Blast", Structural Research Series No. 149, University of Illinois, April 1958. (UNCLASSIFIED)
- 7-3 Norris, Hansen, Holley, Biggs, Namyet, and Minami, "Structural Design for Dynamic Loads", McGraw-Hill, 1959. (UNCLASSIFIED)
- 7-4 Hammer, J. G. and Dill, A. F., "Failure Criteria as Applied to Atomic Defense Engineering", NAVDOCKS P 290, Department of the Navy, Bureau of Yards and Docks, January 1957. (UNCLASSIFIED)

CHAPTER 8. PROPERTIES OF STRUCTURAL ELEMENTS

8.1 INTRODUCTION

In this chapter there are presented procedures for determining the properties of basic structural elements significant in the design of protective structures. Included in these significant properties are yield resistance in each of the several possible failure modes, stiffnesses, and natural periods of vibration.

Each symbol is defined when first introduced. For convenience the nomenclature is summarized in Appendix D.

8.2 REINFORCED CONCRETE BEAMS AND ONE-WAY SLABS

8.2.1 Introduction. Reinforced concrete flexural members may fail in any one of four possible modes of failure: flexure, diagonal tension, pure shear, and bond. Of these modes, only the flexural mode and the diagonal tension mode, if properly reinforced, possess any significant degree of ductility. In protective structures, it is of utmost importance that structural elements be so proportioned as to insure ductile response under load.

In protective construction it is frequently necessary, because of the very high pressures to be resisted, to design reinforced concrete beams and slabs having span-to-thickness ratios much smaller than those commonly used in conventional structures. Because of the limited amount of data that are available on the strength and behavior of very deep reinforced concrete

members, the procedures presented herein are necessarily based on studies, largely experimental, of the behavior of beams and slabs of conventional proportions.

An indication of the applicability of these procedures to deeper sections is given in Refs. 8-30 and 8-31, which are reports of static and dynamic tests of simply supported, reinforced concrete beams having span to depth ratios of 2, 3, and 4. Summarizing the results of the studies of flexural strength and behavior of these deep beams, it is stated in Ref. 8-30 that "the behavior of deep reinforced concrete beams under static load can be predicted reasonably well. The well-known straight line formulas can be used to predict the yield load capacity. The ultimate capacity can be predicted using existing ultimate strength concepts but using a crushing strain equal to 0.008 instead of 0.003 to 0.004 as usually assumed for beams of conventional span-depth ratios."

In summary of the shear strength studies of deep sections, while indicating the continuing difficulty of predicting with confidence the shear or diagonal tension strength of such elements, it is stated in Ref. 8-31 that "the susceptibility of a deep beam to failure in shear does not seem to present the problem that was envisioned at the beginning of this investigation. For beams tested in this study, shear failures occurred only in those beams in which the concrete strength was low ($f'_c = 3000$ psi), the steel percentage was fairly high (1.67 and 2.58 percent) and the L/d ratios were low ($L/d = 2$). The cracking load and 'shear-moment' criteria used to determine the shear strengths of conventional beams underestimated the ultimate strength of the

beams failing in shear. The fact that several beams failed in shear at or near their flexural capacity and with large deflections before failure serves only to illustrate further that shear is not the problem in deep beams that it is in ordinary beams."

On the basis of these studies, it may be concluded that the flexural resistance of deep beams can be computed reliably by conventional methods and that the shear resistance of deep beams is greater than that given by the expressions developed for beams of normal proportions. However, since general criteria of demonstrated reliability for shear resistance of deep elements is not yet available, it is recommended that the conventional methods presented herein be used even though, in some cases, they may yield excessively conservative results.

8.2.2 Flexural Strength of Beam Sections. The characteristics of the flexural mode of failure are heavily dependent upon the percentage of tensile steel employed. If insufficient steel is used, when the concrete on the tensile side cracks, the steel is incapable of picking up the tensile force carried by the concrete before cracking. For such under-reinforced members, at the point of concrete cracking, the load deflection relationship is characterized by a sudden rapid increase in deflection under a reduced load intensity. If, on the other hand, an excessively large percentage of steel is used, the concrete crushes on the compression side before the tensile steel yields. When this happens the member loses practically all of its load carrying capacity and a very brittle failure results.

To avoid either of these undesirable failure characteristics and to insure ductile response, reinforced concrete flexural members should be

proportioned to have a reinforcing index less than 40. The reinforcing index is given by $(\Phi - \Phi') (f_{dy}/f'_{dc})$ where Φ is the percentage of tensile steel, Φ' is the percentage of compression steel, f_{dy} is dynamic yield strength of steel, and f'_{dc} is the dynamic compressive strength of concrete. In no case should the amount of steel on any face of a beam or slab exceed 2.0 percent of the cross-sectional area of the element .

Under dynamic loadings, the yield strengths of concrete and steel are increased because of the strain-rate effect discussed in Chapter 6. The basic shape of the load-deflection relationship under dynamic loading does not differ significantly from the same relationship found under static loads. Thus, to obtain the dynamic moment-resistant capacity of a reinforced concrete section, it is necessary only to substitute the dynamic properties of the materials into the equation for the static moment capacity. The ultimate moment capacity (Ref. 8-3) is therefore

$$M_p = A_s f_{dy} d \left(1 - \frac{k_2}{k_1} \frac{\frac{\Phi}{100} f_{dy}}{0.85 f'_{dc}} \right) \text{ in.-lbs.} \quad (8-1)$$

where A_s = the tensile steel area, sq. in.

d = the effective depth of the section, in.

f_{dy} = the dynamic yield strength of the steel, psi

f'_{dc} = the dynamic strength of the concrete, psi

Φ = the percentage of tensile reinforcement

k_1 = the ratio of the average compressive stress to $0.85 f'_c$

and k_2 = the ratio of the distance between the extreme fiber and the resultant of compressive stresses to the distance between the

extreme fiber and the neutral axis.

Using the commonly accepted values for the constants (equivalent to a rectangular stress block for the compressive concrete stresses), this equation can be written as:

$$M_p = \frac{\phi a d^2}{100} f_{dy} \left[1 - \frac{\phi f_{dy}}{170 f_{dc}} \right] \text{ in.-lbs.} \quad (8-2)$$

where a is the width of the beam section in in.

Over the range of recommended steel percentages and obtainable concrete strengths, Eq. (8-2) can be approximated, with little error, by Eq. (8-3)

$$M_p = 0.009 \phi f_{dy} a d^2 \text{ in.-lbs.} \quad (8-3)$$

Thus, for a simply supported beam of length L (in.), the uniformly distributed load intensity, q_f , required to produce flexural yielding of the beam is:

$$q_f = 0.072 \phi f_{dy} \left(\frac{a}{b}\right) \left(\frac{d}{L}\right)^2 \text{ psi} \quad (8-4)$$

where b (in.) is the width over which q_f is applied. For a one-way slab, b is equal to a ; for a tee-beam, or a beam that supports a slab, b is greater than a .

For continuous beams, the uniform load corresponding to flexural yielding of a beam with equal end moment capacities is given by:

$$q_f = \frac{8}{L^2} (M_p^c + M_p^e) = 0.072 (\phi_c + \phi_e) f_{dy} \left(\frac{a}{b}\right) \left(\frac{d}{L}\right)^2 \text{ psi} \quad (8-5)$$

where ϕ_c and ϕ_e are the percentages of tensile steel at the center and ends

and M_p^c and M_p^e and fully plastic moment capacities at the center and ends, respectively. Equations applicable to other support and load conditions are given in Fig. 8-1.

8.2.3 Diagonal Tension. This failure mode is characterized by diagonal cracks which propagate through the beam from a point near the tensile steel toward the compression face. When the crack has penetrated to the point where the remaining compression zone of the concrete is insufficient to sustain the bending stresses, the concrete crushes and the member fails.

The uniformly distributed load, q_y , required to produce yielding in diagonal tension can be defined for simply-supported and continuous beams by Eq. (8-6), which is derived from Eqs. (5-14) and (5-17) of Ref. 8-2,

$$q_y = 100 \left(1 + \frac{3}{2} \frac{\phi_{e \text{ avg}}}{\phi_c} \right) \left(\frac{1}{2 + \gamma} \right) \sqrt{\phi_c f_c'} \left(1 + \frac{2\phi_v f_{dy}}{10^5} \right) \left(\frac{d}{L} \right)^2 \left(\frac{a}{b} \right) \text{ psi} \quad (8-6)$$

where $\phi_{e \text{ avg}}$ is the average of the percentages of tensile steel at the ends of the member, ϕ_v the percentage of web steel, f_c' the static concrete strength in psi, γ the ratio of compression to tension steel at midspan, and f_{dy} , a , and b are as previously defined. Eq. 8-6 defines the upper limit on the resistance that the member can be expected to supply without the possibility of a diagonal tension failure.

When applying this equation to design, the ductility factor should not be permitted to exceed 1.5 unless a web steel percentage, ϕ_v , in excess of 0.25 is used. When applying this equation to a T-beam section, a rectangular beam whose width is equal that of the stem should be considered.

No shear or diagonal tension failures have been observed during static tests when the classically defined diagonal tension stress was less than $2\sqrt{f'_c}$ (See Ref. 8-2). Therefore, if the required resistance of a member with symmetrical support conditions is less than

$$q_y = 3.5\sqrt{f'_c} \left(\frac{d}{L}\right) \left(\frac{a}{b}\right) \text{ psi,} \quad (8-7)$$

flexure will govern regardless of the value determined from the diagonal tension equation (Eq. 8-6). When the member has unsymmetrical support conditions this limit is given approximately, but with acceptable accuracy, by the following:

$$q_y = 3.5\sqrt{f'_c} \left[\frac{1}{1 + \frac{1}{4} \left(\frac{\phi_{e \max} - \phi_{e \min}}{\phi_c} \right)} \right] \left(\frac{d}{L}\right) \left(\frac{a}{b}\right) \text{ psi} \quad (8-8)$$

where $\phi_{e \max}$ and $\phi_{e \min}$ are the maximum and minimum tensile steel percentages at the supports and ϕ_c is the tensile steel percentage at midspan.

Expressions for the diagonal tensile resistance of uniformly loaded reinforced concrete beams are summarized for convenience in Fig. 8-2(b).

8.2.4 Pure Shear. Tests have shown that a concrete section, when subjected to pure shear, will fail when the average shearing force over the section exceeds $0.2f'_c$. In other words, the intercept of the Mohr envelope of rupture on the shear axis corresponds to $0.2f'_c$.

Failure of a beam or slab in this mode is at least theoretically possible even though the section may be adequately reinforced in diagonal tension. This failure mode is characterized by the rapid propagation of a

more or less vertical crack through the depth of the beam or slab in the region near the support. A failure of this type is quite brittle; thus any design should be such that this behavior is not initiated during the response of the member. No rational theory for determining the yield resistance in this shear mode has yet been developed; however, the procedure given below, based on Ref. 8-1, is recommended.

The average shear stress on a vertical section through a beam or slab at a specified critical location should not exceed $0.2f'_c$. Therefore, assuming that the effective depth d is equal to 0.9 times the total depth D , the total shear force on the critical section should not exceed the value given by Eq. (8-9).

$$V_{ult} = 0.22 f'_c d a, \text{ lbs.} \quad (8-9)$$

The critical section is defined in Ref. 8-1 to be at a distance of $d/2$ or $0.1L$ away from the support, whichever is smaller. Thus, for symmetrical support conditions, a beam or slab has a pure shear resistance, expressed in terms of a uniformly distributed load, of

$$q_v = 0.44 f'_c \frac{d/L}{1 - d/L} \left(\frac{a}{b}\right) \text{ psi for } \frac{d}{L} \leq 0.2 \quad (8-10)$$

$$= 0.55 f'_c (d/L) \left(\frac{a}{b}\right) \text{ psi for } \frac{d}{L} \geq 0.2 \quad (8-11)$$

when inclined steel is supplied over the support, the resulting increased resistance (Ref. 8-1) is approximated by assigning to the inclined steel a shear resistance equal to its yield capacity and to the concrete a

shear resistance equal to one-half that of the uncracked concrete section.

Thus, for a member with inclined web steel,

$$q_v = 0.44 f'_c \frac{d/L}{1 - d/L} \left(\frac{1}{2} + \frac{\phi_v^i}{20} \frac{f_{dy}}{f'_c} \right) \left(\frac{a}{b} \right) \text{ psi} \quad (8-12)$$

when d/L is less than 0.2 and, when d/L is greater than 0.2,

$$q_v = 0.55 f'_c \left(\frac{d}{L} \right) \left(\frac{1}{2} + \frac{\phi_v^i}{20} \frac{f_{dy}}{f'_c} \right) \left(\frac{a}{b} \right) \text{ psi} \quad (8-13)$$

where ϕ_v^i is the percent of steel (inclined at 45°) crossing a surface inclined at 45° . If $\phi_v^i (f_{dy}/f'_c)$ is less than 10.0, q_v should be computed from Eqs. (8-10) and (8-11).

If the member has unsymmetrical support conditions, the pure shear capacity for a section without inclined web steel can be written with acceptable accuracy in the following form:

$$q_v = 0.44 f'_c \left(\frac{d/L}{1 - d/L} \right) \left[\frac{1}{1 + \frac{1}{4} \left(\frac{\phi_{e \max} - \phi_{e \min}}{\phi_c} \right)} \right] \left(\frac{a}{b} \right) \text{ psi} \quad (8-14)$$

when d/L is less than 0.2 and

$$q_v = 0.55 f'_c \left(\frac{d}{L} \right) \left[\frac{1}{1 + \frac{1}{4} \left(\frac{\phi_{e \max} - \phi_{e \min}}{\phi_c} \right)} \right] \left(\frac{a}{b} \right) \text{ psi} \quad (8-15)$$

when d/L is greater than 0.2. In these equations the ϕ quantities are as

defined in Sect. 8.2.3 for diagonal tension.

The pure shear resistance of unsymmetrically supported sections with inclined web steel can be closely approximated by multiplying Eqs.

$$(8-14) \text{ and } (8-15) \text{ by } \left(\frac{1}{2} + \frac{\phi_v^i}{20} \frac{f_{dy}}{f_c'} \right).$$

For convenience, the preceding expressions for the pure shear resistance of beams with various support conditions are summarized in Fig. 8-2(a).

8.2.5 Stiffness. The stiffness factors for beams with various end supports are given in Fig. 8-1. For beams and slabs which have idealized bilinear resistance-deflection relationships, the stiffness factors are determined directly from the common elastic deflection formulas. When the resistance-deflection relationship is approximately trilinear in shape, (as for a fixed-ended beam), it is replaced by an equivalent bilinear shape. The initial slope of this bilinear replacement system is taken so that the area under the resistance-displacement diagram for the replacement system is equal to the area under the actual system at the point of inception of fully plastic behavior of the beam.

8.2.6 Natural Period. The fundamental period of vibration of reinforced concrete beams and one-way slabs is given theoretically by

$$T = R_o L^2 \sqrt{\frac{m}{EI}} \quad (8-16)$$

where R_o , which is a function of the support conditions, can be evaluated using expressions given in Ref. 8-2. The precision of computation implied

in the use of Eq. (8-16) cannot usually be justified. The following approximate but much simpler expressions, taken from Ref. 8-2, are recommended for general use.

$$\text{For Simple Support: } T = \frac{1}{42,500 \text{ (in per sec)} \sqrt{\phi_c}} \frac{L^2}{d} \text{ secs.} \quad (8-17)$$

For Fully Fixed-Fixed ($\phi_c = \phi_e$):

$$T = \frac{1}{85,000 \text{ (in per sec)} \sqrt{\phi_c}} \frac{L^2}{d} \text{ secs.} \quad (8-18)$$

$$\text{For Hinged-Fixed: } T = \frac{1}{63,800 \text{ (in per sec)} \sqrt{\phi_c}} \frac{L^2}{d} \text{ secs.} \quad (8-19)$$

in which L and d are taken in inches. The above expressions for the period of a distributed mass beam, as well as similar expressions for the period of a beam with the mass concentrated at the center, are summarized for ready reference in Fig. 8-3.

These formulas are based upon a cracked-section analysis, and assume no additional mass in the vibrating system in excess of that of the element alone. If any soil or other mass moves with the member, the period as given by Eqs. (8-17), (8-18), or (8-19) must be modified to account for the additional mass and the increased stiffness corresponding to it. The new period is defined by

$$T' = T \sqrt{\left(\frac{m'}{m}\right) \left(\frac{K}{K_T}\right)} \quad (8-20)$$

where T is the period of the member alone, m and K are the mass and stiffness of the member alone, and m' and K' are the mass and stiffness, respectively, of the entire vibrating system. At the present time little data, either

theoretical or experimental, are available on which to base estimates of the values of m' and K' that should be used for buried structural elements. For a cylindrical structure in a fluid, it has been shown that the fluid within about one cylinder radius should be assumed to move with the vibrating cylinder. Consequently, for such a case, m' should be taken as, m , the mass of the cylinder, plus the mass of the fluid within one radius of the cylinder. Also, in such a case, since the fluid has no shear strength, K' is equal to K .

For a structure buried in soil, since no better basis is available, m' can be estimated on the basis of the behavior of vibrating systems in a fluid. Thus, for the roof or wall of a buried structure, m' should include not only the mass of the structural element, but also the mass of the soil that vibrates with it. It is recommended that the depth of soil used in computing this added mass be taken as the average depth of soil above the element, but not to exceed a depth equal to the span of the element.

Since soils, as contrasted to fluids, do possess internal shearing strength, it is appropriate that an increase in stiffness of the responding soil-structure system, resulting from the mobilization of the shear strength of soil, also be considered. Thus, K' should be equal to K , the stiffness of the structural element alone, plus an additional stiffness produced by the soil. Unfortunately, at the present time, there is no basis on which to estimate, even with reasonable confidence, the magnitude of this increase in stiffness.

Two recent studies (Refs. 8-32 and 8-33), though rather crude, indicate that for buried arches, the increase in resistance, as earth cover

is increased, is of approximately the same relative magnitude as the increase in mass of the responding systems. Consequently, it is suggested that, until additional studies and tests make possible the development of a more rational procedure, the period of a buried structural element be taken the same as the period of the same element above ground; this will usually be conservative, from a design point of view. In any given case, however, the designer should modify this suggested procedure as may be appropriate in special cases where m' and K' can be estimated with reasonable confidence. For example, if the soil surrounding the structure possesses little or no shearing strength, it is obviously appropriate that the mass, m' , of the system include the soil, while the resistance of the system should include only the resistance of the structural element.

8.3 TWO-WAY SLABS

8.3.1 Flexural Strength. Tests have verified that the yield-line theory predicts the static ultimate flexural load capacity with reasonable accuracy. Furthermore, according to Hognestad (Ref. 8-4), it is always on the conservative side, the calculated ultimate load being 80 to 90 percent of the actual ultimate load. It is thought that this results from strain hardening of the reinforcement together with membrane action of the slab when the slab has relatively large deflections near failure. No attempt is made to refine this conservatism.

Except for the case of a square slab with equal reinforcement in both directions, the critical set of yield lines can be located only by

trial and error. Thus, to be directly useful in design, some approximations are necessary. For rectangular slabs of reasonable relative dimensions and steel percentages, the critical yield line pattern will not differ markedly from that indicated in Fig. 8-4. For the indicated set of yield lines, the yield resistance, expressed as a uniformly distributed load, can be computed for segments A and B (Fig. 8-4) by applying the conditions of equilibrium to each segment independently. On this basis, the yield resistance of segment A is

$$q_A = 0.216 (\phi_{Le} + \phi_{Lc}) f_{dy} \left(\frac{d}{L_s}\right)^2 \quad (8-21a)$$

and that of segment B is

$$q_B = 0.216 (\phi_{se} + \phi_{sc}) \left(\frac{1}{3-2\alpha}\right) f_{dy} \left(\frac{d}{L_s}\right)^2 \quad (8-21b)$$

where α is the ratio of the short span to the long span and the subscripts on the ϕ 's indicate the position and direction of the reinforcement. (For example, ϕ_{se} is the average percentage of negative moment steel perpendicular to the long edge of the slab).

If the assumed yield lines are in fact the correct ones, q_A and q_B , as determined from Eqs. (8-21a) and (8-21b) respectively, will be equal. That this situation should exist would be largely a matter of coincidence since, for a fixed value of α , equality of q_A and q_B implies also a definite relationship between the steel percentages in the two directions. Even though q_A and q_B , when evaluated from the given equations, are not equal, an

estimate of the flexural yield resistance of the slab can be obtained as an average of q_A and q_B , weighed on the basis of the areas of the two segments. The resulting yield resistance is given by Eq. (8-22).

$$q_f = 0.108 (\phi_{se} + \phi_{sc}) \left[\alpha \left(\frac{\phi_{Le} + \phi_{Lc}}{\phi_{se} + \phi_{sc}} \right) + \frac{2-\alpha}{3-2\alpha} \right] f_{dy} \left(\frac{d}{L_s} \right)^2, \text{psi} \quad (8-22)$$

Results of this approach may in some instances overestimate the resistance of the slab, but generally not in amounts sufficient to warrant redesign by a more refined application of the yield line theory (Ref. 8-4 and 8-5).

Edge panels, however, or other cases where unsymmetrical support conditions exist, should be checked for adequacy. If Eq. (8-22) is compared with Eq. (8-5), it is seen that the former can be written as some constant (for any particular slab geometry and reinforcement placement), Ω , times Eq. (8-5), where the constant Ω is

$$\Omega = 1 + \alpha \left[\frac{1}{6 - 4\alpha} + \frac{3}{2} \left(\frac{\phi_{Lc} + \phi_{Le}}{\phi_{sc} + \phi_{se}} \right) \right] \quad (8-23)$$

This constant Ω is thus a conversion factor which relates the resistance of a two-way slab numerically to that of a one-way slab spanning the short dimension of the two-way slab. Recognizing this fact, the maximum pressure that a two-way slab can resist is that of a one-way slab (with span and reinforcement corresponding to the short dimension of the two-way slab) times the conversion factor Ω .

8.3.2 Shear Strength. The shear and diagonal tension resistance of a two-way slab is taken as $(2/3)(1 + \alpha)$ times that for a one-way slab spanning in the short direction when α is greater than $1/2$ and the same as the one-way slab when α is less than $1/2$.

8.3.3 Supporting Beams. The beams supporting a two-way slab must be designed for flexure to be consistent with the actual load distribution on the beam, which varies as the edge shear of the supported slab. Thus, for a square slab, the flexural yield resistance of the supporting beams, with symmetrical support restraints, can be determined on the basis of a triangular distribution of load, the maximum intensity of which exists at the center of the beam. For this case,

$$q_f = 0.108 (\varphi_e + \varphi_c) f_{dy} \left(\frac{a}{b}\right) \left(\frac{d}{L}\right)^2, \text{ psi} \quad (8-24)$$

where q_f is a uniform pressure over the surface of the slab, b is the center-to-center distance between adjacent slabs, a is the beam width, d is the effective depth of the beam, L is the length of the beam, and φ_e and φ_c are the beam steel percentages at the end and center, respectively.

For the beam under the long side of a two-way slab, the loading may be assumed trapezoidal, which leads to

$$q_f = 0.072 (\varphi_e + \varphi_c) f_{dy} \left(\frac{a}{b}\right) \left(\frac{d}{L}\right)^2 \left(\frac{1}{1 - \frac{1}{3}(\alpha)}\right), \text{ psi} \quad (8-25)$$

where the terms are as previously defined except that b is center-to-center distance between adjacent long beams.

The resistance of a beam supporting the short side of a two-way slab can be determined from Eq. (8-24) if b is taken as defined for Eq. (8-25).

The above equations apply to interior beams only. If the beams support only a single panel, these expressions must be modified accordingly.

The resistance in pure shear and diagonal tension of beams supporting a two-way slab can be determined using the equations of Section 8.2.3 and 8.2.4 by assuming the beam to be a one-way slab and taking q_y and q_v as average pressures on the beam that will produce total forces on the beam (and, consequently, maximum shears in the beam) corresponding to the triangular or trapezoidal load distributions used above for flexure.

8.3.4 Stiffness. Assuming the material to be elastic and the supports to be rigid, the stiffness of a two-way slab may be computed from the Tables of Ref. 8-6. The stiffnesses (load per unit area to produce unit center elastic deflection) thus computed (Ref. 8-1), for slabs with simply supported and with fully fixed supports, for varying $\alpha = (L_s/L_L)$ ratios, are:

	<u>Simple Supports</u>	<u>Fixed Supports</u>
	$K = 252 \frac{E_c I}{(L_s)^3 L_L}$	$K = 810 \frac{E_c I}{(L_s)^3 L_L}$
$\alpha = 1.0$		
$\alpha = 0.9$	= 230 "	= 742 "
$\alpha = 0.8$	= 212 "	= 705 "
$\alpha = 0.7$	= 201 "	= 692 "
$\alpha = 0.6$	= 197 "	= 724 "
$\alpha = 0.5$	= 201 "	= 806 "

where E_c is the modulus of elasticity of concrete and I is the average of the moments of inertia of the uncracked and transformed sections, per unit of width of slab. For slabs with either 1, 2, or 3 sides fixed, the stiffness may be estimated by interpolating between the values given above, or, with greater precision, by use of the Tables given in Ref. 8-6.

8.3.5 Natural Period. The classical equation for the period of plates simply supported on rigid beams (Ref. 8-7) is

$$T = \frac{2}{\pi} \left(\frac{1}{\frac{i^2}{L_L^2} + \frac{j^2}{L_S^2}} \right) \sqrt{\frac{w}{gD}} \quad (8-26)$$

where i is number of waves in the long span direction, j is the number of waves in the short span direction, w is the total weight per unit of slab area, and D is the flexural stiffness of the slab. For the fundamental period, this equation may be approximated (Ref. 8-1) by

$$T = 5.3 \sqrt{\frac{w}{Kg}}, \text{ sec.} \quad (8-27)$$

where K is the stiffness per unit of slab area taken from the table above, and w is the weight per unit of slab area. The corresponding equation for fixed supports is

$$T = 4.5 \sqrt{\frac{w}{Kg}}, \text{ sec.} \quad (8-28)$$

The period of vibration of slabs with other combinations of support conditions may be found by procedures given in Ref. 8-8.

For buried slabs, the effects of the added soil mass on the period of the system are given by

$$T' = T \sqrt{\left(\frac{m'}{m}\right) \left(\frac{K}{K'}\right)} \quad (8-29)$$

where m' and K' should be evaluated as discussed in Section 8.2.6.

8.4 REINFORCED CONCRETE COLUMNS

8.4.1 Axially Loaded Reinforced Concrete Columns. Under axial load, the limiting static strength of reinforced concrete columns is given as:

$$P_u = 0.85 f'_c A_c + f_y A_s \quad (8-30)$$

where A_c is the cross-sectional area of the concrete and A_s is the total steel area. For a tied column, this represents the ultimate capacity, the resistance dropping off sharply after this load is reached. A spirally reinforced column, on the other hand, can undergo substantially larger deformations prior to losing its load carrying capacity (Ref. 8-5). The spiral column thus exhibits more ductile behavior than the tied column.

Because of the strain rate influence associated with dynamic loading, the strength characteristics of the steel and of the concrete should increase in the amounts recommended in Chapter 6. Thus, the axial load capacity of a dynamically loaded column is

$$P_u = \left(0.85 f'_{dc} + \frac{\phi_t}{100} f_{dy}\right) A_c \quad (8-31)$$

where ϕ_t is the total percentage of reinforcing steel, and f'_{dc} and f_{dy} are respectively the dynamic yield strengths of concrete and steel.

In view of the particularly serious consequences of a column failure, when the column supports a roof subjected to blast loading, it is recommended that the resistance of the column be either twice the peak blast pressure times the tributary roof area, or the maximum resistance of the supported elements, whichever is smaller.

If the ratio of the unsupported length of the column, L , to the least width of the column, t , exceeds 15, the ultimate capacity must be adjusted to the long column formula (Ref. Appendix of ACI Code)

$$P_u^l = P_u \left(1.6 - 0.04 \frac{L}{t} \right) \quad (8-32)$$

8.4.2 Combined Flexure and Axial Loads. The existence of a combined state of flexure and axial load is commonly met in protective construction. The behavior of a member in such a state of loading encompasses both those of a beam and of a column; the degree to which either behavior predominates depends upon the relative magnitudes of the two loadings and the sectional properties of the member. The entire range of limiting combinations of moment and axial load may be summarized on an interaction diagram (Ref. 8-5) as shown in Fig. 8-5.

It is evident from Fig. 8-5 that, for an under-reinforced member which carries a small axial load, the presence of the axial load increases the bending capacity of the member. This increase may be substantial.

The interaction diagram of Fig. 8-5 was developed for a member of rectangular cross section with reinforcing steel symmetrically placed in single rows about the bending axis. In this figure, P_u is ultimate axial

load capacity of the member when carrying no moment (Eq. 8-31), and M_p is the ultimate moment capacity when no axial forces are present (Eq. 8-3). M and P , as used in the diagram, are the values of moment and thrust computed for a given loading condition.

The effects of axial compressive forces acting in combination with flexure on the strength of a beam-column in shear have not been well established. Qualitatively, axial compressive forces increase the stress normal to potential shear failure surfaces and, consequently, increase the shear resistance; however, the nature and extent of this increase is not known. Conservatively, it is recommended that the resistance in shear be determined without regard to the axial forces.

8.4.3 Period. The period of vibration of a beam is increased by the presence of an axial compressive load (Ref. 8-7). For a member under combined load, the flexural period is equal to that of the member without axial force divided by $\sqrt{1 - (P/P_{cr})}$, where P is the axial force present and P_{cr} is the Euler buckling load.

8.5 STEEL BEAMS

8.5.1 Introduction. In designing steel members to resist blast effects many of the concepts and equations developed for the plastic analysis of steel structures under static loads are utilized. Therefore, an understanding of the conditions and equations governing the static behavior is essential. A number of references (such as Ref. 8-12 and 8-13) contain discussions of plastic analysis and design of steel structures for static loads.

8.5.2 Flexural Strength. As for reinforced concrete, the dynamic flexural capacity of a steel beam section is related to its static flexural capacity by the ratio of the dynamic to the static yield stresses of the material. Thus, the dynamic moment resisting capacity of a steel section is given by

$$M_p = f_{dy} Z \quad (8-33)$$

where f_{dy} is the dynamic yield strength for the steel in question and Z is the plastic section modulus. For standard I-sections, the plastic section modulus is approximately 1.15 times the elastic section modulus. The useable load capacity or resistance of a beam is found by substituting the moment capacity as given by Eq. (8-33) into the appropriate limit analysis formula. For beams with various support conditions, loaded either by a uniform load over the entire span or by a concentrated load at midspan, the resulting expressions for yield resistance are as given in Fig. 8-6.

8.5.3 Shear Strength. Shear is of interest primarily because of its possible influence on the plastic moment capacity of a steel member. At continuous supports, where combined bending and shear exist, the assumption of an ideal elasto-plastic stress-strain relationship indicates that during the progressive formation of a plastic hinge there is a shrinkage of the web area available for shear. This reduced area might then result in the initiation of shear yielding and thus reduce the moment capacity. However, since "I" sections carry moment predominately through the flanges and shear through the web, and furthermore, because combinations of high shear and high moment generally occur at points where the moment gradient is steep,

it has been found experimentally that the member will achieve its fully plastic moment capacity if the average shear stress over the full web area is less than the yield stress in shear (Ref. 8-14).

The yield capacity of an "I-shaped" steel beam in shear is given by:

$$V = v_{dy} A_w, \text{ lbs.} \quad (8-34)$$

where V is the ultimate shear capacity, v_{dy} is the dynamic shear yield strength of the steel in psi (see section 6.2.2), and A_w is the area of the web in sq. in. For several particular load and support conditions, Fig. 8-7 gives the shear yield resistance of a beam in terms of the applied load required to produce shear yielding in the beam web.

When a built-up section is designed with reliance being placed on the web to carry a significant part of the total moment requirements of the section, the shear influence cannot be neglected and the member should be investigated for possible moment loss through shear yield. It is recommended that the moment capacity of such a section (Ref. 8-15) be defined by:

$$M = bt_f(d + t_f) f_{dy} + (1/4) t_w d^2 \sqrt{f_{dy}^2 - 3v^2} \quad (8-35)$$

where b is the flange width, t_f is the flange thickness, d is the depth of the web, t_w is the web thickness, f_{dy} is the dynamic tensile yield stress, and v is the average web shear stress.

8.5.4 Local Buckling. To insure the ability of a steel beam to sustain fully plastic behavior and thus to possess the assumed ductility at

plastic hinge formations, it is necessary that the elements of the beam section meet minimum thickness requirements sufficient to prevent a local buckling failure. Based upon theoretical and experimental data which are summarized in Ref. 8-14, the beam section must satisfy the following thickness requirements if premature local buckling is to be prevented:

$$\text{For Flanges: } \frac{\text{flange width, } b}{\text{flange thickness, } t_f} < 17$$

$$\text{For webs without longitudinal stiffeners: } \frac{\text{web depth, } d}{\text{web thickness, } t_w} < 70 \quad (8-36)$$

$$\text{For stiffeners: } \frac{\text{stiffener width, } b_s}{\text{stiffener thickness, } t_s} < 8.5$$

These thickness ratios were developed for the static load case; however, lacking evidence to the contrary, they are also applied to the dynamic case. Since G. Haaijer and B. Thurlimann developed these relations through the analysis of buckling of orthotropic plates whose properties were those of A-7 steel stressed into the strain hardening region, they should be adjusted when the material being used has characteristic values of the stress-strain relationship differing substantially from those of A-7 steel. Adjustments for other materials can be made on the basis of the procedures used in Ref. 8-14.

8.5.5 Stiffness. Stiffness factors are given in Fig. 8-6 for beams with various support and load conditions. The stiffnesses for the simply supported beams are the standard relationships given in any structural text. For the restrained beams, the stiffnesses given correspond to load-deflection relationships that have been idealized as bilinear

functions with initial slopes so defined that the areas under the idealized load-deflection diagrams are equal to the areas under the actual diagrams at the point of inception of fully plastic behavior of the beam.

8.5.6 Natural Period. The natural periods of beams with uniformly distributed mass and various support conditions are given in most vibration texts. These periods are, however, for purely elastic beams. For a restrained beam, stressed into the inelastic region, the load-deflection relationship should be idealized as a bilinear system as described above, and the period of the beam should be adjusted to agree with the idealized resistance function. Beam periods adjusted accordingly are given in Fig. 8-8. This figure includes periods for various load and support conditions. It should be noted that the beam periods are given in terms of the total supported weight. Therefore, for beams in an underground structure, the effects of soil cover should be included as discussed in Sect. 8.2.6 for reinforced concrete beams and slabs.

8.6 STEEL COLUMNS

8.6.1 Axially Loaded Columns. Columns designed for structures which must resist the blast effects of nuclear weapons usually have sufficiently small slenderness ratios that the buckling occurs plastically rather than elastically. Recent studies (Lehigh University) have indicated that residual stresses have a prominent influence on the ultimate load capacity of steel columns (Refs. 8-12 and 8-16). It has been found for rolled wide-flange sections that, because of the typical pattern of

residual stresses, the reduction in capacity is more sharply felt about the weak axis than about the strong axis. Formulas for the capacity of axially loaded columns for the static case are given in Ref. 8-12 for buckling about both the weak and the strong axes.

Because dynamic application of loads tends to suppress the occurrence of buckling, it is conservative to adapt the static formulas to the dynamic case by replacing the static yield stress by its comparable dynamic value. Thus the buckling stress of dynamically loaded column sections of A-7 steel can be taken as:

$$f_{cr} = 42,000 - 1.44 \left(\frac{\alpha L}{r_g} \right)^2, \text{ psi} \quad (\text{strong axis})$$

$$f_{cr} = 42,000 - 155 \left(\frac{\alpha L}{r_g} \right), \text{ psi} \quad (\text{weak axis})$$

(8-37)

where L is the column length, r_g is the radius of gyration and α is the effective length factor (Ref. 8-17). These relationships are summarized for several common end support conditions in Fig. 8-9.

For other materials having stress-strain relationships similar to that of A-7 steel, the critical buckling stresses may be found by referring to the basic relations given in Ref. 8-12, using the dynamic yield stress instead of the static value.

8.6.2 Local Buckling. To avoid the possibility of local buckling, and insure that a column has the ability to sustain loads at ultimate capacity, the section should be proportioned to meet the following thickness ratios:

$$\frac{\text{flange width}}{\text{flange thickness}}, \frac{b}{t_f} < 17$$

(3-38)

$$\frac{\text{column depth}}{\text{web thickness}}, \frac{d}{t_w} < 43$$

8.7 CIRCULAR ARCHES

8.7.1 Introduction. For the design of arch structures, two components of loading, and corresponding response, should be considered. The first component is a uniform radial load which produces a vibration mode identified by uniform radial motions. This mode, designated as the uniform compression mode, is the only mode considered in the case of fully-buried underground arches. The second loading component is unsymmetrical, consisting of a uniform radial load inward on one-half the arch and outward on the other half. The vibration mode corresponding to this component of load is the first unsymmetrical mode. This mode produces primarily flexural stresses in the arch. For arches which do not meet the fully buried criterion, this mode must be considered to occur in combination with the uniform compression mode. A more complete description of these recommended loadings is presented in Chapter 5.

The nomenclature used in the following discussion of arch properties is shown in Fig. 8-10.

8.7.2 Natural Period.

(a) Uniform Compression Mode. The natural period of vibration of this mode is approximated for design by that of the pure radial vibration of a complete ring. In Ref. 8-7 the formula for this pure

compression period is given as

$$T_c = 2\pi r \sqrt{\frac{m}{EA}}, \text{ sec.} \quad (8-39)$$

where A is the cross-sectional area of the arch, m is the mass per unit of arch length, r is the radius of the arch, and E is the modulus of elasticity. For convenience, this expression can be converted into the form

$$T_c = 2\pi r/c \quad (8-40)$$

where c is the velocity of sound in the material of which the arch is made. For reinforced concrete arches, therefore, the period may be approximated (Ref. 8-2) by the following simplified formula,

$$T_c = \frac{r}{1800} \text{ (seconds)} \quad (8-41)$$

where r is the radius of the arch in feet.

This approach neglects the effect of any restraint at the boundary. Thus, both fixed and hinged arches are considered to have the same period. The inclusion of some support restraint would induce a flexural mode superimposed upon that of the uniform radial motion. However, discrepancies resulting from neglect of the support restraint are not considered to be significant. In addition, for fully buried arches, the superimposed flexural motions are inhibited by the presence of the soil.

Equation (8-41) should not be applied to arches having central angles of less than 90° . For such cases, even for buried arches, flexural behavior is the dominant factor and should control the design.

(b) Flexural Mode. When the arch vibrates in this mode, the stresses within the arch are predominately of a flexural nature. The period of this mode is therefore approximated by that of a substitute straight beam whose span is equal to one-half the developed arc length of the arch. The support conditions for this substitute beam are: at one end, the same as that existing on the original arch; and at the other end, hinged. Thus, for a hinged arch, the substitute is a simply supported beam. The cross-sectional properties of the beam are taken to be those of the arch. For a constant section, the flexural period of the substitute straight beam is:

$$T_f = \frac{2L^2}{\pi} \sqrt{\frac{m}{EI}} \quad (8-42)$$

where $L = r\beta$, m is the mass per unit of arch length, and I is the moment of inertia of the section. For an arch, this period must be corrected for the effect of curvature by multiplying by a correction factor ψ (Ref. 8-9).

This factor, given by

$$\psi = \frac{n^2 + 1.5}{n^2 - 1} \quad (8-43)$$

where $n = \frac{\pi}{\beta}$, is obtained from the ratio of the period of the first antisymmetrical mode of the unloaded arch to the first mode of the substitute straight beam. The factor, ψ , is taken at full value when earth cover over the arch is zero. However, the arch action upon which this factor is based can not be developed unless the crown of the arch is allowed to displace laterally. Therefore, for a buried arch, ψ , as given by Equation (8-43),

must be modified to account for restraint offered by the soil. Reference 8-1 recommends the following modification: (1) When the earth cover over the crown is zero, use ψ as given by Equation (8-43). (2) When the earth cover at the crown is greater than 0.1 times the arch span, the factor, ψ , may be reduced to 1.0. (3) Between these two limits of earth cover, a linear interpolation should be used. Thus, for an arch pinned at the springing line, the flexural period is given by Equation (8-44), which can be used directly for steel arches.

$$T_f = \frac{2(r\beta)^2}{\pi} \sqrt{\frac{m}{EI}} (\psi), \text{ sec.} \quad (8-44)$$

For reinforced concrete arches, the flexural period formula can be simplified, as was the pure compression period, by use of the velocity of sound in concrete. Simplified in this manner, Ref. 8-2 recommends the following form,

$$T_f = \frac{L^2}{42,500 d \sqrt{\phi}} \psi, \text{ sec.} \quad (8-45)$$

where L , the arch span, and d , the effective depth, are in inches, and ϕ is the percentage of circumferential steel on one face of the arch.

For a fixed arch, the substitute beam is fixed at one end and simply-supported at the other end. The period for such a beam is 0.64 times that of a simply supported beam of the same span and cross-section. The correction factor for arch action is, for the fixed ended case,

$$\psi = \frac{n^2 + 1.0}{n^2 - 0.5} \quad (8-46)$$

where $n = \pi/\beta$. As for the simply supported case, this factor must be varied

according to the earth cover over the crown.

(c) Soil Mass Effect. The periods as determined above are those for the bare structural elements. If the arch has any soil cover, the influence of the additional mass and stiffness on the period must be considered. As for beams and slabs, the adjusted period, T' , is given by:

$$T' = T \sqrt{\left(\frac{m'}{m}\right) \left(\frac{K}{K'}\right)} \quad (8-47)$$

The discussion of Sect. 8.2.6 relative to the evaluation of m' and K' for buried beams and slabs is equally applicable to arches.

8.7.3 Resistance.

(a) Uniform Compression Mode. In this mode, the effect of radial distortions on the reactions is assumed to be small; therefore, the stresses in the arch are considered to be only those produced by the axial thrust. The thrust which must be sustained by the arch is given by the hoop stress equation for a circular ring. Therefore, the ultimate thrust capacity, per unit length of arch, is given by

$$P_u = f_{cr} A, \text{ lbs. per in.} \quad (8-48)$$

where f_{cr} is the usable compressive stress capacity of the material composing the arch and A is effective cross sectional area per unit of arch length.

For reinforced concrete arches, this is equivalent to

$$P_u = (0.85 f'_{dc} + 0.009 \phi_t f_{dy}) D, \text{ lbs. per in.} \quad (8-49)$$

where ϕ_t is the total percentage of circumferential steel and D is the thickness of the arch, in inches. Thus, the resistance of the arch, expressed in terms of a uniform radial pressure, is

$$q_c = \frac{f_{cr} A}{r}, \text{ psi} \quad (8-50)$$

For steel arches, this may be written as

$$q_c = \frac{f_{dy} A}{r}, \text{ psi}$$

where f_{dy} is the dynamic yield stress of steel in psi, and A and r are in inches.

For reinforced concrete arches of uniform thickness, Eq. (8-50) is equivalent to

$$q_c = (0.85 f'_{dc} + 0.009 \phi_t f_{dy}) \frac{D}{r}, \text{ psi} \quad (8-52)$$

where f_{dy} and f'_{dc} are the dynamic yield strengths of steel and concrete in psi, ϕ_t is the total steel percentage, D is the total arch thickness in inches, and r is the arch radius in inches.

(b) Flexural Mode. The criterion governing the adequacy of an arch in its flexural mode is the ultimate moment resisting capacity, M_p , of its cross-section. For a hinged arch, the applied moment is the simple beam moment of the substitute beam defined earlier, corrected to take account of curvature of the arch. Thus, expressed in terms of applied radial pressure, the yield resistance in flexure of a hinged arch is

$$q_f = \frac{8M_p}{(\beta r)^2} \left(1 - \frac{1}{n^2}\right) \quad (8-53)$$

where $n = \pi/\beta$, and consistent units are used. This equation will give the yield resistance of a steel arch directly. For a reinforced concrete arch of constant thickness, the resistance is more conveniently expressed as

$$q_f \approx 0.072 \phi_c f_{dy} \frac{d^2}{(\beta r)^2} \left(1 - \frac{1}{n^2}\right) \quad (8-54)$$

where d = depth to the tension steel, and consistent units are used.

For an arch with fixed supports, the substitute beam to be analyzed is simply supported at the point corresponding to the crown and fixed at the abutment. The limiting capacity of this beam occurs when plastic hinges have formed both at the fixed support and at a point between the crown and the abutment. The uniform intensity of pressure required to produce this condition, including a correction for curvature, is

$$q_f = 11.7 \frac{M_p}{(\beta r)^2} \left(1 - \frac{0.6}{n^2}\right) \quad (8-55)$$

This equation is again directly applicable to steel sections. For reinforced concrete, the equation is conveniently rewritten as

$$q_f \approx 0.036 (2 + \theta') \phi_c f_{dy} \left(\frac{d}{r\beta}\right)^2 \left(1 - \frac{0.6}{n^2}\right) \quad (8-56)$$

where θ' is the ratio of the negative steel percentage at the support to the positive moment steel near the haunch.

(c) Combined Loading. When the depth of burial of the arch is less than that required for full burial, the arch must be designed for the effects of both the above modes simultaneously. For purposes of design, a

reasonable estimate of the combined effect of the two load components can be made as described below. Under combined flexure and direct compression, a steel arch section can be designed as a beam column, the governing equation for which is

$$\frac{M'_p}{M_p} + \frac{P}{P_u} = \frac{q}{q_f} + \frac{qr}{f_{cr}A} = 1 \quad (8-57)$$

where M'_p and P are the ultimate values of moment and thrust acting in combination, q is the resistance (in terms of uniform pressure) under combined direct compression and flexure, and the other terms are as previously defined. For reinforced concrete, the interaction diagram given in Fig. 8-5 can be used to determine the resistance under combined loading.

8.7.4 Buckling. Even though an arch has been proportioned, on the basis of yield stress and permissible inelastic deformation, to withstand a given level of applied pressure, it is still necessary that consideration be given to the possibility of a premature buckling failure. For a bare arch, the determination of the critical buckling pressure is reasonably straightforward, at least for static loads. In the absence of information related specifically to dynamic buckling loads for arches, the criterion for the static case can be applied also to the dynamic case; such a procedure is conservative.

For earth-covered arches, the effect of the restraint offered by the surrounding soil on the critical buckling pressure of an arch is not well defined. Qualitatively, it is clear that soil restraint increases the buckling resistance; however, no rational basis has been developed on which

to estimate this increase. The recommendations presented below are believed to be conservative.

For a hinged arch having an average depth of earth cover equal to or greater than 0.25 times the span, the stability criterion is satisfied if the uniform radial pressure is less than the static critical buckling pressure given by the formula (Ref. 8-11)

$$q_{cr} = (n^2 - 1) \frac{EI}{r^3} \quad (8-58)$$

where $n = \pi/\beta$.

To avoid the possibility of premature buckling failures, the buckling pressure should be at least as large as the ultimate capacity of the section. Thus, for a 180° arch, the proportions needed to prevent buckling may be stated as follows:

$$\text{For concrete arch: } \frac{D}{r} \geq 0.001 \sqrt{f'_{dc}} \quad (8-59)$$

$$\text{For steel arch: } I \geq 0.00011 \frac{f_{dy}}{10,000} Ar^2$$

These expressions might at first appear unreasonable in that they seem to indicate an increased buckling resistance with increased material strength; however, this is not the case. Instead, they indicate that as the ultimate strength of the section is increased, the parameter D/r or I must also be increased to prevent buckling before the capacity is reached.

For an above-ground arch, it is recommended that the critical buckling pressure be taken no greater than about 2/3 of that given by

Equation (8-58). The critical pressure for arches with a depth of cover intermediate between full burial and the above-ground positions can be estimated by assuming a linear variation in critical pressure between these two conditions. For depths greater than that required for full burial, buckling of the arch need not be considered.

The critical buckling pressure for a fixed arch is approximated as $(2 + 1/n)$ times the critical pressure for the corresponding hinged arch (Ref. 8-10).

8.7.5 Ductility Factor. In the uniform compression mode the entire arch section is considered to be under a uniform stress intensity equal to the thrust divided by the area. Thus, in a reinforced concrete arch, the stresses approach the ultimate capacity of the concrete; the probability of failure over large areas of the arch is high. Therefore, it is necessary that a low ductility factor be used in design; μ -values between 1.3 and 1.5 are reasonable.

There are several aspects of the behavior of a concrete arch as it approaches its ultimate capacity which tend to add some ductility to the structure. First, concrete is not linearly elastic up to its maximum stress intensity but rather takes on increasingly larger deformation increments as the stresses approach the maximum. Also, once the maximum stress is reached, the resistance does not immediately drop to zero but decays on a finite slope. Finally, if end walls are used to close an arch area, some shell behavior will be induced.

8.8 DOMES

8.8.1 Introduction. As in the design of arches, two components of loading and their associated response modes must be considered in the design of a dome to resist blast effects. The prominence of either component depends upon the position of the dome relative to the ground surface. For a fully-buried dome, the loading tends to be of a more symmetrical nature and as such produces predominately compressive stresses within the dome. On the other hand, when the dome is on the ground surface, the reflection and drag phases of the loading pulse generate more of an unsymmetrical loading. This latter case, for convenience of identification, is referred to as the flexural mode, even though the stresses produced by it are primarily membrane stresses.

These two loading cases have different optimum opening angles for the shell. For above-ground domes, it is advantageous to keep the profile as low as the headroom requirements will permit in order to minimize the reflection and drag components of the loading pulse. This has a further advantage in that the covering efficiency (ratio of floor area to surface area of the shell) increases as the opening angle of the dome decreases. Underground, however, unsymmetrical loading is not as severe, and the variation in covering efficiency is not sufficient to outweigh the undesirable edge-effect forces associated with shallow angles. In the hoop direction these edge-effect stresses may be tensions several times as large as the maximum compressive stresses experienced over the major portion of the shell. It is therefore desirable, when underground, to use domes of as nearly hemispherical a shape as possible.

The terms used in the dome analysis are identified in Fig. 8-11.

The membrane stress analyses presented herein are theoretical solutions which indicate a precision greater than is consistent with the certainty of the loading. The dome should be designed on the basis of the maximum values of stress; the variation in stress intensity over the dome, as given by the equations, should be considered only a rough guide. Design techniques are presently being studied in an effort to establish a method wherein the precision of the stress calculations will be consistent with the other design steps.

When the shell rebounds, tension may exist over some areas of the dome. Investigation of this may be treated by the method presented in Appendix B.

8.8.2 Ductility. The selection of a doubly-curved surface for a structure is based primarily on the structural efficiency of this shape; that is, the ability of this shape to carry load by the nearly-full utilization of the material throughout the surface. As a consequence, any ductility considered for this structure must be a property of the material rather than of the total structure. Since the compression stress-strain relationship for concrete does show a non-linear behavior for stresses near the maximum and does not drop to zero immediately after the maximum is reached, a ductility factor on the order of 1.0 - 1.5 is reasonable for a dome. In steel, a larger ductility can be used but possible failure by buckling may be more critical.

8.8.3 Natural Period. The natural period of a dome, computed for use in design, is the period associated with uniform radial motion of the

shell, regardless of load intensity variations over the surface of the dome.

The differential equation of the radially vibrating dome can be written in the following form if only membrane forces are considered.

$$\ddot{w} + \alpha^2 w = 0$$

where w is the radial displacement of the dome and $\alpha^2 = \frac{2E}{\rho r^2(1-\nu)}$. Thus the period is given by:

$$T = \pi r \sqrt{\frac{2\rho(1-\nu)}{E}}, \text{ sec.} \quad (8-60)$$

where r is the radius of the dome, ρ is mass per unit of volume, and ν is Poisson's ratio, all quantities being taken in consistent units.

For reinforced concrete, this equation can be approximated by

$$T \approx \frac{r}{2500} \text{ sec.} \quad (8-61)$$

where r is the radius of the dome in feet. In the case of a buried structure the period computed by either of the above formulas should be adjusted for the additional mass and resistance of the soil by the same methods recommended for similar modification of the periods for beams, slabs, and arches. The same period should be used for both the flexural and compression modes since in both modes the predominate behavior is membrane action.

8.8.4 Compression Mode. The loading associated with this mode is a uniform radial load which is discussed in Chapter 5 and shown in Fig. 8-11(b). If the dome is assumed to deflect into a shape consistent with a

membrane stress state, a state of uniform compression exists everywhere within the dome. These compression forces per unit width are

$$T_{\psi} = T_{\theta} = \frac{P_o r}{2} \quad (8-62)$$

where P_o is any uniform radial pressure.

The yield resistance of the dome, for uniform radial pressure, is given by

$$q_c = (1.7 f'_{dc} + 0.018 \phi_t f_{dy}) \frac{D}{r} \quad (8-63)$$

As mentioned above, the membrane stresses are contingent upon the shell's ability to deform into the proper shape and the support's ability to sustain the proper reactions. For an opening angle in the dome of less than 180° , it may be quite difficult to support the horizontal component of the T_{ψ} force at the reaction. If the edge of the dome is free to move horizontally rather severe hoop tensions will develop. In such a case, a footing can be tied to the dome in such a way that the footing acts as a ring girder for the dome. The stresses induced in the dome by the influence of the ring girder may be studied by means of Figs. 8-12, 8-13 or 8-14. These figures, taken from Ref. 8-18, are based upon an approximate elastic analysis similar to that given in Chapter 16 of Ref. 8-19. Since these figures are based upon a truly elastic material, it is expected that they will overestimate the edge influence when applied to a concrete shell with the high design stresses associated with protective construction. In addition, when using the charts in design, it should be kept in mind that

they are based upon a "thin" shell theory which may become somewhat inaccurate when applied to shells with a radius to thickness ratio significantly smaller than about 20. Unfortunately no adequate "thick" shell theory has been advanced to the state where it is amenable to design. An alternate solution to develop the proper reaction is to use a bell shaped footing axially oriented with respect to the T_ψ force. In this case the major movement of the dome is radial and the hoop force remains compressive. Even if the bell shaped footing is employed, a nominal amount of steel should be placed to account for possible tensile T_θ hoop forces and also nominal steel should be placed for possible moment along the meridian, M_ψ .

8.8.5 Flexural Mode. The drag and reflection phases of the blast wave generate an unsymmetrical loading on the dome. For design purposes this loading may be approximated as a radial force varying sinusoidally, in both longitudinal and circumferential directions, as shown in Fig. 8-11(c). These pressures are discussed in Chapter 5.

At any point, the intensity of the sinusoidal load is given as $P_1 \sin (\beta - \psi) \cos \theta$; and the corresponding membrane forces per unit width are given by:

$$\begin{aligned} T_\psi &= -\frac{P_1 r}{3} \left[2 + \cos (\beta - \psi) \right] \cot (\beta - \psi) \tan^2 \left(\frac{\beta - \psi}{2} \right) \cos \theta \\ T_\theta &= -\frac{P_1 r}{3} \left[3 + 4 \cos (\beta - \psi) + 2 \cos^2 (\beta - \psi) \right] \frac{\tan^2 \left(\frac{\beta - \psi}{2} \right)}{\sin (\beta - \psi)} \cos \theta \quad (8-64) \\ T_{\theta\psi} &= -\frac{P_1 r}{3} \left[2 + \cos (\beta - \psi) \right] \frac{\tan^2 \left(\frac{\beta - \psi}{2} \right)}{\sin (\beta - \psi)} \sin \theta \end{aligned}$$

In these equations, P_1 should be taken as the maximum value of p_f (See Sect. 5.2.5) divided by $\sin \beta$. For domes with central angles of less than 180° , this results in a small departure from the pure half sine wave of load along a meridian recommended in Sect. 5.2.5; however, considering the approximate nature of the load recommendations, the resulting error is not of particular importance.

As in the uniform compression mode, the existence of the forces given by Eq. (8-64) assumes that the dome can take a shape consistent with them. In other words, it is assumed that the support conditions are such as to permit edge deformations consistent with the stresses given by the above equations at the edge.

Even with the rather simple loading chosen to approximate the real unsymmetrical loading component, the computation of the boundary influences is quite lengthy (Ref. 8-23 through 8-27). T. Van Langendonck suggests in Ref. (8-26) a procedure whereby these corrective edge forces may be computed. This development is based on the technique of superposing on the membrane stresses and displacements additional stresses and displacements of such a magnitude as to fit the edge of the dome to the actual support conditions.

According to Van Langendonck, the membrane displacements due to the unsymmetrical load are:

$$\begin{aligned} u &= \frac{P_1 r^2}{3ED} (1 + \nu) \left[\log \left\{ 1 + \cos (\beta - \psi) \right\} - 1 - \frac{1}{1 + \cos (\beta - \psi)} \right] \sin \theta \\ v &= \frac{P_1 r^2}{3ED} (1 + \nu) \left[-\cos (\beta - \psi) \log \left\{ 1 + \cos (\beta - \psi) \right\} + 1 + \frac{1}{1 + \cos (\beta - \psi)} \right] \cos \theta \\ w &= -\frac{P_1 r^2}{3ED} (1 + \nu) \left[\sin (\beta - \psi) \log \left\{ 1 + \cos (\beta - \psi) \right\} + \frac{1 - 2\nu}{1 + \nu} \sin (\beta - \psi) + \right. \\ &\quad \left. \left\{ 1 - \cos (\beta - \psi) \right\} \cot (\beta - \psi) \right] \cos \theta \end{aligned} \quad (8-65)$$

where u = tangential displacement of a point in the circumferential direction
 v = tangential displacement of a point along the meridian
 w = radial displacement
 D = thickness of the dome
 ν = Poisson's Ratio

Having established the membrane displacements, corrective boundary forces are applied at the edge of the dome to return it to its proper position. The corrective edge displacements and forces may be approximated by combinations of functions of the type:

$$\varphi_c = e^{-\alpha\psi} \cos \alpha\psi$$

$$\varphi_s = e^{-\alpha\psi} \sin \alpha\psi$$

where

$$\alpha = \sqrt[4]{\frac{1-\nu^2}{4} \frac{1+(D^2/12r^2)}{D^2/12r^2}} \approx 1.3 \sqrt{\frac{r}{D}} \quad (8-66)$$

In such cases, all displacements and stresses associated with the boundary disturbances can be represented by the function

$$\left[k_c \varphi_c + k_s \varphi_s \right] f(\theta)$$

where k_c and k_s are constants which have the values given in Table 8-1. This table is a slightly modified form of the one given in Ref. (8-26).

Along the edge of the dome there are four possible force boundary conditions, four possible displacement boundary conditions, or combinations

of these. With the loading considered, however, the four force boundary conditions are not independent and can be reduced to 2 by making use of the equilibrium relations that require the horizontal resistance along the support circle to balance the horizontal thrust of the loading, and the moment, about a diameter, of the applied loading to balance that of the boundary forces. In the displacement boundary conditions, a corresponding reduction is achieved by eliminating the rigid body movements. Thus, Van Langendonck was able to represent the force boundary conditions simply by:

$$\frac{M}{ErD} = -k_1 B_1 - k_2 B_2 \quad (8-67)$$

$$\frac{H}{ED} = -\frac{T_{\psi_0}}{ED} \cos \beta - \frac{\alpha - \cot \beta}{\sin \beta} k_1 - \frac{\alpha}{\sin \beta} k_2 \quad (8-68)$$

where H is the horizontal component of the boundary reactions, and the zero subscript on T_{ψ} designates the membrane solution. The corresponding displacement boundary conditions are:

$$x_c = x_o - \frac{\eta_o}{r \sin \beta} - 2\alpha^3 k_1 + 2\alpha^2 k_2 (\alpha - \cot \beta) \quad (8-69)$$

$$\frac{\xi_c}{r} = \frac{\xi_o + u_o}{r} - k_1 (1 + \nu) \left(\alpha \cos \beta - \frac{1}{\sin \beta} \right) + k_2 \left[2\alpha^2 \sin \beta - \alpha (1 + \nu) \cos \beta \right] \quad (8-70)$$

where x is the change of slope at a point on a meridian, η the vertical displacement and ξ the horizontal displacement.

Thus employing the above force, displacement, or proper combination of force and displacement relations in the boundary condition equation establishes a set of simultaneous equations which can be solved for k_1 and k_2 . k_s and k_c can then be computed. With the previous table, all the internal forces in the dome are then determined.

As was true of the treatment for the uniform boundary influence, elastic thin shell theory underlies the method presented for the unsymmetrical component of loading. Consequently it becomes subject to question when the shell has a radius to thickness ratio smaller than 20. Also the analysis shows the boundary influence to be quite local in nature, damping out at about 5 to 10 degrees away from the boundary. The distance from the edge at which the effect becomes unimportant increases as the radius to thickness ratio decreases. If the dome is tied to the foundation in such a manner that the footing acts as a ring girder to the dome, the equality of the displacements of the dome and the footing establishes the boundary influence upon the dome. Since the analysis of the displacements of the dome neglects its rigid body motion, the analysis of the footing should also neglect the rigid body components of the footing displacement.

8.8.6 Buckling. A static critical uniform radial pressure on a spherical dome as given in Ref. 8-11 is

$$q_{cr} = \frac{1.2 E_c D^2}{r^2} \quad (8-71)$$

As in the case of arches, the static equation is applied directly to the dynamic case.

Experimentally determined critical pressures for thin shells deviate considerably from the classical elastic value given by Eq. (8-71). The two principal reasons claimed for these differences are that small deflection theory, although adequate for the computation of the buckling loads for plates and bars, breaks down when applied to shells, and that the initial imperfections in shape have a rather pronounced influence on reducing the critical load. For concrete shells, creep must also be considered. Because of these factors, the present thinking of shell roof designers is that actual buckling loads are about 1/2 to 1/3 those given by Eq. (8-71). However, since relatively thick shells which have a low dead load to design load ratio are generally the type found in protective construction; reductions in the critical pressure^{are}/not expected to be as severe.

For a fully-buried dome, the critical buckling pressure can be taken as that given by Eq. (8-71), and for an above-ground dome, the buckling pressure is considered to be only 2/3 of that value. For intermediate depths, interpolate linearly between these two limits. When the depth of burial is greater than that necessary to constitute the fully-buried case, the possibility of buckling need not be investigated.

8.9 SILOS AND TUNNELS

The resistance capacities, periods, etc. of cylinders can be computed as for an arch with a central angle of 180° .

8.10 FOOTINGS

8.10.1 Flexural Resistance. The flexural capacity of a square reinforced concrete footing may be computed using the usual cantilever moment. Thus, for isolated square footings, the resistance is

$$q_f = 0.072 \phi f_{dy} \left(\frac{d}{L - a} \right)^2 \quad (8-72)$$

where d is the depth to the tension steel, a is the width of the column or base plate, and L is the plan dimension. Clearly d , L , and a must be in the same length units. Likewise, the resistance for a wall footing is

$$q_f = 0.018 \phi f_{dy} \left(\frac{d}{\ell} \right)^2 \quad (8-73)$$

where ℓ is the projection of the footing outside the wall.

8.10.2 Shear. At present it is impossible to compute the shearing resistance of a square or rectangular footing on the basis of a rational theory; consequently, an alternate approach making use of an empirical equation must be relied upon. The ultimate resistance of an isolated footing is taken as the value proposed by Hognestad in Ref. 8-34:

$$q_v \cdot \frac{L^2 - a^2}{3.5 a d f'_{dc}} = 0.035 + \frac{130}{f'_{dc}} + 0.07 \frac{q_f}{q_v} \quad (8-74)$$

Since it is desirable to have the shearing strength equal to the flexural strength, the above equation can be rewritten as

$$\frac{L^2 - (a + 2d)^2}{3.5 a d} q_v = 0.105 f'_{dc} + 130 \quad (8-75)$$

Since the wall footing is a cantilever slab, the diagonal tension equation (Eq. 8-6) of Section 8.2.3 is assumed to be applicable even though this is an extension beyond the empirical basis on which it was developed. Applied to a wall footing, the diagonal tension resistance can be approximated as:

$$q_y \approx 25 \sqrt{f'_c \phi} \left(\frac{d}{L}\right)^2 \quad (8-76)$$

8.11 REFERENCES

- 8-1 Newmark, Hansen and Associates, "Protective Construction Review Guide, (Hardening)" Volume I, prepared for the Office of the Assistant Secretary of Defense, Properties and Installations, June 1961. (UNCLASSIFIED)
- 8-2 Merritt, J. L. and Newmark, N. M., "Design of Underground Structures to Resist Nuclear Blast," Structural Research Series No. 149, University of Illinois. (UNCLASSIFIED)
- 8-3 "Report of ASCE-ACI Joint Committee on Ultimate Strength Design," Proceedings of Structural Division, American Society of Civil Engineers, Volume 81, Paper No. 809. (UNCLASSIFIED)
- 8-4 Hognestad, E., "Yield-Line Theory for the Ultimate Flexural Strength of Reinforced Concrete Slabs," ACI Journal, March 1953. (UNCLASSIFIED)
- 8-5 Ferguson, P. M., "Reinforced Concrete Fundamentals, With Emphasis on Ultimate Strength," Wiley, 1958. (UNCLASSIFIED)
- 8-6 Timoshenko, S., "Theory of Plates and Shells," McGraw-Hill, 1940. (UNCLASSIFIED)
- 8-7 Timoshenko, S., "Vibration Problems in Engineering," D. Van Nostrand, 1955. (UNCLASSIFIED)
- 8-8 Hearmon, R. F. S., "The Frequency of Vibration of Rectangular Isotropic Plates," Journal of Applied Mechanics, Volume 19, 1952. (UNCLASSIFIED)
- 8-9 Newmark, N. M., "Vulnerability of Arches, Preliminary Notes," Paper for Physical Vulnerability Division, USAF, revised 21 May 1956. (UNCLASSIFIED)
- 8-10 Williamson, R. A., Letter 10 June 1959 to N. M. Newmark. (UNCLASSIFIED)
- 8-11 Timoshenko, S., "Theory of Elastic Stability," McGraw-Hill, 1936. (UNCLASSIFIED)
- 8-12 Beedle, L. S., "Plastic Design of Steel Frames," John Wiley and Sons, 1958. (UNCLASSIFIED)
- 8-13 Beedle, L. S., Thurlimann, B., and Keeter, R. L., "Plastic Design in Structural Steel, Lecture Notes Summer Course, September 1955," American Institute of Steel Construction. (UNCLASSIFIED)

- 8-14 "Commentary on Plastic Design in Steel: Additional Design Considerations-I, Chapter 6," Journal of the Engineering Mechanics Division, American Society of Civil Engineers, October 1959. (UNCLASSIFIED)
- 8-15 Baker, J. F., Horne, M. R. and Heyman, J., "The Steel Skeleton," Vol. 2, Cambridge University Press, 1956. (UNCLASSIFIED)
- 8-16 Thurlimann, B., "New Aspects Concerning Inelastic Instability of Steel Structures," Journal of the Structural Division, American Society of Civil Engineers, January 1960. (UNCLASSIFIED)
- 8-17 Johnston, B. G., "Digest of the Guide to Design Criteria for Metal Compression Members," Journal of the Structural Division, American Society of Civil Engineers, April 1960. (UNCLASSIFIED)
- 8-18 "Effect of Edge Loads on Domes," Portland Cement Association. (UNCLASSIFIED)
- 8-19 Timoshenko, S. and Woinowsky-Krieger, S., "Theory of Plates and Shells," McGraw-Hill Book Company, 1959. (UNCLASSIFIED)
- 8-20 Flügge, W., "Stresses in Shells," Springer Verlag, 1960. (UNCLASSIFIED)
- 8-21 Goldenveiser, A. L., "The Theory of Elastic Thin Shells," Pergamon, 1961. (UNCLASSIFIED)
- 8-22 Born, J., "Praktische Schalenstatik," Verlag Von Wilhelm Ernst and Son, Berlin, 1960. (UNCLASSIFIED)
- 8-23 Schwerin, E., "Über Spannungen in Symmetrisch and Unsymmetrisch Belasteten Jugelschalen (Kuppeln) insbesondere bei Belastung durch Winddruck," Armierter Beton, 1919. (UNCLASSIFIED)
- 8-24 Gondikas, P. and Salvadori, M. G., "Wind Stresses in Domes," Engineering Mechanics Division Journal, ASCE, October 1960. (UNCLASSIFIED)
- 8-25 Lichtenstein, S., "Elastically Supported Spherical Segments Under Antisymmetrical Loads," Columbia University Report No. 37, June 1960. (UNCLASSIFIED)
- 8-26 Van Langendonck, T., "Spherical Domes Under Unsymmetrical Loading," International Association for Bridge and Structural Engineers Publications, 1960. (UNCLASSIFIED)

- 8-27 Havers, A., "Asymptotische Biegetheorie der unbelasteten Kugelschale," Ingenieur-Archiv, v. 6, 1935. (UNCLASSIFIED)
- 8-28 Toebes, G. H., Discussion to Reference 8-24, Engineering Mechanics Division Journal, Proceedings of American Society of Civil Engineers, April 1961. (UNCLASSIFIED)
- 8-29 Singell, T. W., "Wind Forces on Structures: Forces on Enclosed Structures," Structural Division Journal, ASCE, July 1958. (UNCLASSIFIED)
- 8-30 Untrauer, R. E. and Siess, C. P., "Strength and Behavior in Flexure of Deep Reinforced Concrete Beams Under Static and Dynamic Loads," University of Illinois, Structural Research Series No. 230, a report to Research Directorate, Air Force Special Weapons Center, October 1961. (UNCLASSIFIED)
- 8-31 dePaiva, H. A. R. and Siess, C. P., "Strength and Behavior of Deep Reinforced Concrete Beams Under Static and Dynamic Loads," University of Illinois, Structural Research Series No. 231, a report to Research Directorate Air Force Special Weapons Center, October 1961. (UNCLASSIFIED)
- 8-32 Whipple, C. R., "The Dynamic Response of Shallow-Buried Arches Subjected to Blast Loading," Report for Air Force Special Weapons Center, Contract No. AF 29(601)-2591, Project 1080, University of Illinois, 1961. (UNCLASSIFIED)
- 8-33 Whipple, C. R., "Numerical Studies of the Dynamic Response of Shallow-Buried Arches Subjected to Blast Loading," Draft of report for Air Force Special Weapons Center Contract Nos. AF 29(601)-2591 and AF 29(601)-4508, Project No. 1080, University of Illinois, 1961. (UNCLASSIFIED)
- 8-34 Hognestad, E., "Shearing Strength of Reinforced Concrete Column Footing," Journal, American Concrete Institute, Vol. 25, No. 3, November, 1953. (UNCLASSIFIED)

TABLE 8-1

VALUES OF k_c AND k_s FOR VARIOUS COMPONENTS OF DISPLACEMENT AND STRESS

Displacement or Stress	k_s	k_c	$f(\theta)$
w	$2\alpha^2 r k_1$	$2\alpha^2 r k_2$	$\cos \theta$
v	$\alpha r(1+\nu)(k_2-k_1)$	$-\alpha r(1+\nu)(k_2+k_1)$	$\cos \theta$
u	$-r(1+\nu)k_2 \operatorname{cosec} \beta$	$r(1+\nu)k_1 \operatorname{cosec} \beta$	$\sin \theta$
x	$2\alpha^3(k_2+k_1)$	$2\alpha^3(k_2-k_1)$	$\cos \theta$
T_{ψ}/ED	$\alpha(k_1-k_2) \cot \beta + \frac{1}{\sin^2 \beta} k_2$	$\alpha(k_1+k_2) \cot \beta - \frac{1}{\sin^2 \beta} k_1$	$\cos \theta$
$T_{\psi\theta}/ED$	$B_4 = \frac{1}{\sin \beta} \left[\alpha(k_1-k_2)+k_2 \cot \beta \right]$	$B_5 = \frac{1}{\sin \beta} \left[\alpha(k_1+k_2)-k_1 \cot \beta \right]$	$\sin \theta$
M_{ψ}/ED	$r(B_1 k_2 - B_2 k_1)$	$-r(B_1 k_1 + B_2 k_2)$	$\cos \theta$
$M_{\psi\theta}/ED$	$-B_5 r \frac{1-\nu}{2\alpha^2}$	$B_4 r \frac{1-\nu}{2\alpha^2}$	$\sin \theta$
M_{θ}/ED	$r(B_6 k_2 - B_7 k_1)$	$-r(B_6 k_1 + B_7 k_2)$	$\cos \theta$
$\frac{T_{\theta}}{ED} = \left[\frac{w}{r} - \frac{T_{\psi}}{ED} \right] \cos \theta$	$B_6 = -B_1 + 1 + \nu$	$B_7 = -B_2 + \frac{1-\nu}{2\alpha^2}$	
$B_1 = -\frac{1-\nu}{2\alpha} \cot \beta$	$B_2 = (\alpha \cot \beta + 1 - \frac{1-\nu}{\sin^2 \beta} \frac{1-\nu}{2\alpha^2})$		

Member	Flexural Capacity	Stiffness
	$q_f b = 0.072 \phi_c f_{dy} a \left(\frac{d}{L}\right)^2$	$K = \frac{384 E_c I}{5 L^3}$
	$Q_f = 0.036 \phi_e \frac{a d^2}{L} f_{dy}$	$K = \frac{48 E_c I}{L^3}$
	$q_f b = 0.072 \left(\phi_c + \frac{\phi_e}{2}\right) f_{dy} a \left(\frac{d}{L}\right)^2$	$K = \frac{160 E_c I}{L^3}$
	$Q_f = 0.036 \left(\phi_c + \frac{\phi_e}{2}\right) \frac{a d^2}{L} f_{dy}$	$K = \frac{106 E_c I}{L^3}$
	$q_f b = 0.072 (\phi_c + \phi_e) f_{dy} a \left(\frac{d}{L}\right)^2$	$K = \frac{307 E_c I}{L^3}$
	$Q_f = 0.036 (\phi_c + \phi_e) \frac{a d^2}{L} f_{dy}$	$K = \frac{192 E_c I}{L^3}$

Where:

ϕ_e = Percentage Of Tensile Steel At The Support Section.

b = Width Of Contributory Load Area; a = Beam Width.

ϕ_c = Percentage Of Tensile Steel At Midspan.

$E_c = 1000 f'_c$ From ACI 318-56

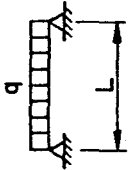
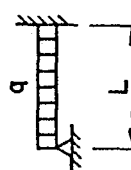
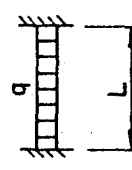
$$I = \frac{b(k'd)^3}{3} + \frac{nb\phi d^3}{100} (1-k')^2$$

$$n = \frac{E_s}{E_c} = \frac{30,000}{f'_c}$$

VALUES OF k'

ϕ	$f'_c = 3000$	$f'_c = 5000$
0.5	0.27	0.22
1.0	0.36	0.29
1.5	0.42	0.34

FIG. 8-1 FLEXURAL CAPACITY AND STIFFNESS OF REINFORCED CONCRETE BEAMS.

Member	PURE SHEAR	
	$d/L \leq 0.2$	$d/L \geq 0.2$
	$q_v b = 0.44 f'_c a \frac{d/L}{1-d/L}$	<u>Without Inclined Steel</u> $q_v b = 0.55 f'_c (\frac{d}{L}) a$
	<u>With Inclined Steel</u> $q_v b = 0.44 f'_c a \frac{d/L}{1-d/L} (\frac{1}{2} + \frac{\phi'_v f_{dy}}{20 f'_c})$ But Not Less Than $q_v b = 3.5 \sqrt{f'_c} \frac{a d}{L}$	$q_v b = 0.55 f'_c a (\frac{d}{L}) (\frac{1}{2} + \frac{\phi'_v f_{dy}}{20 f'_c})$ But Not Less Than $q_v b = 3.5 \sqrt{f'_c} \frac{a d}{L}$
	$q_v b = 0.44 f'_c \frac{d/L}{1-d/L} a \lambda_s$	<u>Without Inclined Steel</u> $q_v b = 0.55 f'_c (\frac{d}{L}) a \lambda_s$
	<u>With Inclined Steel</u> $q_v b = 0.44 f'_c a (\frac{d/L}{1-d/L}) \lambda_s (\frac{1}{2} + \frac{\phi'_v f_{dy}}{20 f'_c})$ But Not Less Than $q_v b = 3.5 \sqrt{f'_c} \frac{a d}{L} \lambda_s$	$q_v b = 0.55 f'_c a (\frac{d}{L}) \lambda_s (\frac{1}{2} + \frac{\phi'_v f_{dy}}{20 f'_c})$ But Not Less Than $q_v b = 3.5 \sqrt{f'_c} \frac{a d}{L} \lambda_s$
	$q_v b = 0.44 f'_c \frac{d/L}{1-d/L} a$	<u>Without Inclined Steel</u> $q_v b = 0.55 f'_c (\frac{d}{L}) a$
	$q_v b = 0.44 f'_c a \frac{d/L}{1-d/L} (\frac{1}{2} + \frac{\phi'_v f_{dy}}{20 f'_c})$ But Not Less Than $q_v b = 3.5 \sqrt{f'_c} \frac{a d}{L}$	<u>With Inclined Steel</u> $q_v b = 0.55 f'_c a (\frac{d}{L}) (\frac{1}{2} + \frac{\phi'_v f_{dy}}{20 f'_c})$ But Not Less Than $q_v b = 3.5 \sqrt{f'_c} \frac{a d}{L}$

Where:

q_v = Shear Resistance Capacity.

b = Width Of Loading Area.

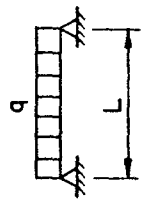
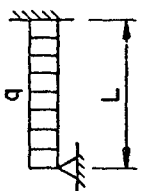
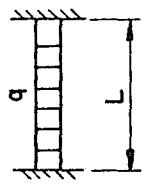
a = Beam Width.

d = Effective Depth Of The Beam.

ϕ'_v = Inclined Web Steel For Pure Shear

$$\lambda_s = \frac{1}{1 + \frac{1}{4} (\phi_e \max. - \phi_e \min.) \phi_c}} = \frac{1}{1 + \frac{1}{4} (\phi_e)} , \text{ For Hinged-Fixed Span.}$$

FIG. 8-2a PURE SHEAR RESISTANCE OF REINFORCED CONCRETE BEAMS.

Member	Diagonal Tension
	$q_y b = 100 \left(\frac{1}{2 + \frac{\phi}{\phi_c}} \right) \left(1 + \frac{2 \phi_v f_{dy}}{10^5} \right) a \sqrt{\phi_c f'_c} \left(\frac{d}{L} \right)^2$ <p>But Not Less Than</p> $q_y b = 3.5 \sqrt{f'_c} \frac{a d}{L}$
	$q_y b = 100 \left(1 + \frac{3}{4} \frac{\phi_e}{\phi_c} \right) \left(\frac{1}{2 + \frac{\phi}{\phi_c}} \right) \left(1 + \frac{2 \phi_v f_{dy}}{10^5} \right) a \sqrt{\phi_c f'_c} \left(\frac{d}{L} \right)^2$ <p>But Not Less Than</p> $q_y b = 3.5 \sqrt{f'_c} \frac{a d}{L} \left(\frac{1}{1 + \frac{1}{4} \left(\frac{\phi_e}{\phi_c} \right)} \right)$
	$q_y b = 100 \left(1 + \frac{3}{2} \frac{\phi_{eavg}}{\phi_c} \right) \left(\frac{1}{2 + \frac{\phi}{\phi_c}} \right) \left(1 + \frac{2 \phi_v f_{dy}}{10^5} \right) a \sqrt{\phi_c f'_c} \left(\frac{d}{L} \right)^2$ <p>But Not Less Than</p> $q_y b = 3.5 \sqrt{f'_c} \frac{a d}{L}$

Where:

q_y = Shear Resistance Capacity.

b = Width Of Loading Area.

a = Beam Width.


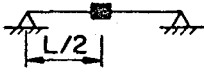

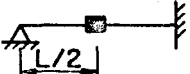

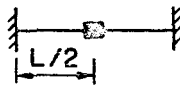
d = Effective Depth Of Beam.

ϕ_v = Vertical Web Steel For Diagonal Tension.

ϕ_c = Percent Tensile Steel At Center Of Beam.

ϕ'_c = Percent Compressive Steel At Center Of Beam.

FIG. 8-2b DIAGONAL TENSILE RESISTANCE OF REINFORCED CONCRETE BEAMS.

Member	Period
	$T = \frac{L^2}{42,500 d \sqrt{\phi}}$
	$T = 0.91 \sqrt{\frac{W_c}{g} \frac{L^3}{E_c I}}$
	$T = \frac{L^2}{63,800 d \sqrt{\phi}}$
	$T = 0.61 \sqrt{\frac{W_c}{g} \frac{L^3}{E_c I}}$
	$T = \frac{L^2}{85,000 d \sqrt{\phi}}$
	$T = 0.45 \sqrt{\frac{W_c}{g} \frac{L^3}{E_c I}}$

Where;

T = Period, sec.

L = Span, in.

d = Depth To Steel, in.

W_c = Total Weight Concentrated At Midspan, lbs.

NOTE:

For Underground Structures Increase Period By $\sqrt{\left(\frac{m'}{m}\right)\left(\frac{K}{K'}\right)}$
(See Section 8.2.6)

I Computed From Transformed Section.

FIG. 8-3 NATURAL PERIOD OF VIBRATION FOR REINFORCED CONCRETE BEAMS

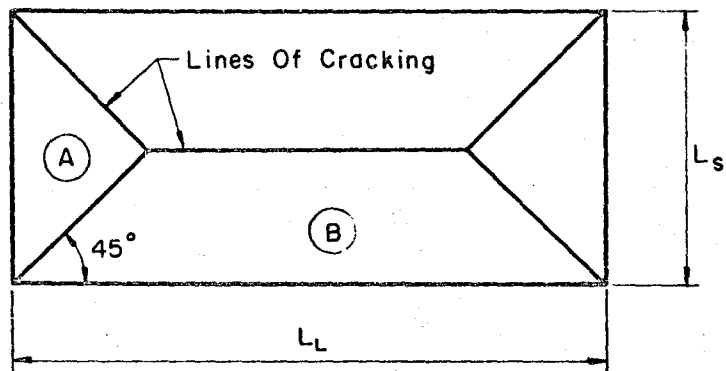


FIG. 8-4 ASSUMED CRACK PATTERN FOR TWO-WAY SLABS

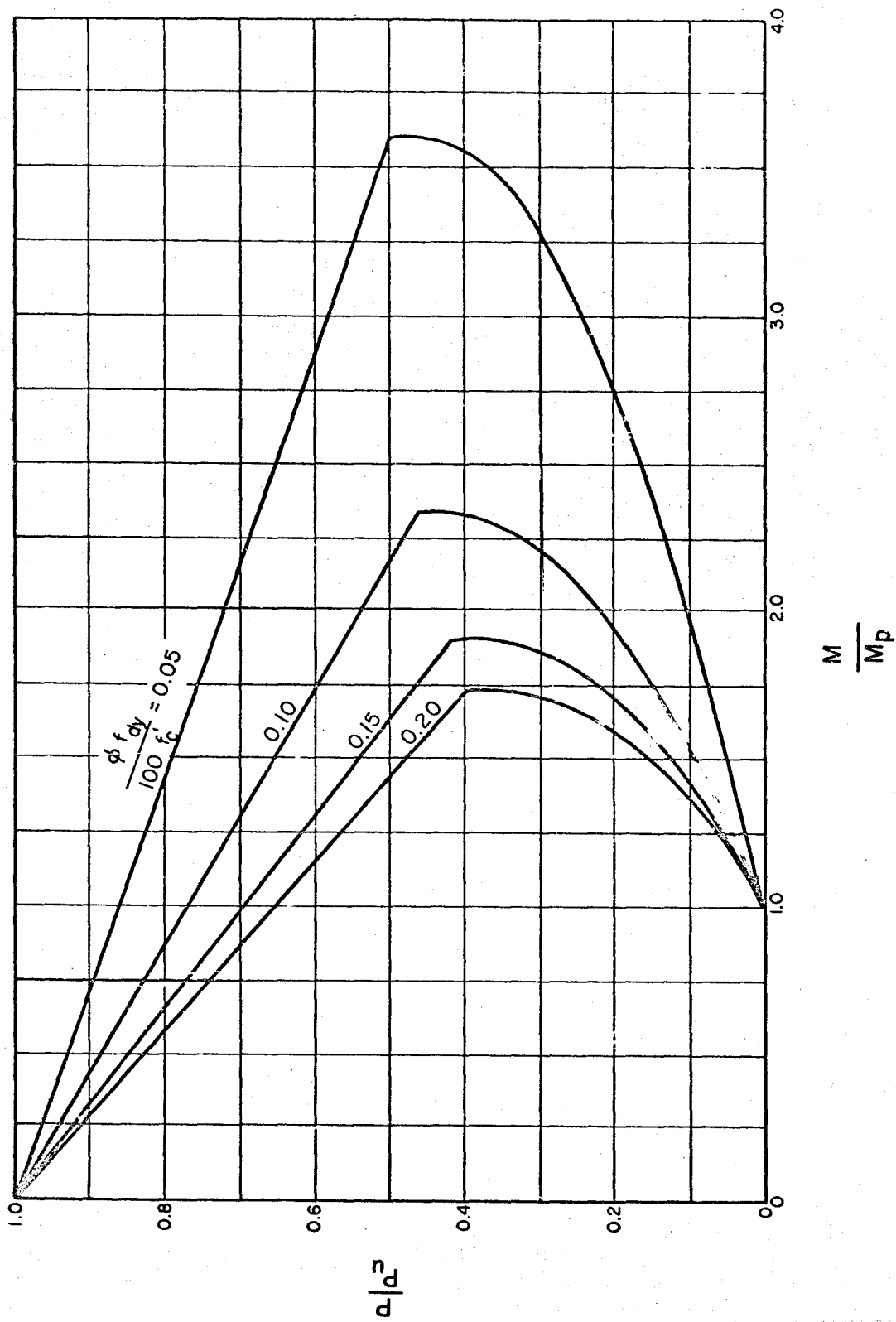
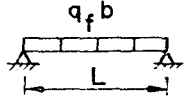
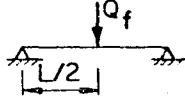
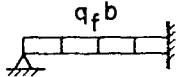
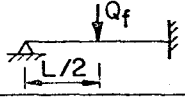
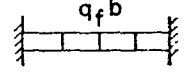
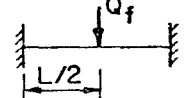


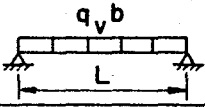
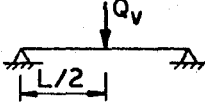
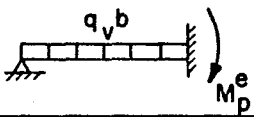
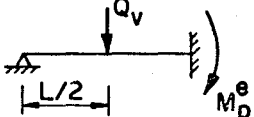
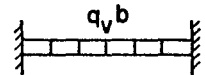
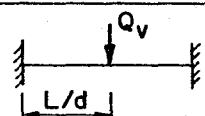
FIG. 8-5 INTERACTION DIAGRAM FOR REINFORCED CONCRETE BEAM-COLUMNS

Member	Flexural Capacity	Stiffness
	$q_f b = 9.20 \frac{f_{dy} S}{L^2}$	$K = \frac{384 EI}{5 L^3}$
	$Q_f = 4.6 \frac{f_{dy} S}{L}$	$K = \frac{48 EI}{L^3}$
	$q_f b = 11.7 \frac{f_{dy} S}{L^2}$	$K = \frac{160 EI}{L^3}$
	$Q_f = 6.9 \frac{f_{dy} S}{L}$	$K = \frac{106 EI}{L^3}$
	$q_f b = 18.4 \frac{f_{dy} S}{L^2}$	$K = \frac{307 EI}{L^3}$
	$Q_f = 9.2 \frac{f_{dy} S}{L}$	$K = \frac{192 EI}{L^3}$

Where:

b = Width Of Contributory Loading Area.
S = Elastic Section Modulus.

FIG. 8-6 FLEXURAL CAPACITY AND STIFFNESS OF STEEL BEAMS.



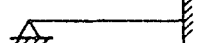
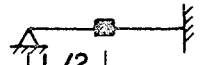
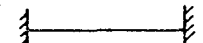
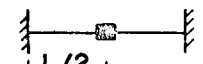
Member	Shear Capacity
	$q_v b = \frac{2V}{L}$
	$Q_v = 2V$
	$q_v b = \frac{2V}{L} - \frac{2M_p^e}{L^2}$
	$Q_v = 2V - \frac{2M_p^e}{L}$
	$q_v b = \frac{2V}{L}$
	$Q_v = 2V$

Where :

b = Width Of Loaded Area.

V = Total Shear Resistance Of Beam.

FIG. 8-7 SHEAR CAPACITY OF STEEL BEAMS.

Member	Period
	$T = 0.64 L^2 \sqrt{\frac{W}{gEI}}$
	$T = 0.91 \sqrt{\frac{W_c}{g} \frac{L^3}{EI}}$
	$T = 0.42 L^2 \sqrt{\frac{W}{gEI}}$
	$T = 0.61 \sqrt{\frac{W_c}{g} \frac{L^3}{EI}}$
	$T = 0.28 L^2 \sqrt{\frac{W}{gEI}}$
	$T = 0.45 \sqrt{\frac{W_c}{g} \frac{L^3}{EI}}$

Where:

T = Period, sec.

W = Supported Weight (Including Beam) Per Unit Length.


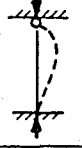



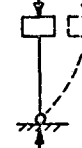
W_c = Total Weight Concentrated At Midspan.

E = Modulus Of Elasticity.

I = Moment Of Inertia.

g = Gravitational Constant.

FIG. 8-8 NATURAL PERIOD OF VIBRATION
FOR STEEL BEAMS.

COLUMN	α	CRITICAL STRESS	
		Strong Axis	Weak Axis
	0.65	$f_{cr} = 42,000 - 0.61 \left(\frac{L}{r}\right)^2$	$f_{cr} = 42,000 - 100 \left(\frac{L}{r}\right)^2$
	0.80	$f_{cr} = 42,000 - 0.92 \left(\frac{L}{r}\right)^2$	$f_{cr} = 42,000 - 124 \left(\frac{L}{r}\right)^2$
	1.20	$f_{cr} = 42,000 - 2.07 \left(\frac{L}{r}\right)^2$	$f_{cr} = 42,000 - 186 \left(\frac{L}{r}\right)^2$
	1.00	$f_{cr} = 42,000 - 1.44 \left(\frac{L}{r}\right)^2$	$f_{cr} = 42,000 - 155 \left(\frac{L}{r}\right)^2$
	2.10	$f_{cr} = 42,000 - 6.35 \left(\frac{L}{r}\right)^2$	$f_{cr} = 42,000 - 326 \left(\frac{L}{r}\right)^2$
	2.00	$f_{cr} = 42,000 - 5.76 \left(\frac{L}{r}\right)^2$	$f_{cr} = 42,000 - 310 \left(\frac{L}{r}\right)^2$

Where:

f_{cr} = Critical Buckling Stress Of The Column.

L = Column Height.

r = Radius Of Gyration Of Column Section.

Local Buckling,

$$\frac{\text{flange width}}{\text{flange Thickness}}, \frac{b}{t_f} < 17$$

$$\frac{\text{column depth}}{\text{web thickness}}, \frac{d}{t_w} < 43$$

FIG. 8-9 BUCKLING STRESSES FOR AXIALLY LOADED A-7 OR A-36 STEEL COLUMNS.

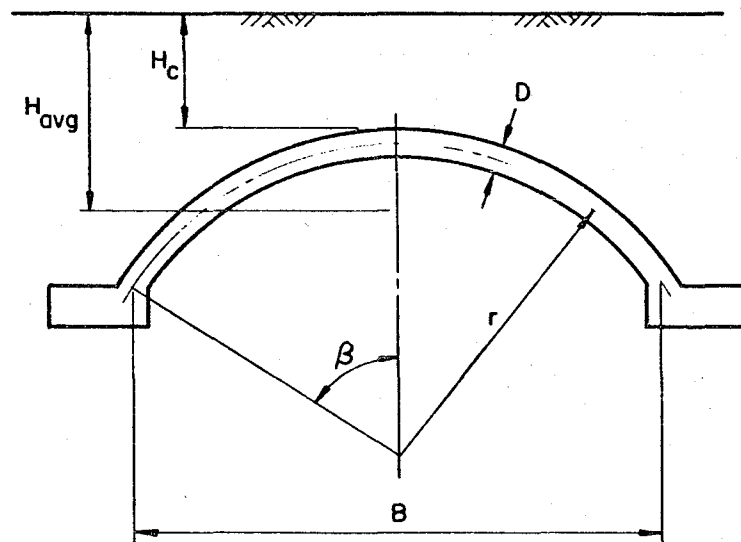
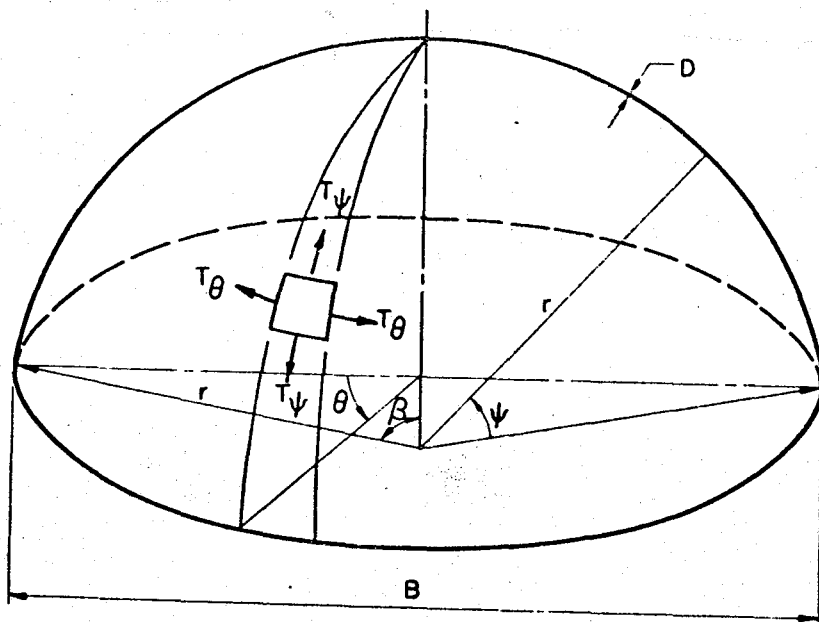
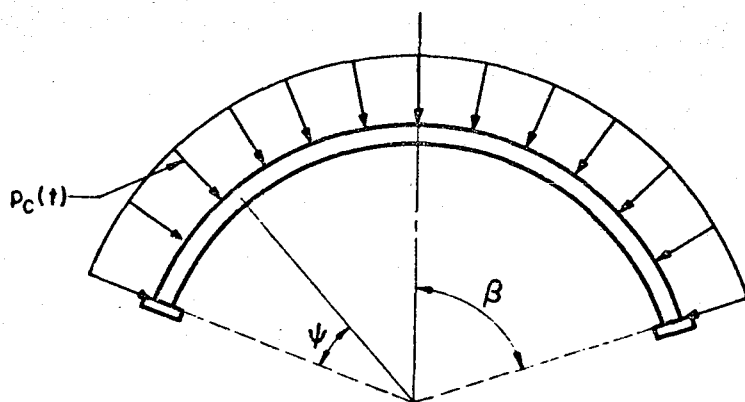


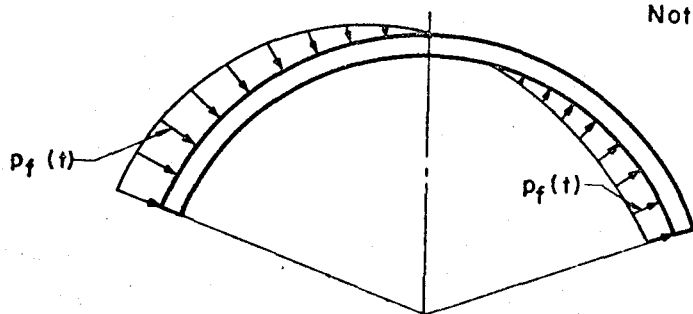
FIG. 8-10 ARCH NOTATION USED IN ANALYSIS.



(a) Dome Notation



(b) Uniform Radial Component. (For Variation With Time See Fig. 5-6(a) For Arch.)



Note:

$p_f(t)$ Varies Sinusoidally With Latitude From Maximum At $\psi=0$ To Zero At $\psi=\beta$; It Also Varies Sinusoidally With Longitude From Maximum At $\theta=0$ To Zero At $\theta=90^\circ$.

(c) Flexural Component. (For Variation With Time See Figs. 5-6 (b and c) For Arch.)

FIG. 8-II A BLAST LOADING ON AN ABOVE-GROUND DOME.

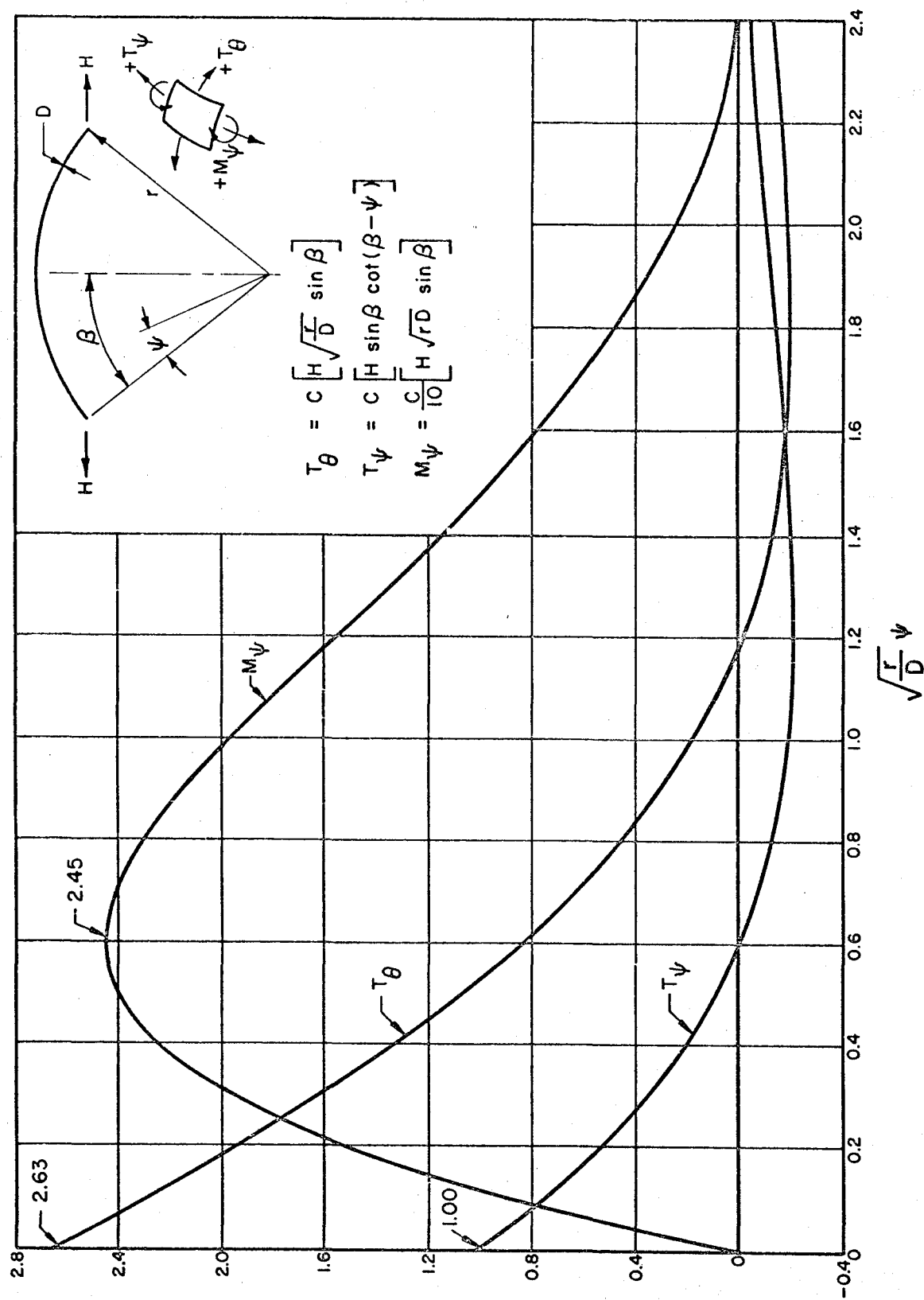


FIG. 8-12 EFFECTS OF LINE LOAD H—EDGE FREE TO ROTATE.

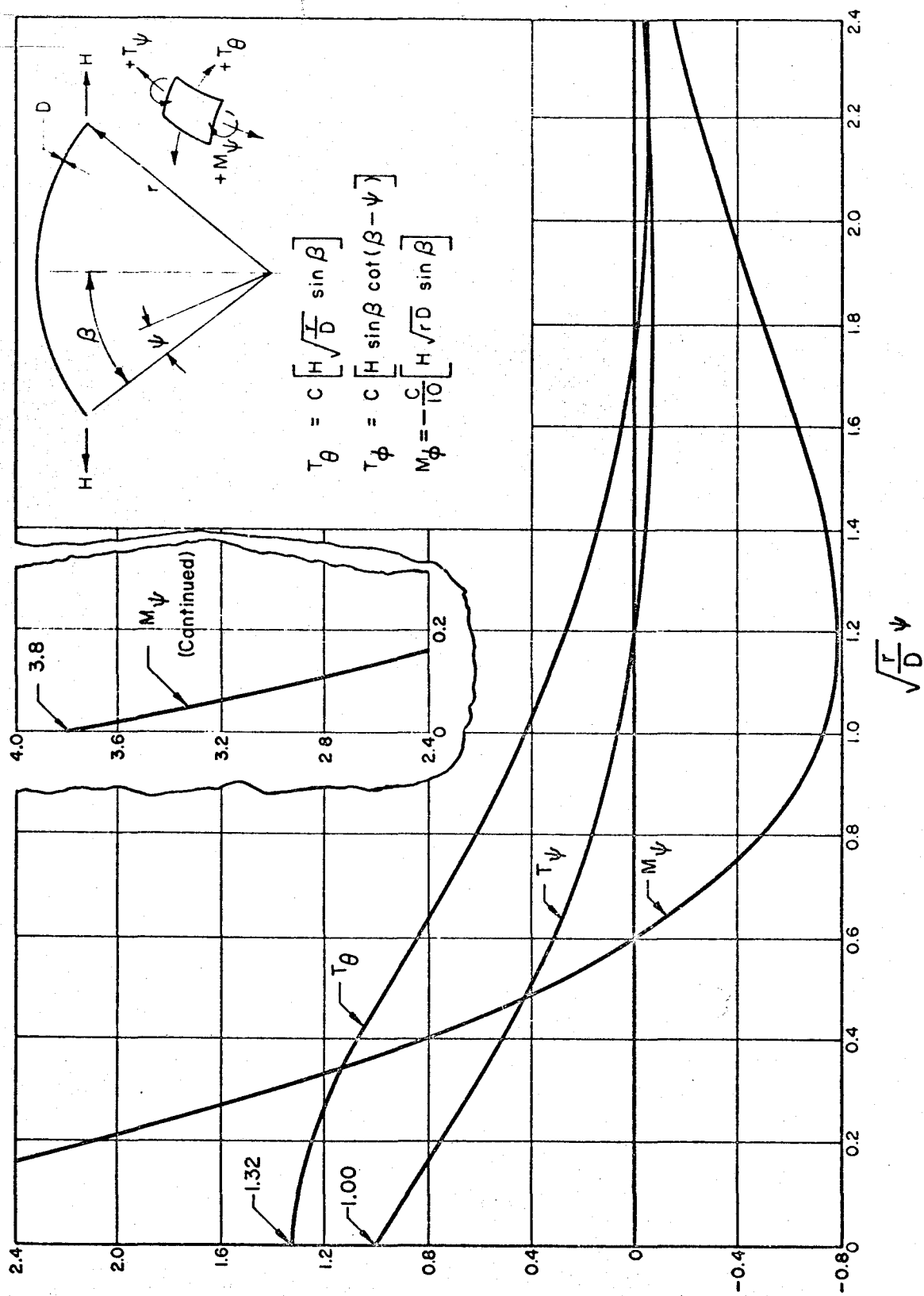


FIG. 8-13 EFFECTS OF LINE LOAD H — ROTATION OF EDGE PREVENTED

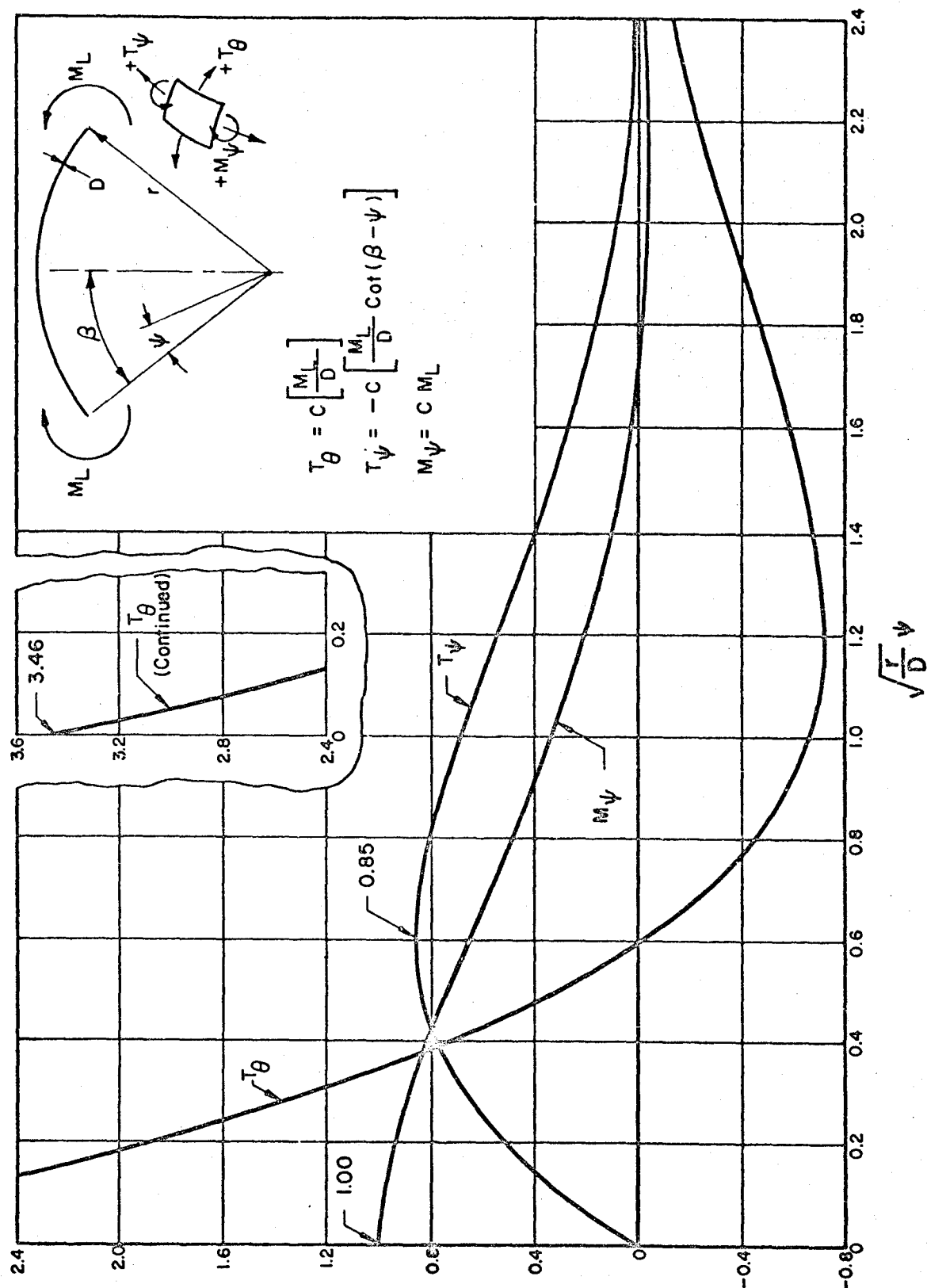


FIG. 8-14 EFFECTS OF EDGE MOMENTS M_L — EDGE FREE TO MOVE.

9.1 INTRODUCTION

In this chapter methods are presented for the design of the structure based upon the loadings of Chapter 5, dynamic properties of the material from Chapter 6 and the resistance capacities, periods etc. of the structural sections as given in Chapter 8. For a preliminary design it is suggested that the structure be designed to have a static resistance equal to the peak force applied by the blast. Because the duration of the loading is generally long compared with the period of vibration of the structure and the ductility factor is usually at least 3.0, revisions of this preliminary design will usually be found to be quite minor.

In some instances, where the loading lasts for a short time compared with the period of vibration of the structure, this procedure will result in an overly conservative structure. For cases where it is considered necessary to restrict the ductility to a low value (near 1.0), for example, in some aspects of the design of arches and domes, a structure designed on this basis will be found to be inadequate. In these cases a redesign will be necessary using a more accurate analysis of the dynamic effect of the loading.

The factor of safety should be selected in accord with the concepts presented in Chapter 7.

Using the principles described above, the preliminary design is evolved by normal static design procedures or by employing design aids such as the figures at the end of this chapter. The majority of these figures were taken from Ref. 8-1.

It must be emphasized that the charts given herein (Figs. 9-2 through 9-38) can not properly be called "Design Charts". They can be used very effectively as an aid in preliminary design. However, they were prepared on the assumption that the duration of the blast-induced load was long in comparison to the period of vibration of the structural element (adjusted if necessary for any additional mass that vibrates with it). Furthermore, they presumed specific values for the ductility factor as indicated on the figures. If the effective load duration is about 3.0 times the period of vibration, the effect of the actual load duration becomes relatively insignificant and can usually be ignored, that is considered to be infinite. Similarly, if the ductility is taken as large as 3.0, a further increase will reflect only very small changes in the resistance required of a structural element for a given blast load.

If, in a given case, the effective load duration is relatively short (less than about 3.0 times the period) or if the ductility factor chosen differs from that stipulated on the charts, the charts should be used only for preliminary estimates of required proportions of structural elements which should then be carefully checked using the time-dependent loadings that can be determined by methods given in Chapter 5 and the dynamic analysis methods presented in Appendix B.

If preliminary designs are made simply by setting the resistance as given by the equations of Chapter 8 equal to the peak blast-induced force, the ductility factor will have effectively been set at a high value (theoretically infinite, but practically at about 10) and the load duration

will have been taken as being very large relative to the period of vibration. Since the charts do consider specific ductility factors, the results obtained from the charts should not be expected to agree exactly with those obtained from the equations of Chapter 8.

The rebound behavior of the structure must not be overlooked and a method for estimating the necessary rebound strength is given in Appendix B.

9.2 REINFORCED CONCRETE BEAMS AND ONE-WAY SLABS

Once the loading has been established, the preliminary proportioning of the slab or beam may be accomplished directly from the resistance formulas given in Chapter 8 considering the peak pressure as a static load or by charts similar to those given at the end of this chapter following the sequence of operations listed below:

1. The percentage of positive reinforcing steel at midspan, ϕ_c , and the effective negative steel at the supports, ϕ_e , must be assumed initially. If the supports can be considered as simple supports, the latter is taken as zero. If the beam or slab frames into another element which restrains its rotation at the support, ϕ_e must be taken to be consistent with either the moment that the member itself can develop or the moment that the restraining slab or element can develop, whichever is smaller.

2. Set the value of f_{dy} equal to the dynamic yield stress selected for the steel type to be used.

3. If the structure is buried such that dead load may not be ignored and the preliminary design is being developed by use of the charts,

it is expedient to convert the dead load to an equivalent blast loading. Since the blast loading has been increased by 1.20 when dealing with those aspects for which a $\mu = 3.0$ is selected, and by 1.62 for those where μ is restricted to 1.3, a soil cover weighing $120\#/ft^3$ is converted to an equivalent blast pressure by multiplying the μ equal 3.0 cases by 0.69 times the depth of earth in feet and the μ equal 1.3 cases by 0.51 times the depth of earth in feet. The slab or beam weight may be handled in the same way. If other μ values are considered more reasonable and design charts for these μ are available a similar conversion may be used.

4. Assume the required resistance to be equal to the maximum applied pressure. For slabs find the d/L necessary in flexure by Eq. (8-4) or (8-5), or Fig. 9-2. For beams, Eq. (8-4) or (8-5), or Fig. 9-9 are used. Establish preliminary proportions of the slab or beam on the basis of d/L thus determined.

5. Check the adequacy of the section established in step 4 against a pure shear failure by the Eqs. of Sect. 8.2.4, or Fig. 9-3 for slabs and 9-11 for beams. If pure shear governs the member under consideration, increase d/L or add inclined steel. Fig. 9-4 gives the inclined steel factor. When inclined steel is used it will normally require reasonably large amounts to be effective. The reason for this is that before the steel is effective the deformations are such that the concrete shear strength is reduced. If the depth is increased, it is then possible to reduce the percentage of flexural steel used, provided that in doing so it is not dropped below 0.5 percent.

6. Check the adequacy of the slab or beam for its resistance to diagonal tension using Eq. (8-6), (8-7), and (8-8), or Fig. 9-5 if it has been decided to restrict u to 3.0. The web reinforcement factor needed is taken from Fig. 9-6. The influence of the support conditions and flexural steel is taken from Fig. 9-7. If web reinforcement is required, at least 0.5 percent should be used to insure ductility.

7. When the preliminary design is completed, the adequacy of the section can be checked using the resistances and periods of vibration as given by the appropriate equations of Chapter 8, the actual time-dependent load function defined in Chapter 5 idealized as equivalent triangular pulses, and the analysis procedures of Appendix B. The section can then be revised if necessary, and the analysis repeated.

9.3 REINFORCED CONCRETE TWO-WAY SLAB AND SUPPORTING BEAMS

Design of two-way slabs and supporting beams by the equations or charts is accomplished by converting them to equivalent uniformly loaded one-way elements. For the slab the flexural resistance is Ω (given in Fig. 9-8) times that of a one-way slab. The diagonal tension strength and pure shear resistance of the slab are taken to be $(2/3)(1 + \alpha)$ times those of a one-way slab but this factor is not to be taken less than one. The supporting beams are designed using the factors given in Figs. 9-10 and 9-13.

Slab Design

1. The steel percentages ϕ_{Le} , ϕ_{Lc} , ϕ_{sc} and ϕ_{se} must be assumed.

The comments in Item (1) of Section 9.2 apply.

2. Dynamic yield properties of the reinforcement are selected.
3. The weight of the slab and earth cover may be taken into account by the method given in Step 3 of Section 9.2.
4. For a resistance assumed equal to the peak applied pressure, find the d/L necessary for flexure from Eq. (8-22) or Fig. 9-2. Figure 9-2 should be entered using the peak applied pressure divided by Ω (Eq. (8-23) or Fig. 9-8) as p_m . Using d/L thus determined, select the slab thickness.
5. Check the pure shear resistance of the slab chosen in Step 4 by the method of Sect. 8.3.2. If found to be inadequate, increase the thickness and repeat the flexural analysis to reduce the reinforcement.
6. Follow the procedure of Step 6, Sect. 9.2 to check diagonal tension strength, taking note that the shear resistance of a two-way slab is $(2/3)(1 + \alpha)$ times that of a one-way slab spanning in the short direction when α is greater than $1/2$, and the same as a one-way slab when α is less than $1/2$. If the slab is not nearly square, and if web reinforcement is needed along the long edges, the short edges should be investigated using $\alpha = 1.0$.
7. Review the design thus obtained and revise it using the same methods described in Step 7 of Sect. 9.2 for one-way slabs.

9.4 STEEL BEAMS

The flexural resistance of steel beams is given in Fig. 8-6 for the static case. Fig. 9-14 gives the specific resistance values when $\mu = 3.0$ if an infinite duration of the blast loading is applicable. Fig. 9-15 gives

the comparable values for the shear resistance. If the duration of the load is relatively short or a ductility factor different from 3.0 is used, revise the preliminary design obtained from Figs. 9-14 and 9-15 using the analysis procedure of Appendix B, equivalent triangular loads based on the actual time-dependent loads of Chapter 5, and resistances and periods as given in Sect. 8.5.

9.5 ARCHES

If an underground steel or concrete arch is to be designed and the depth of burial meets the requirements of "full-burial", only the compression mode is considered to be significant. The resistance in this mode, q_c , is given in Sect. 8.7.3. A preliminary value of D/r for concrete arches may be determined by summing those values from Fig. 9-16 and Fig. 9-17 or 9-18 which correspond to the dynamic strength parameters for the design in question. In a steel underground arch, the analogous value f_{dy} (A/r) may be obtained from Fig. 9-23 or 9-24.

The value of peak pressure, p_m , to be used in the charts should be taken as the attenuated pressure at a depth $z = H_{av}$ (See Fig. 4-3). The period, T_c , is then computed for this arch (Sect. 8.7.2) and compared with the rise time and the effective duration of the actual loading as given in Chapter 5. If the ratios of the rise time (see Fig. 9-39) and duration (see Fig. 9-1) to the period yield a value of $p_m/q_c = K_r p_m/q$ ratio that is different from that of the design figures, the arch should be revised by use of Eq. (8-51) or (8-52). The weight of the arch and earth cover may be included by the method of Section 9.2.

For above-ground arches, or those whose depth of burial do not meet the requirements of "full burial", both modes of loading must be considered simultaneously.

A preliminary design for the above-ground reinforced concrete arch may be obtained from Fig. 9-21 or 9-22 and for the steel arches from Fig. 9-27 or 9-28. Factors are included on the above-ground reinforced concrete arch figures for the conversion to several concrete strengths and steel percentages.

Having selected the preliminary thickness, compute the flexural and uniform compression periods from the appropriate equations of Section 8.7.2. Determine the effective load durations for the two loading components as defined in Chapter 5. For the uniform compression mode, use single or multiple triangular representations (Figs. 3-7, 3-8, and 3-9) of the pressure pulse as may be needed, depending on the relative magnitude of T_c . For the flexural component use a double triangle replacement pulse as discussed in Sect. B.2.3f. Since the flexural mode loading is not a precisely known time function, inclusion of the rise time in the double triangle replacement system is not considered justified. Consequently for design purposes, the flexural loading is considered as an initially peaked pulse of magnitude $(0.5 + \beta/\pi)p_{s0}$ decaying linearly to $\beta/\pi C_d p_d$ at a time $(1 + 3\beta/\pi)$ times the transit time. Compute the p_m/q values separately for the flexural and uniform compression modes by the methods of Sect. B.2.3f. Calculate the thrust in the arch consistent with the required resistance, q_c , as found for the uniform compression mode, and also the ultimate thrust

capacity P_u of the arch by Eq. (8-48) or (8-49). Knowing P/P_u , q/q_f is determined in the steel arch case by the use of the interaction formula, Eq. (8-57), and for the concrete arch by use of the Fig. 8-5.

Some judgment must be used in selecting the appropriate P/P_u value to use particularly when dealing with concrete because the shape of the concrete interaction diagram gives increasing q/q_f values as P/P_u increases, until P/P_u is approximately one-half. Reliance should not be placed upon a specific value of P/P_u which gives a significant increase in q/q_f since this value of P/P_u may not be active in the arch when the maximum flexural resistance is needed. Once q/q_f is found, q_f is calculated by the appropriate equation of Sect. 8.7.3, "Flexural Mode," and the solution for q determined by these values is compared with the assumed flexural loading. Comparison of the q 's determines the adequacy of the design. An attempt should not be made to shave the section in order to get exceedingly close agreement because of the uncertainty existing in the required q .

For the partially-buried case, the general procedure is the same as for the above ground case except that the increased soil mass and resistance effects as discussed in Sect. 8.2.6 must be included in the period computation. It should also be noted that the design charts for "Partially Buried Arches" were prepared for a given depth and a flexural loading simpler in form than that given in Chapter 5. Therefore, the charts can yield only preliminary designs.

The fully buried arches need not be checked against buckling, but the above-ground and partially-buried cases must be checked for buckling

stability in accordance with the formulas of Sect. 8.7.4 "Buckling".

9.6 DOMES

When the placement of the dome meets the full burial requirements given in Chapter 5, the preliminary design is accomplished in the same manner as with arches. Initially the total steel percentage in each face in each direction must be assumed and the dynamic material properties must be selected. A preliminary thickness of the dome may then be found from Fig. 9-17 or 9-18 for arches simply by taking one-half of the value read from the chart.

The period of the dome including the soil mass influence and the actual load (Sect. 5.3.6), idealized with equivalent triangles, should be computed. The design can then be revised to reflect the p_m/q value (Fig. 9-1) consistent with the selected μ and the calculated t_d/T parameters. The revised thickness may be found from Eq. (8-63) and the proper p_m/q value. Buckling need not be investigated for fully buried cases.

For a dome it is also desirable to investigate the interaction between the dome and the footing. A method is given in Sect. 8.8.4 if the dome and footing are to have consistent deformations. Because of possible tensile forces around the circumference at the base resulting from a non-uniform load distribution over the dome at least 0.5 percent steel should be used circumferentially at the base.

For partially buried and above-ground domes, the flexural mode with its loading as discussed in Chapter 5 must also be considered. Preliminary thickness may be found from Fig. 9-29 or 9-30 for a partially

buried dome. In the case of the above-ground domes, Fig. 9-31 or 9-32 apply. Having the preliminary thickness, a period can be computed, including the soil mass effect for the partially buried dome. The durations of the flexural and uniform compression loads can be found in the same manner as for arches. In computing the pressure p_{im} for the flexural mode, refer to Chapter 3 for the appropriate reflection factor. Having the peak pressures and the duration-to-period ratios for each mode, the corresponding p_m/q values may be found as described in Sect. 9.5 for an arch. Substituting for the q values the resistances given in Sects. 8.8.4 and 8.8.5, the required thicknesses can be found for each mode separately. Since both of these modes result predominately in membrane or axial forces, the total required thickness is the sum of the flexural mode and compression thicknesses.

For the compression mode a uniform compression exists throughout the dome and there is no specific critical point. Eq. (8-63) may be used directly for the uniform compression mode q_c . For the flexural mode, the region near the foundation is critical; therefore Eq. (8-64) should be converted to an expression for q_f by setting $\psi = 0$ and the normal forces, T_ψ and T_θ , to their axial force capacities, i.e., for reinforced concrete,

$$T_\psi = (0.85 f'_{dc} + 0.009 \phi_t f_{dy})D$$

When P_1 is taken equal to $(q_f/\sin \beta)$ and the resulting expressions are equated to the axial force capacities as defined above, the desired relation for q_f is derived. Since the only significance of the thickness upon the period computations occurs in the soil mass effect, even if there is some variation

between the preliminary thickness and the final thickness, it will generally not be necessary to revise this section.

Finally, the resulting dome should be checked against buckling by Eq. (8-65) or its increased value for the partially buried case, and the effects of foundation restraints should be evaluated as discussed in Sect. 8.8.5.

As stated previously, the methods of Appendix B may, if appropriate, be used to evaluate more carefully the resistances required in each of the modes.

9.7 VERTICAL SHAFTS AND SILOS

The circumferential behavior of the silo under the various loadings discussed in Chapter 5 is predictable within acceptable tolerances by considering the behavior of a ring of the same geometry as the silo cross section. The resistance capacities and periods of vibration of the silo are therefore the same as those discussed in Sect. 8.7 for arches.

Below a depth of one diameter the required cross sectional properties of the silo are governed by the hoop forces from the sum of the dead load and uniform compression load discussed in Chapter 5. The preliminary design steps to follow are therefore the same as those for arches. The dynamic character of the uniform compression is taken into account by Fig. 9-1 with the ductility factor, μ , and the ratio of the duration to period having been established. It is then possible to revise the design in the same manner as discussed in Sect. 9.4. Because of possible irregularities and variations in soil properties, some bending may be induced in both the circumferential and longitudinal directions. Therefore steel in the amount of at least

0.25 percent in each face in each direction should be used.

The region of the silo from the surface to a depth of one diameter is subjected to a flexural loading as discussed in Chapter 5 in addition to the uniform compression and dead loads. This additional loading produces predominately flexural stresses and is treated in the same manner as the flexural mode in the arch. The designer is again cautioned in using the interaction diagram not to rely upon the simultaneous existence of maximum compressive hoop forces and maximum flexural forces.

In addition to the bending developed by the pressure variation resulting from soil irregularities etc. discussed in the previous paragraph, the propagation of the pressure pulse down the side of the silo generates a longitudinal bending moment. Because of the restraining influence of the soil and the fact that the cracking associated with this moment does not significantly affect the structural integrity of the silo, it is generally considered sufficient if 0.25 to 0.50 percent longitudinal steel is placed in each face.

9.8 FOOTINGS

A discussion of some of the general aspects of the design of foundation elements is given in Sect. 11.5. As mentioned there, very little information is available in this area. Since some design value must be selected in spite of lack of information, it is suggested that the dynamic bearing pressures used for design be taken as follows:

For rock use the in-place crushing strength.

For granular soil use a bearing pressure which
if applied statically would produce a settlement

of one inch.

For cohesive soil use a bearing pressure of three-quarters of the failure load.

If detailed soil information is not available, the bearing pressure may be taken as the sum of twice the conventional allowable static value plus the peak free-field soil pressure existing at the foundation level.

Having selected the allowable bearing pressure the plan size of the footing may be chosen to carry a force equal to the maximum dynamic column load or arch thrust. The footing thickness and steel percentages may then be computed in accordance with the resistance capacities presented in Sect. 8.10.1 or by Figs. 9-33 through 9-36. Even though the dynamic material properties are included in determining the resistance capacity of the footing, it is suggested that the load be treated as static.

9.9 COLUMNS

The ultimate dynamic strengths of axially loaded reinforced concrete and steel columns may be determined by Figs. 9-37 and 9-38. The latter gives the strength of steel columns in terms of the flange width and weight per foot. As mentioned in Chapter 8 the dynamic strength of a column is taken to be the static strength with the significant stress parameters increased by set percentages. No period or p_m/q values are necessary. When the column supports a roof subjected to blast loading the column loading should be taken as twice the peak blast pressure times the tributary area or the maximum resistance of the supported elements, whichever is smaller.

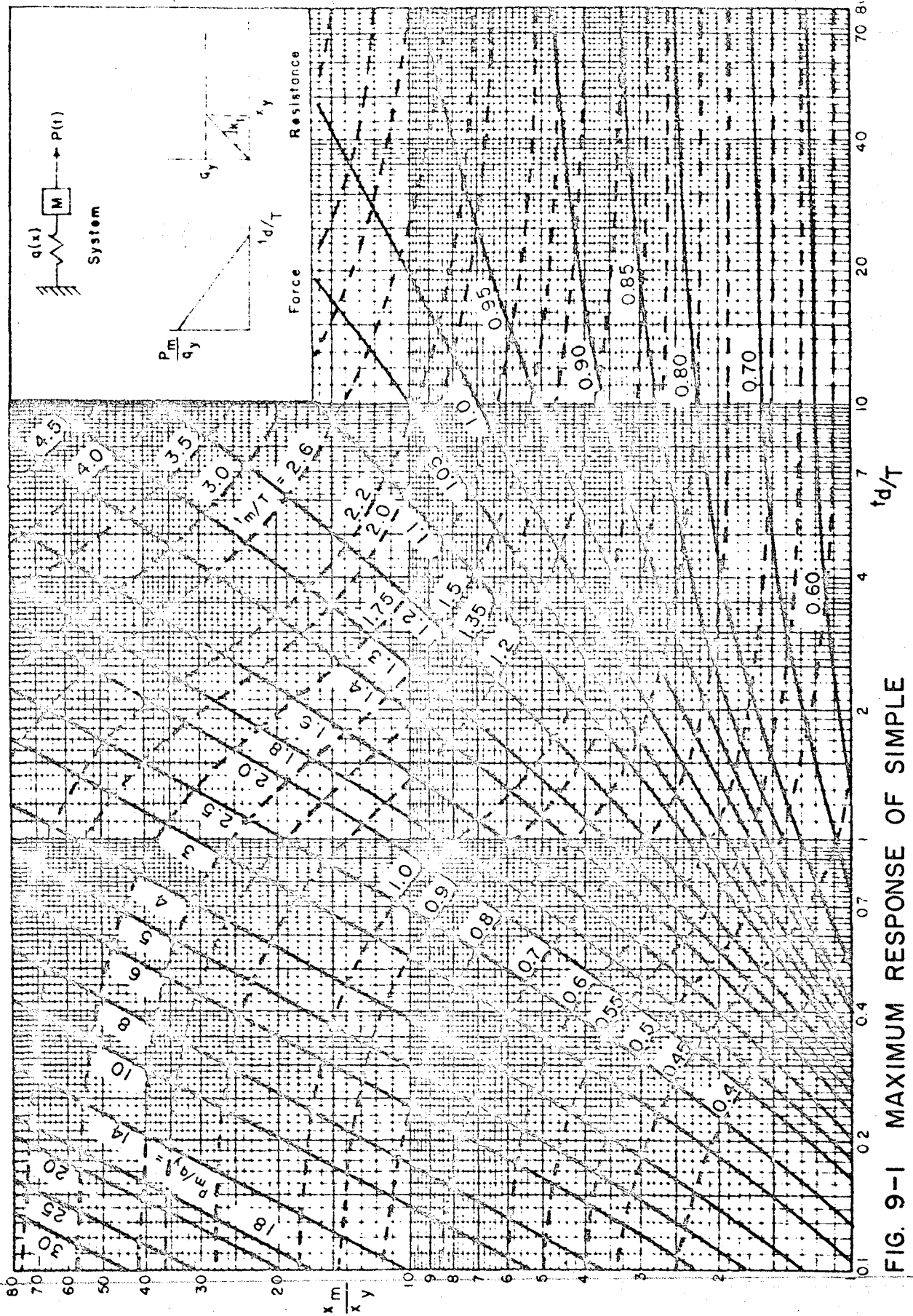


FIG. 9-1 MAXIMUM RESPONSE OF SIMPLE SPRING-MASS SYSTEM TO INITIALLY PEAKED TRIANGULAR FORCE PULSE.

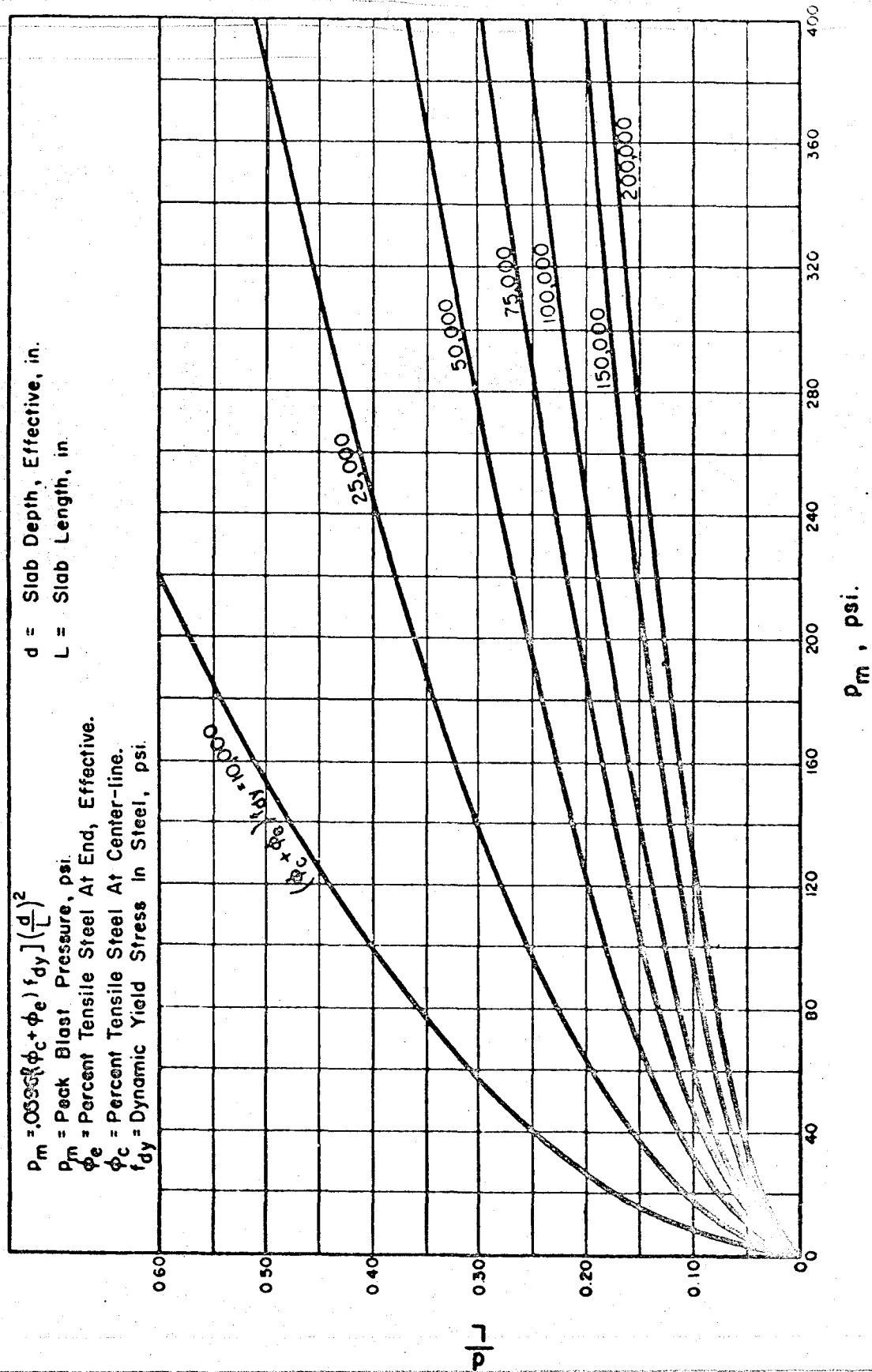


FIG. 9-2 FLEXURAL RESISTANCE OF SIMPLY SUPPORTED AND CONTINUOUS ONE-WAY SLABS ($\mu = 3.0$)

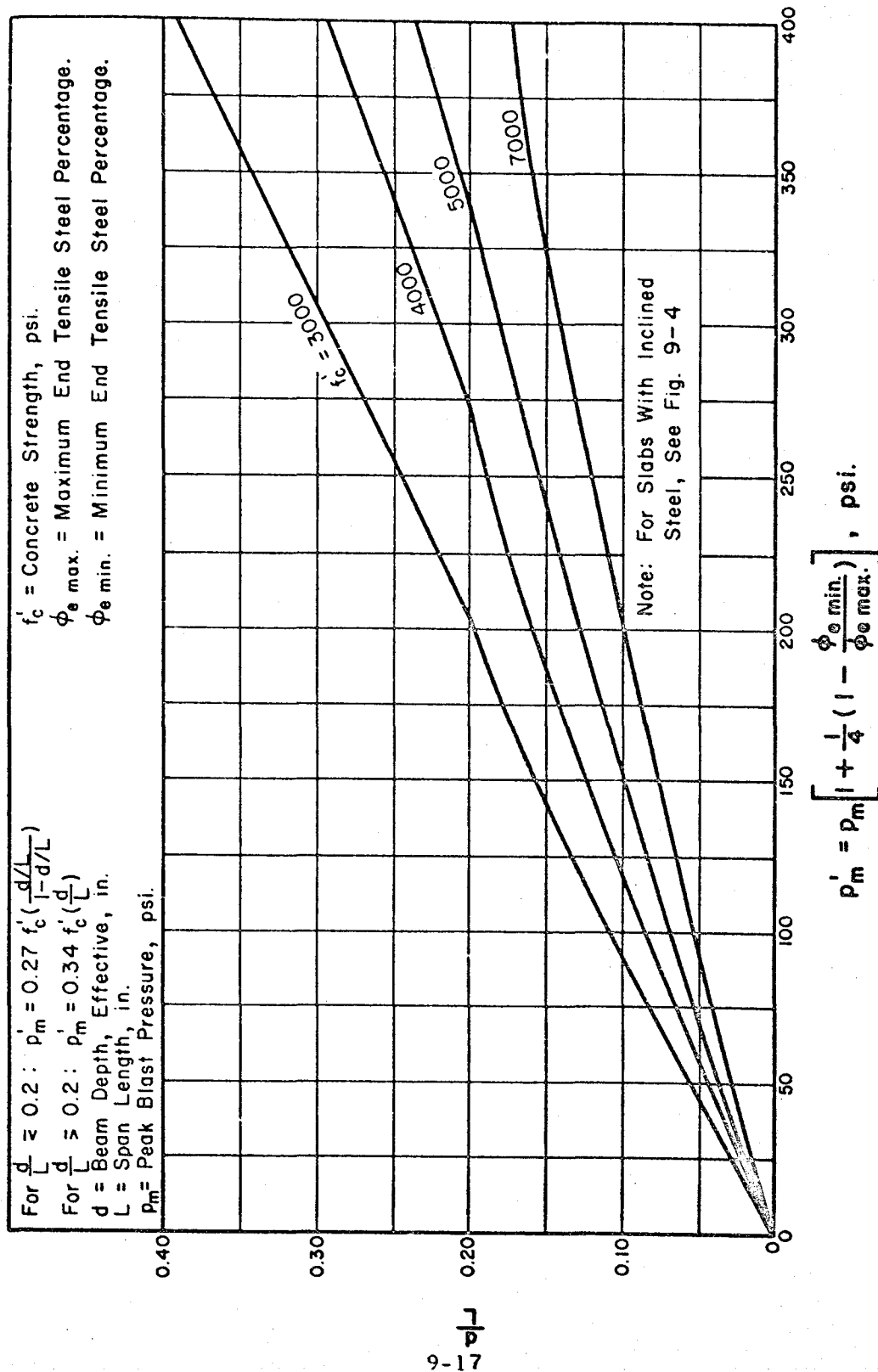


FIG. 9-3 RESISTANCE IN PURE SHEAR OF ONE-WAY SLABS WITHOUT INCLINED WEB STEEL ($\mu = 1.3$)

$$\lambda_s = \frac{1}{2} \left[1 + \frac{1}{10} \left(\phi_v' \frac{f_{dy}}{f_c'} \right) \right]$$

λ_s = Pure Shear Factor: Ratio Of Pure Shear Resistance Of Slab or Beam With Inclined Steel To That Of Same Slab or Beam Without Inclined Steel

f_{dy} = Dynamic Yield Stress In Steel, psi

f_c' = Concrete Strength, psi

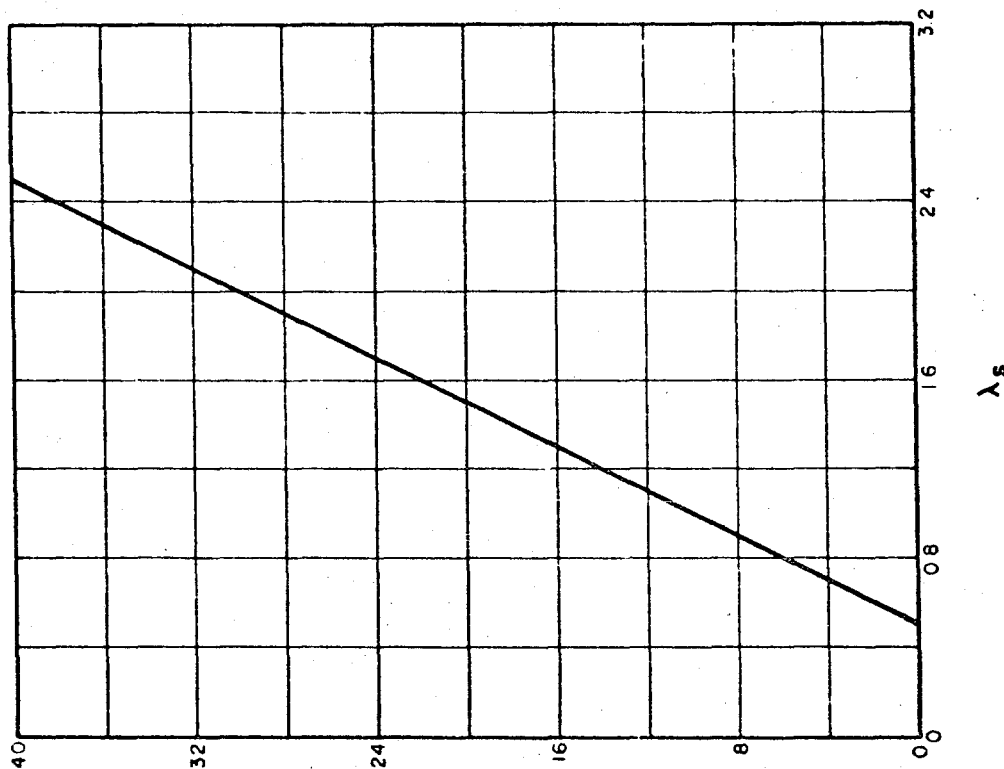
ϕ_v' = Percent Of Inclined Steel Intersecting a 45° Surface Through Beam or Slab At End Of Beam or Slab. Express As Percentage Of Concrete Area On 45° Surface.

NOTE:

(1) To Obtain Resistance In Pure Shear, Consult First Fig. 9-3 or 9-11.

Multiply Value Thus Obtained By λ_s If $\lambda_s > 1.0$

(2) If λ_s Is Less Than 1.0, The Inclined Steel Is Ineffective.



$$\frac{\phi_v' f_{dy}}{f_c'} = \lambda_s$$

FIG. 9-4 PURE SHEAR RESISTANCE — FACTOR FOR SLABS AND BEAMS WITH INCLINED STEEL AT ENDS

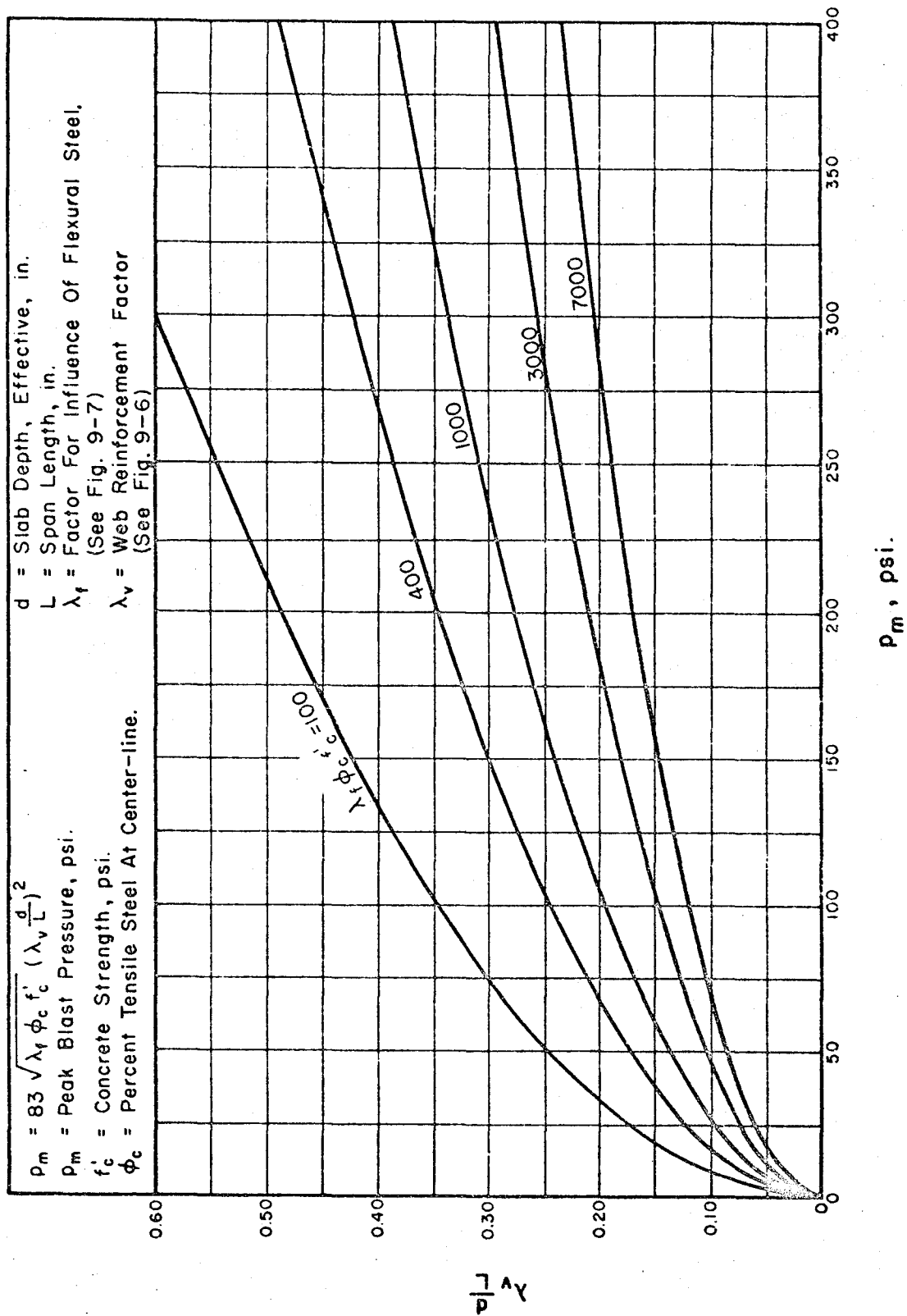


FIG. 9-5 RESISTANCE IN DIAGONAL TENSION OF ONE-WAY SLABS
($\mu = 3.0$)

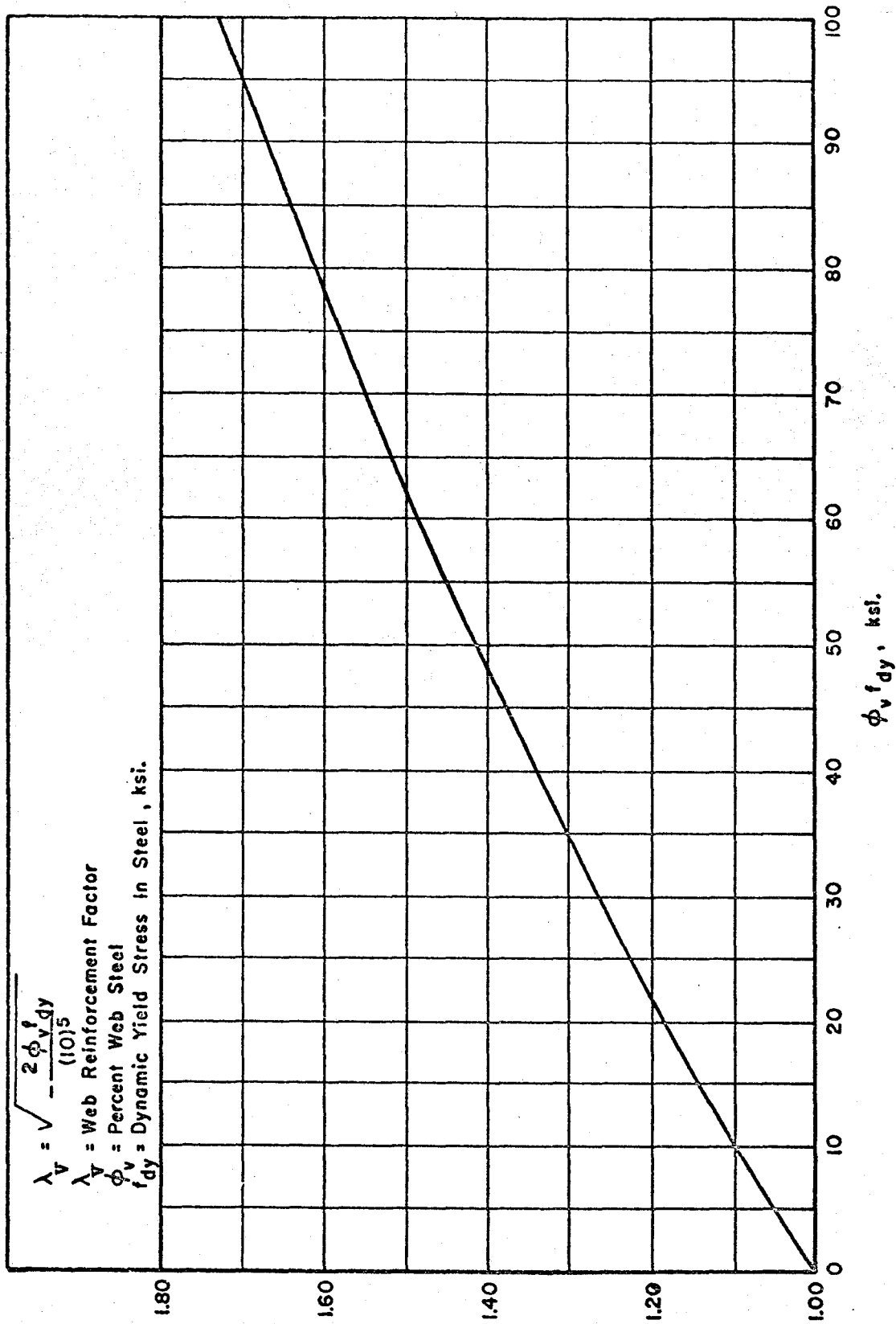


FIG. 9-6 WEB REINFORCEMENT FACTOR

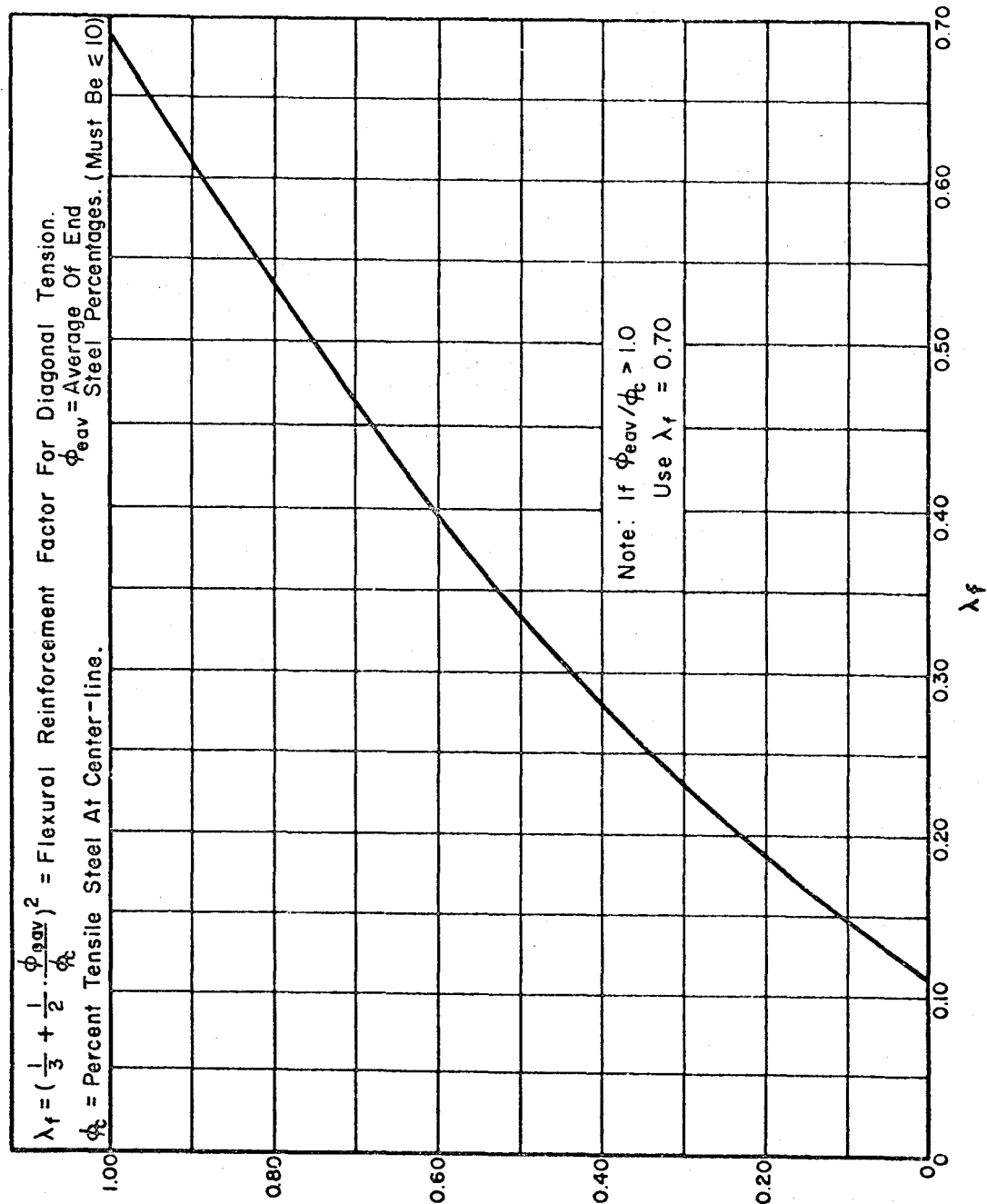


FIG. 9-7 RESISTANCE IN DIAGONAL TENSION FOR ONE-WAY SLABS AND BEAMS — FACTOR FOR INFLUENCE OF FLEXURAL STEEL.

ϕ_c
 ϕ_{avg}

$$\Omega = 1 + \alpha \left[\frac{1}{6-4\alpha} + \frac{3}{2} \left(\frac{\phi_{LC} + \phi_{LE}}{\phi_{SC} + \phi_{SE}} \right) \right]$$

Ω = Two-Way Slab Factor

α = Ratio Of Short Side To Long Side

ϕ_{LC} = Percent Tensile Steel In Long Direction at Center-line

ϕ_{LE} = Percent Tensile Steel, Long Direction, At End, Effective.

ϕ_{SC} = Percent Tensile Steel In Short Direction, At Center-line.

ϕ_{SE} = Percent Tensile Steel In Short Direction, At End, Effective.

NOTE:

Flexural Strength Of Two-Way Slabs Can Be Determined As Follows.

- (1) Treat As One-Way Slab Spanning Short Direction
- (2) Determine Corresponding Strength From Figure 9-2.
- (3) Multiply Value From (2) above By Ω .

Restrict Relative Steel Percentages In Both Directions To Insure Development Of Yield Lines.

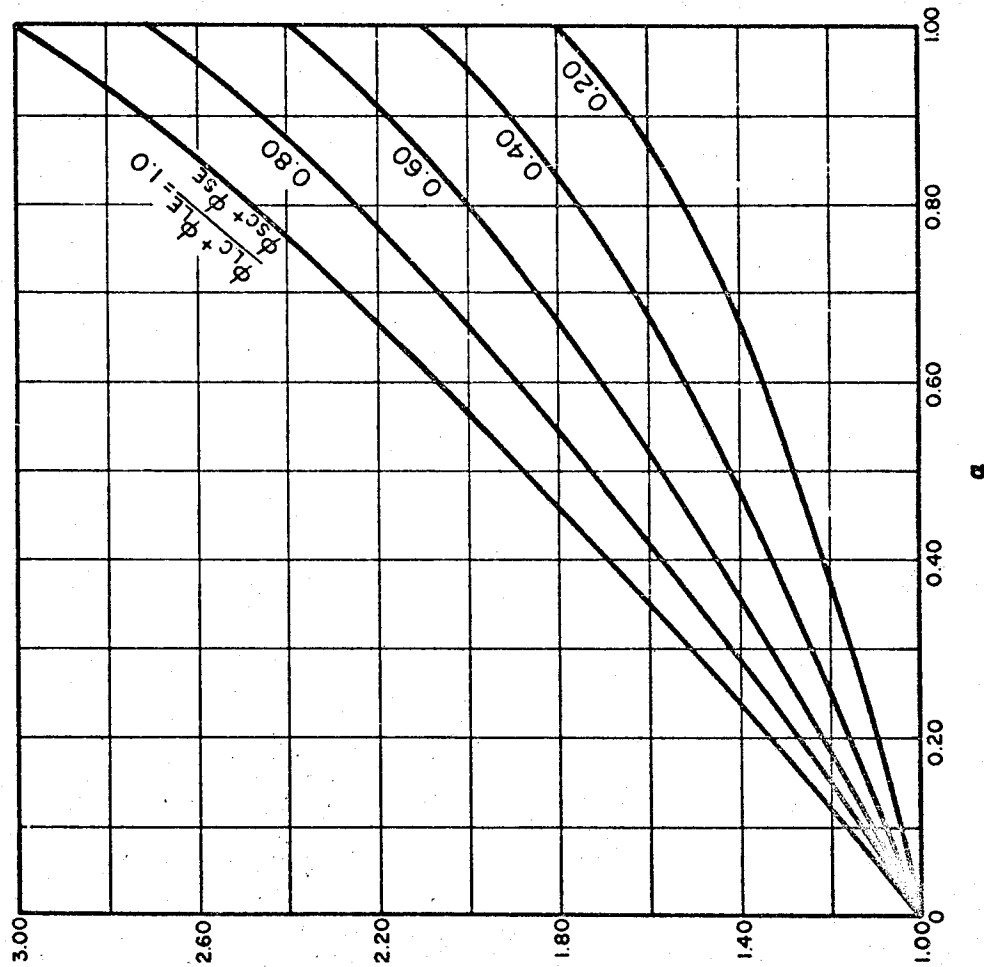


FIG. 9-8 FLEXURAL RESISTANCE — TWO-WAY SLAB FACTOR

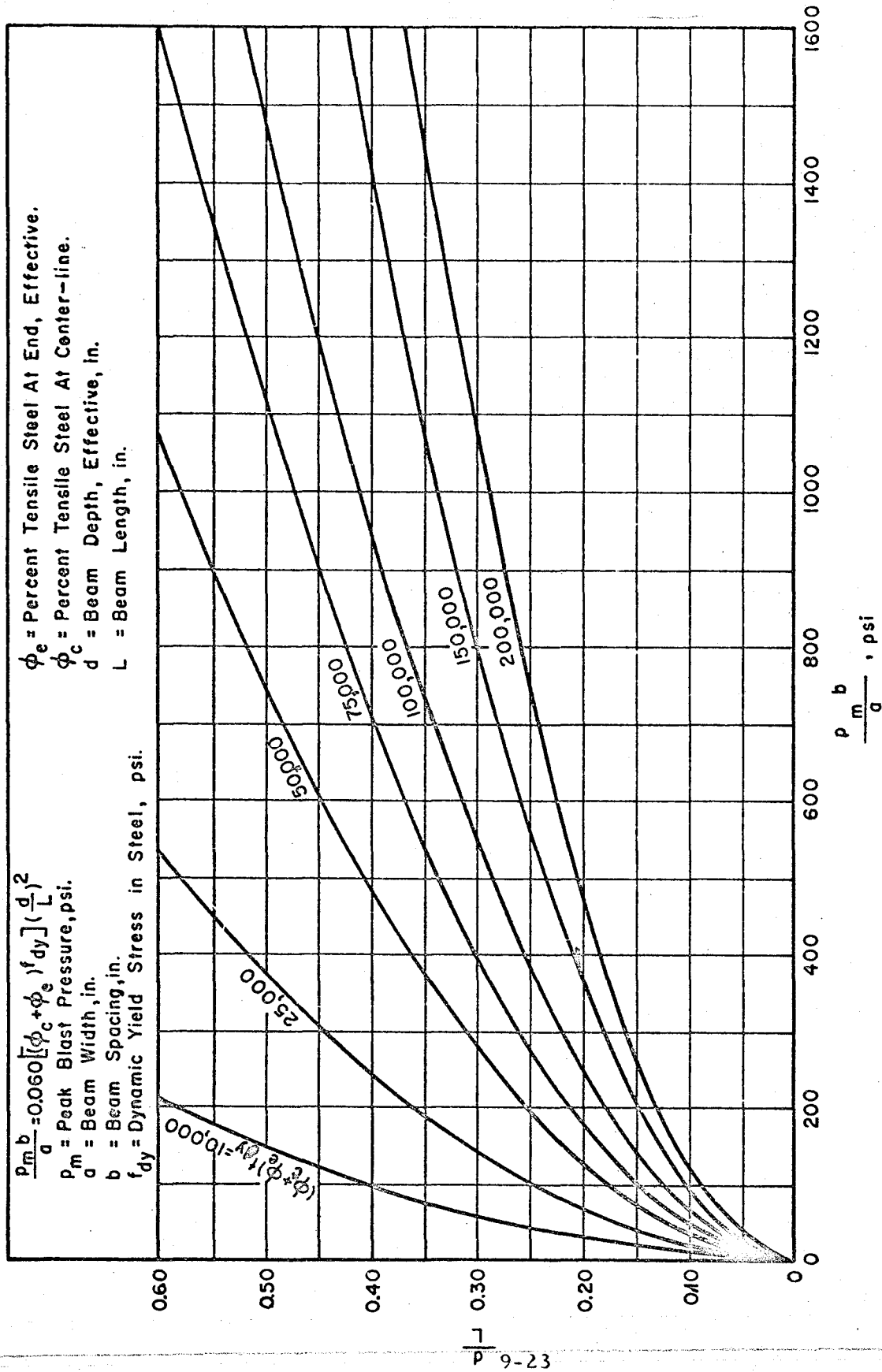


FIG. 9-9 FLEXURAL RESISTANCE OF SIMPLY SUPPORTED OR CONTINUOUS
 REINFORCED CONCRETE BEAMS SUPPORTING ONE-WAY SLABS
 ($\mu = 3.0$)

$$\gamma = \frac{1}{1 - \frac{1}{3} \alpha^2 (1 - \frac{a}{b})}$$

γ = Ratio Of Flexural Resistance Of Beam Supporting Two-Way Slab To That Of The Same Beam Supporting A One-Way Slab
 α = Ratio Of Short Side To Long Side Of Two-Way Slab.
 a = Width Of Beam.
 b = Spacing Center To Center Of Beams.

NOTES:

- (A) To Obtain Resistance Of Beams Under Square Two-Way Slabs And Of Long Beam Under Non-Square Slabs:
 (1) Treat As Beam Under A One-Way Slab. Get Resistance From Figs. 9-9 or 9-14.
 (2) Multiply Value From (1) Above By γ .
- (B) To Obtain Resistance Of Short Beams Under Non-Square Two-Way Slab:
 (1) Treat As Beam Under A Square Two-Way Slab Of Span Equal To That Of Short Beam Being Considered.

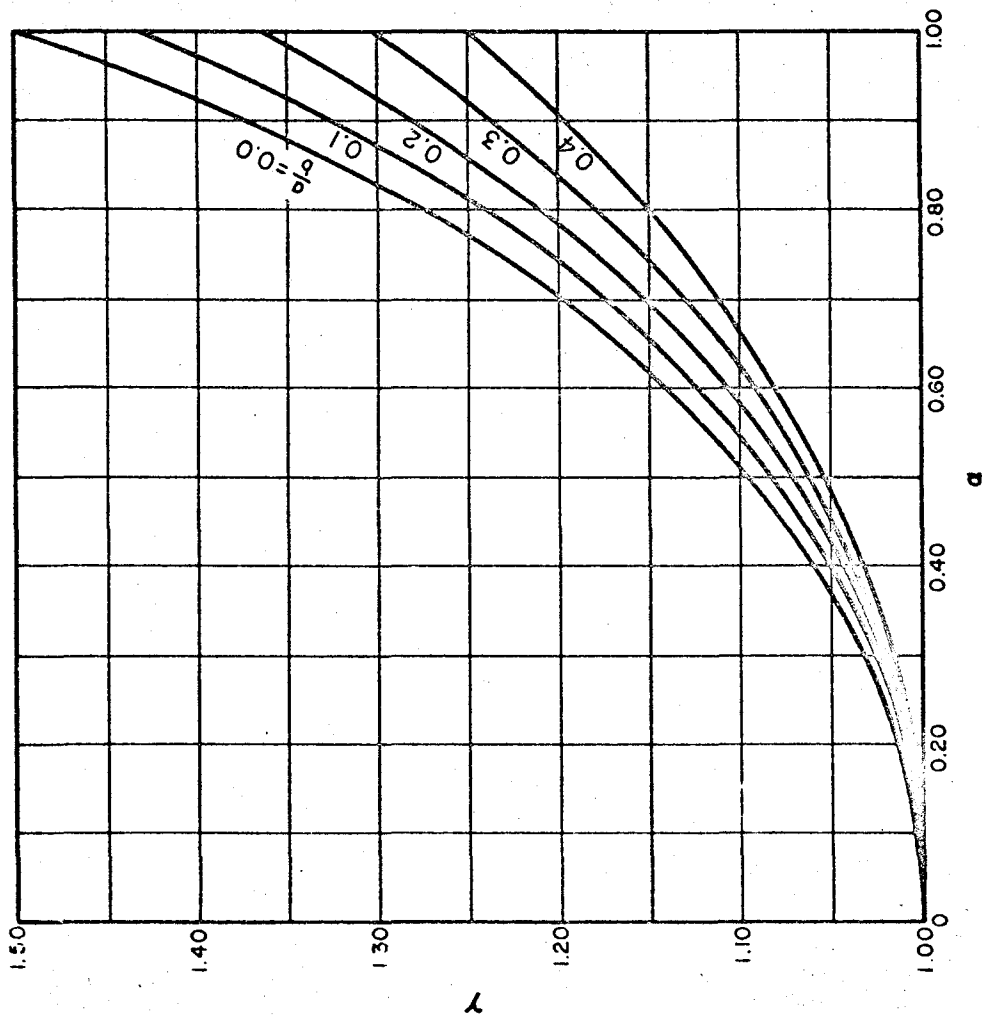


FIG. 9-10 FLEXURAL RESISTANCE — FACTOR FOR BEAMS SUPPORTING NON-SQUARE TWO-WAY SLABS.

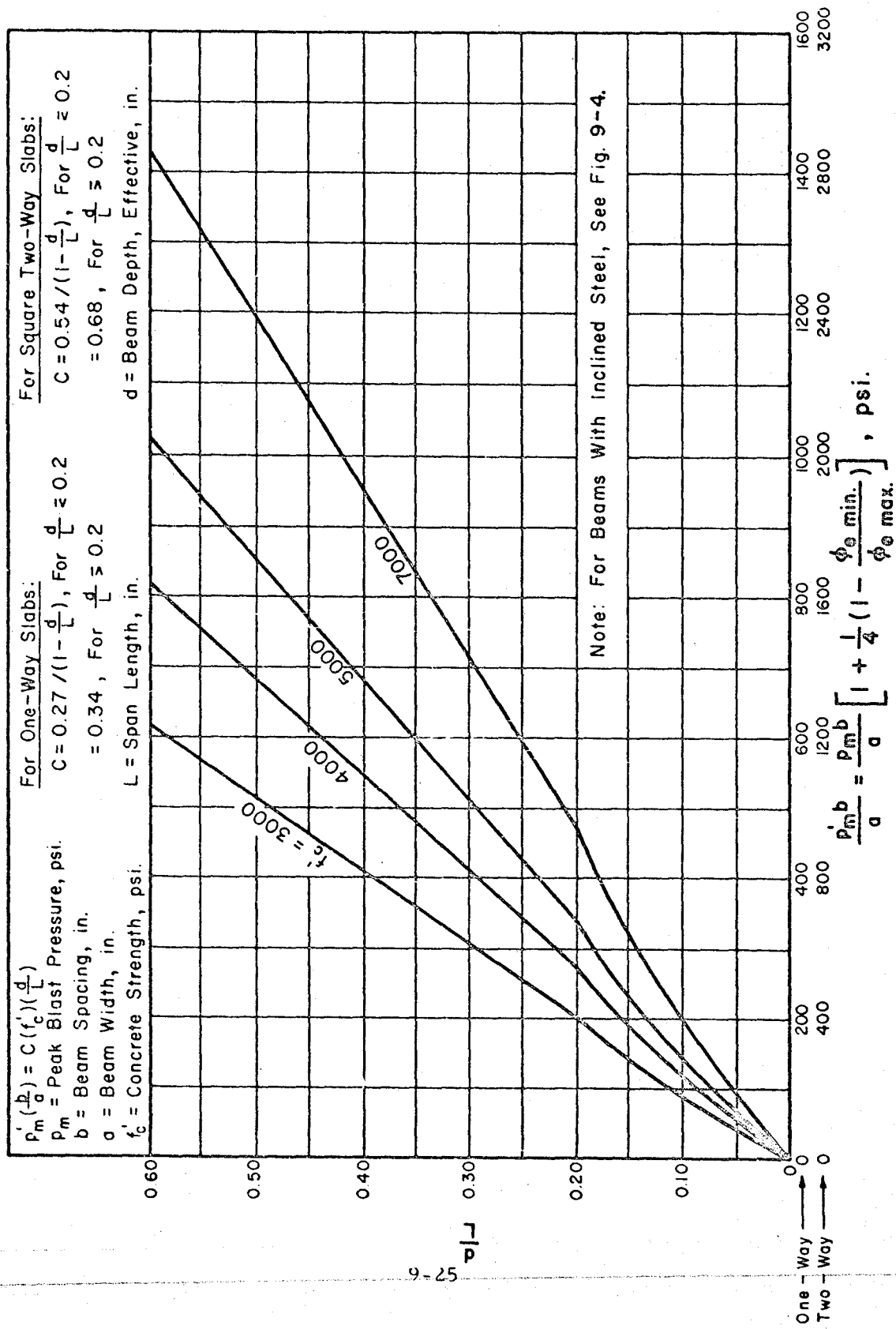


FIG. 9-11 RESISTANCE IN PURE SHEAR OF REINFORCED CONCRETE BEAMS SUPPORTING ONE-WAY AND SQUARE TWO-WAY SLABS ($\mu = 1.3$).

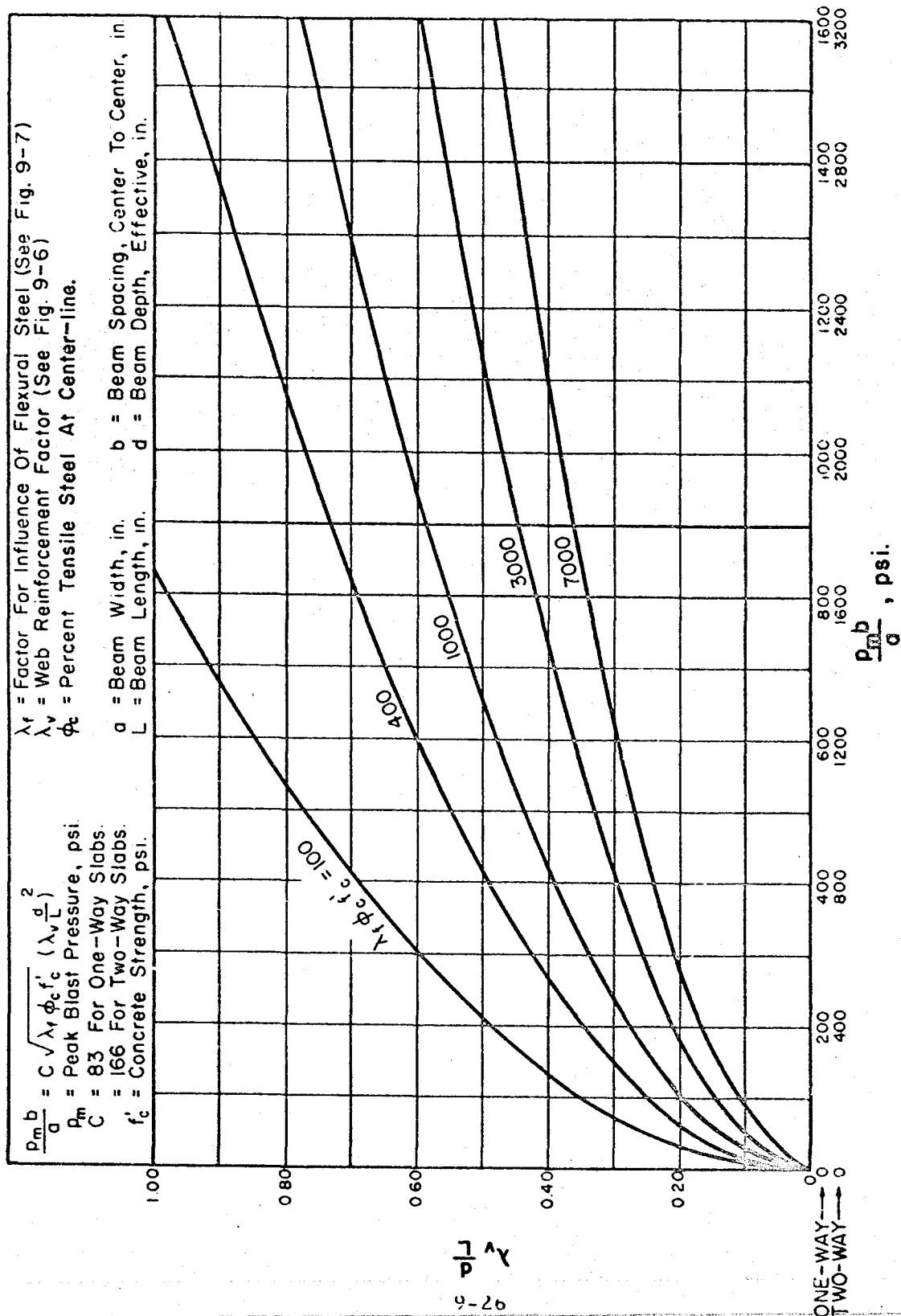


FIG. 9-12 RESISTANCE IN DIAGONAL TENSION OF REINFORCED CONCRETE BEAMS SUPPORTING ONE-WAY AND SQUARE TWO-WAY SLABS ($\mu=3.0$)

$$\eta = \frac{2}{2-a}$$

η = Correction Factor For Resistance in Shear Or Diagonal Tension Of Long Beam Under Two-Way Slab

a = Ratio Of Short Side To Long Side Of Two-Way Slab

NOTE

To Obtain Resistance in Shear And/Or Diagonal Tension For Long Beam Under Two-Way Slab

- (1) Treat As Beam Under One-Way Slab. Get Resistance From Figures 9-11, 9-12, And 9-15.
- (2) Multiply Value From (1) Above By η

Resistance Of Short Span Beam is Same As For Beam Under a Square Slab Of That Span (See Figures 9-11, 9-12, And 9-15).

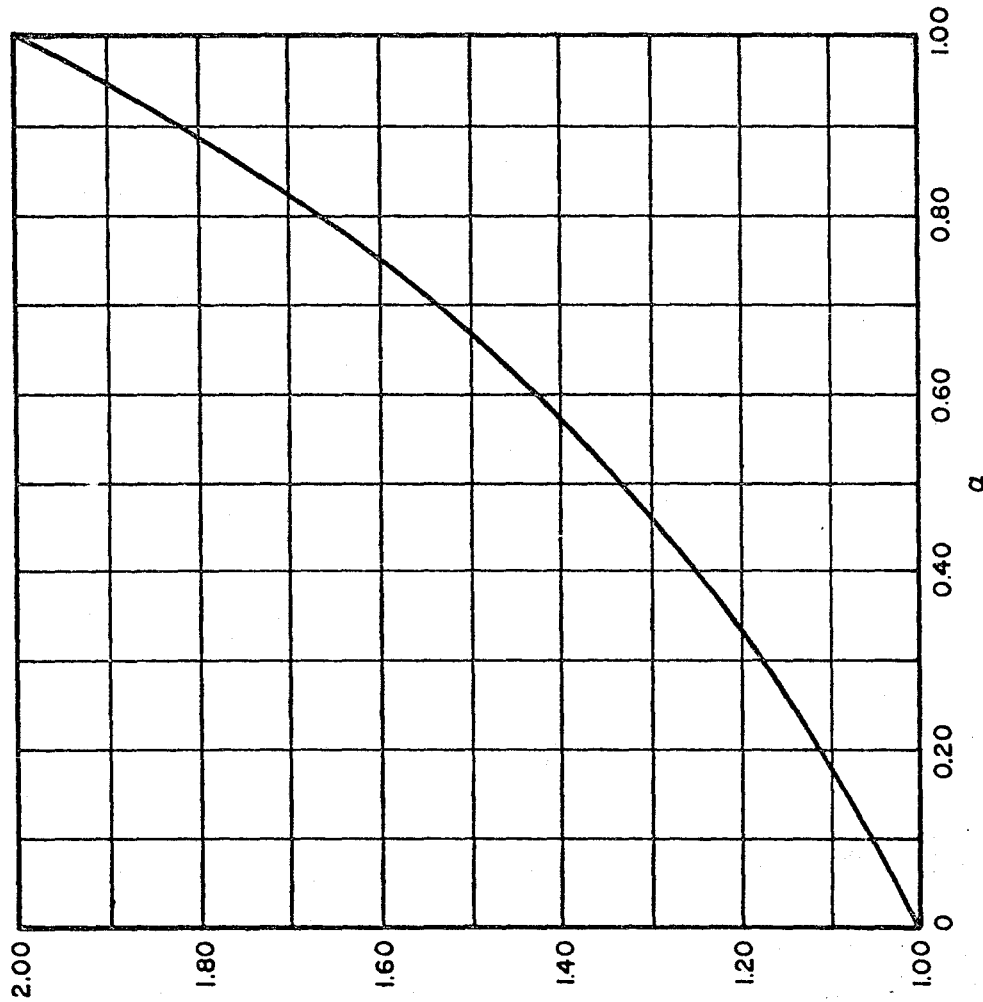


FIG 9-13 RESISTANCE IN SHEAR AND DIAGONAL TENSION — FACTOR FOR BEAMS SUPPORTING NON-SQUARE TWO-WAY SLABS

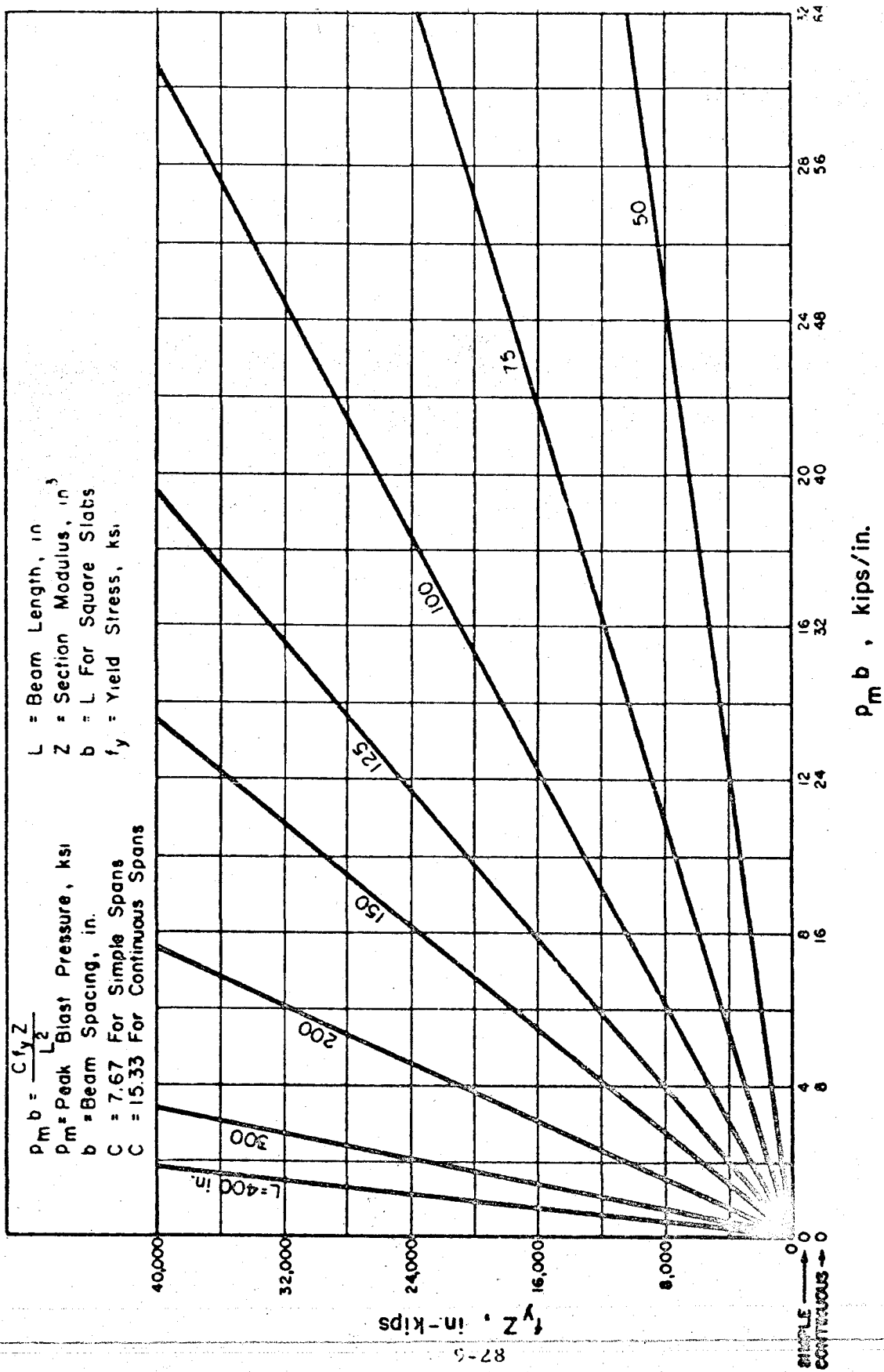


FIG. 9-14 FLEXURAL RESISTANCE OF STEEL BEAMS SUPPORTING ONE-WAY SLABS ($\mu = 3.0$)

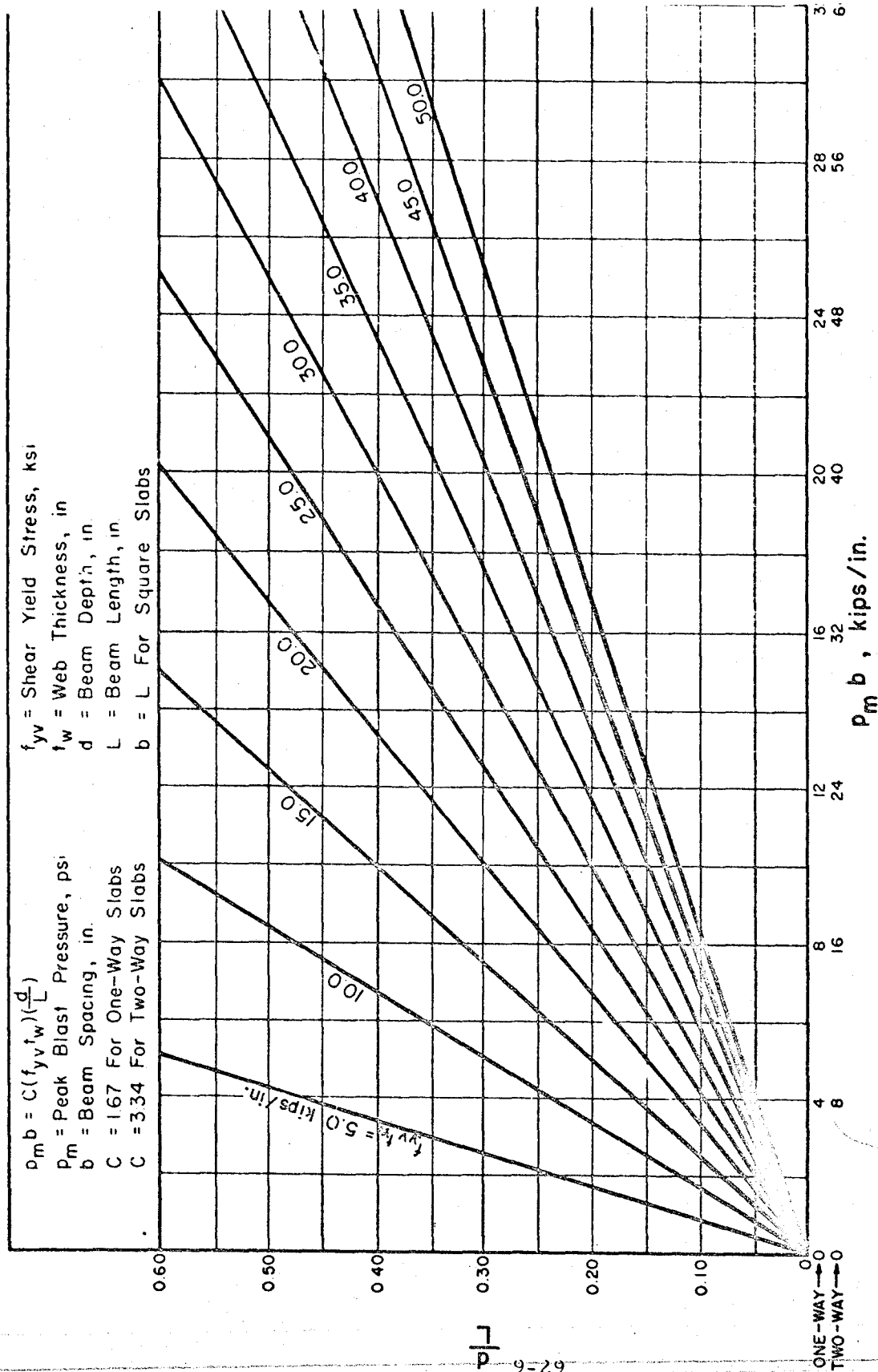


FIG. 9-15 SHEARING RESISTANCE OF SIMPLE AND CONTINUOUS STEEL BEAMS SUPPORTING ONE-WAY AND SQUARE TWO-WAY SLABS ($\mu = 3.0$)

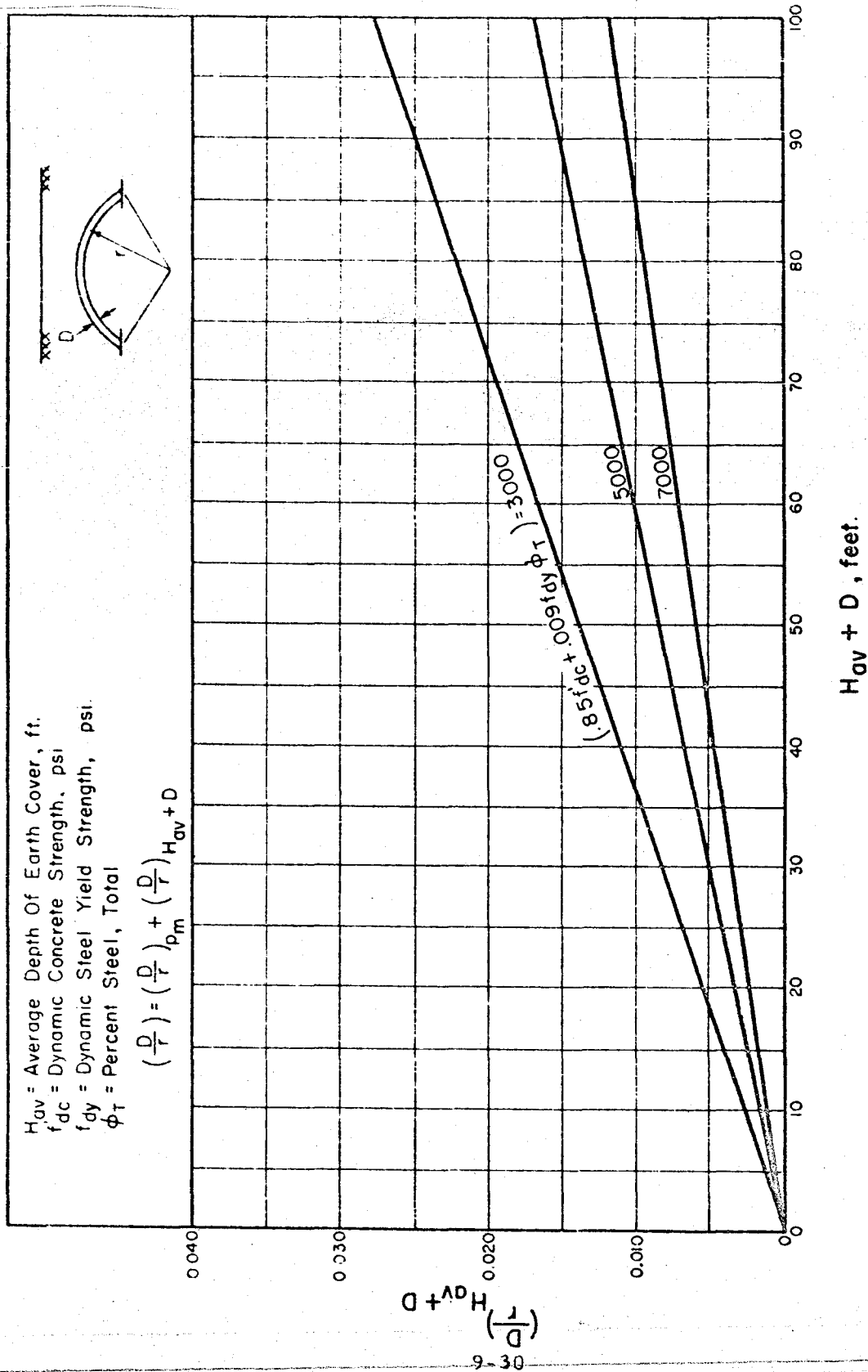


FIG. 9-16 REQUIRED THICKNESS OF FULLY-BURIED REINFORCED CONCRETE ARCHES FOR DEAD LOAD

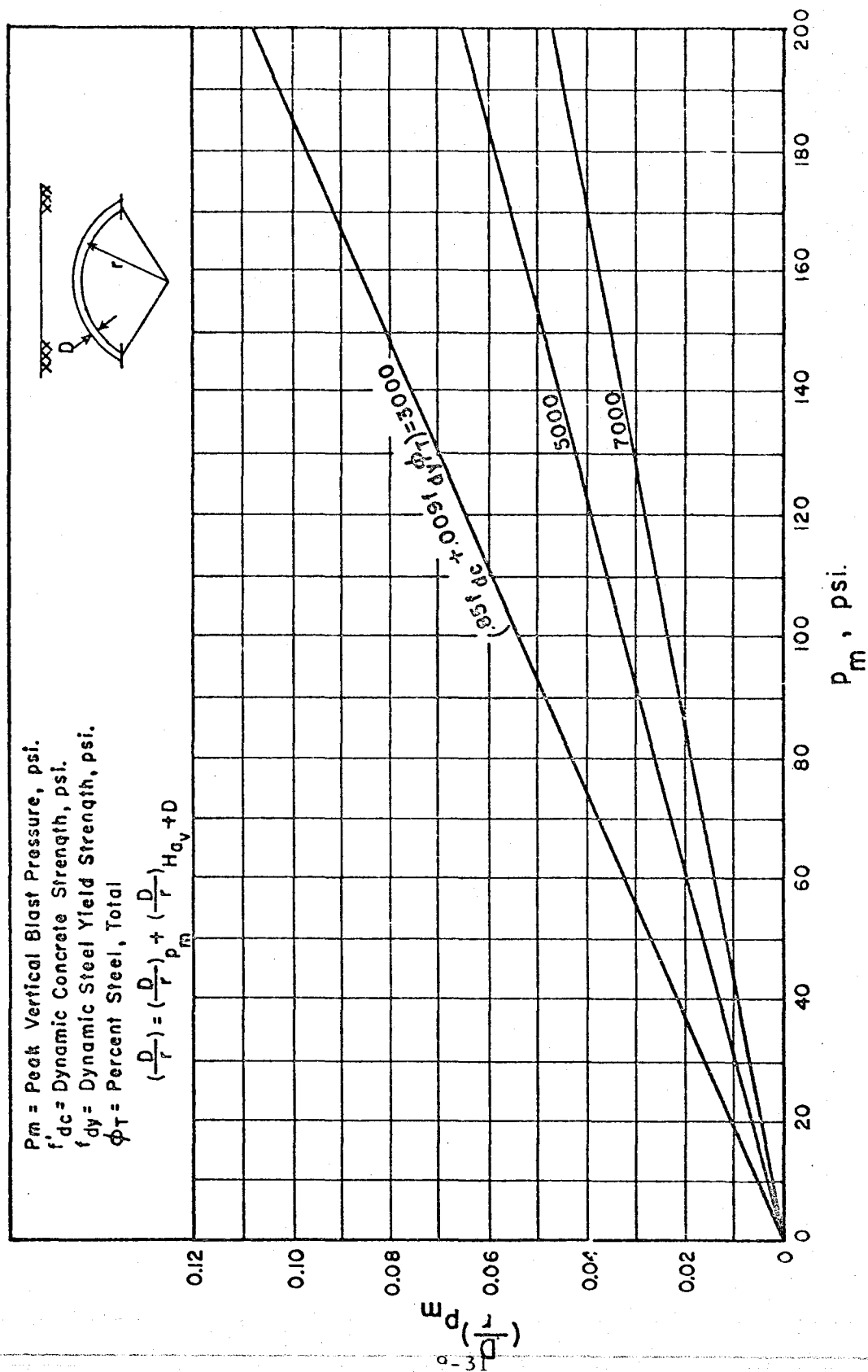


FIG. 9-17 REQUIRED THICKNESS OF FULLY-BURIED REINFORCED CONCRETE ARCHES FOR BLAST LOAD ($\mu = 1.3$)

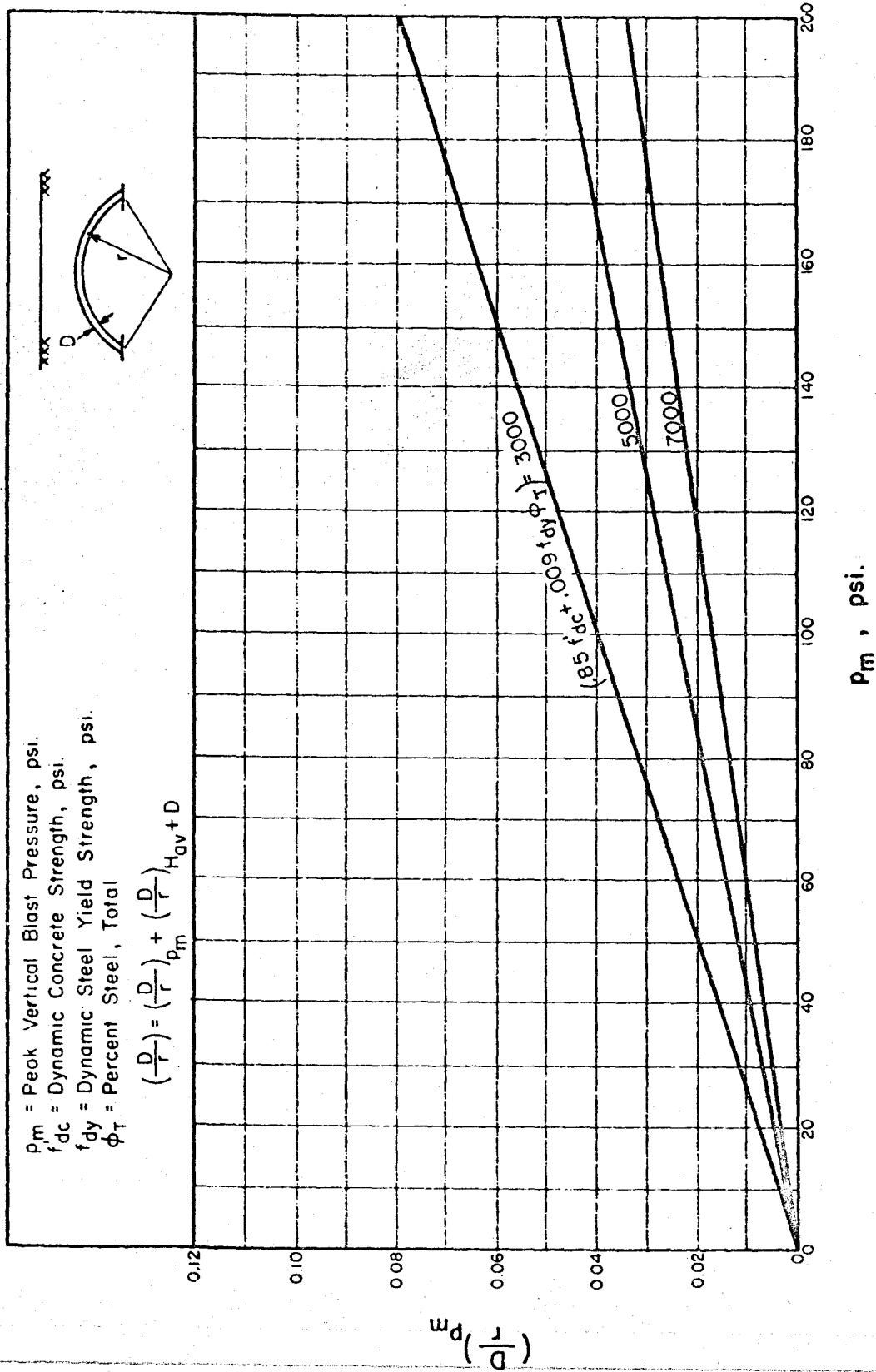


FIG. 9-18 REQUIRED THICKNESS OF FULLY-BURIED REINFORCED CONCRETE ARCHES FOR BLAST LOAD ($\mu = 3.0$)

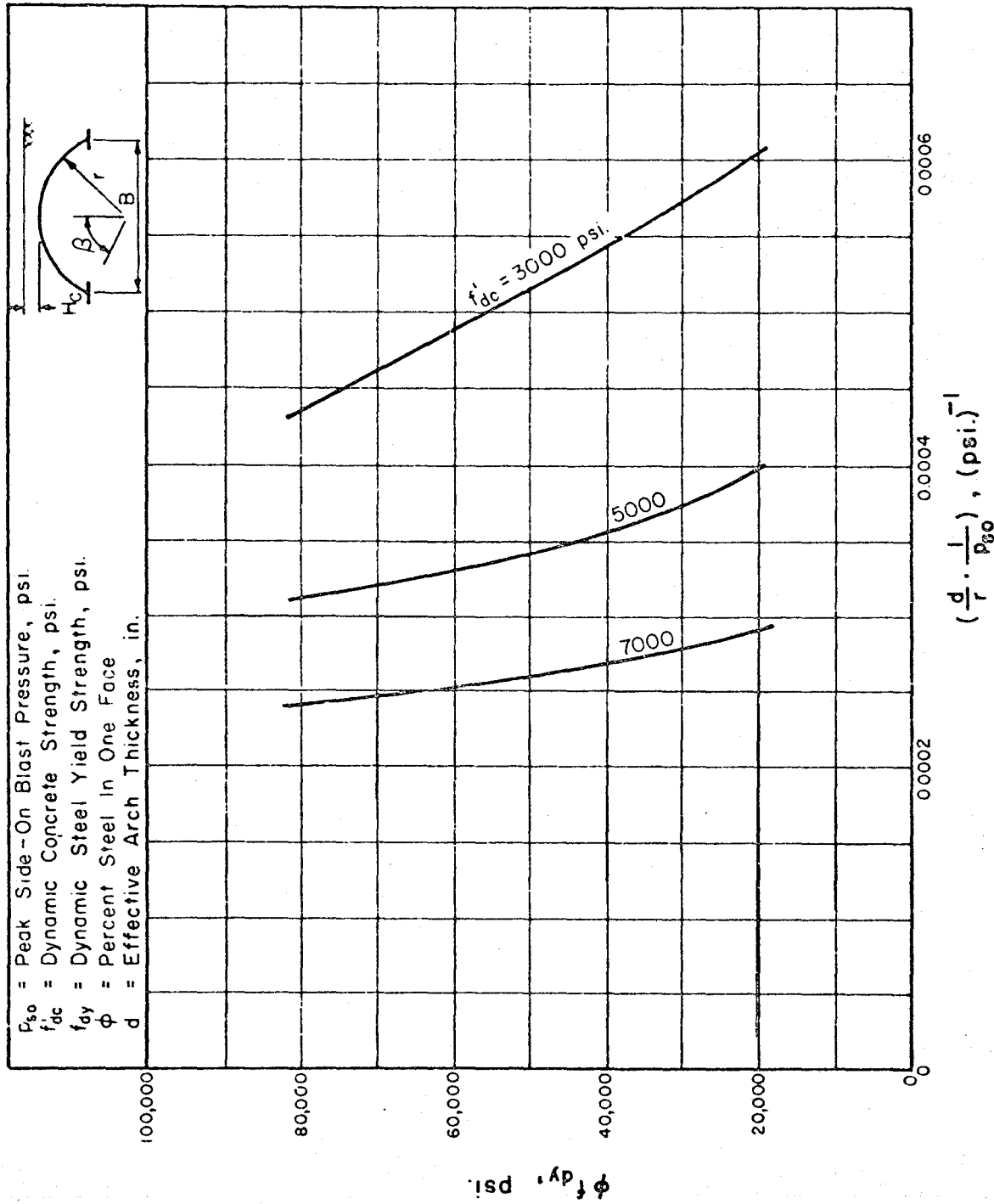


FIG. 9-19 REQUIRED THICKNESS OF PARTIALLY-BURIED ($H_c=0 \rightarrow 0.062B$) REINFORCED CONCRETE ARCHES ($\mu=1.3$)

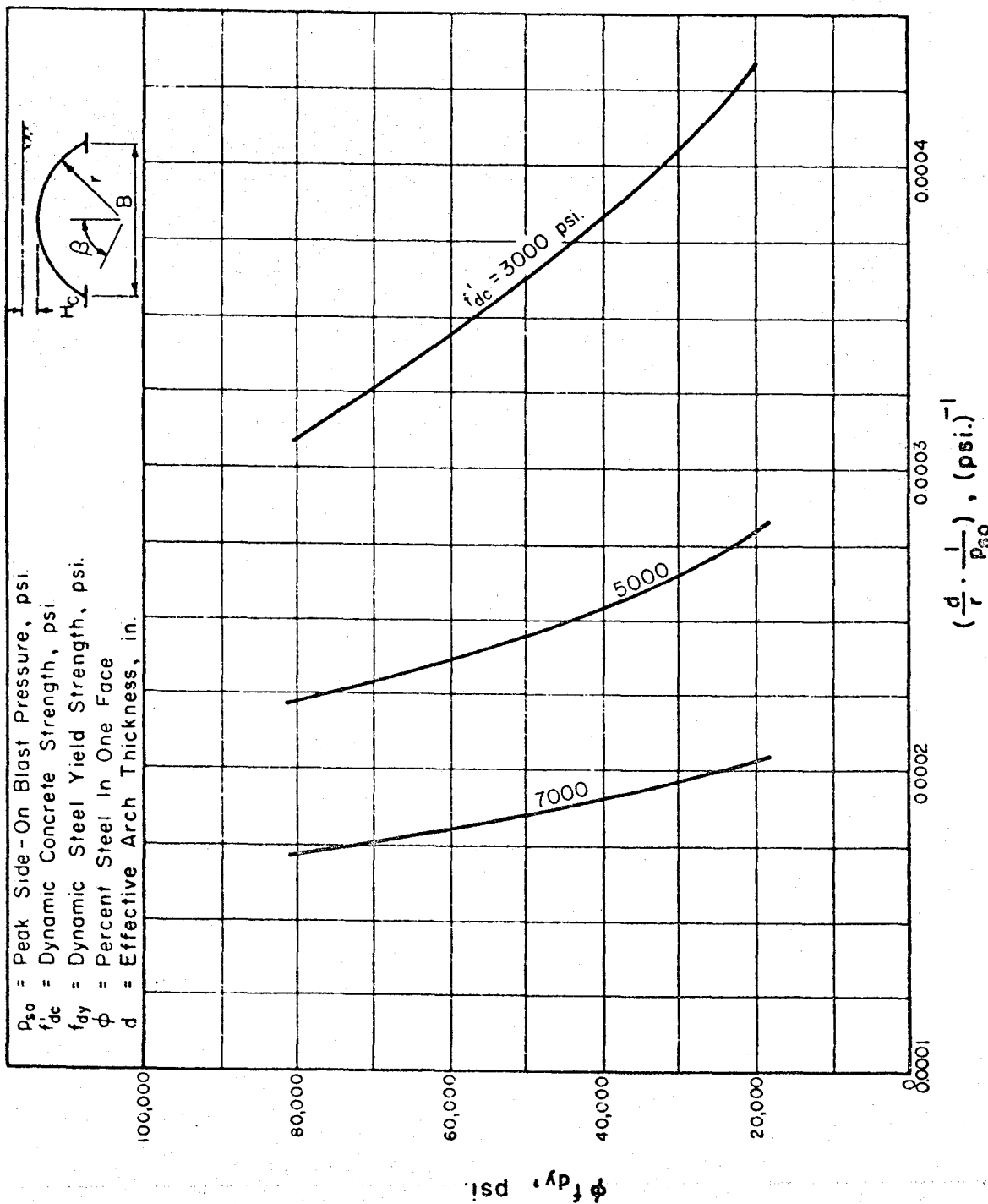


FIG. 9-20 REQUIRED THICKNESS OF PARTIALLY-BURIED ($H_c=0 \rightarrow 0.062B$) REINFORCED CONCRETE ARCHES ($\mu=3.0$)

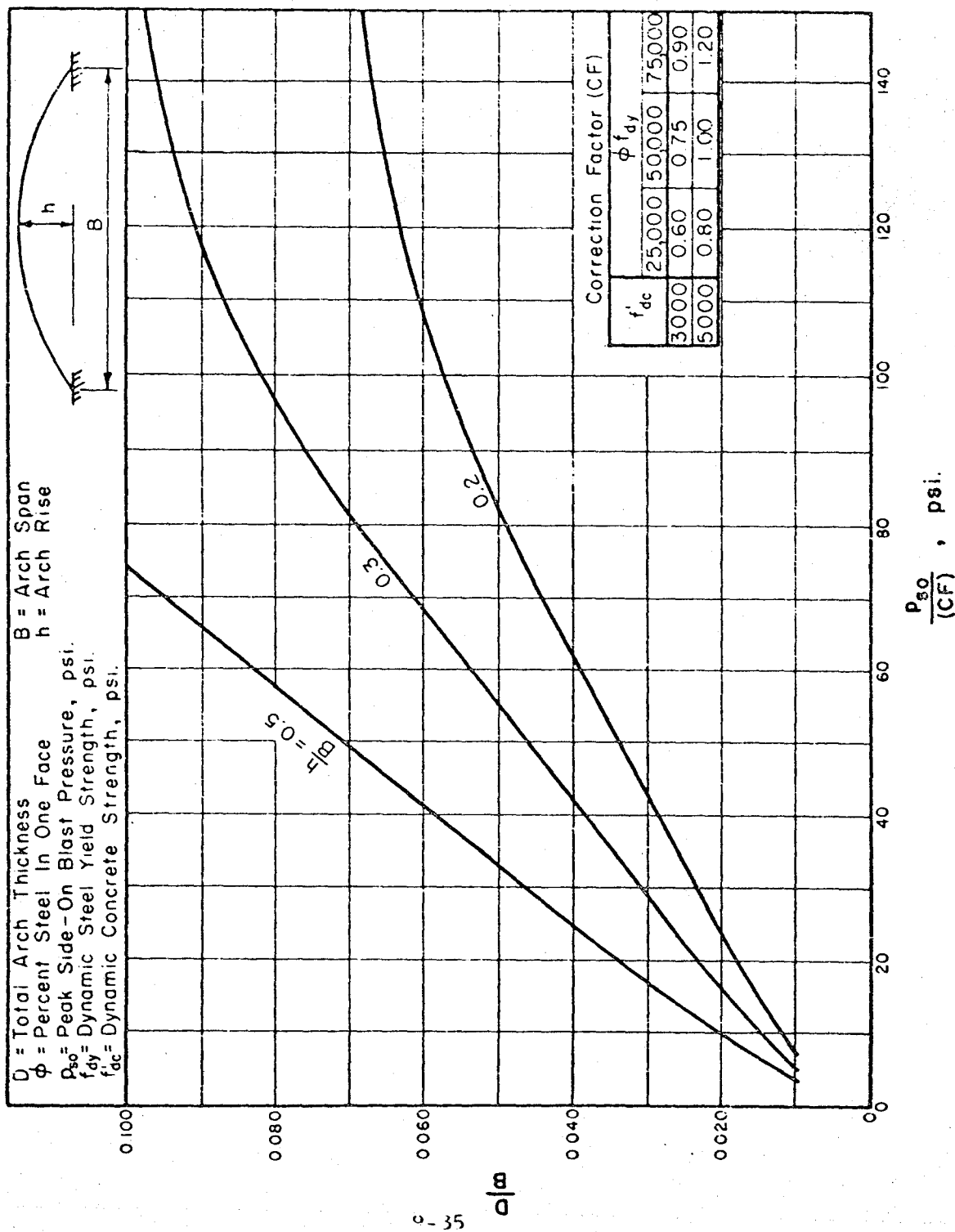


FIG. 9-21 REQUIRED THICKNESS OF ABOVEGROUND REINFORCED CONCRETE ARCHES ($\mu = 1.3$)

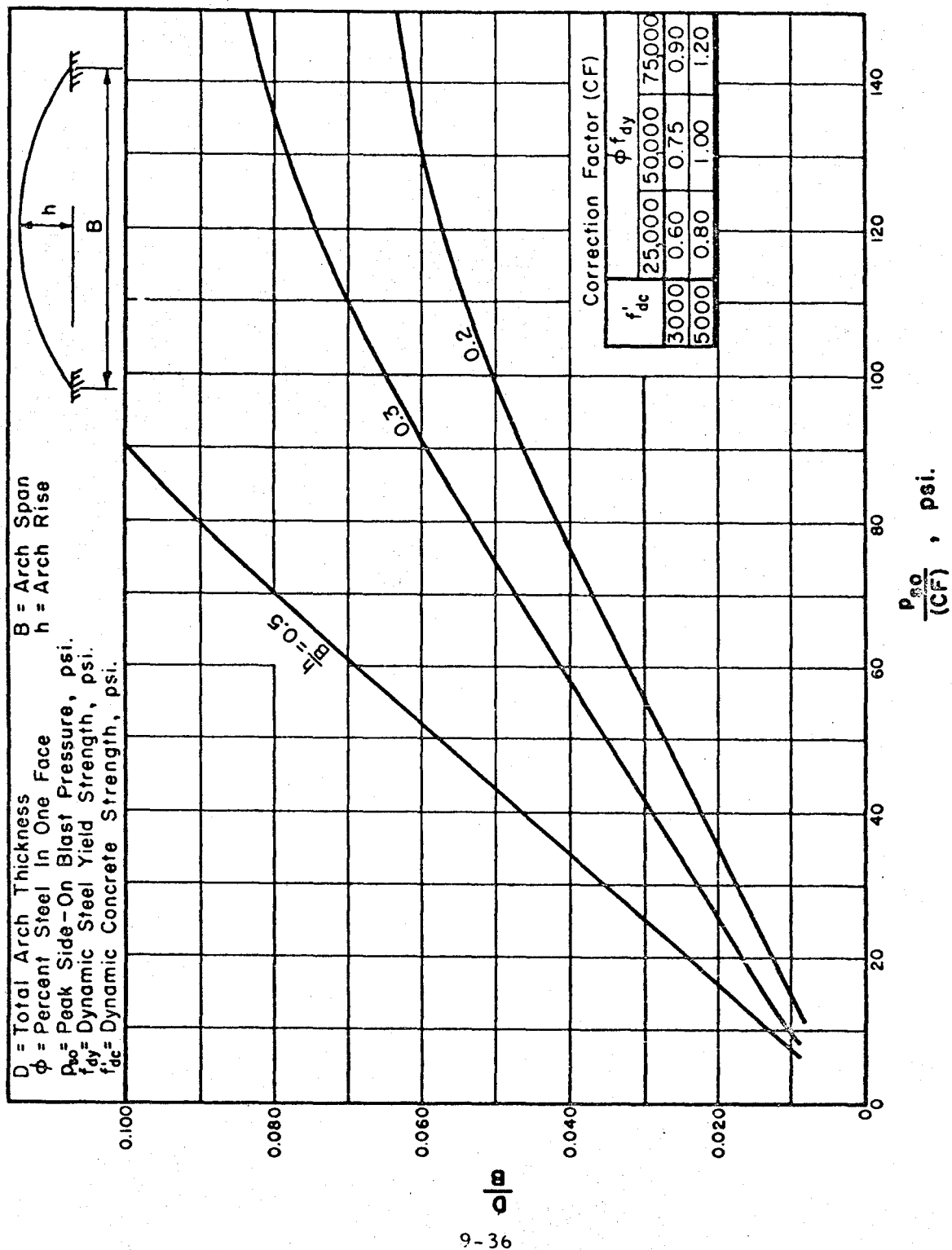


FIG. 9-22 REQUIRED THICKNESS OF ABOVEGROUND REINFORCED
 CONCRETE ARCHES ($\mu = 3.0$)

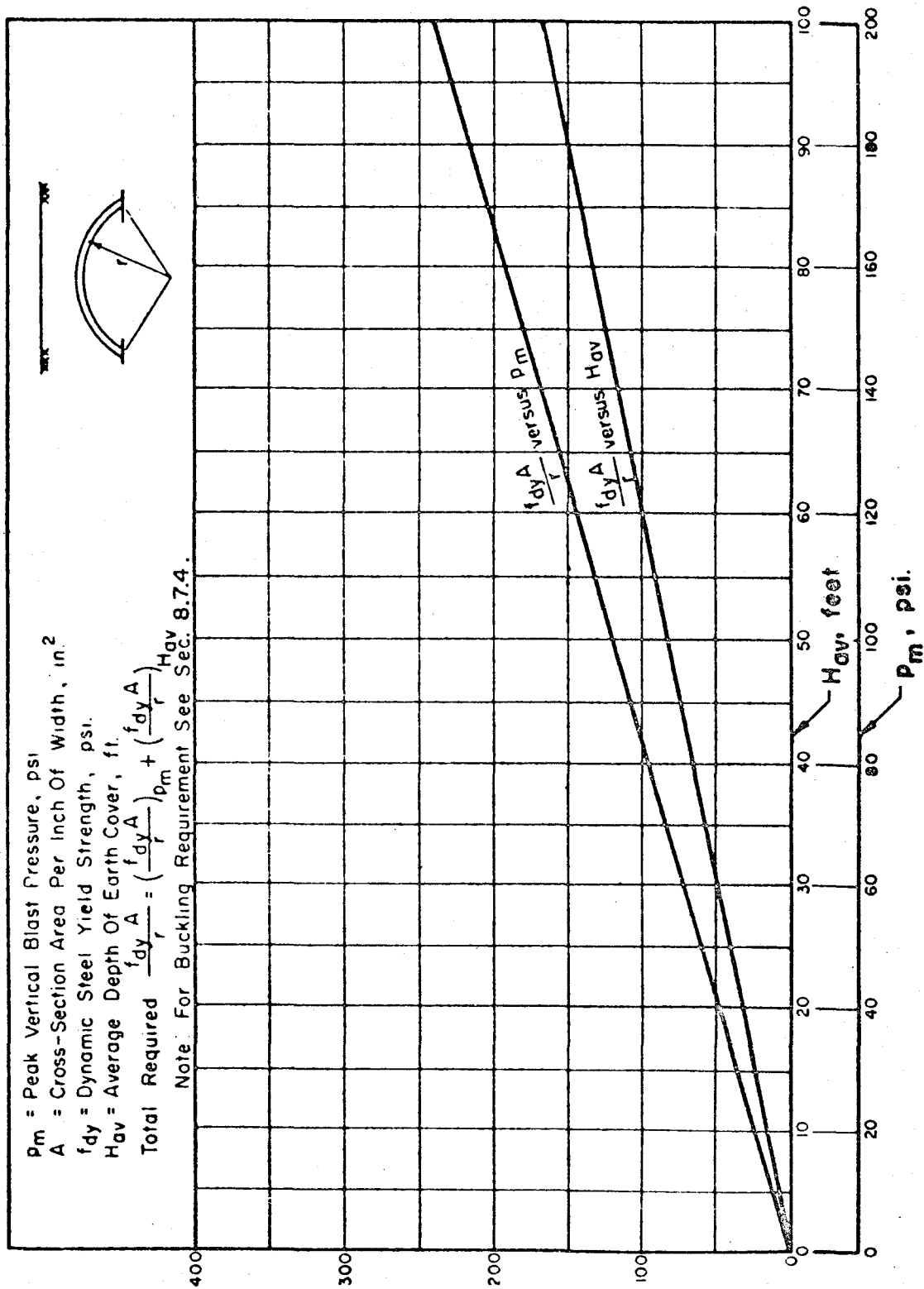


FIG. 9-23 REQUIRED AREA OF FULLY-BURIED STEEL ARCHES ($\mu = 3.0$)

$\frac{f_{dy} A}{r}$, lbs./in.

p_m = Peak Vertical Blast Pressure, psi
 A = Cross-Section Area Per Inch Of Width, in.²
 f_{dy} = Dynamic Steel Yield Strength, psi.
 H_{av} = Average Depth Of Earth Cover, ft.

$$\text{Total Required } \frac{f_{dy} A}{r} = \left(\frac{f_{dy} A}{r} \right) p_m + \left(\frac{f_{dy} A}{r} \right) H_{av}$$

Note: For Buckling Requirement See Sec. 8.7.4

100'



$\frac{f_{dy} A}{r}$, lbs./in.

9-38

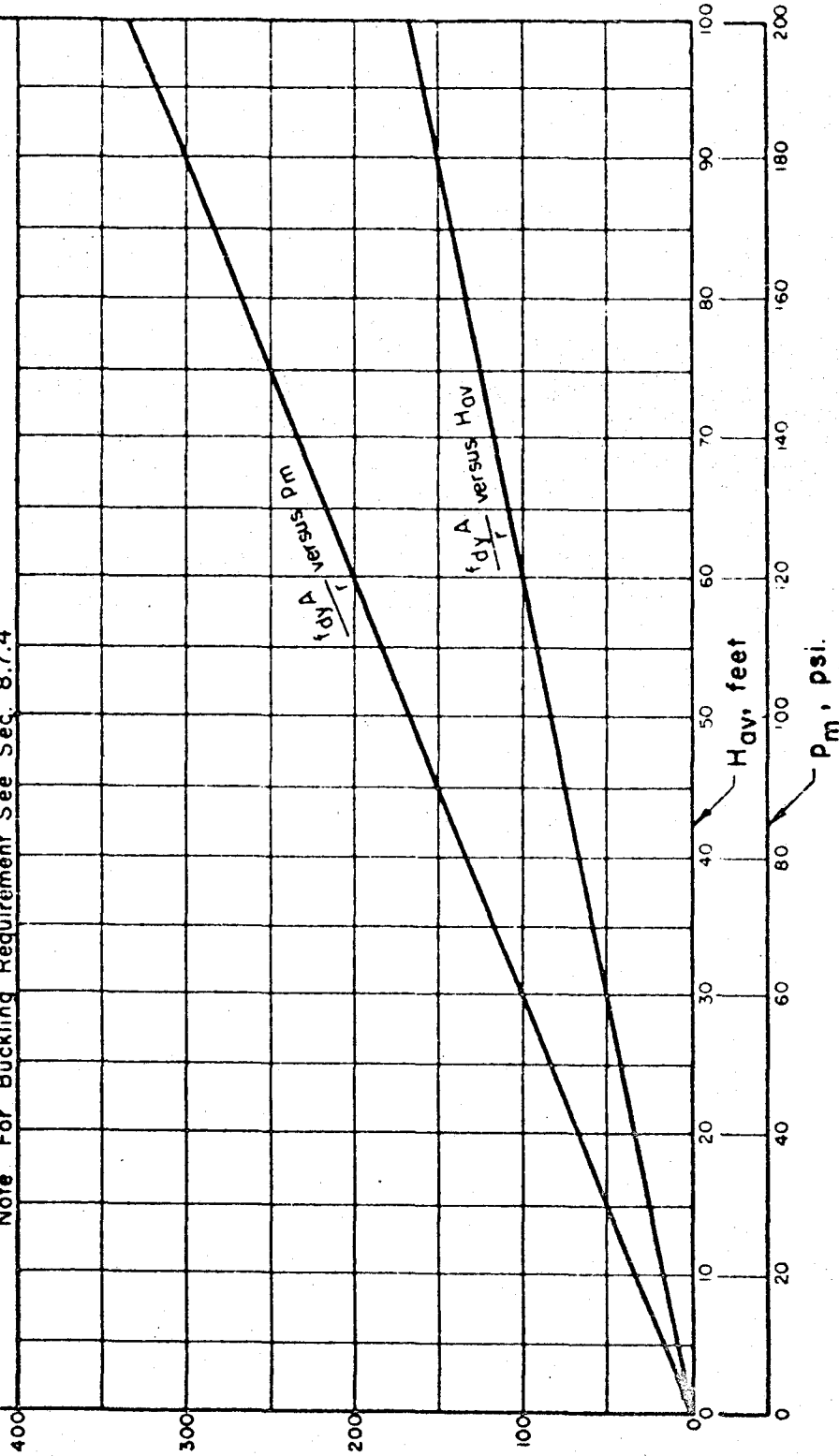


FIG. 9-24 REQUIRED AREA OF FULLY-BURIED STEEL ARCHES ($\mu = 1.3$)

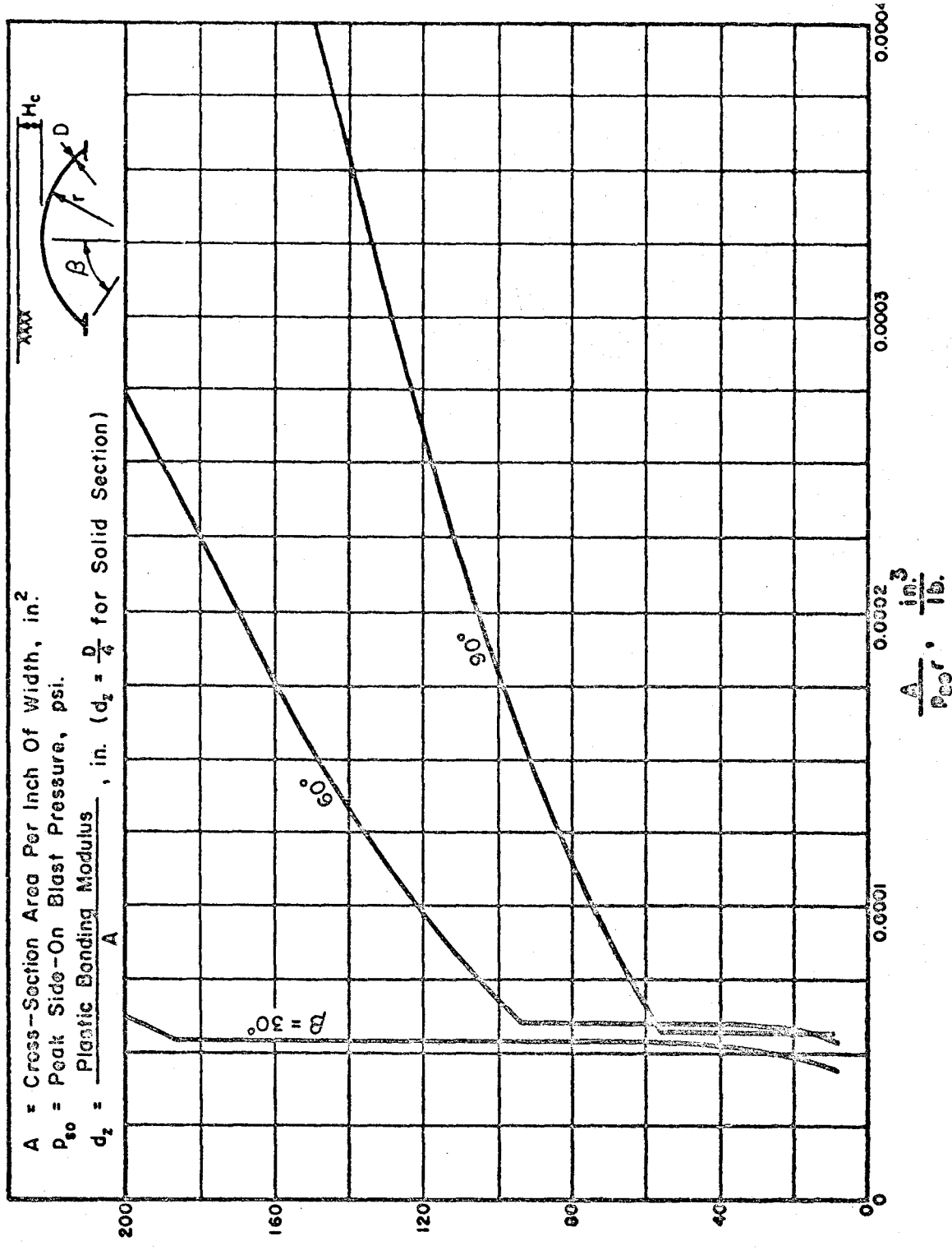


FIG. 9-25 REQUIRED AREA OF PARTIALLY-BURIED STEEL ARCHES
 ($H_c = 0 \rightarrow 0.062D$), ($\mu = 1.3$)

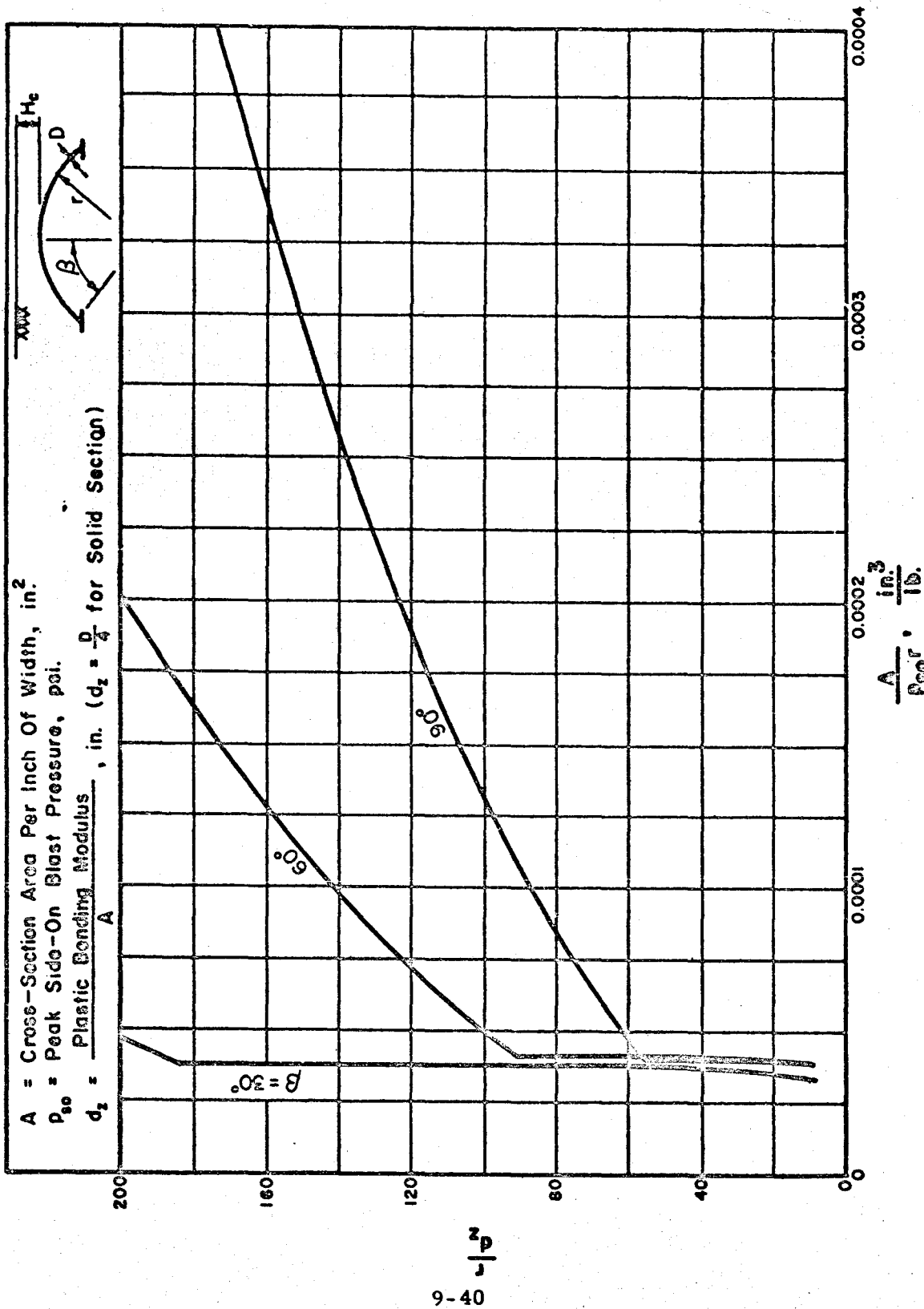


FIG. 9-26 REQUIRED AREA OF PARTIALLY-BURIED STEEL ARCHES
 ($H_c = 0 \rightarrow 0.062B$), ($\mu = 3.0$)

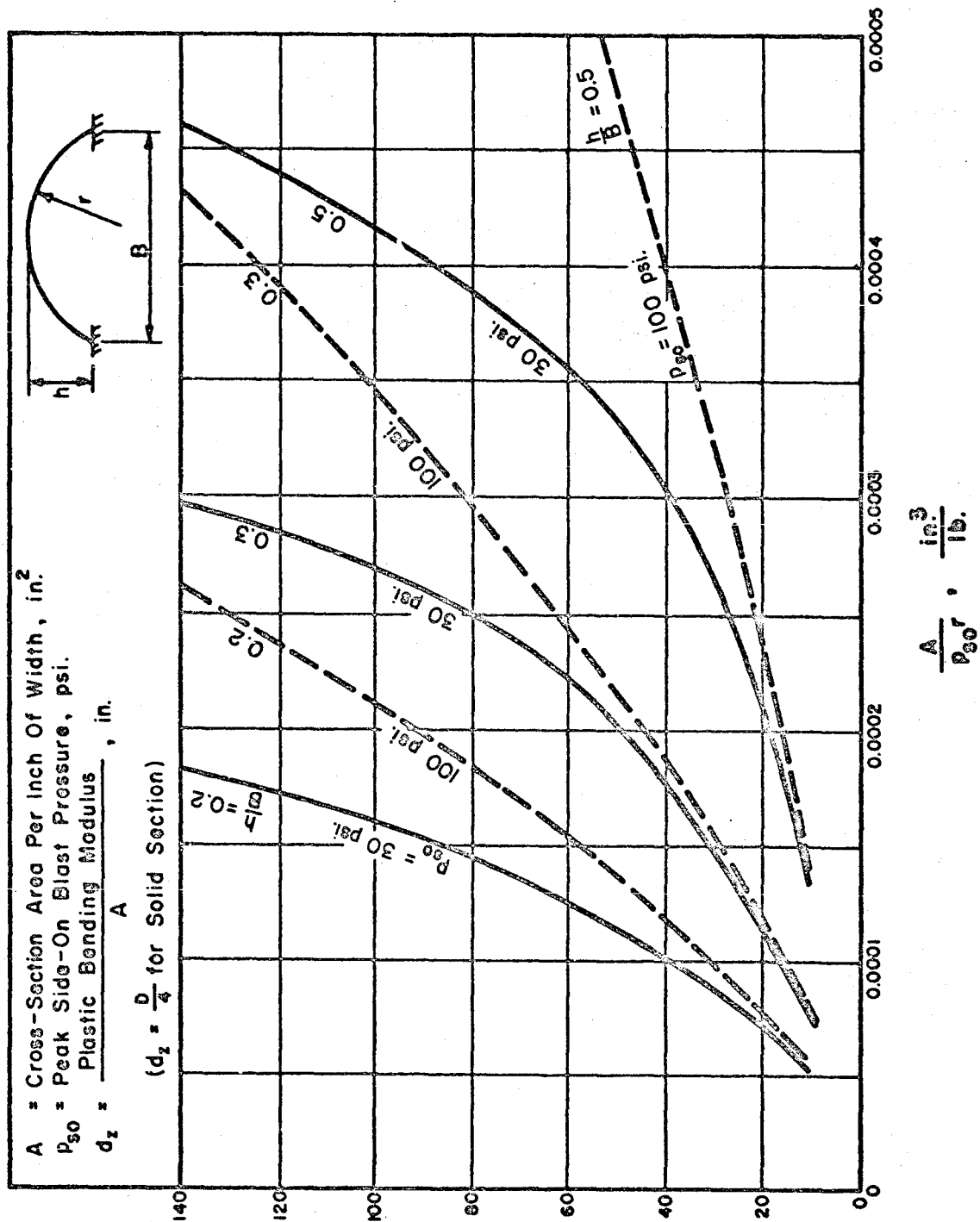


FIG. 9-27 REQUIRED AREA OF ABOVEGROUND STEEL ARCHES
($\mu = 1.3$)

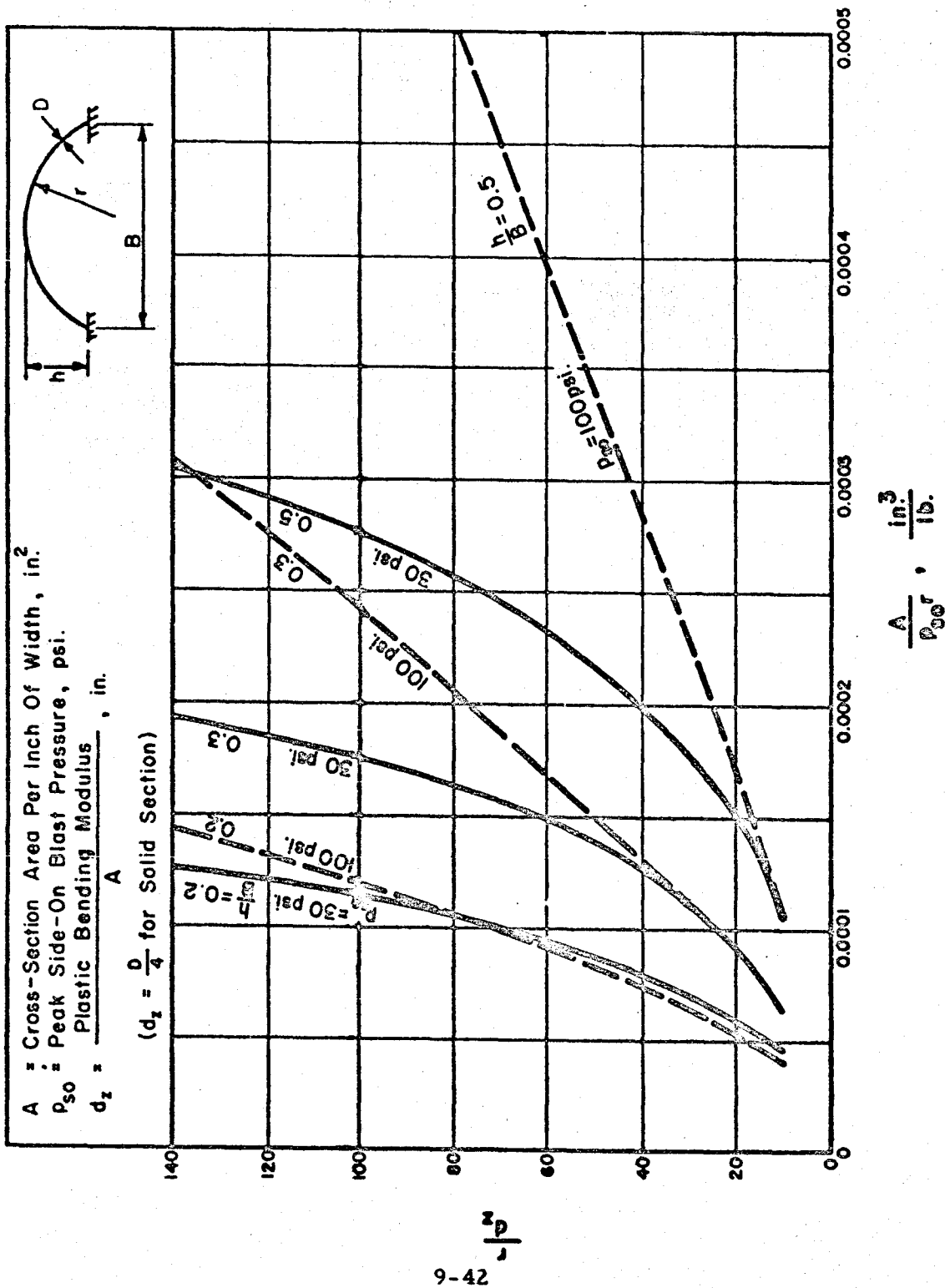


FIG. 9-28 REQUIRED AREA OF ABOVEGROUND STEEL ARCHES
 ($\mu = 3.0$)

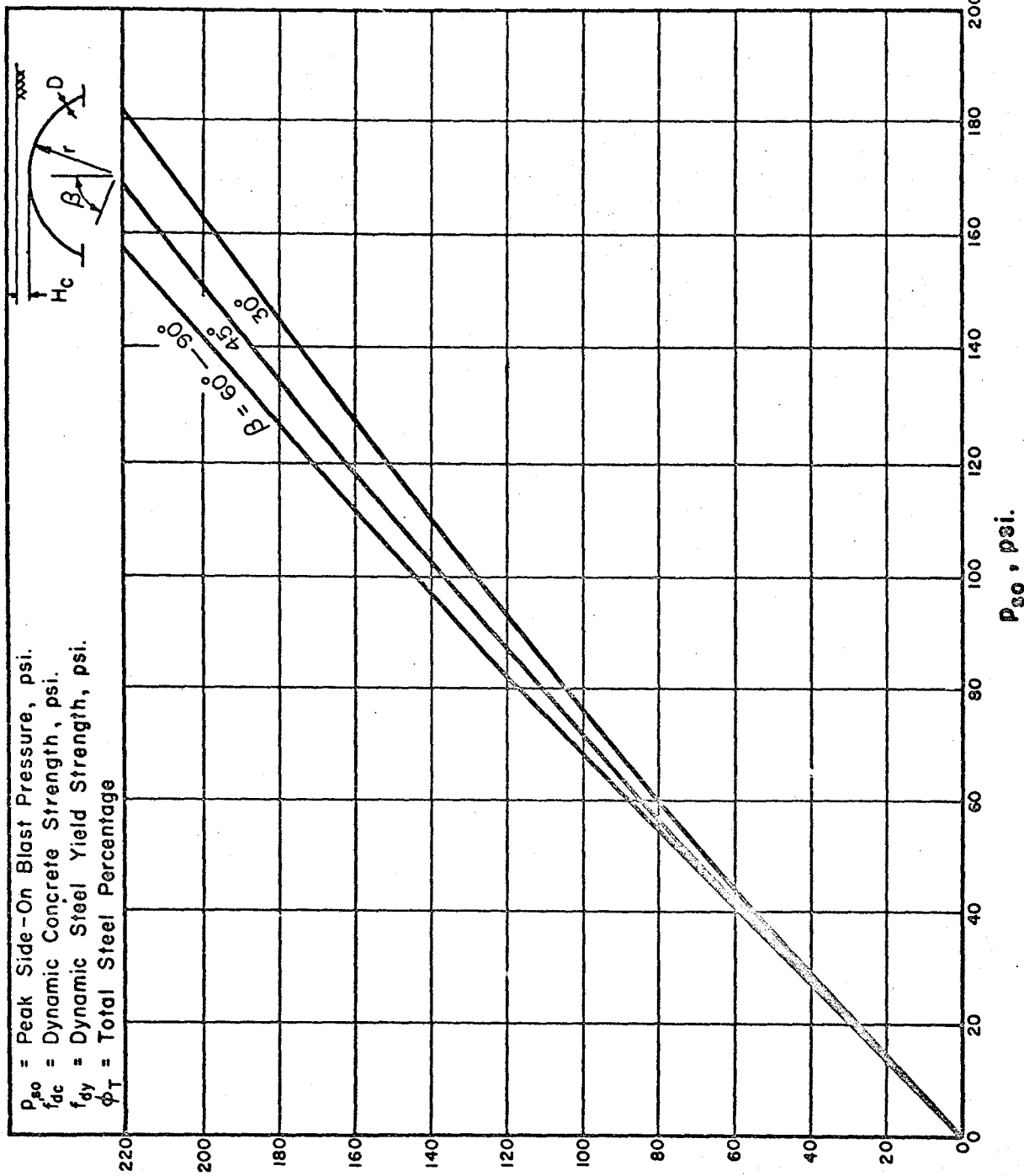


FIG. 9-29 REQUIRED THICKNESS OF PARTIALLY-BURIED R/C DOMES ($\mu = 1.3$)

$$\frac{r}{D} (0.85 f'_{dc} + 0.009 \phi_T f_{dy}) \leq P_{so} \text{ , psi.}$$

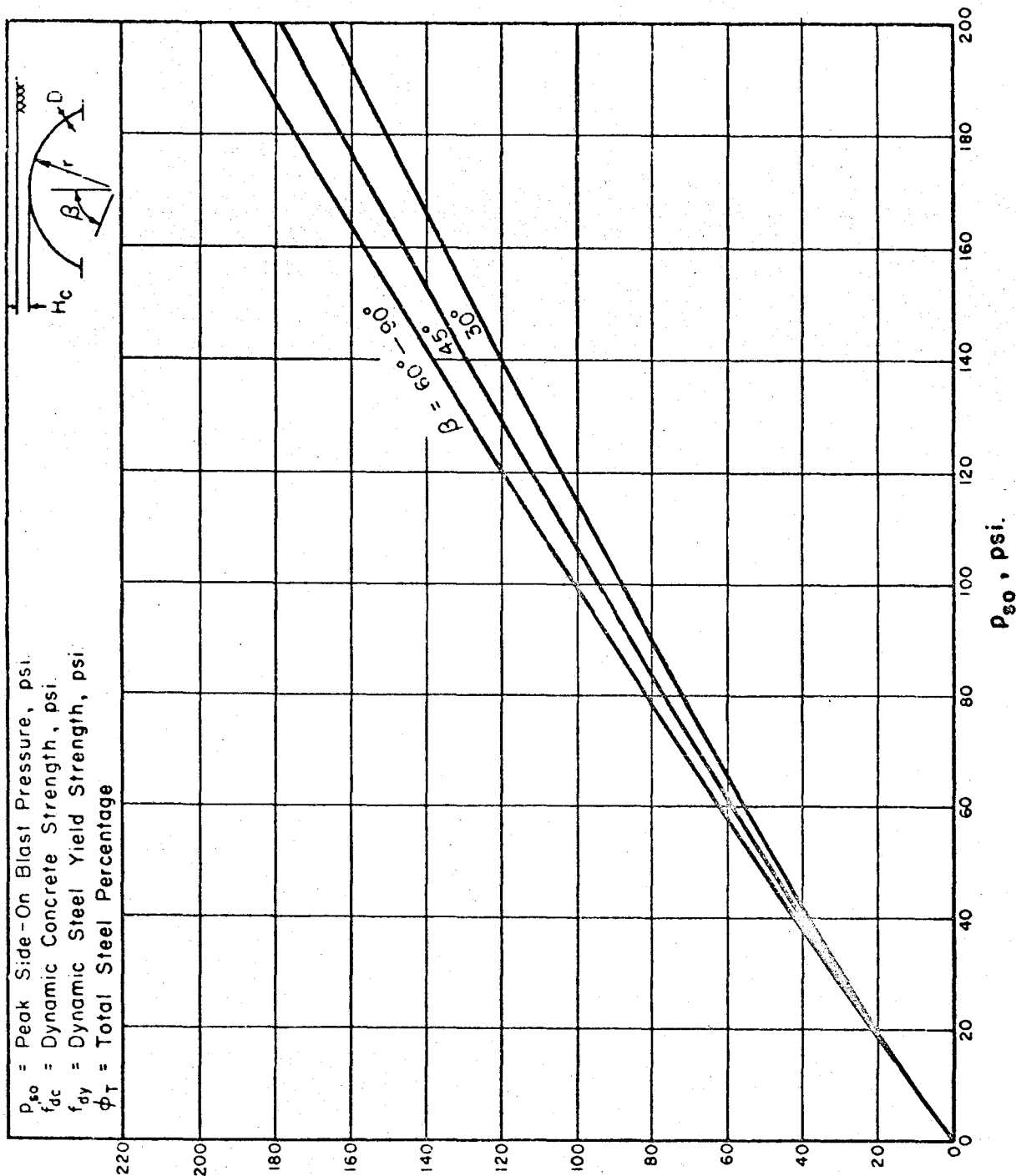


FIG. 9-30 REQUIRED THICKNESS OF PARTIALLY-BURIED R/C DOMES ($\mu = 3.0$)

$$\frac{1}{0} (0.85 f'_{dc} + 0.009 \phi_T f_{dy}), \text{ psi.}$$

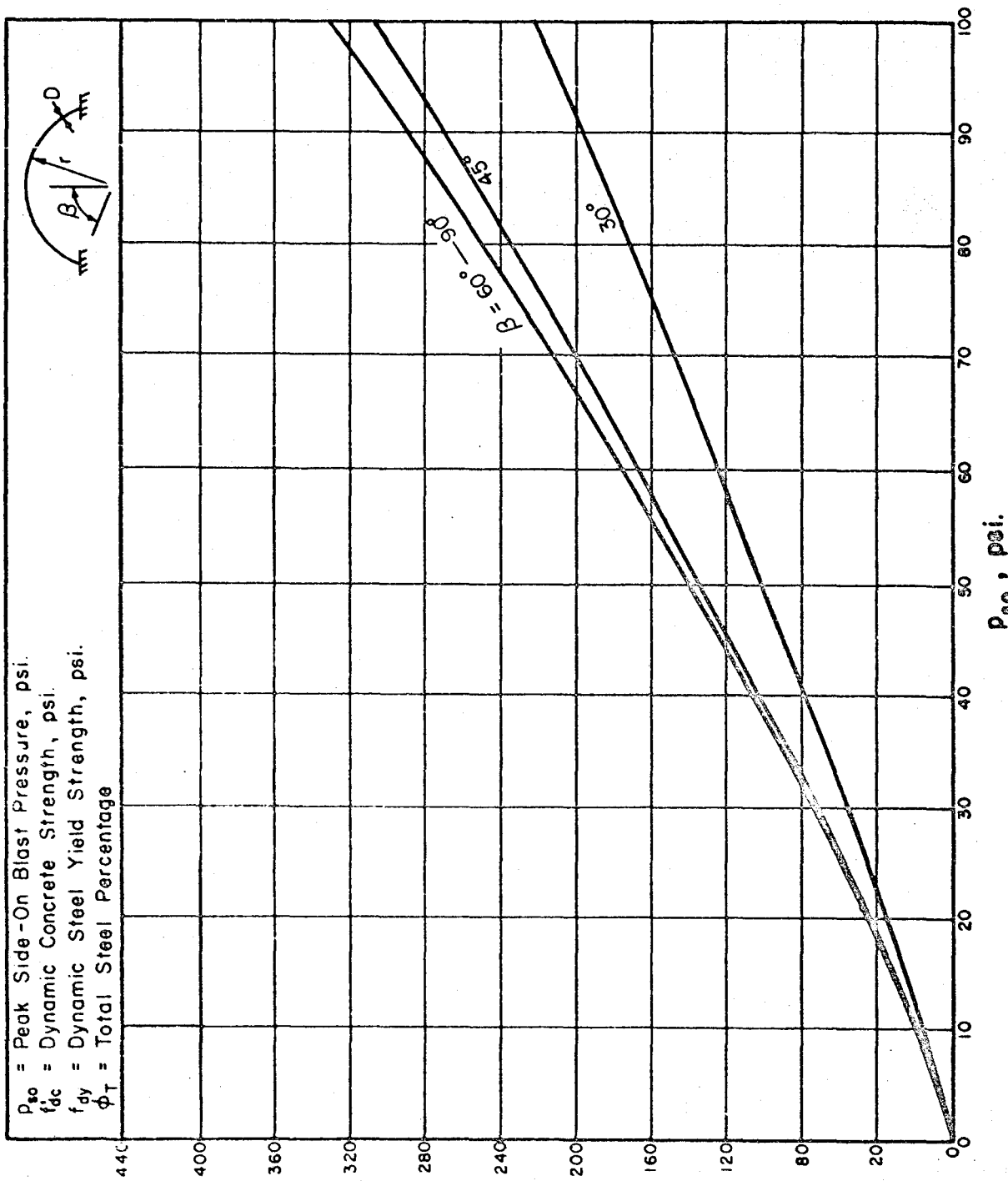


FIG. 9-31 REQUIRED THICKNESS OF ABOVEGROUND R/C DOMES ($\mu=3.0$)

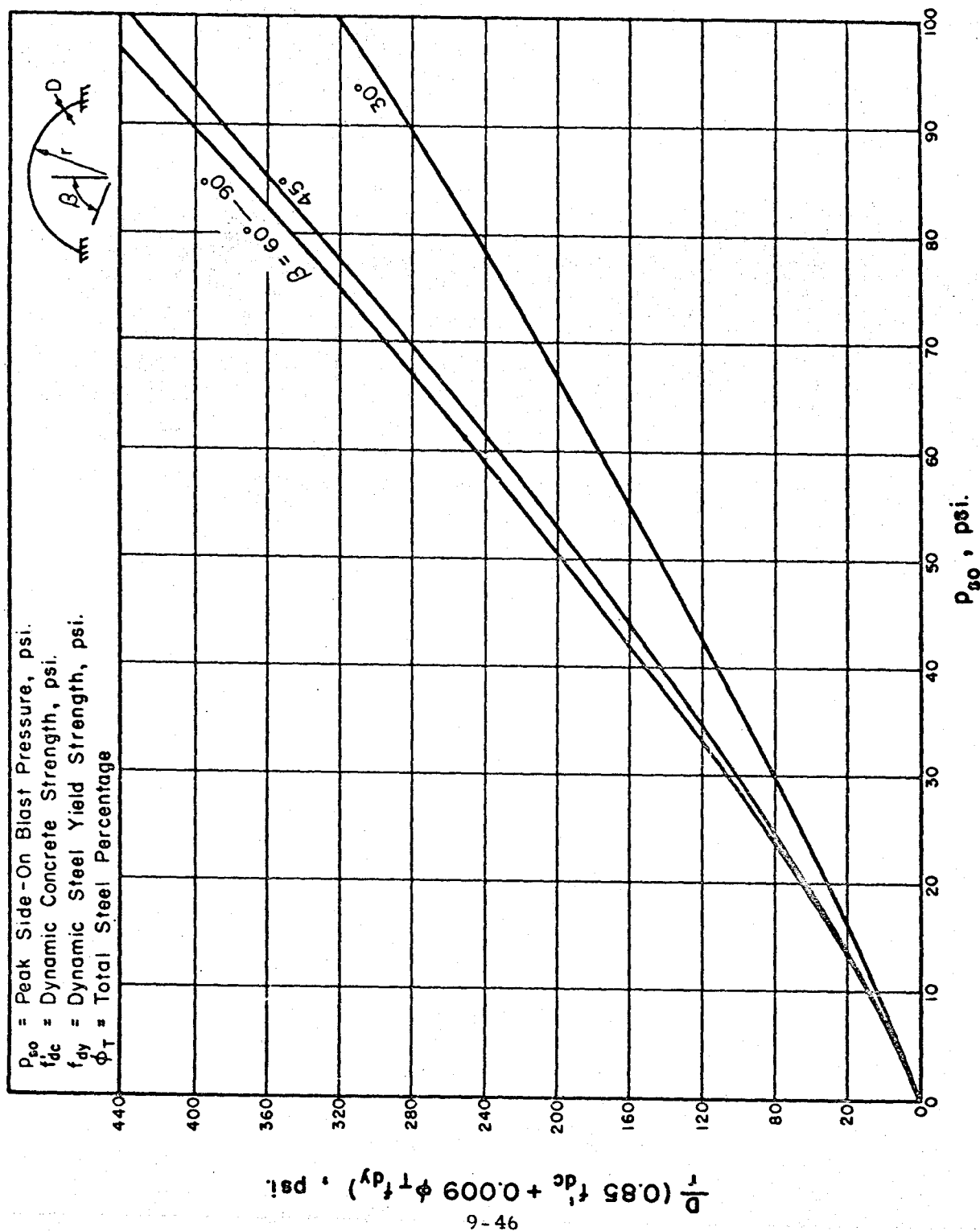


FIG. 9-32 REQUIRED THICKNESS OF ABOVEGROUND R/C DOMES ($\mu = 1.3$)

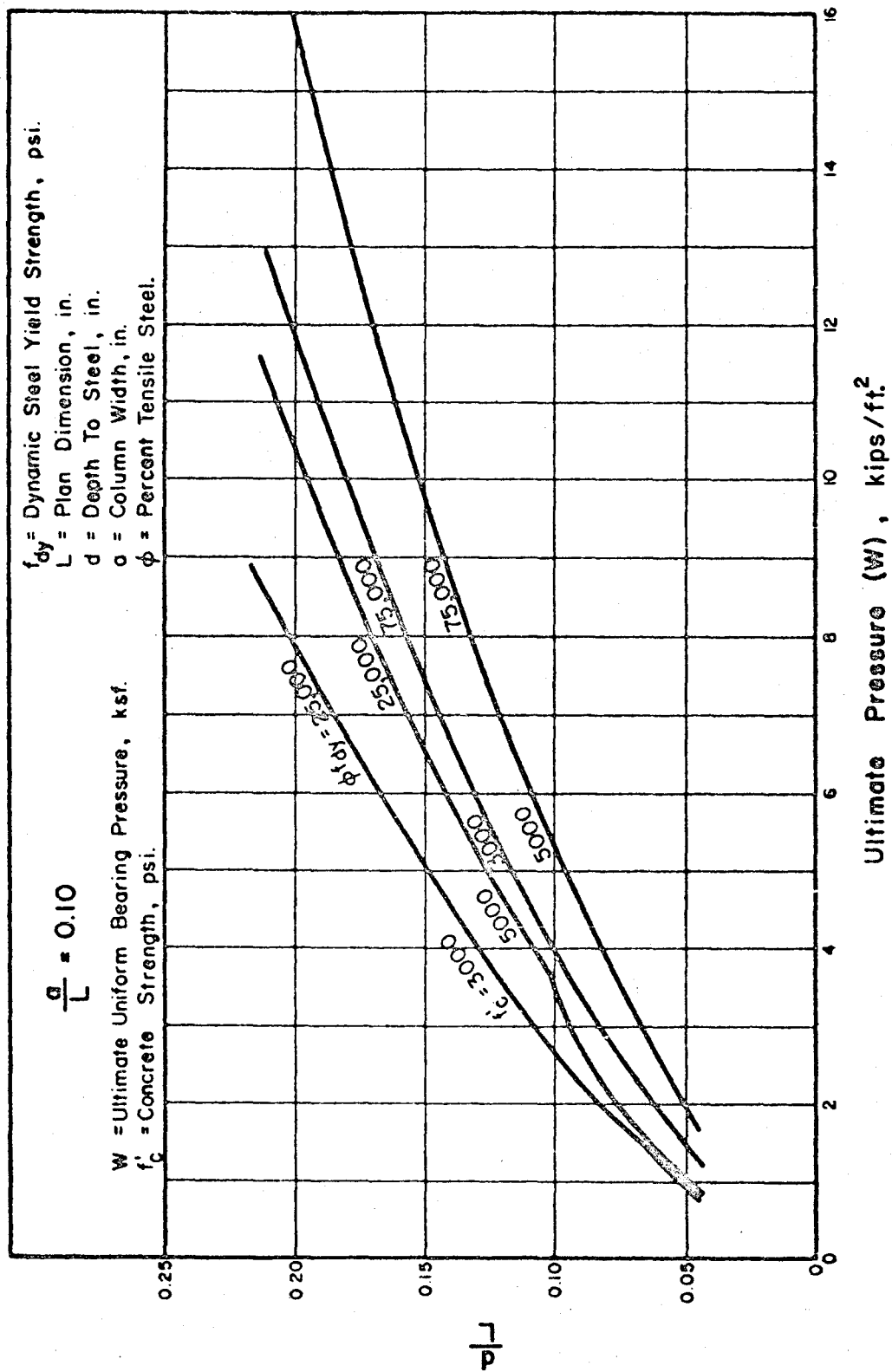


FIG. 9-33 RESISTANCE OF SQUARE COLUMN FOOTINGS

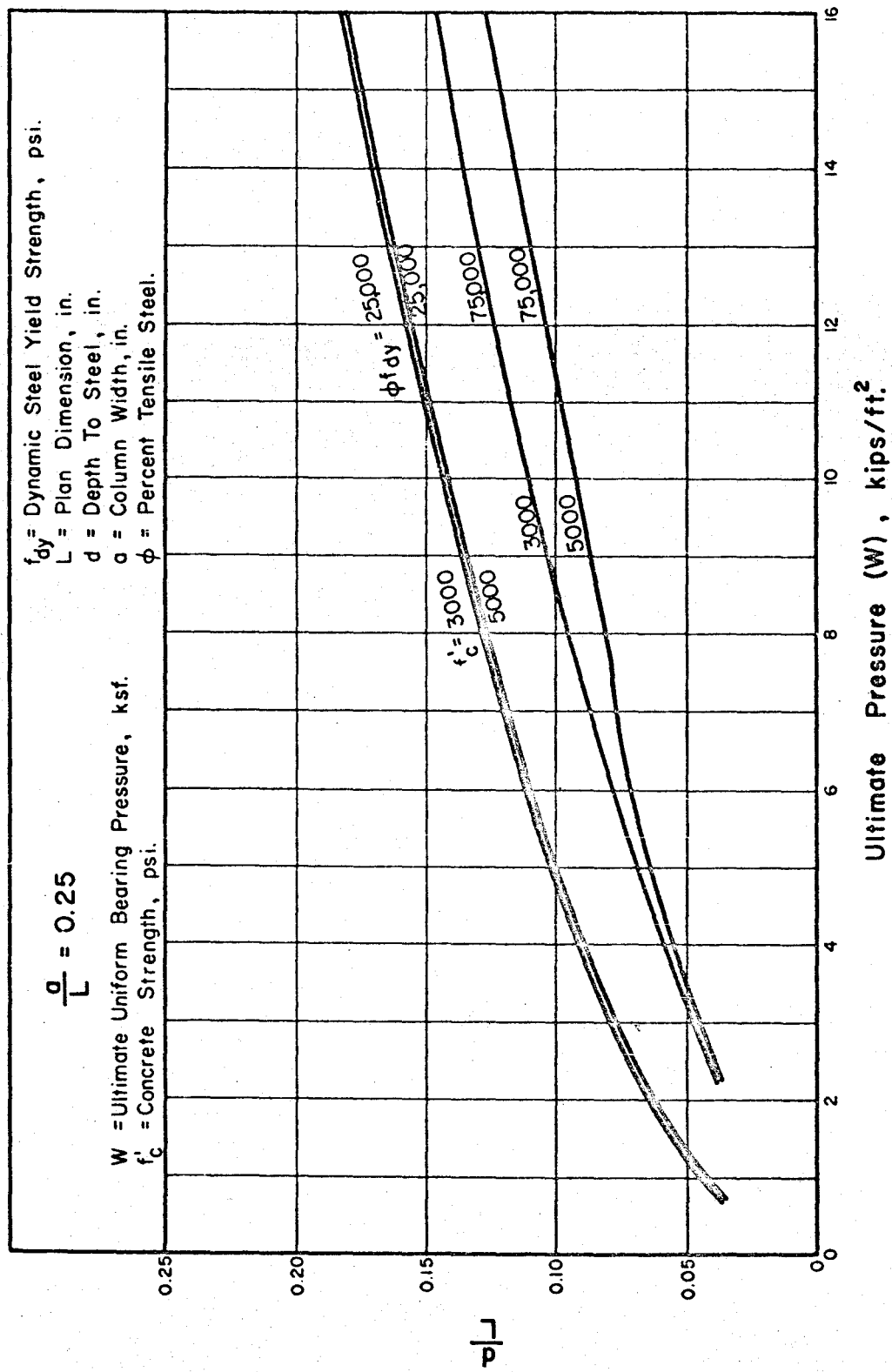


FIG. 9-34 RESISTANCE OF SQUARE COLUMN FOOTINGS

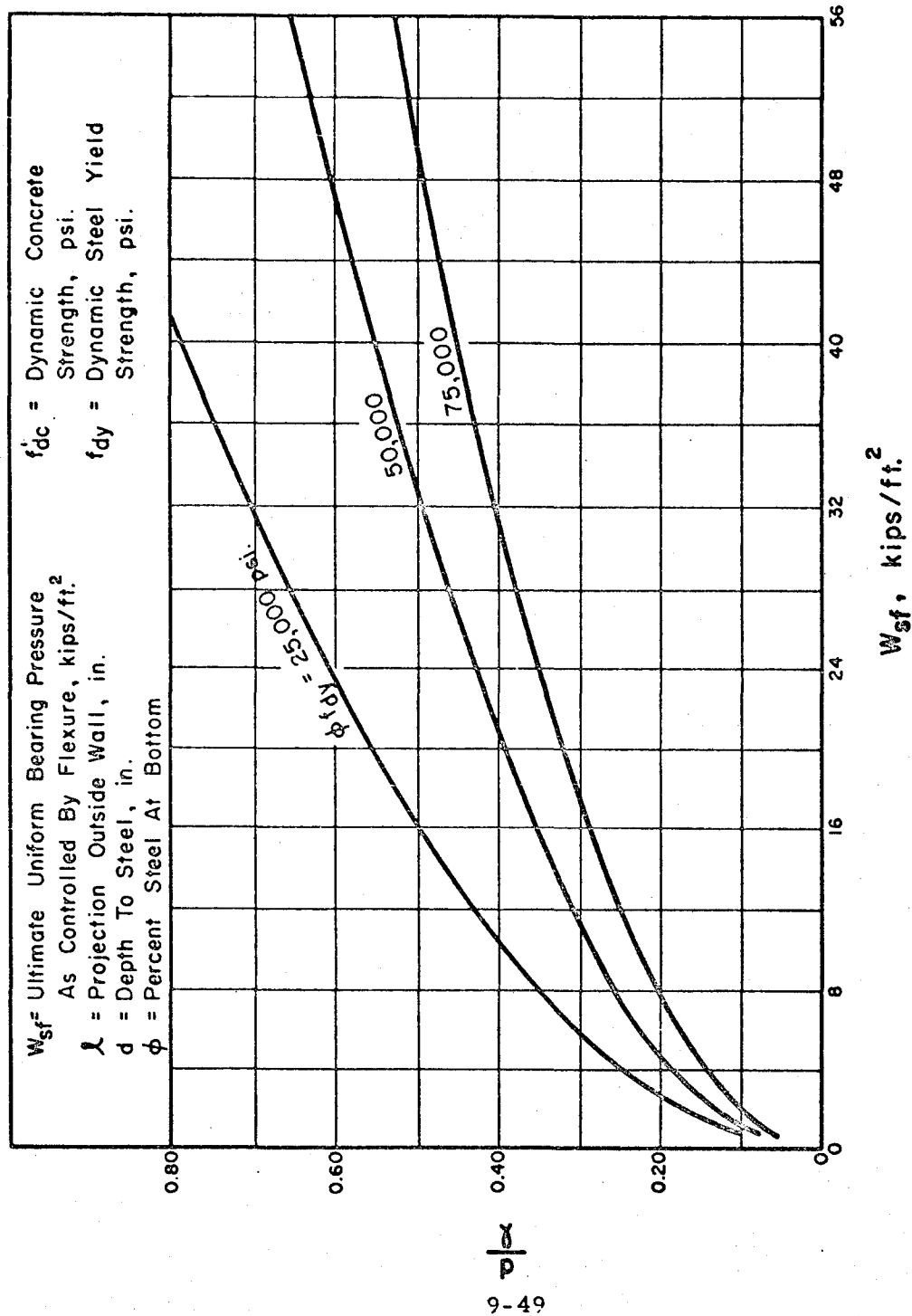


FIG. 9-35 FLEXURAL RESISTANCE OF WALL FOOTINGS

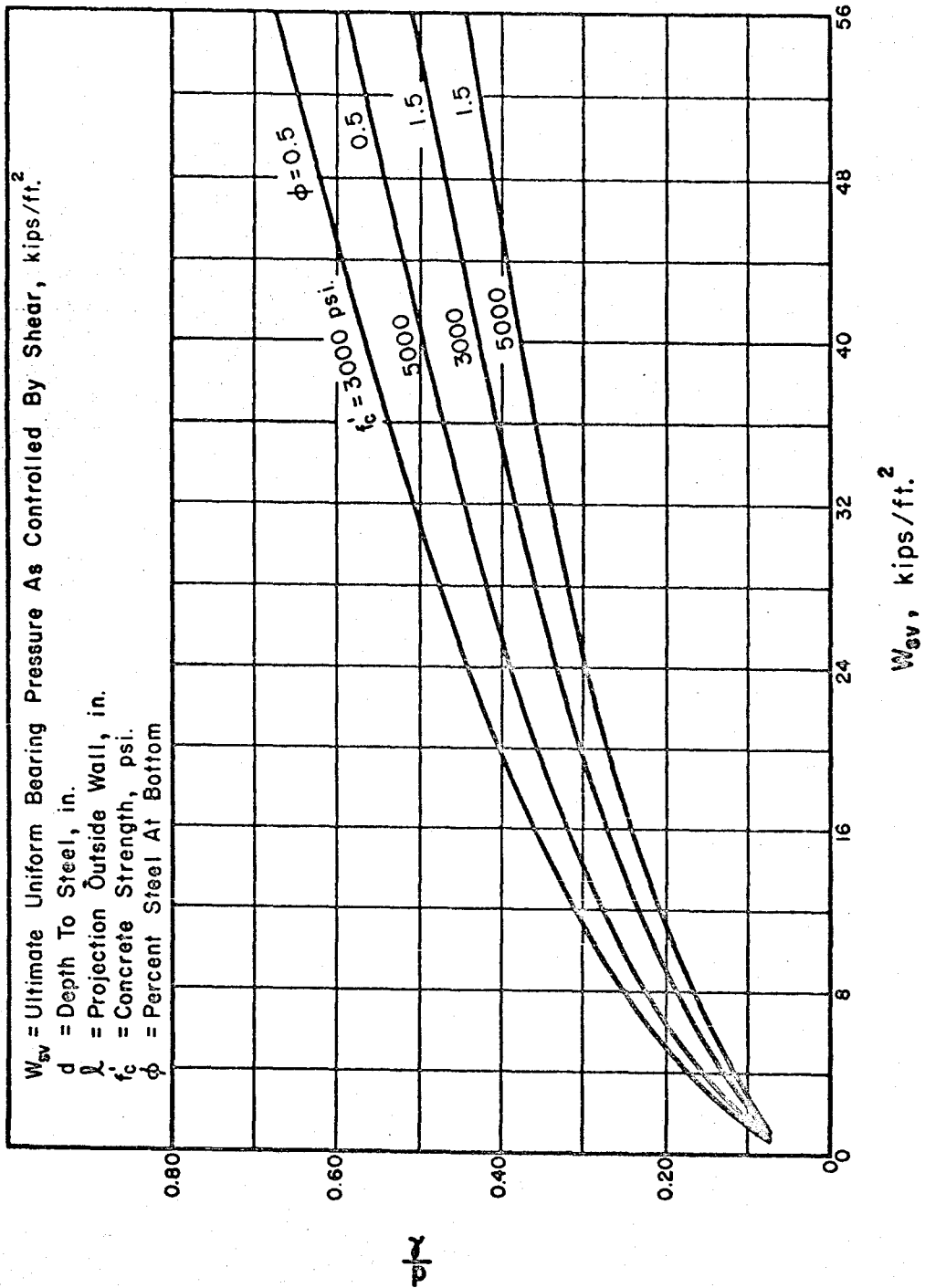


FIG. 9-36 SHEAR RESISTANCE OF WALL FOOTINGS
WITHOUT WEB REINFORCEMENT.

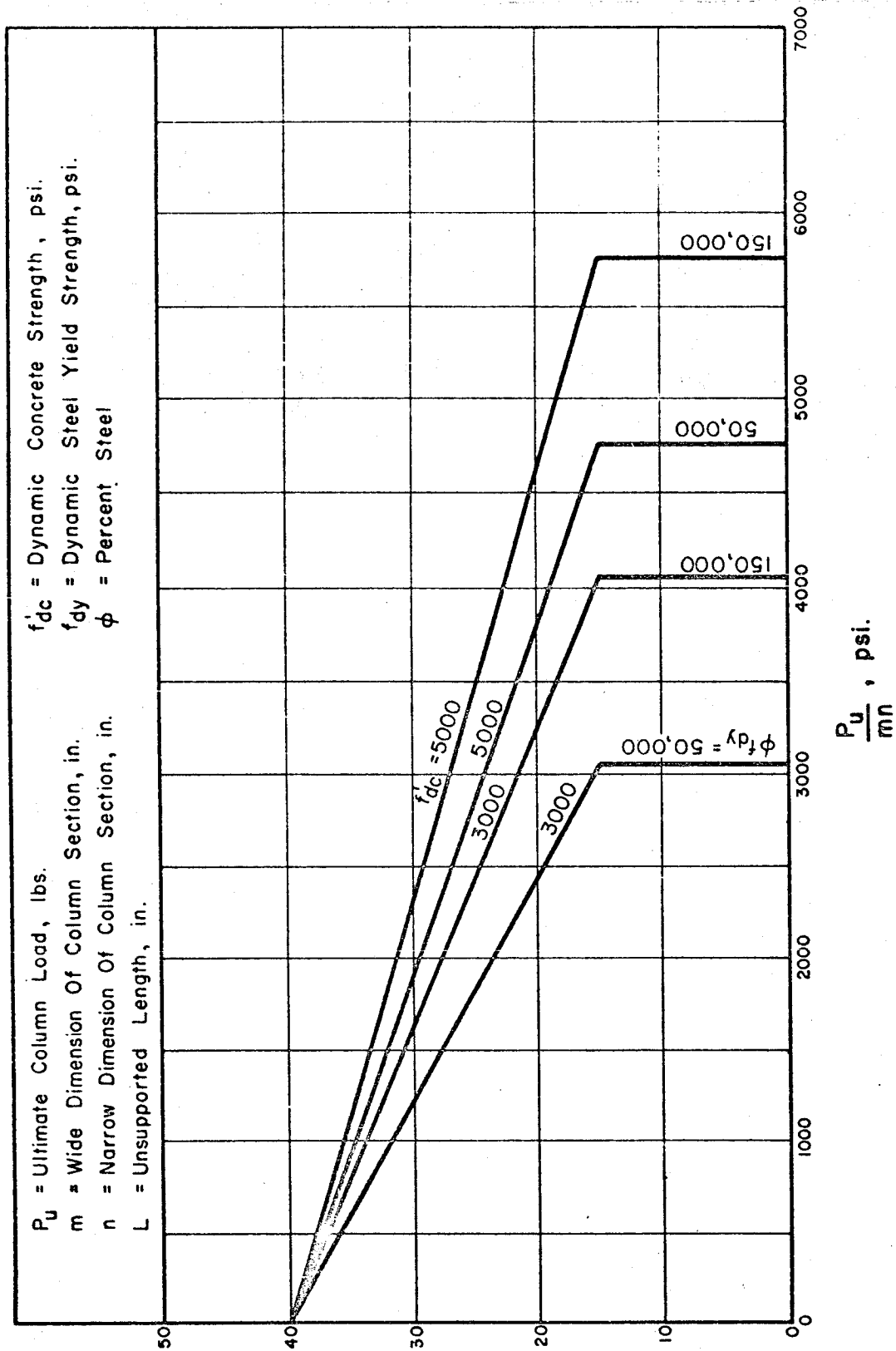


FIG. 9-37 STRENGTH OF AXIALLY-LOADED RECTANGULAR REINFORCED CONCRETE COLUMNS

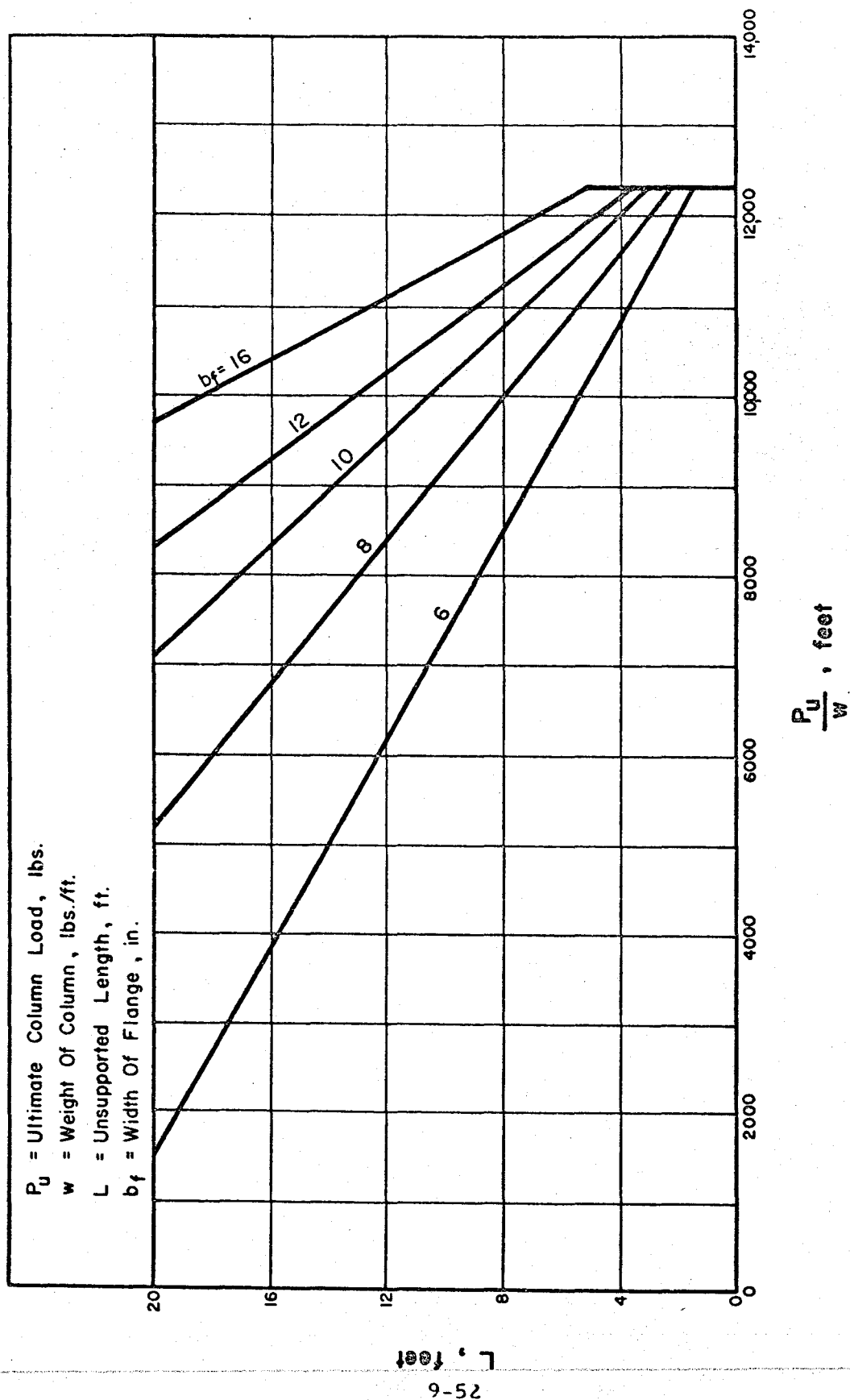


FIG. 9-38 ULTIMATE STRENGTH OF AXIALLY-LOADED I-SECTION
 STEEL COLUMNS

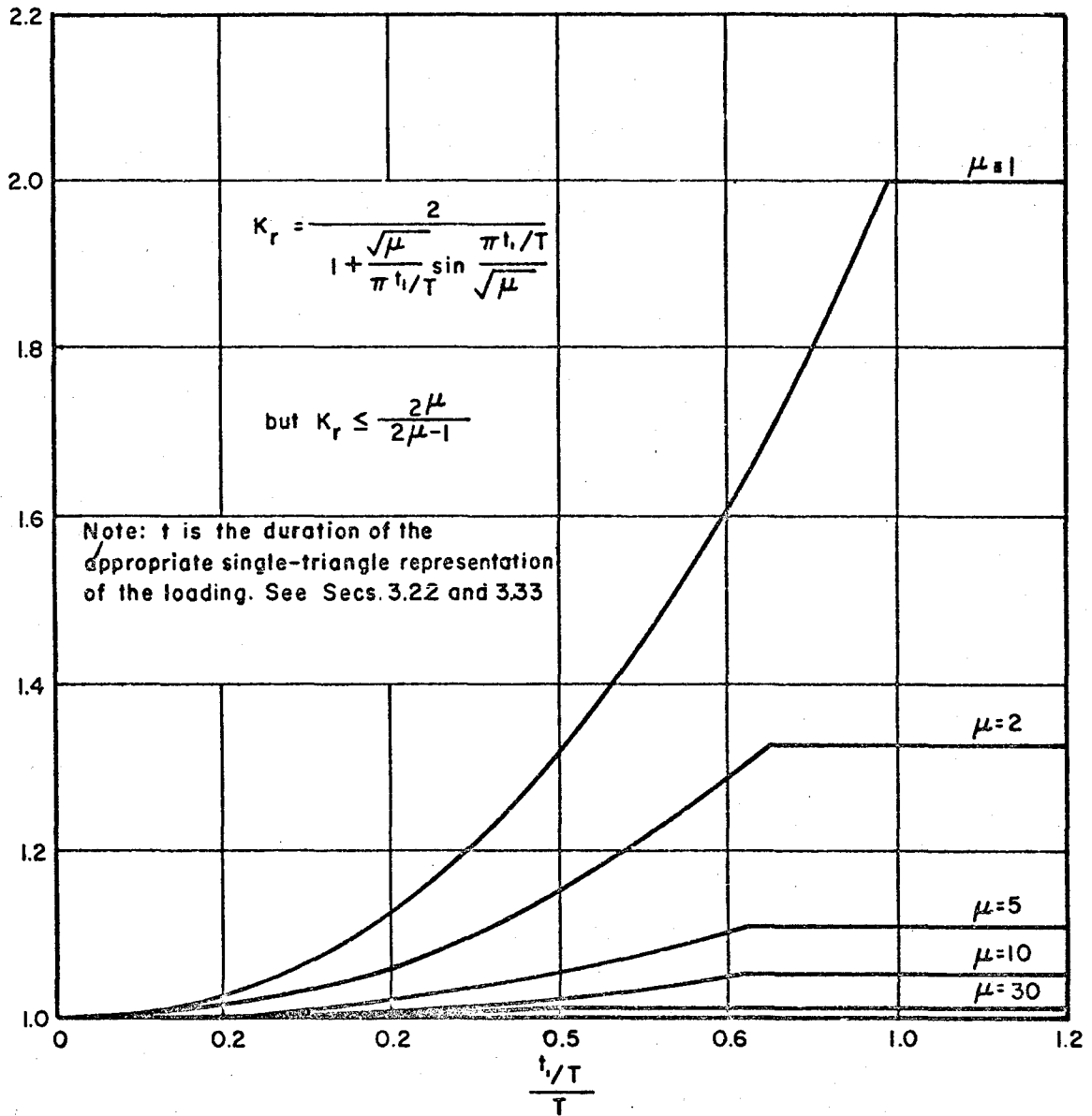


FIG. 9-39 RISE TIME FACTOR (K_r) VERSUS RISE TIME.

CHAPTER 10. EARTH SHOCK AND SHOCK MOUNTING

The material presented in this chapter is taken largely from Refs. 10-1, 10-2, 10-11 and 10-12, supplemented as considered necessary for the more general use ascribed to this manual. In numerous instances, the text of parts of Refs. 10-1 and 10-11 have been used almost unchanged.

10.1 INTRODUCTION

The ground motion resulting from a nuclear detonation is a complex combination of many effects, including air-induced shock, direct-transmitted ground shock, surface and reflected waves, coupled effects, and random motions. Because of the complex nature of the situation, it is convenient for design purposes to consider the earth shock resulting from a nuclear explosion as producing both systematic and random effects. Systematic effects can further be divided into two major types: (1) air-induced shock associated with the passage of an air-shock wave over the surface of the ground, the overpressure at the surface above the structure being transmitted downward with such attenuation and dispersion as may be consistent with the physical conditions at the site; and (2) direct-transmitted ground shock arising from direct energy transfer from surface, near surface, or underground bursts. Random effects commonly include high frequency ground-transmitted shock, surface wave effects, reflections, refractions, etc. Which particular effect is dominant and controls the design is dependent on such factors as weapon yield, point of detonation, range from ground zero,

depth of the structure, and geologic conditions.

At present it is possible to make reasonable estimates of the maximum free-field values of displacement, velocity and acceleration that are associated with the air-induced shock effects, and in more restricted cases, for the direct-transmitted ground shock effects as discussed in Chapter 4.

When structural systems or equipment are subjected to a base disturbance, as for example that arising from the ground motion associated with a nuclear blast, the response of the system is governed by the distribution and magnitudes of the masses and resistance elements. A knowledge of the response of systems subjected to such loadings is important from the standpoint of design in order to proportion the structure so that it will not undergo complete collapse, and to protect the structure, equipment, and personnel from shock damage.

For purposes of assessing the effects of shock on structures or elements in direct contact with the soil, one of the simplest interpretations of ground motion data involves the concept of the response spectrum, which is a plot against frequency of the maximum response of a simple linear oscillator subjected to a given input motion. Studies of the many shock spectra that have been determined from ground motion measurements, from both blast and earthquake sources, suggest that response spectra can be described in a relatively simple way in terms of the maximum values of displacement, velocity or acceleration. Concepts relating to the use of shock spectra for the design of structures and shock isolation systems are

given in this chapter.

10.2 SHOCK RESPONSE SPECTRA

The principal effects of blast-induced ground shock on structural components and equipment can be described adequately by means of a shock response spectrum. As stated in Section 10.1, a response spectrum is a plot against frequency of the maximum response of a simple linear oscillator subjected to a given input motion. Clearly, then, a response spectrum depicts only maximum response values, not a time-dependent history of the motion of the oscillator. However, it is usually sufficient to have only the maximum values.

Response spectra have been used extensively (Refs. 10-3, 10-4 and 10-5) in studies of the response of structures to earthquake ground motions. Applications of the response spectrum technique to shock problems arising from blast have also been published for elastic systems (Refs. 10-6, 10-7, 10-11 and 10-12) and extensions of the spectrum concept to elasto-plastic systems have been made for earthquake motions (Ref. 10-8), and for blast effects (Refs. 10-11 and 10-12).

10.2.1 Response Spectra for Elastic Systems. Consider a piece of equipment or a structural element in an under-ground structure which is subjected to ground motions from a nuclear blast. The equipment or structural element can be considered to be the mass of a simple oscillator. The spring constant of the oscillator can be characterized by the load-deflection properties of the structural system which connects the mass to

ground, or base, at which point it is subjected to the ground motion. The maximum displacement of the mass relative to the base is called the spectrum displacement, D , and the maximum acceleration of the mass is called the spectrum acceleration, A . The maximum velocity of the mass is approximately equal to the following more useful quantity called the spectrum pseudo-velocity, V , where

$$V \approx 2\pi f D \quad (10-1)$$

f being the natural frequency of vibration of the oscillator.

For a system with zero damping, D and A are related by

$$A = (2\pi f)^2 D \frac{g}{387 \text{ in/sec}^2} \quad (10-2)$$

which also holds, though only approximately, even when damping is present.

For a given input motion of the base, D , V , and A are functions only of the frequency of the system considered. Plots of these three quantities against frequency are, then, response spectra. They may be plotted individually or, more conveniently, on a single plot by means of the type of chart shown in Fig. 10-1.

Clearly, the nature, or shape, of the response spectrum is dependent only upon the nature of the input motion. Ordinarily the input for blast-induced ground motion consists of two parts, a systematic portion on top of which is superimposed a series of random oscillations. The magnitudes of the peaks of the random components may be either small or large compared

to the systematic portion. The random part may exist over the entire range of the systematic portion, only part of the range, or even prior to the systematic portion. Schematically the parts may be related as in Fig. 10-2 where the actual input at any time is the sum of the two input curves.

For a random series of pulses, the relative velocity peak of the spectrum compared with the maximum input velocity can be high, but is unlikely to be much higher than about 3 times the maximum input velocity unless an almost resonant condition is obtained with several pulses of alternate positive and negative sign of exactly the same shape and duration. Such a resonant condition for velocity is extremely unlikely from blast loading, and has not been observed even in earthquake phenomena. Even if for some reason partial resonance is achieved, damping will reduce the peaks considerably.

In general the combined effect of the two input motions, systematic and random, depends on their individual effects. In Fig. 10-3 are shown sketches of the response curves corresponding to each of the parts of Fig. 10-2. The response spectrum corresponding to the systematic component (a) is a relatively smooth, somewhat triangular curve, generally having its peak at a relatively low frequency, while the response spectrum corresponding to input (b), the random component, is flatter and broader. The combination of the two spectra will be roughly of the same general shape as (b) but with a longer base. There may be a higher peak as well.

It can be shown rigorously that the combined spectrum will in all cases be either equal to or less than the sum of the spectra corresponding

to the individual inputs. In general, although it has not been rigorously proven, it appears reasonable that the combined spectrum can be expected to be equal approximately to the square root of the sums of the squares of the individual spectra, point by point. In most practical cases of the type under consideration, because of the fact that in the range of frequencies for which one spectrum is a maximum the other spectrum is relatively low, and vice-versa, the sums of the spectra and the square root of the sums of the squares are nearly the same.

From studies of many earth shock response spectra, it has been found that approximate spectrum envelopes can be plotted on the chart of Fig. 10-1 if only the maximum values of free-field displacement, velocity, and acceleration are known. That is to say, one does not need the complete time history of the input motions - only the maximum values of the three motion parameters.

While generally irregular throughout its length, a response spectrum envelope can be approximated adequately for most purposes as a trapezoid such as is shown on Fig. 10-1 by the lines labeled D, V and A. The three sides of this trapezoid can be related to the maximum free-field input motion parameters of displacement, velocity, and acceleration.

Recent studies of the relationships between spectrum envelope bounds and the characteristics of the time-dependent free-field input motions (displacements, velocities, and accelerations) have been reported in Refs. 10-11 and 10-12. A study of these references indicates clearly that as the

definition of the variation with time of the free-field motion parameters is improved, the definition of the corresponding spectrum envelope can be refined. However, in the general case of blast-induced motions, the input motions can not usually be described in significant detail. Consequently, based on the results given in Ref. 10-12, it is recommended that, for systems responding elastically, the spectrum be defined by the following three straight-line bounds, as illustrated in Fig. 10-1.

(a) A line "D", drawn parallel to lines of constant displacement, at a displacement magnitude equal to the maximum free-field displacement.

(b) A line "V", drawn parallel to lines of constant velocity (actually, pseudo velocity, as discussed earlier), at a value equal to 1.5 times the maximum free-field velocity.

(c) A line "A", drawn parallel to lines of constant acceleration, at an acceleration value equal to twice the maximum free-field acceleration.

A spectrum defined in this manner is clearly an approximation; however, its accuracy is considered to be consistent with that of the input free-field motions on which it is based. In special cases where the input motions can be defined with greater confidence, the spectrum identified above can be refined by the methods presented in Refs. 10-11 and 10-12.

10.2.2 Response Spectra for Inelastic Systems. For an elastic system, the maximum response produced by a given blast-induced excitation of the base can be read from the response spectra plotted as described in the preceding section. If, however, the spring becomes plastic before the

maximum deflection has been reached, it is necessary to consider the effect of this inelastic behavior on the response of the mass to the same input base excitation. The procedures that follow were taken from Ref. 10-11 and represent the results of the most recent studies on this question.

The shock response of a simple system having an inelastic force-displacement relation is considered here. A typical inelastic relationship is shown in Fig. 10-4, with an initial "elastic" portion continued above the "inelastic" curve. For an elastic system, with a frequency corresponding to the line *oc* in Fig. 10-4, the response spectrum for a typical shock input, when plotted on a form illustrated by Fig. 10-1, may have a shape similar to that shown in Fig. 10-5.

Recent studies indicate that the following relationships are applicable for the inelastic system of Fig. 10-4.

- (1) Along the D-line of Fig. 10-5, the total displacement of the system is the same for the inelastic system as for the corresponding elastic system.
- (2) Along the V-line, the total energy (or velocity) of the system is nearly the same for the inelastic system as for the elastic system.
- (3) Along the A-line, the maximum acceleration (or force) is nearly the same for the inelastic system as for the elastic system.

These three relations imply certain relations among forces or accelerations and displacements which can be clarified by reference to Fig. 10-4. Consider the case when the elastic system has a force R_c (and a

corresponding acceleration), and a displacement u_c , corresponding to point c on the "elastic" line.

For case (1) where displacement is conserved, the inelastic system would have a displacement of u_d , and a force (or acceleration) R_d , corresponding to point d on the "inelastic" curve.

For case (2), where velocity or energy is conserved, the inelastic system would have a displacement u_v and a force R_v , corresponding to a point v, up to which the total area under the force-displacement curve is the same as that up to point c for the elastic case.

For case (3), where acceleration is conserved, the inelastic system would have a force R_a and a displacement u_a , corresponding to a point a.

However, in cases (2) and (3), the principles stated overestimate the response of the inelastic system. A correction is needed which refers the energy in case (2) to a line probably intermediate between V and v_b in Fig. 10-5, and which refers the acceleration in case (3) to a line probably intermediate between A and a_b in the same figure.

It is suggested that this interpolation between A and a_b or between V and v_b be linear, based on the proportion of the total energy lost at the maximum deflection considered. For example, at a point such as a, the total energy is the area o-d-a- u_a -o and the area lost is o-d-a-a'-o, the difference being the recoverable elastic energy at point a.

To illustrate the use of the concepts just described, they will be applied to a simple elasto-plastic system. However, any other force displacement relationship can be approximated by an elasto-plastic relationship in

which the energy is conserved up to the point of maximum deflection and roughly also up to the point of yielding, in the replacement system. These relationships are expressed in Fig. 10-6. The area under the force displacement curve up to the point u_y should be the same for the two curves, and they should also be the same up to the point u_m . (It appears, therefore, that the frequency for the equivalent elasto-plastic curve will be changed slightly from the frequency corresponding to the initial part of the inelastic curve. The modified frequency is the one that should be used, however, in the calculations.)

If the recovery from the point of maximum deflection for the elasto-plastic curve is along a line parallel to the equivalent initial elastic portion, the ratio of the lost energy to the total energy can be expressed as follows:

$$\frac{\text{lost energy}}{\text{total energy}} = \frac{R_y(u_m - u_y)}{R_y(u_m - \frac{1}{2}u_y)} = \frac{2(\mu - 1)}{2\mu - 1} \quad (10-3)$$

For $\mu = 1.5$, this factor has the value 0.5; for $\mu = 2$, it is 0.67; for $\mu = 4$, 0.86; and for $\mu = 10$, it is 0.95. Without serious error, therefore, for values of μ greater than 3 one can base further calculations on the lines v_b and a_b rather than V and A in Fig. 10-5.

Consider now an elasto-plastic system with a given value of μ . In case (1) the total displacement is conserved, but because the elastic component of displacement is $1/\mu$ times the total, the acceleration is reduced by the factor $1/\mu$.

In case (2), the energy is conserved, hence

$$R_y (u_m - \frac{1}{2} u_y) = \frac{R_y u_y}{2} (2\mu - 1) = \frac{R_c u_c}{2} \quad (10-4)$$

However, $R_c/R_y = u_c/u_y$.

Therefore

$$\frac{u_c}{u_y} = \sqrt{2\mu - 1} \quad (10-5)$$

It follows that $u_v = \mu u_y$ is related to u_c as follows:

$$\frac{u_v}{u_c} = \frac{u_v}{u_y} \cdot \frac{u_y}{u_c} = \frac{\mu}{\sqrt{2\mu - 1}} \quad (10-6)$$

and

$$\frac{R_v}{R_c} = \frac{R_y}{R_c} = \frac{u_y}{u_c} \frac{1}{\sqrt{2\mu - 1}} \quad (10-7)$$

In case (3), the force is conserved, and hence the accelerations are the same, but the displacement is increased for the elasto-plastic case, compared with the elastic case, by the factor μ .

For the elasto-plastic design, or for any inelastic condition, two sets of lines must be drawn on the response spectrum chart. One set is used for determining relative displacement, and the other set is used for determining acceleration. In the case of an elasto-plastic spring, however, the latter can also be interpreted as the elastic component of the total elasto-plastic relative displacement.

As an example, consider the following maximum base motions due to shock:

$$\text{Displacement} = d_b = 1.0 \text{ in.}$$

$$\text{Velocity} = v_b = 100 \text{ in./sec}$$

$$\text{Acceleration} = a_b = 200 \text{ g}$$

and an "elastic" spectrum having the following bounds

$$D = 1.0 \text{ in.}$$

$$V = 150 \text{ in./sec}$$

$$A = 400 \text{ g}$$

Now consider an elasto-plastic system having a value of μ of 5.

The proportion of energy lost is, from Eq. (10-3), 0.889, and one could use v_b and a_b as a base for calculations; however, the example which follows illustrates a more refined approach.

Hence the line used between V and v_b lies at a distance 0.889 of the way from V to v_b , or at

$$105.6 \text{ in./sec.}$$

Correspondingly, the line used between A and a_b is

$$222 \text{ g}$$

With these lines used as a basis, one finds the following bounds for the elasto-plastic spectrum:

	<u>For Displacements Only</u>	<u>For Accelerations Only</u>
"Defl" Bound	$D = d_b = 1.0 \text{ in.}$	$\frac{1.0}{5} = 0.20 \text{ in.}$
"Veloc" Bound	$5 \times 35.2 = 176 \text{ in./sec}$	$\frac{105.6}{\sqrt{10-1}} = 35.2 \text{ in./sec}$
"Accel" Bound	$5 \times 222 = 1110 \text{ g}$	222 g

The spectrum for this elasto-plastic system is sketched on Fig. 10-7 for comparison with the spectrum for the elastic system used as a basis for the calculations.

Similar calculations, as well as more accurate studies of response reported in Ref. 10-8 and elsewhere, show that in general for small ductility factors, say 5 or less, the displacement can be considered as conserved over the whole spectrum, and consequently it is necessary only to reduce the elastic spectrum uniformly by the factor $1/\mu$ to obtain the acceleration values, or N values, for design.

This procedure is not entirely conservative for high frequency elements, but this may not be a serious deficiency. However, more careful determination of the bounds of the spectra is desirable when μ is greater than 5.

10.3 DESIGN OF SIMPLE STRUCTURES FOR GROUND SHOCK

Ground shock, as such, is normally of little or no significance as far as the design of simple one-story structures are concerned. More correctly stated, any structural element that must be designed to resist blast-induced pressures will be affected only to a small extent by the inertial forces resulting from ground shock accelerations.

In a given case, the magnitude of the inertial force can be determined quite readily by reading from a response spectrum the maximum acceleration that the element will experience and multiplying this acceleration by the mass of the structural element being studied. In most cases, the

Inertial force thus determined will be quite small in comparison with the blast-induced pressure for which the element is being designed. Furthermore, the inertial force will be of short duration and will usually occur in time so as not to be directly additive to the peak pressure.

10.4 DESIGN OF MULTI-STORY STRUCTURES FOR GROUND SHOCK

The discussion of Section 10.3 is applicable also to the design of exterior wall, roof, and base slab elements since these elements are subjected directly to blast-induced pressures regardless of the number of stories in the building. However, the interior floors, which are not subjected to blast pressure, must be designed for inertial forces in addition to their normal dead and live loads. Furthermore, if the structure is free-standing within a protected cavity, either natural or man-made, it must be designed for the effects of ground shock imparted to it at its base. Though response spectra are plotted only for single-degree-of-freedom systems, the spectrum technique can be used, as discussed in the paragraphs that follow, for the design of multi-story structures.

10.4.1 Design for Horizontal Motions. The use of the single-degree-of-freedom response spectrum for a multi-story building represents an approximation which requires study. The background of experience with earthquake resistant design indicates that the approximation can be useful. Rigorous use of the spectrum concept is possible only by consideration of the individual modes of dynamic response of the multi-story structure. An exact method for the elastic analysis of a complex system is outlined in Section 10.6.

There are several reasons why a design spectrum can be lower in value than the response spectrum plotted as described in Section 10.2. Before failure of a building frame occurs, plastic action will develop, and the inertial forces will, therefore, be reduced. Response is further reduced by damping.

There is another influence about which little is yet known. This concerns the interaction of relatively heavy structures with the ground when ground motion occurs. Although the interaction is relatively slight, calculations that have been made in a preliminary fashion indicate that there is a series of peaks and valleys in the response spectra and that the valleys correspond to the true response of the actual structure for which the input motions are measured whereas the peaks correspond to responses of structures with slightly different physical properties.

Because of these factors, it is believed reasonably conservative to use, as a basis for design, a spectrum plotted as described in Section 10.2, with envelopes determined on the basis of the amount of plastic deformation that is permissible.

Insofar as a building frame itself is concerned, structural design can be accomplished with a reasonable degree of conservatism by using the design recommendations proposed for earthquake design (Ref. 10-9). The recommendations of Ref. 10-10 are similar to those of Ref. 10-9 and are more generally available. In general, for building frames, these recommendations consist of two parts: (1) a specification for the maximum base shear for which the design should be made; and (2) a specification for the distribution

of this shear over the height of the building frame.

The recommended force distribution over the height of the building corresponds to a linear distribution of acceleration ranging from zero at the base to a maximum at the top of the building. The accelerations corresponding to the design force distribution are shown in Fig. 10-8. Shown in this figure is a derivation of the equation for force distribution given in Refs. 10-9 and 10-10, in which the force at any elevation is given by

$$\frac{F}{V} = \frac{Wh}{\sum Wh} \quad (10-8)$$

in which F = lateral force at any height h above the base, corresponding to the mass of the building or weight of the building at that height

V = total lateral design shear at the base

W = the weight at the height h

h = the height above the base of the building

From the design spectrum which has been modified to account for inelastic action, one can read the accelerations and therefore the seismic coefficients to be applied to the total weight of the building to determine the maximum base shear, V . The base shear so obtained can then be distributed over the height of the building as outlined in Fig. 10-8 to determine the design shear at any elevation in the building.

In using the spectrum for a multi-story building, the frequency that corresponds to the lowest natural period should be used. Although a more accurate analysis taking account of the modal deformation of the building

can be made, such an analysis is not warranted in the light of present knowledge for the building frame design itself.

10.4.2 Design for Vertical Motions. In the vertical direction the situation is more complex. The high frequency of the building in the vertical direction, particularly in the vertical oscillation of the columns, makes it possible for the forces to be transmitted almost directly through the building to the intermediate floors. The floors will then oscillate as systems having a frequency corresponding to their frequency when partly fixed at the ends or simply supported, depending upon their connections, in accordance with their own mass and that of the weight which they carry. The maximum acceleration to which such floors will be subjected can be read from a spectrum plotted as described in Section 10.2.

Because the blast shock in the vertical direction may be greater than in the horizontal direction, there may be a necessity for investigating more carefully the vertical effects on the building. However, some brief study of this problem will indicate that ordinarily, unless the design accelerations are quite large, this will be unnecessary.

For vertical loads, ordinary elastic design procedures employing the usual factors of safety will produce a structural element having a dynamic yield resistance of approximately $2.2 (DL + LL)$, in which DL is the dead load magnitude measured in terms of force per unit of area, and LL is the live load magnitude measured in the same way. The factor 2.2 is an estimate of the ratio between the dynamic yield stress of the material and

the normal working stress. For static yield values the factor would be only about 1.7. With a redistribution of moments corresponding to limit loading conditions, the factor may be increased to as much as 2.5.

For a vertical acceleration of Ng , the design of the intermediate floors must be made for a downward load of N times the weight, plus the weight itself, or, in effect, a load of $(N + 1)(DL + FL)$, in which FL is the "fixed" live load or the live load actually in existence rather than the design live load. This might be taken as a sort of average value, because the local values are not of as great importance in determining the stresses as the average over-all value that actually is in place at the time of the shock.

The larger of these two relationships governs the design. If the fixed live load, FL , is equal to the design live load, LL , then in order for the dynamic effect to govern, the critical acceleration factor N must be greater than 1.2. But in general, FL is less than LL and N must be even larger. For $FL = 0.5 LL$, and $LL = 2DL$, which are reasonable average values, then the static design corresponds to a magnitude of 6.6 DL and the dynamic vertical design would correspond to $(N + 1)(2 DL)$, in which case, in order for the dynamic vertical design to govern, the factor N must be greater than 2.3. In general it will be seen that only in rare circumstances, for extremely high accelerations, will it be necessary to take into account the vertical dynamic effect if the design is made under the usual static requirements for the dead load and live load effects.

10.5 SHOCK EFFECTS ON MOUNTED EQUIPMENT

10.5.1 Basic Considerations in Shock Mounting. This section is concerned with the problem of the attachment of equipment (mechanical, electrical, hydraulic, etc.) to the protective structure. The equipment must remain attached throughout a blast and must function in the post-blast state. It is obvious that the attachments must have sufficient strength to transmit the forces which are associated with the equipment accelerations and with the relative distortions of structure and equipment. The stiffness of attachments must be considered not only in relation to its influence on the magnitudes of transmitted forces but also from the point of view of possible limits of acceptable relative displacements of equipment and structure.

Since the problem relates to the mounting of equipment, rather than to the articulation of major structural components, it can be assumed that the attached mass is relatively small in comparison with the mass of the structure. It follows that the attachment forces are negligible in comparison with the direct effects of the blast, and the motion of the structure is nearly independent of the forces transmitted through the attachments. Motion of the structure is taken as the basic input for which the mounting must be designed. These input data must be obtained from an analysis of the response of the structure to ground shock and air blast, or must be assumed.

Maximum accelerations or displacements which can be tolerated by the equipment must be known or computed. For complex items, such as electronic equipment, this information should be supplied by the manufacturer. The permissible accelerations and distortions of many other items, such as piping, ductwork, machinery bases, etc., often can be investigated directly by the mounting designer.

10.5.2 Provision for Relative Distortion of Equipment and

Structure. When equipment must be connected to the structure at two or more points, and when significant relative displacements of these points are anticipated, the capacity of the equipment and attachments to accommodate such displacements must be investigated. Cases of this kind are not limited to the obvious situation in which the equipment is attached to two structures having independent motion components. Quite often structures are designed to undergo substantial distortion, particularly in flexural modes.

It should be emphasized that the relative displacement of attachment points may be accommodated by elastic or elasto-plastic distortion of the equipment, by flexible joints, slip-couplings or other devices incorporated in the equipment, by elastic or elasto-plastic distortion of the attachment, or by some combination of these factors. It may be quite unrealistic to attempt to supply all of the required accommodation in the attachments. In the case of piping or conduit, for example, provision of bends or loops rather than a straight run between the connected points may permit the entire relative motion to be absorbed by flexural distortion of the pipe.

10.5.3 Nature of Elastic Systems Comprised of Mounted Equipment.

In general any piece of mounted equipment comprises a multi-degree-of-freedom elastic system (or elasto-plastic system) which responds to the motion of its support points (points of attachment to the structure). If the equipment is so connected to the structure that relative distortions of the structure can be accommodated without serious stresses in equipment and attachments, a desirable condition, the stresses in the equipment and forces transmitted

through the attachments will be primarily a function of accelerations of the equipment. The major problem of analysis thus is the determination of equipment accelerations. The products of equipment masses (concentrated or distributed) and corresponding accelerations represent loadings for which the corresponding stresses and support forces can be found by conventional methods of stress analysis.

Every system has many degrees of freedom and corresponding modes of motion, and the total motion is comprised of the sum of the responses in each mode. Fortunately most systems have only a very few, easily recognized modes of predominant significance which contribute most of the response in a specified direction of support motion. Consequently, it usually is sufficient to determine the response in each (often only one) of these predominant modes. When it is deemed necessary to determine the response in more than one mode, advantage should be taken of the fact that peak values of stresses and reactions in the separate modes are unlikely to occur simultaneously. Thus the combination of values from the separate modes should be based on probability considerations.

In some instances the flexibility of a piece of equipment and its attachments may be limited almost entirely to the latter. This would, for example, be the case if an electric motor were attached to the structure by relatively soft spring mountings. In other cases the attachments may be very rigid and the equipment may be relatively flexible. An example of the latter would be piping having a relatively small ratio of diameter to distance between points of support.

In many instances for which the equipment has a mass distributed over considerable length, or area, it is convenient to approximate the distributed mass by one (or a few) mass concentrations.

If a light piece of equipment is mounted on a mass M , and if the equipment mass is so small that it does not affect the response of M , in general the equipment acts like a system subjected to a revised base motion, which is the time-dependent motion of the mass M . Unfortunately, this absolute motion of M cannot be obtained from a spectrum such as Fig. 10-1. However, it can be inferred that the maximum motion of M can range from a minimum value of $x_m - u_m$ to a maximum value of $x_m + u_m$ where x_m is the maximum displacement of the base and u_m is the maximum displacement of M with respect to the base, though this range is probably too large to be useful.

Nevertheless, a value of maximum acceleration can be obtained from the spectrum, and this value provides an upper limit of acceleration for the equipment. Under the worst possible conditions, the response of mass M , which is the base of the equipment, will be a simple harmonic motion of magnitude corresponding to the maximum acceleration determined from the response spectrum. If the equipment is subjected to such an input, its response is a function of the ratio of the equipment frequency to the frequency of the motion of mass M .

The ratio of the equipment acceleration a_e to the "structure" acceleration a_s is given by the expression

$$\frac{a_e}{a_s} = \frac{1}{1 - (f_s^2/f_e^2)} \quad (10-9)$$

where f_e = frequency of the equipment
 f_s = frequency of the structure

This relation is not valid when f_e is nearly equal to f_s . However, it indicates that the acceleration of the equipment will be less than twice that of the structure (or of mass M) when the frequency of the equipment is more than 1.4 times that of the structure, or less than about 0.8 times that of the structure. In other words, high acceleration in the equipment can be avoided by not "tuning" the equipment to the same frequency as the structure.

For example, for a structural frequency of 3 cps and the response spectrum of Fig. 10-1, the equipment acceleration will be less than 5g, provided that the equipment frequency is less than 2.4 cps or greater than 4.2 cps. This frequency range may be avoided by appropriate shock mounting of the equipment, or it may have been implicitly avoided by the very nature of the equipment itself.

10.5.4 Response of Light Equipment Mounted on Building Frame Members. For equipment mounted on the bottom floor, if the floor is supported directly on rock, or for equipment near points of support such as columns (for vertical motion), the equipment will be subjected to the same intensities of input motion as is the base; consequently, the response spectrum drawn for the base input motions should be used directly for the equipment. However, if the equipment is mounted on interior elements which are themselves flexible or which may become plastic, the response spectrum for the equipment

should be modified because the equipment base is now subjected to a revised input motion which is, in fact, the absolute motion of the structural element to which it is attached.

Only preliminary studies are available for this problem. They indicate that, for frequencies outside the range in which the structure or structural element becomes plastic, the part of the structure which acts as a base for the equipment responds in the same manner as if the structure remained elastic. However, this motion is now different from the original structural base motion, and the response spectrum of the equipment is thereby affected.

At the present time it is not possible to develop a simple, generally applicable design procedure for the equipment mounted on flexible interior elements without a complete analysis of the system consisting of the structure and the equipment. It is therefore recommended that each problem of this type be considered individually using the more rigorous procedures outlined in paragraph 10.6.

10.5.5 Shock Effects on Heavy Equipment. The procedures described above for determining the response of light equipment are not unreasonable, although in some circumstances the response may be even greater because of resonance. One should avoid particularly a frequency of the equipment equal to the frequency of the member on which it is mounted. When the equipment is heavy, however, there is a feedback mechanism in which the response is less than it would be by the methods described above. This problem is under study. No definitive analytical means are yet available

for handling the problem in a simple fashion. Consequently, it is recommended that the same procedures be used as for light equipment, although it is recognized that such procedures may be over-conservative. In special cases, an analysis can be made of the actual system.

10.6 THEORETICAL APPROACH FOR COMPLEX LINEAR SYSTEMS

In general, the analysis for a multi-degree-of-freedom system subjected to blast shock can be made analytically with a procedure which involves a number of steps as follows:

(1) For the complex system, find the modes and frequencies. For each mode find the stress, or other quantity desired, at the point considered.

(2) If the system is one which is subjected only to base motion, find the excitation coefficient for each mode. This is defined as the expansion of a unit deflection of all the masses, in the direction of the base motion, into a series of modal deflection shapes. The excitation coefficient is the coefficient of the particular modal shape in this expansion. For other kinds of input motion, the excitation coefficients have to be defined in a different fashion. This is not discussed here.

(3) Now determine the response spectrum for the quantity desired for a single-degree-of-freedom system.

(4) The modal response is then determined as the product of the stress, or other specified quantity in each mode, times the excitation coefficient for that mode, times the response spectrum value for the frequency of that mode.

(5) The maximum response of the system for the particular response quantity that is desired is less than the sum of the modal maxima.

(6) For a system with several degrees of freedom, the actual maximum response will not ordinarily exceed greatly the square root of the sums of the squares of the modal responses. Even in a two-degree-of-freedom system the excess will be less than thirty percent. Consequently, the root mean square value can be used as a design basis rather than the sum of the modal maxima, particularly where the number of modes is three or greater.

10.7 REFERENCES

- 10-1 Newmark, Hansen and Associates, "Protective Construction Review Guide - Hardening, Volume I," Revised June 1, 1961, for Office of the Assistant Secretary of Defense. (UNCLASSIFIED)
- 10-2 Committee on Structural Dynamics, Engineering Mechanics Division, ASCE, "Design of Structures to Resist Nuclear Weapons Effects," Manual of Engineering Practice No. 42, 1961. (UNCLASSIFIED)
- 10-3 Biot, M. A., "Analytical and Experimental Methods in Engineering Seismology," Trans. ASCE, Vol. 108, 1943, pp. 365-408. (UNCLASSIFIED)
- 10-4 Hudson, D. E., "Response Spectrum Techniques in Engineering Seismology," Proc. World Conf. on Earthquake Engineering, Earthquake Engineering Research Institute, Berkeley, California, 1956, pp. 4-1 to 4-12. (UNCLASSIFIED)
- 10-5 Housner, G. W., "Behavior of Structures During Earthquakes," Journ. Engineering Mechanics Division ASCE, Vol. 85, No. EM-4, October 1959, pp. 109-129. (UNCLASSIFIED)
- 10-6 Fung, Y. C., "Shock Loading and Response Spectra," Colloquium on Shock and Structural Response, ASME, November 1960, pp. 1-17. (UNCLASSIFIED)
- 10-7 Barton, M. V., "Ground Shock and Missile Response," Colloquium on Shock and Structural Response, ASME, November 1960, pp. 69-79. (UNCLASSIFIED)
- 10-8 Veletsos, A. S. and Newmark, N. M., "Effect of Inelastic Behavior on the Response of Simple Systems to Earthquake Motions," Proceedings Second World Conference on Earthquake Engineering, Tokyo, 1960, Science Council of Japan, Veno Park, Tokyo, Japan. (UNCLASSIFIED)
- 10-9 Structural Engineers Association of California, "Recommended Lateral Force Requirements," Draft copy, 2 October 1960. (UNCLASSIFIED)
- 10-10 Anderson, A. W., Blume, J. A., et al, "Lateral Forces of Earthquake and Wind," Trans. ASCE, Vol. 117, 1952, pp. 716-780. (UNCLASSIFIED)
- 10-11 Newmark, N. M. and Hall, W. J., "Preliminary Design Methods for Underground Protective Structures," AFSWC-TDR-62-6, June 1962. (SECRET)
- 10-12 Veletsos, A. S. and Newmark, N. M., "Design of Shock Isolation Systems for Underground Protective Structures, Vol. 2 - Response Spectra," Interim Report, June 1962; prepared for Air Force Special Weapons Center. (UNCLASSIFIED)

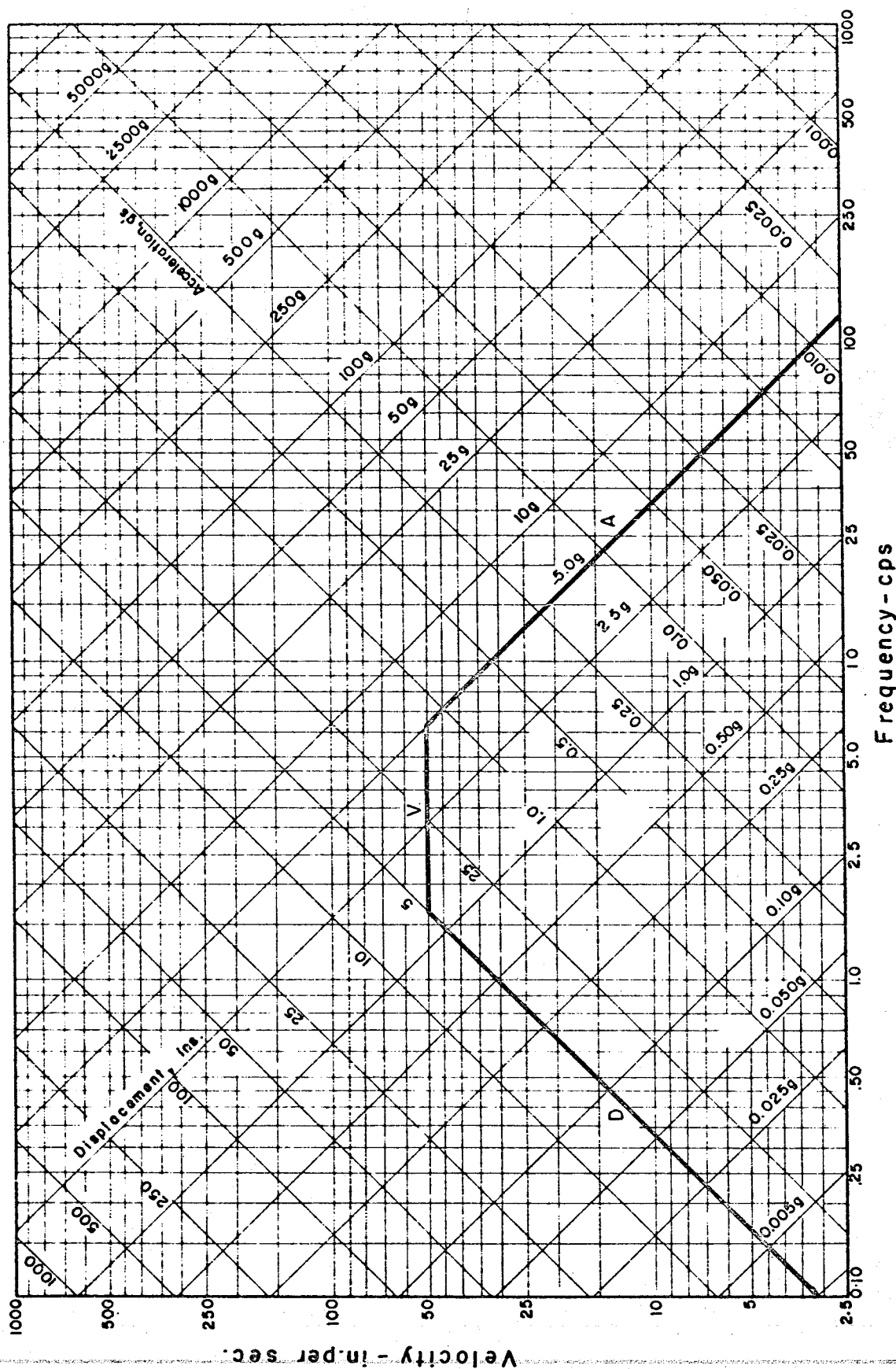
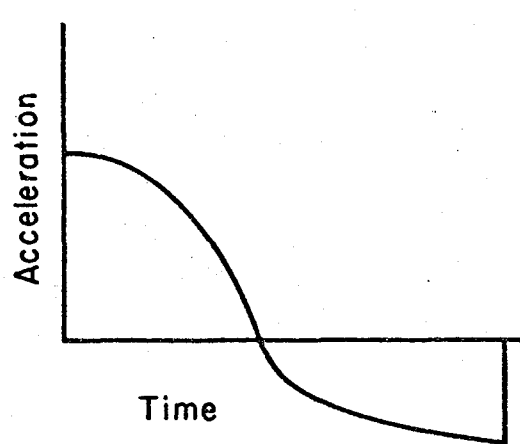
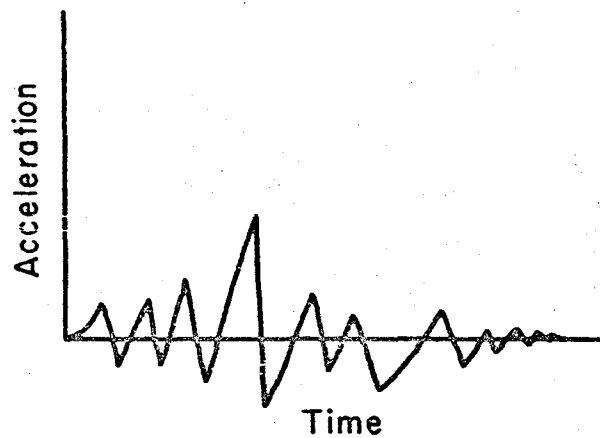


FIG. 10-1 TYPICAL RESPONSE SPECTRUM. (Values shown have no physical significance - they are used for illustration only.)

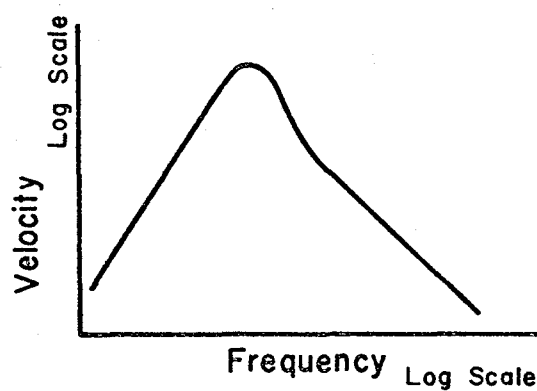


(a) Systematic

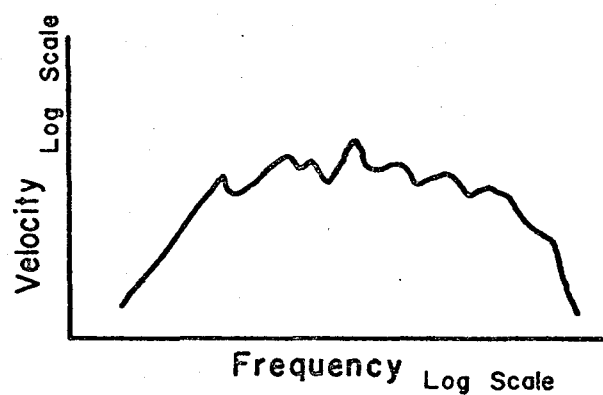


(b) Random

FIG. 10-2 COMPONENTS OF GROUND MOTION

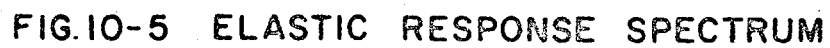
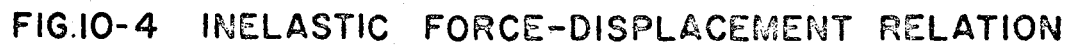


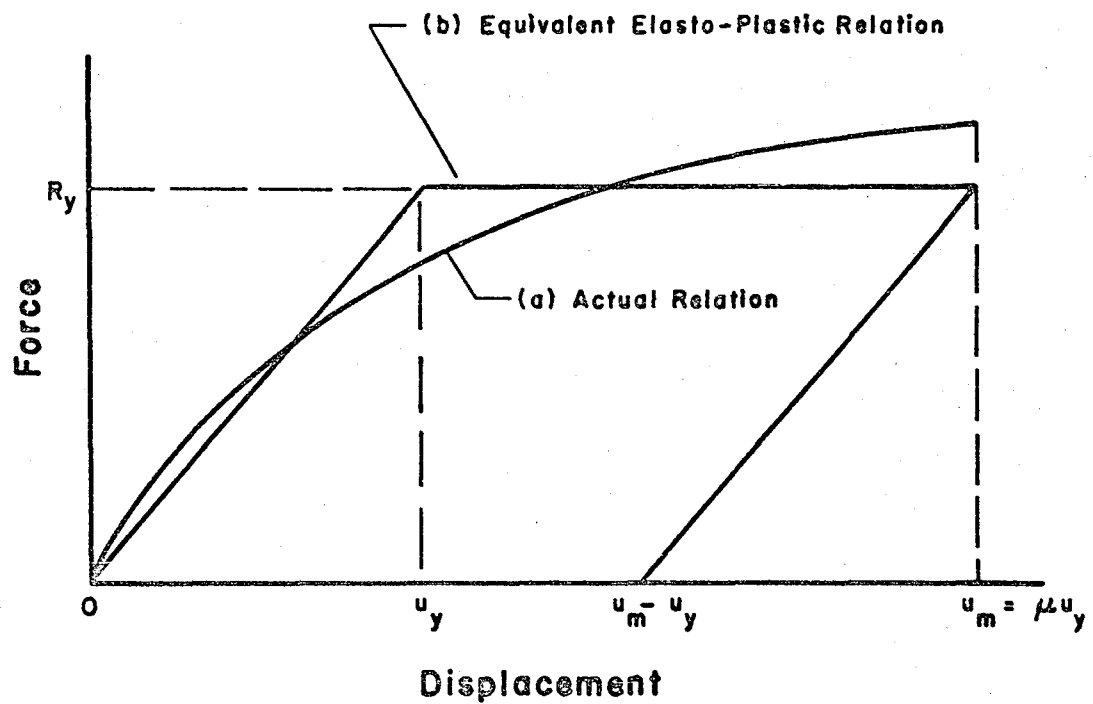
(a) Systematic



(b) Random

FIG. 10-3 RESPONSE SPECTRA





**FIG.10-6 REPLACEMENT OF AN INELASTIC
LOAD-DEFLECTION RELATION BY
AN ELASTO-PLASTIC RELATION.**

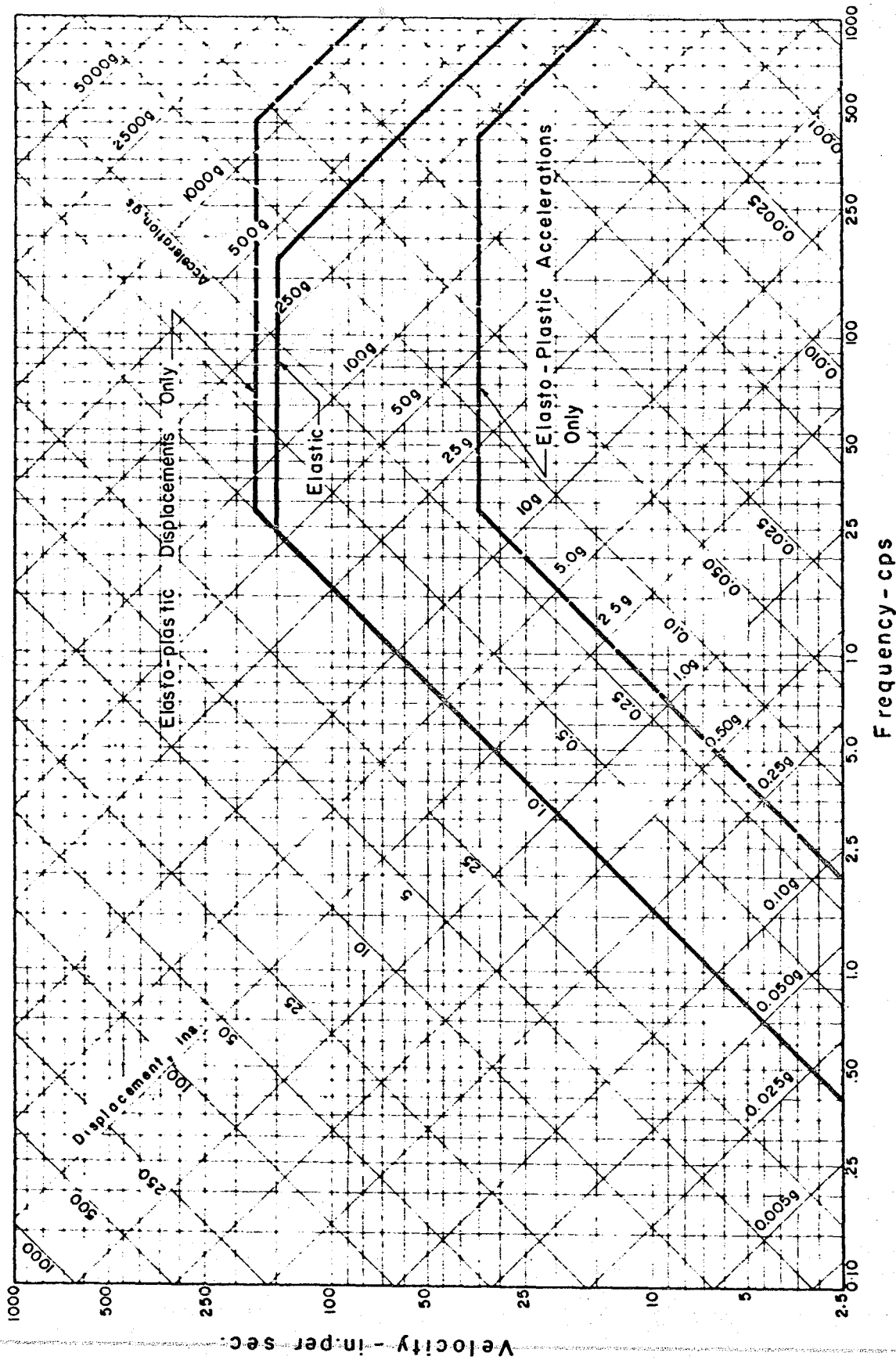
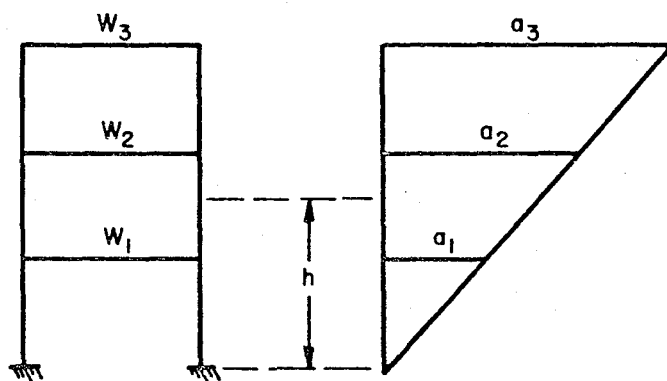


FIG. 10-7 ELASTO-PLASTIC RESPONSES FOR A SYSTEM WITH A DUCTILITY FACTOR OF 5.



$$a = ch$$

$$F = ma = \frac{W}{g} ch$$

$$\therefore F = CWh$$

$$V = \sum F = C \sum Wh$$

$$\therefore \frac{F}{V} = \frac{Wh}{\sum Wh}$$

FIG. 10-8 ACCELERATION CORRESPONDING TO DESIGN
FORCE DISTRIBUTION OVER HEIGHT OF
BUILDING FRAME

CHAPTER 11. ARCHITECTURAL CONSIDERATIONS

11.1 GENERAL APPROACH

In planning a facility to resist the effects of nuclear weapons, consideration must be given to the following factors: (1) the immediate nuclear and thermal radiation; (2) the shock transmitted through the ground; (3) the blast forces; (4) the radiation from fallout and the induced radiation resulting from the immediate neutron effects on materials. Because of the increase in weapon yields and potential devastation by these factors, it is becoming increasingly necessary to consider the design and construction methods for buried protective structures. For this reason most of the emphasis in this section will be on underground structures. However, as there will still be some cases where above-ground hardened facilities must be provided, this type of construction will also be covered from the standpoint of doors and entranceways, architectural and structural details, foundations, and cost comparisons.

Shielding criteria and the relative merits of various structural materials as a means of reducing radiation will not be discussed in this section.

Totally buried structures and those partially buried with a mounded earth cover are obviously more readily concealed and are less susceptible to flying debris. The earth cover is less efficient than heavier structural materials as a protecting medium against radiation but it is usually the most economical material for this purpose. The increased earth cover decreases the effective loading under given blast conditions and, in addition,

blast reflections and drag forces are considerably reduced by the silhouette of the mound.

Naturally there are disadvantages in using buried structures in preference to surface structures. Among these are the difficulty of providing easy access, the problem of possible ground water leakage, and the necessity of providing artificial ventilation even for normal conditions of use. Yet, in many instances, the underground structure maintains an advantage over the surface structure.

Under certain conditions, it might be found justifiable to make use of existing tunnels and mines or newly excavated and reinforced tunnels. It has been reported that there are hundreds of millions of square feet of mine space suitable for shelters.

An additional factor in planning a facility which may be significant is the possibility of fire conflagrations or "fire-storms" in the area of the shelter. It was learned in World War II that many people died in shelters under such conditions due to CO poisoning or suffocation.

It is essential also that careful consideration be given to the selection and design of the utility system and services that are necessary to insure full operational capability of the facility at all times.

After considering function, importance of operation, damage to what items and to what degree would constitute "failure", and probabilities of attack and survival, it is then necessary to compare relative costs of alternate types of structures in order to make the best selection for the particular conditions.

This section will include discussions and recommendations for: entranceways, doors, ventilation and blast-valves, foundations and sealing, structural details, miscellaneous architectural considerations and costs.

Much of the material was taken directly from Ref. 11-2, as this was believed to be the best available source presenting a comprehensive and concise discussion of the items listed above. Additional references are listed at the end of this chapter.

11.2 ENTRANCEWAYS

Where it is possible to do so, entrances should be shielded such that radiation and reflection of the blast will be a minimum. Right angle turns in entranceways are effective in attenuating radiation but a continuous entranceway, preferably a ramp, which can be entered from either end has the advantage of no reflecting surfaces and consequent "pressure-traps".

If below the water-table, the entranceway may encounter the same problems of drainage and waterproofing as discussed in the section on "Foundations".

11.3 DOORS

11.3.1 Protective Doors. The intended function of a protective installation may be achieved or lost according to the attention that is given to the doors. It cannot be overemphasized that doors, particularly large doors, represent a major structural-mechanical design problem, and that door requirements often may influence the type or proportions of the main structure. Door proportions may be such as to significantly affect

the structural integrity of the basic structure, as in the case of domes. Careful study of this problem is further necessitated by the fact that the total cost of a large door, including its mechanical and electrical components, can represent a significant fraction of the total cost of the protective installation. It follows that door studies should be initiated at the outset of the over-all planning and design. As a corollary, the reviewer of a proposed protective installation should scrutinize the door provisions most carefully.

It should not be inferred that every door requires detailed design study. On the contrary, small doors, particularly those which are not so located as to experience all of the weapons effects, should be standardized types whenever possible. Such small doors occur frequently throughout the field of protective construction (in most cases as emergency personnel exists), and standardization is highly desirable to minimize costs and construction delays. For personnel entrances or emergency exits in underground structures, closures of the type used in bulkheads of ships or of the type used in submarine hatches may be adequate.

11.3.2 Types of Doors. In general, doors may be classed in accordance with their attitude: either horizontal, vertical or inclined; and with respect to their method of opening: sliding or rolling, hinged on one side, or opening from hinges on both sides with a joint down the center. A third method of classification involves the configuration: whether the door is flush with a surface, or in a recess where, under certain conditions, advantage may be taken of the containing element in supporting the door when it is subjected to blast forces.

There are advantages and disadvantages in each type of configuration, method of opening, or attitude. Horizontal doors have the advantage that they are subjected only to side-on overpressures whereas inclined or vertical doors may be subjected to the much higher reflected pressures rising from a blast. On the other hand, horizontal doors may have to be larger than vertical doors to provide entrance to certain items of equipment or personnel although they may have advantages in openings for missile silos where only a vertical ingress to or exit from the enclosure is needed.

Sliding flush doors have certain advantages in mechanical simplicity although some difficulties are presented with regard to the exposed free edge in the direction of the sliding opening. Such a free edge is exposed to blast forces and drag pressures for which provision must be made in the supports of the door. Difficulties are also encountered in providing for the seals against blast pressure and dust. Provision must be made for removal of debris either by the door itself as it slides forward, or through auxiliary means in order to permit opening of the door when the surrounding area is covered with the debris resulting from a close-in burst. Some of these disadvantages are overcome by doors which swing on hinges of the single or double-leaf type. Such doors may be made to be practically self cleaning of debris, but generally require more careful attention to detail in the mechanical arrangements at the hinges than do sliding doors. Special provision must be made in double leaf doors for the sealing of the enclosure where the free edges meet. The relief of the hinges from blast loading also presents mechanical

problems which can be solved, although not simply. Doors which must remain open for operations in severe wind storms present additional problems. Flush sliding doors provide less resistance to winds and less turbulence in the region of the enclosure than do doors which stand up in the wind stream when they are open.

Vertical doors may also be hinged or may slide. Sliding vertical doors are usually supported at their bottom surface. Hinges for vertical doors are usually most conveniently provided at the bottom so that the door swings open as in a drawbridge, or at the top in which case the door may swing either outward or inward. However, heavy doors are difficult to swing from hinges at the top and to support when they are closed.

In addition to the door types discussed above, there may be other unusual types of doors that may offer many special advantages for particular uses. For very high overpressures, doors may be used which are relatively thick and slide into place against a solid wall so that the door itself is not subjected to high stresses under blast conditions. When the door is slid to one side into a pocket, a right-angled entranceway is formed which may be adequate for personnel and for small vehicles but is generally not capable of being made adequate for large vehicles or equipment. Other types of doors may involve plugs of rock or earth which can be removed after a blast, but not quickly. Such doors would not ordinarily be adequate for installations which require a short reaction time. Other energy absorbing doors such as doors involving masses of water or mechanical energy absorbers may find particular uses. In general such doors involve a great deal more complexity than do simpler and more rugged, although possibly

more massive, doors.

11.3.3 Functional Requirements.

(a) Existence of Alternate Openings of Similar Function.

Is the installation such that more than one opening is desired under day-to-day or attack conditions? If necessary, can the installation function after an attack with less than the total number of doors operable? If so, can alternate openings be oriented to avoid or minimize the probability of full weapons effects at all locations?

(b) Exposure. Is the opening at an exposed (i.e., surface) location or is it within a tunnel or other shielded location? In the latter case some weapons effects (thermal, radiation, reflection increments to shock pressure, dust and rubble) may not have to be taken into account in the door design.

(c) Day-to-Day Function. Does the door have to operate fairly frequently, in day-to-day functioning of the installation? Only infrequently? Only rarely (as a check on readiness)?

(d) Time Available for Operation. What is the maximum time that can be permitted for door opening and for door closing under attack conditions? In day-to-day operation?

(e) Number of Post-Attack Operations. Is it only required that the door survive one attack, or must the closing-survival-opening cycle be guaranteed through several successive attacks?

(f) Orientation Requirements. Is the purpose of the opening such that the door must be horizontal? Or vertical? Or can the orientation be selected to minimize door loading without regard to function?

(g) Susceptibility of Installation Contents to Various Weapons Effects. For the human or material contents of the installation, is protection required against all attack effects (blast, heat, radiation, chemical and biological contamination)? Are the contents insensitive to one or more of these effects? Is the occurrence of one or more of these effects deemed improbable?

(h) Required Size and Shape of Opening. Although size and shape of opening are obvious criteria, it seems necessary to emphasize that an underestimate of these requirements may impair the function, and an over-estimate will needlessly increase costs.

(i) Operational Limits on Position of Opened Door. To avoid interference with operations, are there limitations on positions of the opened door?

11.3.4 Important Door Characteristics.

(a) Strength and Stiffness. If some plastic deformation can be accepted, this will reduce the strength required to resist the given blast pressures. The extent to which such deformation can be tolerated depends not only upon the failure mode of the door but also upon the influence of distortion on subsequent operation. In particular, excessive distortion may jam the door so that it cannot be opened, or cannot subsequently be closed; may break joint seals or make a tight seal in subsequent closing impossible. Also, due to the door's large mass, latches and hinges may be severely damaged by the force of the door in motion due to ground shock.

(b) Weight. The required thickness may be governed by required resistance to radiation effects, in which case the weight may not

be subject to measurable control by skillful structural design. When thickness is governed by blast loading, however, the weight may vary widely with door form (dome, slab, etc.), method of support (full perimeter, two-edge, points, etc.), materials (steel, concrete, or combination), internal structure (solid, cored, sandwich).

The size and cost of mechanical components of large doors may be very sensitive to the weight of door structure. This would be particularly true in those door types for which the (unbalanced) mass must be lifted. It is to be noted that the cost of mechanical-electrical components (trunnions, rollers, jacks, power cylinders, linkages, gears, motors, tracks, etc.) may be a large fraction of the total cost. Accordingly, an increase in cost of door structure to reduce weight, may reduce the overall cost of a large door. In addition, reduction in weight of door structure may be significant in terms of reduced power requirements.

(c) Shape of Exposed Surface. In many cases, the most appropriate solution of the door structure is a flat slab of concrete or steel, and the major exposed surface is a large flat plane. For more effective use of the material, dome types also have been considered. In the latter type much of the inherent strength advantage may be lost because of a more severe loading associated with reflection and drag effects on the dome surface, in contrast with loading on the plane surface of the slab type. This difference in loading is particularly pronounced when the slab type door is recessed to make its outer surface flush with the outer surface of the main structure. This arrangement is particularly effective for horizontal doors (vertical entrance) designed for resistance to the blast

effects of a surface burst. In this situation the two advantages achieved by a flush surface (with adequate sealing of the perimeter joint) are: elimination of reflection effects in the blast loading; elimination of forces in the door plane due to drag and due to blast pressure on the vertical edges. When the door must be vertical (horizontal entrance) the dome shape is not at a disadvantage with respect to forces normal to the plane of the protected opening; however, it is less satisfactory than the recessed slab type with respect to forces in the plane of the opening.

Door designs of the dome type where the door is actually an integral part of a structural dome are being investigated at this time. The basic idea is for the door to be a spherical segment with rib edges which meet and attach to ribs at the jambs to assure structural integrity and transmit moment and direct stress. A connecting device similar to this has been built at the David Taylor Model Basin to hold the cover on a tank 12 feet in diameter at pressures up to 1500 psi.

It has been suggested that large doors designed for high overpressures may be of the "catenary-arch" type to prevent excessive horizontal thrust to the vertical ribs on arch structures as in the case of dome-shaped doors. This door consists mainly of a vertical end rib of the same shape as the main arch rib and a horizontal rib of the same shape at ground level. Curved plates, possibly of a double-membrane for energy absorption, are suspended between these two ribs providing catenary-arch action to resist loads primarily by membrane stresses. Earth cover would be virtually impossible, though, and horizontal forces to the vertical-rib due to reflection and drag pressures could still be a serious problem.

(d) Degree of Protection Afforded Door Mechanism.

Exposed parts of a door mechanism may be damaged, and the door rendered inoperable by heat, fragment missiles, rubble, or dust. Whether one or more of these hazards must be considered depends upon door location (at surface or well within a tunnel or other shielding), nature of adjacent terrain surface, proximity to other buildings or equipment which might furnish fragment missiles, and assumed weapon size and range.

When these hazards are present, preference should be given to designs which place all of the door mechanism within the protected space. In general, such complete protection is feasible. In the rare case of doors so enormous that a practical method of operation must involve rolling on exterior tracks, the protection of these elements may be a major problem.

Protection of the door mechanism involves not only the direct weapons effects listed above but also the effects of the very large forces transmitted by the door structure, and the distortions and motions which the door structure may experience. Door forces during blast are very much larger than dead weight forces. Thus, while the mechanism can be designed to work against the latter, it is not feasible to provide even static resistance to the former. For this reason, and because resistance to distortion and relative motion requires large mechanism forces, the operating mechanism should be isolated from these forces and motions when the door is in the closed position. Support for the closed door structure should be independent of the trunnions, rollers, struts, and other elements of the door mechanism. In addition, the mechanism must be resistant to the effects of ground shock.

(e) Reliability of Mechanism Power Source. Small blast valves and doors may incorporate integral power sources in the form of compressed springs, explosive cartridges, and power cylinders. Because of the small door mass in these cases, the power requirements are small and emergency hand-operation often may be provided.

Large doors often require very large power expenditures for short periods of time. For day-to-day operations, this power can be drawn from a central source, even a source exterior to the installation. In such cases, however, a parallel standby power source should always be provided within the protected space. Consideration should be given to the use of hydraulic-pneumatic power systems which have the advantage of requiring relatively small electric power input to a pressure accumulator.

In some cases, it may be possible to utilize counterweighting to reduce the power required for door operation. In other cases, gravity forces may be employed to open (or close) the door without power input.

(f) Reliability of Warning and Triggering Devices. It is essential that remote warning devices and circuits be provided to initiate door closure, and that these provisions be matched with the door closure time. Consideration should be given to "fail safe" circuitry which will initiate door closure in the event of failure or malfunction of devices or circuitry.

11.4 VENTILATION AND BLAST VALVES

Ten cfm per person is generally regarded as sufficient fresh-air requirements for personnel for prolonged "buttoned-up" periods. For short

periods of a few days, it may be as low as three cfm per person if little physical activity is required, but supplementary odor removal equipment would be required. In the event of a prolonged attack, or prolonged high radiation above the filtering capacity, "fire-storm", or the presence of gas, an independent air source must be on hand to provide minimum personnel needs for extended periods of complete shelter sealing.

Vents for air intake and exhaust provide the same problems as doors if closures are to be provided. It is very simple, however, to provide protection for covers over small openings even for high overpressures. A "poppet" type closure valve has been tested and has functioned satisfactorily at overpressures up to 100 psi with no appreciable damage. To be effective, the valve must close before or immediately after the arrival of the shock wave, and it was learned that larger valves don't operate quickly under short duration blasts due to the inertia of the moving parts. Although large valves may be complex and expensive, they permit ventilation during a prolonged threat and after attack. They are obviously more economical than fully-enclosed air purifying units such as are used on submarines. Important closure features are: (1) closing time; (2) pressure level that must be withstood; (3) control of pressure build-up and radioactive intake during all phases of an attack. A latching device would probably be needed to retain the disk in a closed position when negative pressures could damage equipment or collapse ductwork. Also, it should remain closed until the radiation level is tolerable. Inspection and operating maintenance of the valve would be essential.

For very small ducts, it may be possible to allow the blast to pass through into the structure by reducing the blast pressure by means of a perforated straight pipe, or preferably, a perforated pipe plus a housing ("muffler" type). These are much more efficient attenuators than right-angle bends in a duct or pipe system and they are indifferent to orientation.

In many cases, a large bed of sand may be used to attenuate blast pressures without providing a mechanical closure. Such expedients may be desirable for air-supplies to power generating equipment, particularly where housed separately from personnel.

Pressures transmitted through ducts may be computed by means of a procedure given in Ref. 11-12.

To preclude chemical, radiological or biological contamination, it is necessary to filter outside air drawn into the facility. It will not be necessary to filter air for combustion engines if such air can be in an isolated circuit. If the blast pressures can be adequately attenuated in the duct system, relatively inexpensive filters might be used for fallout protection. Commercial fiberglass filters will only show moderate damage at 0.5 psi; AEC filters will show moderate damage at 3.0 psi and no damage at less than 2.5 psi. A series of such filters may provide an extra safety feature in that such filters also reduce the pressure. Electrostatic filters can withstand higher pressures and are effective but they are more expensive and require a constant power source. Under subsequent blast loadings, electrostatic plates lose most of their original dust holdings. For BW and CW protection, standard Chemical Corps filters are used. These may be preceded by ordinary dust filters in order to prolong their effective

life but use of more complex and repeated filtration is not warranted.

11.5 FOUNDATIONS AND SEALING

Very little information is available on the design of foundations for structures subjected to blast. The usual criteria stated in terms of allowable footing pressure or allowable pile load are not applicable. The soil generally has greater shearing strength or bearing capacity under high speed loading than under static loading; a bearing failure corresponding to overturning of a wedge or cylinder of soil beneath the footing is partly resisted by the inertia of the large mass of soil that must be moved. Both of these factors should be taken into account. Moreover, one must note that the blast loads a large area of soil nearly uniformly to pressures sometimes considerably greater than those allowed by static design considerations. The presence of this loading affects the bearing capacity for additional load, but does not necessarily reduce it.

In no case is it necessary for blast loading that the total area of the footings supporting the walls and columns of a structure exceed the area of the roof. At the worst, even in a soft soil, the structure can be built as a box with a base slab of the same strength as the roof. Such a structure will behave in the same way as the surrounding soil in general, regardless of the blast pressure to which it is subjected.

Where the structure is founded on or in a cohesionless material, or even a moderately stiff but unsaturated cohesive material, the area of the footings may be considerably less than the area of the roof. In such a soil, the resistance to penetration of the foundation increases with the

movement as friction develops in the material. If moderate amounts of motion are permissible, no special provision for bearing pressure under dynamic load need be made. However, the foundations must be adequate for the static load at the usual allowable soil pressures.

As a rough guide in proportioning foundations for cohesionless or stiff unsaturated cohesive materials, it is permissible to neglect for dynamic loading the uniform pressure equal to the applied surface loading on the ground since this uniform force would act even if the structure were not present. To provide for the additional pressure above this value, design the footings for twice the usual static allowable values.

For soft or saturated materials, the provision that the total footing area be equal to the roof area may be used. However, care should be taken that individual footings be proportioned to maintain a uniform bearing pressure. There will be little or no shear on the outer edges of the footings at the walls due to the balanced dynamic loading above and below the footing projection, but the shear as a result of the dynamic loading through the wall to the footing must be considered.

In the case of above-ground structures, additional resistance to overturning is gained to some extent by the exterior wall-footing cantilever, if large, as this "lip" on the windward side would be loaded before the corresponding areas on the opposite side of the structure. If the projection is large enough to be significant in this manner, then it would have to be designed to withstand the resisting moment. In most cases, sliding of the foundation will not be a problem.

If the water table is below the structure, the floor slab should be separated from the side walls, and it should be designed to support the floor loads resulting from the use of the structure.

When the water-table is above the floor of the structure, the floor must be supported by the side walls to resist the static uplift produced by the water pressure. Since the side walls support the floor in this case, the side walls also transmit the total dynamic roof force to the floor. Therefore, in this case, the floor essentially becomes part of the footing area as described above and should be designed for the same forcing function as used in the roof design.

Where the floor slabs are not integral with the walls, and where construction of contraction joints is necessary, sealing is a common problem. Sealers may have to withstand excessive deformations and high pressures. The most common sealers today are elastomers whose tolerance to radiation is being studied. Other sealers are asbestos, rubber, metals and pneumatic seals, the last being effective for sealing large clearances but of questionable reliability under severe conditions.

11.6 STRUCTURAL DETAILS

Since structural elements in a blast-resistant structure are required to develop their full plastic strengths, particular attention must be paid to what are ordinarily considered details as discussed here for concrete and steel construction. It is emphasized, however, that these so-called details are extremely important in developing dynamic resistance.

Reversals of stress and reaction direction may occur. Accordingly, unless otherwise specified by analysis, all members should be designed to have rebound strengths of at least 25 percent of the normal design strength specified by the blast loading.

11.6.1 Concrete Construction. Reinforced concrete is an excellent material for blast-resistant construction. It has large mass, inherent continuity and assures lateral strength. In addition, it has good shielding properties and is the best material for rigid shear and fire walls. Curved concrete structures have become more competitive with the increased use of pneumatically applied concrete. Strict attention must be paid to details in order to assure continuity, ductility, and resistance to loads in either direction. Thus continuity of reinforcement by adequate lapping or welding is desirable, but welding may be difficult for certain steels. Shear reinforcement, which is more necessary in blast-resistant construction than in ordinary construction, should be perpendicular to the axis of the member since inclined stirrups or main bars designed to carry shear become planes of weakness if the direction of loading or bending is reversed. Doubly-reinforced members with the reinforcing adequately tied have much more ductility than singly reinforced members and, accordingly, offer great advantage for blast-resistant construction. Joints are particularly important. They should be detailed and fabricated in a way which will insure ductile behavior of the completed element. Further, the ultimate strength of the least strong connecting element should be developed in the joint, if at all practicable. This would include the use

of diagonal bars across the joint to resist shear. In no case should the amount of reinforcing used on any face of the beam or slab exceed two percent of the cross sectional area of the element, in order to avoid brittle behavior. Further, if other than billet steel bars of structural or intermediate grade are used, particular attention must be paid to avoid brittle behavior.

11.6.2 Steel Construction. Steel also can be used very economically for certain types of blast-resistant construction. Arch or circular sections for underground construction, steel beams for composite construction, high strength columns, and steel doors for personnel or equipment entrances are elements which may be more economically constructed of steel than of reinforced concrete.

Ductility, continuity, and development of full plastic strengths at joints are also recommended for steel construction. Fully continuous beam-to-column connections also assure the adequate transfer of lateral shear without excessive distortion at the connection. Steel members designed for maximum plastic resistance should be able to experience large deflections without reduction in load capacity.

In the design of vertical members of continuous frame construction, fixed column bases, if combined with a suitable strong foundation, will increase the plastic resistance of the entire frame. Continuous welded frame construction has several times the plastic lateral strength of a corresponding truss-frame and the use of heavier roof construction increases the dynamic lateral resistance. In addition, if the column top is

restrained against rotation about both axes by members that frame in both directions, the plastic strength capacities of the column will be increased by reducing tendencies toward lateral buckling. Diagonal stiffeners can be used in corner connections to prevent large local angle change between connecting members due to shear yielding.

Though not likely, there may be cases where a structure is designed to resist an anticipated blast level while permitting the possible destruction of frangible panels. The use of such light panels over a steel frame virtually "levels-off" the peak blast load to the extent that the drag force on the frame becomes the significant design criterion. With such construction, it should be noted that long, slender columns would undergo local bending along with the stresses and distortions from translation and vertical forces. Fire protection may be a problem since exposed, loaded columns and trusses can collapse when directly exposed to fire for only 10 - 15 minutes.

Above-ground steel frames can have their effective lateral resistance increased by the simple, though sometimes awkward, expedient of wire-cable "stays".

11.7 UTILITY SYSTEMS

In this section, attention is called to the more important utility systems and building services that must be considered in the design of a hardened facility, and particularly pertinent summary recommendations are presented. For a comprehensive discussion of these items, the reader is

referred to Sec. 5.7 of Ref. 11-2 in which detailed consideration is given to all aspects of utility needs, including electrical power, heat units, air supply and conditioning, water supply and sanitation needs, and fire protection.

11.7.1 Utility Service Loads. Unnecessarily high utility loads result in oversized and costly equipment, consequently additional space and emergency standby material. An overestimate of equipment cooling requirements, for example, will pyramid into oversized and costly refrigeration and ventilation equipment, electric power equipment and excess emergency storage of ice or cooling water. The following factors are important:

(a) Ventilation. (See recommended requirements under section "Ventilation and Blast Valves".)

(b) Refrigeration. Cooling requirements for all equipment, particularly electronic, should be carefully established in order not to require excess cooling capacity. This problem is critical enough to warrant the acceptance of upper limits of operating temperatures. Above-ground cooling towers which are exposed to blast will be lost at relatively low overpressures. They should be backed up by appropriately sized ice or water storage which will provide sufficient cooling to permit emergency operation of equipment. In some cases, surface water reservoirs may be adequate.

The air-cooling loads must be reduced to account for tolerable temperature rise during "buttoned-up" periods and for losses to surroundings, particularly in the case of under-ground installations in rock.

(c) Heating and Air-Conditioning. Normal comfort (i.e. 75°F, 50% to 60% relative humidity) should be maintained for personnel for peace-time operations; but considerable, though not extreme, discomfort is acceptable during "buttoned-up" operations (50°F to 90°F, 20% to 80% relative humidity).

(d) Door Opening Mechanism. Since the opening of a door must be certain, and in many cases in a short period of time, use of hydraulic and pneumatic accumulators should be considered to minimize power requirements and to insure reliability of power for opening.

11.7.2 Water Supply. The absolute minimum water supply is one gallon of drinking water per man-day. It is recommended, however, that a minimum supply of 10 gallons per man-day be planned for the "buttoned-up" period and a more normal requirement is 100 gallons per man-day. Water may also be required for industrial or cooling purposes and for sanitary flushing. The latter will normally amount to 10 gallons per man-day. Chemical toilets can be provided as back-up during "buttoned-up" periods in order to provide greater water supply for other uses. Water supply is generally best obtained from wells within the protected installation. If wells within the installation are not feasible, water-well fields should be provided with blast-resistant construction and a certain power source for pumping.

11.7.3 Water Storage. Storage of water for both domestic and industrial purposes will generally be required. Storage of domestic water and a portion of the industrial water should be located within the installation protected against blast, chemical, bacteriological and radiological

agents. A portion of the water for industrial purposes may be located in surface reservoirs if contamination from fallout can be accepted in this system.

11.7.4 Lighting, Electric Power. Lighting should be provided at approximately 40 foot-candles in administrative areas, and may range from 5 to 50 foot-candles in other areas. A portion of the lighting system should be on an emergency circuit with automatic transfer switch. Portable emergency lighting units of the rechargeable battery-powered type should be provided in areas of heavy personnel concentration and areas of critical functions. For communication and other operational facilities which require large generating capacity and especially close power regulation, diesel engine and nuclear powered generators should be studied as the primary source of power.

11.7.5 Sanitary Sewers. The sewerage system should be designed so that the contaminated wastes may be delivered to a treatment facility, or in the event of its destruction, to a dumping area in such a manner that blast and chemical, bacteriological and radiological agents cannot enter the protected installation through the pipe. Check valves should be used if possible. Auxiliary chemical toilets should be provided.

11.7.6 Fire Protection. Fires in confined spaces are difficult to control and likely to be devastating. Accordingly, all precautions against the initiation and spread of fires should be taken in the planning of the installation. Areas which contain equipment or operations of extreme fire hazard should be isolated from others and the spread of fire and/or

fumes controlled by adequate blast and fire doors. Careful attention must be paid to all paths between areas, including ventilation, ducting, etc. Non-toxic hand fire-fighting equipment should be available.

11.7.7 Equipment Mounting, Utility Connections. Consideration must be given to shock mounting of all equipment. Generally, items which must remain in the same relation to each other should be mounted on a common rigid base. The base itself may be shock-mounted. Where relative motions can be anticipated, bends can be put in piping, slack can be provided in electrical cable, etc. Frame supported machinery (cranes, pulley lines, etc.) should be avoided, if possible, or designed to withstand the blast forces. Examination of Japanese factories in nuclear blast areas showed considerable damage to such items. Where exterior utilities pass through exterior walls, provision must be made for the relative motion between the structure and the adjacent earth in order to avoid rupture of the pipe or conduit. This may be done by encasing the utility line in a larger, more rigid sleeve extending a short distance from the base of the structure. This will protect the utility line at the critical point and permit some bending to take place without rupture.

11.7.8 Psychological Treatment. Ten to fifteen square feet per person is recommended as a desirable standard for the size of personnel shelters exclusive of operational space, air-locks, decontamination chambers, equipment areas, etc.

Acoustics may be a serious problem for personnel, particularly in concrete shelters with noise from operating mechanical equipment under prolonged "buttoned-up" periods. This can be relieved considerably by the

relatively inexpensive wall treatment of sprayed asbestos, or similar acoustic material.

11.7.9 Miscellaneous Facilities. Personnel decontamination facilities should be provided in at least two locations convenient to personnel movement.

The following additional facilities may be found necessary: food storage and preparation facilities, first-aid equipment and oxygen, emergency communications, functional equipment for personnel, emergency gear (shovels, hand-tools, etc.), radiac equipment and radiological safety gear.

11.8 COSTS

As in the case of conventional construction, the ultimate decision regarding the structural type to be used for a given design condition must be based on the relative economy of the appropriate types available. The desired result is optimum protection, considering degree of resistance and importance of survival, within economic capabilities.

Experience in costs of protective construction is limited to a very small number of actual construction projects and relatively few design studies. Three types of estimates may be made from data presently available: gross facility, limited costs and detailed costs.

11.8.1 Gross Facility Estimate. This provides a single unit cost (\$ per sq. ft.) for an entire facility, including all structural, mechanical, electrical elements, access, utilities, etc. It can be used only in cases where the facility in question is typically the same as one for which actual

construction cost experience is available.

Facilities for which there are sufficient data to permit use of gross facility estimates are listed in Table 5-6 of Ref. 11-21. Cost experience has been adjusted to reflect fiscal year 1961 cost indices, with geographical or location factors of 1.0. These costs may be used in estimating the cost of a proposed facility only if there is close similarity in all elements listed. In some cases adjustments may be possible if only a few elements are different. Other gross facility estimates may be found in Ref. 11-13.

Layout, cost and operational data for three types of industrial installations (two manufacturing and one storage) have been estimated and compared for the following three methods of housing:

- (a) Above-ground construction (conventional)
- (b) Suitable existing mine. Utilization of a suitable mine presented no element protection problems. Cooling was generally required where there were mechanical operations and dust-free areas were sometimes required. This type of installation initially cost 20 to 35 percent more than the same installation above ground for the operational plants but 20 percent less for storage areas. If figured on the annual operating cost, this type was said to be only 2 to 4 percent over the above-ground costs.
- (c) New excavations. The same plants in under-ground structures requiring new excavations were 45 to 60 percent more than the above-ground structures in the cases of operational units and 50 percent more for storage only. If figured on an annual operating cost basis, this

type would be approximately 3 to 6 percent more than the above-ground.

These estimates were made during the early post-war years and were based on limited examples of conventional (non-hardened) construction. It would seem, therefore, that if estimates were made for blast-resistant installations to perform the same size and type of functions, the annual operating costs of the mine installations would be less than the hardened structures above ground.

11.8.2 Limited Cost Breakdown. This reduces the total facility costs to nine elements, for each of which unit costs are provided as discussed. This method is applicable to cases where the level of protection, size and general configuration of the facility are known but advanced designs are not available and no direct experience data are available. It will be the most commonly used method in review of protective construction projects.

(A Detailed Cost Breakdown requires a near-final design for the facility and consists of the procedures used conventionally in cost estimating. It will not be discussed further here. It is, of course, the most reliable method. Special consideration must be given to the mechanical/ electrical costs and to access requirements.)

Table 11-1 presents a list of the major elements which should be included in a limited cost breakdown and suggested unit costs to be used in evaluating the contribution of each element. In some cases it is necessary to indicate ranges of unit costs and the estimator's judgment of the particular case will be required to select reasonable values within such ranges.

The costs of excavation and the structure itself have been shown as two separate items because depth of structure can vary over a wide range and excavation costs rise rapidly with depth of cover. The separation of the first three items of Table 11-1 requires that the estimator start with a minimum design concept. This concept must include the following items: type and size of basic structure, and depth of cover. From these he must determine at least approximate excavation and fill quantities and size of entrance structure. Figures 11-1 and 11-2 show the variation of cost of base structures as a function of type of structure. Figures 11-3, 11-4 and 11-5 show the variation for a particular structural type as a function of span or column spacing.

The additional costs of stairs or ramps in mounded or buried construction is to be included under Item 3 of Table 11-1. These items can be almost as costly as the basic structure, (Ref. 11-4) particularly when the basic structure is relatively small. Figures 11-1 and 11-2 are alike except that the curves of Fig. 11-2 include costs of entrance structures whereas Fig. 11-1 does not. For larger structures of a given type the cost of entrance structure should not increase appreciably with size of structure, any increase being primarily due to increase in depth of cover (if any) required by the larger basic structure. For example, a buried rectangular structure can be increased in size (plan area) without increase in depth of cover, and therefore without increase in cost of entrance structure. On the other hand, increase in the size of a buried dome requires an increase in the distance from the surface to the basic structure which must be provided for by the entrance structure. Thus the cost of entrance

structure must be increased in this latter case. To obtain an estimate of entrance structure for a structure of different size than is represented by the curves of Figs. 11-1 and 11-2, the following approach is suggested.

(a) By subtracting cost on the appropriate curve of Fig. 11-1 from the corresponding curve of Fig. 11-2, a cost-of-entrance-structure per square foot of the basic structure for which these curves are drawn is obtained.

(b) By multiplying the figure obtained in "a" by the area of the corresponding basic structure (listed in Fig. 11-1), a cost of entrance structure is found corresponding to the size of basic structure represented in Figs. 11-1 and 11-2.

(c) The cost found in "b" must be multiplied by the ratio of entrance size for the structure of interest to the entrance size for the structure represented in Figs. 11-1 and 11-2.

Figure 11-6 gives approximate costs of protective doors, per square foot of opening, as a function of pressure and size. The cost curves also consider the attitude or orientation of the door in terms of whether it will be subjected to side-on or reflected pressure. Costs of stairs, ramps or other access are not included in Fig. 11-6.

11.8.3 Principal Factors Affecting Costs.

(a) Level of Protection. The strength and cost of structural components must increase with the overpressure level to be resisted, and the results of design studies of cost often have been presented in the form of cost factors vs. design overpressure (Refs. 11-4, 11-5, 11-6). The

cost factors may be dollars, or dollars per square foot, or ratios of cost at given overpressure level to cost of conventional (non-hardened) construction. When data given in this form are intended to reflect total costs (structural, mechanical-electrical including air conditioning where required, etc.) they must necessarily be more approximate and less reliable because total costs cannot be expressed as simple functions of overpressure. On the other hand, data of this kind covering only the structural costs, and for specifically defined structural types, can be sufficiently accurate to be useful if properly combined with estimated costs of the appropriate non-structural items. When dollars per square foot are presented as the cost factor, the estimator should make certain that the areas used in computing such factors correspond to areas which are useful for the intended function. For example, in arch and dome construction perimeter areas may have to be discounted because of insufficient head room.

It is noted that overpressure is not always the governing factor in costs from the point of view of protection level. In particular, for surface structures designed to low overpressure levels, protection against radiation hazards (in the form of minimum thicknesses of structural components and provision for air filtering) may be much more important than overpressure levels.

The increase in structural resistance to blasts of an underground structure plus the economy in the use of earth cover for radiation protection may be enough to make the underground structure more economical despite the additional complexities of construction. Figure 11-7 shows the relative cost

factors vs. design overpressure for above-ground and below-ground structures.

(b) Size. From the point of view of direct structural costs, the required size, particularly the required clear span, is highly important. Figure 11-3 indicates the influence of clear span on cost for a simple rectangular form of structure. It must be emphasized that the question of size cannot very well be separated from the question of function. This may be illustrated by the fact that floor space provided in arched and domed structures is related to size of the structure and to whether multi-level floor systems can be utilized. If such utilization is feasible, larger spans in structures of this kind may be attractive.

For certain special cases, such as aircraft shelters, the necessary spans, and particularly the correspondingly large exits and entrances, dominate the cost (Ref. 11-7).

It is impossible to give rules as to the type of construction to be used in any particular case although some criteria for economy hold true in most cases. If clear spans greater than 20 to 30 feet are required (depending on the overpressure), arch or dome construction definitely should be considered as an alternative to slab construction. Also, as in conventional design, flat-slab type construction has the advantage of less depth compared to slab-and-beam systems which often offsets the cost of additional concrete. This might be of more significance in underground structures due to the cost of increased excavation.

(c) Number of Personnel and Duration of Occupancy. Human occupancy adds much to the cost of protective construction. Utilities, messing facilities, food and water storage, air-conditioning, are costly items dependent upon the number of people who must live in the protected structure and the anticipated duration of their occupancy.

(d) Function. It is apparent that all other listed factors are directly or indirectly related to the function of the protected installation. Both day-to-day and attack conditions of operation may be significant from the point of view of costs. The requirements for utilities, air conditioning, entrances, etc., may vary from a minimum in the case of a warehouse to a maximum in the case of a missile base or command center.

(e) Geographical Area and Specific Site Location. Factors which influence the cost of conventional construction are at least equally significant to the cost of protected construction. Proximity to transportation, power and water, and the local availability of labor and materials are pertinent considerations. To a certain extent these can be accounted for by the application of "Location Factors" such as those tabulated in Ref. 11-8. Wherever possible, however, cost estimates should be based on designs which give full consideration to local conditions, and location factors should be used only when better information is not available.

The cost of protective construction may be very sensitive to conditions at the specific site. The type of soil to be handled is a major factor in costs of excavation and foundations; the importance of this factor increases with depth of construction. Ground water may add greatly to the costs of construction operations and entail additional expense for waterproofing the structure.

Whether a particular structure is isolated or part of a complex, may influence direct construction costs as well as mechanical and electrical costs for the finished installation. Similarly the distances between structures in a complex may also influence direct and indirect construction costs.

(f) Other. A number of factors other than those mentioned above can affect the cost of protective construction. These include the following.

1. The degree of certainty in the design of the operational system to be protected.
2. The time urgency of construction.
3. Weather conditions at the construction site.

To cover the above costs, contingency items are included in budget estimates as well as allowance for government costs of engineering and design, supervision and inspection, and overhead. A factor of 21 percent of the basic contractors bid price has been applied to the curves presented herein.

11.9 REFERENCES

- 11-1 Merritt, J. L. and Newmark, N. M., "Design of Underground Structures to Resist Nuclear Blast," Volume II, Civil Engineering Studies, Structural Research Series No. 149, University of Illinois, Urbana, Illinois, April 1958. (UNCLASSIFIED)
- 11-2 Newmark, Hansen and Associates, "Protective Construction Review Guide-Hardening," Volume 1, prepared for the Office of the Assistant Secretary of Defense (Installations and Logistics), 1 June 1961. (UNCLASSIFIED)
- 11-3 Saunders, L. N., "Designing Entrances for Protective Shelters," BuDocks Technical Digest No. 80, September 1957. (UNCLASSIFIED)
- 11-4 "Engineering Study of Atomic Blast Resistant Design for Several Building Types," draft by Ammann and Whitney, Final Report, DA 49-129-eng-317, March 1960. (UNCLASSIFIED)
- 11-5 Curione, C., "Cost Guidance for Protective Construction," Technical Study No. 24, Department of the Navy, Bureau of Yards and Docks, 20 August 1958. (UNCLASSIFIED)
- 11-6 Koike, R. S., Morrison, T. G., and Tuggle, W., "Cost Planning Information," American Machine and Foundry Co., Contract AF 33(616)-2457 with Air Force Special Weapons Center, ARDC, October 1956. (CONFIDENTIAL)
- 11-7 "A Protective Alert Shelter for Strategic Air Command," Associated Research Design, Contract AF 18(600)-1636 with Air Force Special Weapons Center, ARDC, 1 April 1957. (SECRET, RESTRICTED DATA)
- 11-8 "USAF Pricing Guide for Permanent Construction on Continental U.S.," Directorate of Installations DCS Operations, Hdq. USAF, October 1958. (UNCLASSIFIED)
- 11-9 "The Effects of Nuclear Weapons," U.S. Atomic Energy Commission, April 1962. (UNCLASSIFIED)
- 11-10 "Nuclear Blast Design," Holmes and Narver, Inc. (UNCLASSIFIED)
- 11-11 Hammer, J. G. and Dill, A. F., "Improvement of Conventional Designs to Resist Blast Loadings," and "Personnel Protective Shelters," Studies in Atomic Defense Engineering, NavDocks P-290, January 1957. (UNCLASSIFIED)

- 11-12 Chilton, A. B., "Blast Pressure Leakage into Closed Structures Through Small Openings," Studies in Atomic Defense Engineering, NavDocks P-290.1, August 1958. (UNCLASSIFIED)
- 11-13 DaDeppo, D. A., Sherlock, T. E., and Tazelaar, R. D., "Protective Arch Structures," (U), University of Michigan Research Institute, March 1958. (SECRET)
- 11-14 Curione, C., "European Protective Shelters," Studies in Atomic Defense Engineering, NavDocks P-290.1, August 1958. (UNCLASSIFIED)
- 11-15 "Fourteenth Meeting of the Panel on Blast Effects on Buildings and Structures, and Protective Construction," Volume 1, SWC-9S-53500, Air Force Special Weapons Center Kirtland Air Force Base, New Mexico, October 1958. (SECRET, FORMERLY RESTRICTED DATA)
- 11-16 DaDeppo, D. A. and Sherlock, T. E., "Doors and Access Openings to Protective Structures," (U), University of Michigan Research Institute, October 1958. (CONFIDENTIAL)
- 11-17 Taylor, W. J., Curtis, W. E., and Clark, R. O., "Devices for Reducing Blast Effects in Ventilating Systems," Ballistic Research Laboratories Technical Note No. 869, (AFSWP No. 730), February 1954. (UNCLASSIFIED)
- 11-18 "Proceedings of the Conference on Building in the Atomic Age," Massachusetts Institute of Technology, June 1952. (UNCLASSIFIED)
- 11-19 "Blast Effects on an Air-Cleaning System," ITR 1475, Civil Effects Test Group-Operation Plumbbob, November 1957. (UNCLASSIFIED)
- 11-20 "Retest and Evaluation of Antiblast Valves," ITR 1717, Civil Effects Test Operations--Operation Hardtack, March 1959. (UNCLASSIFIED)
- 11-21 Newmark, Hansen and Associates, "Protective Construction Review Guide-Hardening," Volume 11, prepared for the Office of the Assistant Secretary of Defense (Installations and Logistics), 1 June 1961. (SECRET)

TABLE 11-1

COST DATA - LIMITED COST BREAKOUT*

Cost (cy = cubic yard, SF = sq. ft., L.F. = Lin. ft.)					
Item	Above Ground	Mounded or Shallow u/g (25' Cover)	Deep Underground	Remarks	
<u>1. Excav. and Backfill</u>	\$/cy	\$/cy	\$/cy		
Backfill					
Excav. - Earth	2	3	-		
" - Soft Rock	3	3	6		
" - Hard Rock	6	6	15		
" - Added cost if ground water problem	10	10	25		
	-	Add 50%	Add 100%		
<u>2. Structural</u>	\$/SF	\$/SF	\$/SF		
Walls, roof, floors, and foundations; bldg. frame and cladding exclusive of interior partitions, finishes and excavation.	9 (soft) See Figs. 11-1, 11-3	See Figs. 11-1, 11-3 11-4, 11-5 11-6	Unlined 20 Lined 25	Structural costs vary with structural type, span, and design overpressure	
<u>3. Entrances, Doors</u>	(See Figs. 11-1, 11-2 and 11-6) Add 3 \$/SF of door for or ramps radiation shielding at 25 psi	(See Figs. 11-1, 11-2, and 11-6) Add for stairs	(See Figs. 11-1, 11-2, and 11-6) Multiply by factor 1.5; access tunnels under Item 7		

* From Ref. 11-2.

TABLE 11-1 (Continued)
COST DATA - LIMITED COST BREAKOUT

Costs (cy = cubic yard, SF = sq. ft., L.F. = Lin. ft.)				
Item	Above Ground	Mounded or Shallow u/g (25' Cover)	Deep Underground	Remarks
4. <u>Architectural</u> (Interior finishes partitions, etc.)	\$/SF 4-9	\$/SF 4-9	\$/SF 10-22	Lower figures apply to simple interior layout higher figures to multi-partitioned layout, acoustic treatment, etc.
5. <u>Mechanical</u> (Heating, ventilating, air conditioning, air filtration, plumbing)	\$/SF 4-7	\$/SF 4-7	\$/SF 5-8	Includes 1.50 \$/SF for decon: air filt., blast valves, etc. Refrigeration costs for cooling computers and other electronic equipment, and ice storage for emergency use must be added
6. <u>ELECTRICAL</u> (Lighting, electrical outlets, normal power connections)	\$/SF 3-5	\$/SF 3-5	\$/SF 4-6	Includes 1.0 \$/SF for minimum administrative standby. For operational standby add 300 \$/Kw for generators and switchgear..

TABLE 11-1 (Continued)

COST DATA - LIMITED COST BREAKOUT

Costs (cy = cubic yard, SF = sq. ft., L.F. = Lin. ft.)

Item	Above Ground	Mounded or Shallow u/g (25' Cover)	Deep Underground	Remarks
7. <u>Water Supply; Sanitary; ventilation shafts and tunnels; personnel shafts and tunnels</u>	250 \$/person for water 350 \$/person for sewerage, 200 \$/L.F. (for D > 10') 300 \$/L.F. (for D < 10')	same as for above ground	350 \$/person for water, 450 \$/person for sewerage	For shafts and tunnels, cost of excav. or tunneling must be added.

8. Site Improvements

Access roads, power transmission, communications tie-in, fencing, physical security features, heliports, tone-down, radar countermeasures etc.

Note: A breakdown of these items is not provided since the cost will vary widely for specific installations, depending upon the type of construction, geographical location, mission, existence of or proximity to other facilities and many other factors. However, the importance of considering the costs for such items during the initial planning stages cannot be overemphasized. On small projects they may amount to substantial increases in unit costs and greatly affect the validity of cost comparisons with other projects.

TABLE 11-1 (Continued)
COST DATA - LIMITED COST BREAKOUT

Item	Total Excavation Cu. Yards	Total Cost	Labor	Costs per Cubic Yard		
				Materials	Explo- sives	Power Total
9. Detailed cost breakdown for excavation in hard rock accomplished by the U.S. Bureau of Mines during 1955-58 for a deep underground installation						
Access Tunnels	33,337	352,000	6.82	1.95	1.30	0.51
Main Chambers	172,475	1,670,260	5.84	1.93	1.41	0.52
Gross Cuts and Misc.	32,922	506,659	10.31	2.86	1.68	0.54
(Subtotal)	238,734	2,528,919	6.61	2.07	1.39	0.53
Rock Bolting	16,500 / (cost per bolt):	119,980	0.26 (3.61)	0.24 (3.42)	-	0.01 (0.21)
Mining Equipment	--	371,813	-	1.56	-	-
Engineering and Overhead	--	345,038	1.32	0.12	-	0.01
Totals	238,734	3,365,750	8.19	3.99	1.39	0.55
						14.12

Note: With the exception of Item 9, all costs are referred to fiscal year 1961 indices and Geographical Factor of 1.0. Costs consist of contract costs plus about 20% for contingencies and inspection.

Unit Costs	30 \$/cu yd, Concrete 250 \$/ton, Reinforcement 0.40-1.25 \$/sq. ft., Forms
------------	---

25 Percent For Overhead And Profit, + 21 Percent For Contingencies And Government Costs

- | | — Two-Story Administration Building — | 34,800 Sq. ft | — Column Spacing Varies | — Above Ground |
|---|---------------------------------------|---------------|----------------------------------|----------------|
| ① | — Two-Story Administration Building — | 34,800 Sq. ft | — " " " | — Above Ground |
| ② | — One-Story Communication Building — | 5,350 Sq ft | — " " " | — Above Ground |
| ③ | — One-Story Warehouse — | 14,790 Sq ft | — " " " | — Above Ground |
| ④ | — Single-Arch Igloo — | 1,628 Sq ft | — Span Of Approx. 28 ft. | — Above Ground |
| ⑤ | — One-Story Rectangular Building — | 3,200 Sq ft. | — Col. Spacing Of Approx. 20 ft. | — Mounded Over |
| ⑦ | — Hemispherical Dome — | 492 Sq ft. | — Span Of Approx. 25ft. | — Mounded Over |
| ⑧ | — One-Story Rectangular Building — | 3,200 Sq. ft | — Col Spacing Of Approx 20 ft | — Buried |
| ⑩ | — Hemispherical Dome — | 492 Sq ft | — Span Of Approx 25 ft. | — Buried |
| ⑪ | — Single-Arch Igloo — | 1,628 Sq. ft. | — Span Of Approx. 28 ft. | — Buried |

Note: Reference Numbers Of Structures Are The Same As In Reference 11-4.

Included Items:

- a. Earthwork, Concrete And Reinforcement, Formwork, Steel Blast Doors, For All Structures.
- b. Roofing, Insulation, Waterproofing, Interior Doors, Partitions And Finishes
For Structures ①, ②, ③.
- c. Waterproofing For Structures ④ - ⑪.

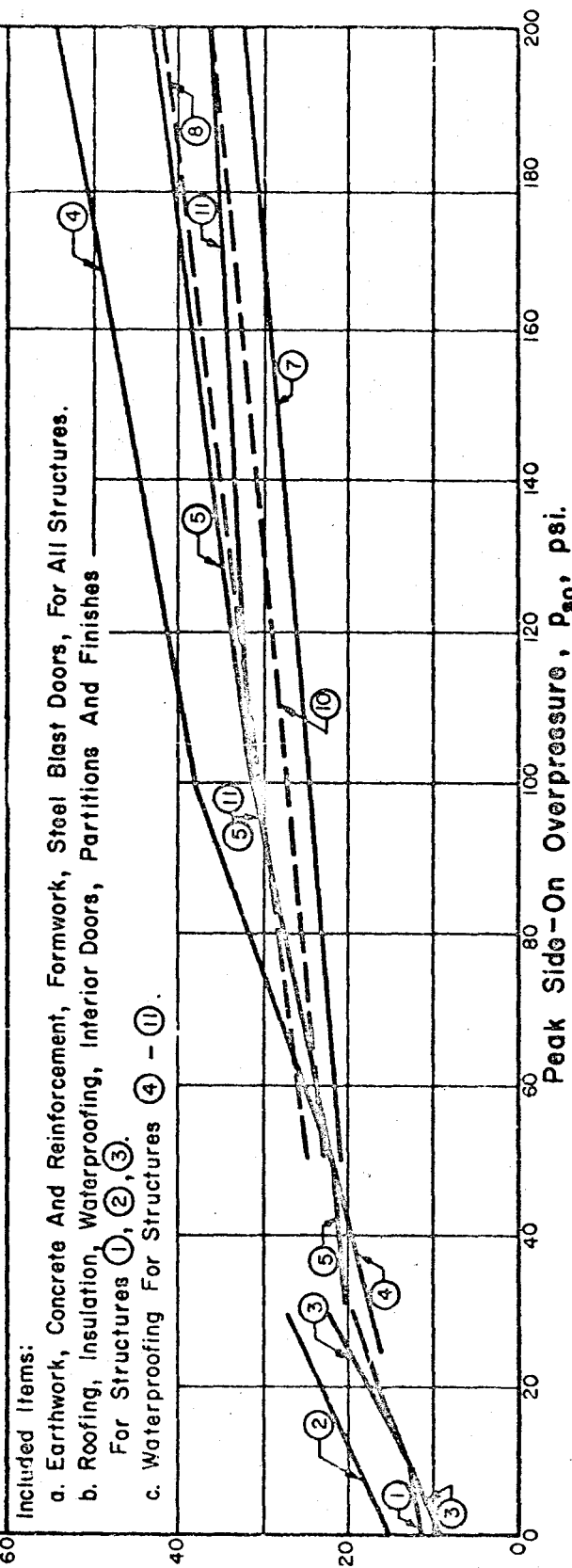


FIG. 11-1 ESTIMATED COST OF BARE STRUCTURE, EXCLUDING ENTRANCE STRUCTURES

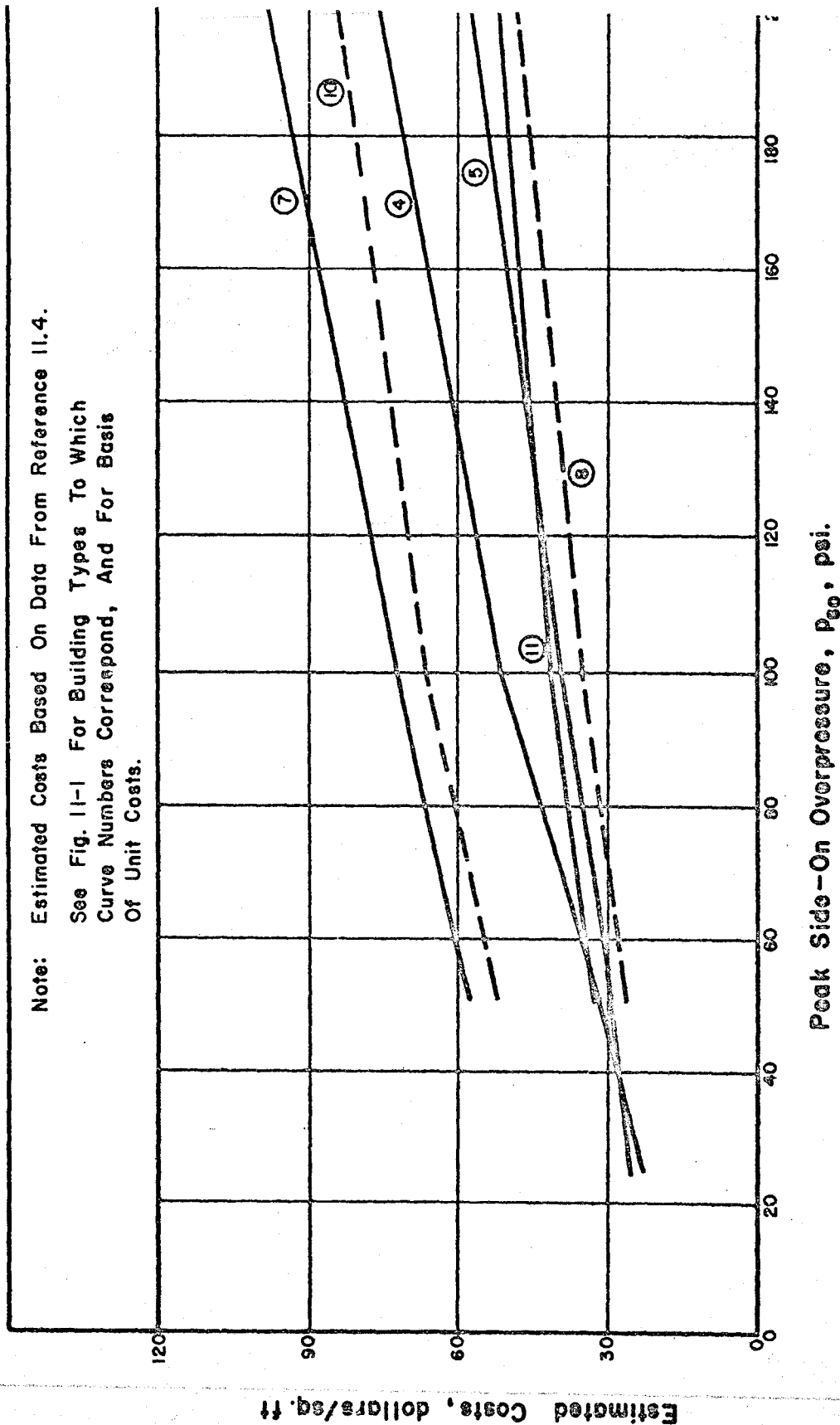


FIG. 11-2 ESTIMATED COST OF BARE STRUCTURE, INCLUDING SPECIAL ENTRANCE STRUCTURES.

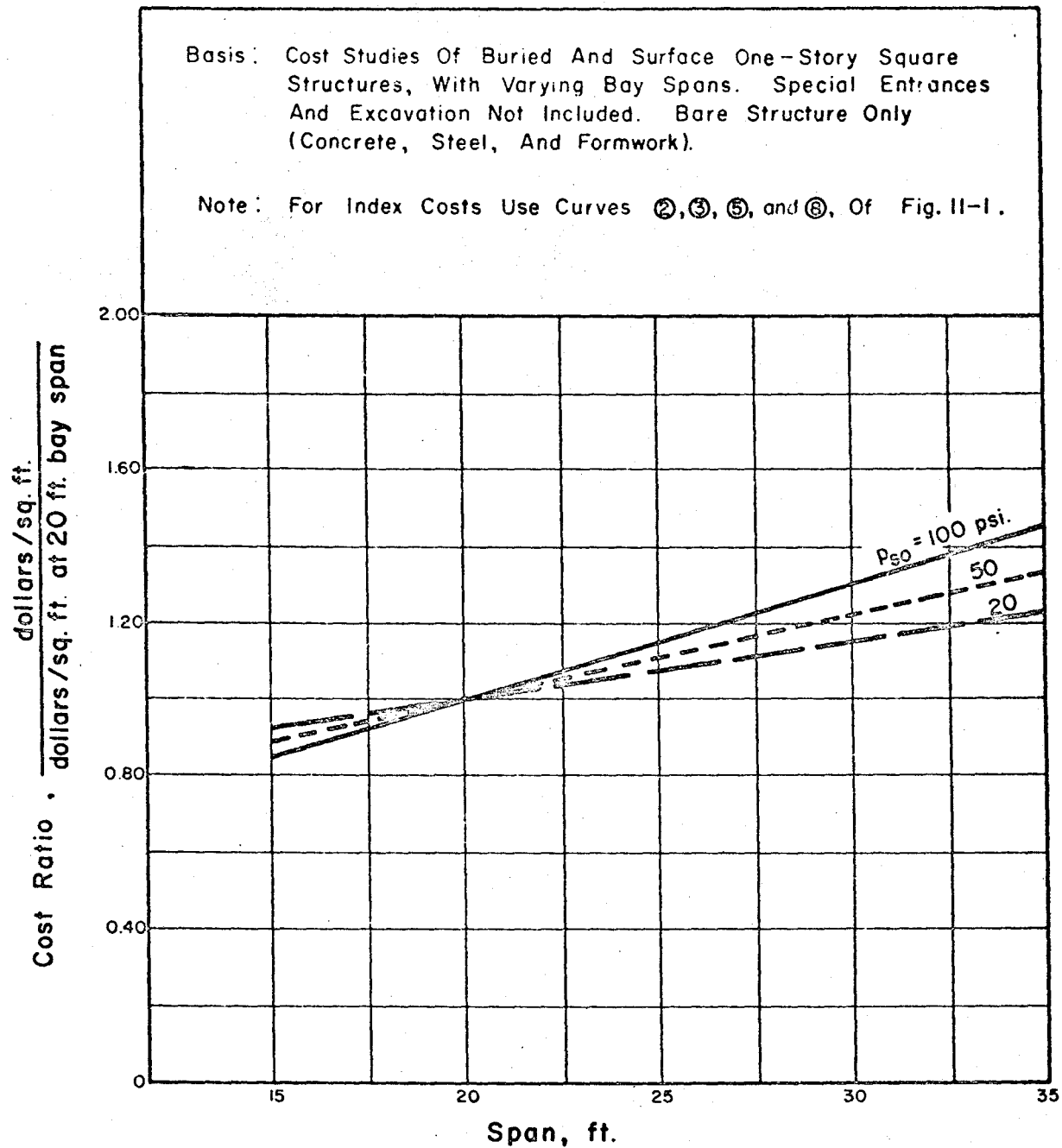


FIG. II-3 COST RATIO VERSUS SPAN FOR ONE-STORY RECTANGULAR STRUCTURES

Basis: Cost Studies For Buried, Hemispherical Domes. Special Entrances And Excavation Not Included. Bare Structure Only (Concrete, Steel, And Formwork).

Note: For Index Costs Use Curves ⑦ And ⑩ Of Fig. II-1.

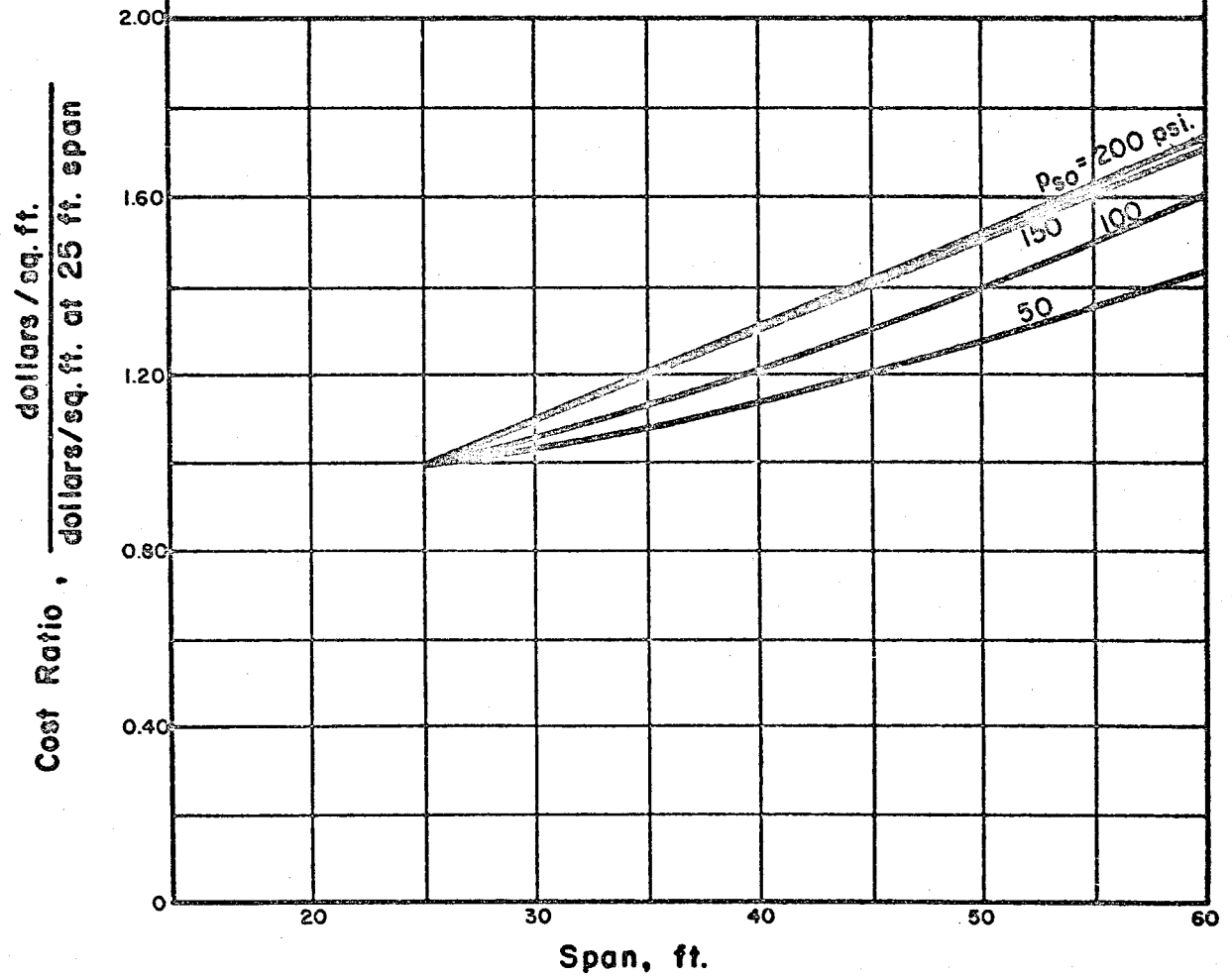


FIG. II-4 COST RATIO VERSUS SPAN FOR DOME STRUCTURES

Basis: Cost Studies For Buried, Single-Arch, Igloo With Length Equal To Twice The Span. Special Entrances And Excavation Not Included. Bare Structure Only (Concrete, Steel, And Formwork).

Note: For Index Costs Use Curves ④ And ⑪ Of Fig. 11-1.

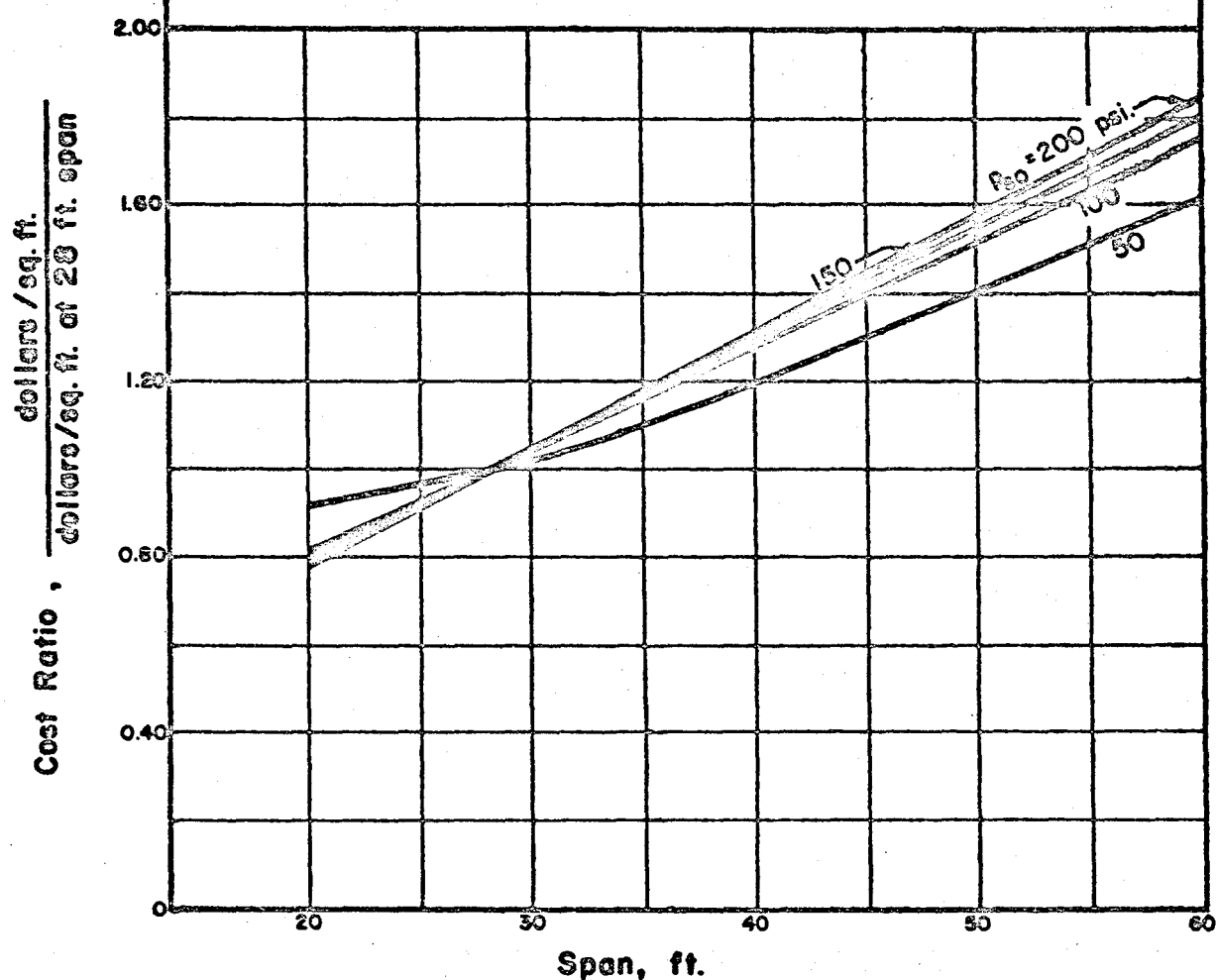


FIG. 11-5 COST RATIO VERSUS SPAN FOR ARCH (IGLOO) STRUCTURES

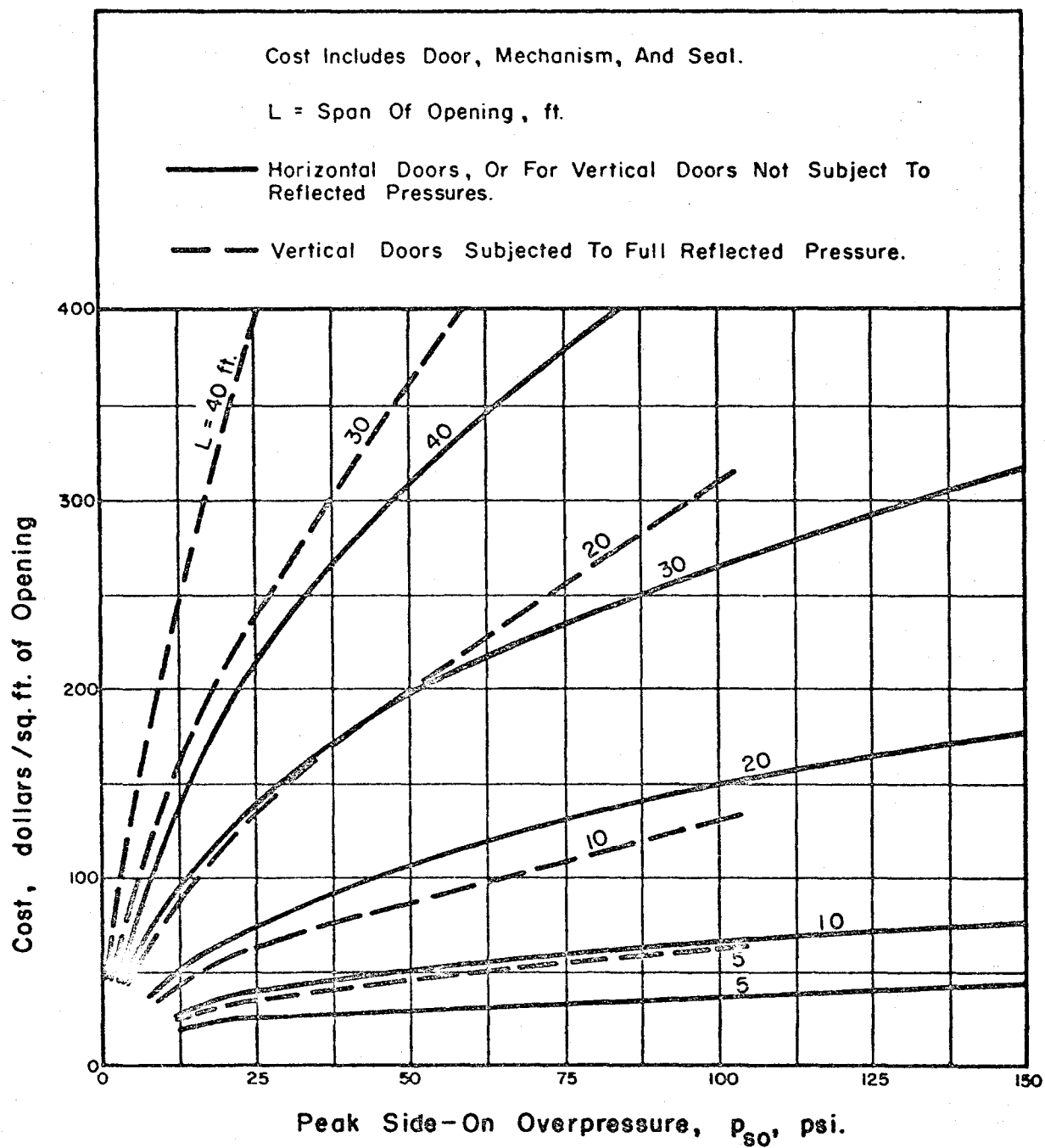


FIG. II-6 COST OF PROTECTIVE DOORS

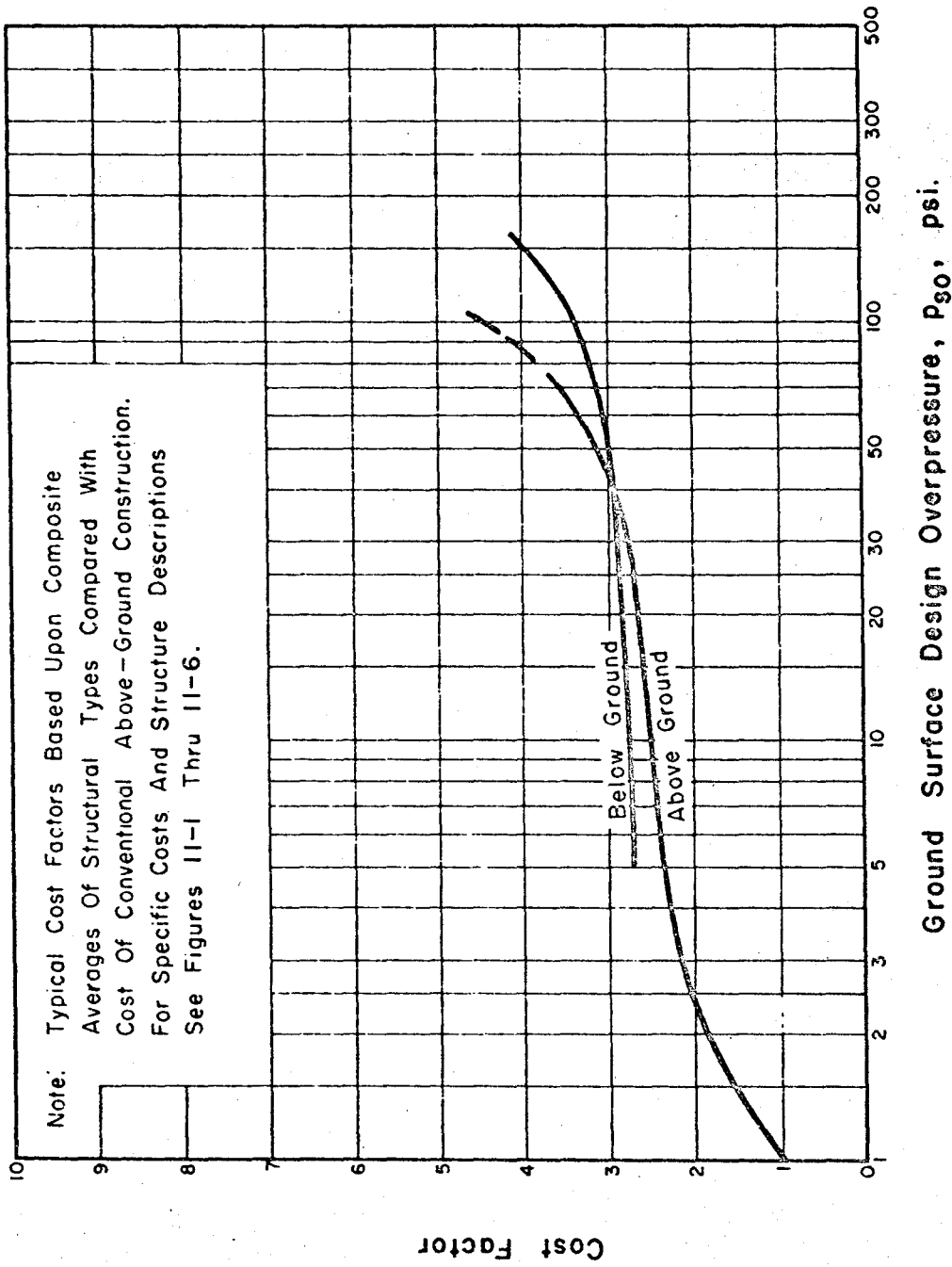


FIG. 11-7 COST FACTOR VERSUS DESIGN OVERPRESSURE

CHAPTER 12. NUCLEAR RADIATION

12.1 INTRODUCTION

In both fusion and fission reactions some of the energy released appears in the form of nuclear radiation. This section is concerned with nuclear radiations, their effects, and protection against them. The discussions contained herein are not intended to be comprehensive, but rather to identify the problems associated with protection against nuclear radiation, both prompt and residual. For a presentation of basic nuclear radiation phenomenology, the reader is encouraged to study Chapters 8 through 11 of Ref. 12-4. A more complete treatment of structure shielding is contained in Ref. 12-5.

Some nuclear radiation is produced at the instant of fission or fusion, and some is emitted by radioactive nuclei over a long period of time. By definition, that emitted in the first minute after detonation is called prompt or initial radiation, and, that emitted afterward, residual radiation. The sources and characteristics of both vary according to the relative extent to which fission and fusion contribute to the yield of the weapon.

Nuclear radiations can be classified, however, and general conclusions can be drawn as to their behavior and effects. Two general types are present: those consisting of high-energy particles with or without electric charge; and those electro-magnetic in nature similar to that of light. These will be discussed in greater detail.

12.2 DESIGN IMPORTANCE

Nuclear radiation becomes an important factor in design when it presents a threat to personnel, equipment, or structures. Normally, radiation considerations will not be the governing factor in a design, but it is not improbable that modifications will be required in design to insure adequate radiation protection. This entails first a prediction of radiation levels at the structural site; second, an estimate of the critical tolerance of personnel and equipment; and finally, provision for attenuation so as to make the level compatible with the tolerances. Prediction of the radiation levels can be made from experimental data coupled with several assumptions. Usually the assumptions will be such as to insure safety of the design and should be consistent with the level of blast protection provided or desired. The experience and judgment of the designer or planner play an important part, and he should make use of all available information as to prevailing weather, winds, and atmospheric conditions. The critical tolerances of personnel and equipment must be established on the basis of existing test data and Japanese experience.

12.3 PROTECTION

Some forms of radiation can be absorbed completely by a barrier; however, the types of radiation of primary interest here, i.e., gamma and neutrons, have great penetrating power. Attenuation is possible with suitable shielding materials or a sufficient interval of air. The amount and kind of material required for attenuation to safe levels are a function of the energy

of radiation, the intensity and cumulative value of the radiation, the atomic characteristics of the shielding material used, and the emergent level desired.

12.4 RADIATION CHARACTERISTICS

12.4.1 Kinds of Radiation.

(a) Alpha. Alpha particles are emitted by heavy elements as they undergo radioactive decay. Alpha particles are essentially ionized helium nuclei with a charge of plus two (esu). Because they are charged, alpha particles travel only a few feet in air. They can be stopped by thin layers of material such as paper and therefore do not constitute an external hazard.

(b) Beta. Beta particles are emitted by most fission products. Beta particles are similar to electrons in electrical charge and mass. Like alpha particles, beta particles can be absorbed and do not constitute an external hazard to sheltered personnel.

There is some danger, however, to personnel from alpha- or beta-emitters if these particles gain entry to the body in some manner. Strontium 90 is an example of a Beta emitter, having a half-life of about 25 years. (Sr⁹⁰, 0.6 Mev)

(c) Gamma. Gamma radiation is a form of electromagnetic wave radiation with characteristics similar to X-rays, but with greater energies. A beam of gamma rays may be considered to consist of a large number of small packets of energy called photons or quanta. In addition

to wave-like qualities, each photon has the properties of a small particle with an effective mass, momentum, and energy which may be calculated from its wave length or frequency. Gamma rays are produced by a rearrangement of nucleons in the nucleus of an atom. This can occur: (1) during the fusion or fission process, (2) in the nuclei of fission products which have been formed, (3) in the nuclei of atoms made radioactive by neutron bombardment. The first occurs within seconds following a nuclear explosion; the latter may continue over long periods of time.

Gamma photons have energies measured in millions of electron volts (mev), an electron volt being a unit equivalent to the energy attained by an electron "falling through" a potential difference of one volt. Thus, a 1-mev photon has an energy equal to that gained by an electron accelerated by a potential of 1,000,000 volts.

(d) Neutrons. Neutrons are electrostatically neutral particles which are part of atomic nuclei. They have approximately the same mass as a proton which is exceedingly small (1.661×10^{-24} gm.) but which is still about 1840 times the mass of an electron. Neutrons are released during the fission or fusion process primarily. In the fission process about 99 percent of the emitted neutrons are released immediately, probably within 1 microsec., and the balance subsequently. In the fusion process 100 percent of the emitted neutrons are released immediately. Neutrons travel at high speed but less than that of light.

Neutrons can cause biological damage to the human body and the effects can be equated to damage from gamma radiation. In addition, neutron radiation can cause damage to electronic equipment.

Neutron emission can be classified according to the particle energy. "Thermal" neutrons have energies of the order of 0.03 ev.; "Slow" neutrons have energies in the range 1-100 ev.; "Intermediate" neutrons have energies in the range 100 ev.-1 mev.; and "Fast" neutrons have energies of over 1 mev. The method of protection against neutron flux is dependent upon the energies, as will be discussed later. In the fission process, virtually all of the neutrons initially released are fast neutrons; however, because of various interactions with nuclei of matter comprising the earth and the atmosphere some lose energy with the result that at some distance from the point of detonation the energy spectrum is quite broad. In the fusion process the same is true, except the resulting emission has a larger proportion of fast neutrons than in the case of the fission process. The energy spectrum varies from one weapon to another. Hence, a single curve is an inaccurate compromise. However, the proportion of neutrons in any particular energy range appears to be essentially the same at all distances of interest.

To summarize, the kinds of radiation of primary concern to a structural designer are prompt gamma, residual gamma, and neutrons.

12.4.2 Units of Measure. In order to establish necessary protection against radiation, it is necessary to correlate intensities, energies, and total dosage with tolerances of humans and equipment. To do this some units of measurement are needed other than those previously discussed.

(a) Exposure Dose. A measure of the strength of a radiation field at a given location is given by the "roentgen". The roentgen

is not a measure of energy of radiation nor of the type of radiation but rather of its capabilities under specific conditions. The roentgen is defined as that amount of X- or gamma radiation which produces ions carrying one electrostatic unit of charge in one cubic centimeter of air under standard conditions of temperature and pressure. The total or cumulative dose in roentgens is commonly used for prompt or instantaneous radiation. For residual radiation, the dosage rate, i.e., roentgens per unit time, is a useful measurement. At energies appreciably above 2 mev. it becomes difficult to measure the dose in roentgens, and units of erg/gram are used to indicate the radiation energy which 1 gm. of tissue would absorb.

(b) Absorbed Dose. The absorbed dose is expressed in "rep" (roentgens equivalent physical) and "rad". Rep is defined as an absorbed dose of 97 ergs per gram of body tissue of any nuclear radiation. This is not always useful because the number of ergs absorbed is not determinable and can change. The unit "rad" is defined as an absorbed dose of any nuclear radiation accompanied by the liberation of 100 ergs of energy per gram of absorbing material. The difference between rep and rad for soft tissue is negligible.

(c) Biological Dose. The unit of biological dose is the rem (roentgen equivalent mammal). The rem is related to the rad by a factor called the RBE (relative biological effectiveness).

$$\text{Dose in rems} = \text{RBE} \times \text{Dose in rads}$$

The RBE is approximately unity for gamma radiation although it varies with the energy of radiation.

For gamma radiation and soft tissue it can be said that:

$$\text{No. rems} \approx \text{No. rads} \approx \text{No. r}$$

This equality does not exist for other nuclear radiations.

The expected biological effect, however, can be related approximately to the exposure dose. Neutrons can be measured in rads and converted to rems and thus combined with gamma effects in rems.

12.5 VULNERABILITIES

Both humans and equipment are vulnerable to nuclear radiation. The exact maximum dosage to which personnel may be exposed is a rather arbitrary figure best established by executive or military decision for the specific instance. The designer, once given this limiting dosage, and knowing the design weapon parameters, can then undertake the provision of adequate shielding in the given structure.

The effects on humans are roughly as follows:

170-220 r	prolonged sickness of 50 percent no deaths
220-330 r	severe prolonged sickness to all, 20 percent deaths
400-750 r	60-100 percent deaths

While these values are based on cumulative doses received, the time over which this dose is received has some bearing on the effects on humans. The body is somewhat more resistant to a given amount of radiation if the radiation is spread over a long period. Table 12-1 shows estimated medical effects of radiation doses.

At the present time there is not a great deal of information on the vulnerability of equipment to radiation. Some data are available in Ref. 12-2.

12.6 PREDICTION OF LEVELS AT SITE

Both for above-ground and under-ground construction it is necessary to estimate the radiation levels which will occur at the ground surface. For above-ground construction this is of direct importance in determining wall thicknesses and architectural features; for under-ground construction it is important to know the surface intensities to insure sufficient earth cover and to insure adequate design of exposed ventilators, intakes, and portals.

(a) Initial Gamma. The intensity of prompt gamma radiation decreases with distance from the point of detonation. This reduction is due to spherical divergence (inverse-square law) and interactions between the gamma photons and the gas molecules comprising the atmosphere. The path of radiation deviates locally from simple line-of-sight because of these scattering interactions. For this reason more than a simple shield is required for protection. Figure 12-1 shows the total amount of initial gamma radiation which would be measured at various horizontal distances from surface bursts of various yields. These data were obtained by applying scaling relationships to the information in Ref. 12-2. As an example, if it were required to erect a structure at a location which was 15,000 feet from the most probable Ground Zero and if the design criteria specified a 10 MT weapon; one could estimate from Fig. 12-1 that the total initial gamma radiation would be of the order of 100 roentgens.

(b) Residual Gamma and Fallout. The term "residual" gamma usually refers to all gamma radiation not given off as prompt or initial. For practical purposes this is primarily "fallout" gamma radiation. Fallout is the name given the deposits of air-borne particles which have been transported from the explosion site. These particles, swept aloft with the fireball, include explosion products, earth, and other fragments. Many of these particles are radioactive. The distances from the point of detonation at which fallout can be deposited are great and depend upon factors such as wind velocity, particle size, atmospheric and topographical conditions, etc. The fallout pattern may be idealized to elliptical contours extending downwind from Ground Zero. The ellipses are narrow and extend for many miles, e.g., for a 1-MT surface burst the intensity or dose rate 180 miles downwind (15 knot wind, 12 hours following the explosion) is approximately 1.6 r/hr. On the other hand, the intensities upwind or crosswind will be only a fraction of those downwind at corresponding distances from Ground Zero. The designer must consider the relationship of his construction site to the most probable Ground Zero. To assume the structure to be downwind is, of course, the most conservative for design, but may be too conservative in many cases.

For an observer downwind from an explosion, two things are happening which tend to affect the amount of radioactivity to which he is exposed:

(1) The airborne particles are being deposited continually so that the number of particles reaching him is less the farther away his position is.

(2) Depending on the wind velocity, it takes a finite time for the particles which do reach him to get there. During this time the radio-

active elements have been undergoing decay and for some of them with short half-lives this time is sufficient to cut down their intensities appreciably.

The problem for the designer is to determine the accumulated radiation dose for a given location beginning at the time the first fallout occurs and extending to the time when the last particle ceases to give off radiation. This latter time, obviously, would be infinite; and for practical purposes an extrapolation is made.

The depositing of air-borne particles is a function of particle size, wind velocity, and air density. The radioactive decay is a function of time. These two actions are going on simultaneously. It is difficult to devise a curve or graph to show this. What is generally done is to establish a reference value of wind velocity and a reference time for radioactive intensity, and to show the fictitious fallout radiation intensities based on these references at various downwind locations from given surface bursts. Figure 12-2 is such a curve for a wind velocity of 15 knots and a reference time of one hour following the explosion. The values read directly from Fig. 12-2 would only be correct for a location 15 nautical miles downwind. Values for other locations further downwind must be corrected to take into account the radioactive decay between the one-hour reference and the actual time of arrival. The actual time of arrival can be taken as the downwind distance divided by the wind velocity. For velocities other than 15 knots the scaling factors shown should be applied to the one-hour intensities shown, and the true velocity used in computing the arrival time. Figure 12-2 is

based on the assumption that the fission yield equals the total yield. This is not usually true for large weapons. Therefore the radiation intensities shown in Fig. 12-2, such as 3000 r/hr, must be multiplied by the ratio of fission yield to total yield.

A radioactive decay curve could be used as a means of converting the one-hour reference doses read from Fig. 12-2 to the true values at the time of arrival. However, since total dosage rather than intensity is the important value, it is convenient to use a curve such as Fig. 12-3. Figure 12-3 gives the ratio of total cumulative dose to the one-hour intensity or dose rate for various times following the explosion. The total dose accumulated in any time interval can be obtained by subtracting the ratio obtained at the time that the interval ends from that obtained at the time the interval begins and multiplying the difference by the one-hour reference dose rate.

(c) Neutrons. The production and emission of neutrons are closely related to weapon design. In general the thermonuclear processes (fusion) produce more high energy neutrons than do the fission processes. The energy spectrum and total number of neutrons will vary with the weapon design. This makes scaling risky and representation of intensities by a single curve an over-simplification.

Experimental data and measurements of neutron flux produced by nuclear explosions are incomplete and unreliable. Although it is customary to find neutron intensity vs. distance curves presented in a manner analogous to those for initial gamma radiation, each source carefully points out the unreliability of the data and the doubtful validity of scaling laws. One is, however, usually obliged to use such over-simplified representations.

The various detection methods such as boron counters, fission chambers, and foil activation can give measurements in absorption units (rad). These must be converted to units of biological dosage (rem) before the effects on humans can be assayed. The conversion factor, RBE, has not been definitely established. It is different for different energies. A value of about 1.7 seems reasonable and is derived from limited tests on animals and study of human experiences in Japan.

In spite of the preceding deficiencies it is necessary to make a determination for design purposes. At the present time Ref. 12-3 should be used for the prediction of neutron intensities if no better information is available.

12.7 GAMMA RADIATION SHIELDING

The amount of attenuation or absorption of gamma radiation depends roughly on the mass of material between the source and observation point. The effectiveness of wood, water, soil, concrete, steel and iron, and lead for shielding from initial and residual gamma radiation is shown in Figs. 12-4 and 12-5 respectively. The effectiveness is given by the dose or dose rate transmission factor which is the ratio of the transmitted to the incident radiation intensity. When the shielding is provided by two or more materials such as earth and concrete, the appropriate dose transmission factor is the product of the individual factors of each material.

Figure 12-4 and 12-5 were taken from Ref. 12-1 and were originally derived from the data in Ref. 12-4. Strictly speaking, they should be applied only to monoenergetic gamma radiation in a narrow beam or when the shielding

material is relatively thin. However, they can be used as an indication of the attenuation to be expected in under-ground structures and will give a conservative estimate of the protection afforded by the structure being analyzed.

12.8 NEUTRON RADIATION SHIELDING

Neutron attenuation is a more complex phenomenon than that of gamma attenuation, since several phenomena are involved in the former. First, the very fast neutrons must be slowed down to the moderately fast range; this requires a suitable (inelastic) scattering material, such as one containing barium or iron. Then, the moderately fast neutrons have to be decelerated to the slow range by means of an element of low atomic weight. Water is very satisfactory, since its two constituent elements, i.e., hydrogen and oxygen both have low atomic weights. The slow (thermal) neutrons must then be absorbed. This is not a difficult matter since the hydrogen in water will serve the purpose. Unfortunately, however, most neutron capture reactions are accompanied by the emission of gamma rays. Consequently, sufficient gamma attenuating material must be included to minimize the escape of capture gamma rays from the shield.

Rough attenuation data for fast neutrons are given in Ref. 12-1 based on actual measurements. These have been reduced to usable form and are presented in Fig. 12-6. It must be emphasized that the thermal neutrons must be captured (by water, parafin, etc.) and that gamma radiation induced by the capture process must be attenuated. The "iron-concrete" aggregate shown in

Fig. 12-6 is limonite (iron oxide ore).

Two cases of induced gamma radiation may be distinguished.

Case A applies to sustained radiation from the material in the shield that becomes radioactive as a result of neutron bombardment. Case B refers to the neutron-gamma radiation which occurs immediately. The gamma radiation emitted immediately has a higher energy level in general.

(a) Case A. The effect on steel, cement, virtually all aggregates, and on water is minor. The induced gamma is about 10 percent of the radiation that actually penetrates the shield for close-in bursts (overpressure as much as two or three hundred psi). At greater distances this proportion is even less, being about one percent for ranges where initial gamma is low but still significant.

(b) Case B. Some measurements have shown that the induced gamma through the shield is 2 to 7 times as great as the transmitted initial gamma, and even greater at very high overpressures. No better data are available. This matter must be rechecked when a particular project is reviewed.

12.9 REFERENCES

- 12-1 Newmark, Hansen and Associates, "Protective Construction Review Guide, (Hardening)," Volume I, prepared for the Office of the Assistant Secretary of Defense, Properties and Installations, June 1961. (UNCLASSIFIED)
- 12-2 Newmark, Hansen and Associates, "Protective Construction Review Guide, (Hardening)," Volume II, prepared for the Office of Assistant Secretary of Defense, Properties and Installations, June 1961. (SECRET, RD)
- 12-3 "Capabilities of Atomic Weapons," AFM-136-1A, Armed Forces Special Weapons Project, Washington, D. C., Revised June 1960. (CONFIDENTIAL)
- 12-4 "The Effects of Nuclear Weapons," U.S. Atomic Energy Commission, Washington, D. C., April 1962. (UNCLASSIFIED)
- 12-5 "Design of Structures to Resist Nuclear Weapons Effects," ASCE Manual of Engineering Practice No. 42, 1961. (UNCLASSIFIED)

TABLE 12-1 ESTIMATED MEDICAL EFFECTS OF RADIATION DOSES EXPRESSED
AS PROBABILITY OF SICKNESS OR DEATH

Early Effects For Periods of Time Over Which Total Dose is Received

Measured Dose (r)	1 Day		3 Days		1 Week		1 Month		3 Mo. or more		Significant Late Effect
	Sick- ness %	Death %	Sick- ness %	Death %	Sick- ness %	Death %	Sick- ness %	Death %	Sick- ness %	Death %	
0 to 75	0	0	0	0	0	0	0	0	0	0	None
100	2	0	0	0	0	0	0	0	0	0	None
125	15	0	2	0	0	0	0	0	0	0	None
150	25	0	10	0	2	0	0	0	0	0	None
200	50	0	25	0	15	0	2	0	0	0	Some
300	100	20	60	5	40	0	15	0	0	0	Some
450	100	50	100	25	90	15	50	0	5	0	Some
650	100	95	100	90	100	40	80	10	10	0	Some

This table applies to healthy, young adults under usual working conditions. The probability of fatalities will be decreased with adequate medical treatment. The casualty estimates are based on an interpretation of the best current available evidence and may be changed as more information is accumulated.

NOTE: Data from Ref. 12-1

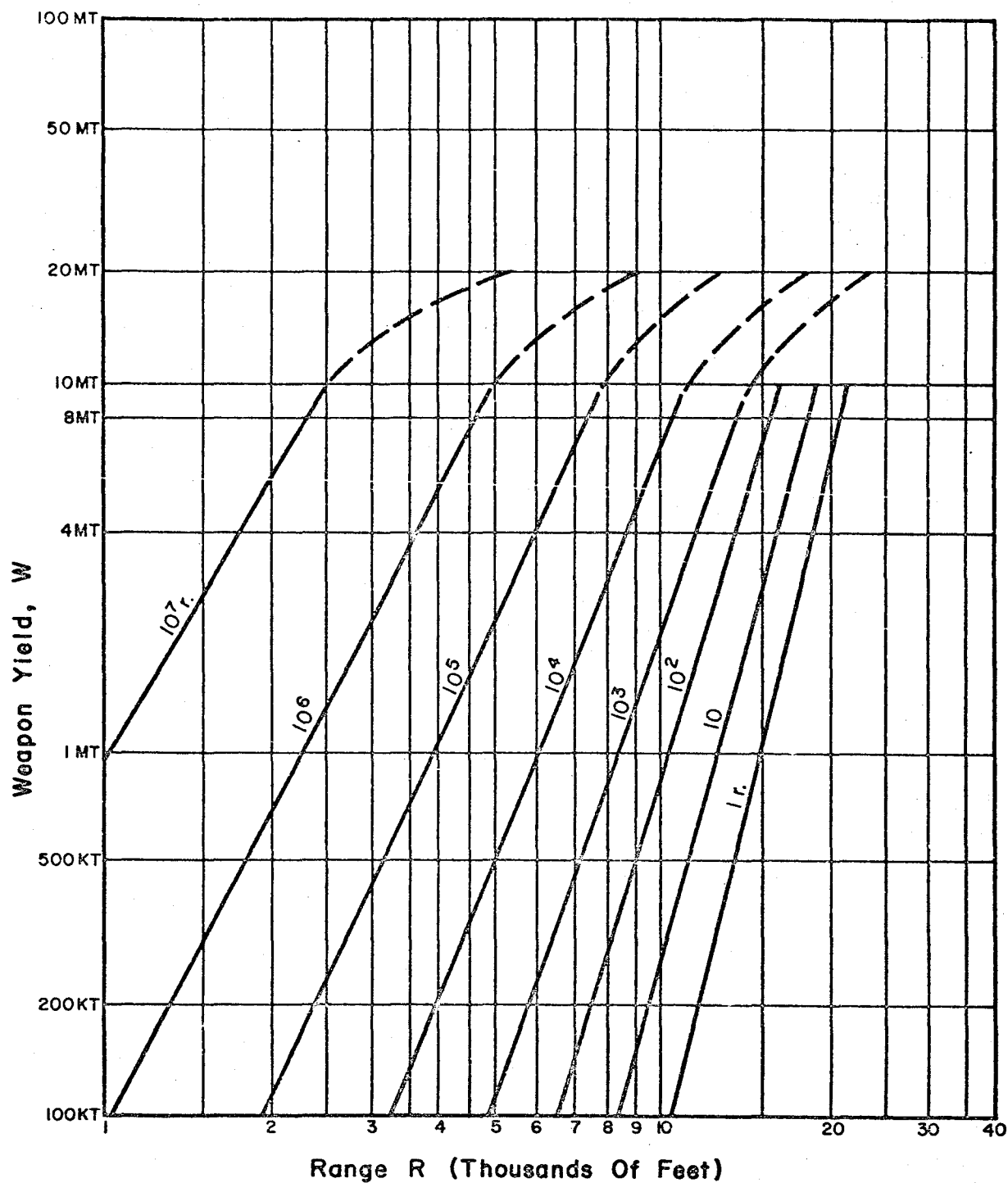


FIG. 12-1 WEAPON YIELD VERSUS VULNERABILITY
RADIUS FOR VARIOUS LEVELS OF
INITIAL GAMMA RADIATION — SURFACE
BURST

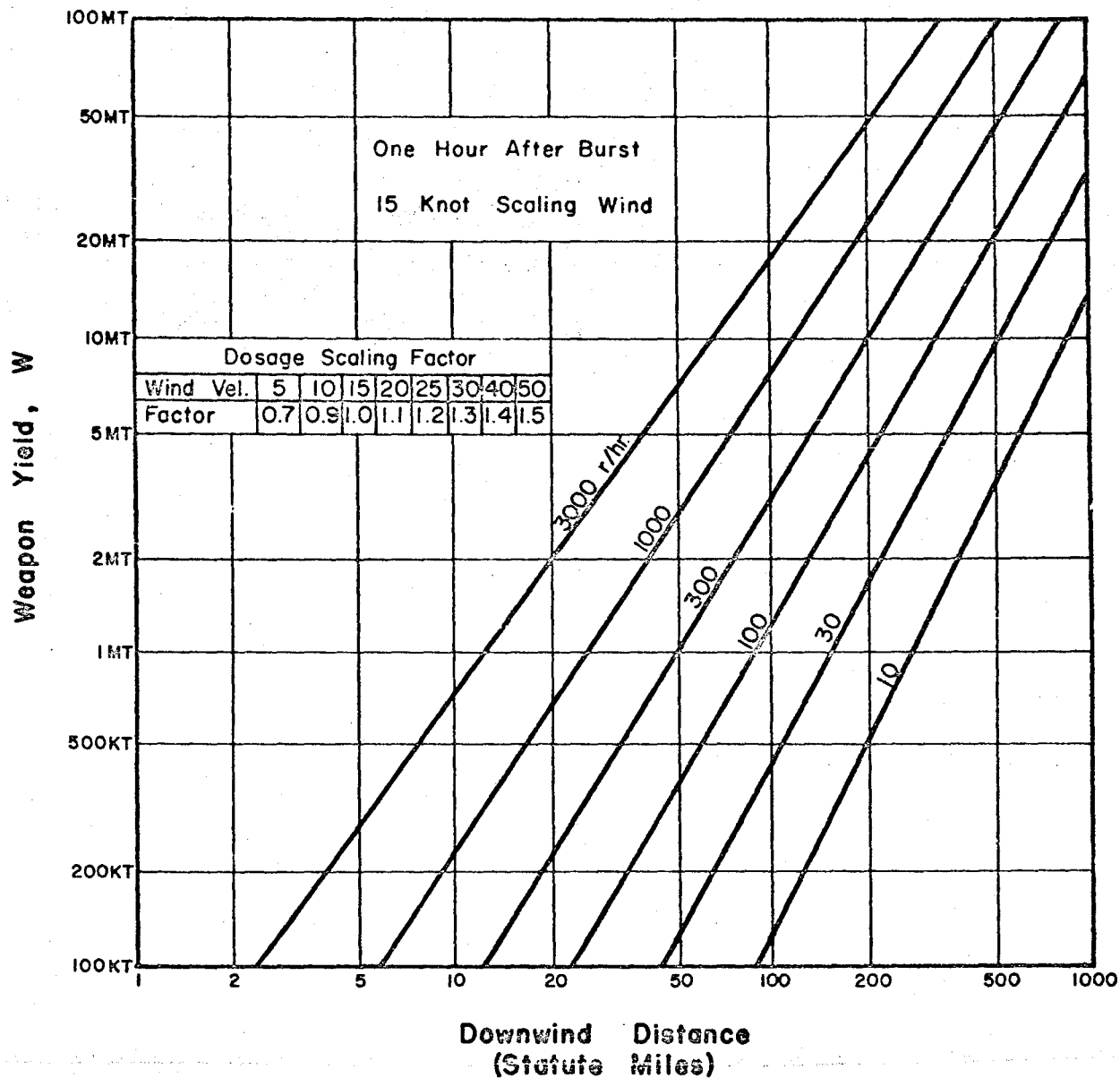


FIG. 12-2 FALLOUT INTENSITIES (1 HOUR REFERENCE DOSE) AT DOWNWIND DISTANCES FROM GZ FOR VARIOUS WEAPON YIELDS (SURFACE).

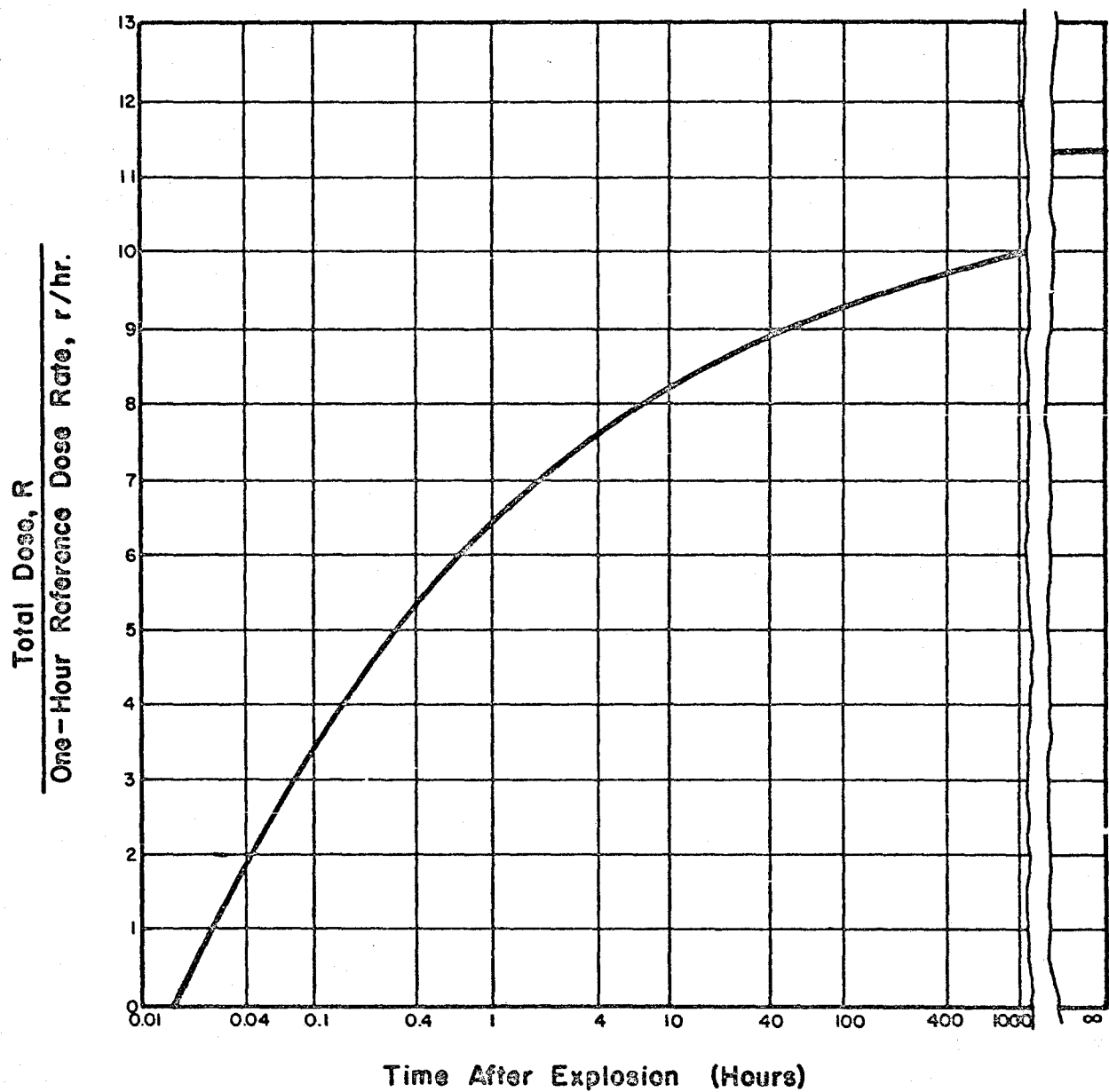


FIG. 12-3 ACCUMULATED TOTAL DOSE OF RESIDUAL RADIATION FROM FISSION PRODUCTS FROM 1 MINUTE AFTER THE EXPLOSION

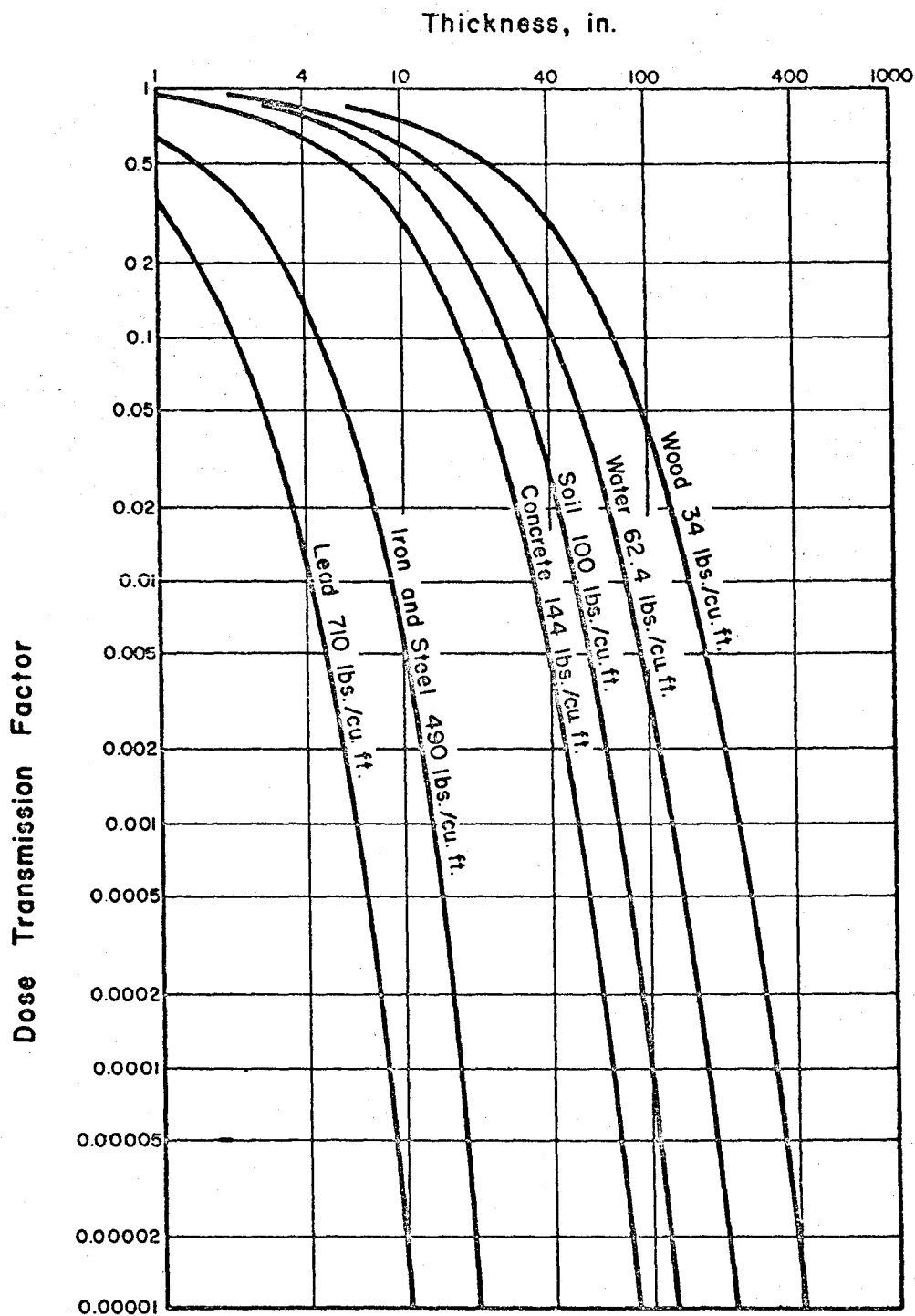


FIG. 12-4 SHIELDING FROM INITIAL GAMMA RADIATION

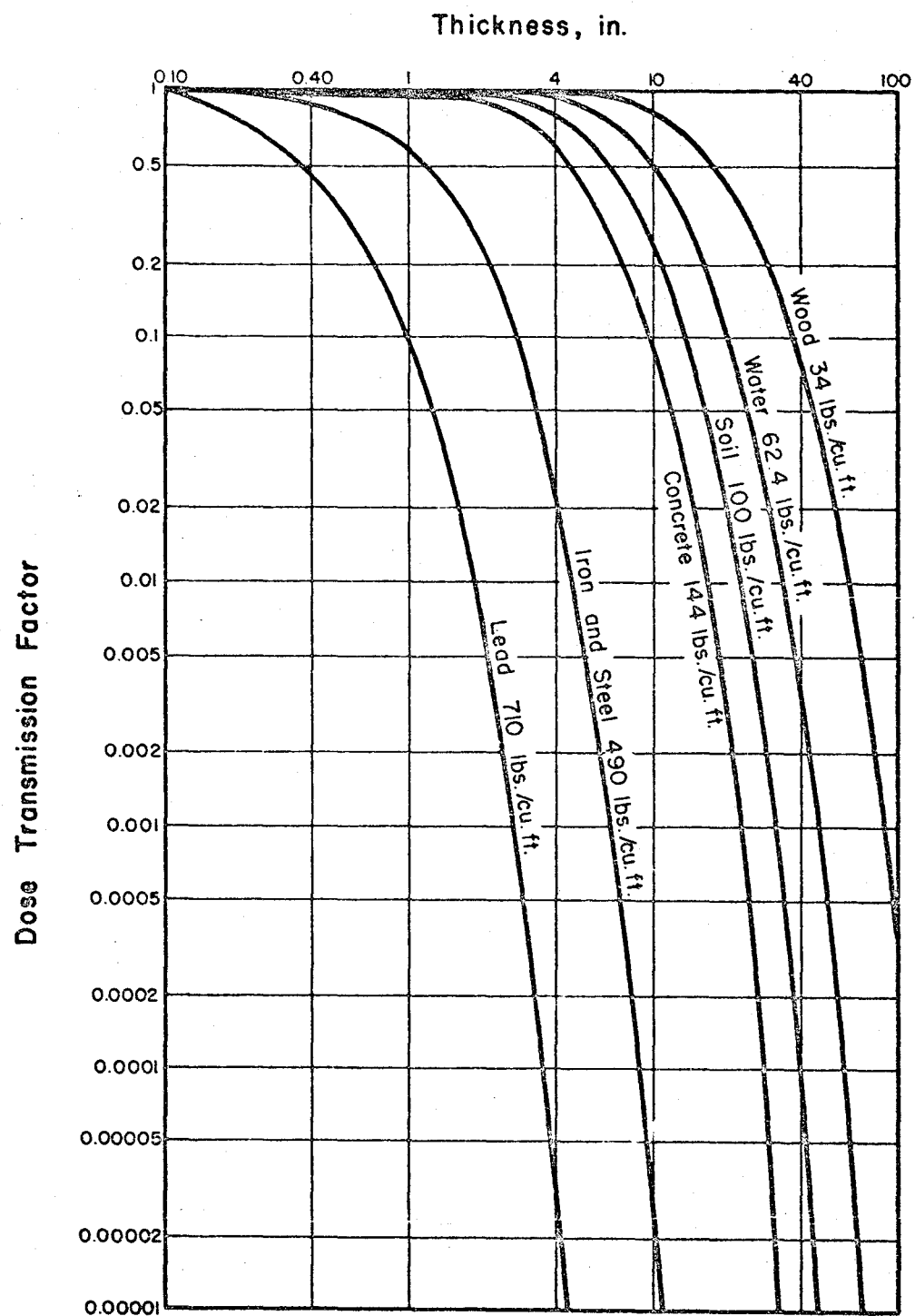


FIG. 12-5 SHIELDING FROM RESIDUAL GAMMA RADIATION

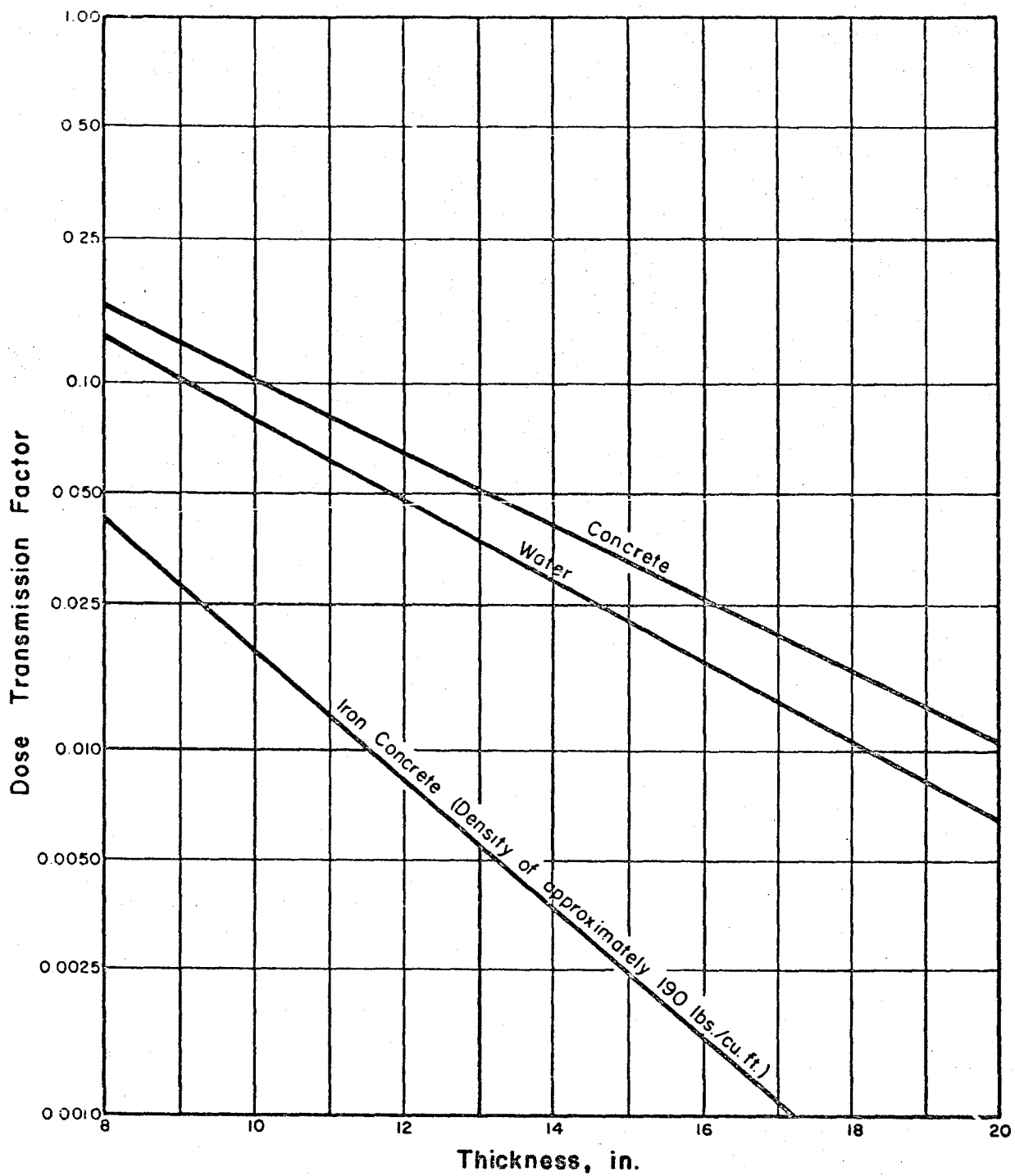
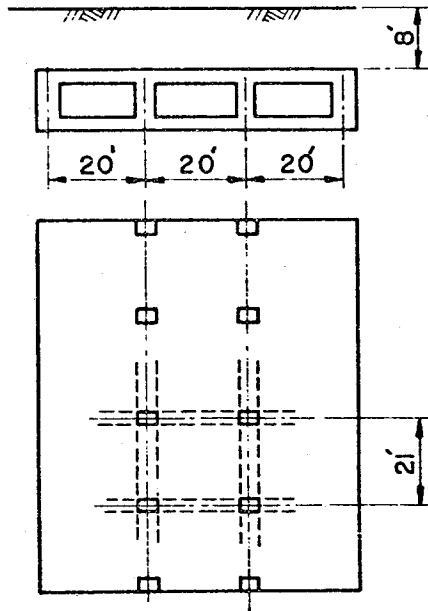


FIG. 12-6 ATTENUATION OF FAST NEUTRON RADIATION—BROAD BEAM IN THICK SHIELDS

APPENDIX A
DESIGN EXAMPLES

A.1 BURIED RECTANGULAR STRUCTURE

Consider a buried, single-story, rectangular structure, 60 ft. by 84 ft. in plan, with 8 ft. of earth cover over it, as shown in the accompanying sketch. To illustrate the design procedures presented herein, the roof will be proportioned as a two-way slab supported on beams that span between columns spaced as shown. The other structural elements (walls, base slab, etc.) can be designed in a similar manner.



Given Data:

Loading

$$p_{so} = 200 \text{ psi, on ground surface}$$

$$W = 1 \text{ MT, Surface Burst}$$

Ductility Factors

$$\mu = 3.0 \text{ for ductile response}$$

$$\mu = 1.3 \text{ for brittle response}$$

Yield Stresses

$$f'_c = 4000 \text{ psi}$$

$$f'_{dc} = 5000 \text{ psi}$$

$$f_y = 40,000 \text{ psi}$$

$$f_{dy} = 50,000 \text{ psi}$$

A.1.1 Design of Two-Way Roof Slab (See Sect. 9.3). Assume the beams to be approximately 4 ft. wide; therefore the side dimensions of the slab are 16 ft. x 17 ft.

$$\alpha = \frac{\text{Short Span}}{\text{Long Span}} = \frac{16}{17} = 0.94$$

Flexural Requirements

Because the slab is nearly square, it is reasonable to assume equal reinforcement in both directions. Therefore:

$$\frac{\phi_{Lc} + \phi_{Le}}{\phi_{sc} + \phi_{se}} = 1.0$$

and, from Fig. 9-8, $\Omega = 2.85$ = ratio of the resistance of the two-way slab to that of a one-way slab having the same cross-section and a span equal to the short side of the two-way slab.

Estimate DL + LL: (Use reduced DL; See Sect. 9.2, Step 3)

Neglecting attenuation with depth, blast load = 200.0 psi

Earth cover, 8 ft. of soil = $8(0.69)$ = 5.6 psi

Assuming 3 ft. slab depth, est. slab wt. = $3(0.84)$ = 2.5 psi

208 psi

Because of the shallow depth of soil, arching can be neglected.

The design pressure for equivalent one-way slab is, then,

$$p_m = \frac{208}{2.85} = 73 \text{ psi}$$

Take $(\phi_{Lc} + \phi_{Le}) = (\phi_{sc} + \phi_{se}) = (\phi_c + \phi_e) = 1.0$. Then $(\phi_c + \phi_e)f_{dy}$ = 50,000 psi, and from Fig. 9-2, $(d/L) = 0.16$ for flexure. Check other

modes of failure.

Because of the shallow depth of soil, arching can be neglected.

Pure Shear Resistance

Equivalent resistance for one-way slab: (See Sect. 8.3.2)

$$\frac{2}{3} (1 + \alpha) = 1.3$$

The peak applied pressure for an equivalent one-way slab is, therefore,

$$\frac{208}{1.3} = 160 \text{ psi}$$

From Fig. 9-3, for $f'_c = 4000$, $(d/L) = 0.13$ for pure shear; therefore, $(d/L) = 0.16$ as determined above for flexure is adequate.

Diagonal Tension

Equivalent one-way slab pressure = 160 psi

Assume $\phi_{e \text{ avg}} = \phi_c$; from Fig. 9-7, $\lambda_f = 0.7$

If $\phi_c = \phi_e = 0.5$, consistent with $(\phi_c + \phi_e) = 1.0$, then, from Fig. 9-5, with $\lambda_f \phi_c f'_c = 1400$, $\lambda_v \frac{d}{L} = 0.23$.

Hence,

$$\lambda_v = \frac{0.23}{0.16} = 1.44, \text{ for } \frac{d}{L} = 0.16,$$

and, from Fig. 9-6,

$$\phi_v f_{dy} = 52 \text{ ksi}$$

Therefore,

$$\phi_v = 1.04, \text{ say } 1.0$$

Compute Period (Considering shallow depth of earth cover, neglect soil re-

distance but include soil mass). Assuming fixed edge conditions:

$$T = 4.5 \sqrt{\frac{W}{Kg}}, \text{ from Eq. (8-28),}$$

and

$$K \approx 770 \frac{E_c I}{L_s^3 L_L} = 3.87 \text{ psi}$$

Taking the total depth of slab ≈ 2.86 ft., and assuming the unit wt. of soil to be 120 pcf:

$$W = \left(\frac{150}{144} \times 2.86\right) + \left(\frac{120}{144} \times 8.0\right) = 9.7 \text{ psi} \approx 0.010 \text{ Ksi}$$

$$g = 386 \text{ in/sec}^2$$

$$T = 4.5 \sqrt{\frac{0.010}{3.87 (386)}} = 0.0116 \text{ sec}$$

Load Duration

Assume that the effective duration of the load is equal to the initial slope duration:

$$t_d = t_{\infty} = 0.075 \text{ sec., (from Fig. 3-7)}$$

$$\frac{t_d}{T} = \frac{75}{11.6} = 6.5; \text{ consequently, an infinite duration may be reasonably}$$

assumed. Therefore the preliminary design is adequate; no revision is necessary. However, greater economy may result if depth is increased, thereby reducing the web steel requirement.

Slab Summary

$$d = 2.56', \text{ say } 2' 7"; \quad D = 2' 10''$$

$$\phi_{Lc} = \phi_{Le} = \phi_{sc} = \phi_{se} = 0.5; \quad \phi_v = 1.0$$

A.1.2 Design of Supporting Beams (See Sect. 9.3). For beam under long side of slab, converting load on slab to uniform load on beam;

$$\text{With } a = 4', \frac{a}{b} = \frac{4}{20} = 0.2$$

From Fig. 9-10, with $\alpha = 0.94$, $\gamma = 1.31$.

Estimating the effective pressure on the slab to be 210 psi (208 psi from slab computation plus effect of supporting beam):

$$p_m = \frac{210}{1.31} = 160 \text{ psi}$$

$$\text{Thus, } \frac{p_m b}{a} = 160 \times 5 = 800 \text{ psi on equivalent beam under one-way slab.}$$

$$\text{Assume } \phi_c = \phi_e = 1.0$$

$$\text{Then, } f_{dy} (\phi_c + \phi_e) = 100,000$$

$$\text{From Fig. 9-9, } \frac{d}{L} = 0.37 \text{ for flexure}$$

$$\text{Hence, } d = (0.37) (17 \times 12) = 76''$$

Check Pure Shear

From Fig. 9-13, for $\alpha = 0.94$, $\eta = 1.9$

Then, $p_m = \frac{210}{1.9} = 110 \text{ psi}$, $\frac{p_m b}{a} = 550 \text{ psi}$, for equivalent beam under one-way slab.

From Fig. 9-11, assuming equal end steel percentages, $\frac{d}{L} = 0.40$, which is greater than 0.37 as required for flexure.

Therefore, use $d = 0.40 (17 \times 12) = 82 \text{ in.}$ Redetermine flexural steel as $\phi_c = \phi_e = 0.85$.

Check Diagonal Tension

Since $\phi_e / \phi_c = 1.0$, $\lambda_f = 0.7$ (from Fig. 9-7)

Using $\lambda_f \phi_c f'_c = 2380$, and $\frac{p_m b}{a}$ (one-way slab) = 550, then from

Fig. 9-12, $\lambda_v \frac{d}{L} = 0.38$; $\lambda_v = \frac{0.38}{0.37} \approx 1.00$.

Therefore, from Fig. 9-6, $\phi_v = 0$, no web steel needed.

Compute Period

$$T = \frac{1}{85,000 \sqrt{\phi_c}} \frac{L^2}{2} = .0065 \text{ sec. for beam alone.}$$

Correcting for the added mass of slab and soil:

$$\text{Wt. of beam} = 150 (4.0 \times 7.25 \times 17.0) = 76,500 \text{ lbs.}$$

$$\text{Wt. of slab} = 150 (2.83 \times 8.0 \times 17.0) = 57,800 \text{ lbs.}$$

$$\text{Wt. of soil} = 120 (8.0 \times 8.0 \times 17.0) = \underline{130,500 \text{ lbs.}}$$

$$\text{Total} \quad 264,800 \text{ lbs.}$$

Then,

$$T' = 0.0065 \sqrt{\frac{m'}{m}} = 0.0065 \sqrt{\frac{264,800}{76,500}} = 0.0065 \sqrt{3.47} = 0.012 \text{ sec.}$$

Compute Ratio of Load Duration to Period

$$t_d/T = \frac{75}{12} = 6.3$$

Thus, the load can be assumed to be of long duration, and the preliminary design given above does not need revision.

Beam Summary

$$d = 6' 10''; D = 7' 3''$$

$$\phi_c = \phi_e = 0.85, \phi_v = 0.0$$

A.2 BURIED ARCH (See Sect. 9.5)

Give Data (See Sketch)

$$P_{so} = 200 \text{ psi}; W = 1 \text{ MT}; \text{ Cohesionless soil, } \phi \approx 35^\circ$$

$$f_c^I = 3000 \text{ psi}; f_{dc}^I = 3750 \text{ psi}; f_y = 40,000 \text{ psi}; f_{dy} = 50,000 \text{ psi}$$

Semicircular arch of radius $r = 30'$; Depth of cover over crown = 20 ft.

Check Depth of Burial

$$H_{av} = \frac{60(20 + 30) - \frac{\pi}{2}(30)(30)}{60} = 26.4 \text{ ft.}$$

$$26.4 > \left(\frac{L}{4} = 15\right) \text{ (See Sect. 5.3.5)}$$

Therefore "FULLY BURIED"

Determine Load

Peak pressure at depth $z = H_{av} = 26.4'$:

From Fig. 4-3, $\alpha = 0.87$

$$p_m = 0.87 \times 200 = 174 \text{ psi}$$

For preliminary design, assume a long duration load, and take

$t_d = t_{oo}$ corresponding to $p_{so} = 200 \text{ psi}$.

From Fig. 3-7, $t_{oo} = 0.075 \text{ sec.}$; neglect rise time.

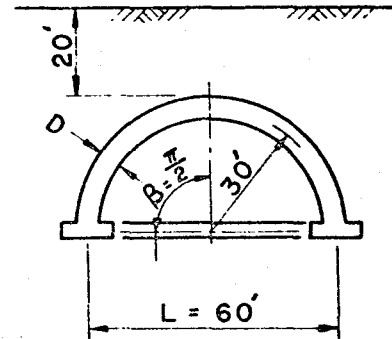
Effects of Soil Arching (Sect. 5.3.2):

Estimate δ_o , considering only deformation of arch. Footing motion cannot be computed with confidence, and its neglect

$$\text{is conservative. } \delta_o \approx \mu r (f_c^I / E_c) = (1.3)(30') \left(\frac{3000}{3,000,000} \right) =$$

0.03' which is less than $0.02(60) = 1.2'$.

From Eq. (5-36), $\frac{p_o}{p_{vp}} \approx 1.00$; therefore, arching effect is negligible.



Trial Section

Assume $\phi_t = 1.0 = 0.5\%$ circumferentially on each face.

$0.85 f'_{dc} + 0.009 \phi_t f_{dy} = 3640$ psi. Then, for $(H_{av} + D) \approx 27$,

Fig. 9-16 gives $\left(\frac{D}{r}\right) (H_{av} + D) = 0.007$ and, for $p_m = 174$ psi, Fig. 9-17 gives

$$\left(\frac{D}{r}\right) (p_m) = 0.080; \Sigma \frac{D}{r} = 0.087.$$

Therefore, $D_{(Preliminary)} = 0.087 \times 30' = 2.61'$, say $2' 8''$

Compute Period

$$T_c = \frac{r}{1800} = \frac{30}{1800} = 0.0167 \text{ sec., from Eq. (8-41)}$$

As discussed in Chapter 8, neglect conservatively a possible modification of T_c for the effects of surrounding soil.

Check Adequacy of Trial Section

Assume the effective load duration to equal the initial slope duration.

From Fig. 3-7, $t_d = t_{\infty} = 0.075$ sec.

$$\frac{t_d}{T} = \frac{0.075}{0.0167} = 4.6$$

For $\frac{t_d}{T} = 4.6$, and $\mu = 1.3$, from Fig. 9-1, $\frac{p_m}{q} = 0.61$.

Since the preliminary design charts were prepared on basis of $\frac{p_m}{q} = 0.61$ (for $t_d/T = \infty$ and $\mu = 1.3$), the preliminary design is adequate for final section. Therefore, use $D = 2' 8''$ and $\phi_t = 1.0$.

A.3 FULLY BURIED DOME (See Sect. 9.6)

Given Data

$p_{so} = 100$ psi; $W = 10$ MT; Hemispherical dome ($\beta = \pi/2$);
Radius, $r = 20$ ft.; Depth of earth cover over crown = 6.0 ft., with
ground surface level; μ selected as 1.3; $f'_c = 3000$ psi; $f'_{dc} = 3750$ psi;
 $f_y = 40,000$ psi; $f_{dy} = 50,000$ psi.

Check Depth of Burial

For full burial, $H_{av} > \frac{1}{4} L$ where $L = 40'$, but not less than
 $\frac{L}{8} = 5.0$ ft.

$$H_{av} = \frac{400\pi (20 + 6) - \frac{2}{3}\pi (8000)}{400\pi} = 12.7 \text{ ft.}$$

which is greater than $\frac{40}{4} = 10.0$ ft. and $\frac{L}{8} = 5.0$ ft.

Therefore, consider the dome to be fully buried, and design only for
the compressive component of loading.

Loading

Uniform Compression Loading = $p_{so} = 100$ psi, from blast

plus dynamic equivalent of DL = 7 psi = (0.51×12.7) from
earth cover.

Total = 107 psi; neglect weight of dome

Preliminary Design

With $\beta = 90^\circ$, $p_{so} = 100$ psi, and $(0.85 f'_{dc} + 0.009 \phi_t f_{dy}) = 3630$,
which assumes nominal steel of 0.5% in each face, read $\frac{D}{r}$ for blast load =
0.044 from Fig. 9-17 for corresponding arch. For dome: $\frac{0.044}{2} = 0.022$. For
 $(H_{av} + D) \approx 13$ ft., read $\frac{D}{r}$ for dead load = 0.004 from Fig. 9-16 for
corresponding arch. For dome: $\frac{0.004}{2} = 0.002$. Then $\frac{D}{r}$ total = 0.024, and
 $D = 0.48'$. Try $D = 6''$.

Check Adequacy of Trial Section

Compute the natural period,

By Eq. (8-61), $T = \frac{r_1 \text{ ft.}}{2500} = .008 \text{ sec.}$

Uniform Compression Mode Load Duration

Assume an effective duration, $t_d = t_\infty$, the initial slope duration, for $p_{so} = 100 \text{ psi.}$

From Fig. 3-7, $t_\infty = 0.15 \left(\frac{10}{1}\right)^{1/3} = 0.32 \text{ sec.}$

$\frac{t_d}{T} = \frac{320}{8} = 40$. Thus, the assumption that $t_d = t_\infty$ is reasonable, and load duration can be taken as infinite. Therefore, the preliminary design is adequate. Use $D = 6''$ and $\phi_t = 1.0$.

Study of Interaction Between the Foundation and the Dome

If the dome were free to slide over the footing in such a manner as to take a deflected shape consistent with the stresses computed above, the design of the dome shell would be complete; however, it is necessary to investigate the effects of the footing acting as a ring girder on the dome if relative motion between the shell and the footing is not permitted.

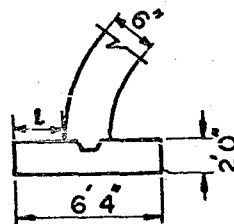
Design of Footing

The footing must support a peak load of $252 \frac{k}{ft}$ of length, including dead load and dynamic magnification factor for $\mu = 1.3$ of 1.62. Assume the allowable dynamic soil pressure to be 40 ksf (See Section 9.8).

Hence, a footing width of $\frac{252}{40} = 6.3 \text{ ft.}$ is required.

To find the footing depth enter

Fig. 9-35 with a soil pressure of 40 ksf and $\phi = 1$ (therefore $\phi f_{dy} = 50,000$); find $\frac{d}{L} = 0.55$.

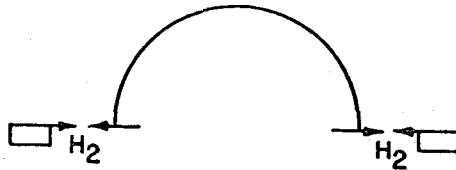


Since $l = \frac{1}{2} (6.3 - 0.5) = 2.9$ ft., $d = 0.55 (2.9) = 1.60$ ft. for flexure.

Check shear requirement in footing. From Fig. 9-36, with $W = 40$ ksf and $f'_c = 3000$ psi, read $\frac{d}{l} = 0.58$. Therefore, increase d to 1.68 ft., or 1'8".

Use total thickness 2'0".

Dome and footing displacements are not consistent; a force H_2 , as shown in the sketch, is required to pull them together.



Determine Force H_2

To evaluate the force H_2 required to make the radial displacements of the dome and footing equal, set the hoop stresses in the footing produced by H_2 equal to the T_θ stresses in the dome produced by a combination of the applied external loads and H_2 .

Assuming a nominal amount (1%) of ring steel in the footing, the effective cross-section of the footing is:

$$\text{Concrete} = 6.33 \times 2.00 \times 144 = 1824 \text{ sq. in.}$$

$$\text{Ring Steel} = (0.01)(1824) \left(\frac{E_s}{E_c} \right) = \underline{182}$$

$$\text{Total} = 2006 \text{ sq. in. of concrete}$$

$$\text{where } \frac{E_s}{E_c} = \frac{30,000,000}{3,000,000} = 10$$

As indicated on Fig. 8-12, the circumferential force, T_θ , in the dome produced by a force such as H_2 , is given by:

$$T_\theta = \left[H \sqrt{\frac{r}{D}} \sin \beta \right] C \text{ lbs per ft.}$$

At the base of the dome, $\psi = 0$, and, from Fig. 8-12, $C = 2.63$.

Under uniform radial pressure, neglecting edge restraint effects, the dome is subjected to uniform compressive stresses in all directions which, for this problem, are (refer to footing design computations above):

$$\frac{252,000}{6.0 \times 12} = 3500 \text{ psi}$$

Then, equating the hoop stresses in the footing to the corresponding stresses at the base of the dome yields:

$$\frac{(H_2)(20 \times 12)}{2006} = \frac{252,000}{6.0 \times 12} - \frac{\left[(H_2) \sqrt{\frac{20 \times 12}{6}} \sin 90^\circ \right] (2.63)}{6.0 \times 12}$$

from which $H_2 = 10,000 \text{ lbs/ft.}$

Effect of H_2 on T_θ Stresses

Due to external load: circumferential stress = 3500 psi in compression, as indicated above.

$$\text{Due to } H_2: T_\theta = \left[10,000 \sqrt{\frac{20 \times 12}{6}} \sin 90^\circ \right] (2.63)$$

$$= 166,000 \text{ lbs/ft. in tension.}$$

The corresponding tensile stress is $\frac{166,000}{6.0 \times 12} = 2300$ psi tension.

Therefore, the net circumferential stress at the base of the dome is:

$$3500 - 2300 = 1200 \text{ psi, compression.}$$

Effect of H_2 on T_ψ Stresses

Due to the external loads, the stress is equal in all directions and, for the case being studied, it is 3500 psi, compression.

Reference to Fig. 8-12 indicates that, for a hemispherical dome, the longitudinal, T_ψ , stresses can be neglected.

Thus, the net longitudinal stress in the dome is 3500 psi, compression.

Effect of H_2 on M_ψ

Due to the uniform external loads, the moment is zero.

As indicated in Fig. 8-12, the longitudinal moment resulting from H_2 is:

$$M_\psi = \left[H \sqrt{rD} \sin \beta \right] \left(\frac{C}{10} \right)$$

where C has a maximum value of 2.45 at a point defined by $\sqrt{\frac{r}{D}} \psi = 0.6$, which corresponds to:

$$\psi = \frac{0.6}{\sqrt{\frac{20 \times 12}{6}}} = \frac{0.6}{6.33} = 0.095 \text{ rad.} = 5.5^\circ$$

Thus, the maximum value of M_ψ occurs at $\psi = 5.5^\circ$, and is given by

$$\begin{aligned} \text{Max. } M_\psi &= \left[(10,000) \sqrt{20 \times 0.5} \sin 90^\circ \right] \left(\frac{2.45}{10} \right) \\ &= 7,850 \text{ ft-lbs/ft.} \end{aligned}$$

Analyze a longitudinal strip one ft. wide under the combined effects of T_ψ and M_ψ .

Actual thrust = $P = 252,000$ lbs/ft.

Ultimate thrust, acting alone = P_u

$$P_u = (0.85 f'_{dc} + 0.009 \phi_t f_{dy}) (6 \times 12) \\ = 262,000 \text{ lbs/ft.}$$

$$\text{Therefore, } \frac{P}{P_u} = \frac{252}{262} = 0.96$$

With 0.5% steel on each face,

$$\frac{\phi f_{dy}}{100 f'_c} = \frac{(0.5)(50,000)}{(100)(3000)} = 0.083$$

Entering Fig. 8-5, read $\frac{M}{M_u} = 0.18$

Thus, to be adequate, the ultimate moment capacity, acting alone, must be at least

$$M_u = \frac{7,850}{0.18} = 43,600 \text{ ft-lbs/ft.}$$

For the 6-in. dome selected on the basis of the preliminary analysis, with $\phi = 0.5$ on each face:

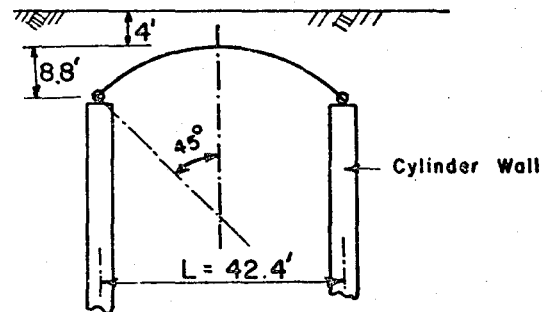
$$M_u = 0.009 \phi f_{dy} d^2 \\ = (0.009)(0.5)(50,000)(4.5)^2 = 4,550 \text{ ft-lbs/ft.}$$

Since the actual moment capacity is much less than that required, the dome should be redesigned with an increased thickness, unless substantial cracking in the dome can be tolerated. Reference to Fig. 8-12 indicates that the intensity of bending moment induced by the H_2 forces diminishes quite rapidly as the angle ψ increases. Hence, the severe cracking will be

local in nature. Furthermore, the local inelastic behavior tends to permit the development of relative displacement between the dome and its footing, thereby reducing the force H_2 and the moment produced by it.

A.4 SHALLOW BURIED DOME

Design a dome with an opening angle of 90° and a radius of $30'$, which is attached to the top of a cylinder as shown in the sketch. The depth of earth cover over the crown is $4'$. Design for $p_{so} = 100$ psi from a 10 MT, surface burst. Use ductility factor, $\mu = 1.3$.



Average Depth of Earth Cover

$$H_{av} = \frac{\pi (21.2)^2 (12.8) - \frac{\pi}{3} (8.8)^2 [3(30) - 8.8]}{\pi (21.2)^2}$$

$$= 8.1 < \frac{L}{4}; \text{ therefore, consider the dome to be partially buried.}$$

Loading (See Sect. 5.4.4)

Uniform compression (peak value):

$$\text{Blast pressure} = 100 \text{ psi}$$

$$\text{Blast equivalent of D.L}_1 = \frac{4 \text{ psi}}{104 \text{ psi}} = 0.51 \text{ (8.1)}$$

Neglect weight of dome.

Flexural Component (peak value):

$$\left[1 - 4 \left(\frac{H_{av}}{L} \right) \right] p_{so} = \left[1 - 4 \left(\frac{8.1}{42.4} \right) \right] (100) = 24 \text{ psi}$$

Preliminary Design

To obtain a reasonable section to be checked by further calculation, use Fig. 9-29.

With $\beta = 45^\circ$ and $p_{so} = 100$ psi, enter Fig. 9-29

and read: $\frac{D}{r} (0.85 f'_{dc} + 0.009 \phi_t f_{dy}) = 135$ psi

Selecting $f'_c = 3000$ psi, $f'_{dc} = 3750$ psi,

$f_y = 40,000$ psi, $f_{dy} = 50,000$ psi

and $\phi_t = 1.0$,

$$\text{compute } \frac{D}{r} = \frac{135}{3630} = 0.0372$$

Thus, $D = 0.0372 (30 \times 12) = 13.4$ in.

Try $D = 1'2''$ with $\phi_t = 1.0$ (0.5% each face)

Period of Vibration (See Sect. 8.8.3)

The same period should be used for both components of load. As recommended in the referenced section, the effect of the soil mass is neglected.

$$T \approx \frac{r, \text{ ft}}{2500} = \frac{30}{2500} = 0.012 \text{ sec.}$$

Load Durations

For the uniform compression component, try an effective duration equal to the initial slope duration of the overpressure pulse. Then, from Fig. 3-7

$$t_d = t_\infty = 0.15 \left(\frac{10}{1}\right)^{1/3} = 0.32 \text{ sec.}$$

Since $\frac{t_d}{T} = \frac{0.32}{0.012} = 27$, the assumption that $t_d = t_\infty$ is reasonable.

For the flexural component of load, the duration is given by

(Sect. 5.4.3)

$$t_d = \left(1 + 3 \frac{\beta_s}{\pi}\right) \tau$$

where $\tau = L/U$, U being the shock front velocity, which can be determined from basic data sources such as "Effects of Nuclear Weapons". For $p_{s0} = 100$ psi, $U \approx 3000$ fps.

Since the ground surface is level, $\beta_s = 0$. Therefore, for the flexural component:

$$t_d = \tau = \frac{L}{U} = \frac{42.4}{3000} = 0.014 \text{ sec.}$$

$$\text{and } \frac{t_d}{T} = \frac{0.014}{0.012} = 1.17$$

Required Resistances (Fig. 9-1, with $\mu = \frac{x_m}{x_y} = 1.3$):

Uniform compression:

$$\text{For } \frac{t_d}{T} = 1.17, \frac{p_m}{q} = 0.61$$

$$\text{Hence, } q_c \text{ (required)} = \frac{104}{0.61} = 170 \text{ psi}$$

Flexural component:

$$\text{For } \frac{t_d}{T} = 1.17, \frac{p_m}{q} = 0.77$$

$$\text{Hence, } q_f \text{ (required)} = \frac{24}{0.77} = 31 \text{ psi}$$

Compute Stresses Corresponding to Required Resistances

For the uniform compression mode, the membrane forces are constant throughout, and are given by Eq. (8-62) as

$$T_\theta = T_\psi = \frac{p_o r}{2} = \frac{170(30 \times 12)}{2} = 30,600 \text{ lbs/in}$$

in compression. The corresponding stress is

$$\sigma_\theta = \sigma_\psi = \frac{T_\theta = T_\psi}{D} = \frac{30,600}{14} = 2,180 \text{ psi}$$

For the flexural mode, the membrane forces are given by Eq.

(8-64) as follows:

$$T_{\psi} = \frac{P_1 r}{3} \left[2 + \cos (\beta - \psi) \right] \cot (\beta - \psi) \tan^2 \left(\frac{\beta - \psi}{2} \right) \cos \theta$$

$$T_{\theta} = \frac{P_1 r}{3} \left[3 + 4 \cos (\beta - \psi) + 2 \cos^2 (\beta - \psi) \right] \frac{\tan^2 \left(\frac{\beta - \psi}{2} \right)}{\sin (\beta - \psi)} \cos \theta$$

$$T_{\theta\psi} = \frac{P_1 r}{3} \left[2 + \cos (\beta - \psi) \right] \frac{\tan^2 \left(\frac{\beta - \psi}{2} \right)}{\sin (\beta - \psi)} \sin \theta$$

$$\text{where } P_1 = q_f / \sin \beta = 31 \text{ psi} / \sin 45^\circ = 44 \text{ psi}$$

These forces have their maximum values at the edge of the dome ($\psi=0$).

Therefore:

$$T_{\psi} = \frac{44(30 \times 12)}{3} \left[2 + \cos 45^\circ \right] \cot 45^\circ \tan^2 22.5^\circ \cos 0^\circ$$

$$= 5280 (2.707) (1.0) (0.414)^2 (1.0)$$

$$= 2450 \text{ lbs/in compression}$$

and the corresponding stress, σ_{ψ} , is $\frac{2450}{14} = 175 \text{ psi}$

$$T_{\theta} = \frac{44(30 \times 12)}{3} \left[3 + 4 \cos 45^\circ + 2 \cos^2 45^\circ \right] \frac{\tan^2 22.5^\circ}{\sin 45^\circ} \cos 0^\circ$$

$$= 5280 (6.83) \frac{(0.414)^2}{0.707} (1.0)$$

$$= 8730 \text{ lbs/in compression}$$

and the corresponding stress, σ_{θ} , is $\frac{8730}{14} = 623 \text{ psi}$

$$T_{\theta\psi} = \frac{44(30 \times 12)}{3} \left[2 + \cos 45^\circ \right] \frac{\tan^2 22.5^\circ}{\sin 45^\circ} \sin 90^\circ$$

$$= 5280 (2.707) \frac{(0.414)^2}{0.707} (1.0)$$

$$= 3460 \text{ lbs/in shear}$$

and the corresponding shear stress, $\tau_{\theta\psi}$, is $\frac{3460}{14} = 247 \text{ psi}$

Resultant Maximum Stresses

$$\Sigma \sigma_{\psi} = 2180 + 175 = 2355 \text{ psi compression}$$

$$\Sigma \sigma_{\theta} = 2180 + 623 = 2803 \text{ psi compression}$$

$$\Sigma \pi_{\theta\psi} = 0 + 247 = 247 \text{ psi shear}$$

These stresses are based on the assumption that the edge of the dome is not restrained but is free to deform in a manner consistent with these stresses.

Investigate Edge Restraint Effects

The following analysis is based on the assumption that the cylinder walls on which the dome is supported are rigid. This is, of course, an unreal assumption and will lead to edge-restraint stresses in the dome that are greater than they actually would be.

Consider first only the uniform compression mode.

Assume that the cylinder wall is rigid and that there is no relative displacement between the dome and the cylinder, though rotation is permitted at their juncture. Under this condition, T_{θ} must be zero at the edge of the dome, instead of 30,600 lbs/in in compression as computed earlier. Therefore, from Fig. 8-12, the edge force H necessary to establish this condition is given by

$$H \sqrt{\frac{r}{D}} (\sin \beta) C = 30,600 \text{ lbs/in, tension.}$$

from which

$$H = \frac{30,600}{\sqrt{\frac{30 \times 12}{14}} (0.707) (2.63)} = 3230 \text{ lbs/in}$$

The T_v force produced by this value of H is, from Fig. 8-12:

$$T_v = [H \sin \beta \cot \beta] C$$

$$= (3230)(0.707)(1.00)(1.0) = 2280 \text{ lbs/in tension}$$

and the corresponding stress is

$$\sigma_v = \frac{2280}{14} = 163 \text{ psi in tension.}$$

The bending moment produced by this value of H is, from Fig. 8-12

$$M_v \text{ max.} = [H \sqrt{rD} \sin \beta] \frac{C}{10}$$

$$= 3230 \sqrt{(30 \times 12) / 14} (0.707)(0.245)$$

$$= 39,600 \text{ in-lbs/in}$$

which occurs at $\psi \approx 7^\circ$

Consider now the flexural component of load. As for the uniform compression mode just considered, assume, by virtue of the rigidity of the cylinder, that there are no displacements at the base of the dome, though rotation is possible. Consequently, the previously computed flexural component stresses must be modified.

From Eq. (8-66) compute

$$\alpha \approx 1.3 \sqrt{\frac{30 \times 12}{14}} = 6.6$$

The support conditions for the dome (as assumed above) are:

$$M_v = 0 \text{ and } \xi = 0 \text{ (no horizontal displacement)}$$

From Eq. (8-67), the zero moment support condition yields

$$\frac{M_{\downarrow}}{ED_r} = - \left[\left(1 - \frac{1-\nu}{2\alpha} \cot \beta \right) k_1 + \left(\alpha \cot \beta + 1 - \frac{1}{\sin^2 \beta} \right) \frac{1-\nu}{2\alpha^2} k_2 \right] = 0$$

Since the dome is to be constructed of concrete, ν is assumed to be zero. Thus

$$\left[1 - \frac{1}{2(6.6)} (1.0) \right] k_1 + \left[6.6(1.0) + 1 - \frac{1}{\frac{1}{2}} \right] \left(\frac{1}{2(6.6)^2} \right) k_2 = 0$$

and $k_2 = -14.4 k_1$

From Eq. (8-70), the second support condition stipulating zero horizontal displacement is

$$\frac{\xi_c}{r} = \frac{\xi_o + u_o}{r} - k_1 \left[\alpha \cos \beta - \frac{1}{\sin \beta} \right] + k_2 \left[2\alpha^2 \sin \beta - \alpha \cos \beta \right] = 0$$

where ξ_o and u_o represent membrane displacements. The quantity ξ_o is the horizontal displacement accompanying the membrane stresses and is therefore

$$\xi_o = w \sin \beta + v \cos \beta$$

and, substituting for w and u their values from Eq. (8-65),

$$\frac{\xi_o}{r} = \frac{P_1 r}{3ED} \left\{ - \left[\sin \beta \log (1 + \cos \beta) + \sin \beta + \cot \beta (1 - \cos \beta) \right] \cos \theta \sin \beta \right. \\ \left. + \left[- \cos \beta \log (1 + \cos \beta) + 1 + \frac{1}{1 + \cos \beta} \right] \cos \theta \cos \beta \right\}$$

With $\beta = 45^\circ$, and $\theta = 0^\circ$, $\frac{\xi_o}{r} = -0.0402 \frac{P_1 r}{ED}$

Similarly:

$$\frac{u_o}{r} = \frac{P_1 r}{3ED} \left[\log (1 + \cos \beta) - 1 - \frac{1}{1 + \cos \beta} \right] = - 0.3504 \frac{P_1 r}{ED}$$

Therefore, for $\beta = 45^\circ$ and $\theta = 0^\circ$,

$$\frac{\xi_o + u_o}{r} = - 0.3906 \frac{P_1 r}{ED}$$

Then

$$-\left[\alpha \cos \beta - \frac{1}{\sin \beta} \right] k_1 + \left[2 \alpha^2 \sin \beta - \alpha \cos \beta \right] k_2 = 0.3906 \frac{P_1 r}{ED}$$

$$-\left[6.6(0.707) - 1.414 \right] k_1 + \left[2(43.6)(0.707) - 6.6(0.707) \right] (-14.4 k_1) = 0.3906 \frac{P_1 r}{ED}$$

$$- 825 k_1 = 0.3906 \frac{P_1 r}{ED}$$

$$k_1 = - 0.000474 \frac{P_1 r}{ED}$$

$$\text{and } k_2 = - 14.4 k_1$$

$$= 0.00682 \frac{P_1 r}{ED}$$

With the values of k_1 and k_2 now known, the magnitudes of M_ψ , T_ψ , T_θ , and $T_{\psi\theta}$, which result from the boundary effects, can be determined from the equations of Table 8-1.

$$\frac{M_\psi}{EDr} = \left\{ \left[\left(1 - \frac{1}{2\alpha} \cot \beta \right) k_2 - \left(\alpha \cot \beta + 1 - \frac{1}{\sin^2 \beta} \right) \frac{1}{2\alpha^2} k_1 \right] \varphi_s \right.$$

$$\left. - \left[\left(1 - \frac{1}{2\alpha} \cot \beta \right) k_1 + \left(\alpha \cot \beta + 1 - \frac{1}{\sin^2 \beta} \right) \frac{1}{2\alpha^2} k_2 \right] \varphi_c \right\} \cos \theta$$

where $\phi_s = e^{-\alpha\psi} \sin \alpha\psi$ and $\phi_c = e^{-\alpha\psi} \cos \alpha\psi$. For maximum, at $\theta = 0^\circ$,

$$\frac{M_\psi}{EDr} = \left[\left(1 - \frac{1}{13.2}\right) \left(0.00682 \frac{P_1 r}{ED}\right) - \left(6.6 + 1.0 - \frac{1}{0.5}\right) \frac{1}{2(6.6)^2} \left(-0.000474 \frac{P_1 r}{ED}\right) \right] e^{-\alpha\psi} \sin \alpha\psi$$

$$- \left[\left(1 - \frac{1}{13.2}\right) \left(-0.000474 \frac{P_1 r}{ED}\right) + \left(6.6 + 1.0 - \frac{1}{0.5}\right) \frac{1}{2(6.6)^2} \left(0.00682 \frac{P_1 r}{ED}\right) \right] e^{-\alpha\psi} \cos \alpha\psi$$

$$M_\psi = \left\{ \left[(0.9243)(0.00682) + (5.6) \frac{1}{87} (0.000474) \right] e^{-\alpha\psi} \sin \alpha\psi - \left[-(0.9243)(0.000474) + (5.6) \frac{1}{87} (0.00682) \right] e^{-\alpha\psi} \cos \alpha\psi \right\} P_1 r^2$$

$$M_\psi = \left\{ \left[0.00630 + 0.00003 \right] e^{-\alpha\psi} \sin \alpha\psi - \left[-0.00044 + 0.00044 \right] e^{-\alpha\psi} \cos \alpha\psi \right\} P_1 r^2$$

$$= \left[0.00633 e^{-\alpha\psi} \sin \alpha\psi \right] P_1 r^2$$

The position of the maximum moment M_ψ is obtained from:

$$\frac{\partial M_\psi}{\partial \psi} = 0.00633 P_1 r^2 \frac{\partial (e^{-\alpha\psi} \sin \alpha\psi)}{\partial \psi} = 0$$

Therefore,

$$\frac{\partial (e^{-\alpha\psi} \sin \alpha\psi)}{\partial \psi} = -\alpha e^{-\alpha\psi} \sin \alpha\psi + \alpha e^{-\alpha\psi} \cos \alpha\psi = 0$$

$$\text{and } \sin \alpha\psi = \cos \alpha\psi$$

Therefore, the maximum moment occurs at an angle

$$\alpha\psi = 45^\circ \text{ or } \psi = \frac{45}{(6.6)} = 6.8^\circ$$

which is at the same location as the uniform compression moment previously computed.

$$e^{-\alpha\psi} \sin \alpha\psi = e^{-0.785} (\sin 45^\circ) = 0.321$$

Therefore,

$$M_{\psi \max} = (0.00633)(0.321) P_1 r^2 = 11,600 \text{ in-lbs/in.}$$

From Table 8-1,

$$\begin{aligned} \frac{T_{\psi}}{ED} = & \left\{ \left[\alpha(k_1 + k_2) \cot \beta - \frac{1}{\sin^2 \beta} k_1 \right] \varphi_c \right. \\ & \left. + \left[\alpha(k_1 - k_2) \cot \beta + \frac{1}{\sin^2 \beta} k_2 \right] \varphi_s \right\} \cos \theta \end{aligned}$$

for which a maximum exists at $\theta = 0^\circ$.

$$\begin{aligned} \frac{T_{\psi}}{ED} = & \left[(6.6) (0.00635 \frac{P_1 r}{ED}) (1.0) - \frac{1}{0.500} (-0.00047 \frac{P_1 r}{ED}) \right] e^{-\alpha\psi} \cos \alpha\psi \\ & + \left[(6.6) (-0.00729 \frac{P_1 r}{ED}) (1.0) + \frac{1}{0.500} (0.00682 \frac{P_1 r}{ED}) \right] e^{-\alpha\psi} \sin \alpha\psi \\ T_{\psi} = & \left[0.0428 e^{-\alpha\psi} \cos \alpha\psi - 0.0345 e^{-\alpha\psi} \sin \alpha\psi \right] P_1 r \end{aligned}$$

The location of $T_{\alpha \max}$ is given by

$$\begin{aligned} \frac{\partial T_{\psi}}{\partial \psi} = & 0.0428 P_1 r (-\alpha e^{-\alpha\psi} \cos \alpha\psi - \alpha e^{-\alpha\psi} \sin \alpha\psi) \\ & - 0.0345 P_1 r (-\alpha e^{-\alpha\psi} \sin \alpha\psi + \alpha e^{-\alpha\psi} \cos \alpha\psi) = 0 \\ & - 0.0773 \cos \alpha\psi - 0.0083 \sin \alpha\psi = 0 \\ & \cos \alpha\psi = -0.107 \sin \alpha\psi \end{aligned}$$

Thus, for $T_\psi = \text{max.}, \text{ or min.}$

$$\alpha\psi = 96^\circ \text{ and } \psi = 14.5^\circ$$

Also, $T_\psi \text{ max or min. may occur at } \alpha\psi = 0^\circ$

$$\begin{aligned} \text{Then, } T_{\psi \text{ max}} &= \left[0.0428 \cos (96^\circ) - 0.0345 \sin (96^\circ) \right] P_1 r e^{-1.675} \\ &= \left[0.0428 (-0.105) - 0.0345 (0.994) \right] (0.187) P_1 r \\ &= - 0.0073 P_1 r \\ &= - 0.0073 (44) (30 \times 12) = - 116 \text{ lbs/in.} \end{aligned}$$

The corresponding stress is

$$\sigma_\psi = \frac{116}{14} = 8 \text{ psi, compression}$$

At the edge $\alpha\psi = 0$

$$T_{\psi \text{ max}} = (0.0428) P_1 r = 678 \text{ lbs/in}$$

$$\sigma_\psi = \frac{678}{14} = 48 \text{ psi tension}$$

The T_θ forces are given by Table 8-1 as:

$$\frac{T_\theta}{ED} = \left[\frac{w}{r} - \frac{T_\psi}{ED} \right] \cos \theta$$

$$\text{where } \frac{w}{r} = \left[2\alpha^2 k_2 \varphi_c + 2\alpha^2 k_1 \varphi_s \right] \cos \theta$$

$$= 2\alpha^2 (k_2 \varphi_c + k_1 \varphi_s) \cos \theta; \text{ and, for } \theta = 0^\circ,$$

$$= 87.2 \left[0.00682 e^{-\alpha\psi} \cos \alpha\psi - 0.00047 e^{-\alpha\psi} \right] \frac{P_1 r}{ED}$$

$$\text{and } \frac{T_{\psi}}{ED} = \left[0.0428 e^{-\alpha\psi} \cos \alpha\psi - 0.0345 e^{-\alpha\psi} \sin \alpha\psi \right] \frac{P_1 r}{ED} \text{ for } \theta = 0^\circ.$$

Therefore,

$$T_{\theta} = \left[0.552 e^{-\alpha\psi} \cos \alpha\psi - 0.0054 e^{-\alpha\psi} \sin \alpha\psi \right] P_1 r$$

and its maximum occurs at:

$$\begin{aligned} \frac{\partial T_{\theta}}{\partial \psi} &= 0.552 P_1 r (-\alpha e^{-\alpha\psi} \cos \alpha\psi - \alpha e^{-\alpha\psi} \sin \alpha\psi) \\ &\quad - 0.0054 P_1 r (-\alpha e^{-\alpha\psi} \sin \alpha\psi + \alpha e^{-\alpha\psi} \cos \alpha\psi) = 0 \end{aligned}$$

from which

$$\cos \alpha\psi = -0.982 \sin \alpha\psi$$

$$\cot \alpha\psi = 0.982$$

and $\alpha\psi \approx 135^\circ$.

$$\text{Thus } \psi \text{ for } T_{\theta \text{ max}} = \frac{135}{6.6} = 20.5^\circ$$

The T_{θ} force thus becomes

$$\begin{aligned} T_{\theta} &= \left[0.547 \right] \left[\cos \alpha\psi \right] e^{-\alpha\psi} P_1 r \\ &= \left[0.547 \right] \left[0.707 \right] \left[0.095 \right] \left[44 \right] \left[30 \times 12 \right] = 572 \text{ lbs/in. comp.} \end{aligned}$$

The corresponding stress is

$$\sigma_{\theta} = \frac{572}{14} = 42 \text{ psi compression}$$

The $T_{\psi\theta}$ as given in Table 8-1 is

$$\frac{T_{\psi\theta}}{ED} = \frac{1}{\sin \beta} \left\{ \left[\alpha(k_1 + k_2) - k_1 \cot \beta \right] \varphi_c + \left[\alpha(k_1 - k_2) + k_2 \cot \beta \right] \varphi_s \right\} \sin \theta$$

For maximum at $\theta = 90^\circ$:

$$\begin{aligned} T_{\psi\theta} &= 1.414 \left\{ \left[6.6(0.00635) + 0.00047 \right] e^{-\alpha\psi} \cos \alpha\psi + \left[6.6(-0.00729) + \right. \right. \\ &\quad \left. \left. 0.00682 \right] e^{-\alpha\psi} \sin \alpha\psi \right\} P_1 r \\ &= 1.414 \left[0.0424 e^{-\alpha\psi} \cos \alpha\psi - 0.0413 e^{-\alpha\psi} \sin \alpha\psi \right] P_1 r \end{aligned}$$

The max. $T_{\psi\theta}$ occurs at

$$\begin{aligned} \frac{\partial T_{\psi\theta}}{\partial \psi} &= 1.414 P_1 r \left\{ 0.0424 (-\alpha e^{-\alpha\psi} \cos \alpha\psi - \alpha e^{-\alpha\psi} \sin \alpha\psi) - 0.0413 (-\alpha e^{-\alpha\psi} \sin \alpha\psi \right. \\ &\quad \left. + \alpha e^{-\alpha\psi} \cos \alpha\psi) \right\} = 0 \end{aligned}$$

Therefore,

$$\begin{aligned} -0.0837 \cos \alpha\psi - 0.0011 \sin \alpha\psi &= 0 \\ \cos \alpha\psi &= -0.0132 \sin \alpha\psi \\ \cot \alpha\psi &= -0.0132 \text{ or } \alpha\psi \approx 90^\circ \\ \text{and } \psi &= \frac{90}{6.6} = 13.6^\circ \end{aligned}$$

Another possible max of $T_{\psi\theta}$ is at $\alpha\psi = 0$

For $\alpha\psi = 90^\circ$

$$\begin{aligned} T_{\psi\theta} &= 1.414 \left[-0.0413 \right] e^{-\alpha\psi} P_1 r \\ &= -1.414 (0.0413) (0.208) (44) (30 \times 12) \\ &= -192 \text{ lbs/in} \\ \tau_{\psi\theta} &= -\frac{192}{14} = -13.7 \text{ psi shear} \end{aligned}$$

For $\alpha\psi = 0$

$$T_{\psi\theta} = 1.414 (0.0424) (44) (30 \times 12)$$

$$\approx 950 \text{ lbs/in}$$

$$\tau_{\psi\theta} = \frac{950}{14} = 68 \text{ psi shear}$$

Stress Summary

The several maximum stresses, and the points at which they occur are summarized below. Tension is indicated as positive and compression as negative.

<u>Membrane Stresses</u>			<u>Edge Effects</u>	
	<u>Uniform Compression</u>	<u>Flexural Mode</u>	<u>Uniform Compression</u>	<u>Flexural Mode</u>
$\sigma_{\theta} =$	-2180 psi	-623 psi	+ 2180 psi	-42 psi
$\psi =$	all	0	0	20°
$\theta =$	all	0	all	0
$\sigma_{\psi} =$	-2180 psi	-175 psi	+ 163 psi	+ 48 psi; -8 psi
$\psi =$	all	0	0	0 ; 14.5°
$\theta =$	all	0	all	0 ; 0
$\tau_{\psi\theta} =$	0	247 psi	0	68 psi
$\psi =$	all	0	all	0
$\theta =$	all	90°	all	90°
$M_{\psi} =$	0	0	39,600 in-lbs/in	12,200 in-lbs/in
$\psi =$	all	all	7°	6.8°
$\theta =$	all	all	all	0

A review of these tabulated stresses indicates clearly that, except for the bending moment induced, the edge effects are of relatively little consequence.

To study the influence of the edge-effect moment, note that it acts in combination with the σ_ψ stresses. Since σ_ψ , for the flexural mode edge effects, is obviously quite small and varies from + 48 psi at $\psi = 0$ to -8 psi at $\psi = 14.5^\circ$, it may reasonably be neglected at $\psi \approx 7^\circ$, the point of maximum moment. Thus, the thrust may be taken as:

$$\begin{aligned} T_{\psi \max} &= (-2180 - 175 + 163) \text{ psi} \times D \\ &= (-2192)(14) = 30,600 \text{ lbs/in} \end{aligned}$$

and the maximum moment is:

$$\begin{aligned} M_{\psi \max} &= (39,600 + 11,600) \text{ in-lbs/in} \\ &= 51,200 \text{ in-lbs/in} \end{aligned}$$

The ultimate thrust capacity is:

$$\begin{aligned} P_u &= (0.85 f'_{dc} + 0.009 \phi_t f_{dy}) D \\ &= (3630)(14) = 50,800 \text{ lbs/in} \end{aligned}$$

Then,

$$\frac{T_{\psi \max}}{P_u} = \frac{30,600}{50,800} = 0.60$$

Entering Fig. 8-5 with

$$\frac{\phi f_{dy}}{100 f'_c} = \frac{(0.5)(50,000)}{(100)(3000)} = 0.083$$

read $\frac{M}{M_p} \approx 2.0$

Therefore, the required ultimate moment capacity is:

$$M_p = \frac{M_{\psi \text{ max}}}{2} = \frac{51,200}{2} = 25,600 \text{ in-lbs/in}$$

With $\phi_t = 1.0$ (0.5% each face), and assuming $d = 12''$ (2" cover on steel), the ultimate moment capacity of the trial section is

$$\begin{aligned} M_p &= 0.009 \phi f_{dy} d^2 \\ &= (0.009)(0.5)(50,000)(12)^2 \\ &= 32,400 \text{ in-lbs/in} \end{aligned}$$

which is greater than required.

It may be concluded that the trial section ($D = 14''$, $\phi = 0.5$ on each face) is adequate, and somewhat conservative. The section could be reduced slightly.

It should be noted that this analysis assumed the supporting cylinder walls to be rigid; consequently, the computed edge effects are somewhat greater than they would actually be if the cylinder walls deformed. After the side walls of the cylinder have been designed, the dome should be investigated allowing for movement of the support. The boundary conditions to impose are that the dome and the cylindrical side wall have equal displacements at their edge. Reference 8-24 contains a method for accomplishing this.

APPENDIX B
DYNAMIC THEORY OF STRUCTURES

B.1 INTRODUCTION

B.1.1 Single Versus Multi-Degrees-of-Freedom Systems. Most structures are exceedingly complex in their dynamic behavior. There is an interplay of elastic and inelastic vibrational modes, and different parts do not necessarily respond in phase with each other. The complete configuration of a deforming complex structure usually defies accurate mathematical description.

Mathematical analysis is possible for structural systems having only limited degrees of freedom, but for more than a few degrees of freedom the solution becomes exceedingly tedious. By "degree of freedom" is meant the number of generalized coordinates necessary to describe the deflected configuration of a structure. Even something as elementary as a beam actually has an infinite number of degrees of freedom. Fortunately, the contributions of the higher modes are slight and good approximations can be made without them.

As might be expected, the systems most attractive for mathematical solutions are too simple to be found in practical situations. The single-degree-of-freedom system is an example. It consists of a lumped mass constrained to move without friction in a single direction normal to gravity forces, a linearly increasing resistance to displacement, and a concentrated time-dependent force applied to the mass in the direction of permissible

movement. This system is susceptible to analytical solution when the forcing function is simple, but there are few important practical cases of such a simple system. However, many real structures can be approximately described by the single-degree-of-freedom system and can be thus solved with sufficient accuracy for engineering purposes. This means that if the distortion of the element or structure in the mode of expected failure can be expressed mathematically as a function of one variable, then the system can be approximated by the single-degree-of-freedom system.

If there is an ideal correspondence between an actual structural system deforming in an assumed pattern and the single-degree-of-freedom system model, the following will be true:

- (1) The displacement, velocity, and acceleration of the model are at all times equal to the displacement, first time-derivative, and second time-derivative of the governing dimension of the actual structural system.
- (2) The kinetic energy, strain energy, and work done by external loads for the model are equivalent at all times to the corresponding total energies for the actual structural system.

From the above sets of conditions, "equivalence" factors can be obtained for the mass, stiffness, and load parameters of the actual system so that these parameters may be used in the equation for the single-degree-of-freedom model. For each type of element or system the equivalence factors will generally be different. These have been worked out for a great number of elements and conditions of support.

For an actual structural system vibrating in a single mode without load and a single-degree-of-freedom model in free vibration, equivalence can be obtained by adjusting the period of the actual structure to account for the distributed mass and stiffness. Then, if the structural resistance is defined in the same units as the applied loading, and the structure deforms in the shape of the mode assumed, the solution for the model will be a solution for the actual structure. If the structure does not deform in the shape of the mode assumed, the model solution will be only an approximate solution for the actual structure. The effectiveness of the single-degree-of-freedom model approximation depends on the correctness of the assumed configuration. This is the approach of Ref. B-1, which gives general procedures for design.

The same equivalence relationship between actual system and model does not generally hold for both the elastic and plastic ranges. One therefore might select two equivalent models, one for the elastic range and one for the plastic range. Another approach would be to use the equivalence corresponding to the predominant action, i.e. mostly elastic or mostly plastic.

The single-degree-of-freedom approximation is fortunately better for design than for analysis. The error sensitivity is less, when starting with a desired maximum deformation and solving for the required static yield resistance in terms of the peak overpressure, than in the reverse situation. Therefore, an error introduced in the desired maximum deflection by the single-degree-of-freedom approximation will not produce a significantly large error in the computed design strength required.

B.2 METHODS OF ANALYSIS OF SIMPLE SYSTEMS

B.2.1 Introduction. There are two fundamental methods available for treating simple systems subject to dynamic forces. The first of these methods is concerned with solving the differential equations of the system either by classical, numerical, or graphical means. The differential equation approach is, of course, not restricted to simple systems. The second method of analysis depends on solutions which have been accumulated by use of the first method, and is an approximate method. The method of solution which is most desirable for a particular problem depends on the character of the problem, the accuracy desired, and the time available for finding the solution.

All notations are defined when first used in this Appendix and are summarized for reference in Section B.3.

B.2.2 Methods of Analysis.

(a) Differential Equation Approach.

1. Equations of Motion. The equation of motion for a simple system takes the form:

$$m \frac{d^2 x}{dt^2} + c \frac{dx}{dt} + q(x) = p(t) \quad (B-1)$$

where m is the mass, c the coefficient of damping, $q(x)$ the resistance function, and $p(t)$ the forcing function. If attention is restricted to the undamped case, $c = 0$ and the resulting equation of motion is:

$$m \frac{d^2 x}{dt^2} + q(x) = p(t) \quad (B-2)$$

(b) Classical Solution. For some very elementary problems the equation of motion can be solved easily by the methods of classical differential equation analysis. Unfortunately, practical problems are not often elementary problems, and although the classical analysis can usually be made, the solution tends to be a lengthy proposition, yielding results in quite complicated forms.

(c) Graphical Solution. There are two distinct types of graphical solution, the gyrogram method and the method of graphical integration. The first of these methods, the gyrogram method, has found a great deal of favor in the past, and has been discussed in great detail in the literature. A thorough treatment is included in Ref. B-2. The second method, that of graphical integration, has been applied to a variety of problems, but is really useful in only a few applications. For problems in which the resistance is constant, such as the sliding problem, this method is probably the simplest way of finding the solution. Since the sliding problem is not a typical underground problem, a thorough discussion of the method of graphical integration will not be given here. The method is discussed in detail in Ref. B-3.

(d) Numerical Integration. The method of numerical integration is probably the most generally applicable method of analysis in structural dynamics problems. It can be applied to any system with a finite number of degrees of freedom, and can treat any force-displacement-time relationship, ranging from linear elastic to non-linear visco-elasto-plastic relations. The method of numerical integration has found wide application

on electronic computing devices for compiling the solutions to simple problems, and for the rapid solution of problems in the dynamics of complicated systems. For hand computation the method is best suited to systems of a few degrees of freedom with simple force-resistance relations, such as the bilinear elastic or elasto-plastic resistances. In the following material many of the results of theorems on stability and convergence will be stated without proof for reasons of length and simplicity. The reader is referred to the many excellent papers in this field for a more complete discussion of these subjects.

The differential equations of motion of a system of a finite number of degrees of freedom may be written in the form:

$$\ddot{x}^i = \frac{p^i(t) - q^i(x) - r^i(\dot{x})}{m^i}, \quad i = 1, 2, \dots, N \quad (B-3)$$

where $p^i(t)$ is the applied force on the i^{th} mass, $q^i(x)$ is the resistance due to displacement of the i^{th} mass, and $r^i(\dot{x})$ is the resistance due to velocity (i.e. viscous damping) of the i^{th} mass. The resistance could also include functions of higher order time derivatives, but these are not usually of interest in structural problems.

The bases of the method of numerical integration are the subdivision of time into intervals Δt , and the assumption of the nature of the variation of the acceleration during the time interval. The procedure recommended herein was developed by N. M. Newmark and presented in Refs. B-5 and B-7. It is convenient to adopt the notation developed in Ref. B-5; thus the velocity and displacement of the i^{th} mass and of the $(n+1)^{\text{th}}$ time interval

are given by:

$$\dot{x}_{n+1}^i = \dot{x}_n^i + \frac{1}{2} \Delta t (\ddot{x}_n^i + \ddot{x}_{n+1}^i) \quad (B-4)$$

$$x_{n+1}^i = x_n^i + \Delta t \dot{x}_n^i + \frac{(\Delta t)^2}{2} \ddot{x}_n^i + \beta (\ddot{x}_{n+1}^i - \ddot{x}_n^i) (\Delta t)^2 \quad (B-5)$$

If $\beta = 1/6$ the variation of the acceleration is linear, while $\beta = 1/4$ corresponds to a constant acceleration which is the average of \ddot{x}_n^i and \ddot{x}_{n+1}^i . Values of β of 0, 1/12, and 1/8 can also be given simple geometric interpretations.

The method then proceeds as follows: For $t = 0$ the acceleration, velocity, and displacement are computed from the given initial condition and the differential equation. Then, for $t = \Delta t$, the acceleration \ddot{x}_1^i is assumed. Using Eqs. (B-4) and (B-5), the velocity and displacement \dot{x}_1^i and x_1^i are computed. Knowing \dot{x}_1^i and x_1^i , the resistances $q^i(x)$ and $r^i(\dot{x})$ can be evaluated. These values are then substituted into the differential equations, Eq. (B-3), and the assumed accelerations checked. If the resultant and assumed accelerations are not in agreement, the resultant acceleration can be used for the next trial until the procedure converges.

The important questions which arise in the application of numerical integration are convergence, rate of convergence, stability, length of time interval, and choice of β . All of the questions are interrelated and have been studied fairly extensively. Some of the results of these studies are presented in Tables B-1 and B-2. In Table B-1 the rate of convergence for

an undamped single degree of freedom system is presented for various values of β and $\Delta t/T$ (the time interval scaled by the natural period of vibration). The smaller the value of the rate of convergence, the more rapid the convergence. In Table B-2 the stability and convergence limits for an undamped single-degree-of-freedom system are given for common values of β . The scaled time interval $\Delta t/T$ must be less than both these limits to insure both stability and convergence. For systems with several degrees of freedom, the stability and convergence limits must be applied in terms of the natural period of the highest mode of vibration, i.e., the minimum natural period.

The choice of β , of course, governs the accuracy and ease of application of the method. Extensive work in the application of this method has brought the following conclusions: When $\beta = 1/6$, the method is best suited to forced vibrations with damping and with initial velocity and displacement. The best results in amplitude of response are obtained for an undamped system using $\beta = 1/4$. For $\beta = 1/12$ the method is most rapid and accurate for an undamped system without initial velocity. For very rapid results, where accuracy is not of primary importance, $\beta = 0$ often proves useful.

B.2.3 Approximate Analysis of Simple Systems Subject to Dynamic Loads.

(a) Introduction. As noted before, the differential equation of motion of an undamped, single-degree-of-freedom system takes the form:

$$m \frac{d^2 x}{dt^2} + q(x) = p(t) \quad (B-6)$$

The functions $q(x)$ and $p(t)$ that characterize the problem can be restricted to a limited number of forms for the usual blast analysis problem.

For the large majority of structures, the resistance function, $q(x)$, can be adequately idealized to a bilinear form, i.e., a continuous function composed of two straight line segments as shown in Fig. B-1. In Fig. B-1, q_y is the yield resistance and x_y the yield displacement. For $x \geq x_y$ the resistance may increase, decrease, or remain constant as indicated by the three lines in the figure. Also, when $x > x_y$, unloading will occur along a line parallel to the elastic portion, leaving a permanent displacement in the system.

One of the important parameters in dynamic analysis is the natural period of vibration of the structure for elastic deformations. This quantity, T , can be computed from the mass of the system and the slope of the elastic portion of the resistance curve, and is defined as:

$$T = 2\pi \sqrt{\frac{mx_y}{q_y}} \quad (B-7)$$

(b) Force Functions. The nature of the loading produced on a structure by nuclear blast is dependent upon the weapon size, distance from the point of detonation, and the geometry and orientation of the structure. However, the force functions can usually be idealized to one of the forms shown in Fig. B-2. For simplicity in computation the pressure and time coordinates have been reduced to dimensionless form by scaling pressure by the

yield resistance, time by the natural period of vibration, and concentrated impulses, I , by the product $q_y T$.

(c) Response of an Elasto-Plastic System to an Initially Peaked Triangular Force. Probably the most commonly used force function is the initially-peaked triangle. This simple force function has been studied extensively, and the results have been used in the approximate analysis of the effect of the other more complicated force functions shown in Fig. B-2. The maximum response of a simple system with elasto-plastic resistance subject to an initially-peaked triangular force pulse is shown in Fig. B-3. This chart is a convenient plot of solutions made by numerical integration of the equations of motion of the system using the ILLIAC, the electronic digital computer of the University of Illinois. Given any two of the three parameters on this chart, the third can be found immediately. For instance, if the response, u , and the duration of the force are specified, then the ratio of the maximum pressure to the yield resistance can be read from the chart.

The chart in Fig. B-3 can be extended to resistances other than the elasto-plastic with the introduction of only minor errors (of the order of 5 per cent or less).

(d) Replacement Resistances. Although the methods are similar, it is convenient to treat the strain hardening and decaying resistances separately. The strain hardening resistance can be replaced by an equivalent elasto-plastic resistance in a number of ways. The method found to be most convenient and accurate is that known as the constant period

replacement. The criteria for the replacement are:

1. The energy absorbed during the displacement of the elasto-plastic replacement resistance ^{and the original resistance} up to maximum displacement must be the same. In essence, this requires that the area under the two resistance curves must be equal.

2. The initial slope (k_1) of both resistances must be the same. Thus, the natural period remains unchanged. The constant period replacement is illustrated in Fig. B-4. The equality of the energies is affected by equating the two shaded areas "A" and "B". The yield resistance and displacement of the replacement system (primed symbols) are related to the corresponding quantities of the original system by the following relations:

$$q'_y/q_y = \mu - (\mu - 1)(1 - k)^{1/2} \quad (B-8)$$

where k is defined as $\frac{k_2}{k_1}$

$$\mu' = \mu q_y/q'_y \quad (B-9)$$

Using the above formulas, a system having a strain hardening resistance subject to an initially peaked triangular load can be analyzed by first replacing the resistance with an elasto-plastic one and then using Fig. B-3.

When the resistance is decaying the same method of replacement, i.e. elasto-plastic, can be used as for the strain hardening resistance with the exception that the pressure level computed for a specified maximum response may be less than the pressure level necessary to cause a maximum displacement

less than that specified. This phenomenon generally occurs only when the duration of the force is long.

In the case of a long duration load, there is a maximum pressure level, p_α , and a corresponding maximum response called the apparent maximum response, μ_α , which is less than the collapse response, μ_c . This apparent maximum response, μ_α , is the largest finite response obtainable for a given load duration since any pressure level greater than p_α will cause an infinite response.

If the maximum displacement of interest is less than μ_α , then Eqs. (B-8) and (B-9) can be used to make the elasto-plastic replacement and the pressure-time-response relations of Fig. B-3 employed. On the other hand, if the maximum response is greater than μ_α , then p_α is the controlling maximum pressure. The simplest method for determining p_α and μ_α is to plot the pressure versus response for several values of response such as that shown in Fig. B-5. The curve ABC represents the proper pressure-displacement relation, while the curve ABD is that obtained using the replacement resistance. The values of μ_α and p_α are the coordinates of the maximum of curve ABC.

(e) Damage Pressure Level Equation. Another approximate method for determining the pressure necessary to cause a specified response is the so-called damage pressure level equation developed by Newmark. The equation takes the form:

$$p_m/q_y = p'_m/q_y + \frac{p''_m/q_y}{1 + 0.7 \frac{T}{t_d}} \quad (B-10)$$

where

$$p_m''/q_y = \frac{T}{\pi t_d} \left\{ \left[2\mu - 1 + k(\mu - 1)^2 \right]^{1/2} - \frac{\pi I_o}{q_y T} \right\} \quad (B-11)$$

and

$$p_m''/q_y = 1 - \frac{1}{2\mu} + k \frac{(\mu - 1)^2}{2\mu} - \frac{1}{2\mu} \left[\frac{\pi I_o}{q_y T} \right]^2 \quad (B-12)$$

Equation (B-10) is directly applicable for an initially-peaked, triangular force with an initial impulse I_o acting on elasto-plastic systems ($k = 0$), strain hardening systems ($k > 0$), or decaying systems ($k < 0$). In a decaying system p_α and μ_α must be found in the same manner as described in the section on the elasto-plastic replacement of a decaying resistance. The maximum detected difference between the approximate damage pressure level equation (Eq. B-10) and the exact theoretical solution is less than eight percent.

(f) Maximum Dynamic Response to a General Decaying Force.

For an initially-peaked triangular force pulse, the dynamic behavior of a simple system is defined by either Fig. B-3 or the damage pressure level equation. For other initially-peaked decaying pulses, a technique developed by Newmark is applicable.

Consider the force pulse shown in Fig. B-6a, which is acting on an elasto-plastic system. The approximate peak pressure necessary to cause a specified response is given approximately by:

$$\frac{f_1}{F_1} + \frac{f_2}{F_2} = p_m/q_y \left[\frac{c_1}{F_1} + \frac{c_2}{F_2} \right] = 1 \quad (B-13)$$

where $f_1 = c_1 p_m/q_y$ is the peak pressure of the upper triangular component; $f_2 = c_2 p_m/q_y$ is the peak pressure of the lower triangular component; F_1 is the pressure level ratio, p_m/q_y , required to give the specified response if only the upper triangle were acting; and F_2 is the pressure level ratio required to give the specified response if only the lower triangle were acting. F_1 and F_2 may be found from Fig. B-3.

If an initially-peaked decaying force is approximated by a number of triangular components as illustrated in Fig. B-6b, Eq. (B-13) can be generalized to the form:

$$p_m/q_y \sum_{i=1}^N \frac{c_i}{F_i} = 1 \quad (B-14)$$

Peak pressures computed from Eqs. (B-13) and (B-14) are lower bounds to the actual pressure consistent with the specified maximum response. The errors in this averaging technique are generally less than 10 percent, while the maximum possible error is 20 percent, which occurs when this technique is used to predict the damage pressure level for an infinite duration step pulse with an initial impulse.

If the shape of the force pulse is such that it can be approximated by two straight lines, then an upper bound solution is given by:

$$\left[\frac{f_1}{F_1} \right]^2 + \frac{f_2}{F_2} = \left[\frac{c_1}{F_1} \frac{p_m}{q_y} \right]^2 + \frac{c_2}{F_2} \frac{p_m}{q_y} = 1 \quad (B-15)$$

This equation is exact when Eq. (B-13) has its maximum error and has its greatest error when Eq. (B-13) is exact, i.e., when both components are

either of very short duration, of very long duration, or of equal duration.

The maximum calculated error in Eq. (B-15) is approximately 23 percent.

An upper bound solution for an initially peaked decaying force pulse which is approximated by more than two triangular components may be obtained by squaring the impulsive components. It is, however, usually very difficult if not impossible to detect which components are to be treated as "impulses".

(g) Maximum Response to a Delayed-Rise Triangular Force.

Consider the force pulse shown in Fig. B-7. A small change in the rise time, t_1/T can have a significant effect on the response of a system subject to such a pulse. Fortunately, however, the damage pressure level is usually only slightly affected by a variation in rise time.

The effect of rise time on damage pressure level is given approximately by:

$$\left[p_m/q_y \right]_{t_1} = K_r \left[p_m/q_y \right]_{t_1=0} \quad (B-16)$$

$$K_r = \frac{2}{1 + \frac{\sqrt{\mu}}{\pi t_1/T} \sin \frac{\pi t_1/T}{\sqrt{\mu}}}, \text{ but always } K_r \leq \frac{2\mu}{2\mu-1} \quad (B-17)$$

where $\left[p_m/q_y \right]_{t_1}$ is the damage pressure level for the rise time pulse, and

$\left[p_m/q_y \right]_{t_1=0}$ is the damage pressure level for a pulse of the same duration as

the rise time pulse, but having zero rise time, i.e., an initially peaked triangular pulse. This value is given by Fig. B-3 or the damage pressure level equation.

For a more complete discussion of the topics covered in this section, see Ref. B-4.

B.2.4 Sliding, Overturning and Rebound of Simple Systems. Of these three problems, the first two arise primarily in the consideration of above-ground structures, while the third, rebound, is of interest in both above-ground and under-ground structures.

(a) Sliding Systems. The simplest type of sliding system (which is the one to be considered here) is one in which no motion can take place until the applied force is greater than the sliding resistance, the sliding resistance being a constant. In this case the differential equation of motion becomes:

$$\frac{d^2x}{dt^2} + q = p(t) \quad (B-18)$$

or

$$\ddot{x} = \frac{1}{m} [p(t) - q] \quad (B-19)$$

From Eq. (B-19), the acceleration-time diagram for the system can be plotted as in Fig. B-8. Note that both the positive acceleration, $p(t)/m$, and the negative acceleration q/m have been plotted above the t -axis for convenience.

The velocity, \dot{x} , can be obtained from Eq. (B-19) by integration, thus:

$$\dot{x} = \frac{1}{m} \int_0^t [p(\tau) - q] d\tau + \dot{x}_0 = \frac{1}{m} \int_0^t p(\tau) d\tau - \frac{q}{m}t + \dot{x}_0 \quad (B-20)$$

The maximum displacement will occur when the velocity is zero. When the initial velocity, \dot{x}_0 , is zero, the condition for a maximum is:

$$qt_m = \int_0^{t_m} p(\tau) d\tau \quad (B-21)$$

This implies that the cross-hatched areas A and B in Fig. B-8 are equal.

The displacement is obtained from Eq. (B-20) by integrating, thus:

$$x = \frac{1}{m} \int_0^t \int_0^{\tau} p(\tau') d\tau' d\tau - 1/2(q/m)t^2 + \dot{x}_0 t + x_0 \quad (B-22)$$

or for zero initial conditions:

$$x = \frac{1}{m} \int_0^t \int_0^{\tau} p(\tau') d\tau' d\tau - 1/2(q/m)t^2 \quad (B-23)$$

Eq. (B-23) is equivalent to taking the first moment of areas A and B about t maximum.

When a sliding system is to be designed, the above analysis would prove much too laborious, so that it is more convenient to use the following approximate formula developed for an initially peaked triangular load, at least for the preliminary work. The approximate formula (see Ref. B-4) is:

$$\frac{p_m}{q} = 1 + \frac{2}{t_d} \sqrt{\frac{2mx_m}{q}} \quad (B-24)$$

The design made by use of Eq. (B-24) can then be checked by use of the more exact procedure outlined above.

(b) Overturning Systems Without Sliding. In this problem it is assumed that the structure will be seriously damaged if it overturns. Thus, it is necessary to consider only the conditions which will cause the structure to be on the verge of overturning. In the following the structure is considered to offer (from its own weight only) resistance to overturning. The force pulse is assumed to act laterally on the structure and to be of short duration so that the structure will not move appreciably while the force is acting. For the system shown in Fig. B-9, the damage-pressure level for a triangular force is given approximately by the formula:

$$p_m/q_y = 1 + \frac{2}{t_d} \sqrt{\frac{J_o}{WD}} \quad (B-25)$$

where J_o is the polar moment of inertia of the structure about point O of Fig. B-9, W is the weight of the structure, and D is the distance from point O to the center of gravity of the structure. No more elaborate analysis is presented in this problem because of the complicated nature of the interaction between the structure and the loading.

(c) Rebound of Simple Systems. In the design of members subjected to dynamic loading, the member must be designed to resist the negative displacement, or rebound, which can occur after the member has reached its maximum positive displacement.

For an undamped single-degree-of-freedom system subjected to an initially-peaked triangular force pulse, the ratio of the required rebound resistance to the yield resistance, r/q_y , such that the system will remain

elastic during rebound, is given by the formula:

$$\frac{r}{q_y} = s \left[1 + \left(\frac{\phi}{2\pi y_d s} \right)^2 + \frac{2\phi \sin(2\pi y_d - \alpha)}{2\pi y_d s} \right]^{1/2} \quad (B-26)$$

where

$\phi = p_o/q_y$, p_o being the magnitude of the applied force at the time of maximum positive displacement, t_m ,

$$y_d = \frac{t_d - t_m}{T}$$

$$s = \sqrt{(1 - \phi)^2 + \left(\frac{\phi}{2\pi y_d} \right)^2}$$

and

$$\alpha = \arcsin \frac{\phi}{2\pi y_d s}$$

For design purposes, Fig. B-10 has been prepared which gives approximate values of the rebound resistance required for an undamped single-degree-of-freedom system subjected to an initially peaked triangular force pulse. The maximum error in Fig. B-10 is approximately $0.20 q_y$ and is on the conservative side in all cases. Entering the chart with the value of the ductility factor (x_m/x_y) and the ratio of the duration of the load pulse to the natural period of the system (t_d/T), it is possible to read directly the required rebound resistance, r , in terms of the originally

designed yield resistance, q_y .

As a general observation connected with Fig. B-10, it may be noted that if the loading is applied in a relatively short time compared with the period of vibration of the structure, the required rebound resistance may be equal to the resistance in the normal design direction. However, when the loading is applied for a relatively long time, the structure reaches its maximum deflection when the positive forces are still large, and the rebound is reduced.

B.3 NOTATION

The symbols used are defined as they appear in the text, and are assembled here for reference.

- c = coefficient of viscous damping
- c_i = ratio of f_i to p_m
- f_i = peak force of i^{th} component of multi-triangular force pulse
- F_i = value of p_m/q_y necessary to cause a given response by the i^{th} component of a multi-triangular force pulse acting alone
- I_o = initial concentrated impulse
- J_o = polar moment of inertia of overturning structure about point of rotation
- k = ratio of second slope to initial slope in bilinear resistance
- k_i = i^{th} slope of multi-linear resistance-displacement function
- K_r = rise time correction factor
- m = mass
- $p(t)$ = force function

- P_{α} = maximum applied pressure that is consistent with a finite maximum displacement for system with decaying resistance function
- p_m = peak pressure of pressure-time variation
- Δp_s = peak pressure in Brode type pressure-time functions
- $q(x)$ = resistance function
- q_y = yield resistance
- q'_y = yield resistance of equivalent elasto-plastic system
- r = required rebound resistance
- $r(x)$ = damping resistance
- t = time
- t_d = duration of force pulse
- t_m = time at which maximum response occurs
- t_l = rise time of pressure pulse
- T = natural period of vibration
- x = displacement
- x_m = maximum displacement
- x_y = yield displacement
- β = numerical integration parameter
- $\mu = x_m/x_y$ = response parameter
- μ' = ratio of maximum displacement to yield displacement of equivalent elasto-plastic system
- μ_{α} = maximum finite response obtainable in a system with decaying resistance, under a load pulse of given duration
- μ_c = value of μ consistent with zero resistance for system with decaying resistance function

8.4 REFERENCES

- B-1** Newmark, N. M., "An Engineering Approach to Blast Resistant Design," Transactions American Society of Civil Engineers, Vol. 121, 1956. (UNCLASSIFIED)
- B-2** Jacobsen, L. S. and Ayre, R. S., "Engineering Vibrations," McGraw-Hill Book Company, New York, 1958. (UNCLASSIFIED)
- B-3** Newmark, N. M., "Analysis and Design of Structures Subjected to Dynamic Loading," Proceedings of the Conference on Building in the Atomic Age, Massachusetts Institute of Technology, Cambridge, Massachusetts, 1952. (UNCLASSIFIED)
- B-4** Melin, J. W. and Sutcliffe, S., "Development of Procedures for Rapid Computation of Dynamic Structural Response," Civil Engineering Studies, Structural Research Series No. 171, University of Illinois, Urbana, Illinois, 1958. (UNCLASSIFIED)
- B-5** Newmark, N. M., "Computation of Dynamic Structural Response in the Range Approaching Failure," Proceedings of the Symposium on Earthquake and Blast Effects on Structures, Los Angeles, California, 1962. (UNCLASSIFIED)
- B-6** Melin, J. W., "Numerical Integration by Beta Method," ASCE Conference on Electronic Computation, Kansas City, Missouri, 1958. (UNCLASSIFIED)
- B-7** Newmark, N. M., "A Method of Computation for Structural Dynamics," Journal, Engineering Mechanics Division, ASCE, EM 3, July 1955. (UNCLASSIFIED) - Note: To be published in Transactions, ASCE, 1962.

TABLE B-1
RATE OF CONVERGENCE
(From Ref. B-7)

$\Delta t/T$	$\beta = 0$	$\beta = 1/12$	$\beta = 1/8$	$\beta = 1/6$	$\beta = 1/4$
0.05	0	0.008	0.012	0.016	0.025
0.10	0	0.033	0.049	0.066	0.099
0.20	0	0.132	0.197	0.263	0.395
0.25	0	0.206	0.308	0.411	0.617
0.318	0	0.333	0.500	0.667	1.000
0.389	*	0.500	0.750	1.000	1.500
0.450	*	*	1.000	1.333	2.000

TABLE B-2
STABILITY AND CONVERGENCE LIMITS

	$\beta = 0$	$\beta = 1/12$	$\beta = 1/8$	$\beta = 1/6$	$\beta = 1/4$
Stability Limit, $\Delta t/T$	0.318	0.389	0.450	0.551	∞
Convergence Limit, $\Delta t/T$	∞	0.551	0.450	0.389	0.318

* $\Delta t/T$ exceeds the limits for convergence or stability.

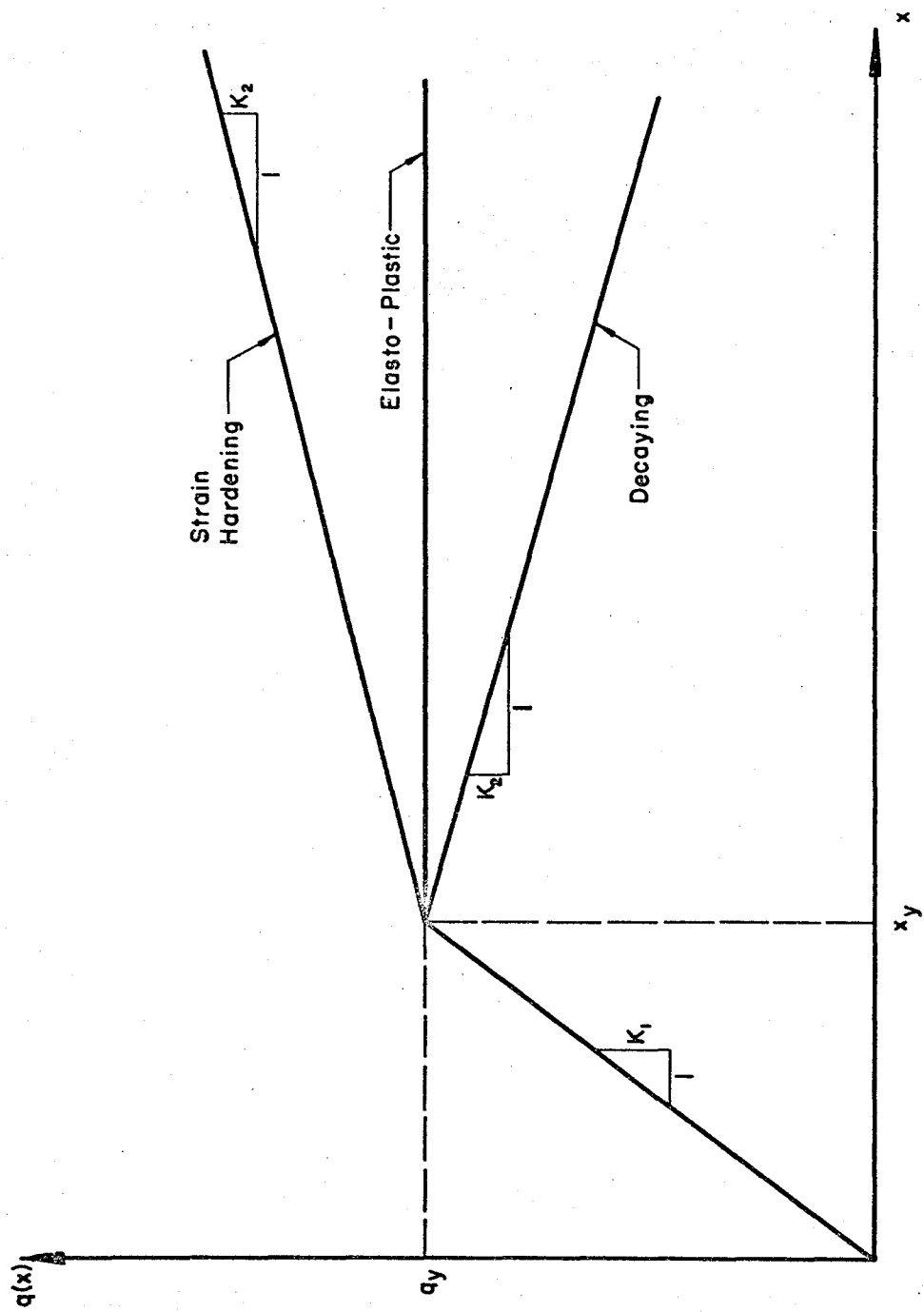
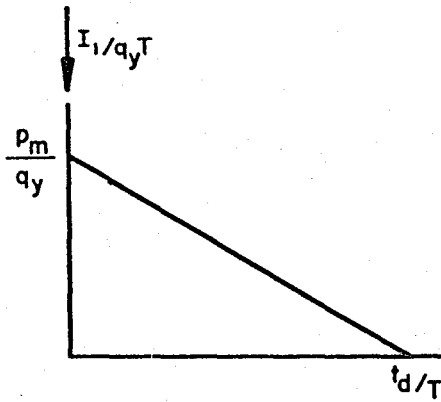
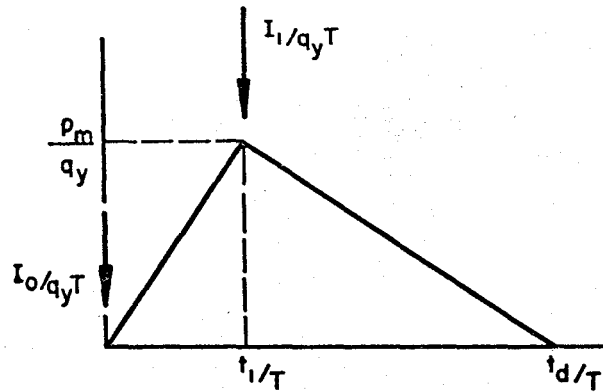


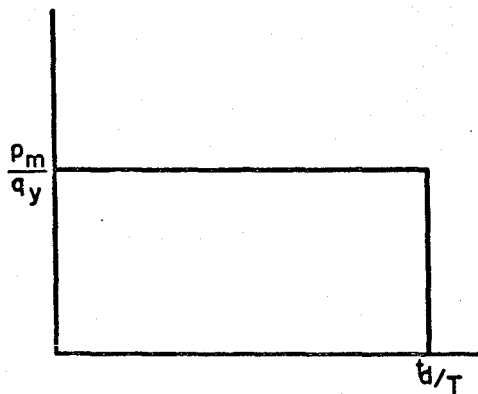
FIG. B-1 IDEALIZED RESISTANCE FUNCTIONS



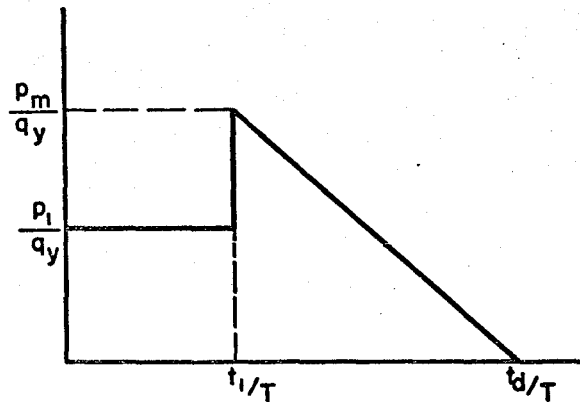
(a) Initially Peaked Triangular Force Pulse With Impulse



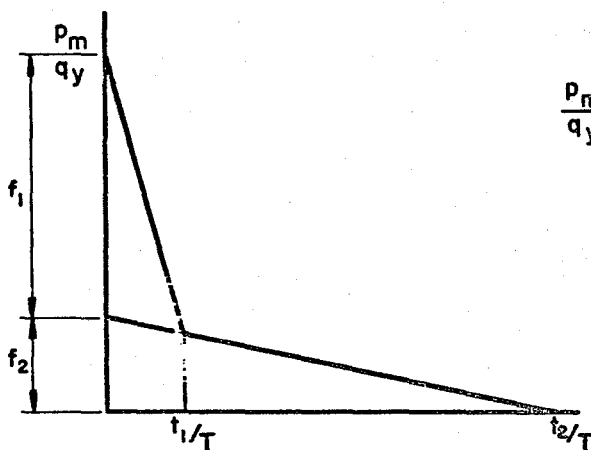
(b) Delayed Rise Triangular Force Pulse With Impulse



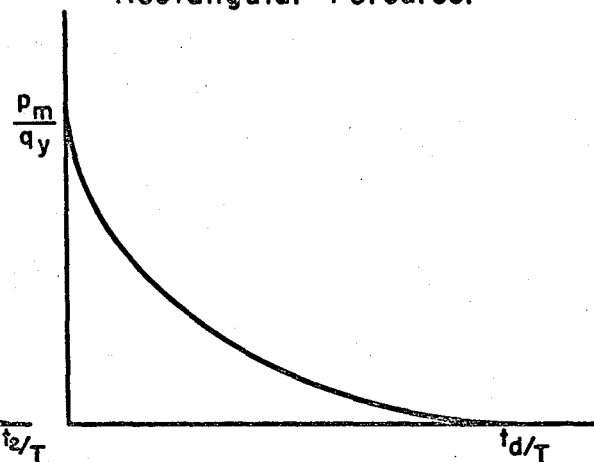
(c) Finite Duration Step Pulse



(d) Triangular Pulse With Rectangular Precursor



(e) Double Triangle Force Pulse



(f) Spherical Blast Wave

FIG. B-2 FORCE PULSES

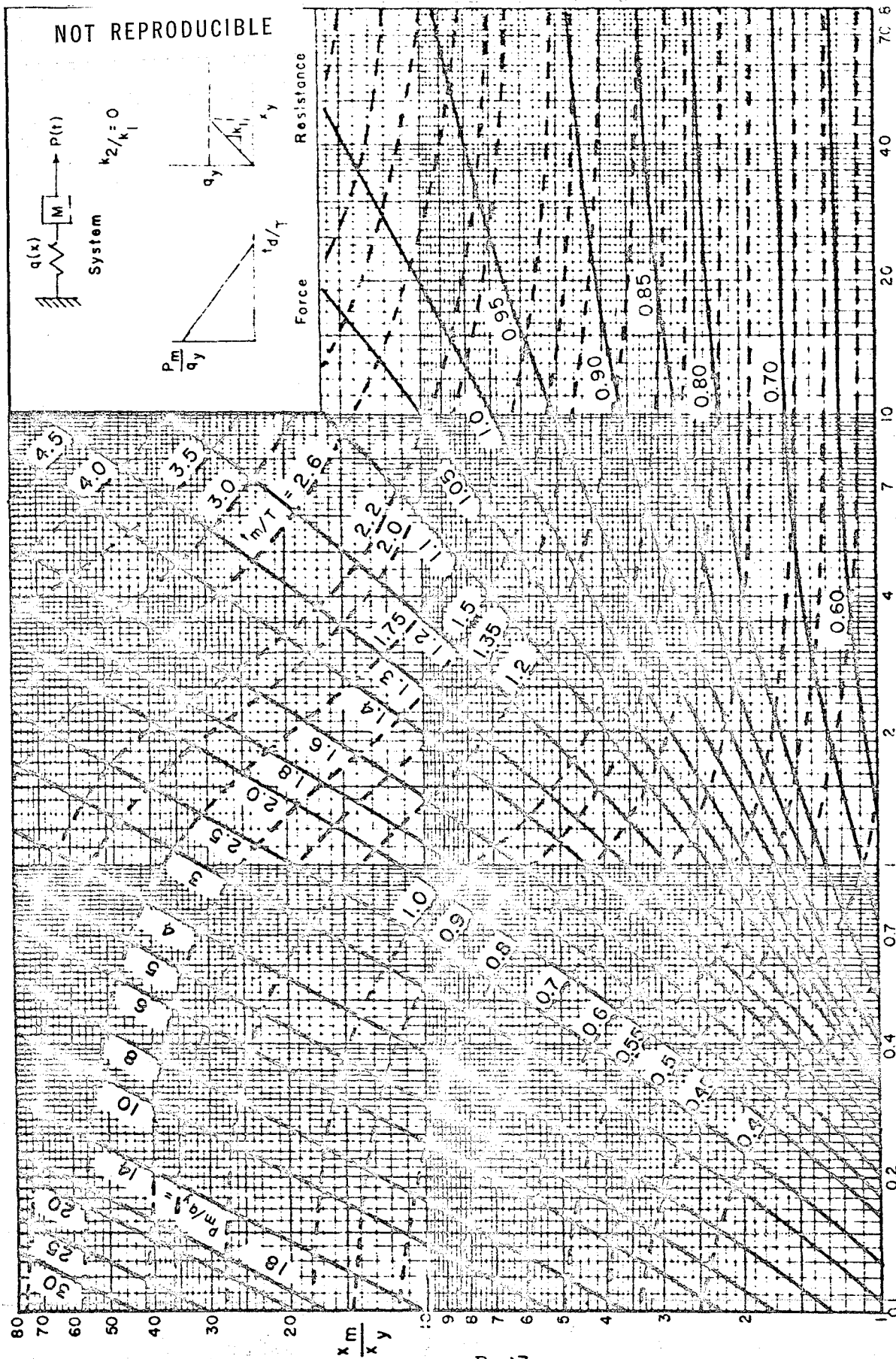


FIG. B-3 MAXIMUM RESPONSE OF SIMPLE SPRING-MASS SYSTEM TO INITIALLY PEAKED TRIANGULAR FORCE PULSE.

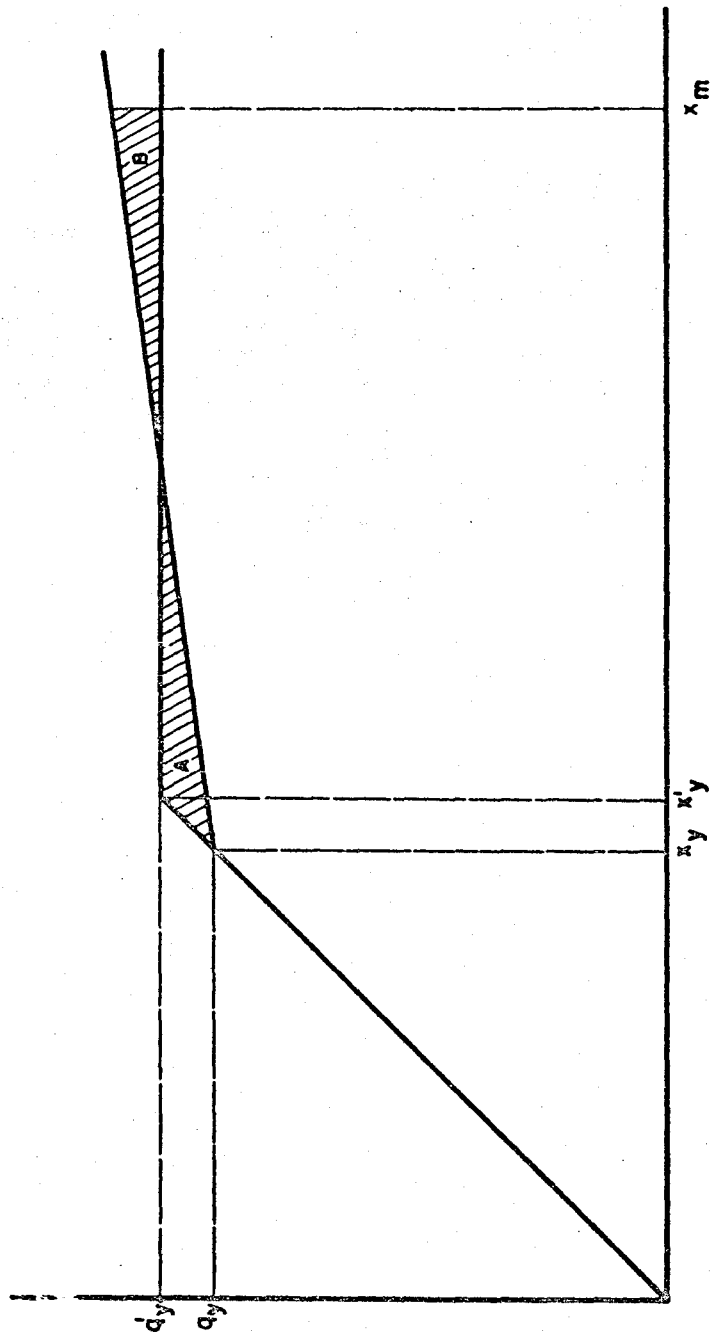
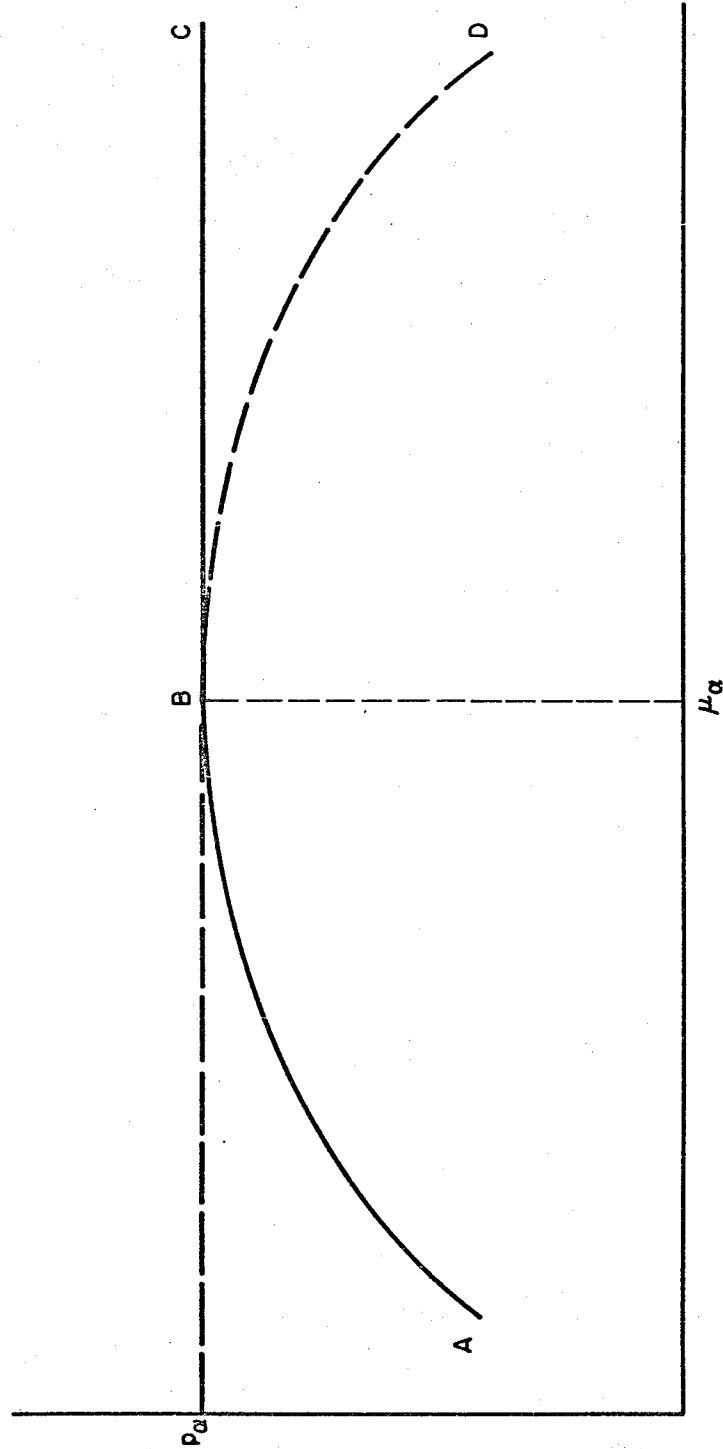
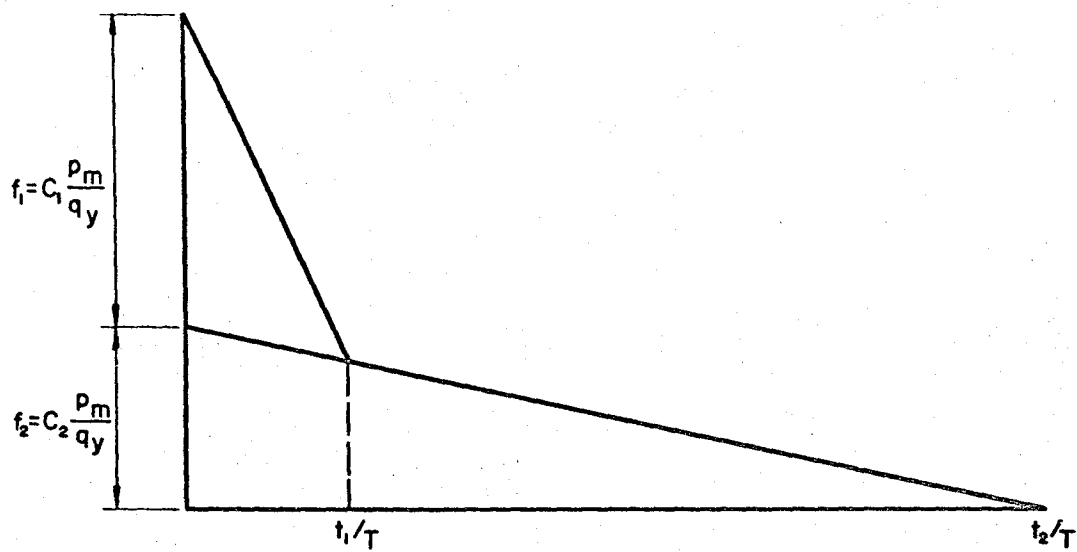


FIG. B-4 ELASTO - PLASTIC REPLACEMENT RESISTANCE

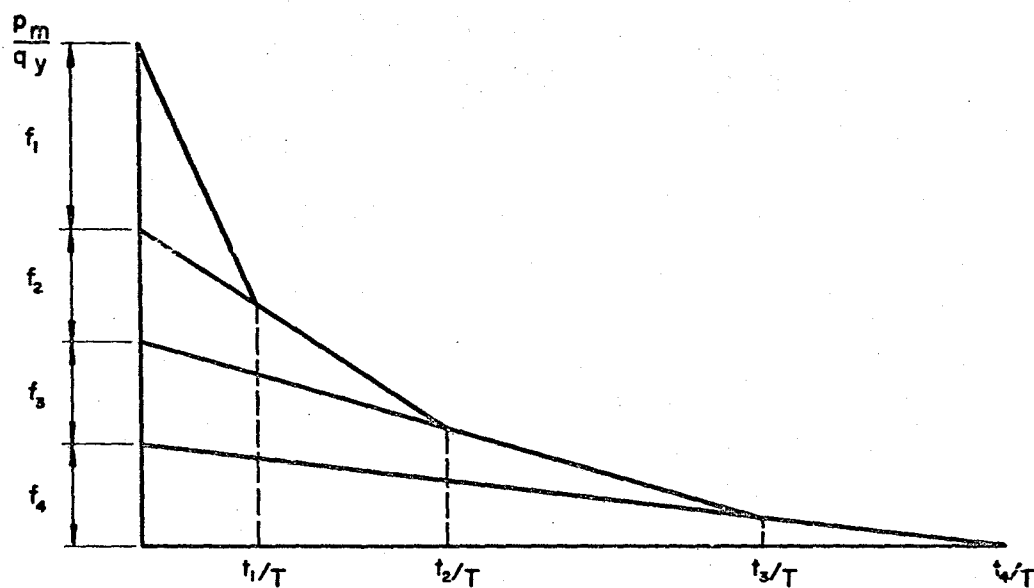


B-29

FIG. B-5 PRESSURE-RESPONSE CURVE FOR DECAYING RESISTANCE.



(a) Double Triangle Force Pulse.



(b) Multiple Triangle Force Pulse

FIG. B-6 MULTIPLE TRIANGLE FORCE PULSES

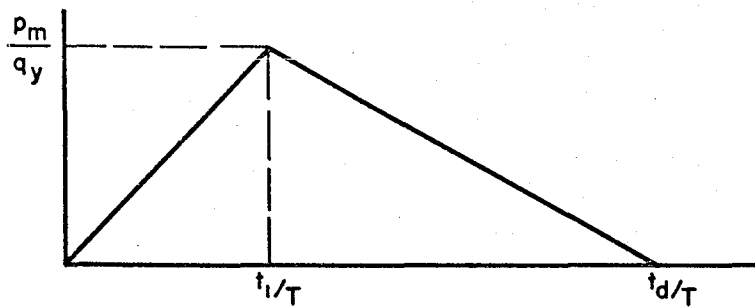


FIG. B-7 DELAYED RISE TRIANGULAR FORCE PULSE.

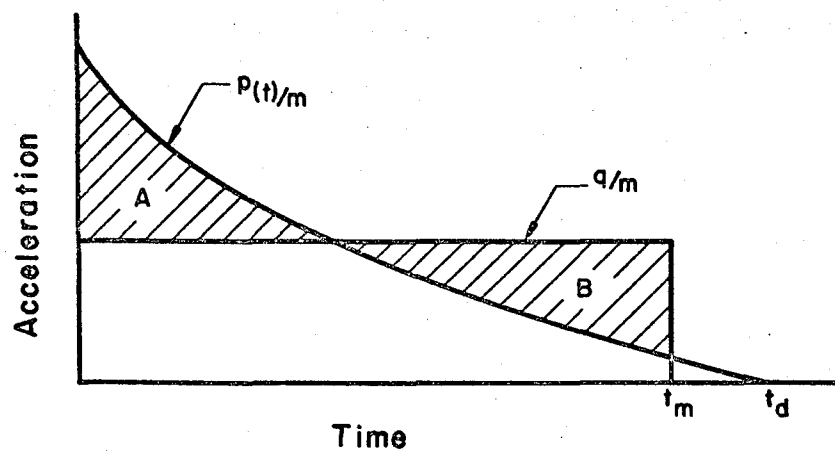


FIG. B-8 ACCELERATION-TIME DIAGRAM FOR SLIDING SYSTEMS.

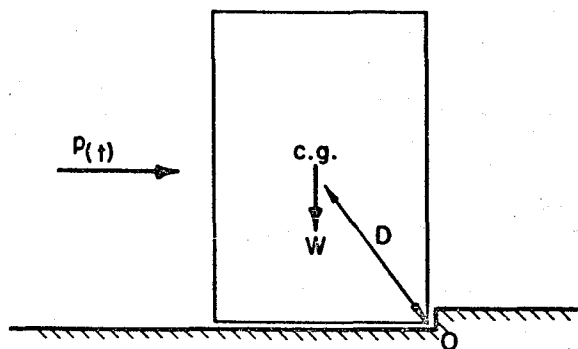
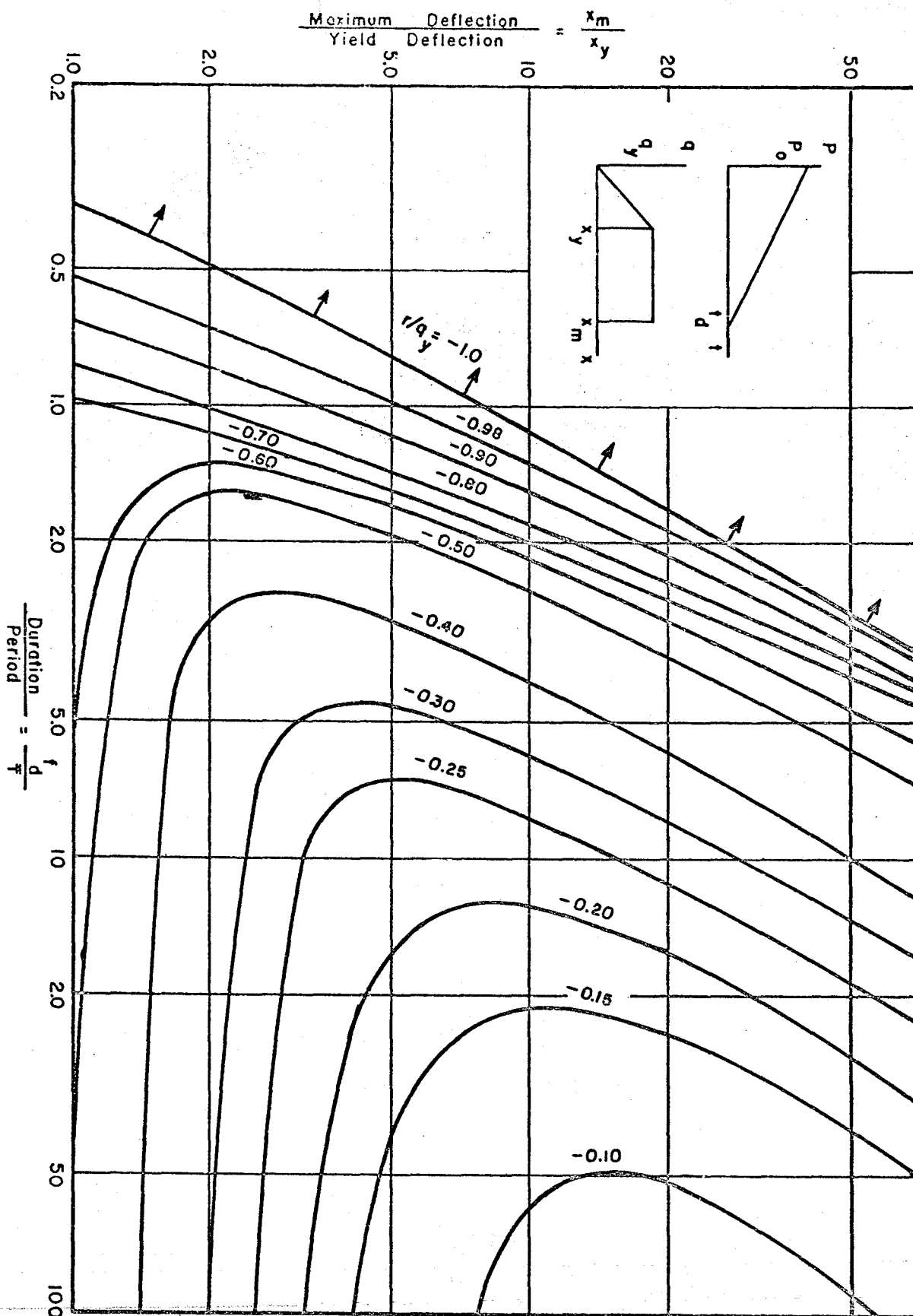


FIG. B-9 OVERTURNING SYSTEMS.

FIG. B-10. DESIGN CHART FOR ELASTIC REBOUND



APPENDIX C

THEORETICAL BACKGROUND FOR PREDICTIONS OF FREE-FIELD GROUND MOTIONS

C.1 INTRODUCTION

The ground motions produced by nuclear explosions are functions of the characteristics of the nuclear weapon, its location relative to the ground surface and the properties of the earth materials in the area affected. The stresses producing the ground motions are transmitted as stress waves which can be grouped into general categories, P waves or dilatational waves, S waves or shear waves, and surface waves or Rayleigh and Love waves. The characteristics of these wave types are briefly discussed below from a phenomenological point of view. For a rigorous definition of their character a standard reference, such as Ref. C-1, should be consulted.

A dilatational wave is a wave form which does not produce shearing strains in the medium through which it travels; it is typified by the air-blast wave in the air. A significant proportion of the air-induced and direct-transmitted ground motions are attributable to stresses propagated in this manner. The dilatational wave has the greatest velocity of propagation of all the wave types; for an elastic solid the velocity of propagation, c , is given by

$$c^2 = \frac{E(1 - \nu)}{\rho(1 + \nu)(1 - 2\nu)} \quad (C-1)$$

The notation is defined in Section C.3.

A shear wave is a wave form which does not produce volume changes or volumetric strain in the medium through which it passes. Shear waves contribute to both air-induced and direct-transmitted ground motions, but the influence of dilatational waves is generally more significant. The velocity of propagation of the shear wave, c_s , is given by

$$c_s^2 = \frac{E}{2(1 + \nu)\rho} \quad (C-2)$$

Rayleigh surface waves, comparable to the waves produced in still water by dropping in a stone, can occur when an interface such as the air-ground boundary exists. The Rayleigh wave motion occurs in a radial plane extending outward from the source of the disturbance. The particle motion at the surface produced by a Rayleigh wave is such that the particle describes a roughly elliptical path with a horizontal axis approximately two-thirds of the vertical axis. At the surface the initial horizontal motion of the particle is opposite to the direction of wave propagation. Rayleigh wave motions reduce rapidly with increasing depth, but because the wave is propagated at the surface, or in two dimensions, it attenuates, due to spatial dispersion of its energy, much more slowly with distance from the point of burst than do dilatational or shear waves. For this reason the Rayleigh wave is responsible for the most severe earthquake ground motions, however, the importance of the Rayleigh wave in ground motions produced by nuclear explosions is not clear. A detailed study of the results of nuclear tests, Ref. C-2, finds no evidence of prominent Rayleigh wave effects;

however, theoretical studies, Ref. C-3, and drop weight tests have indicated that a surface burst of a nuclear weapon should efficiently produce Rayleigh waves. The velocity of propagation of a Rayleigh wave is $0.9194 c_s$ for $\nu = 0.25$.

Love surface waves differ from the Rayleigh waves in that the particle motions take place in a horizontal plane. Shearing energy input and reflective containment resulting from the presence of a low seismic velocity layer over a high seismic velocity layer are required for the formation of Love waves. Love waves are not considered to have much influence on ground motions due to nuclear explosions since the horizontally symmetrical disturbance produced by a nuclear explosion does not provide significant horizontal shearing energy.

Theoretical descriptions of the ground stresses and motions produced by nuclear explosions using wave theories have been and are being made. Exact solutions have long been available for simple loadings and homogeneous elastic media, but the analytical problems involved in evaluating the motions due to a pressure distribution moving at a varying velocity over the surface of a nonuniform non-elastic medium are severe. In this appendix reference is made to some of the wave propagation situations which have been formulated and solved and a development of the equations for the stresses and motions due to a one-dimensional dilatational wave is presented. This latter is the simplest case of wave propagation and provides the basis for the techniques of free-field ground motion prediction which are presented in Chapter 4.

The energy input of a nuclear explosion to the ground is essentially axisymmetric when the explosion occurs above or near the surface of the earth. The general wave forms induced by such loading are termed three-dimensional since spatial dispersion of the wave energy occurs in three-dimensions. At great distances from the point of burst, where the radius of the air blast wave front is large compared to the depth of interest in the earth, the ground disturbance can be considered to be produced by a plane wave, that is the air blast wave front can be considered to be a straight line on the ground surface. When the velocity of the air blast front is great compared to the wave propagation velocity in the earth, a one-dimensional wave formulation can be applied. The assumption is made that at a given time the surface loading is everywhere the same, so that no shear waves are induced, and only a dilatational wave travels into the earth.

An additional complication is introduced into the theoretical study of ground motions because of the non-elastic behavior of real earth media. Even for the ideal situation of horizontally uniform soil or rock the strain must be considered to be a non-linear function of the stress and strain history in order to describe the observed behavior of real materials. The stress-strain-time characteristics of soils and rocks are not yet well defined but some simple visco-elastic, elasto-plastic and locking soil stress-strain-time functions have been considered in theoretical studies of wave propagation. Obviously, such considerations considerably complicate the analytical problem.

Comprehensive surveys of the present theoretical capability to analyze the ground motions due to nuclear explosions are presented in Refs. C-2, C-4, and C-5. Some of the solutions available and other references of interest are mentioned in the material which follows.

C.2 TWO AND THREE-DIMENSIONAL STUDIES OF AIR-INDUCED GROUND MOTIONS

C.2.1 Three-Dimensional Studies. The one-dimensional loading, while offering desirable simplicity of formulation and solution, is not a generally valid representation of the loading applied to the ground by an air blast pulse. A real air blast loading is distributed with reasonable horizontal symmetry about ground zero, so a solution for an axisymmetric loading producing axisymmetric ground motions promises to provide a good representation of actual conditions. Such a solution for the problem is particularly desirable for study of motions at points of large ratios of depth to radius from ground zero. The equations governing the response of a medium for such loading conditions are presented in Refs. C-2 and C-5, but the solutions are not yet available for study.

C.2.2 Two-Dimensional Studies. The two-dimensional study of air-induced ground motions considers the loading function to be a plane wave, that is that the wave front when viewed from above appears as a straight line. Under these circumstances the medium is in a condition of plane strain; displacements parallel to the wave front are identically zero. This formulation is more susceptible to solution than the three-dimensional problem and gives a reasonable approximation of the actual conditions when

the ratio of the depth of interest to the radius from ground zero is small. Solutions for stress, displacement, and velocities for a plane wave condition in which the air blast wave has unchanging form and velocity are presented in Refs. C-4, C-5 and C-6.

The form of the solution for the plane wave loading depends upon the relation between the air shock velocity U and the dilatational and shear wave velocities of the medium.

Dilatational Wave Velocity

$$c^2 = \frac{E}{\rho} \frac{1 - \nu}{(1 + \nu)(1 - 2\nu)}$$

Shear Wave Velocity

$$c_s^2 = c^2 \frac{1 - 2\nu}{2 - 2\nu}$$

The solutions must be presented for three conditions

$U > c > c_s$	Supersismic condition
$c > U > c_s$	Transismic condition
$c > c_s > U$	Subseismic condition

The supersismic condition is of interest for high overpressures and has received considerable study. Reference C-6 presents a solution for a visco-elastic medium for supersismic conditions. A numerical example for a rock-like medium for a peak overpressure of 2000 psi is presented which demonstrates considerable attenuation due to the viscous behavior. However, the data available are not yet sufficiently extensive to provide a basis for the

definition of attenuation due to spatial distribution of energy and absorption of energy through inelastic response.

References C-4 and C-5 provide equations for stresses and motions produced by a plane wave acting upon an elastic medium for superseismic conditions and in C-5 for transeismic and subseismic conditions. Because of the unchanging wave form and velocity, these solutions are actually one-dimensional solutions; the peak stress value does not attenuate with increasing depth for superseismic conditions. Figure C-1, after Ref. C-4, shows the wave form and the traces of the dilatational and shear wave fronts with depth.

C.3 GROUND MOTIONS BY ONE-DIMENSIONAL WAVE THEORY

In one-dimensional wave theory a time dependent disturbance is considered to act uniformly over a surface of infinite extent. Therefore, only vertical motions occur and simple relationships can be established between stress, displacement, velocity, and acceleration. No shearing stress or shear wave is induced in the medium. Although the situation is highly idealized compared to the conditions resulting from nuclear blast, the theory provides an understanding of the basic relationships between stresses and ground motions and can be corrected to provide a reasonable representation of actual free-field conditions.

C.3.1 Uniform Elastic Medium. Figure C-2 shows an element of unit area of a uniform elastic medium of infinite extent. The terms used to define the undisturbed location of a given particle of the medium and the displacement of that particle with time are as follows.

- t** time variable
x undisturbed location of a given particle
u displacement of a given particle in the x direction,
 a function of x and t
 σ_x normal stress in x direction, tension considered to be positive
 σ_y normal stress in y direction (any direction normal to x)
 tension positive
E Young's modulus
v Poisson's ratio
c velocity of propagation of a dilatational wave
 c_s velocity of propagation of a shear wave
 ρ mass density of the medium
 p_s side-on overpressure at the surface
 ϵ_x engineering strain in x direction

For equilibrium of an element of the medium of unit area and of thickness dx

$$\frac{\partial \sigma_x}{\partial x} dx - \rho \frac{\partial^2 u}{\partial t^2} dx = 0$$

To obtain an equation in terms of u alone, the strain is expressed

$$\epsilon_x = \frac{\partial u}{\partial x}$$

and considering that all displacements normal to the direction x are zero,
 from Ref. C-7

$$\sigma_x = E \epsilon_x \frac{1 - v}{(1 + v)(1 - 2v)} = \frac{E(1 - v)}{(1 + v)(1 - 2v)} \frac{\partial u}{\partial x}$$

Substitution for $\frac{\partial \sigma_x}{\partial x}$ in the differential equation of equilibrium yields

$$\frac{\partial^2 u}{\partial t^2} - c^2 \frac{\partial^2 u}{\partial x^2} = 0 \quad (C-3)$$

where c is the velocity of propagation of the wave form

$$c^2 = \frac{E(1-\nu)}{\rho(1+\nu)(1-2\nu)} \quad (C-1)$$

The general solution for Eq. (C-3) is

$$u = f\left[t - \frac{x}{c}\right] + g\left[t + \frac{x}{c}\right]$$

Where $f\left[t - \frac{x}{c}\right]$ denotes some function of the quantity $\left[t - \frac{x}{c}\right]$ and $g\left[t + \frac{x}{c}\right]$ some function of the quantity $\left[t + \frac{x}{c}\right]$. The function f represents a wave form moving in the positive x direction at the velocity c , while the function g represents a wave form moving in the negative x direction at the velocity c .

For an infinitely deep elastic uniform medium loaded by surface pressure, such as is shown in Fig. C-2, the solution is given by

$$u = f\left[t - \frac{x}{c}\right] \quad (C-4)$$

In terms of Eq. (C-4) the quantities of stress, strain, and particle velocity become

$$\text{Stress } \sigma_x = \rho c^2 \frac{\partial u}{\partial x} = -\rho c f'\left[t - \frac{x}{c}\right]$$

$$\text{Strain} \quad \epsilon_x = \frac{\partial u}{\partial x} = -\frac{1}{c} f' \left[t - \frac{x}{c} \right]$$

$$\text{Particle Velocity} \quad \dot{u} = \frac{\partial u}{\partial t} = f' \left[t - \frac{x}{c} \right]$$

where

$$f' \left[t - \frac{x}{c} \right] = \frac{d \left[f \left(t - \frac{x}{c} \right) \right]}{d \left[t - \frac{x}{c} \right]}$$

To relate the quantities to the overpressure, the boundary conditions at $x = 0$ require that

$$\sigma_x = -p_s(t) \text{ at } x = 0$$

Defining a time quantity t^* such that

$$t^* = t - \frac{x}{c}$$

then

$$f' \left[t - \frac{x}{c} \right] = \frac{p_s \left[t^* \right]}{\rho c}$$

where $p_s \left[t^* \right]$ is the surface overpressure at the time $t = t^*$.

The expressions for stress, strain, and particle velocity become

$$\text{Stress} \quad \sigma_x = -p_s \left[t^* \right]$$

$$\text{Strain} \quad \epsilon_x = -p_s \left[t^* \right] / \rho c^2 \quad (C-5)$$

$$\text{Particle Velocity} \quad \dot{u} = p_s \left[t^* \right] / \rho c = -\epsilon_x c$$

Note that stress, strain, and particle velocity are linearly related to the overpressure p_s .

The acceleration at a point can be determined by differentiating the equation for particle velocity

Acceleration

$$\ddot{u} = \frac{1}{\rho c} \frac{\partial}{\partial t} (p_s [t^*]) \quad (C-6)$$

The peak acceleration will depend upon the shape of the overpressure - time variation. For a vertical shock front the acceleration will be infinite.

The absolute displacement of a point x_a at a given time t_a can be obtained in two manners.

- (1) By an integration of the particle velocity at the point x_a

Displacement

$$u(x_a, t_a) = \frac{1}{\rho c} \int_0^{t_a} p_s [t_a^*] dt \quad (C-7)$$

where

$$p_s [t_a^*] = p_s \left[t - \frac{x_a}{c} \right]$$

- (2) By integration of strain from infinite depth to the depth x_a at the time t_a

Displacement

$$u(x_a, t_a) = - \frac{1}{\rho c^2} \int_{x_a}^{\infty} p_s (t_a^*) dx \quad (C-8)$$

where

$$p_s(t_a^*) = p_s(t_a - \frac{x}{c})$$

Either integration can be conveniently performed graphically on the overpressure-time curve. The integral

$$\int_0^{t_a} p_s(t_a^*) dt$$

of Eq. (C-7) is the area under the overpressure-time curve $p_s(t^*)$ between the times $0 < t^* < t_a - x_a/c$. The integral

$$- \int_{x_a}^{\infty} p_s(t_a^*) dx$$

of Eq. (C-8) is c times the same area.

The relative displacement between points x_a and x_b at a given time t_c can be determined by integrating the strain between the points at the given time.

For

$$x_b > x_a$$

$$t_a^* = t_c - x_a/c$$

$$t_b^* = t_c - x_b/c$$

Relative Displacement

$$u_b - u_a = - \frac{1}{\rho c} \int_{t_b^*}^{t_a^*} p_s(t^*) dt^* \quad (C-9)$$

The integral

$$\int_{t_b^*}^{t_a^*} p_s(t^*) dt^*$$

represents the area under the overpressure-time curve $p_s(t^*)$, or impulse, in the time interval $t_a^* > t^* > t_b^*$. The length of the time interval is not a function of the time in question t_c but equals $(x_b - x_a)/c$. Therefore, the maximum relative displacement can readily be estimated by obtaining the maximum impulse for the time interval.

Horizontal Motions - do not occur for this ideal one-dimensional loading.

The stress in any horizontal direction is given by the theory of elasticity as

Horizontal Stress

$$\sigma_y = \frac{\nu}{1 - \nu} \sigma_x \quad (C-10)$$

Note that for the one-dimensional wave theory no attenuation of stress occurs with increasing depth.

C.3.2 Layered Elastic Medium. Changes in the properties of the medium through which a one-dimensional wave travels influence the character of the motions and stresses induced. Consider the influence of a change in properties of horizontal strata such as are shown in Fig. C-3.

A wave in the upper stratum incident to the boundary is given by the equation

$$u = f(t - \frac{x}{c})$$

At the boundary a reflected wave

$$u = g(t + \frac{x}{c})$$

will form and travel in the negative x direction in the upper stratum. A transmitted wave

$$u = F(t - \frac{x}{c})$$

will also form at the boundary and will travel in the positive x direction in the lower stratum.

Two conditions must be applied at the boundary to define the reflected and transmitted waves in term of the incident wave.

(a) For equilibrium

$$\sigma_1 + \sigma_r = \sigma_t$$

$$- \rho c f' (t - \frac{x}{c}) + \rho c g' (t + \frac{x}{c}) = - \bar{\rho} \bar{c} F' (t - \frac{x}{c})$$

(b) For compatible displacement

$$u_1 + u_r = u_t$$

$$f (t - \frac{x}{c}) + g (t + \frac{x}{c}) = F (t - \frac{x}{c})$$

Defining coefficients of reflection r , and transmission, s , where r and s are constants with respect to time,

$$g(t + \frac{x}{c}) = r f(t - \frac{x}{c})$$

$$F(t - \frac{x}{c}) = s f(t - \frac{x}{c})$$

Then, from (b)

$$1 + r = s$$

and, from (a), by substituting the time partial derivatives of the above definitions of r and s ,

$$-1 + r = -\frac{\partial c}{\partial c} s$$

Defining $\psi = \frac{\partial c}{\partial c}$

(C-11)

$$s = \frac{2}{1 + \frac{1}{\psi}} \quad r = \frac{\psi - 1}{\psi + 1}$$

The reflected and transmitted stresses are

$$\sigma_r = \frac{1 - \psi}{1 + \psi} \sigma_1$$

(C-12)

$$\sigma_t = \frac{2}{1 + \psi} \sigma_1$$

If the lower stratum is stiffer than the upper, and of equal or greater density, ψ will be less than one. For these conditions a reflected compressive stress and a transmitted compressive stress will result from an

incident compressive stress. The transmitted compressive stress will be greater than the incident compressive stress.

The above expressions are valid for any number of strata. The quantities E , c , and ρ are used to represent the properties of the stratum in which the incident wave is traveling.

C.3.3 Non-elastic Media. Most of the studies concerned with the influence of non-linear elastic soil properties on the propagation of waves have been carried out for the one-dimensional situation. It is an effective technique for studying the influence of the variation of the soil stress-strain-time function since no effects of spatial dispersion of energy are present and the equation of motion is in the simplest possible form.

The studies of Ref. C-10, providing numerical solutions of the one-dimensional wave equation for visco-elastic and elasto-plastic soils, are discussed in Section 4.2.2. Studies of the effects of bi-linear stress-strain relations with the second modulus greater than the first which approximate the behavior of confined granular soils, are given in Refs. C-8 and C-9.

Formulations for the propagation of plane and three-dimensional waves in visco-elastic materials may be found in previously mentioned Refs. C-2, C-4, C-5, and C-6. The problems of solution are considerable, but Ref. C-6 does present the results of some solutions showing the marked reductions in peak stress at depth resulting from the energy absorption due to viscous response of the soil.

Additional study of the influence of non-elastic soil behavior on displacements is required. It is necessary that such work be accompanied by studies of soil behavior since the mathematical formulations the stress-strain-time properties of soils must be demonstrated to represent reasonably their behavior.

C.4 REFERENCES

- C-1 Kolsky, H., "Stress Waves in Solids," Oxford, Clarendon Press, 1953. (UNCLASSIFIED)
- C-2 Sauer, F. M., "Ground Motion Produced by Aboveground Nuclear Explosions," AFSWC-TR-59-71, April 1959. (SECRET FRD)
- C-3 Baron, M. L. and Lecht, C., "Elastic Rayleigh Wave Effects due to Nuclear Blasts," Journal of the Engineering Mechanics Division, ASCE, Vol. 87, EM5, October 1961. (UNCLASSIFIED)
- C-4 Baron, M. L., Bleich, H. H., and Weidlinger, P., "Theoretical Studies on Ground Shock Phenomena," The Mitre Corporation, SR-19, October 1960. (UNCLASSIFIED)
- C-5 Cinelli, G. and Fugelso, L. E., "Theoretical Study of Ground Motion Produced by Nuclear Blasts," AFSWC-TR-60-8, 30 October 1959. (UNCLASSIFIED)
- C-6 Weidlinger, Paul, "A Study on the Effect of a Progressing Surface Pressure on a Visco-Elastic Half-Space," The Mitre Corporation, SR-22, 20 February 1961. (UNCLASSIFIED)
- C-7 Timoshenko, S. and Goodier, J. N., "Theory of Elasticity," McGraw-Hill Book Company, Inc., New York, 1951. (UNCLASSIFIED)
- C-8 Skalak, R. and Weidlinger, P., "Attenuation of Stress Waves in Bi-Linear Materials," Journal of the Engineering Mechanics Division, ASCE, Vol. 87, EM3, June 1961. (UNCLASSIFIED)
- C-9 Salvadori, M. G., Skalak, R. and Weidlinger, P., "Waves and Shocks in Locking and Dissipative Media," Journal of the Engineering Mechanics Division, ASCE, Vol. 86, EM2, April 1960. (UNCLASSIFIED)
- C-10 Smith, R. H. and Newmark, N. M., "Numerical Integration for One-Dimensional Stress Waves," Civil Engineering Studies, Structural Research Series No. 162, University of Illinois, Urbana, Illinois, August 1958. (UNCLASSIFIED)

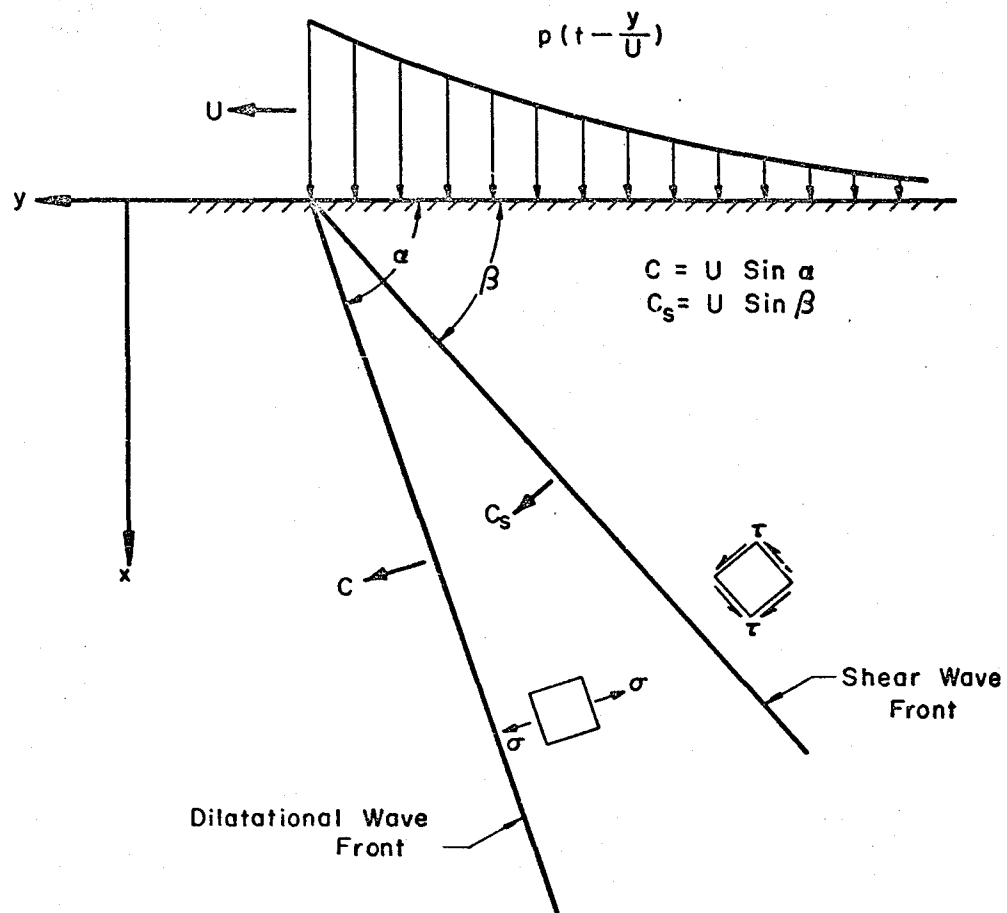
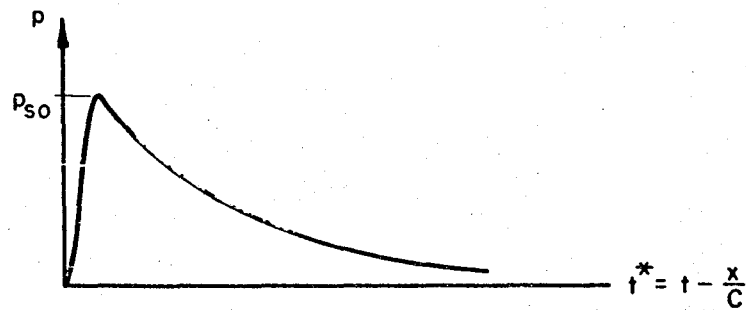
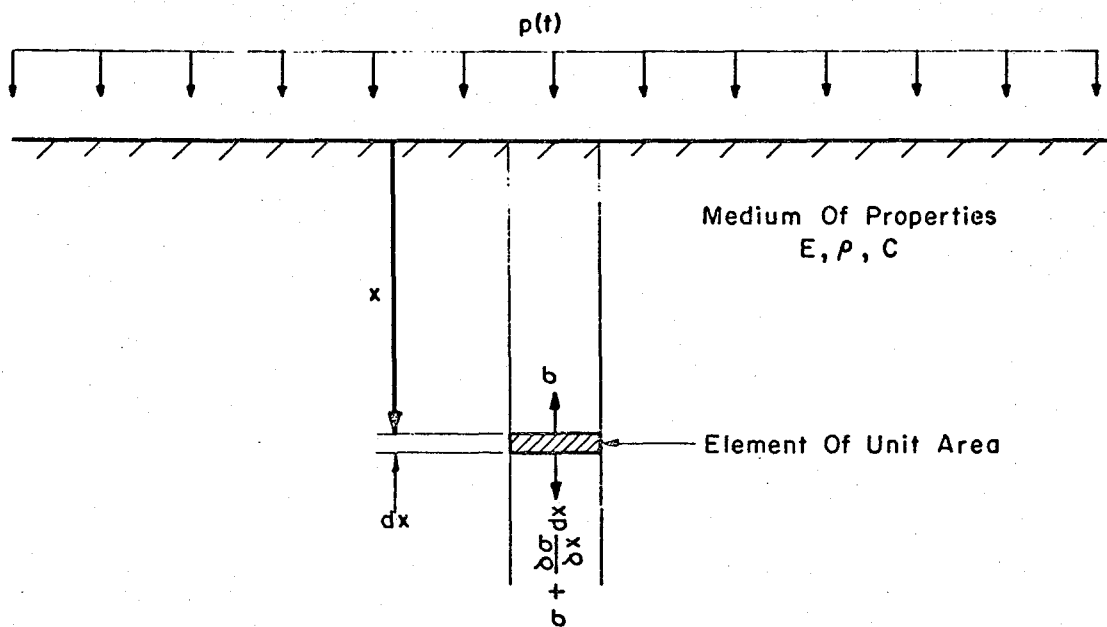


FIG. C-1 DILATATIONAL AND SHEAR WAVE FRONTS
FOR A SUPERSEISMIC PLANE WAVE OF
CONSTANT VELOCITY OF PROPAGATION.

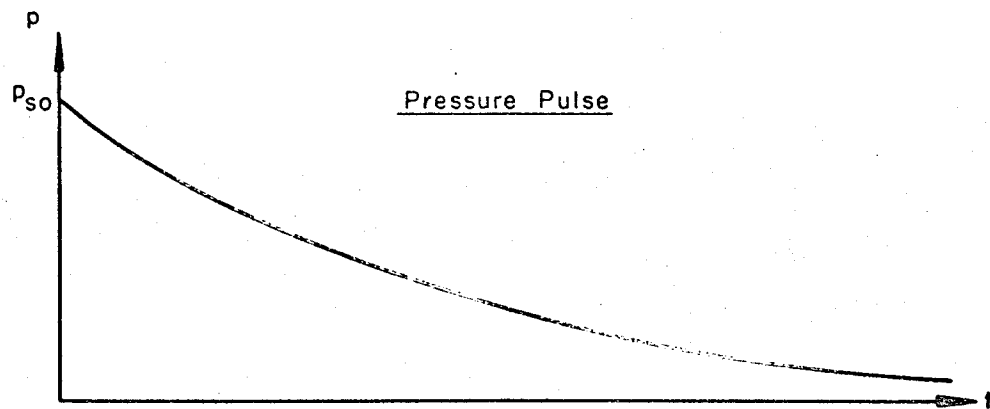


Overpressure - Time Variation



Stresses On An Element Of The Medium

FIG. C-2 ONE-DIMENSIONAL WAVE CONDITIONS.



Location Of Wave Front With Respect To
Depth (x) And Time (t)

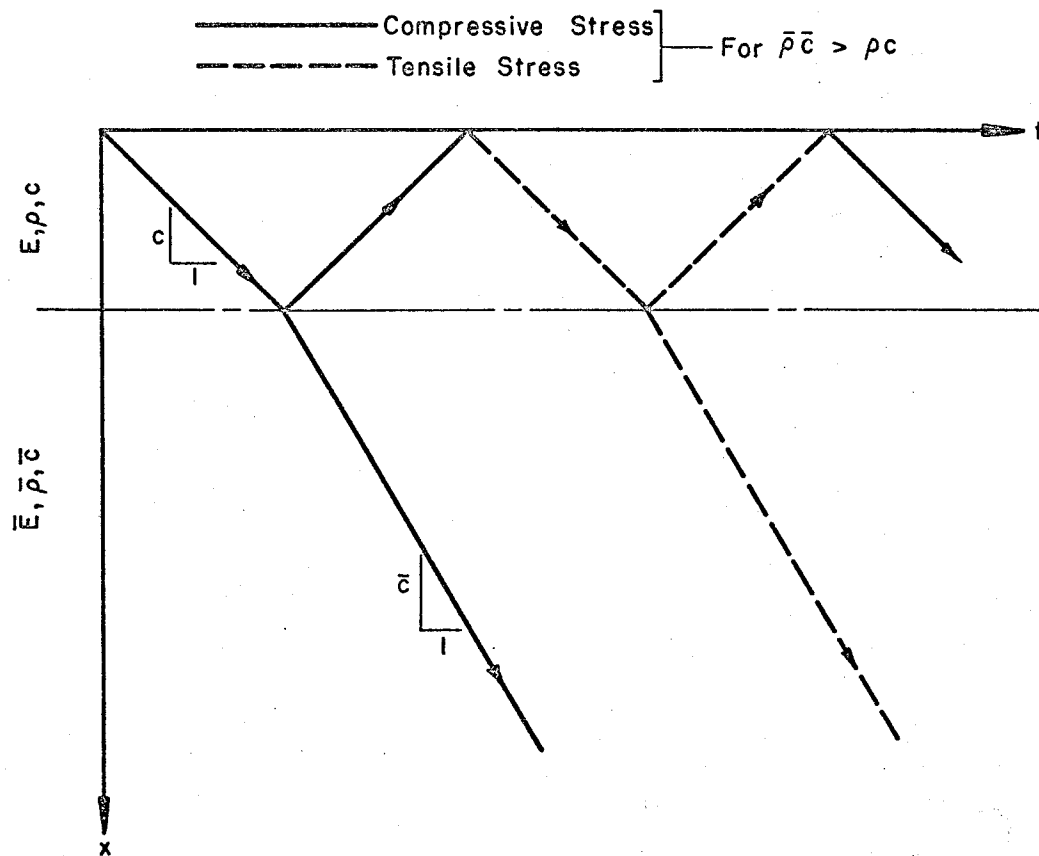


FIG. C-3 ONE-DIMENSIONAL WAVE IN A LAYERED MEDIUM

APPENDIX D

NOMENCLATURE

a	=	width of beam
a_p	=	peak vertical acceleration of soil in free-field, air-induced shock
a_r	=	maximum radial acceleration in free-field, direct transmitted shock
A	=	cross sectional area of an arch; also Response Spectrum Acceleration
A_c	=	cross-sectional area of concrete column
A_s	=	area of steel in a reinforced concrete member
A_w	=	area of steel beam web
b	=	width of loaded area; also flange width of steel beam
b_s	=	width of stiffener
B	=	span of an arch
c	=	static cohesive strength of soil; also, seismic velocity in elastic medium
c_i	=	seismic velocity consistent with M_i
c_o	=	ambient sound velocity in dry air
c_p	=	seismic velocity consistent with M_p
c_r	=	seismic velocity consistent with M_r
C	=	lateral seismic coefficient
C_d	=	drag coefficient
C_{do}	=	drag coefficient for an object
C_{dp}	=	drag coefficient for a point pressure

C_{ds}	=	drag coefficient for a surface
C_f	=	drag coefficient on front face
C_r	=	reflection coefficient = p_{ro}/p_{so} ; also drag coefficient on rear face
C_r^i	=	drag coefficient on roof
d	=	effective depth of steel in concrete members; also depth of web in steel beams
d_p	=	peak transient vertical displacement of soil, air-induced shock
d_{pe}	=	elastic component of relative displacement over depth z , air-induced shock
d_r	=	residual displacement, air-induced shock; also, maximum radial displacement in free-field, direct-transmitted shock
d_{rs}	=	residual displacement of ground surface, air-induced shock
d_{rz}	=	residual displacement at depth z , air-induced shock
d_{se}	=	peak elastic displacement at surface, air-induced shock
D	=	total depth or thickness of a member; also Response Spectrum Displacement
D_p^+	=	duration of overpressure positive phase
D_u^+	=	duration of dynamic pressure positive phase
e	=	void ratio of soil
e_o	=	void ratio of soil in situ
ev	=	electron volt
E	=	modulus of elasticity
E_c	=	effective modulus of elasticity for concrete
E_i	=	initial tangent modulus
f	=	frequency

f_{cr}	=	critical buckling stress; also usable stress capacity of material composing arch
f_c^i	=	28 day compressive strength of concrete
f_{dc}^i	=	dynamic compressive strength of concrete
f_{dy}	=	dynamic yield stress of steel
f_y	=	static yield stress of steel
F	=	lateral force at floor of multistory building resulting from base motion
g	=	acceleration of gravity
h	=	depth from ground surface to top of structure; also, height above base of multistory building
H	=	effective wave length in feet; also, the smaller of $(h-0.25L)$ or $(2L)$ for soil arching study; also horizontal boundary force on dome
H_{av}	=	average depth of earth cover
H_c	=	critical depth of soil overburden to produce creep
I	=	moment of inertia
I_c	=	moment of inertia at cracked concrete section
I_p^+	=	overpressure impulse
I_u^+	=	dynamic pressure impulse
K	=	stiffness factor; also ratio of horizontal to vertical soil pressure for general case
K^i	=	stiffness factor including soil resistance
K_h	=	fraction of \bar{p} considered to act on wall of mounded structure
K_o	=	ratio of horizontal to vertical soil pressure for zero lateral strain
K_r	=	rise-time factor

K_v	=	fraction of \bar{p} considered to act on roof of mounded structure
L	=	span length for beam, or length of structure; also, least plan dimension of structure for soil arching study
L_L	=	length of <u>long</u> span for two-way slab
L_s	=	length of <u>short</u> span for two-way slab
m	=	mass of structural element per unit length
m'	=	mass of structural element plus soil per unit length
mev	=	million electron volts
M	=	constrained modulus of deformation of soil; also, bending moment
M_i	=	initial tangent modulus during loading (Fig. 4-9)
M_p	=	fully plastic moment; also, idealized modulus during loading (Fig. 4-9)
M_p^t	=	fully plastic moment with axial load
M_r	=	idealized modulus during unloading (Fig. 4-9)
M_F^c	=	fully plastic moment at center of span
M_p^e	=	fully plastic moment at end of span
n	=	$1 - (0.02L/\delta_0)$ for soil arching study; also, π/β for arch flexural computations
o_p	=	preconsolidation ratio for soil (Sect. 4.2.3)
o_s	=	overstress ratio for soil (Sect. 4.2.3)
P_c	=	compressive mode pressure for arch, dome, or silo
P_{cr}	=	elastic buckling pressure
P_d	=	dynamic pressure
P_{dm}	=	peak value of drag component of flexural load on arch or dome
P_{do}	=	peak dynamic pressure

P_{im}	=	peak value of initial component of flexural load on arch or dome
P_f	=	flexural mode pressure for arch, dome, or silo
P_{f1}	=	initial component of P_f
P_{f2}	=	drag component of P_f
P_h	=	free-field horizontal pressure in soil at depth z
P_m	=	peak value of loading pressure on structure
P_o	=	ambient atmospheric pressure; also, uniform pressure on roof of buried structure = p_{vp} minus arching effect; also, in-situ soil overburden pressure
p_o'	=	previous maximum value of soil overburden pressure
P_{∞}	=	static radial pressure on silo at infinite depth
P_{ro}	=	peak reflected pressure
P_s	=	side-on overpressure on ground surface
P_{so}	=	peak side-on overpressure on ground surface
P_v	=	free-field vertical pressure in soil at depth z
P_{vp}	=	maximum free-field vertical pressure at depth z or, for soil arching, at depth h
P_z	=	static radial pressure on silo at depth z
\bar{p}	=	pressure on windward slope of embankment
P	=	thrust in arch or column
P_{cr}	=	buckling strength in direct compression
P_u	=	ultimate strength in direct compression
q	=	yield resistance of member, general
q_c	=	compression mode resistance
q_f	=	flexural mode resistance

q_u	=	ultimate resistance; also, unconfined compressive strength of soil
q_v	=	shear resistance
q_y	=	diagonal tension resistance of a reinforced concrete member
r	=	radius of arch, dome, or silo; also, roentgen, measure of strength of radiation field (Sect. 12.4.2)
r_g	=	radius of gyration
rad	=	unit of absorbed dose of nuclear radiation (Sect. 12.4.2)
rem	=	unit of biological dose of nuclear radiation (Sect. 12.4.2)
R	=	effect of rise time on required resistance; also, for arching computation, plan area divided by perimeter of structure; also, range from point of detonation
R_o	=	natural period factor due to support conditions
s	=	horizontal distance per unit rise of side slope
S	=	least distance from stagnation point to edge of obstruction
t	=	time; also, least width of column
t_d	=	effective duration
t_f	=	thickness of steel beam flange
t_i	=	impulse duration for overpressure
t_o	=	positive phase duration of overpressure at tunnel entrance
t_{∞}	=	the duration of an initially peaked triangular replacement with decay defined by tangent to the overpressure-time curve at p_{so}
t_r	=	rise time of pressure pulse
t_s	=	thickness of stiffener
t_w	=	thickness of steel beam web
t_{50}	=	the duration of an initially peaked triangular replacement with decay line passing through p_{so} and $0.5 p_{so}$ on the original overpressure-time curve

t_i'	=	impulse duration for dynamic pressure
t_o'	=	positive phase duration of pressure in tunnel
t_{∞}'	=	the duration of an initially peaked triangular replacement with decay defined by tangent to dynamic pressure-time curve at p_{do}
t_{50}'	=	the duration of an initially peaked triangular replacement with decay line passing through p_{do} and $0.5 p_{do}$ of the dynamic pressure-time curve
T	=	natural period of vibration; also, temperature
T'	=	natural period modified by soil mass effect
T_c	=	uniform compression mode period
T_f	=	flexural mode period
u	=	particle velocity
U	=	velocity of air blast shock front
v	=	average shear stress in flexural member
v_{dy}	=	dynamic shear yield stress in steel
v_{hp}	=	peak horizontal velocity of soil in free-field, air-induced shock
v_p	=	peak vertical velocity of soil in free-field, air-induced shock
v_r	=	peak radial velocity of soil in free-field, direct-transmitted shock
V	=	total shear; also, Response Spectrum Velocity
w	=	total weight per unit of slab area; also, unit weight of soil
W	=	weapon yield in megatons; also, weight of multistory building concentrated at floor levels
z	=	depth below ground surface in feet

z_1	=	depth of penetration of wave front
z_p	=	depth of penetration of wave peak
Z	=	plastic section modulus of steel beam
α	=	ratio of short to long spans of a two-way slab; also, side slope factor for mounded arches or domes (Sect. 5.4.3); also, effective column length
α_z	=	attenuation at depth z
β	=	one-half central angle of an arch or dome
β_s	=	one-half central angle of circular arc approximating ground surface over buried arch or dome
γ	=	factor for long beam under two-way slab; also, in-situ density of soil
δ_o	=	deflection of structural element under load p_o
ϵ	=	strain
η	=	correction factor for shear or diagonal tension resistance of a long beam under a two-way slab = $2/(2-\alpha)$
θ	=	horizontal angle
θ'	=	ratio of negative to positive reinforcement percentages
μ	=	ductility factor, ratio of maximum deflection to deflection at yield
ν	=	Poisson's ratio
ρ	=	mass density
τ	=	transit time of shock front across structure or element; also, shear stress in soil
ϕ	=	tensile steel percentage; also, static angle of internal friction in soil
ϕ'	=	compressive steel percentage
ϕ_c	=	tensile steel percentage at midspan

ϕ_e	=	tensile steel percentage at support
$\phi_{e \text{ avg}}$	=	average of tensile steel percentages at ends of beam
ϕ_{Lc}	=	tensile steel percentage at midspan in long direction of two-way slab
ϕ_{Le}	=	tensile steel percentage at supports in long direction of two-way slab
ϕ_{sc}	=	tensile steel percentage at midspan in short direction of two-way slab
ϕ_{se}	=	tensile steel percentage at supports in short direction of two-way slab
ϕ_t	=	total steel percentage
ϕ_v	=	web reinforcement percentage
ϕ_v'	=	percent of steel (inclined at 45°) crossing a surface inclined at 45°
ψ	=	correction factor to modify substitute beam for flexure mode of an arch
ψ	=	relative acoustic impedance of two adjacent strata (used only in Appendix C)
Ω	=	two-way slab factor for flexural resistance

